

40/8-91 JS (2)

ornl

ORNL-6624

**OAK RIDGE
NATIONAL
LABORATORY**

MARTIN MARIETTA

**FUSION ENERGY
DIVISION**



**ANNUAL PROGRESS
REPORT**

MANAGED BY
MARTIN MARIETTA ENERGY SYSTEMS, INC.
FOR THE UNITED STATES
DEPARTMENT OF ENERGY

Period Ending December 31, 1989

DISTRIBUTION OF THIS DOCUMENT IS UNLIMITED

This report has been reproduced directly from the best available copy.

Available to DOE and DOE contractors from the Office of Scientific and Technical Information, P.O. Box 62, Oak Ridge, TN 37831; prices available from (615) 576-8401, FTS 626-8401.

Available to the public from the National Technical Information Service, U.S. Department of Commerce, 5285 Port Royal Rd., Springfield, VA 22161.

This report was prepared as an account of work sponsored by an agency of the United States Government. Neither the United States Government nor any agency thereof, nor any of their employees, makes any warranty, express or implied, or assumes any legal liability or responsibility for the accuracy, completeness, or usefulness of any information, apparatus, product, or process disclosed, or represents that its use would not infringe privately owned rights. Reference herein to any specific commercial product, process, or service by trade name, trademark, manufacturer, or otherwise, does not necessarily constitute or imply its endorsement, recommendation, or favoring by the United States Government or any agency thereof. The views and opinions of authors expressed herein do not necessarily state or reflect those of the United States Government or any agency thereof.

Dist. Code ORNL--6624

DE92 000388

FUSION ENERGY DIVISION ANNUAL PROGRESS REPORT

Period Ending December 31, 1989

J. Sheffield
C. C. Baker
M. J. Saltmarsh

Fusion Energy Division Staff

Date Published: July 1991

Prepared for the
Office of Fusion Energy
Budget Activity No. 25 19 00 00 0

Prepared by the
OAK RIDGE NATIONAL LABORATORY
Oak Ridge, Tennessee 37831-6285
managed by
MARTIN MARIETTA ENERGY SYSTEMS, INC.
for the
U.S. DEPARTMENT OF ENERGY
under contract DE-AC05-84OR21400

MASTER

JMP

Report previously issued in this series are as follows:

ORNL-2693	Period Ending January 31, 1959
ORNL-2802	Period Ending July 31, 1959
ORNL-2926	Period Ending January 31, 1960
ORNL-3011	Period Ending July 31, 1960
ORNL-3104	Period Ending January 31, 1961
ORNL-3239	Period Ending October 31, 1961
ORNL-3315	Period Ending April 30, 1962
ORNL-3392	Period Ending October 31, 1962
ORNL-3472	Period Ending April 30, 1963
ORNL-3564	Period Ending October 31, 1963
ORNL-3652	Period Ending April 30, 1964
ORNL-3760	Period Ending October 31, 1964
ORNL-3836	Period Ending April 30, 1965
ORNL-3908	Period Ending October 31, 1965
ORNL-3989	Period Ending April 30, 1966
ORNL-4063	Period Ending October 31, 1966
ORNL-4150	Period Ending April 30, 1967
ORNL-4238	Period Ending October 31, 1967
ORNL-4401	Period Ending December 31, 1968
ORNL-4545	Period Ending December 31, 1969
ORNL-4688	Period Ending December 31, 1970
ORNL-4793	Period Ending December 31, 1971
ORNL-4896	Period Ending December 31, 1972
ORNL-4982	Period Ending December 31, 1973
ORNL-5053	Period Ending December 31, 1974
ORNL-5154	Period Ending December 31, 1975
ORNL-5275	Period Ending December 31, 1976
ORNL-5405	Period Ending December 31, 1977
ORNL-5549	Period Ending December 31, 1978
ORNL-5645	Period Ending December 31, 1979
ORNL-5674	Period Ending December 31, 1980
ORNL-5843	Period Ending December 31, 1981
ORNL-5919	Period Ending December 31, 1982
ORNL-6015	Period Ending December 31, 1983
ORNL-6111	Period Ending December 31, 1984
ORNL-6234	Period Ending December 31, 1985
ORNL-6332	Period Ending December 31, 1986
ORNL-6452	Period Ending December 31, 1987
ORNL-6528	Period Ending December 31, 1988

CONTENTS

SUMMARY	xi
1. TOROIDAL CONFINEMENT ACTIVITIES	1
SUMMARY OF ACTIVITIES	3
1.1 THE ATF PROGRAM	4
1.1.1 Overview	4
1.1.2 Confinement Studies	4
1.1.3 Fluctuation Studies	6
1.1.4 Impurity Studies	9
1.1.4.1 Gettering and impurity radiation	10
1.1.4.2 Effects of gettering on plasma performance	12
1.1.4.3 Impurity injection	16
1.2 EDGE PHYSICS AND PARTICLE CONTROL PROGRAM	19
1.2.1 Edge Plasma Studies and Particle Control in ATF	20
1.2.1.1 Initial measurements of edge plasma turbulence using a fast reciprocating Langmuir probe	20
1.2.1.2 Gettering techniques	22
1.2.2 Helium Removal Experiments and H_{α} Studies on ALT-II in TEXTOR	23
1.2.2.1 Helium exhaust and transport studies	23
1.2.2.2 Modeling of H_{α} emission and plasma confinement	24
1.2.2.3 Analysis of recycling energy distributions from H_{α} measurements	25
1.2.3 Pump Limiter Studies on Tore Supra: Measurements of Pressure Buildup and Particle Fluxes	26
1.2.4 The DIII-D Advanced Divertor Program	27
1.2.4.1 Neutral particle modeling	27
1.2.4.2 The pre-VORTEX code	28
1.2.4.3 Diagnostics	30
1.2.4.4 Divertor pumping	31
1.3 ATF-II STUDIES	32
1.3.1 Transport Code Development	33
1.3.2 Effect of the Electric Field	33
1.3.3 Results of Reactor Surveys	34
1.3.4 Conclusions	35
REFERENCES	35

2. ATOMIC PHYSICS AND PLASMA DIAGNOSTICS	
DEVELOPMENT	37
SUMMARY OF ACTIVITIES	39
2.1 EXPERIMENTAL ATOMIC COLLISIONS	41
2.1.1 Electron Capture in $O^{3+} + H(D)$ and $O^{4+} + H(D)$ Collisions Using Merged Beams	41
2.1.2 Dissociation and Ionization of CD_4^+ by Electron Impact	42
2.1.3 Studies of Angular Dependence and Line Shapes for Auger Electron Emission in Low-Energy $He^{9+} + He$ Collisions	43
2.1.4 Auger Spectroscopy of Low-Energy Multicharged Ion-Atom Collisions	45
2.1.5 Electron Spectroscopy of Multicharged Ion-Surface Interactions	47
2.1.6 Merged-Beams Experiment for Electron-Impact Excitation of Ions	49
2.1.7 Electron-Impact Ionization of Ta^{8+}	49
2.2 ATOMIC COLLISION THEORY	50
2.2.1 Abstract of "Strong-Field Laser Ionization of Alkali Atoms Using 2-D and 3-D Time-Dependent Hartree-Fock Theory"	50
2.2.2 Abstract of "Coupling Effects for Electron-Impact Excitation in the Potassium Isoelectronic Sequence"	50
2.2.3 Abstract of "Indirect Processes in the Electron Impact Ionization of Atomic Ions"	50
2.2.4 Abstract of "Correlation Enhancement of the Electron-Impact Ionization Cross Section for Excited State Ne-Like Ions"	50
2.2.5 Time-Dependent Hartree-Fock Studies of Ion-Atom Collisions	51
2.3 CONTROLLED FUSION ATOMIC DATA CENTER	51
2.4 ADVANCED PLASMA DIAGNOSTICS DEVELOPMENT	53
2.4.1 Small-Angle CO_2 Laser Thomson Scattering Diagnostic for D-T Fusion Product Alpha Particles	53
2.4.2 Multichannel Far-Infrared Interferometer and Scattering System for the Advanced Toroidal Facility	53
2.4.3 Feasibility Studies of a Two-Color Interferometer/Polarimeter for the Compact Ignition Tokamak	55
2.4.4 Optics Damage and Irradiation Studies	57
REFERENCES	58
3. FUSION THEORY AND COMPUTING	61
SUMMARY OF ACTIVITIES	63
3.1 EQUILIBRIUM AND STABILITY	65
3.1.1 Overview	65

3.1.2	Highlights of 1989	66
3.1.2.1	ATF operation in the second stability regime	66
3.1.2.2	Stability of helical-axis stellarators	67
3.1.3	Advanced VMEC Equilibrium Analysis	67
3.2	TURBULENCE	69
3.2.1	Overview	69
3.2.2	Highlights of 1989	70
3.2.2.1	The hybrid fluid-kinetic model	70
3.2.2.2	Trapped-electron modes	71
3.2.2.3	Edge turbulence modeling	71
3.3	KINETIC THEORY	72
3.3.1	Cause and Effect of Electric Fields in Toroidal Devices	72
3.3.2	Ripple Losses of Alpha Particles in ITER	73
3.3.3	Benchmark Studies of Neutral Beam Injection for Stellarators/Heliotrons	73
3.3.4	Beam Deposition and TF Ripple in TEXT	73
3.4	TRANSPORT AND CONFINEMENT MODELING	77
3.4.1	General Transport Studies	77
3.4.2	ITER Studies	77
3.4.3	CIT Studies	77
3.4.4	ATF Studies	78
3.4.5	Pellet Injection Studies on JET	78
3.5	RF HEATING	79
3.5.1	Global ICRF Wave Propagation in Edge Plasma and Faraday Shield Regions	80
3.5.2	Fast-Wave Current Drive Modeling for ITER and DIII-D	80
3.5.3	Electron Heating and Static Sheath Enhancement in Front of Energized RF Antenna	82
3.6	COMPUTING AND OPERATIONS	84
	REFERENCES	85
4.	PLASMA TECHNOLOGY	89
	SUMMARY OF ACTIVITIES	91
4.1	PLASMA FUELING PROGRAM	93
4.1.1	Pellet Injector Development	93
4.1.1.1	Electron-beam rocket pellet injector	94
4.1.1.2	CIT and ITER fueling	96
4.1.1.3	Tritium injector	97
4.1.1.4	Two-stage light gas gun	98
4.1.2	Pellet Injector Applications	103
4.1.2.1	ATF pellet injector	103
4.1.2.2	Tore Supra pellet injector	104
4.1.2.3	JET	105

4.1.3	Pellet Projects: High-Speed Injector	107
4.1.4	Work for Others	107
4.2	RF TECHNOLOGY	108
4.2.1	Basic Development	108
4.2.1.1	Faraday shield studies	108
4.2.1.2	Plasma-materials interactions	110
4.2.1.3	Fast-wave current drive	111
4.2.1.4	Folded waveguide	113
4.2.1.5	RF modeling	115
4.2.2	RF Projects	119
4.2.2.1	Tore Supra antenna	119
4.2.2.2	Alcator C-Mod ICRF antenna project	120
4.2.2.3	Fast-wave current drive antenna for DIII-D	123
4.2.2.4	CIT antenna	124
4.2.3	ICRH Experiments on TFTR	124
4.3	NEUTRAL BEAMS	125
4.3.1	Ion Sources	125
4.3.1.1	Enhancement of negative ion extraction and electron suppression by a magnetic field	125
4.3.1.2	Measurement of the H ⁻ thermal energy by two-laser photodetachment	126
4.3.1.3	Analysis of the initial stages of H ⁻ evolution	126
4.3.2	RFQ-Accelerated High-Energy Beams	129
4.3.2.1	Ion source	129
4.3.2.2	Low-energy beam transport system	130
4.3.2.3	RF accelerator	130
4.3.2.4	Neutralizer	130
4.3.2.5	Beam dump	131
4.3.3	Negative Ion Beams	131
4.3.4	Upgrade of the T-15 Long-Pulse Ion Source	132
	REFERENCES	136
5.	SUPERCONDUCTING MAGNET DEVELOPMENT	139
	SUMMARY OF ACTIVITIES	141
5.1	EXPERIMENTAL WORK	142
5.1.1	Superconducting Magnet Design	142
5.1.2	Quench Propagation, Pressure Rise, and Thermal Expulsion of Helium from a Cable-in-Conduit, Forced-Flow Superconductor	142
5.1.3	Magnetic Heat Pump Test	142
5.1.4	Large Coil Task	143

5.2	THEORETICAL RESEARCH	143
5.2.1	The Gorter-Mellink Pulsed-Source Problem in Cylindrical and Spherical Geometry	143
5.2.2	Propagation of Normal Zones of Finite Size in Large, Composite Superconductors	144
	REFERENCES	144
6.	ADVANCED SYSTEMS PROGRAM	145
	SUMMARY OF ACTIVITIES	147
6.1	CIT	149
6.1.1	Ex-Vessel Remote Maintenance	149
6.1.1.1	Remote maintenance systems	149
6.1.1.2	Graphic modeling	149
6.1.1.3	Task evaluations	151
6.1.1.4	Special tools	153
6.1.2	Vacuum System and Shield	153
6.1.2.1	Vacuum system	153
6.1.2.2	Thermal shield	154
6.1.3	Ion Cyclotron Resonance Heating System	154
6.1.4	Fueling System	155
6.1.5	Insulation for the TF Coils	157
6.1.6	MHD Equilibrium and Poloidal Field System Studies	158
6.1.7	Plasma Disruption Simulations	159
6.1.8	Structural Materials	160
6.2	ITER	160
6.2.1	Plasma Engineering	160
6.2.1.1	Systems analysis	161
6.2.1.2	Plasma disruption simulations	161
6.2.2	Engineering	163
6.2.2.1	Configuration and maintenance	164
6.2.2.2	Electromagnetic and structural analysis	165
6.2.2.3	Fast-wave current drive system	166
6.2.2.4	Pellet injection system	167
6.2.3	Physics	172
6.2.3.1	ITER physics design guidelines	172
6.2.3.2	ITER confinement capability	173
6.2.3.3	ITER global stability limits	173
6.3	ARIES	174
6.3.1	MHD Equilibrium and Stability	174
6.3.2	Pellet Fueling	177
	REFERENCES	177

7. FUSION MATERIALS RESEARCH	179
SUMMARY OF ACTIVITIES	181
7.1 STRUCTURAL MATERIALS	182
7.1.1 Austenitic Stainless Steels: The U.S.–Japan Collaborative Program	182
7.1.2 ITER Design Database	183
7.1.2.1 Tensile properties	184
7.1.2.2 Swelling	186
7.1.3 Reduced-Activation Steels	187
7.1.4 Conventional Ferritic Steels	189
7.1.5 Copper	192
7.1.6 Vanadium Alloys	193
7.1.7 Corrosion Studies	194
7.2 GRAPHITE AND CARBON-CARBON COMPOSITES	195
7.3 CERAMICS	196
7.4 HFIR EXPERIMENTS	198
REFERENCES	199
8. NEUTRON TRANSPORT	201
SUMMARY OF ACTIVITIES	203
8.1 RADIATION SHIELDING INFORMATION CENTER	204
8.2 DATA EVALUATION AND PROCESSING FOR FUSION NEUTRONIC DATA NEEDS	205
8.3 REACTION RATE DISTRIBUTIONS AND RELATED DATA IN THE FUSION NEUTRON SOURCE PHASE II EXPERIMENTS: COMPARISON OF MEASURED AND CALCULATED DATA	205
REFERENCES	206
9. NONFUSION APPLICATIONS	207
SUMMARY OF ACTIVITIES	209
9.1 MICROWAVE PROCESSING OF RADIOACTIVE WASTES	210
9.2 MICROWAVE SINTERING	212
9.2.1 Background	212
9.2.2 Technical Progress	213
9.3 PLASMA PROCESSING	215
9.4 DIAMOND FILMS	217
9.5 EHD ION SOURCE	217
REFERENCES	219
10. MANAGEMENT SERVICES, QUALITY ASSURANCE, AND SAFETY	221
SUMMARY OF ACTIVITIES	223
10.1 MANAGEMENT SERVICES	224
10.1.1 General Administration Services	224

10.1.1.1	Personnel	224
10.1.1.2	Procurement	224
10.1.1.3	International agreements and collaboration	225
10.1.2	Engineering Services	225
10.1.3	Financial Services	225
10.1.4	Library Services	226
10.1.5	Publications Services	227
10.2	QUALITY ASSURANCE	228
10.2.1	QA Program Development and Training	228
10.2.2	QA Program Implementation	228
10.3	SAFETY AND ENVIRONMENTAL PROTECTION	228
10.3.1	Safety	228
10.3.2	Environment	228
Appendix 1. PUBLICATIONS AND PRESENTATIONS		231
Appendix 2. ACRONYMS AND ABBREVIATIONS		277
Appendix 3. FUSION ENERGY DIVISION ORGANIZATION CHART		283

SUMMARY

The Fusion Program of Oak Ridge National Laboratory (ORNL) carries out research in most areas of magnetic confinement fusion. The program is directed toward the development of fusion as an energy source and is a strong and vital component of both the U.S. fusion program and the international fusion community.

Issued as the annual progress report of the ORNL Fusion Energy Division, this report also contains information from components of the Fusion Program that are carried out by other ORNL organizations (about 15% of the program effort).

The areas addressed by the Fusion Program and discussed in this report include the following:

- experimental and theoretical research on magnetic confinement concepts,
- engineering and physics of existing and planned devices, including remote handling,
- development and testing of diagnostic tools and techniques in support of experiments,
- assembly and distribution to the fusion community of databases on atomic physics and radiation effects,
- development and testing of technologies for heating and fueling fusion plasmas,
- development and testing of superconducting magnets for containing fusion plasmas,
- development and testing of materials for fusion devices, and
- exploration of opportunities to apply the unique skills, technology, and techniques developed in the course of this work to other areas.

Highlights from program activities follow.

Toroidal Confinement Activities

Experimental research in the toroidal confinement area is concentrated mainly in two programs, the Advanced Toroidal Facility (ATF) Program and the Edge Physics and Particle Control (EPPC) Program. The ATF Program is an element of the U.S. Advanced Toroidal Program, which seeks to study improvements to the mainline fusion confinement concept, the basic first-stability tokamak. ATF, the world's largest stellarator, was designed to explore a broad spectrum of toroidal physics issues, including the second stability regime. The EPPC Program aims to characterize edge plasma behavior and to explore edge modification techniques for improved performance. This program is collaborative in nature and is carried out on a number of major confinement research facilities: TEXTOR (Jülich, Germany), Tore Supra (Cadarache, France, with support from the European Community), DIII-D (San Diego, California), and ATF. In addition, some research on advanced fusion projects is carried out in this area.

The progress of ATF during 1989 was quite satisfactory. Although only modest improvements in the facility and the diagnostics were possible owing to budget constraints, the results of the physics studies were notable. Since the removal of a field error that created large magnetic islands in the plasma, plasma profiles are broader and the operational space is significantly expanded (to longer-lived plasmas, higher density and stored energy, and longer energy confinement time). The plasma parameters are now similar to those of tokamaks of similar size. The flexibility of the magnetic configuration has been used in studies of bootstrap current. Several diagnostics are addressing plasma fluctuations in a coordinated effort

directed toward understanding their effect on transport, in support of the Tokamak Transport Initiative (TTI) of the U.S. Department of Energy (DOE). The behavior of impurities has been much more thoroughly documented. Collaboration continues to be an important part of the ATF program, with many international visitors to ORNL and exchanges with other experimental programs.

In the EPPC area, helium transport and removal studies were the focus of collaborative work on TEXTOR. Additional pump limiter diagnostics were installed and commissioned on Tore Supra. Contributions to the Advanced Divertor Program on DIII-D included predictions of divertor performance, evaluation of possible pumping systems, and preparation of divertor diagnostics.

Advanced project activity was extended to studies extrapolating the ATF-II compact torsatron approach to a reactor.

Atomic Physics and Plasma Diagnostics Development

Activities in the atomic physics and plasma diagnostics development program are divided among atomic collisions research, atomic data compilation and evaluation, and plasma diagnostics development.

Atomic collisions research focuses on inelastic processes that are important for determining the energy balance and impurity transport in high-temperature fusion plasmas and for diagnostic measurements. The electron-ion crossed-beams experiment was equipped with a new high-resolution electron gun as part of a collaboration with Niigata University, Japan, improving the electron energy resolution. In addition, an electron-ion merged-beams apparatus from the Joint Institute for Laboratory Astrophysics was installed on the main electron cyclotron resonance (ECR) beam line. Ejected Auger electron intensities and line shapes from collisions of helium atoms and ions with helium atoms were measured at different emission angles.

Data compilation and evaluation are carried out by the Controlled Fusion Atomic Data Center. Volume 6 of the "Redbook" series, *Atomic Data for Fusion*, was issued. The Data Center also continued its major role in the development and implementation of a universal system for the computer storage, retrieval, and exchange of recommended atomic data.

The plasma diagnostics program concentrates on the development of advanced diagnostics for magnetic fusion experiments. The pulsed-laser Thomson scattering diagnostic for alpha particles, which is being tested on ATF, was commissioned, and the multichannel far-infrared interferometer was installed on ATF and operated on seven channels by the end of the year. A 28- μm water vapor laser and an electro-optic polarization modulator were built and tested for use in a two-color interferometer/polarimeter for the Compact Ignition Tokamak (CIT).

Fusion Theory and Computing

The fusion theory and computing effort is characterized by close interaction with the division's experimental programs and with the national and international fusion programs.

Progress continued in the area of turbulence and confinement degradation in toroidal systems. In support of the TTI mission to characterize, understand, and control anomalous transport losses in toroidal systems, turbulent transport phenomena in the edge regions of

ATF and the Texas Experimental Tokamak (TEXT) were modeled in detail. Cooperative work with the TEXT group led to substantial progress in determining the appropriate models to represent the experimental data.

The influence of the radial electric field on the transition from the L-mode to the H-mode of operation (identified by lower and higher energy confinement times) was studied further. Data from several experiments provided increasing support for the bifurcation theories proposed by ORNL researchers.

Theoretical modeling of the antenna and Faraday shield regions and of the wave propagation and energy deposition processes in the plasma has become increasingly important as heating and current drive systems for new experiments are developed. Results from the ORION and RAYS codes were used in the International Thermonuclear Experimental Reactor (ITER) and CIT programs and in proposals by the DIII-D group at General Atomics and by Princeton Plasma Physics Laboratory (PPPL).

Work to understand the behavior of ATF was a key part of the program. Theoretical calculations were compared with experimental data in studies of the second stability regime and of the dependence of the bootstrap current on geometrical factors.

Existing computational tools were improved and new ones formulated. Examples include expressions for the neoclassical viscosity with strong rotation and plateau regime collisionality, a hybrid fluid-kinetic model for plasma turbulence, methods for speeding up and improving the convergence of the widely used VMEC equilibrium code, and testing and application of orbit-following models.

Experiments undertaken on the Joint European Torus (JET) to refine the theoretical understanding of pellet penetration showed that the velocity dependence of the penetration depth is greater than previously predicted. This improves the likelihood of finding a method of depositing fuel near the center of a device at the ITER and demonstration reactor scales.

In the computing area, efforts focused on improving the ATF data acquisition system and the associated software. New workstation computers are being used to improve the visualization of scientific data and to provide effective analysis.

Plasma Technology

The Plasma Technology Section carries out the division's research into and development of plasma fueling systems, rf technology, and neutral beams.

Development of the centrifuge and pneumatic pellet injector concepts and of advanced concepts to achieve higher pellet speeds for more demanding plasma fueling applications (e.g., CIT and ITER) continued. The centrifugal pellet injector for the Tore Supra tokamak was installed and successfully tested, and an eight-pellet pneumatic injector was installed and operated on ATF. Testing of the tritium proof-of-principle pneumatic injector on the Tritium Systems Test Assembly at Los Alamos National Laboratory was completed, demonstrating the feasibility of tritium fueling for CIT and ITER. The ORNL repeating pneumatic injector continued to be a key in the achievement of impressive plasma parameters on JET. Development of the electron-beam rocket accelerator and the two-stage light gas gun continued. Interest at PPPL in injecting high-velocity impurity pellets to peak the electron density profile in high-temperature discharges in the Tokamak Fusion Test Reactor (TFTR) led to a collaboration in which the two-stage light gas gun was used to accelerate several LiH pellets to velocities of 3.6 to 4.4 km/s.

In the rf technology program, the ion cyclotron range of frequencies (ICRF) heating systems on TFTR were operated at new power levels and pulse lengths; the ORNL antenna reached a power level of >1.0 MW for 1.0-s pulses. The ICRF antenna for Tore Supra was tested in the Radio Frequency Test Facility (RFTF) and then shipped to Cadarache, installed on Tore Supra, and tested. The design of a four-strap, 2-MW ICRF antenna for DIII-D was completed, and construction was under way at year's end; the antenna will be used for a high-field test of current drive and for core plasma heating. The folded waveguide antenna was tested in RFTF, with encouraging results. Studies of interactions between rf power and materials, also conducted on RFTF, were completed, demonstrating that rf power increased plasma edge temperatures and potentials, consistent with modeling results. The electromagnetic properties of several Faraday shield geometries were calculated.

The radio-frequency quadrupole (RFQ) concept for high-energy neutral beams was the focus of a broad collaborative effort that led to the development of an architecture for an ITER-relevant neutral beam line. A collaboration with Ecole Polytechnique (France) on the volume negative ion source continued, as did modeling of negative ion sources and ion beam dynamics.

Superconducting Magnet Development

The Magnetics and Superconductivity Section carries out experimental and theoretical research in applied superconductivity. Activities this year focused on optimization of conductor design, exploration of new applications for technology developed in support of fusion research, and development and application of mathematical techniques for designing and understanding superconducting magnets. Analysis of the extensive data from the international Large Coil Task continued.

Advanced Systems

The Advanced Systems Program was organized in 1987 as a focal point for design studies of future fusion experiments. The Fusion Engineering Design Center (FEDC) is the major engineering resource for this program. The principal activities of the Advanced Systems Program during 1989 were the CIT project, directed by PPPL; the ITER project, under the auspices of the International Atomic Energy Agency; and the Advanced Reactor Innovation and Evaluation Studies (ARIES) project, managed by the University of California at Los Angeles. Some work on the spherical torus concept was carried out.

ORNL continued to have lead responsibility for design integration and for six elements of the CIT design: ex-vessel remote maintenance, vacuum systems, ICRF heating, shielding, external structure, and fueling, with additional responsibility for toroidal field (TF) coil insulation. A conceptual design for a pellet injection system was developed, and candidate TF coil materials were tested.

The conceptual design phase of the ITER project, an international collaboration involving the United States, the U.S.S.R., the European Community, and Japan, continued through 1989. The Design Center led the U.S. effort in configuration development, design integration, mechanical design of plasma-facing components and blankets, facilities, reliability and availability analysis, remote maintenance, design and analysis of heating and current drive, and cost estimating. Design Center representatives participated in the ITER joint work sessions in

Garching. The FEDC designs for the divertor and the plasma vacuum vessel were accepted as the reference designs, and the FEDC interval segmentation approach was identified as the preferred approach. A concept was developed for a fast-wave current drive system. The TETRA systems code, developed and maintained under the direction of the Design Center, was used to examine the operational space for the ITER technology phase.

As input to development of the ARIES-II concept, D-³He ignition and burn criteria were examined. The results were more favorable for a configuration based on a spherical torus than for one based on a second-stability tokamak.

ORNL was asked by Culham Laboratory to analyze the efficacy of Culham's novel compression approach to create spherical torus plasmas with 200-kA plasma currents and aspect ratios of ≈ 1.2 for the small, tight-aspect-ratio tokamak (START) experiments. The request also included a charge to develop collaborative programs for spherical torus research and device design.

Materials Research and Development

The Fusion Materials Program is focused on the development of materials for use in components of a fusion reactor that will be exposed to high neutron fluences during their design life. Austenitic and martensitic steels are being developed for first wall and structural applications; copper alloys, graphite, and carbon-carbon composites for high-heat-flux components; and ceramics for electrical insulators, rf windows, and possible structural applications.

A collaborative program with the Japan Atomic Energy Research Institute to study the properties of austenitic and martensitic steels for fusion entered its sixth year. Four spectrally tailored experiments were designed for the High-Flux Isotope Reactor (HFIR). Data from experiments in the Fast Flux Test Facility appear to indicate radiation-induced depletion of chromium, which increases the susceptibility of austenitic stainless steels to intergranular stress-corrosion cracking. Standard chemical immersion tests showed that reduced-activation austenitic steels are more prone to thermal sensitization and thus to intergranular corrosion than standard 300-series stainless steels. A database on the mechanical properties of austenitic stainless steels is being assembled for ITER under the leadership of ORNL.

In a long-range program to study the effects of transmutation-produced helium on the properties of the ferritic/martensitic steels, it was found that irradiation in HFIR with helium concentrations of 30 to 100 appm produces a large upward shift of the ductile-to-brittle transition temperature. This problem must be addressed before these steels can be considered viable structural materials for fusion.

The fatigue behavior of copper and Glidcop Al-15 is being investigated for the ITER divertor assembly. At room temperature, Glidcop has a lifetime of $\sim 5 \times 10^5$ cycles at 150 MPa, an order of magnitude longer than the fatigue lifetime of copper.

Polycrystalline specimens of spinel and alumina were irradiated at room temperature and at 650°C with either dual or triple ion beams to investigate the effects of simultaneous damage displacement and helium implantation. Catastrophic amounts of cavitation were observed at the grain boundaries in spinel when displacement damage exceeded a critical level (~ 40 dpa) in the presence of a fusion-relevant helium concentration.

Neutron Transport

The Neutron Transport Program, carried out within the Engineering Physics and Mathematics Division, includes three elements: analyses, cross-section evaluation and processing, and the work of the Radiation Shielding Information Center.

The analysis program is part of a joint U.S.–Japan neutronics program and is directed at validating computer codes and cross-section data by comparing calculated results with experimental data obtained from the Fusion Neutron Source facility at the Japan Atomic Energy Research Institute.

The data evaluation and processing program is directed at producing accurate cross-section data for materials that are of interest to fusion reactor designers.

The Radiation Shielding Information Center responds to inquiries about radiation transport problems from an international community. Staff members provide guidance by drawing on a technical database that includes a computerized literature file, a collection of computer programs, and a substantial body of nuclear data libraries.

Nonfusion Applications

In recent years, fusion technology development has been broadened to include nonfusion applications. Challenging opportunities have been identified in many areas in which the technology to be advanced is related to fusion in that advances expected to result from the work will directly benefit future fusion systems, although the initial application may not be directly fusion related.

The nonfusion technology applications are concentrated in four technical fields: (1) energy, (2) U.S. DOE facility environmental restoration and waste management, (3) defense, and (4) technology transfer to industry, through which the competitive position of the United States can be improved. Efforts during 1989 included microwave processing of radioactive wastes, microwave sintering of ceramics, plasma processing for semiconductors, and diamond film growth.

The range of activities, the scope of the collaborative work, and the technical achievements in a variety of areas that are described in this report clearly demonstrate the diversity and strengths of the ORNL Fusion Program.

J. Sheffield

Director, ORNL Fusion Energy Division

C. C. Baker

Associate Director for Development and Technology,
ORNL Fusion Energy Division

M. J. Saltmarsh

Associate Director for Operations,
ORNL Fusion Energy Division

1

**TOROIDAL CONFINEMENT
ACTIVITIES**

J. L. Dunlap, Toroidal Confinement Section Head

S. C. Aceto ¹	S. E. Grebenshchikov ¹⁴	J. Lee ²⁰	K. A. Sarkisyan ¹⁴
D. L. Akers ²	D. E. Greenwood ⁸	U. P. Lickliter ⁶	C. R. Schaich
E. Anabitarte ³	A. D. Guttery ²	K. M. Likin ¹⁴	S. W. Schwenterly ²²
F. S. B. Anderson ⁴	C. L. Hahs ¹⁵	J. W. Lue ²²	K. C. Shaing ¹¹
G. C. Barber ⁵	J. W. Halliwell	V. E. Lynch ⁸	R. C. Shanlever ⁶
L. R. Baylor ⁶	G. R. Hanson ¹⁶	J. F. Lyon	M. G. Shats ¹⁴
G. L. Bell ⁷	J. H. Harris	C. H. Ma ¹⁷	P. L. Shaw ¹⁶
J. D. Bell ⁸	G. R. Haste ⁵	R. Maingi ²³	J. Sheffield ²⁵
R. D. Benson ⁶	C. L. Hedrick ¹¹	L. A. Massengill	T. D. Shepard ⁵
T. S. Bigelow ⁵	M. A. Henderson ⁷	W. S. Mayfield ⁶	J. E. Simpkins
C. B. Brooks ⁷	G. H. Henkel	T. J. McManamy ⁶	P. N. Stevens ²⁰
C. E. Bush	C. Hidalgo ³	M. M. Menon	K. A. Stewart ¹¹
E. J. Byrnes ⁹	D. L. Hillis	D. L. Million ⁸	K. D. St. Onge ⁶
K. Carter ¹⁰	S. Hiroe	P. K. Mioduszewski	S. Sudo ²⁶
B. A. Carreras ¹¹	S. P. Hirshman ¹¹	S. Morita ¹⁹	Y. Takeiri ¹⁸
T. L. Clark ¹²	J. T. Hogan ¹¹	R. N. Morris ⁸	V. I. Tereshin ²⁷
R. J. Colchin	P. A. Holliday ²	M. Murakami	C. E. Thomas ¹⁶
M. J. Cole ⁶	L. D. Horton	G. H. Neilson	M. S. Thompson ²
L. A. Charlton ⁸	W. A. Houlberg ¹¹	B. E. Nelson ⁶	J. S. Tolliver ⁸
K. A. Connor ¹	H. C. Howe ¹¹	R. H. Nelson ⁶	T. Uckan
E. C. Crume, Jr.	D. P. Hutchinson ¹⁷	D. R. Overbey ¹¹	W. I. van Rij ⁸
L. E. Deleanu ⁸	R. C. Isler	L. W. Owen ⁸	M. R. Wade ¹⁶
W. R. DeVan ⁶	T. C. Jernigan	S. L. Painter ²⁰	E. R. Wells ¹⁸
N. Dominguez ¹¹	L. M. Johnson ¹⁸	V. K. Paré ¹⁵	J. A. White ⁶
R. A. Dory ¹	R. L. Johnson ⁶	E. M. Passmore ²	J. B. Wilgen
G. R. Dyer	G. H. Jones ⁶	T. C. Patrick ¹¹	C. T. Wilson ⁶
A. C. England	R. W. Jones ²	J. L. Ping ⁶	W. R. Wing
D. T. Fehling ¹¹	H. Kaneko ¹⁹	A. L. Qualls ²⁰	R. J. Wood ⁶
P. W. Fisher ¹³	K. L. Kannan ⁸	D. A. Rasmussen	A. J. Wootton ¹⁰
J. W. Forseman ⁶	G. T. King ²⁰	T. F. Rayburn	R. E. Wright ⁵
R. H. Fowler ⁸	K. C. Klos ¹⁶	T. M. Rayburn ²⁰	R. B. Wysor ⁶
W. A. Gabbard	C. C. Klepper	W. J. Redmond	H. Yamada ¹⁹
R. F. Gandy ⁷	M. Kwon ¹⁶	T. L. Rhodes ¹⁰	J. L. Yarber
C. A. Giles ⁸	R. A. Langley	R. K. Richards	K. G. Young ¹¹
D. C. Giles ⁸	V. D. Latham ²¹	Ch. P. Ritz ¹⁰	J. J. Zielinski ¹
J. C. Glowienka	E. A. Lazarus	P. S. Rogers ²⁰	
J. M. Gossett ¹²	J. N. Leboeuf ¹¹	J. A. Rome ¹¹	
R. H. Goulding ⁵	D. K. Lee ⁸	M. J. Saltmarsh ²⁴	

-
1. Rensselaer Polytechnic Institute, Troy, N.Y.
 2. Section secretary.
 3. Centro de Investigaciones Energeticas, Medioambientales, y Tecnologicas (CIEMAT), Madrid, Spain.
 4. University of Wisconsin, Madison.
 5. Plasma Technology Section.
 6. Engineering Division, Martin Marietta Energy Systems, Inc.
 7. Auburn University, Auburn, Ala.
 8. Computing and Telecommunications Division, Martin Marietta Energy Systems, Inc.
 9. Quality Department.
 10. Fusion Research Center, University of Texas at Austin, Austin.
 11. Plasma Theory Section.
 12. Tennessee Technological University, Cookeville.
 13. Chemical Technology Division.
 14. General Physics Institute, Moscow, U.S.S.R.
 15. Instrumentation and Controls Division.
 16. Georgia Institute of Technology, Atlanta.
 17. Physics Division.
 18. Management Services Group.
 19. National Institute of Fusion Science, Nagoya, Japan.
 20. University of Tennessee, Knoxville.
 21. Maintenance Division, Y-12 Plant.
 22. Magnetics and Superconductivity Section.
 23. North Carolina State University, Raleigh.
 24. Associate Division Director, Fusion Energy Division.
 25. Division Director, Fusion Energy Division.
 26. Plasma Physics Laboratory, Kyoto University, Uji, Japan.
 27. Kharkov Institute of Physics and Technology, Kharkov, U.S.S.R.

1. TOROIDAL CONFINEMENT ACTIVITIES

SUMMARY OF ACTIVITIES

Experimental research in the toroidal confinement area is concentrated mainly in two programs, the Advanced Toroidal Facility (ATF) program and the Edge Physics and Particle Control (EPPC) program. The ATF program is an element of the U.S. Advanced Toroidal Program, which seeks to study improvements on the mainline fusion confinement concept, the basic first-stability tokamak. The ATF is a stellarator, the world's largest, designed to explore a broad spectrum of toroidal physics topics, including the second stability regime. In the future, it will also be used to investigate steady-state operation at high beta. The EPPC program aims to characterize edge plasma behavior and to explore edge modification techniques for improving performance. This program is collaborative in nature and is carried out on a number of major confinement research facilities throughout the world: TEXTOR (Jülich, Federal Republic of Germany), Tore Supra (Cadarache, France, with support from the European Community), DIII-D (San Diego, California), and ATF.

The progress of ATF has been quite pleasing during this first full year of operation with the field error removed. Only modest facility and diagnostic improvements were possible, but the results of the physics studies were notable. The plasma profiles are broader, and the operational space is significantly expanded (to longer-lived plasmas, higher density and stored energy, and longer energy confinement time). The plasma parameters are now about those of tokamaks of similar size. The flexibility of the magnetic configuration is proving its worth in such studies as that of bootstrap current. Several diagnostics are addressing plasma fluctuations in a coordinated effort directed at understanding their effect on transport. The behavior of impurities is much better documented. Collaboration continues to be an important part of the ATF program.

Helium transport and removal studies were the focus of work on TEXTOR. Additional pump limiter diagnostics were installed and commissioned on Tore Supra. Contributions to the Advanced Divertor Program on DIII-D included predictions of divertor performance, evaluations of possible pumping systems, and preparation of divertor diagnostics.

The advanced project activity was extended to studies extrapolating the ATF-II compact torsatron approach to a reactor.

1.1 THE ATF PROGRAM

1.1.1 Overview

J. L. Dunlap

This report covers the second year of operation of the Advanced Toroidal Facility (ATF). It is the first full year of operation with the field error corrected.

Budget constraints required reducing both personnel- and material-related expenses. Our response was to concentrate on the shorter-term physics returns at the expense of longer-term capabilities of the facility. The ongoing work toward installation of the 2-MW ion cyclotron heating supply and toward installation of the third neutral beam injector was halted. Planned work on particle and power handling was deferred. Facility and diagnostic improvements with high impact on the physics returns were continued, though generally at a slowed pace.

Getter assemblies, improved gas valving, helical field power supply controls necessary for 2-T operation, bus connections to enable use of the mid-vertical field coils (the shaping coils), a second 200-kW, 53.2-GHz gyrotron, and an eight-shot pellet injector are facility improvements that were completed. Diagnostic installations included the scanning mount for the neutral particle analyzer (NPA); a laser ablation impurity injection system; the heavy-ion beam probe (HIBP) primary beam and detector systems, with Rensselaer Polytechnic Institute (RPI); a fast reciprocating Langmuir probe, similar to one used on the Texas Experimental Tokamak (TEXT) and supplied by the University of Texas at Austin; and a microwave interferometer as part of a three-way collaboration with Georgia Institute of Technology and the Centro de Investigaciones Energeticas, Medioambientales, y

Tecnologicas (CIEMAT) in Madrid, Spain. The Thomson scattering system was commissioned to its full radial scan capability with 15 spectrometers, and the far-infrared (FIR) interferometer was commissioned in multiple-channel mode.

A number of these improvements were significant factors in obtaining the results detailed in Sects. 1.1.2–1.1.4.

1.1.2 Confinement Studies

M. Murakami and the ATF Group

Confinement studies in ATF yielded significant results in 1989. Plasma performance has improved substantially with improved wall conditioning and particle fueling. Energy confinement time in ATF has reached a level approximately equal to those in tokamaks of similar size, and the scaling is similar to the gyro-reduced Bohm scaling. The bootstrap current observed during electron cyclotron heating (ECH) is in agreement with predictions of the neoclassical theory.

Extensive gettering (≈ 60 – 80% wall coverage) and better gas programming have led to extended longevity for discharges with neutral beam injection (NBI); discharges lasting up to 0.35 s with a quasi-stationary state for up to 0.15 s were achieved.¹ Figure 1.1 compares plasma performance parameters achieved during NBI operation in 1988 and in 1989. The improvement is substantial. The maximum value obtained for stored energy W_p (27 kJ at $B_0 = 1.9$ T) is 3.5 times the level achieved in 1988, and values of line-average density increased by a factor of 2.5.

Figure 1.2 shows the time evolution of several plasma parameters for a typical discharge with NBI (H^0 into D^+ , 1.2 MW total from co- and counter-injecting beams, $B_0 = 1.9$ T, titanium gettering). “Reheating”

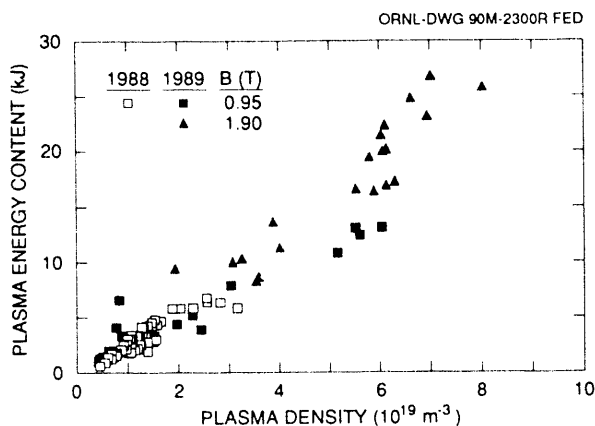


Fig. 1.1. Comparison of plasma parameters obtained during NBI operation in 1988 and 1989.

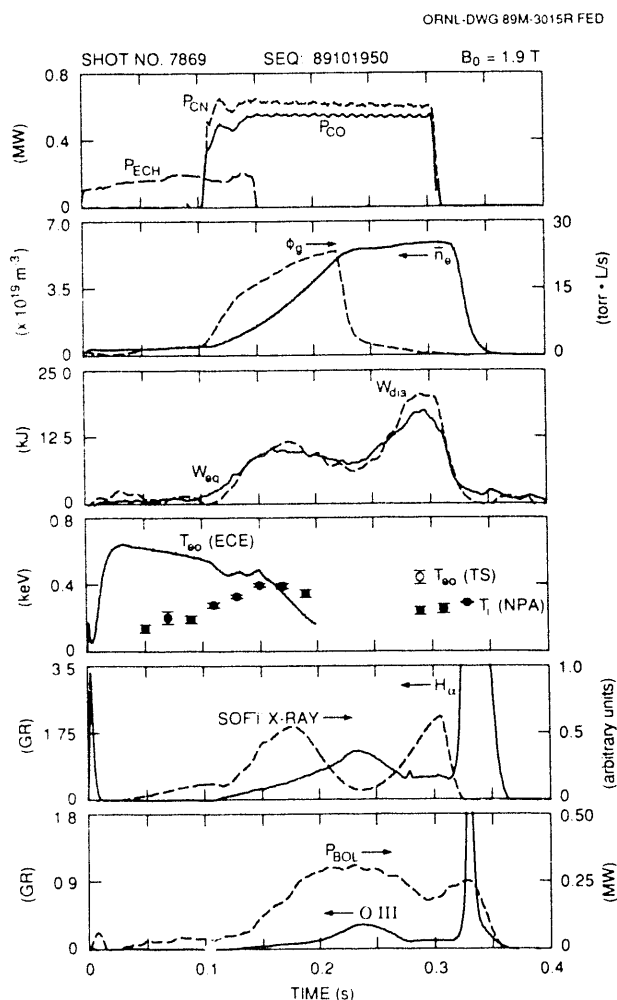


Fig. 1.2. Time evolution of a typical discharge with 1.1-MW NBI at $B_0 = 1.9$ T.

occurs after cessation of the strong gas puff at the beginning of the beam pulse. At the peak of the soft X-ray signal, the line-average density $\bar{n}_e \approx 6.1 \times 10^{19} \text{ m}^{-3}$, the diamagnetically measured plasma stored energy $W_p = 20$ kJ, the global energy confinement time $\tau_E^* = W_p/P_{in} = 16$ ms, and the “apparent” ion temperature obtained from neutral particle analysis is 0.28 keV. Profile analysis based on Thomson scattering profiles taken at this time indicates that the apparent ion temperature is approximately consistent with neoclassical ion conductivity. The analysis yields a stored energy of 17 kJ (with a 5% contribution from the fast-ion component), and a (thermal) gross energy confinement time, $(W_e + W_i)/(P_{be} + P_{bi}) = 15 \text{ ms} \approx \tau_E^*$.

Confinement scaling studies^{1,2} have benefited from the improvements in plasma performance. Global confinement times of ≈ 20 ms have been obtained with injected power > 1 MW. These confinement times are comparable to those obtained in tokamaks of similar size, such as the Impurity Study Experiment (ISX-B). The highest volume-average beta ($= 1.5\%$) was achieved with NBI into a target plasma created with third harmonic ECH at $B_0 = 0.63$ T. Higher densities are possible with NBI, and the positive density dependence (Fig. 1.1) of the energy confinement time offsets the confinement degradation with power. Global confinement in ATF is consistent with the Large Helical Drive (LHD) scaling,³

$$\tau_E^{\text{LHD}} = 0.17 P^{-0.58} n^{0.69} B^{0.84} a^{2.0} R^{0.75}$$

(with τ_E^{LHD} in seconds, P in megawatts, n in particles $\times 10^{20} \text{ m}^{-3}$, B in tesla, and a and R in meters). The ATF (and other stellarator) data also fit the drift wave turbulence (gyro-reduced Bohm) scaling,^{4,5}

$$\tau_E^{\text{dw}} = 10^{-9} P^{-0.6} n^{0.6} B^{0.8} \times a^{2.4} R^{0.6} \kappa A_1^{-0.2} \quad (\text{SI units}),$$

as shown in Fig. 1.3. This suggests that drift waves, in particular trapped-electron instabilities, may be important in stellarator (and tokamak) plasmas. ATF can make a significant contribution to this area because the fraction of confined trapped particles f_t and the magnetic shear can be externally controlled, thereby directly influencing the instabilities.

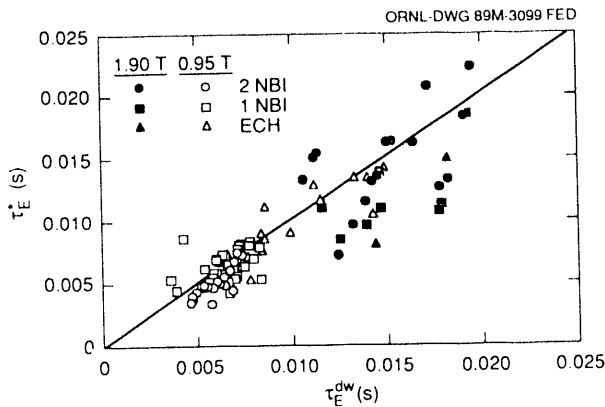


Fig. 1.3. Global energy confinement times observed in ATF vs predictions of gyro-reduced Bohm scaling.

The bootstrap current studies² have made use of the ability to control the magnetic configuration. Neoclassical theory⁶ predicts that, in the low-collisionality limit, the bootstrap current is given by $j_b = -3(f_t/f_c)G_b B_0^{-1} \nabla p$, where G_b is a magnetic geometry factor that depends on the $|B|$ spectrum on a flux surface and changes with the quadrupole (shaping) or dipole (vacuum axis) component of the poloidal field. The toroidal current observed during ECH is predominantly bootstrap current and ranges between +3.5 kA and -1.5 kA. The observed current agrees with neoclassical theory in magnitude (to within 50%) and parametric dependences, as determined by systematic scans of the quadrupole (Fig. 1.4) and dipole poloidal field components and the magnetic field intensity. These results show that the

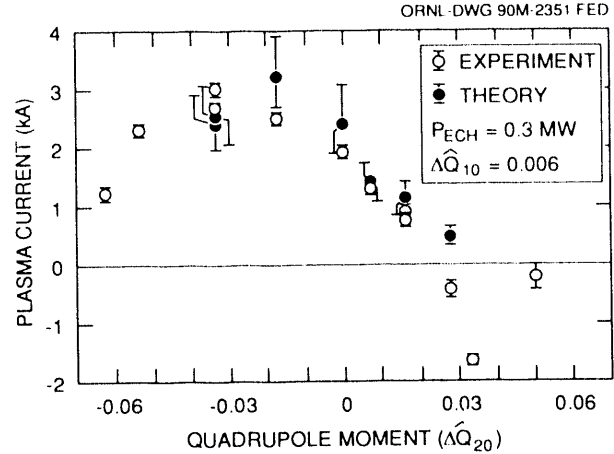


Fig. 1.4. Comparison of the observed plasma current and neoclassical predictions for the bootstrap current in the quadrupole field scan. The quadrupole moment (ΔQ_{20}) of the poloidal field was varied while the dipole moment (ΔQ_{10}) was fixed. The “error” bars shown for theory points correspond to estimates based on $Z_{\text{eff}} = 2.0 \pm 0.5$.

neoclassical theory of bootstrap current gives a good description of the current flow in ATF despite the presence of anomalies in the particle and heat flows. They also demonstrate the ability to reduce the toroidal current to zero, as is desirable for stellarator operation.

1.1.3 Fluctuation Studies

J. H. Harris, E. Anabitarte, J. D. Bell, K. Carter, J. L. Dunlap, G. R. Dyer, G. R. Hanson, C. Hidalgo, K. M. Likin, T. L. Rhodes, Ch. P. Ritz, K. A. Sarksyian, M. G. Shats, C. E. Thomas, T. Uckan, J. B. Wilgen, and A. J. Wootton

During the past year, progress was made in several areas of fluctuation studies on ATF. The studies of edge magnetic fluctuations made in plasmas with the peaked pressure profiles found in ATF before the repair of the field error were extended to the broad profile plasmas obtained after the field

error repair. Microwave reflectometry was used to study plasma density fluctuations in the outer portion of both ECH and NBI plasmas. A reciprocating Langmuir probe system was used to make measurements of plasma edge turbulence for comparison with results from tokamaks. Work was begun on the development of a 2-mm scattering system with which to study drift wave turbulence inside ECH plasmas. In all of these activities, collaboration with teams from other institutions has been essential.

Measurements of fluctuations in the poloidal magnetic field (\tilde{B}_θ) at the plasma edge were used to characterize the behavior of NBI plasmas obtained in ATF since the field error was repaired,⁷ in preparation for experiments to try to reach the second stability regime in full-bore plasmas at high beta in 1990–91. The results (Fig. 1.5) show that with the broader profiles now seen in ATF, the helical resonances seen

in the fluctuations correspond to values of rotational transform in the outer part of the plasma ($\iota \geq 1/2$), as would be expected for broad pressure profiles. In 1990–91, high-beta experiments on ATF with $\langle \beta \rangle \geq 1.5\%$ will attempt to reach the second stability regime with broader pressure profiles (as opposed to the very peaked pressure profiles used in the initial ATF second stability studies⁸).

In collaboration with Georgia Institute of Technology and CIEMAT, a novel diagnostic technique that uses a two-frequency, quadrature-phase detection microwave reflectometer was developed and used to study plasma density fluctuation spectra and radial correlation lengths inside ECH plasmas and at the edge of NBI plasmas. Figure 1.6 illustrates some of the initial results obtained with this system: in NBI discharges in which the plasma stored energy increases, pauses, and then increases again (showing

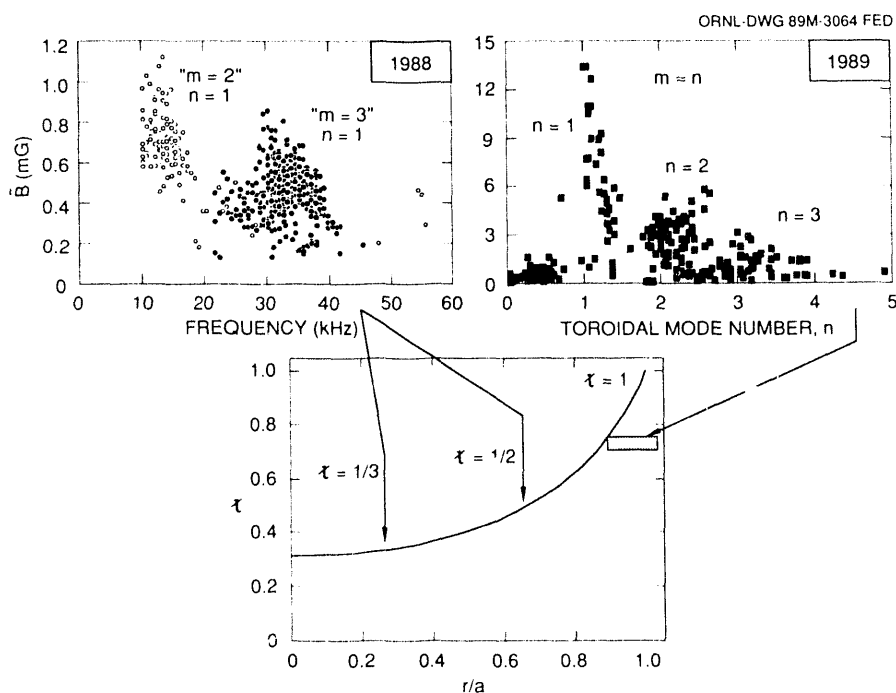


Fig. 1.5. Summary of mode numbers observed for magnetic fluctuations before repair of the field error [1988, peaked $p(r)$] and after repair of the field error [1989, broad $p(r)$].

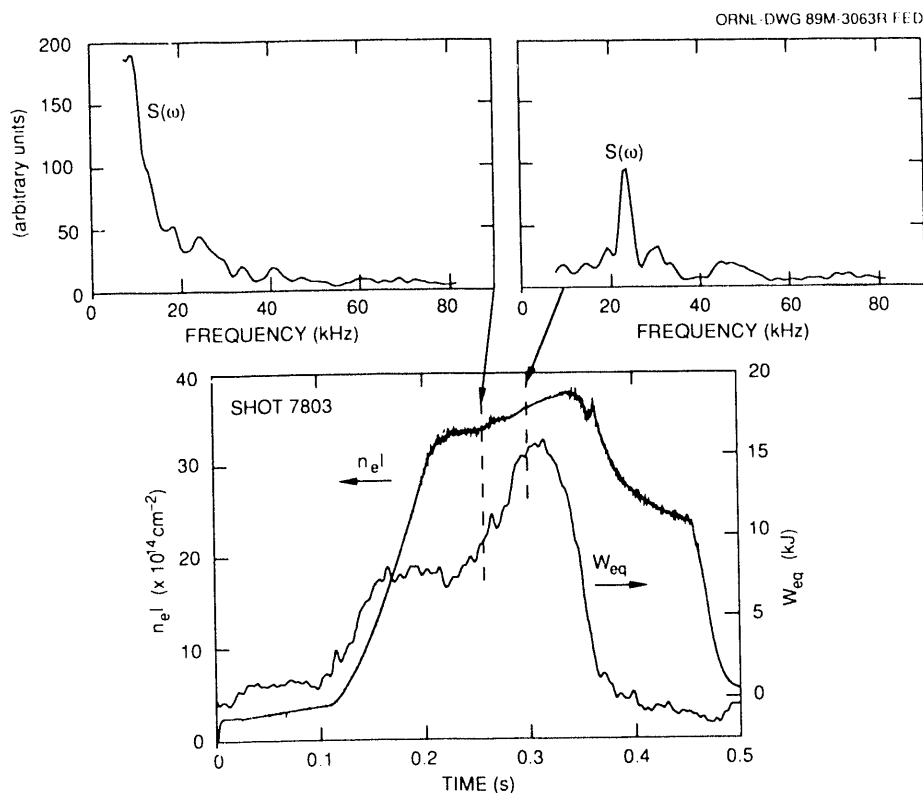


Fig. 1.6. Correlation of change in edge density fluctuation power spectra $S(\omega)$ with improvement in global energy confinement. The time traces show the chordal electron density ($n_e l$) and the stored energy (W_{eq}) determined from poloidal magnetic field measurements. The fluctuation spectra were measured at $r/a \approx 0.9$ using microwave reflectometry at 33 GHz (cutoff density = $1.35 \times 10^{13} \text{ cm}^{-3}$). The spectra were averaged over 12.5-ms intervals centered at the times indicated. The NBI power (balanced injection) was 1.4 MW.

improved confinement), a marked change in the density fluctuation spectrum at the plasma edge is observed. The spectrum measured with the reflectometer changes to a narrow-band spectrum with a strong peak between 20 and 40 kHz. This oscillation is coherent with high- n ($n \geq 3$) components of the \tilde{B}_θ signal. By separately tuning the two frequency channels of the reflectometer to reflect off plasma layers at different radii, it is possible to determine the radial correlation length of density fluctuations. This technique yields correlation lengths of 1–2 cm in ECH plasmas and <0.5 cm at the edge of NBI plasmas. Plans include the extension of the reflectometer studies to

other plasma regimes and higher microwave frequencies.

In collaboration with the TEXT group at the University of Texas, a fast reciprocating Langmuir probe (FRLP) has been installed on ATF and used to measure plasma density and potential fluctuations in the edge region ($T_e \leq 40$ eV) of ECH plasmas.^{9,10} The results show broadband fluctuations in density, $\tilde{n}/n \sim 5\%$, and floating potential, $\tilde{\Phi}/kT_e \sim 10\%$, just inside the last closed magnetic surface ($\bar{r}/\bar{a} \sim 0.95$). The outward particle transport induced by these fluctuations is comparable to that estimated from the global particle balance if the flux is assumed to be poloidally and

toroidally uniform. Figure 1.7 shows that the dominant contribution to the particle flux comes from fluctuations in the frequency range 100–150 kHz. Details of this work are provided in Sect. 1.2.1.

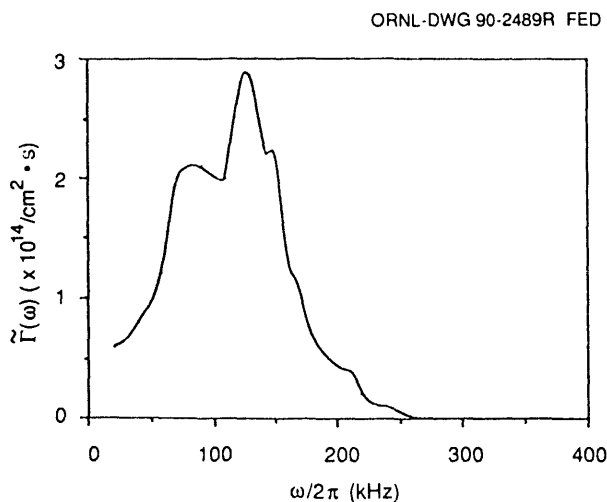


Fig. 1.7. Spectrum of fluctuation-induced particle flux in the edge of ATF as measured by a fast reciprocating Langmuir probe.

Trapped-particle instabilities are thought to play a role in determining anomalous transport in both stellarators and tokamaks, and the configurational flexibility of ATF can be used to vary the trapped-particle populations (as demonstrated in the bootstrap current studies). In order to measure directly the expected plasma drift wave fluctuations, work has begun on the development of a 2-mm microwave scattering diagnostic, in collaboration with the L-2 stellarator group at the Institute of General Physics in Moscow. This instrument will be used to determine frequency and wave number spectra for drift wave turbulence in the low-collisionality ECH plasmas where trapped-particle effects are expected to be important.

1.1.4 Impurity Studies

R. C. Isler, L. D. Horton, E. C. Crume, Jr., S. Hiroe, T. C. Jernigan, and M. Murakami

Although wall conditioning is necessary for obtaining favorable parameters in all types of plasma confinement devices, it appears to be especially important for currentless machines. In the early stages of operating ATF it was found that, without adequate discharge cleaning and baking, discharges generated by ECH alone exhibited rapid, uncontrollable rises in density and low- Z impurity radiation that caused collapses to low-temperature, low-density plasmas.¹¹ Simultaneous glow discharge cleaning (GDC) and baking reduced the amount of impurities and hydrogen evolved from the walls to the point where steady-state operation was obtained for plasmas heated by ECH alone. Nevertheless, when only this type of wall conditioning was employed, NBI plasmas always collapsed within about 50 ms of the start of injection. It was suspected that radiative losses, exacerbated by field errors that generated a large $m = 2$ island and stochastic regions around the $\iota = 1$ surface, might cause this undesirable behavior. However, repair of the field errors did not significantly ameliorate the tendency of NBI plasmas to collapse shortly after the beginning of injection, and during the last year attention was focused on improved wall conditioning as a possible remedy for the problem. As described in Sect. 1.2.1.2, gettering was initiated in the hope that further reduction of low- Z impurities would lead to an improvement of plasma parameters and eliminate collapses in NBI plasmas.

In addition to the expanded use of gettering as a method for assessing the influence of impurities, active impurity injection

experiments were performed to gain more insight into the effects of contaminants on ATF plasmas. A laser ablation system was installed in order to determine the impurity transport coefficients and to permit more accurate modeling of the impurity behavior. Neon injection experiments were also used to assess power losses and to determine the level of radiation that the plasmas could support.

The changes of impurity radiation under various conditions, improvements of plasma parameters as a result of gettering, and impurity injection experiments are described in Sects. 1.1.4.1–1.1.4.3.

1.1.4.1 Gettering and impurity radiation

Radiated power levels determined from spectroscopic analysis and from bolometer measurements are listed in Table 1.1 for plasmas heated by ECH alone and in Table 1.2 for plasmas heated by NBI with the emissions observed for a typical edge ion, O VI. These analyses encompass both nongettered sequences of discharges

and gettered sequences in which chromium and titanium were evaporated with different fractions of wall coverage. The effects of gettering are best evaluated from the quasi-steady ECH plasmas, since the percentage of radiation can vary substantially during NBI. Emissions from the low ionization stages of carbon, nitrogen, and oxygen were lower by factors of 2 to 5 in the discharges with chromium gettering than in the nongettered discharges. This result does not indicate the reduction of the influx of low- Z ions by the same factor owing to the nonlinear response of peripheral emissions to changes of plasma conditions. Indeed, charge-exchange excitation (CXE) signals, which provide a direct measure of the impurity content in the interior of plasmas, indicated a drop of about 30% in the density of carbon immediately after the first getter cycle, but a rise of approximately the same percentage in the oxygen content. Titanium gettering, however, reduced the interior carbon and oxygen densities by factors of 2 to 3, while the emissions from the strongly radiating edge ions were lower by factors of 40 to 60 than in the nongettered cases.

Table 1.1. Spectroscopic analysis of radiated power during discharges with 200-kW ECH

Getters	None	None	2 Cr	2 Cr	4 Cr	4 Ti	6 Ti
$\bar{n}_e \times 10^{12} \text{ cm}^{-3}$	4.1	7.4	6.1	4.5	9.0	5.1	4.9
Emission rate for 1032-Å line of O VI, GR	12	50	16	25	42	2	5
Radiated power, kW							
Oxygen	33	93	70	37	71	4	12
Carbon	48	28	23	11	29	3	6
Nitrogen	8	19	21	5	3	0	0
Iron	16	6	10	8	5	13	25
Chromium	5	2	20	8	7	7	9
Titanium	0	0	0	0	0	12	20
Total power, kW							
Spectroscopy	115	148	144	69	116	45	85
Bolometer	—	60	60	38	75	55	87

Table 1.2. Spectroscopic analysis of radiated power during discharges with NBI

Getters	None	None	4 Cr	4 Ti	4 Ti	6 Ti
Beam power P_{in} , kW	635 ^a	610 ^a	800	900 ^a	900 ^a	800
\bar{n}_e , $\times 10^{12}$ cm ⁻³	10.9	17.6	16.7	8.3	10.0	53.0
Emission rate for 1032-Å line of O VI, GR	150	400	150	12	32	50
Radiated power, kW						
Oxygen	263	364	216	18	69	92
Carbon	298	219	95	7	3	11
Nitrogen	26	93	8	1	1	11
Iron	56	72	100	41	63	22
Chromium	17	20	77	22	18	9
Titanium	0	0	0	55	83	30
Total power, kW						
Spectroscopy	681	798	536	160	261	183
Bolometer	—	—	180	160	235	175

^a 200 kW of ECH power applied during the entire neutral beam pulse.

The total radiated power from a given impurity is determined from spectroscopic data by fitting measured signals from several spectral lines to the output of an impurity transport code in which the free parameters are adjusted to give an acceptable correlation with experiment. Toroidal symmetry is assumed. The uncertainty in evaluating the total radiation from this method is estimated to be $\pm 25\%$.

One obvious effect of gettering over the operational period covered by the sequences presented in Table 1.1 is the strong reduction of low- Z power losses, which raises the plasma edge temperature, and a corresponding increase in the power lost through radiation from the metals as a result of increased sputtering rates. The metal radiation was almost negligible compared to the losses from low- Z ions before gettering, but it accounts for as much as 80% of the radiated power when 70% of the vessel

wall area is covered with titanium. In these low-density ECH discharges, radiated power scales approximately as \bar{n}_e , so that the spectroscopic analyses shown in Table 1.1 imply that chromium and titanium gettering reduce the total radiated power in 200-kW ECH discharges by factors of 1.4 and 2.7, respectively, when normalized to the density. Similar conclusions hold for the 400-kW discharge characterized in Table 1.1 if the radiation is also normalized to the input power. Data from a wide-angle bolometer indicate that gettering has, at most, a small effect on the total radiation. When normalized to the electron density, the losses measured by this diagnostic are a constant fraction of the input power, within $\pm 16\%$, under all conditions of wall conditioning. The spectroscopic and bolometric data are seen to agree well in ECH plasmas when extensive titanium gettering is employed; they diverge by factors of 2 or more when

the low- Z ions dominate the radiative losses. The dichotomy between the two types of analyses remains an unresolved problem.

1.1.4.2 Effects of gettering on plasma performance

Regardless of any uncertainty about the effect of gettering on radiated power, it is clear, at least when titanium is used, that the hydrogen released or recycled from the walls is greatly reduced during a discharge. This feature permits tailored gas puffing and has made high-density operation accessible. At these high densities (up to $1.2 \times 10^{14} \text{ cm}^{-3}$) NBI plasmas can be operated in a quasi-steady mode, although gettering *per se* did not eliminate the collapses in low-density plasmas.

Figures 1.8–1.14 illustrate several characteristics of low-density and high-density

titanium-gettered plasmas. No gas is added during NBI in the low-density case. In fact, the gas puff is reduced throughout the NBI phase, and any increase in n_e comes from beam fueling or from particles released from the walls. Such plasmas manifest the typical evolution observed for nongettered or chromium-gettered plasmas. After the beams are turned on, the electron temperature falls monotonically from 500 eV to less than 20 eV [Fig. 1.10(a)]. The stored energy and the ion temperature rise for about 60 ms after injection begins, but then decay rapidly. Impurity levels increase by a factor of 2 to 3 shortly after injection begins. The rapid increases of emission from the ionization stages depicted in Fig. 1.9 appear to be the result of the falling electron temperature. Although these plasmas collapse, the radiation level remains relatively low, less than 18% of the input

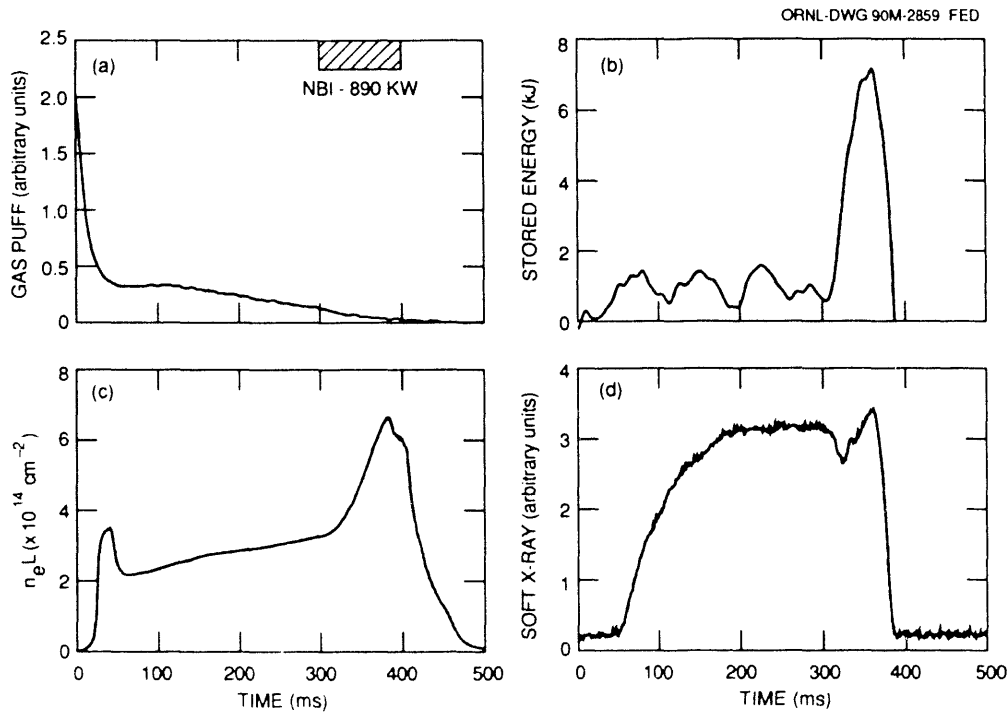


Fig. 1.8. Plasma parameters for a low-density NBI discharge with 200-kW ECH from 0 to 400 ms. The stored energy begins to collapse at 360 ms.

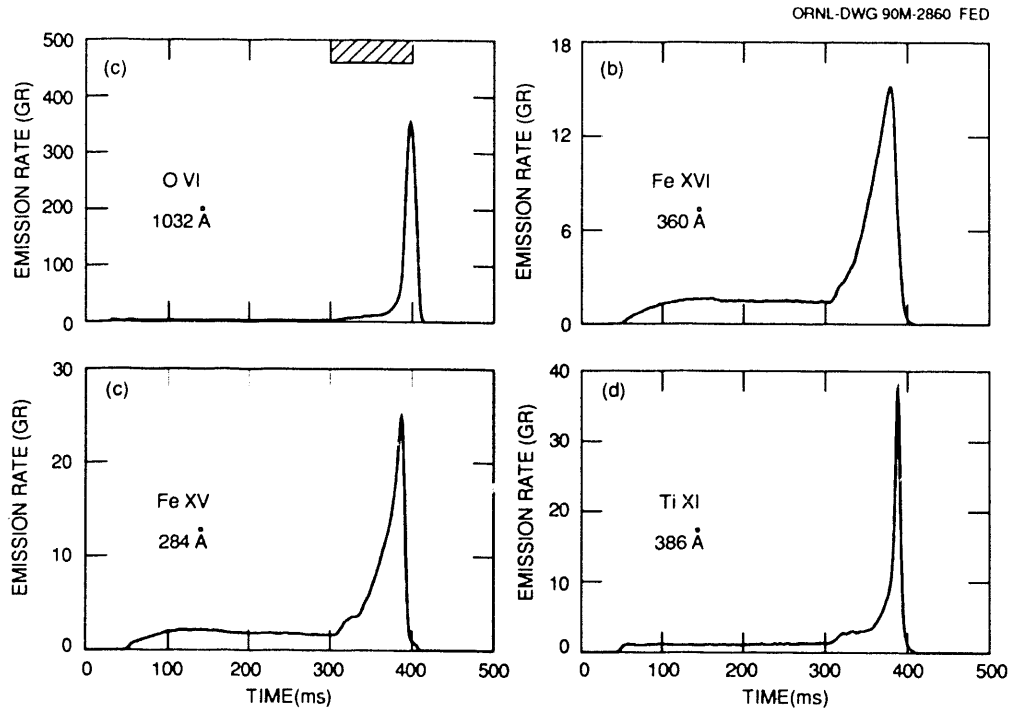


Fig. 1.9. Impurity radiation from a low-density NBI discharge with 200-kW ECH from 0 to 400 ms. The stored energy begins to collapse at 360 ms.

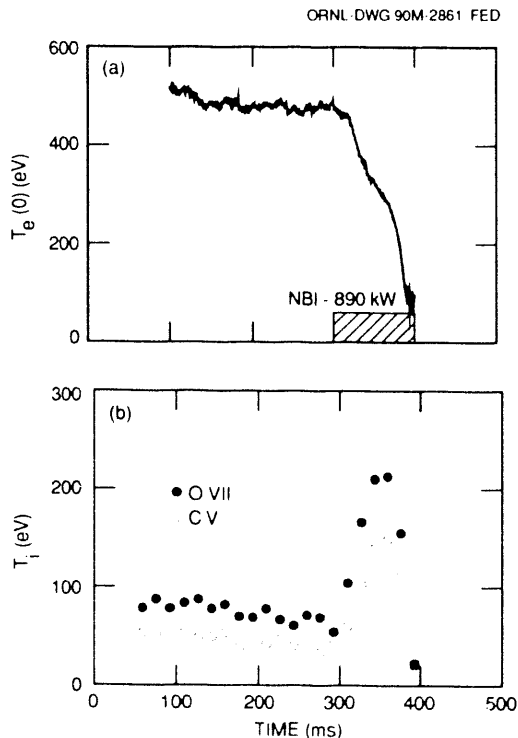


Fig. 1.10. Typical electron and ion temperature evolution in low-density NBI plasmas.

power up to the time of the stored energy maximum. Distinct changes in the slopes of the impurity signals appear first in the innermost ions; this behavior implies that the temperature decay results from confinement losses in the interior rather than from a gradual narrowing of the plasma column as a result of increasing peripheral radiation.

The evolution of the high-density discharges is quite different from that of discharges with no additional gas puff during injection. Figure 1.11(a) shows that the fueling rate is increased strongly at the same time the beams are injected. Initially, the electron temperature cools rapidly, but in the following 50 ms it reheats to 275 eV in the center. The electron temperature behavior is reflected in the soft X-ray signal shown in Fig. 1.11(d), and Thomson scattering profiles are illustrated for various times during the discharges in Fig. 1.13(a). After the initial reheat, the electron temperature and stored

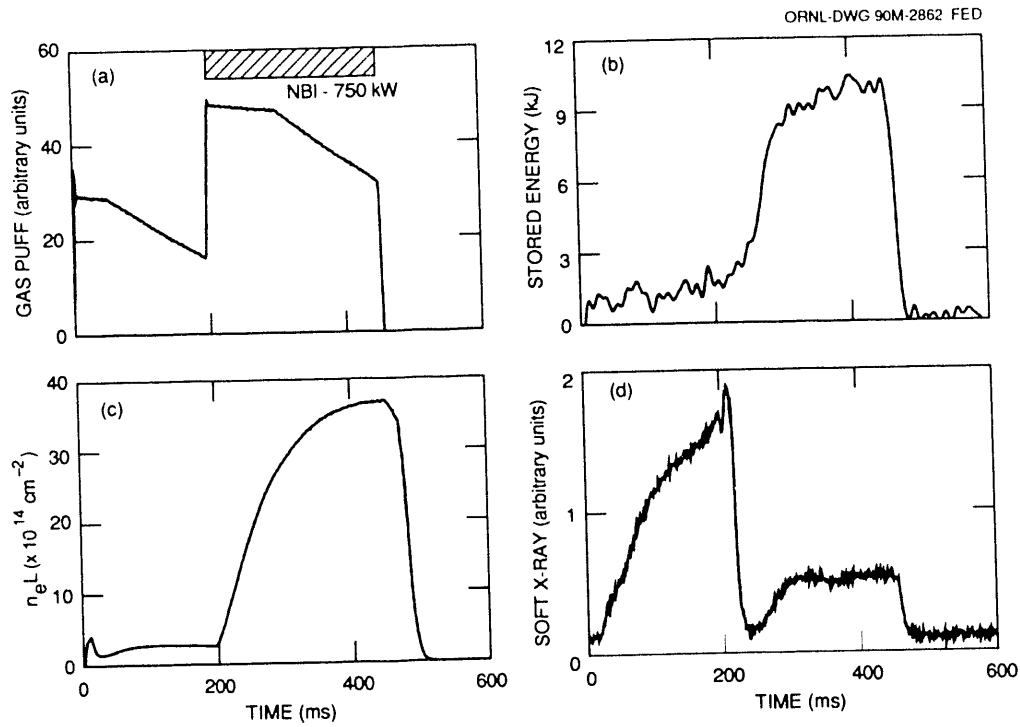


Fig. 1.11. Plasma parameters for a high-density NBI discharge with 200-kW ECH from 0 to 220 ms. No collapse occurs.

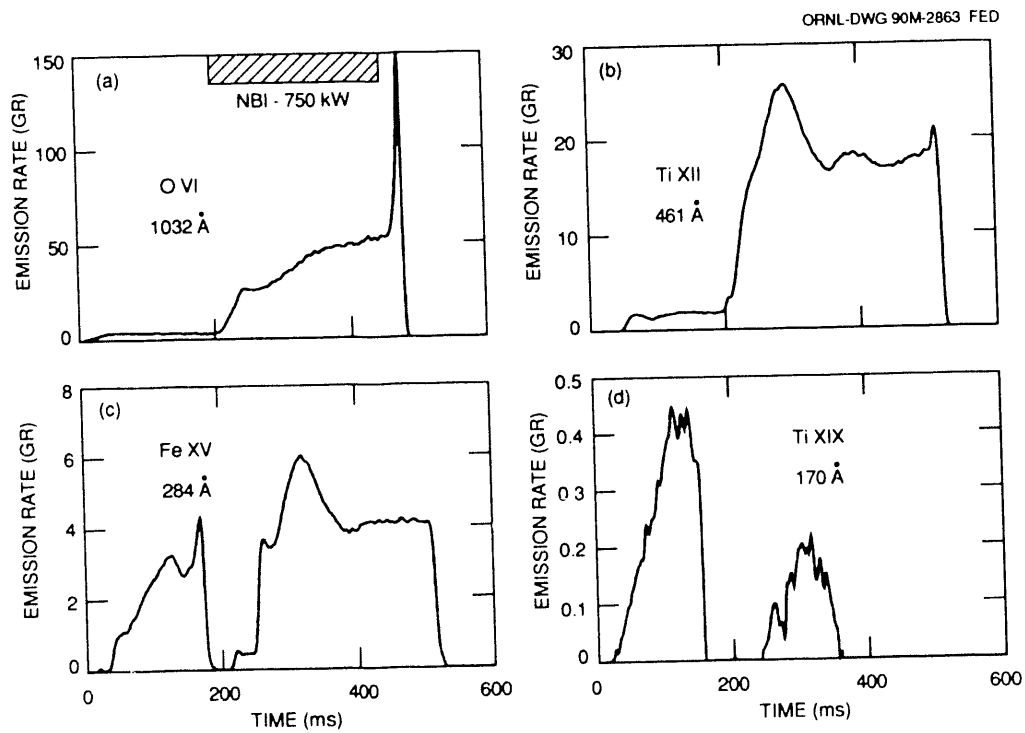


Fig. 1.12. Impurity radiation from high-density NBI discharges with 200-kW ECH (a, b) from 0 to 220 ms and (c, d) from 0 to 180 ms. No collapse occurs.

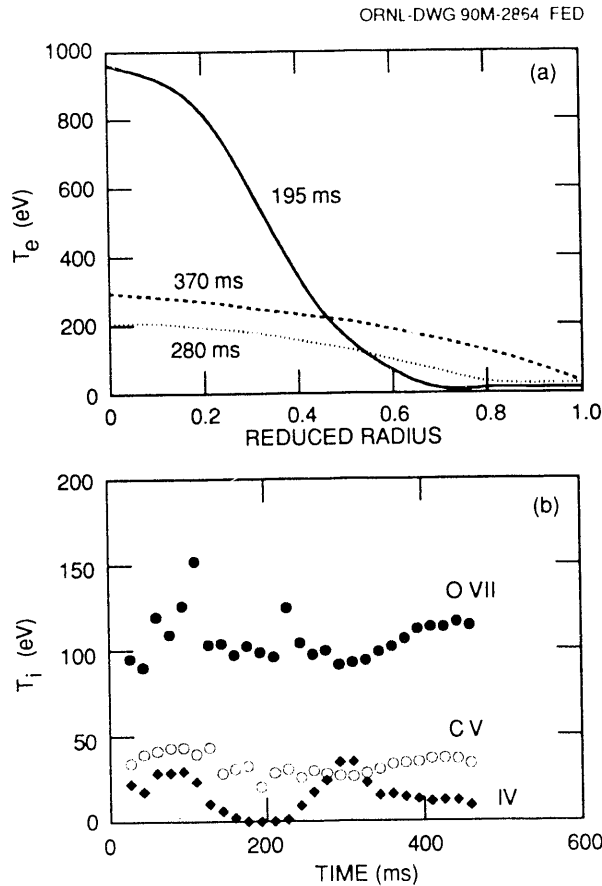


Fig. 1.13. Typical electron and ion temperature evolution in high-density NBI plasmas.

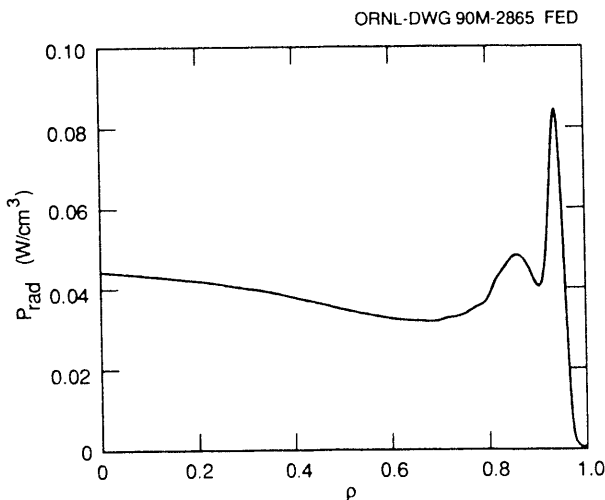


Fig. 1.14. Radiation profile deduced from spectroscopy for a low-density, titanium-gettered sequence of discharges.

energy increase slightly until the end of the NBI pulse with no sign of evolving toward a collapse. The central ion temperature, measured from the Doppler broadening of O VII spectral lines, exhibits a brief rise when the beams are turned on but returns to the preinjection level within 16 ms. Modeling indicates that this ion is spread out over a region where the electron temperature is 200 to 300 eV, and it is not now understood why the electron and ion temperatures should be so different in these high-density, low-temperature plasmas.

Emissions from the lower ionization stages of oxygen, titanium, and iron (Fig. 1.12) are seen to be almost constant after 400 ms. The Ti XIX signal disappears before 400 ms because the electron temperature in the plasma is too low to sustain a measurable density of this ion. (The loss of signals from Fe XV and Ti XIX at 230 ms results from termination of ECH heating before NBI begins in these discharges. Note that the plasma still reheats when the beam turns on.) As in the low-density case, radiated power remains a modest 25% of the input power throughout the discharges. Without gettering, it has not been possible to achieve such high-density, quasi-steady discharges. The comparable fractions of radiated power in the NBI phases of both the transient and the quasi-steady discharges indicate that global radiation losses are not a primary factor in initiating collapses.

Modeling of the profiles of radiated power from the spectroscopic data also indicates that radiation is very unlikely to be responsible for initiating the loss of confinement in the interior inferred from the data of Fig. 1.9. Figure 1.14 shows that the radiated power during low-density discharges is approximately 0.04 W·cm⁻³ from the center of the plasma to a reduced minor radius of 0.8. If all the power from a 1-MW neutral beam is deposited in this

volume, it is more than 10 times this level on average.

1.1.4.3 Impurity injection

Although the global magnitude of the radiated power appears insufficient to explain the collapse depicted in Figs. 1.8 and 1.9, it is obvious that at some level impurity radiation can seriously degrade the plasma confinement. Neon was injected into titanium-gettered plasmas to ascertain the level of radiation that could be supported. Figure 1.15 illustrates the emission from several spectral lines for collapsing (dashed lines) and noncollapsing (solid lines) discharges. The amount of neon introduced in the noncollapsing sequence is marginally

below the level that initiates a continuous drop in the electron temperature. It is introduced in a 7-ms-wide pulse at 200 ms. The emissions from the low stages peak about 80 ms later, then decline until about 350 ms, when a sudden change in the plasma characteristics results in a steady state. Radiation from the intrinsic ions is only about 30% lower in the steady-state phase than it is before neon injection. Table 1.3 shows the power radiated from the dominant impurities before injection, at the maximum of Ne VIII radiation, and in the steady-state interval. Once neon is injected into the plasmas, it doubles the radiative power and becomes the dominant emitter according to the spectroscopic analysis. The bolometer detects almost no change in the

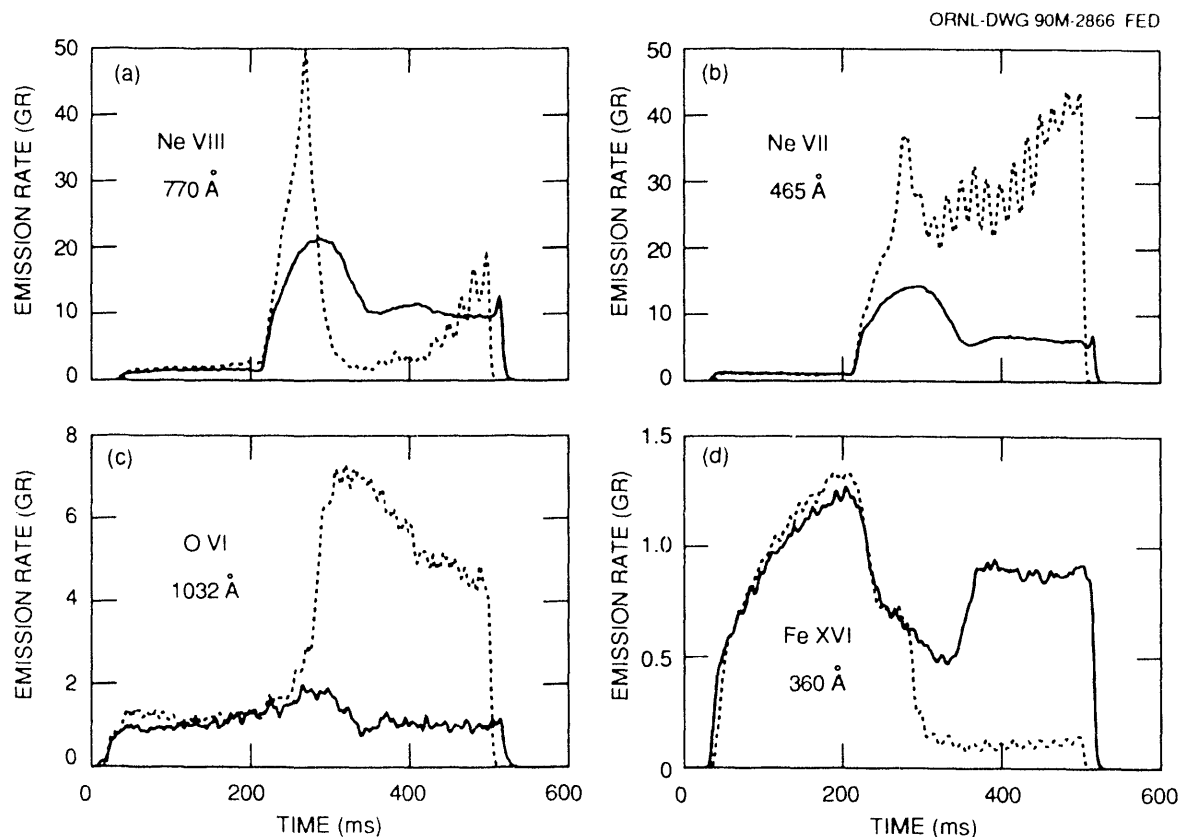


Fig. 1.15. Spectral line radiation from ECH discharges with neon injection at 200 ms. Solid lines: signals from noncollapsing discharges. Dashed lines: signals from collapsing discharges.

Table 1.3. Spectroscopic analysis of radiated power during NBI heating

	Time, ms		
	200	300	400
$\bar{n}_e, \times 10^{12} \text{ cm}^{-3}$	4.2	4.9	4.8
Emission rate for 770-Å line of Ne VIII, GR	1.5	21	11
Radiated power, kW			
Neon	5.2	61.5	27.2
Oxygen	2.6	3.2	1.8
Carbon	1.8	0.8	1.1
Nitrogen	0.5	0.3	0.4
Iron	15.6	6.1	9.8
Chromium	5.6	3.1	4.5
Titanium	0	0	0
Total spectroscopic power, kW	44	87	56

total radiated power, however. The maximum radiated power is 48% of the 200-kW ECH input. Electron temperature profiles measured by means of Thomson scattering at three different times during the neon injection experiments are shown in Fig. 1.16. It is obvious that the profiles are narrower at 320 ms—that is, after neon injection—

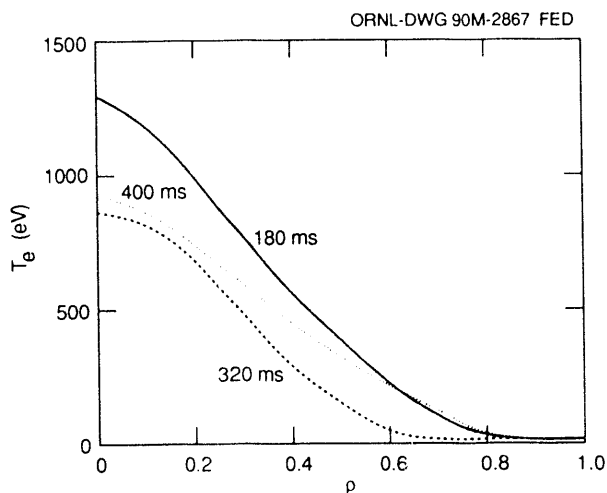


Fig. 1.16. Electron temperature profiles from ECH discharges following neon injection at 200 ms.

than they are at 180 ms before the neon is introduced. This direct observation of edge cooling supports the similar inference from the behavior of the iron emission [Fig. 1.15(d)]. The profile is again relatively broad at 400 ms. A sudden change in the profile around 350 ms is apparently responsible for the transition to the steady-state emission levels observed in the spectral lines.

Lengthening the neon pulse from 7 to 8 ms causes the plasmas to evolve to a collapse, as shown by the dashed lines in Fig. 1.15. The temperatures after the collapse in this experiment are not as low as those usually observed; O VI remains, uncharacteristically, a dominant ion in the afterglow. The erosion of the plasma edge has been proposed as a possible mechanism for the collapse on the basis of predictive calculations using the PROCTR code. The neon injection experiments confirm that this scenario can occur when a strong edge influx narrows the profile; it appears that the total radiation required to trigger this behavior is about 50% of the input power. These results tend to confirm our conclusions that the radiative power losses of 20 to 25% observed during NBI cannot initiate the collapses and imply that some other loss mechanism leads to collapse at low densities.

Although impurities have become less of a problem in ATF as a result of gettering, their influence on plasma behavior is not completely understood. A laser ablation system has been installed on ATF to determine transport coefficients and to model impurity behavior more accurately. For the experiments described here, the injected impurities were aluminum and scandium. The results of these experiments have been modeled with the one-dimensional (1-D) PROCTR transport code, which has been modified to solve the full multi-charge-state impurity equations. The code now

solves for impurity transport in the proper stellarator geometry using arbitrary values of the diffusion coefficient D and of the convective velocity v , both of which can be functions of the reduced minor radius. To model the ECH plasmas, a diffusion coefficient that increased with minor radius was required. The best fit was obtained with $D = 1000 + 4000\rho^2$ cm²/s and with $v = 0$. The results of this fit are shown in Fig. 1.17 for aluminum. If the global impurity particle confinement time is defined as the exponential decay time of the total injected impurity density, then for ECH plasmas the

simulation gives a global impurity particle confinement time $\tau_p^Z = 65$ ms. This is significantly longer than the global energy confinement time, which was approximately 5 ms for these discharges. The results of the fit to the scandium data from NBI plasmas are shown in Fig. 1.18. For these plasmas a centrally peaked diffusion coefficient was required. In this case the best fit was obtained with $D = 5000 - 4500\rho^2$ cm²/s. Again, the convective velocity was set to zero. In this case, $\tau_p^Z = 40$ ms, which is also longer than the energy confinement time. We emphasize that an impurity particle

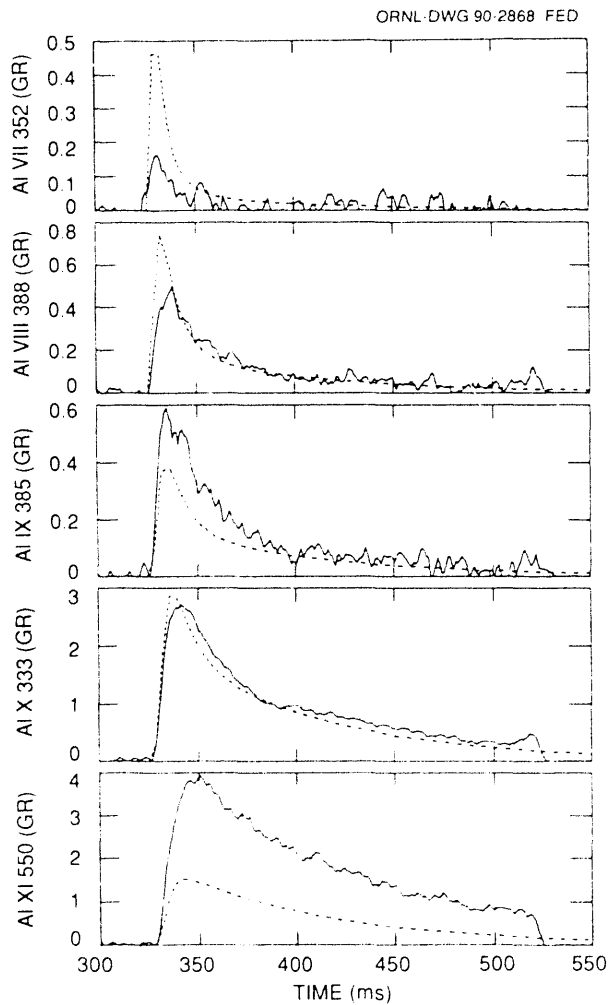


Fig. 1.17. Time histories of laser-ablated aluminum in a discharge heated only by 200-kW ECH.

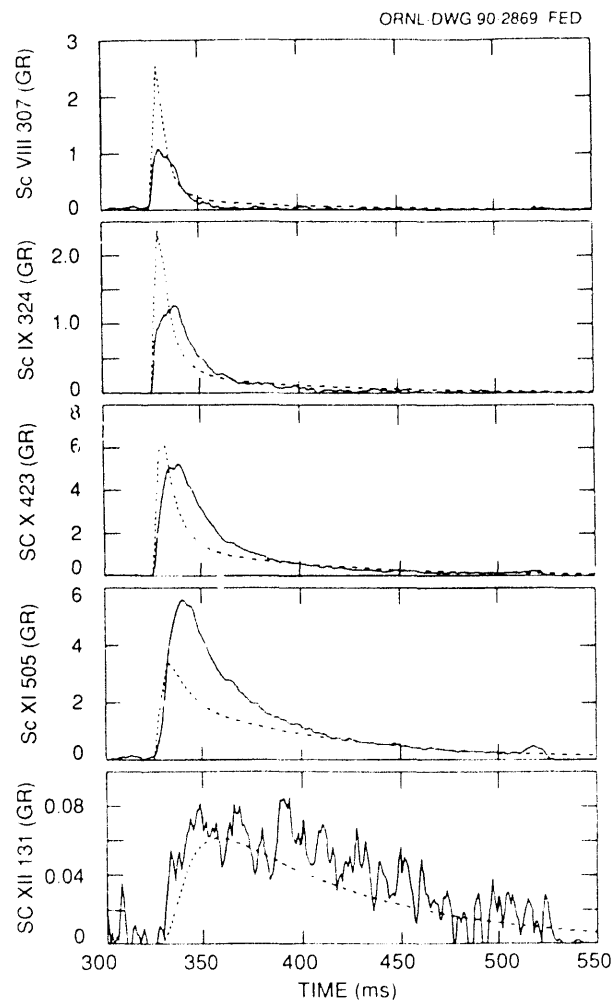


Fig. 1.18. Time histories of scandium injected into discharges heated by 850-kW NBI.

confinement time deduced from the decay time of central impurity radiation such as Sc XIII would be about twice as long as that defined by global losses. The difference in the diffusion coefficients deduced for ECH and NBI plasmas is striking. This type of increased transport in the center of NBI plasmas has been deduced previously from measurements of charge-exchange emission from helium-like ions of light impurities. Such increased transport substantially alters the ionization balance, especially of light impurity species, and contributes to higher radiation levels. Nevertheless, the total radiated power from both spectroscopic and bolometric measurements is only about 25% of the input power for these beam-heated discharges, which are near the effective density limit.

It is difficult in the simulation to reproduce the absolute levels of radiation from ionization stages in the plasma edge. Applying a pinch term to lower the edge radiation to a level in better agreement with the data does not reproduce the observed time behavior of the more central emission. In ATF, the edge rotational transform is unity, in contrast to tokamaks, where generally $q = 3$ at the edge. From the definition of q , it follows that poloidal spreading of edge impurities will be smaller in ATF for each toroidal transit. Since the transit time for these impurities is of the order of 1 ms, poloidal asymmetries may be the cause of the overestimates shown in Figs. 1.17 and 1.18 for the emissions from low ionization stages.

1.2 EDGE PHYSICS AND PARTICLE CONTROL PROGRAM

P. K. Mioduszewski (Program Manager),
D. L. Hillis, J. T. Hogan, C. C. Klepper,
R. Maingi, M. M. Menon, L. W. Owen,

T. F. Rayburn, J. E. Simpkins, and
T. Uckan

The Edge Physics and Particle Control (EPPC) program addresses issues related to characterization of the plasma edge, plasma interactions with the wall, and techniques for edge modification aimed at the improvement of plasma performance. This includes optimization of wall conditioning for particle and impurity control as well as studies of plasma edge properties, pump limiter and divertor operation for density control, confinement improvement, and ash exhaust. Collaborations with TEXTOR, Tore Supra, and DIII-D offer opportunities to study these issues in limiter as well as divertor machines, and in stellarator as well as in tokamak configurations. Application of identical experimental techniques and modeling tools to machines of different sizes and configurations provides maximum payback of investments made and also offers the opportunity for direct comparisons of plasma performance as a function of machine configuration and plasma parameters.

During the past year, activities on ATF were focused on wall conditioning and edge fluctuation studies. On the Advanced Limiter Test-II (ALT-II) in TEXTOR, the emphasis was on helium transport and removal experiments with full pumping of the pump limiter. In addition, particle transport studies by H_{α} measurements were continued. On Tore Supra, additional pump limiter diagnostics were installed and commissioned in preparation for particle transport and exhaust studies with the phase II pump limiter module. Within the collaboration with General Atomics (GA) on the Advanced Divertor Program (ADP) on DIII-D, work was performed in three areas: (1) computer code calculations were carried out to predict the performance of the advanced divertor, (2) possible options for a pumping system

were evaluated, and (3) a set of divertor diagnostics was prepared.

1.2.1 Edge Plasma Studies and Particle Control in ATF

1.2.1.1 Initial measurements of edge plasma turbulence using a fast reciprocating Langmuir probe

T. Uckan, C. Hidalgo, J. D. Bell, J. H. Harris, J. L. Dunlap, G. R. Dyer, P. K. Mioduszewski, J. B. Wilgen, Ch. P. Ritz, A. J. Wootton, T. L. Rhodes, and K. Carter

The electrostatic turbulence on the edge of the ATF torsatron is measured to study the role of this phenomenon in particle transport in this currentless magnetic configuration. Spatial profiles of the plasma electron density n_e , temperature T_e , and fluctuations in density (\tilde{n}_e) and in the plasma floating potential ($\tilde{\phi}$) are measured around the last closed flux surface (LCFS) using an FRLP similar to one on the TEXT tokamak.¹² Measurements are carried out on ECH plasmas at a magnetic field $B = 1$ T. The plasma is created using a gyrotron source at 53 GHz with heating power $P_{\text{ECH}} = 200$ kW. In these ECH plasmas, typical line-average electron densities $\bar{n}_e = (3-6) \times 10^{12} \text{ cm}^{-3}$ and stored energies $W_p \approx 1-2$ kJ.

The FRLP is located one field period away from the instrumented rail limiter. The probe is inserted into the edge plasma from the top, moves 5 cm into the plasma in 50 ms, and remains there for about 40 ms to facilitate the fluctuation measurements. The FRLP head consists of a square array of four tips that are 2 mm long and 2 mm apart. From the double Langmuir probe operation of two tips aligned perpendicular to the local magnetic field, the edge plasma n_e , T_e , and \tilde{n}_e/n_e profiles are measured

inside (about 2 cm) and outside the LCFS. The other tips are used to measure $\tilde{\phi}$ and the wave number k . The data have been analyzed using spectral analysis techniques: the fluctuation signals are digitized at 1 MHz and then, with a conventional fast Fourier transform, their power spectra $S(k, \omega)$ as a function of frequency ω and k are obtained from a two-probe technique.¹³ The ensemble averaging of the spectral distribution of the flux, obtained from the correlation of the density and the floating potential fluctuations (temperature fluctuations are ignored), gives the turbulence-induced radial particle flux:

$$\begin{aligned} \tilde{\Gamma} &= \langle \tilde{n}_e \tilde{v}_r \rangle \\ &= 2 \sum_{\omega > 0} (k/B) \gamma_{n\phi} n_{\text{rms}} \\ &\quad \times \phi_{\text{rms}} \sin \theta_{n\phi} \quad , \end{aligned} \quad (1.1)$$

where $\tilde{v}_r = -ik\tilde{\phi}/B$ is the radial velocity due to the electrostatic fluctuations, $\gamma_{n\phi}$ is the coherence, $\theta_{n\phi}$ is the phase angle between the density and potential fluctuations, and n_{rms} and ϕ_{rms} are the rms values of the fluctuations.

Spatial profiles of the edge plasma density, temperature, and floating potential ϕ are given in Fig. 1.19 for $0.95 < r/\bar{a} < 1.15$, with $\bar{a} = 0.27$ m the average plasma radius at the LCFS, where the safety factor $q \approx 1$. These measurements were made during the steady-state phase of the plasma discharge. Around the LCFS, $r/\bar{a} \approx 1$, $n_e = (1-2) \times 10^{12} \text{ cm}^{-3}$ and $T_e = 30-40$ eV. The characteristic density and temperature scale lengths are $L_n = [-(1/n_e)(dn_e/dr)]^{-1} \approx 2-4$ cm and $L_T \approx 2L_n$, respectively.

The normalized density (\tilde{n}_e/n_e) and floating potential ($\tilde{\phi}/T_e$) fluctuation profiles are given in Fig. 1.20. Typical values around the LCFS are $\tilde{n}_e/n_e \approx 0.05-0.1$ and $\tilde{\phi}/T_e \approx 0.1-0.2$. The fluctuations depart increasingly from the Boltzmann relation ($\tilde{\phi}/T_e = \tilde{n}_e/n_e$)

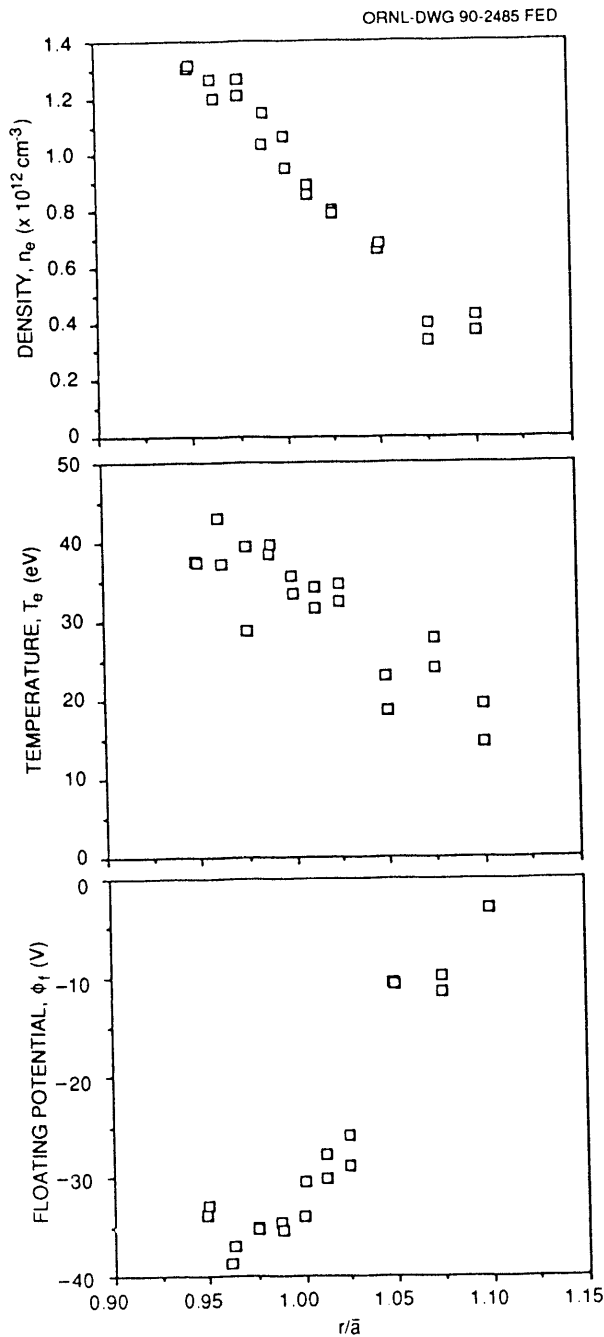


Fig. 1.19. Spatial profiles of the ATF edge plasma density, temperature, and floating potential.

as the probe is moved into the core plasma where $T_e > 20$ eV, and $\tilde{\phi}/T_e \approx 2\tilde{n}_e/n_e$ at $r/\bar{a} \approx 0.95$.

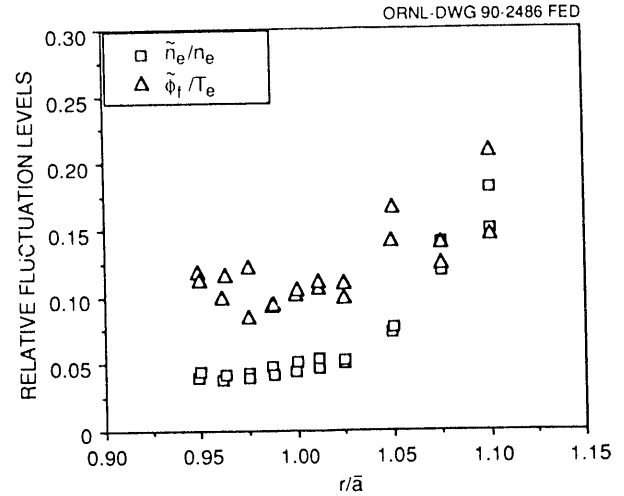


Fig. 1.20. Relative fluctuation levels for edge density and potential.

The fluctuation spectra of \tilde{n}_e and $\tilde{\phi}$ have been examined for frequencies up to 400 kHz. Observed wave number–frequency power spectra $S(k, \omega)$ are broad and mostly in the range 40–300 kHz. The estimated wave numbers $k = 1\text{--}3$ cm $^{-1}$ satisfy $k\rho_s \approx 0.05\text{--}0.1$, where ρ_s is the ion Larmor radius at the sound speed. The propagation of the fluctuations is in the ion diamagnetic direction for $r/\bar{a} > 1$, but it reverses to the electron diamagnetic direction for $r/\bar{a} < 1$.

The fluctuation-induced particle flux is estimated from Eq. (1.1), using $\gamma_{n\phi} \approx 0.8$ up to 150 kHz and $\gamma_{n\phi} \sim 0.2$ beyond 250 kHz. The phase angle is $\theta_{n\phi} \approx 40^\circ$ around 150 kHz. The spatial profile of the total particle flux $\tilde{\Gamma}$ is given in Fig. 1.21 for $\bar{n}_e = 3.5 \times 10^{12}$ cm $^{-3}$. The flux is always outward and at the LCFS has a value $\tilde{\Gamma} \approx 4 \times 10^{15}$ cm $^{-2}$.s $^{-1}$. The corresponding fluctuation-induced particle confinement time is $\tilde{\tau}_p = 0.75(\bar{a}/2)\bar{n}/\tilde{\Gamma} \approx 8\text{--}10$ ms for the assumed parabolic plasma density profile. Using H_α measurements to estimate the particle flux at the LCFS is rather difficult because of the complicated

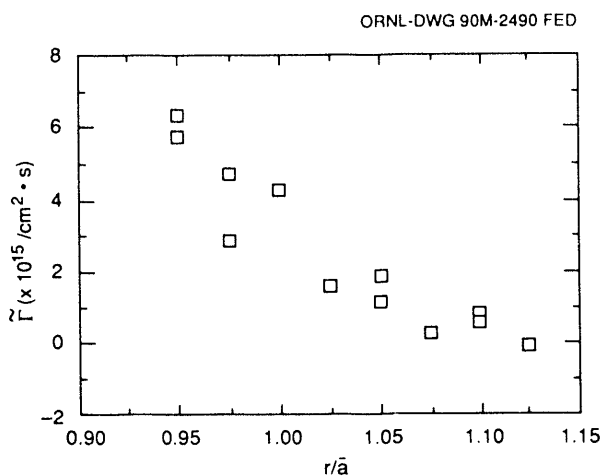


Fig. 1.21. Spatial profile of the fluctuation-induced particle flux at the edge.

geometry of the ATF edge. Instead, the energy confinement time is compared with $\tilde{\tau}_p$. From the stored energy $W_p \approx 2$ kJ, the estimated global energy confinement time is $\tau_E^* = W_p/P_{ECH} \approx 10$ ms, which is comparable to $\tilde{\tau}_p$. The local density diffusion coefficient can be estimated from $D_n = \tilde{\Gamma} L_n/n_e \approx 1.5 \times 10^4$ cm²·s⁻¹, which is about the same order of magnitude as the Bohm diffusion coefficient at $B = 1$ T.

1.2.1.2 Gettering techniques

J. E. Simpkins

Initial gettering in the ATF vacuum vessel was accomplished by subliming chromium from spherical sources fabricated at ORNL. A 30-min getter cycle with two such sources provided a chromium film with an average thickness of 5 monolayers that covered $\sim 30\%$ of the vacuum vessel wall. The results were promising, and two more chromium sources were added to increase the wall coverage to $\sim 50\%$. Reductions in the levels of gaseous impurities were observed in the plasma spectroscopically and in the resid-

ual gas as measured by the quadrupole mass spectrometer (QMS). Initially, P_{rad} was near 100%, causing thermal plasma collapse, but was reduced to less than 40% with $Z_{eff} \leq 2$ after chromium gettering. Since a chromium film can pump only about one monolayer of hydrogen,¹⁴ the recycle coefficient from the walls for this gas is near unity. On the other hand, titanium can pump large quantities of hydrogen by surface adsorption and subsequent bulk diffusion.¹⁴ To aid in the pumping of hydrogen, the chromium sources were replaced by titanium.

At present, seven titanium sources are used on ATF to deposit a film that covers $\sim 70\%$ of the vacuum vessel wall. Improvements to the plasma include the reduction of radiated power to about 25% and longer NBI discharges at higher densities. Gettering is usually performed once each day, just before plasma operations begin. Some of the effects of gettering on the vacuum may be seen in Fig. 1.22. The rates of rise of partial pressures of the gases shown were measured with the pump valves closed. Prior to day 1 (Aug. 18, 1989) no gettering had occurred since an extended opening. Gettering with four chromium sources began on day 10 and was continued as a routine procedure until day 86, when the vacuum vessel developed a large leak. Gettering resumed on day 99 with seven titanium sources. After a few getter cycles, the leak rate could no longer be calculated from either the total pressure rate of rise or the N₂ partial pressure rise because on a "well-gettered" surface the getter film continued to pump N₂, even after 24 h. Instead, the argon rate of rise, identified as mass 40* in Fig. 1.22, was used as the equivalent air leak. For a short time (around day 50), the leak rate decreased by more than an order of magnitude, as shown by the decrease of both N₂ and argon. The H₂ rate of rise from outgassing by the walls remains lower after titanium gettering, indicating the

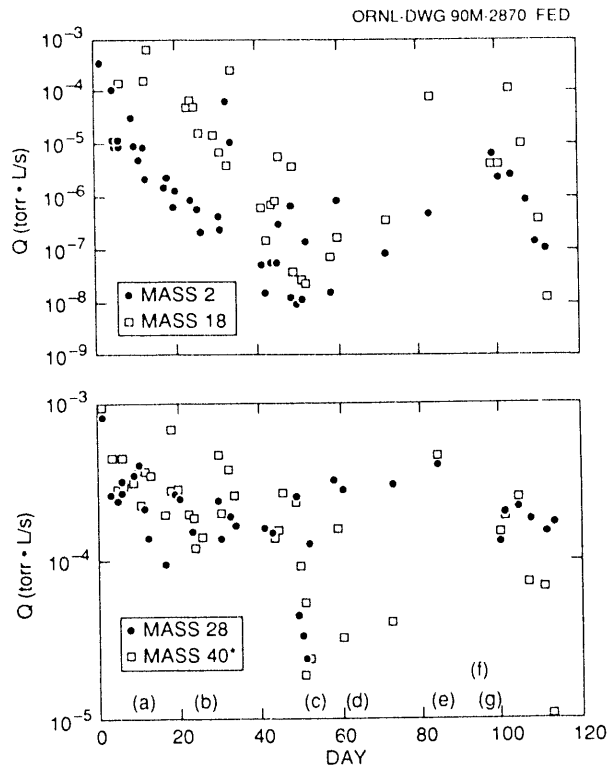


Fig. 1.22. Rate of rise measurements of selected masses in the ATF vacuum vessel following an extended vacuum vessel opening. (a) Gettering with four chromium sources begins (day 10). (b) Gettering with four titanium sources begins. (c) Leak rate decreases. (d) Leak rate increases. (e) Vessel is opened for leak repair. (f) Vessel is closed. (g) Gettering with seven titanium sources begins (day 99).

continued pumping of H_2 by the titanium-coated walls.

1.2.2 Helium Removal Experiments and H_α Studies on ALT-II in TEXTOR

1.2.2.1 Helium exhaust and transport studies

D. L. Hillis, J. T. Hogan, C. C. Klepper,
P. K. Mioduszewski, R. C. Isler, and
L. D. Horton

In future burning fusion devices, the continuous removal of helium ash from the

core with high efficiency is necessary to prevent dilution of the fuel and concomitant extinction of the burn. Exploration of continuous helium removal with a pump limiter is part of the ALT-II experimental program on the TEXTOR tokamak. To simulate the presence of recycled helium ash in a tokamak, concentrations of 3 to 8% helium (relative to n_e) are either premixed into the working gas (H/D) or puffed into the TEXTOR plasma during the discharge. The transport of the helium in the plasma core and its subsequent pumpout using the ALT-II system are followed with CXE spectroscopy, in combination with NBI. The time evolution of the helium concentration is measured at three spatial locations along the plasma minor radius. The exhausted helium in the limiter chamber is detected by a modified Penning gage combined with a spectrally resolving light detector system. Helium transport results have been obtained with plasmas heated both by neutral beams alone (co-injection and co- plus counter-injection up to 3.0 MW) and by neutral beams in combination with up to 1.5 MW of ion cyclotron resonance heating (ICRH).

In helium puffing experiments (with NBI) at low density ($\sim 2 \times 10^{19} \text{ m}^{-3}$), the helium is transported into the plasma core within ~ 100 ms. With ALT-II pumping, up to 90% of the injected helium is subsequently exhausted within 1 s (Fig. 1.23), but the concentration is unchanged when the ALT-II pumps are off. Modeling of the helium transport in the removal experiments has been performed with the MIST impurity transport code: experimental results can be fitted with a spatially dependent anomalous diffusivity [which varies from $D_A(\text{core}) \sim 0.1 \text{ m}^2/\text{s}$ to $D_A(\text{edge}) = 1.0 \text{ m}^2/\text{s}$] added to sawtooth mixing, a pinch term [$V_p(\text{edge}) = -50 \text{ m/s}$], and a global helium recycling coefficient $R_{\text{He}} = 0.92$. This is done by matching both the observed rise time and

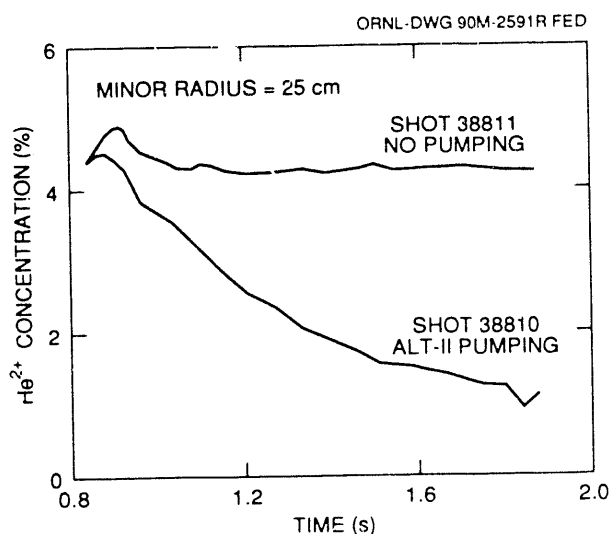


Fig. 1.23. Helium concentration measured with CXE spectroscopy after a short helium puff at 0.7 s with and without ALT-II pumping during NBI.

the longer pumping-induced decay of the helium in the plasma core as a function of the recycling coefficient (Fig. 1.24). The helium exhaust efficiency is about 8%, as estimated from pressure measurements in the ALT-II pumping duct, and is in agreement with these calculations. Combining the helium transport results with energy balance analysis using the TRANSP code for a low-density case gives an estimate of the ratio $\tau_p^{\text{He}^{2+}}/\tau_E \sim 3$. Extrapolations to the parameters of the International Thermonuclear Experimental Reactor (ITER) indicate that more efficient helium removal is required.

These studies are carried out in collaboration with K. H. Finken, K. H. Dippel, A. Pospieszczyk, D. Rübaldt, and H. Euringer of the Kernforschungsanlage (KFA) Jülich; R. A. Moyer and D. S. Gray of the University of California at Los Angeles; K. Akaishi of the National Institute for Fusion Science (Nagoya, Japan); and R. A. Hulse and R. Budny of Princeton Plasma Physics Laboratory.

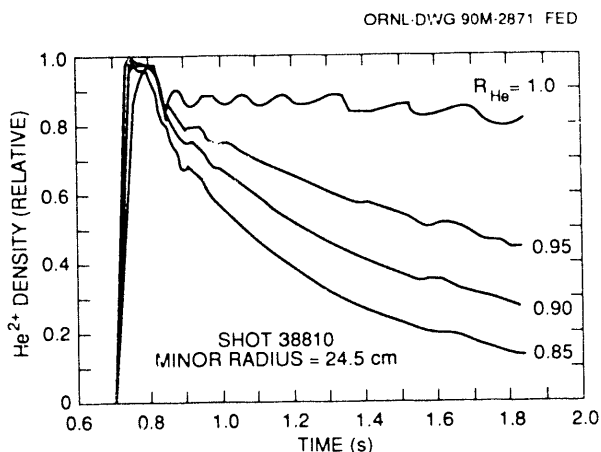


Fig. 1.24. Modeled helium densities. The helium recycling coefficient is varied for a fixed transport model (anomalous diffusivity and pinch) with sawtooth spreading.

1.2.2.2 Modeling of H_α emission and plasma confinement

L. W. Owen, T. Uckan, and
P. K. Mioduszewski

Modeling of H_α emission for Ohmic discharges in TEXTOR was begun during 1988.¹⁵ A semi-empirical model of the edge plasma particle flux incident on the ALT-II blade limiter agreed well with the experimental data. However, the model neglected poloidal asymmetries in the edge particle flux and distributed the plasma flowing under the blade uniformly on the vacuum liner.

During 1989, we attempted to correct these deficiencies by using measured distributions¹⁶ of core plasma density and temperature with scrape-off layer plasma parameters from the scanning probe, the neutral lithium beam diagnostic, and Langmuir probes in the ALT-II scoops to describe the plasma environment for DEGAS neutral transport simulations.

The Langmuir probe measurements¹⁶ of particle flux into the scoops on the electron and ion drift sides of the ALT-II blade indicate a flux asymmetry, favoring the ion drift side, of 2.25 to 1.24 for line-average densities of 1.5×10^{13} to $3.7 \times 10^{13} \text{ cm}^{-3}$. Exponential fits of the scoop flux measurements indicate that the ratio of the decay length on the electron drift side to that on the ion drift side is approximately 1.3. Extrapolation of these distributions to the LCFS gives the tangency point parallel particle flux at the limiter but neglects the effects of local recycling inside the scoops. Direct measurements of the tangency point fluxes are available from the scanning probe (electron drift side) and the lithium beam diagnostic (ion drift side); however, the lithium beam data¹⁷ indicate a pronounced steepening of the density profile as the plasma flows to the blade.

With these uncertainties in mind, we used the scanning probe data for edge plasma density and temperature profiles and the scoop Langmuir probe data (extrapolated) for particle flux to the blade in the DEGAS code to fit the data from the HA3 monitor (viewing the center of blade number 3) and the HA4 monitor (viewing the vacuum liner). The results of these calculations are shown in Fig. 1.25. The corresponding particle confinement times vary from 45 ms at $n_e = 1.5 \times 10^{13} \text{ cm}^{-3}$ to 80 ms at $n_e = 3.7 \times 10^{13} \text{ cm}^{-3}$. These particle lifetimes are in good agreement with those obtained by Goebel et al.¹⁶ with the scanning probe on the outboard midplane.

1.2.2.3 Analysis of recycling energy distributions from H_α measurements

J. T. Hogan, C. C. Klepper, and D. L. Hillis

The energy spectrum of particles reflected from limiter or divertor surfaces is an

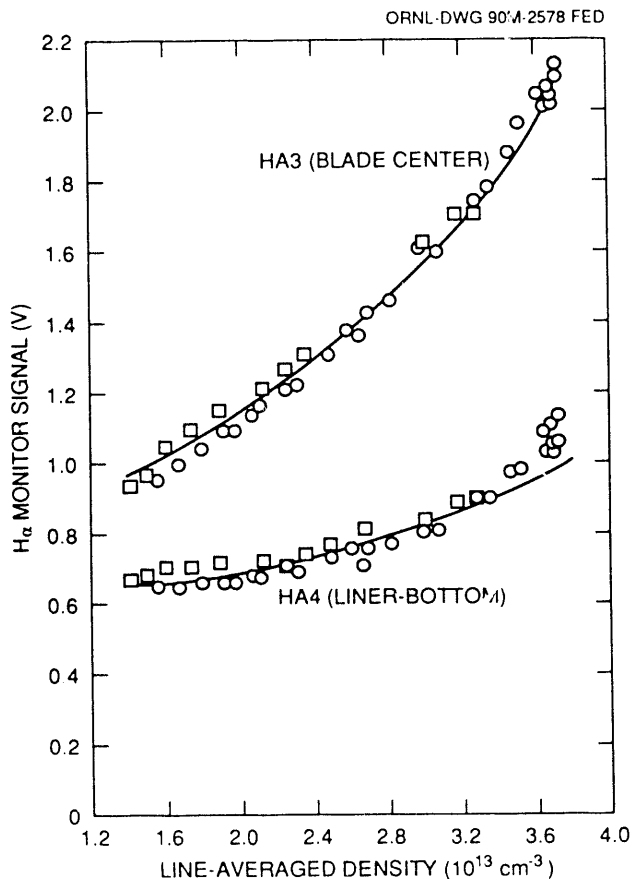


Fig. 1.25. H_α intensity at the ALT-II blade (HA3) and the TEXTOR liner (HA4). Circles: measurements. Curves: fits to the data based on DEGAS calculations.

important quantity in the construction of scrape-off layer models. As part of the ADP, it is important to characterize the flux of recycled high-energy neutrals that might strike the cryogenic pumping system.

Previous work by the TEXTOR group had shown that the wavelength spectrum of H_α light emitted from such surfaces could give a sensitive indication of the velocity distribution of neutral hydrogen as it recycles.¹⁷ Strong features on the red side of the H_α spectrum were found to be well correlated with edge T_e and the existence of particles reflected with an energy of $\sim 3kT_e$.

To explore the feasibility of this technique for the DIII-D application, measurements

were carried out as part of the ALT-II program. A number of poloidal scans of the ALT-II limiter were made with a wavelength-resolved spectrometer. Figure 1.26 shows a typical result. The onset of NBI led to increased recycling of hydrogen from the walls, but no systematic asymmetric (red-side) features were observed on the H_α spectrum. The lack of pronounced asymmetries is probably due to the fact that particle reflection coefficients for graphite surfaces are lower than those for the stainless steel test limiter used in previous work on TEXTOR. Monte Carlo modeling studies of TEXTOR with the Oak Ridge General Geometry code (GEORGE) showed a trend toward diminution of strong reflection peaks in the H_α distribution. If this trend is confirmed, it would support the operation of cryogenic pumping systems near the divertor strikepoint.

Further work is planned on the DIII-D tokamak to extend the observations to higher power (up to 20-MW NBI, compared with

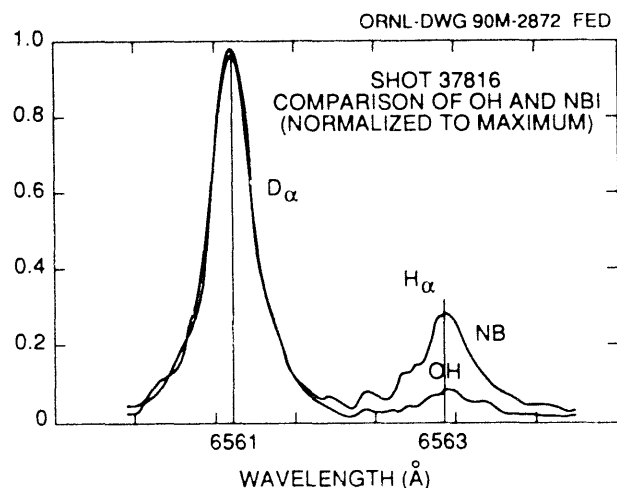


Fig. 1.26. H_α/D_α spectra during the Ohmic (OH) and neutral beam (NB) heating phases of TEXTOR shot 37816. The H_α emission increases, but there are no systematic red-side asymmetries, which would indicate a high-energy component reflected from the ALT-II blade.

1.6 MW on TEXTOR) and to characterize the incoming energetic spectrum for the future DIII-D pumps.

1.2.3 Pump Limiter Studies on Tore Supra: Measurements of Pressure Buildup and Particle Fluxes

C. C. Klepper, P. K. Mioduszewski,
L. W. Owen, J. E. Simpkins, and T. Uckan

The aim of the Tore Supra pump limiter program is to study particle control with a pump limiter system in long-pulse (≈ 30 -s) discharges with high fueling rates and high auxiliary heating. This limiter system consists of six vertical modules located at the bottom of the machine and one horizontal module located at the outboard midplane. It is designed to remove approximately 8 MW of power. The initial pump limiter experiments were carried out in ohmically heated discharges ($B_T = 2$ MW, $I_p = 750$ A, typically), in which the power flux to the edge was low enough to operate on the outboard module only. This module is instrumented with pressure gages, a residual gas analyzer, Langmuir probes in the limiter throat, and a spectrometer viewing the neutralizer plate. The core particle inventory was determined from the density profiles of a five-chord FIR interferometer.

Most experiments were done in helium; H_2 and D_2 plasmas were produced near the end of this first experimental phase. Some of the pump limiter results in helium plasmas are described in ref. 18. Even though the determination of particle balance in the helium discharges is simpler, the pumping effects are only transient, since the 200,000-L/s (nominal) titanium getter pumps, located inside the pumping chamber of the limiter, do not pump the helium. Therefore, the

small set of D_2 discharges with the pump limiter provided the opportunity to study the particle balance with pumping in steady state.

The analysis was done with a global particle model. This model connects the measured changes in core plasma density (Fig. 1.27) and in the edge particle efflux to changes in the pressures inside the pump limiter as pumping is turned on and off (Fig. 1.28). At low densities ($n_e \approx 2 \times 10^{19} \text{ m}^{-3}$) an exhaust flux of about $3 \text{ torr}\cdot\text{L/s}$ was determined, which corresponds to a 6% exhaust efficiency.

Detailed modeling of the processes in the pump limiter with the DEGAS neutral transport code is under way. This work is carried out in collaboration with M. Chatelier and J. L. Bruneau of the Centre d'Etudes Nucléaires, Cadarache, and J. G. Watkins of Sandia National Laboratories, Albuquerque.

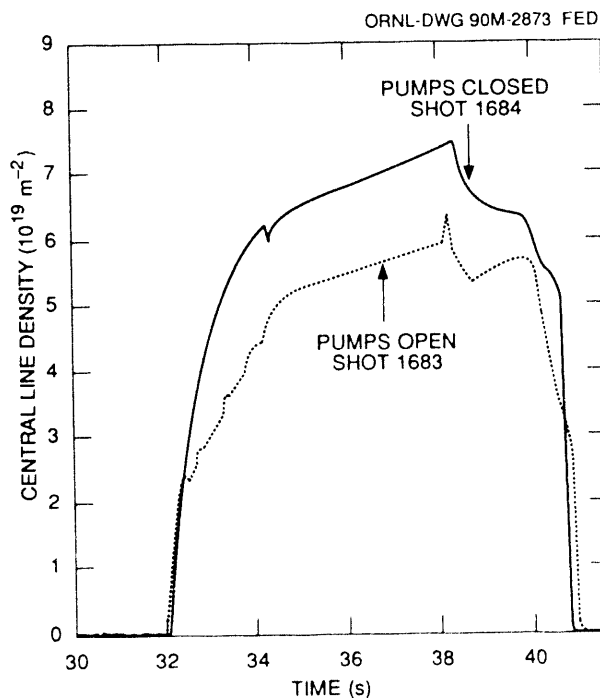


Fig. 1.27. Central line densities (double pass) for a plasma diameter of approximately 1.5 m with titanium getter pumps open and closed.

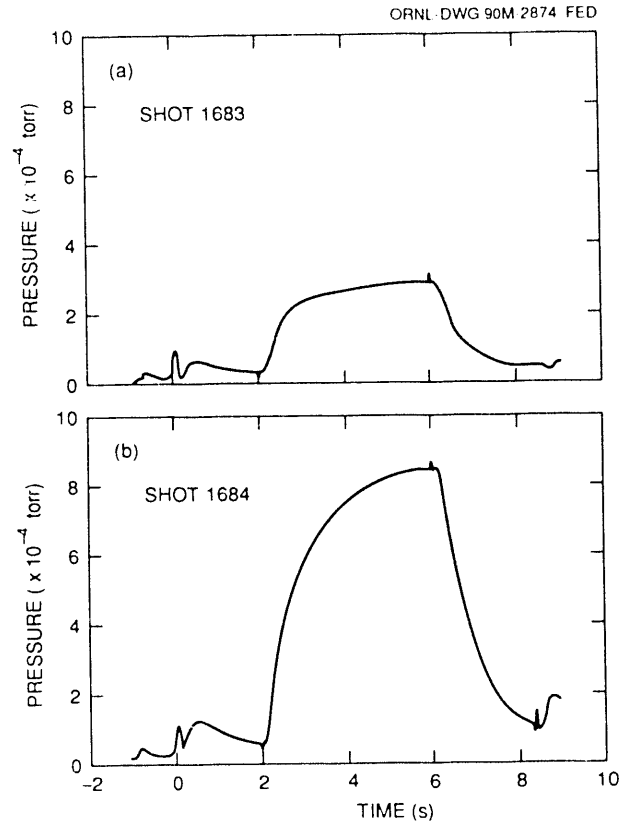


Fig. 1.28. Pressures (measured halfway between the throat and the pumps) for the shots in Fig. 1.27.

1.2.4 The DIII-D Advanced Divertor Program

1.2.4.1 Neutral particle modeling

L. W. Owen, P. K. Mioduszewski,
M. M. Menon, and J. T. Hogan

A principal objective of the collaborative ADP on DIII-D is to achieve density control in H-mode discharges with edge biasing and with continuous particle exhaust at the rate determined by external fueling sources (typically $20 \text{ torr}\cdot\text{L/s}$). The divertor baffle-bias ring system has been optimized with the neutral transport code DEGAS to achieve maximum particle throughput within constraints imposed by other aspects of the DIII-D experimental program. Magnetic flux

surfaces and plasma parameters from the H-mode documentation series are used to establish the dependence of baffle entrance slot conductance, baffle pressure, and particle throughput on the baffle-bias ring geometry.

For typical H-mode discharges, approximately 40 torr·L/s enters the outboard baffle chamber. With an entrance slot conductance of 50,000 L/s, a pumping speed of the same order is required to remove half of the incoming particle flux. Increasing the exhaust fraction with higher pumping speed is self-limiting, because of the reduction of the recycling particle flux with increasing divertor exhaust. The required pumping speed of 50,000 L/s can be achieved with either titanium pumps or cryopumps, but evaluation of both systems, as described in Sect. 1.2.4.4, led to the conclusion that a cryopump will be more compatible with the environment of the DIII-D divertor.

An important consideration in the design of an in-vessel cryopump is the power deposition on the cold surfaces of the pump and radiation shield. No experimental data exist for particle and energy reflection in the energy range (a few electron volts) of neutral atoms in the baffle chamber. Consequently, there is considerable uncertainty in the power deposition estimates from neutral transport simulations in this low-energy regime. Ruzic and Chiu¹⁹ have developed a fractal surface roughness model for use in the TRIM binary collision model code²⁰ and the EAM molecular dynamics code.²¹ Reflection coefficients generated with these fractal codes for deuterium on carbon have been used in DEGAS to calculate the energetic atom-energy flux on the cold surfaces of the pump. Preliminary results indicate that the heat load is somewhat lower than that obtained with reflection coefficients extrapolated from the 100-eV range, where experimental data exist.

A cryopump configuration that meets the objective of removing half of the incoming particle flux is shown in Fig. 1.29. The positions and orientations of the components of the liquid-nitrogen-cooled radiation shield were optimized with DEGAS to maximize the conductance from the baffle entrance to the cryopump and simultaneously minimize the power deposited on the liquid helium tube. For typical quiescent H-mode conditions, the heat load on the cryopump resulting from energetic particles is negligibly small for this configuration.

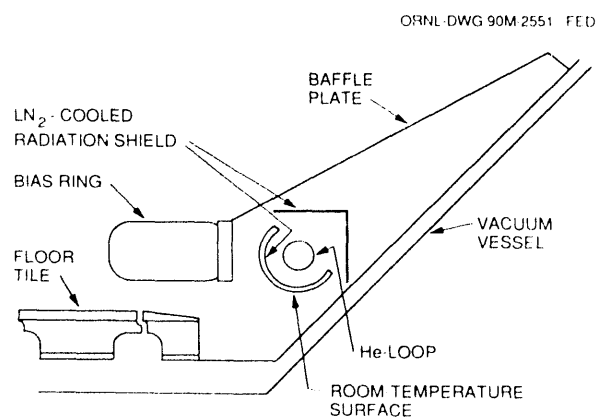


Fig. 1.29. Schematic diagram of the cryocondensation pump inside the baffle chamber.

1.2.4.2 The pre-VORTEX code

J. T. Hogan

To determine the effect of pumping on plasma performance, an internally consistent model for particle transport in an open divertor geometry has been developed. Embodied in a new code, pre-VORTEX, the model couples the particle balance in the plasma core, the scrape-off layer, the open divertor channels, and the vacuum regions. The plasma core is considered to have a relatively quiescent center and a less

well confined outer region characterized by an edge-localized mode (ELM) frequency and amplitude. The radial (1-D) density conservation equation is solved, assuming that all external ionization occurs in the outer (ELM) region and all external fueling (e.g., from neutral beams) occurs in the central region. The scrape-off layer is modeled with 1-D parallel and perpendicular transport, assuming particle influx from the plasma core and ionization of recycling neutrals from the wall and divertors. A two-point divertor channel model integrates the 1-D parallel transport equations between the throat and the divertor plates. It is similar to previous “simple” models, but new physical processes are considered: hydrogen charge exchange, impurity thermal charge exchange, and flux-limited parallel transport. The differing recycling properties of the wall regions and the divertor plates enter in the neutral particle balance, which couples the nine separate regions of the open divertor pumping geometry. No explicit watershed symmetry condition is imposed for the scrape-off layer solutions, and particle balances for the various regions are coupled. A more detailed description of the model is given in ref. 22.

Given local plasma and scrape-off layer diffusivities, wall recycling properties, and magnetic geometry data, the model predicts both divertor properties and the volume-average density and global particle confinement time. The model has been compared as a stand-alone code with typical data from the DIII-D experiment and applied to the proposed ADP.

For the nominal parameters of DIII-D and the pump geometry described in Sect. 1.2.4.1, the effect of pumping on the particle balance in a discharge with 5 MW of injected power at various fueling ratios Σ_{core}

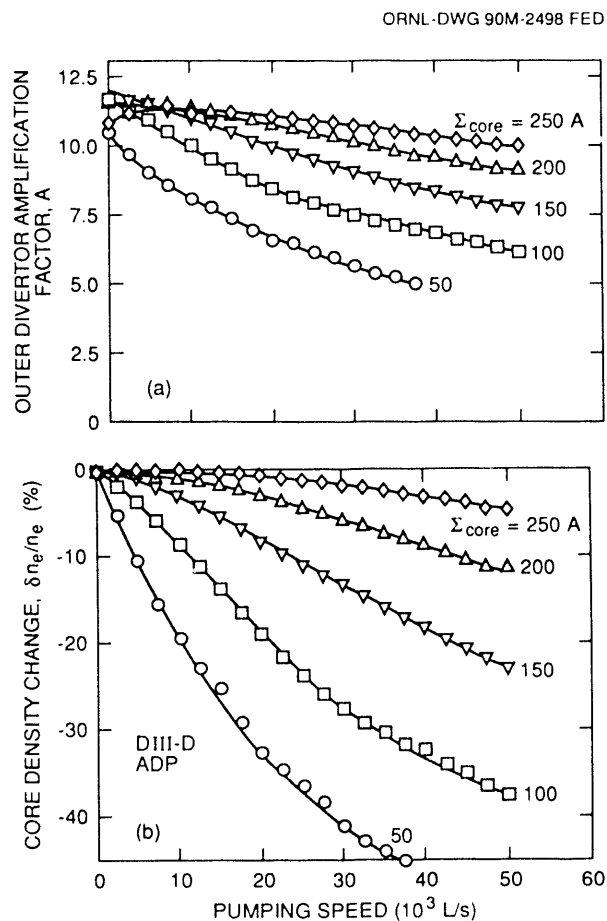


Fig. 1.30. Effect of pumping calculated with pre-VORTEX. (a) Variation of the outer divertor amplification factor, showing $A \sim 9\text{--}12$ for $\Sigma_{core} \sim 150\text{--}250$ A. (b) Change in core density with pumping.

has been examined. Figure 1.30 shows the outer divertor amplification factor A , which is the ratio of divertor particle flux to throat particle flux. Without fueling, A decreases from 12 to 5; with 200–250 A of central fueling, A remains around 10. The core plasma density drop is large ($\sim 50\%$) without core fueling, as shown in Fig. 1.30(b). The pre-VORTEX model predicts particle confinement times of 150 to 350 ms, with an assumed ELM diffusivity of 10^4 $\text{cm}^2\cdot\text{s}^{-1}$.

1.2.4.3 Diagnostics

C. C. Klepper, M. M. Menon, C. L. Haas, J. E. Simpkins, and P. K. Mioduszewski

ORNL is responsible for the diagnostics of the ADP in two areas: fast pressure measurements inside the closed divertor region and visible spectroscopy of the divertor strike region under the biased plate.

Fast pressure gages

The fast gages developed by Gunther Haas of the ASDEX group will be used for fast pressure measurements. Such gages are already employed in DIII-D, where they work more reliably when enclosed in housings that prevent energetic neutrals or ions from arriving directly (or after a single bounce) at the gage. These housings provide a slot where the particles may enter and a set of baffles to ensure that the particles are thermalized before reaching the gage. In designing such housings, care must be taken not to substantially reduce the response time of the system by limiting the conductance. A typical response time of the electronics is 5 ms. Therefore, the maximum response time of the housings should not exceed 5 ms.

Two gages will be used; the second will be employed to detect the effects of the energetic particles. In the design of the pumps for the closed divertor, the modeling included energetic particle fluxes based on assumed reflection fractions and energies at the strike point. These measurements will provide an experimental basis for checking these assumptions.

The gages will be installed in the closed divertor region, near the future location of the cryogenic pump, by means of a re-entrant tube. For the energetic neutrals gage, DEGAS modeling will be used to determine

a relation between the fast particle flux and the corresponding pressure buildup inside the housing.

Visible spectroscopy

Optical measurements of recycling at the divertor strikepoints are made with external optics and direct, vertical views through viewports located on the top part of the machine. When the divertor baffle is added, the outer divertor strikepoint will be inaccessible from external ports. For this reason, special vacuum-compatible, high-temperature optical fibers²³ will be used inside the DIII-D vacuum vessel. The fibers will not be in contact with the plasmas; they will only be inside the closed divertor pumping chamber. At least one fiber may be embedded into a tile at the strikepoint to provide a view perpendicular to the tile. This has the advantage of allowing the fiber to "see" the peak of the distribution of energetic particles reflected off the tile. These reflected particles are expected to follow a cosine law in their angular distribution with respect to the tile.

On the outside, fiber cables (1-mm fiber) that are fully protected with 3.5-mm polyethylene tubing will be attached to the vacuum fibers by means of standard SMA connectors. The connectors of the vacuum fibers will be rigidly attached to a plate to prevent breakage of the vacuum fibers. The light will then be transmitted by the external cables to a spectrometer/OMA, which will be in a room outside the biological shield.

The design of the telescope/fiber holder, shown in Fig. 1.31, includes fused silica lenses to control the viewing volume. Two such telescopes will be employed inside the vacuum vessel. One or both of these holders (telescopes) might be turned to view tangentially at another toroidal location of the strikepoint.

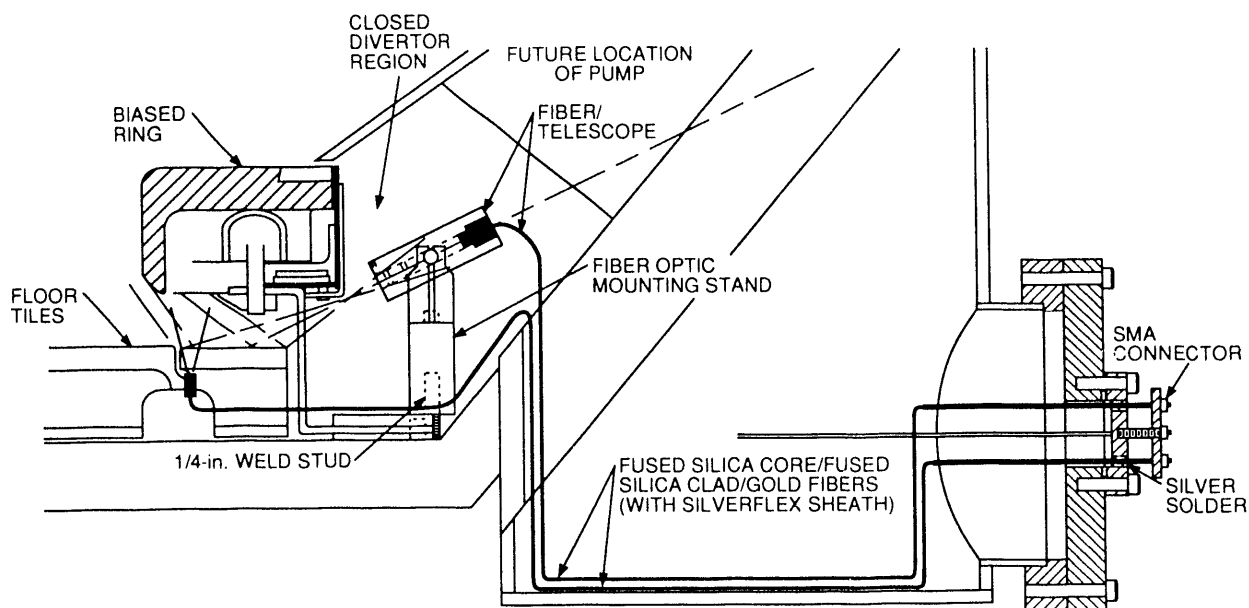


Fig. 1.31. Plan view of the fiber-optics system for the closed divertor of DIII-D.

1.2.4.4 Divertor pumping

M. M. Menon, P. K. Mioduszewski, and
L. W. Owen

As noted in Sect. 1.2.4.1, a pumping speed of about 50,000 L/s is required in DIII-D to exhaust the particles introduced by neutral beams. If pumps external to the tokamak are used, the pumping speed will be limited to <15,000 L/s by the toroidal conductance of the baffle chamber and the number and size of the available ports. Thus, in-vessel pumping is necessary to achieve the required speed. Two different pumping schemes have been investigated: titanium getter pumps and cryopumps.

The titanium getter pump investigated for this application, which is based on the work of Sledziewski and Druaux,²⁴ is made up of an array of annular disks on which a thick layer ($\sim 1 \mu\text{m}$) of titanium is deposited by an axial filament. Our experiments with thick titanium films²⁵ showed that

(1) the pumping speed is not constant but decreases from $>10 \text{ L}\cdot\text{s}^{-1}\cdot\text{cm}^{-2}$ at fluxes corresponding to less than a monolayer to $0.5 \text{ L}\cdot\text{s}^{-1}\cdot\text{cm}^{-2}$ as the cumulative gas loading reaches about $0.015 \text{ torr}\cdot\text{L}\cdot\text{cm}^{-2}$, (2) the pumping surface is poisoned by gases such as O_2 and CO_2 , and (3) rejuvenation of the surface by baking at 380°C for 4 h and depositing a thin ($0.1\text{-}\mu\text{m}$) layer of titanium, as prescribed by Sledziewski and Druaux, did not help to regain the pumping capacity. These results, illustrated in Fig. 1.32, in conjunction with limited access to the pumps after they are installed, suggested that titanium getter pumps are not appropriate for this application.

Cryocondensation pumping is well known and has found wide applications. However, adoption of this technique inside the tokamak is complicated by (1) radiation from high-temperature surfaces, (2) electromagnetic effects that can contribute significant heat loads, (3) plasma disruption forces, (4) energetic particle flux from the

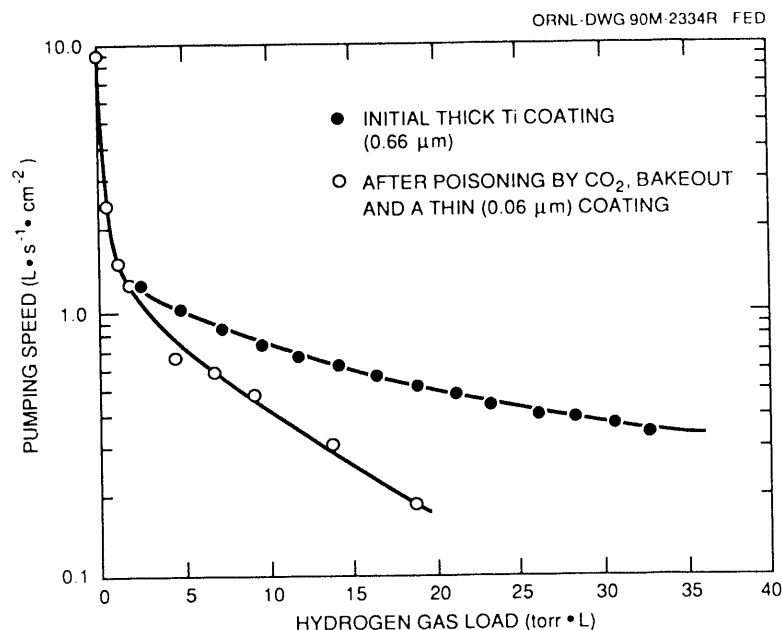


Fig. 1.32. Pumping speed of titanium films as a function of hydrogen loading.

diverted plasma, (5) restrictions on allowable materials imposed by the tokamak, (6) compatibility with glow discharge conditioning of the tokamak, and (7) severe access restrictions.

The cryocondensation pump that is being developed for DIII-D is shown in Fig. 1.29. It consists of a helium-cooled tube that forms the cryocondensation surface, surrounded by a nitrogen-cooled radiation shield. A room-temperature shield around the liquid-nitrogen-cooled surface faces the particle entrance region to prevent desorption of condensible impurities such as water vapor due to the impact of energetic particle flux. To prevent induction of currents in the loop, the pump will be electrically insulated from the tokamak and provided with insulating breaks outside the vacuum vessel. Estimates of all major sources of heat loading have been made in a coaxial geometry,²⁶ and the design is found to be dictated by the need to accommodate the helium glow discharge conditioning performed before each shot

in DIII-D. Current practice is to raise the chamber pressure to about 60 mtorr of helium for a few seconds before the glow strikes. To handle the high heat load during this regime, it may be necessary to allow the pump to regenerate, thereby utilizing the latent heat of vaporization of liquid helium. Electron-assisted glow, where the maximum helium pressure seen by the pump is anticipated to be in the range of 1–2 mtorr, is being investigated in DIII-D.²⁷ If this works, regeneration of the cryopump between tokamak shots may not be necessary.

1.3 ATF-II STUDIES

J. F. Lyon and S. L. Painter

Studies of ATF-II²⁸ during this report period focused on extrapolation of the ATF-II compact torsatron approach²⁹ to a reactor. The relatively open coil geometry

of the $M = 6$ configuration should allow good access for tritium breeding blanket modules and for remote maintenance, but the accompanying field ripple coupled with low-aspect-ratio toroidal effects could lead to an unacceptable level of energetic alpha particle losses and of ripple-induced heat conduction. Revisiting the reactor extrapolation in light of our improved understanding and better computational techniques should help to clarify the issues that ATF-II would have to address.

1.3.1 Transport Code Development

Our previous study of compact torsatron reactors³⁰ used the POPCON (Plasma OPerating CONtours) feature of the WHIST 1-D transport code,³¹ modified for stellarators, to define the reactor operating conditions. This code did not include alpha particle energy losses and, because the POPCON plots were generated by varying the input power P to linearly ramp the temperature at fixed density, the WHIST calculations did not treat the thermally unstable region ($\partial P/\partial T < 0$) properly. A new, fast 1-D transport code, COLTRANE, was written to address these issues. It solves the steady-state radial 1-D power balance equations for electrons and ions in integral form using the spectral collocation method. It assumes fixed forms for the density and potential profiles and varies these forms to test the sensitivity to the forms assumed. This approach is used because there are large uncertainties in the calculation of these profiles, and there are techniques that may be used to control them.

COLTRANE incorporates all relevant physical processes: external heating sources, alpha particle heating (with or without direct-orbit and scattered energy losses), electron-ion Coulomb collisions, radiative losses (hydrogenic bremsstrahlung, impurity radi-

ation assuming a coronal model with fixed fractions of carbon and iron, synchrotron radiation with 90% wall reflectivity), and diffusive losses [Shaing's neoclassical ripple model with electric field including the off-diagonal terms ($\nabla_n, \nabla\Phi$), Chang-Hinton axisymmetric neoclassical losses, and anomalous electron losses based on the Alcator model].

1.3.2 Effect of the Electric Field

The electric field should play a dominant role in reactor-grade stellarator plasmas. Its effect on transport enters through the electric field dependence of the heat diffusivities χ and through the $\nabla\Phi$ term in the heat balance equations. Because the coefficient of the $\nabla\Phi$ term has opposite sign for ions and electrons, this term reduces the heat flux for one species and increases it for the other. These effects lead to two qualitatively different modes of operation, depending on whether the electric field is positive (the electron-root condition, which retards the electron heat flux) or negative (the ion-root condition, which retards the ion heat flux). This is illustrated in Fig. 1.33 for an $M = 6$ compact torsatron reactor with major radius $R_0 = 10$ m, average plasma radius $\bar{a} = 2$ m, and on-axis field $B_0 = 7$ T. Both cases have broad density profiles and parabolic potential profiles parameterized by $\xi_0 = e\Phi(0)/kT_i(0)$. The two POPCON plots show contours of constant auxiliary heating power required for operation at a given value of volume-average density $\langle n \rangle$ and density-average temperature $\langle T \rangle = W/2\langle n \rangle$, where W is the total plasma thermal energy.

For the electron-root case [Fig. 1.33(a) with $\xi_0 = +3$], ignition ($P = 0$ contour) occurs at high temperature (low collisionality ν^*), where the electrons are just entering the $\chi \propto \nu^*$ regime and the ions are deep

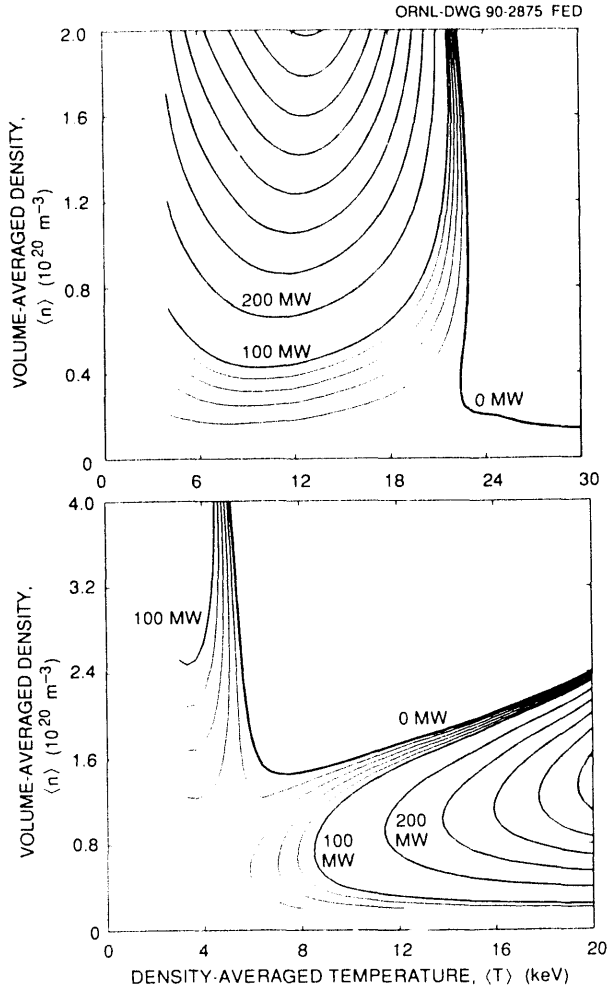


Fig. 1.33. POPCON plots for (a) electron-root operation ($\xi_0 = +3$) and (b) ion-root operation ($\xi_0 = -3$) for an $M = 6$ compact torsatron reactor with $R_0 = 10$ m, $\bar{a} = 2$ m, and $B_0 = 7$ T. The auxiliary heating power contours are equally spaced in 20-MW intervals from 0 to 100 MW and in 100-MW intervals from 100 MW.

in the $\chi \propto \nu^*$ regime, so electron heat conduction is the dominant transport loss. The lowest auxiliary heating path to ignition is at low density. For the ion-root case [Fig. 1.33(b) with $\xi_0 = -3$], ignition occurs at moderate temperature and high density, where the electrons are in the $\chi \propto 1/\nu^*$ regime and the ions are in the $\chi \propto \nu^*$ regime. The lowest auxiliary heating path to ignition is through the saddle point that

occurs between the origin and the vertex of the triangular ignition contour. More startup power is required for the ion-root condition, and simultaneous ramping of the density and temperature is required to minimize this power, as in tokamaks.

1.3.3 Results of Reactor Surveys

The COLTRANE 1-D transport code was used to survey compact torsatron reactors for a wide range of assumptions on ξ_0 , alpha particle losses, R_0/\bar{a} , \bar{a} , B_0 , helical ripple amplitude ϵ_h , anomalous electron heat conductivity $\kappa_e = n_e \chi_e$, and profile shapes for density, potential, and auxiliary power deposition. The reference reactor parameters were $R_0 = 10$ m, $\bar{a} = 2$ m (so the toroidal ripple amplitude $\epsilon_t = \bar{a}/R_0 = 0.2$), $B_0 = 7$ T, $\epsilon_h = 0.2$, and $\xi_0 = \pm 3$. The parameter ranges examined were $\bar{a} = 1-3$ m, $\epsilon_t = 0.1-0.3$, $B_0 = 3-10$ T, $\epsilon_h = 0.05-0.4$, and $\xi_0 = -4$ to -2 and $+1.5$ to $+4$.

The greatest impact is from the value of ξ_0 assumed. For electron-root operation ($\xi_0 > 0$), relatively modest power levels are required for ignition (typically $P < 20$ MW with $\xi_0 > 1.5$). These ξ_0 values are consistent with those expected from balancing the ion and electron neoclassical particle fluxes. Including alpha particle energy losses and varying the device parameters and assumed profile shapes changes the temperature at which the plasma ignites but has relatively little effect on the power required for ignition.

Ion-root operation ($\xi_0 < 0$) is much more sensitive to these assumptions, particularly with regard to the value of ξ_0 ; for example, $\xi_0 = -4$ requires $P = 9$ MW, $\xi_0 = -3$ requires $P = 28$ MW, and $\xi_0 = -2$ requires $P = 545$ MW. Values of $\xi_0 \leq -3$ are more negative than those obtained from neoclassical particle losses; additional

ion losses would need to be induced or a large negative electric field would have to be imposed to sustain these values of ξ_0 , requiring additional power input.

Alpha particle energy losses can also have a significant effect on ion-root operation. The startup power (in megawatts) can be approximated by

$$P \simeq 1.1 \times 10^7 \xi_0^{-5.2} \epsilon_t^{0.57} \epsilon_h^{1.4} B_0^{-1.8} \bar{a}^{-0.4}$$

(with B_0 in tesla and \bar{a} in meters) without these losses and by

$$P \simeq 2.9 \times 10^8 \xi_0^{-6} \epsilon_t^{0.87} \epsilon_h^{1.7} B_0^{-2.1} \bar{a}^{-0.89}$$

when alpha particle energy losses are included, for the range of parameters considered here. For the reference case, this amounts to a requirement for $\simeq 25$ MW of additional power. Varying the shape of the potential profile (and hence the value of the electric field) also has a large effect; for the reference case with alpha particle losses, a parabolic $\Phi(r)$ requires $P = 52$ MW, a parabolic-squared $\Phi(r)$ requires $P = 24$ MW, and a square-root-parabolic $\Phi(r)$ requires $P = 95$ MW.

1.3.4 Conclusions

The electron-root mode of reactor operation appears to be preferable to the ion-root mode. These calculations now need to be applied to the ATF-II case with the same assumptions used in the reactor studies. For this purpose, additional power losses have been included in the COLTRANE code: convection, charge exchange, and ionization through a coupled 1-D neutrals code and additional Bohm-like losses globally when MHD limits on $\langle \beta \rangle$ are violated and locally when stability limits on ∇p are violated. Preliminary results give energy confinement times for ATF parameters that

are close to that seen in the experiment and to that estimated from the LHD scaling.

REFERENCES

1. R. J. Colchin et al., "Overview of Results from the ATF Torsatron," *Phys. Fluids B* **2**, 1347 (1990).
2. M. Murakami et al., "Overview of Recent Results from the Advanced Toroidal Facility," p. 77 in *Proceedings of the 1st International Toki Conference on Plasma Physics and Controlled Nuclear Fusion Research*, NIFS-PROC-3, National Institute for Fusion Science, Nagoya, Japan, 1990; also published as ORNL/TM-11453, Martin Marietta Energy Systems, Inc., Oak Ridge National Laboratory, February 1990.
3. S. Sudo et al., "Scalings of Energy Confinement and Density Limit in Stellarator/Heliotron Devices," *Nucl. Fusion* **30**, 11 (1990).
4. F. W. Perkins, p. 977 in *Heating in Toroidal Plasmas: Proceedings of the 4th International Symposium, Rome, March 1984*, vol. 2, edited by H. Knoepfel and E. Sindoni, International School of Plasma Physics, Varenna, 1984.
5. R. Goldston, " $E \times B$ vs. $v_{\parallel} B / B$ as the Cause of Transport in Tokamaks," *Bull. Am. Phys. Soc.* **34**, 1964 (1989).
6. K. C. Shaing et al., "Bootstrap Current Control in Stellarators," *Phys. Fluids B* **1**, 1663-70 (1989).
7. J. H. Harris et al., "Second Stability in the ATF Torsatron—Experiment and Theory," *Phys. Fluids B* **2**, 1353 (1990).
8. J. H. Harris et al., "Second Stability in the ATF Torsatron," *Phys. Rev. Lett.* **63**, 1249-52 (1989).
9. T. Uckan et al., "ATF Edge Plasma Studies Using a Fast Reciprocating Langmuir Probe (FRLP)," *Bull. Am. Phys. Soc.* **34**, 1948 (1989).
10. Ch. P. Ritz et al., "Comparison of Edge Turbulence of TEXT and ATF," *Bull. Am. Phys. Soc.* **34**, 2153 (1989).
11. R. C. Isler et al., "Spectroscopic Studies of Plasma Collapse in the Advanced Toroidal Facility," *Nucl. Fusion* **29**, 1384-90 (1989).
12. Ch. P. Ritz et al., *Nucl. Fusion* **27**, 1133 (1987).
13. J. M. Beall, Y. C. Kim, and E. J. Powers, *J. Appl. Phys.* **43**, 3993 (1982).
14. J. E. Simpkins, P. K. Mioduszewski, and L. W. Stratton, "Studies of Chromium Gettering," *J. Nucl. Mater.* **111 & 112**, 827-30 (1982).

15. T. Uckan et al., "H α Studies," pp. 25–26 in *Fusion Energy Division Annual Progress Report for Period Ending December 31, 1989*, ORNL-6528, Martin Marietta Energy Systems, Inc., Oak Ridge National Laboratory, February 1990.
16. D. M. Goebel et al., "ALT-II Toroidal Belt Pump Limiter Performance in TEXTOR," *J. Nucl. Mater.* **162–164**, 115 (1989).
17. U. Samm et al., "Plasma Edge Physics in the TEXTOR Tokamak with Poloidal and Toroidal Limiters," *J. Nucl. Mater.* **162–164**, 25 (1989).
18. C. C. Klepper et al., "Spectroscopic Studies of Plasma Surface Interactions in Tore Supra," *Europhys. Conf. Abstr.* **13B**, 1007 (1989).
19. D. N. Ruzic and H. K. Chiu, "Modeling of Particle-Surface Reflections Including Surface Roughness Characterized by Fractal Geometry," *J. Nucl. Mater.* **162–164**, 904 (1989).
20. J. P. Biersack and L. G. Haggmark, "A Monte Carlo computer Program for the Transport of Energetic Ions in Amorphous Targets," *Nucl. Instrum. Methods* **174**, 257 (1980).
21. M. I. Baskes, "Dynamical Calculation of Low Energy Hydrogen Reflection," *J. Nucl. Mater.* **128 & 129**, 676 (1984).
22. J. T. Hogan, *The Pre-VORTEX Code*, ORNL/TM-11562, Martin Marietta Energy Systems, Inc., Oak Ridge National Laboratory, 1990.
23. C. C. Klepper et al., "Application of Modern Optical Fiber Technology in the Study of Closed Divertors and Pump Limiters in Reactors-Relevant Conditions," *Rev. Sci. Instrum.* **61**, 2943 (1990).
24. Z. Sledziewski and J. Druaux, "Titanium Getter Pump for the Tore Supra Neutral Beam Lines," pp. 533–8 in *Fusion Technology: Proceedings of the 14th Symposium, Avignon, 1986*, Vol. 1, Pergamon Press, Oxford, 1986.
25. M. M. Menon and P. K. Mioduszewski, "Pumping Scheme for the DIII-D Collaborative Advanced Divertor Program," *Bull. Am. Phys. Soc.* **34**, 2121 (1989).
26. M. M. Menon and P. K. Mioduszewski, "Particle Exhaust Schemes in the DIII-D Advanced Divertor Configuration," pp. 542–6 in *Proceedings of the 13th IEEE Symposium on Fusion Engineering, Knoxville, 1989*, Vol. 1, IEEE, New York, 1990.
27. G. A. Jackson, General Atomics, personal communication, 1989.
28. J. F. Lyon et al., "Advanced Toroidal Facility II Studies," *Fusion Technol.* **17**, 188 (1990).
29. B. A. Carreras et al., "Low-Aspect-Ratio Torsatron Configurations," *Nucl. Fusion* **28**, 1195 (1988).
30. J. F. Lyon et al., "Compact Torsatron Reactors," *Fusion Technol.* **15**, 1401 (1989).
31. W. A. Houlberg, S. E. Attenberger, and L. M. Hively, "Contour Analysis of Fusion Reactor Plasma Performance," *Nucl. Fusion* **22**, 935 (1982).

2

**ATOMIC PHYSICS AND
PLASMA DIAGNOSTICS
DEVELOPMENT**

R. A. Phaneuf,¹ Program Manager

I. Alvarez ²	J. W. Hale ¹	M. S. Pindzola ²¹
C. F. Barnett ³	C. C. Havener ¹	K. J. Reed ²²
D. Belić ⁴	H. T. Hunter ¹	R. K. Richards
C. A. Bennett ⁵	D. P. Hutchinson ¹	K. Rinn ⁸
C. Bottcher ¹	R. K. Janev ¹³	K. Sommer ²³
G. J. Bottrell ⁶	M. I. Kirkpatrick ¹	N. Stolterfoht ²³
C. Cisneros ²	C. H. Ma ¹	D. Swenson ²⁴
B. DePaola ⁷	E. W. McDaniel ¹⁴	J. K. Swenson ²⁵
G. H. Dunn ⁸	F. W. Meyer ¹	H. Tawara ²⁶
L. K. Fletcher ⁹	T. J. Morgan ¹⁵	E. W. Thomas ¹⁴
Y. M. Fockede ¹⁰	D. W. Mueller ¹⁶	J. S. Thompson ⁸
L. Forand ⁸	A. Müller ¹⁷	C. Timmer ²⁷
H. B. Gilbody ¹¹	M. P. Nesnidal ¹⁸	K. L. Vander Sluis ¹
D. C. Gregory ¹	K. Okuno ¹⁹	E. Wählin ⁸
D. C. Griffin ¹²	F. M. Ownby ²⁰	D. M. Zehner ²⁸

-
1. Physics Division.
 2. Instituto de Física, Universidad Nacional Autónoma de México.
 3. Consultant; deceased.
 4. Belgrade University, Belgrade, Yugoslavia.
 5. University of North Carolina, Asheville.
 6. University of Georgia, Athens.
 7. Kansas State University, Manhattan.
 8. Joint Institute for Laboratory Astrophysics, Boulder, Colo.
 9. Graduate student, Tennessee Technological University, Cookeville.
 10. Catholic University of Louvain, Louvain-la-Neuve, Belgium.
 11. Consultant, Queen's University, Belfast, Northern Ireland.
 12. Research subcontractor, Rollins College, Winter Park, Florida.
 13. Consultant, Institute of Physics, Belgrade, Yugoslavia, and International Atomic Energy Agency, Vienna, Austria.
 14. Consultant, Georgia Institute of Technology, Atlanta.
 15. Consultant, Wesleyan University, Middletown, Conn.
 16. University of North Texas, Denton.
 17. Institut für Kernphysik, University of Giessen, Giessen, Federal Republic of Germany.
 18. ORNL-GLCA/ACM Science Semester Student.
 19. Tokyo Metropolitan University, Japan.
 20. Program secretary.
 21. Consultant, Auburn University, Auburn, Ala.
 22. Lawrence Livermore National Laboratory, Livermore, Calif.
 23. Hahn-Meitner-Institut, Berlin, Federal Republic of Germany.
 24. Los Alamos National Laboratory, Los Alamos, N.M.
 25. University of Tennessee, Knoxville.
 26. Institute of Plasma Physics, Nagoya University, Japan.
 27. Jet Propulsion Laboratory, Pasadena, Calif.
 28. Solid State Division.

2. ATOMIC PHYSICS AND PLASMA DIAGNOSTICS DEVELOPMENT

SUMMARY OF ACTIVITIES

Research in atomic physics and plasma diagnostics development is part of the ORNL Fusion Program and is carried out within the ORNL Physics Division. The principal activities of this program are threefold: atomic collisions research, atomic data compilation and evaluation, and advanced plasma diagnostics development.

The atomic collisions research program focuses on inelastic processes that are critical for determining the energy balance and impurity transport in high-temperature plasmas and for plasma diagnostic measurements. The objective is to obtain a better fundamental understanding of collision processes involving highly ionized impurity atoms at kinetic energies that are characteristic of magnetic fusion plasmas and to determine cross sections for these processes. Close coordination of experimental and theoretical programs guides the selection of key experiments and provides both benchmarks and challenges for theory. Central to the experimental effort is an electron cyclotron resonance (ECR) multicharged ion source, which provides ions for colliding-beams experiments. A crossed-beams approach is applied to the measurement of cross sections for electron-impact ionization of highly ionized ions in initial charge states as high as +16. Electron-impact dissociation of CD_4^+ has also been studied using the crossed-beams approach. Merged beams have been used to study charge-exchange collisions of multiply charged plasma impurity ions (e.g., O^{3+} and O^{4+}) with hydrogen (deuterium) atoms at the lower kinetic energies relevant to the edge plasma. A new collaborative electron-ion merged-beams experiment to measure cross sections for electron-impact excitation of multiply charged ions by energy-loss spectroscopy is in the final testing phase and will be a major part of the experimental effort for the next several years. Ejected-electron spectroscopy has also been applied as a diagnostic tool to the study of electron capture and to the interaction of multiply charged ions with a solid surface. The theoretical effort has focused on the development of close-coupling methods for treating electron-impact excitation of highly charged ions, in support of the planned merged-beams experiments. These calculations require the development and implementation of sophisticated computer codes and depend heavily on the advanced computing capabilities of the National Magnetic Fusion Energy Computer Center.

The Controlled Fusion Atomic Data Center (CFADC) is operated by the atomic physics group, with the assistance of a network of expert consultants under contract. The CFADC searches the current literature and maintains an up-to-date bibliography of fusion-related atomic and molecular processes, which is available for on-line searching. This facilitates

the primary mission of the CFADC: the compilation, evaluation, and recommendation of relevant atomic collision data to the fusion research community. The major effort during the period continued to be directed to the revised and expanded "Redbook" series *Atomic Data for Fusion*. The CFADC actively participates in the International Atomic and Molecular Data Center Network, sponsored by the International Atomic Energy Agency, and cooperates with other data centers in Europe and Japan. Through this network, the CFADC has a major role in the development and implementation of a universal system for the computer storage, retrieval, and exchange of recommended atomic data.

The plasma diagnostics program concentrates on the development of advanced diagnostics for existing and future magnetic fusion experiments, using optical and laser technology. The current emphasis is on the application of pulsed infrared lasers to the diagnostics of alpha particles produced by fusion of deuterium and tritium. A prototype diagnostic system based on small-angle Thomson scattering of a pulsed CO₂ laser beam has been developed and installed on the Advanced Toroidal Facility (ATF) for initiation of proof-of-principle tests. These will consist of measurements of a scattered signal at an angle of $<1^\circ$ from the electrons in a nonburning plasma. A novel multichannel interferometer operating at a wavelength of either 214 or 119 μm has also been developed and installed on ATF. A relatively large number of channels is realized by use of a single reflective cylindrical beam expander, a technique that significantly reduces the number of optical elements needed by a conventional system. The interferometer has been installed on ATF and operated on seven channels to provide a measurement of the plasma electron density profile. To address the issue of optical beam refraction in higher-density plasmas, a two-color infrared interferometer/polarimeter system, which will operate at wavelengths of 10.6 and 28 μm , has been proposed for the Compact Ignition Tokamak. A prototype 28- μm water vapor laser and electro-optic polarization modulator have been constructed and tested in the laboratory. Another laser application is the operation of a facility to quantify radiation damage to optical mirrors and materials. Calorimetry experiments were also initiated to investigate the claims of anomalous heat production in electrolysis cells containing deuterated solutions and palladium cathodes. No evidence was found for the production of neutrons or gamma rays from any of the cells, but evidence for production of excess heat in one cell was found. Improved follow-up experiments are planned to further investigate the effect.

2.1 EXPERIMENTAL ATOMIC COLLISIONS

2.1.1 Electron Capture in $O^{3+} + H(D)$ and $O^{4+} + H(D)$ Collisions Using Merged Beams

C. C. Havener, M. P. Nesnidal, and R. A. Phaneuf

Experimental investigations of electron capture resulting from low-energy collisions of multiply charged ions with neutral hydrogen (deuterium) have continued. Measurements for O^{3+} and $O^{4+} + H(D)$ in the energy range from 1 to 1000 eV/amu were performed at the ORNL Electron Cyclotron Resonance (ECR) Multicharged Ion Research Facility using the ion-atom merged-beams apparatus. We are able to obtain such low collision energies by merging a relatively fast ($\approx q \times 10$ keV) multicharged ion beam with a ground-state neutral hydrogen beam traveling at nearly the same velocity. The primary objective is to obtain a better quantitative understanding of such collisions at energies where the internuclear motion is slow, compared with the orbital motion of the active bound electrons in the system. A quasi-molecular description of the interacting system is appropriate for this study. Our experimental data for $O^{5+} + H$ show an unexpected enhancement at low energies, which may be due to the ion-induced dipole attraction modifying the trajectories of the reactants.¹ No such enhancement, though, was found in subsequent measurements for $N^{3,4,5+} + H$ (ref. 2).

To continue these studies, cross sections have been measured for electron capture for the collision systems $O^{3+} + H(D)$ and $O^{4+} + H(D)$. The data are presented with other experimental and theoretical results in Figs. 2.1–2.3. For collisions with both

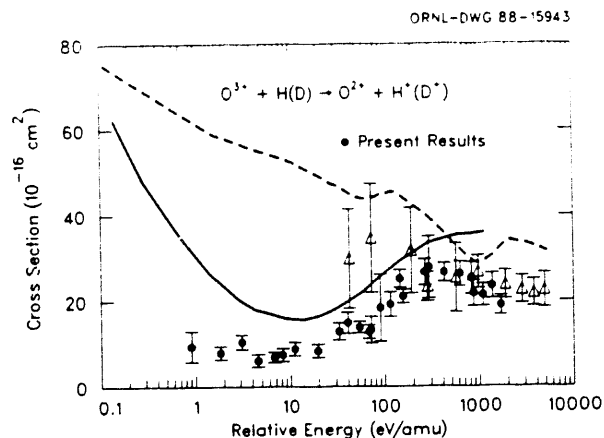


Fig. 2.1. Comparison of merged-beams data for $O^{3+} + H(D)$ with other measurements (Ref. 3) and theoretical calculations (Refs. 4 and 5). The solid curve is from Ref. 4; the dashed curve, from Ref. 5.

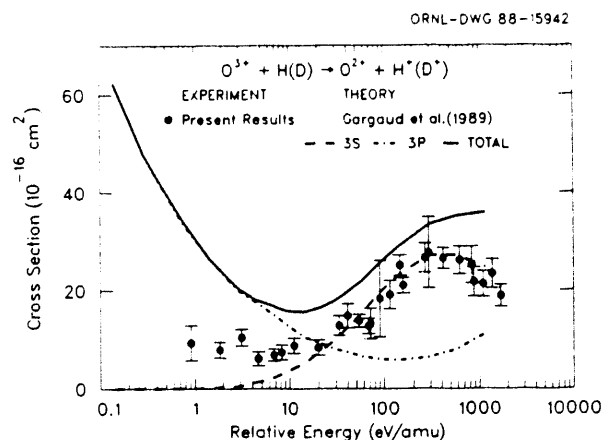


Fig. 2.2. Comparison of merged-beams data for $O^{3+} + H(D)$ with theoretical calculations (Ref. 4) for capture into the $3s$ and $3p$ states.

O^{3+} and O^{4+} , the merged-beams data join smoothly with other measurements³ at the higher energies based on ion-beam-gas-target methods and verify the normalization methods used for the latter. In the $O^{3+} + H$ case, the measurements lie significantly below theoretical calculations^{4,5} at energies below 100 eV/amu where significant contribution from capture to the $3p$ state

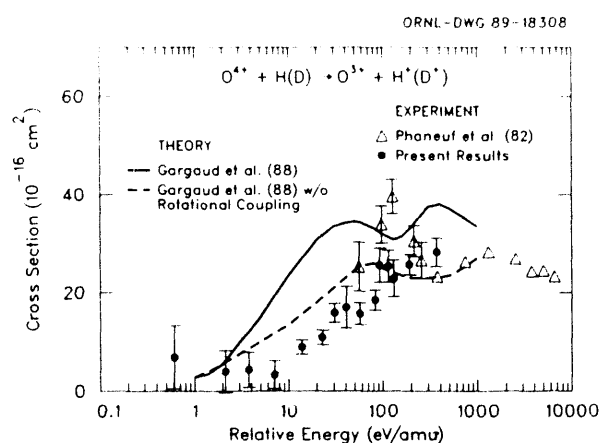


Fig. 2.3. Comparison of merged-beams data for $O^{4+} + H(D)$ with other measurements (Ref. 3) and available theory (Ref. 6).

is predicted. The measured cross section is, in fact, consistent with the calculation for capture to the $3s$ state down to 10 eV/amu and suggests that this calculation may overestimate the $3p$ contribution by roughly a factor of two. For collisions with O^{4+} , the measurements agree with the general trend predicted by the available theory⁶ but suggest that rotational coupling between states may not be as important as previously thought.

2.1.2 Dissociation and Ionization of CD_4^+ by Electron Impact

D. C. Gregory, D. W. Mueller, and H. Tawara

The presence of certain molecular ions near the edges of high-temperature plasma devices has stimulated interest in these ions in the fusion community, adding to the attention received from researchers in plasma processing and flame chemistry. The conventional assumption has been that dissociation of molecular ions should be dominated by removal of a single light particle, with more extreme degrees of dissociation be-

coming increasingly unlikely.⁷ However, the difficulties involved in performing precise absolute cross-section measurements have limited the number of experimental studies on molecular ions. We have measured absolute cross sections for ionization and dissociation of CD_4^+ at collision energies from 4 to 300 eV using the ORNL ECR ion source and crossed electron-ion beams apparatus.⁸

CH_4^+ and CD_4^+ are of particular interest to edge plasma modelers because of the inevitable presence of these molecular ions in devices using carbon limiters and hydrogen (or deuterium) as fuel. An unusual feature of the deuterated form of the ion is that it can be vibrationally excited to a long-lived (metastable) state that is above the dissociation limit, forming what is usually called a "predissociating" ion. We expect the signature of a predissociating component in the ion beam in this experiment to be the measurement of a nonzero cross section at energies far below the 10-eV threshold for dissociation of the "ground-state" CD_4^+ ions. Indeed, the measured cross sections for each dissociation channel studied are finite at the lowest collision energies obtainable, decrease rapidly with increasing collision energy, and are still nonzero just below 10 eV. The fact that the magnitudes of these "below-threshold" cross sections are strongly dependent on ion source conditions indicates that a predissociating component is present in the incident CD_4^+ ion beam.

The cross section for direct ionization of "ground" CD_4^+ (forming CD_4^{2+}) is negligible compared with the competing dissociation channels. As predicted, the resulting CD_4^{2+} is unstable, with a lifetime considerably shorter than the time scale of this experiment. However, the "predissociating" incident ions apparently do ionize, since a finite cross section for production of CD_4^{2+} was observed at energies below 10 eV.

The cross sections for dissociation of "ground" CD_4^+ into C^+ , CD^+ , and CD_2^+ were obtained by subtracting the apparent cross section due to the metastable component in the ion beam from the total cross section for production of the desired fragment ion. The resulting cross section for dissociation of "ground" CD_4^+ to C^+ is shown in Fig. 2.4. The peak cross sections for the three dissociation channels measured in this experiment are all within a factor of 2 (with average value $4.5 \times 10^{-17} \text{ cm}^2$) and are only about a factor of 10 smaller than the predicted cross section for dissociation to CD_3^+ by removal of a single deuterium atom.

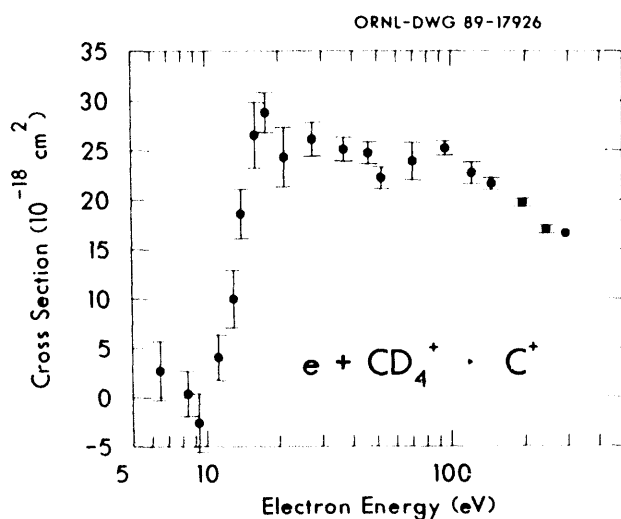


Fig. 2.4. Cross section for dissociation of "ground" CD_4^+ to form C^+ .

The "predissociating" state that has been observed in spectroscopic studies of CD_4^+ has not been seen for CH_4^+ . Follow-up measurements will be made to confirm that the cross section measured below 10 eV is real and due to the small predissociating component of the incident CD_4^+ ion beam.

2.1.3 Studies of Angular Dependence and Line Shapes for Auger Electron Emission in Low-Energy $He^{q+} + He$ Collisions

F. W. Meyer, J. K. Swenson, and C. C. Havener

In a follow-up experiment to our measurements⁹ of Coulomb focusing in low-energy $He^+ + He$ collisions, we studied the energy and angular dependence as well as the line shapes associated with Auger electron emission resulting from low-energy $He^{q+} + He$ collisions. The aim of this study was twofold. The first goal was to investigate the target/projectile electron emission asymmetry resulting from Coulomb focusing as a function of projectile charge. Results of this investigation are illustrated in Fig. 2.5, which shows electron spectra produced in 10-keV collisions of He^0 , He^+ , and He^{2+} projectiles with helium target atoms. As expected, with neutral projectiles (produced by resonant electron capture in an upstream helium gas cell) the Auger electron line shapes are no longer broadened by postcollision interaction (PCI) and, within the uncertainty of the measurement, are equal for target- and projectile-based electron emission (i.e., no asymmetry). On the other hand, for He^{2+} projectiles, significantly increased PCI line broadening is observed, as well as increased target/projectile intensity asymmetry relative to that characterizing the electron spectrum observed for He^+ projectiles.

The second goal of this study was to search for experimental evidence of interference effects that may arise from the existence of two equivalent and indistinguishable trajectories around the "focusing" ion that an Auger electron may take. To increase

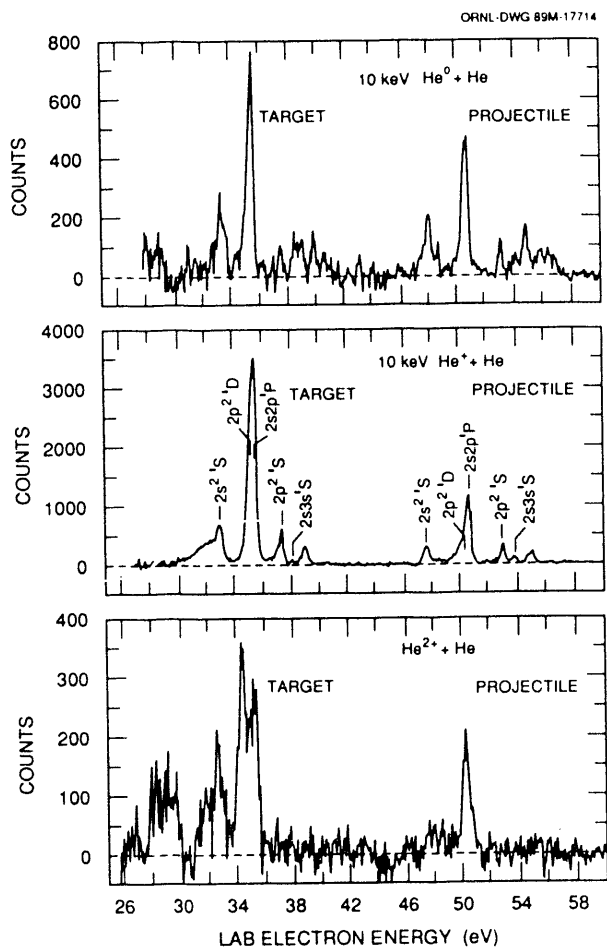


Fig. 2.5. Autoionization electron spectra for 10-keV collisions of He, He⁺, and He²⁺ projectiles with He target gas.

the rate of data acquisition for nonzero observation angles, a new target gas cell was used for these measurements instead of a gas jet. The new cell had, in addition to the entrance and exit apertures for the ion beam, separate openings to permit analysis of Auger electrons emitted at selected nonzero laboratory angles. Figure 2.6 shows typical electron spectra obtained for 5-keV He⁺ + He collisions at four different laboratory observation angles. Pronounced interference structure is observed, particularly in the line shape associated with the Auger decay of the target-based $2s^2\ ^1S$ level. On the basis of a

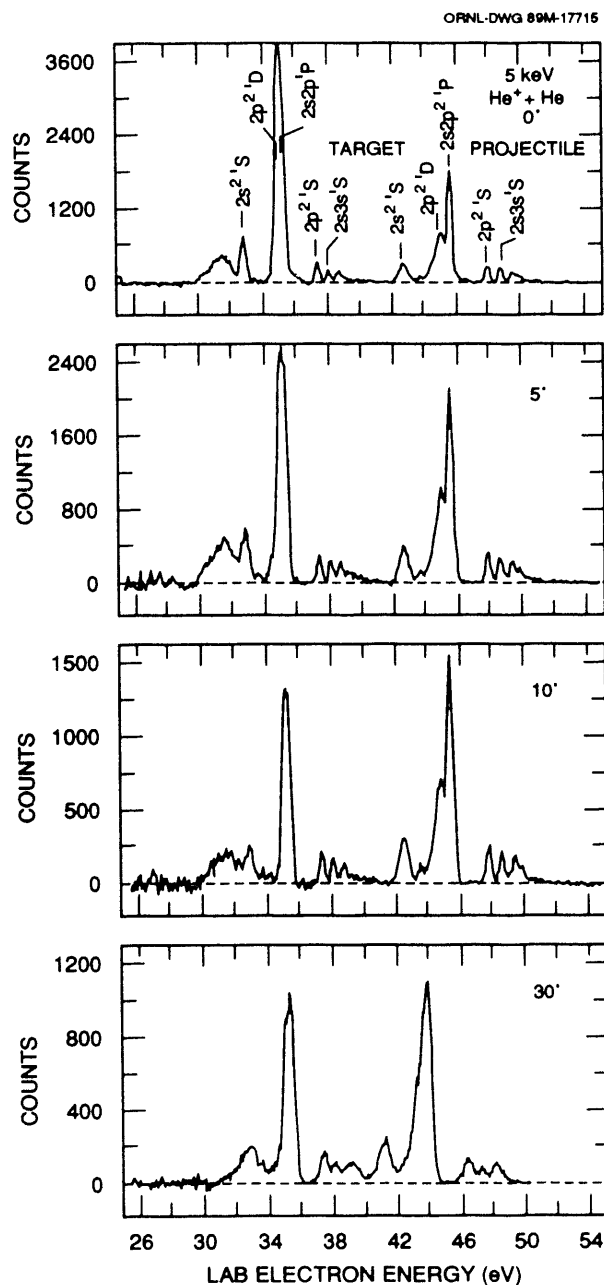


Fig. 2.6. Electron spectra resulting from 5-keV He⁺ + He collisions, observed at four different laboratory angles.

preliminary analysis,¹⁰ the dominant mechanism giving rise to the observed interference structure appears to be interference between contributions from different doubly excited states that overlap in energy because of PCI,

as described, for example, by Morgenstern et al.¹¹ This statement is based on the fact that, when Morgenstern's treatment is used, satisfactory fits are obtained to the line shapes observed for electron emission away from the charged collision partner (e.g., at laboratory angles of 0° in the case of projectile-based transitions or of 180° for target transitions), as illustrated in Fig. 2.7(a). The fits shown in that figure were obtained by assuming interference between the $m_1 = 0$ sublevels of the $2s^2\ ^1S$, $2p^2\ ^1D$, and $2s2p\ ^1P$ initial states and

adjusting the relative amplitudes and phases of the first two states with respect to the third (i.e., four free parameters). While this model predicts that the obtained fitting parameters should equally well describe the line shapes observed for the case of electron emission toward the charged collision partner, it was found that fitting parameters significantly different in amplitude as well as phase were required to obtain reasonable fits for this case [see Figs. 2.7(b) and 2.7(c)]. Similar conclusions were derived from analysis of electron spectra obtained at 10-keV collision energies. The fitting parameter adjustment required for the case of electron emission in the direction of the charged collision partner (i.e., under conditions where Coulomb focusing is possible) may be evidence for a modification of the Auger electron phase evolution or, even more speculatively, for an additional interference mechanism caused by the presence of the He^+ collision partner. Alternatively, the parameter adjustments required may merely reflect the limitations of the model on which the analysis is based. Work is in progress to obtain a better understanding of the assumptions underlying the model used and the ways in which these assumptions might restrict the model's range of validity.

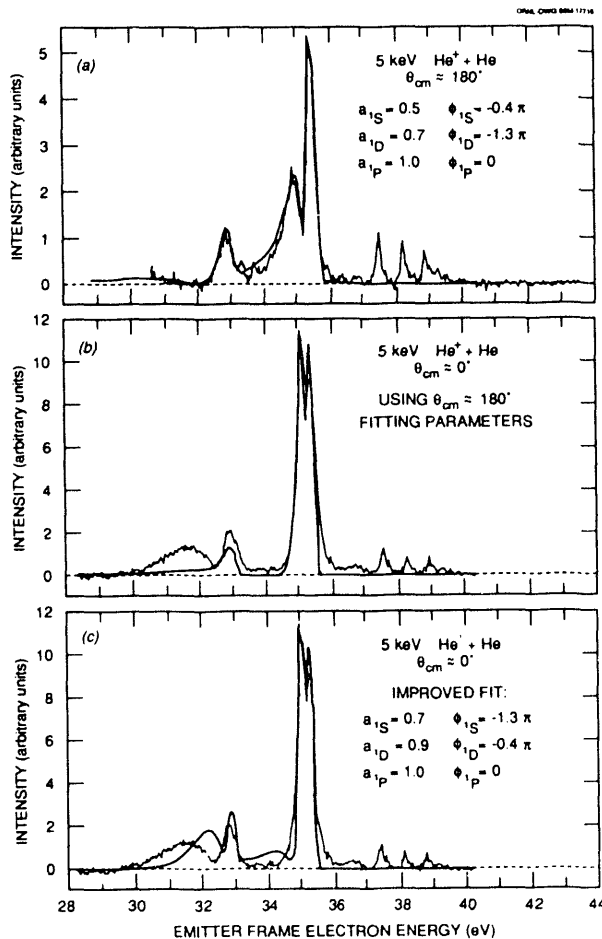


Fig. 2.7. Line shape fits to spectra for electron emission (a) away from and (b), (c) toward the charged collision partner in 5-keV $\text{He}^+ + \text{He}$ collisions.

2.1.4 Auger Spectroscopy of Low-Energy Multicharged Ion-Atom Collisions

F. W. Meyer, C. C. Havener, K. Okuno, J. K. Swenson, K. Sommer, and N. Stolterfoht

During the past year, we have continued the analysis of the Auger electron emission resulting from double-electron capture collisions of 60-keV C^{6+} ions colliding with a helium target. Unlike our previously studied

$O^{6+} + He$ system, in which the nonequivalent $2pnl$ configurations produced by correlation effects decay by very low energy (<20 -eV) Coster-Kronig transitions, which are difficult to measure, the nonequivalent configurations produced in the $C^{6+} + He$ system decay by KLX Auger transitions occurring around 300 eV, which are relatively straightforward to measure. The other attractive feature of the present system is the fact that there are no "hidden" (i.e., nonautoionizing) channels for two-electron capture. Consequently, a more quantitative estimate can be made of the importance of correlation effects in this system (e.g., by comparison of the production of nonequivalent vs equivalent doubly excited configurations). To infer cross sections for the production of the nonequivalent configurations from the KLX Auger electron intensities, it was found, from calculations¹² of Auger and radiative transition rates, that significant corrections had to be made because of Auger yields that were significantly smaller than unity. For example, the calculated average Auger yield for a KLX transition from the $2l7l'$ configuration was found to be 0.11, in sharp contrast to the unity yield found for the corresponding Coster-Kronig transition in the $O^{6+} + He$ system. After this correction was made, very good agreement was found between the O^{6+} and C^{6+} cross sections for the production of nonequivalent configurations.

In addition to the electron spectroscopy studies of double-electron capture by ground state projectiles, we have performed Auger spectroscopy measurements of single- and double-electron capture by helium-like metastable ions in a helium gas target. The goal of the study was to obtain normalized electron capture cross sections, as well as to determine the metastable fractions of helium-like C, N, and O beams extracted from the ECR source. The method used involved the measurement of K-Auger yields in low

resolution as a function of helium target thickness. In the single collision limit, the K-Auger yield is proportional to the product of the electron capture cross section times the metastable fraction. At equilibrium target thicknesses, where each incident metastable ion has a 100% probability of capturing an electron and subsequently filling the initial K-vacancy by Auger decay, the yield is proportional to the metastable beam fraction. From the yields obtained in these two limits, the total (i.e., single plus multiple) electron capture cross section for the helium-like metastable ion can be determined. High-resolution measurements of the K-Auger electrons were also performed to permit separation of single- and multiple-electron capture by identifying the corresponding lithium-like, beryllium-like, etc., K-Auger transitions. Figure 2.8 shows the target

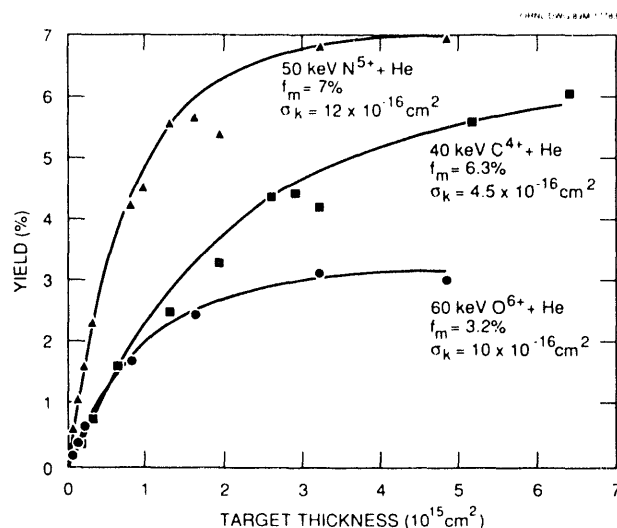


Fig. 2.8. Target thickness dependence of the normalized yields of K-Auger electrons associated with electron capture by metastable He-like ions of C, N, and O. The metastable fractions f_m and capture cross sections σ_K shown in the figure were determined using the asymptotic thick target K-Auger yields and the initial yield slope in the low target thickness limit as described in the text. The solid curves are the calculated yields $Y = f_m \{1 - \exp[-\sigma_K(\pi)]\}$ and do not represent least-squares fits to the data.

thickness dependence of the normalized K-Auger yield for the collision systems studied. The target thickness was calibrated using a capacitance manometer, while the electron spectrometer efficiency was determined by normalizing to the known¹³ Auger electron emission cross section for 10-keV He⁺ + He collisions. The metastable fractions determined from these measurements are consistent with independent measurements of this quantity using ion-surface collisions.¹⁴ For all three ion species investigated, the total electron capture cross sections determined for the metastable ions were in reasonable agreement with the total ground-state electron capture cross sections obtained from the literature. Further work is planned to resolve single- vs multiple-electron capture processes by analysis of the high-resolution K-Auger spectra.

2.1.5 Electron Spectroscopy of Multicharged Ion-Surface Interactions

F. W. Meyer, C. C. Havener, D. M. Zehner, and K. J. Reed

We have continued our collaborative effort to study the interaction of multicharged ions with surfaces. Our previous measurements of a variety of projectile ions incident on copper and gold single crystals have shown electron Auger emission from both the projectile and the target. The projectile Auger electrons result from the decay of inner-shell vacancies either carried into the collision or produced by vacancy transfer from empty outer projectile levels via close collisions with target atoms. If the incident projectile vacancy survives the neutralization process above the surface, subsequent close collisions with the target atoms may lead to the creation of inner-

shell vacancies in the target, which give rise to Auger emission characteristic of the metal. The important time scales of the neutralization of the projectile ion (the rate at which electrons fill the higher levels and the rate of decay of the inner-shell vacancy) are only qualitatively understood.¹⁵

In order to quantitatively determine neutralization times above the surface, we monitor the target Auger emission resulting from collisions of the projectile with the target atoms. The variation of the nitrogen projectile KLL peak and the gold target NVV (69-eV) and NNV (220-eV) peaks were measured for N⁶⁺ incident on gold at various angles of incidence (see Fig. 2.9). If neutralization is assumed to begin at a critical distance¹⁶ above the surface at which the Coulomb barrier between the projectile and the metal falls below the Fermi level (equal to about 16 atomic units for N⁶⁺ ions), each angle of incidence, θ , corresponds to a different above-surface neutralization time t . Since the observed nitrogen KLL peak position is relatively insensitive to incident angle, it is inferred that filling of the upper L levels is accomplished quickly compared to the relevant KLL Auger decay. The disappearance of the 69-eV target line at the lowest angles of incidence indicates that the nitrogen K-vacancy does not survive the neutralization process before interacting with the surface. The areas under the 69-eV and 220-eV gold peaks are plotted in Fig. 2.10 as a function of the above-surface neutralization time. The slopes of both curves are nearly the same and lead to an estimate of the K-vacancy lifetime T above the surface on the order of 1.5×10^{-14} s.

It is hoped that this technique can be applied to a system where the various electron configurations leading to Auger emission may be resolved in the electron emission spectra. Comparison of the observed and calculated decay rates may then lead to a better understanding of the neutralization

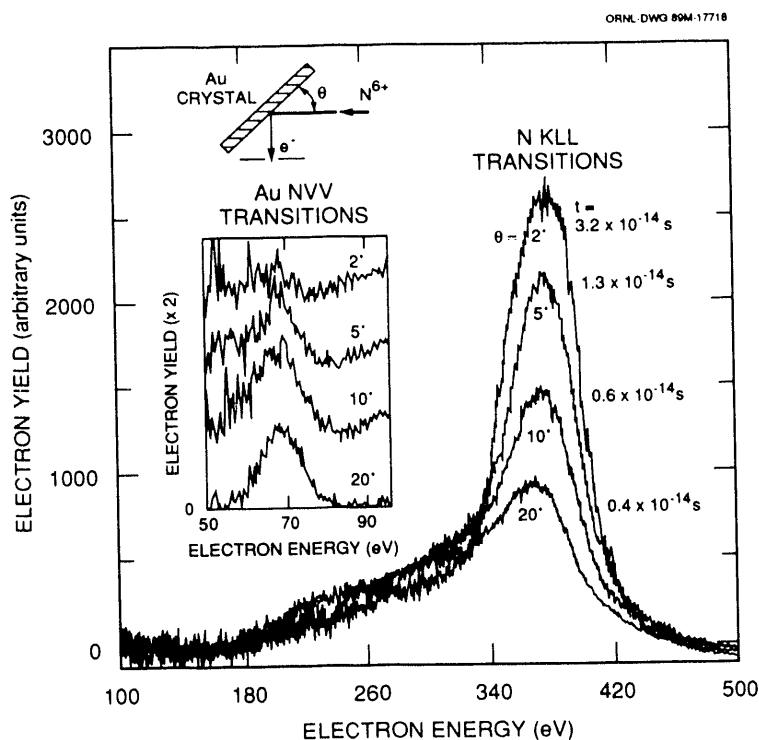


Fig. 2.9. Electron energy distributions for 60-keV N^{6+} ions incident on gold, for four different observation angles θ , and corresponding above-surface neutralization times t .

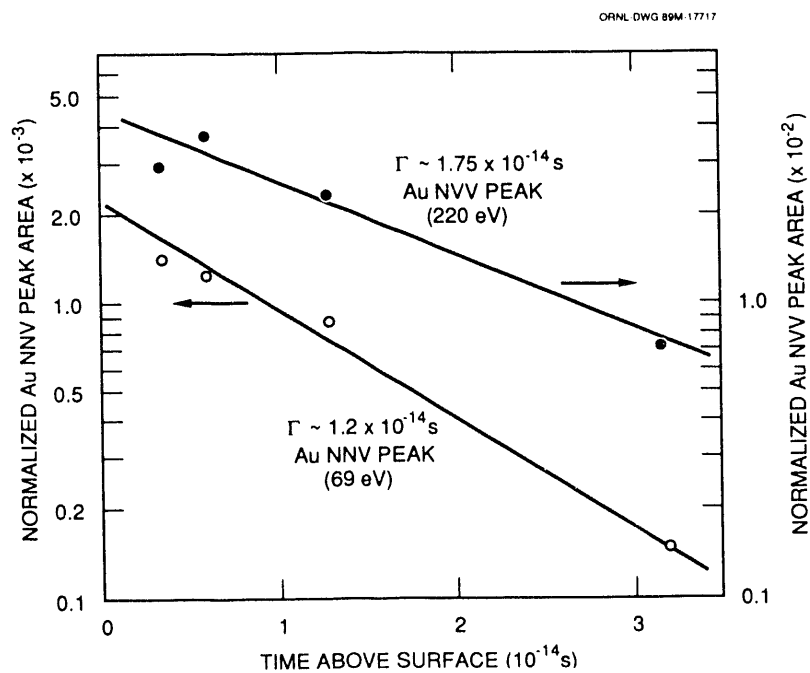


Fig. 2.10. Semi-log plot of the area under the two observed gold lines as a function of above-surface neutralization time. The slopes of the straight-line fit to the data lead to estimates for the lifetime of the nitrogen K-vacancy above the surface.

process, especially the apparent rapid filling of the upper levels.

2.1.6 Merged-Beams Experiment for Electron-Impact Excitation of Ions

E. Wählin, C. Timmer, L. Forand,
D. Swenson, B. DePaola, R. A. Phaneuf,
D. Belić, K. Rinn, J. S. Thompson,
A. Müller, and G. Dunn

Apart from their fundamental importance, cross sections for electron-impact excitation of multiply charged plasma impurity ions are critical to radiative power loss and diagnostics of magnetic fusion plasmas. All such excitation cross-section measurements to date have been based on the crossed-beams approach and on absolute intensity measurements of the radiation emitted as the excited states decay. The number of such measurements has been severely limited by low intensities and efficiencies of photon detection. Resonances are predicted to play a major role in the near-threshold region, but the experiments performed to date have had insufficient energy resolution to adequately test theoretical calculations.

A novel experimental approach to this problem has been under development for a number of years at the Joint Institute for Laboratory Astrophysics (JILA) in Boulder, Colo. This approach involves merging fast beams of electrons and multiply charged ions in a uniform axial magnetic field and using electron energy loss spectroscopy to detect electron-impact excitation events. This experiment has been developed specifically for use in conjunction with the ORNL ECR multicharged ion source. During a six-month assignment of R. A. Phaneuf to JILA during FY 1989, the proof of principle of the technique was established, systematic tests were

completed, and preliminary measurements of excitation of C^+ were initiated.¹⁷

The apparatus will be transported to ORNL in early 1990, with subsequent initiation of collaborative measurements of electron-impact excitation of multiply charged ions. In preparation, modifications were made to the main beam line of the ORNL ECR ion source, and the existing crossed-beams and merged-beams experiments were relocated. Collaborative experiments using this experimental approach will constitute a significant fraction of our experimental effort in electron-ion collisions during the next several years.

2.1.7 Electron-Impact Ionization of Ta^{8+}

D. C. Gregory

In the next generation of magnetic fusion experiments, such as the proposed International Thermonuclear Experimental Reactor (ITER), the power loading at the vacuum vessel walls and divertor plates will exceed the capabilities of low- Z materials such as carbon, which is widely used in current devices. Refractory metals such as tungsten and tantalum are being considered. Such high- Z elements will be only partially ionized in the hot plasma, and radiation from these ions will cool the edge region, insulating the vacuum vessel from the hot core plasma. Line radiation from specific charge states will provide a useful diagnostic of the plasma. Accurate modeling will require knowledge of cross sections for electron-impact ionization and recombination of these high- Z elements.

Preliminary measurements of electron-impact ionization cross sections for Ta^{8+} as a function of collision energy have been made. The experiment used the ORNL ECR ion source and electron-ion crossed-beams

apparatus. This was the first use of heavy refractory metal ion beams from this source in an experiment. The measurements in this preliminary study show that the cross section is approximately 50% larger than that predicted by the simple Lotz formula for collision energies over the energy range from 150 to 900 eV. There are no indications of a high-lying metastable component in the incident ion beam or of sharp features in the cross-section energy dependence. Possible future experiments include a remeasurement of this cross section in greater detail as well as ionization measurements for additional charge states.

2.2 ATOMIC COLLISION THEORY

2.2.1 Abstract of "Strong-Field Laser Ionization of Alkali Atoms Using 2-D and 3-D Time-Dependent Hartree-Fock Theory"¹⁸

M. S. Pindzola, G. J. Bottrell, and C. Bottcher

The time-dependent Schrödinger equation is solved directly for an alkali atom subject to an arbitrarily strong electromagnetic field. Two methods are compared. A tridiagonal finite difference method is used to solve Schrödinger's equation on a three-dimensional (3-D) Cartesian coordinate lattice. Multiphoton ionization cross sections are extracted from the two-dimensional (2-D) calculations for hydrogen and lithium and then compared with previous perturbation theory results. Single-photon ionization probabilities are compared from the 2-D and 3-D calculations for hydrogen.

2.2.2 Abstract of "Coupling Effects for Electron-Impact Excitation in the Potassium Isoelectronic Sequence"¹⁹

M. S. Pindzola, D. C. Griffin, and C. Bottcher

Electron-impact excitation cross sections for outer-subshell transitions in Ca^+ , Sc^{2+} , Ti^{3+} , Cr^{5+} , and Fe^{7+} are calculated in the close-coupling and distorted-wave approximations. Coupling effects, beyond the first-order perturbation included in the distorted-wave approximation, are found to decrease rapidly as one moves to higher Z along the potassium isoelectronic sequence. Only for Fe^{7+} , however, are the close-coupling and distorted-wave results in agreement to 10% or better for all the excitations studied.

2.2.3 Abstract of "Indirect Processes in the Electron Impact Ionization of Atomic Ions"²⁰

M. S. Pindzola, D. C. Griffin, and C. Bottcher

General theoretical methods for the calculation of indirect processes in the electron-impact ionization of atomic ions are reviewed. Theory is compared with the results of recent crossed-beams experiments for several atomic ions.

2.2.4 Abstract of "Correlation Enhancement of the Electron-Impact Ionization Cross Section for Excited State Ne-Like Ions"²¹

M. S. Pindzola, D. C. Griffin, and C. Bottcher

The electron-impact ionization cross section is calculated in the distorted-wave approximation for the neon-like ions Ar^{8+} , Ti^{12+} , Fe^{16+} , Zn^{20+} , and Se^{24+} . For ionization from the $2p^6$ ground state, the contributions from inner-shell excitation followed by auto-ionization are negligible. However, when

these ions are initially in the $2p^53s$ excited configuration, contributions arising from the inner-shell excitations $2p^53s \rightarrow 2p^43snl$ and $2p^53s \rightarrow 2s2p^53snl$ are large. The overall branching ratio for autoionization of the $2p^43snl$ and $2s2p^53snl$ levels increases when the atomic structure calculations are extended beyond the single-configuration approximation to include configuration interaction. The resulting correlation enhancement of the excited state ionization cross section is found to increase as a function of Z . For Se^{24+} the correlation enhancement of the total ionization cross section is found to be 42%.

2.2.5 Time-Dependent Hartree-Fock Studies of Ion-Atom Collisions

G. J. Bottrell and C. Bottcher

We have completed studies on $p + \text{H}$ and $\text{C}^{6+} + \text{Ne}$ collisions using our 3-D time-dependent Hartree-Fock (TDHF) codes. Calculations have been made for $p + \text{H}$ at two ion velocities, $v = 1$ and 2 atomic units, and for $\text{C}^{6+} + \text{Ne}$ at one velocity, $v = 6$. For each velocity and a range of impact parameters, we have extracted excitation and capture probabilities and secondary electron spectra in the target and projectile frames. Typical energy distributions are shown in Fig. 2.11. The $p + \text{H}$ runs at $v = 2$ show evidence of "ridge" electrons, trailing behind the projectile at a relative velocity $v_e = v/2$. We expect that a definitive picture will emerge when the angular distributions are plotted. The amount of data arising from all possible excitations of the five active orbitals of $\text{C}^{6+} + \text{Ne}$ is rather large. Thus far, the results agree with intuition based on the geometry of the orbitals and the extent to which the electrons' velocities match the velocity of the projectile.

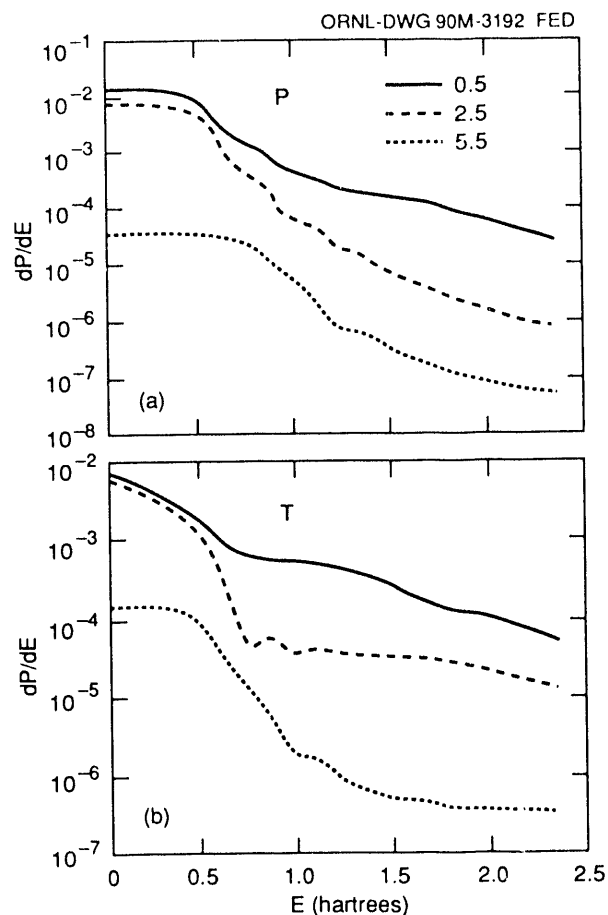


Fig. 2.11. Secondary electron energy distributions in projectile (P) and target (T) frames for a $p + \text{H}$ collision at $v = 1$. The curves refer to three impact parameters: solid line, $v = 0.5$; dashed line, $v = 2.5$; dotted line, $v = 5.5$.

2.3 CONTROLLED FUSION ATOMIC DATA CENTER

I. Alvarez, C. F. Barnett, C. Cisneros, H. B. Gilbody, D. C. Gregory, C. C. Havener, H. T. Hunter, R. K. Janev, M. I. Kirkpatrick, E. W. McDaniel, F. W. Meyer, T. J. Morgan, R. A. Phaneuf, M. S. Pindzola, and E. W. Thomas

The Controlled Fusion Atomic Data Center (CFADC) collects, reviews, evaluates, and recommends numerical atomic collision data that are relevant to controlled thermonuclear fusion research. The CFADC operates

with an equivalent of 1.5 full-time staff members and a number of expert consultants under contract. Members of the Experimental Atomic Physics for Fusion Group also contribute a small fraction of their time to literature searches and categorization of relevant publications.

The major activities of the CFADC are:

- the maintenance of an on-line computer database of fusion-related publications on atomic collision processes and the periodic distribution of updates to other data centers;
- the preparation and publication of compilations of recommended atomic collision data;
- the deduction of scaling laws and parameterization of atomic collision data for ease of application in fusion research;
- the establishment of a computer database of recommended atomic collision data and a data exchange format to facilitate their application in fusion research;
- the review of the existing atomic collision database with respect to current applications in fusion research, identification of data needs, and coordination of research to fill those needs; and
- the handling of individual requests for specific data or literature searches on specific processes.

The CFADC participates in the Atomic and Molecular Data Center Network established by the International Atomic Energy Agency (IAEA) in Vienna and has cooperative agreements with a number of other data centers. These include

- the Atomic and Molecular Processes Information Center at JILA;
- the Data Center for Atomic Spectral Lines and Transition Probabilities at the National Institute for Standards and Technology, Gaithersburg, Md.;
- the IAEA Atomic and Molecular Data Unit in Vienna;

- the Research Information Center at the Institute of Plasma Physics (IPP), Nagoya University, Japan; and
- the Atomic and Nuclear Data Center of the Japan Atomic Energy Research Institute (JAERI), Tokai, Japan.

Updates of our bibliography are sent periodically on computer diskettes to the IAEA and to both Japanese data centers. This forms the basis for the semiannual IAEA *International Bulletin on Atomic and Molecular Data for Fusion*.

During this reporting period, work has continued on preparation of the "Redbook" series of recommended data, *Atomic Data for Fusion*. Volume 6 of this series, entitled *Spectroscopic Data for Titanium, Chromium, and Nickel*, by W. Wiese and A. Musgrove of the National Institute of Standards and Technology (NIST), was published and distributed as ORNL-6551, Vols. 1-3. Data compilation and evaluation have been completed for another volume, entitled *Collisions of H, H₂, He and Li Atoms and Ions with Atoms and Molecules*. Publication and distribution of this volume (ORNL-6086) are planned for 1990. All tabular and graphical data for this series are computer-generated in publication-ready format. Maxwellian rate coefficients are calculated from the cross-section data, and Chebyshev polynomial fits are given for all the recommended data.

The CFADC also participated in two IAEA-sponsored workshops held in Vienna during the period: a specialists' meeting on review of the status of atomic and molecular data for fusion edge plasma studies and the consultants' meeting of the Atomic and Molecular Data Center Network.

A major role of the CFADC is to assist with the implementation of a new atomic data interface program, called ALADDIN, a FORTRAN code designed to facilitate effective exchange of data and the establishment

of a computer database for "users." It can accept a wide range of data formats, including tabular, parameterized, and fitted data, and operates on a wide range of computer systems, including personal computers (PCs). Plans call for a diskette containing the data and the ALADDIN program to be distributed with the next volume of the "Redbook" series.

In collaboration with JAERI, work also has continued on the scaling, parameterization, and fitting of heavy-particle ionization data using functional forms based on analytical physical models for the process. Often the available data are limited to a narrow energy range, and such "physical" fitting formulas permit extrapolation of the data outside this range with some measure of confidence. Such extrapolation of data is impossible with polynomial fits.

The death of C. F. Barnett, the founder of the CFADC, in June 1989 is a most significant loss to the data center. "Barney" served as director of the CFADC until his retirement from ORNL in 1985 and subsequently as a consultant until the time of his death. His keen insights and tireless efforts will be sorely missed.

2.4 ADVANCED PLASMA DIAGNOSTICS DEVELOPMENT

2.4.1 Small-Angle CO₂ Laser Thomson Scattering Diagnostic for D-T Fusion Product Alpha Particles

R. K. Richards, C. A. Bennett, D. P. Hutchinson, L. K. Fletcher, Y. M. Fockede, H. T. Hunter, and K. L. Vander Sluis

The deuterium-tritium (D-T) fusion reaction produces alpha particles at 3.5 MeV. For a fusion reactor to maintain ignition, these

alpha particles must deposit this energy in the plasma fuel. Because of this critical importance, the demonstration of alpha particle heating is the main physics goal of the next generation of fusion reactors.²² To study the behavior of alpha particles in a plasma as they lose energy and produce a distribution characteristic of this energy loss, we have proposed a Thomson scattering diagnostic.²³ With a scattering source at the CO₂ laser wavelength (10.6 μm), the background from electron scattering requires that small-angle (~1°) detection be used to monitor the alpha particle distribution.

As a measure of this diagnostic capability in detecting scattered signals at these small scattering angles, a proof-of-principle test is currently in progress on a nonburning plasma in the Advanced Toroidal Facility (ATF). The goal is to measure a scattered signal (in this case a low-level signal from plasma electrons) at an angle of 0.86°. The major hardware components have been installed at the ATF facility, and preliminary tests have been conducted using the extremely sensitive heterodyne receivers. Tests of the full scattering system to demonstrate proof of principle are scheduled for the second half of FY 1990.

2.4.2 Multichannel Far-Infrared Interferometer and Scattering System for the Advanced Toroidal Facility

C. H. Ma, D. P. Hutchinson, C. A. Bennett, Y. M. Fockede, and K. L. Vander Sluis

During the past year, a multichannel far-infrared (FIR) interferometer system has been fully installed on ATF to measure the line-integrated electron density along 15 vertical chords on the $\phi = 0^\circ$ plane of the ATF plasma. The system is a modification

of the FIR interferometer system that was used on the Impurity Study Experiment (ISX-B) tokamak.²⁴ However, instead of using separate probing beams, a phase image technique²⁵ is used to improve the spatial resolution of the measurement. A schematic diagram of the interferometer system is shown in Fig. 2.12. Briefly, the system employs a pair of cw 214- μm difluoromethane (CH_2F_2) lasers, optically pumped by separate CO_2 lasers. The FIR cavities are tuned so that they oscillate at frequencies differing by Δf of the order of 2 MHz. As shown in the figure, cylindrical parabolic mirrors are used to create a slablike 2- by 45-cm probing beam. The beam is transmitted through almost the whole cross section of the plasma. After passing through the plasma, the probing beam is dissected at the focal plane of the optics system by an array of 15 off-axis paraboloid reflectors, each of which illuminates a single Schottky-diode detector. Part of the beam

from the reference laser is mixed first in a reference detector with a portion of the probing laser beam, which is split off before passing through the beam expansion optics. The remainder of the reference beam is also expanded and is guided to the signal detectors to mix with the probing beam. The detector signals are filtered, amplified, and fed into a digital phase detection circuit to extract the phase shift between the output of the signal detector and the reference signal, which is proportional to the line-integrated electron density. The outputs of the phase detectors are displayed on oscilloscopes for photographic recording and are digitized for computer storage and processing.

A plasma density measurement has been made successfully along one chord of the system. The multichannel system is being tested.

A study has also been carried out to determine the optimum design of an FIR scattering system for measuring spatial and

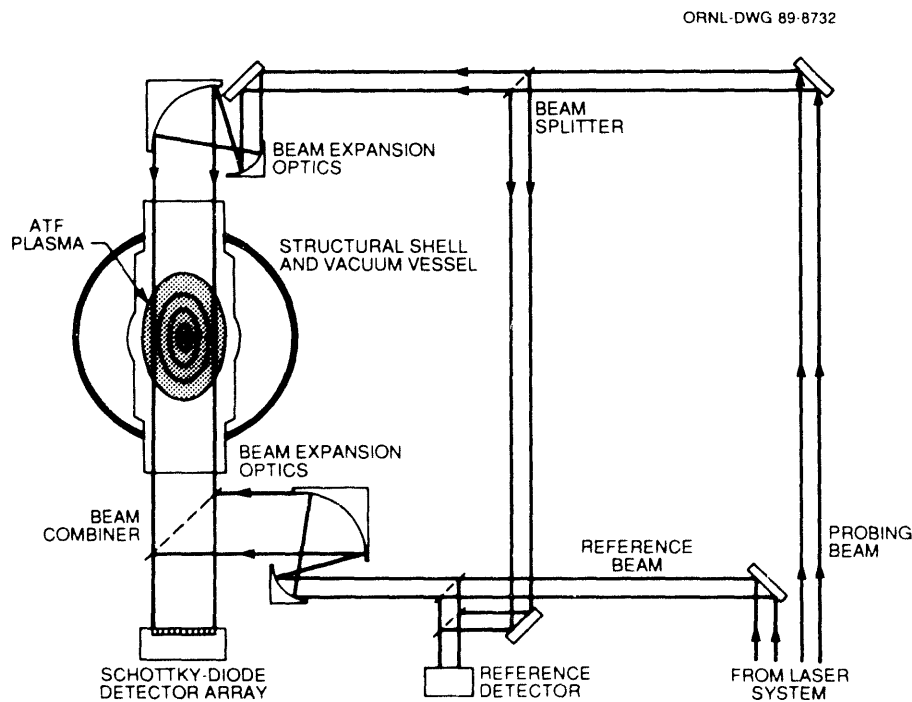


Fig. 2.12 Schematic of the 15-channel FIR interferometer system on ATF.

temporal electron density fluctuations in the ATF plasma. The proposed system may be operated at wavelengths from $447\ \mu\text{m}$ to $119\ \mu\text{m}$. Lasers operated at these wavelengths have been designed, constructed, and tested. Output power levels from 100 to 500 mW have been achieved. A pair of crystal quartz windows, 38 mm by 300 mm, located next to the multichannel FIR interferometer windows, will allow scattering angles of $\pm 15^\circ$ from the incident beam. A single FIR laser beam will be split to provide both the scattering beam and the local oscillator beam in a three- to five-channel detector array. The detector is designed to observe scattering from a single point at three to five different angles or from several points at the same angle. Storage of the scattered signals will be accomplished by a PC-based CAMAC data acquisition system.

2.4.3 Feasibility Studies of a Two-Color Interferometer/Polarimeter for the Compact Ignition Tokamak

C. H. Ma, D. P. Hutchinson, C. A. Bennett, and K. L. Vander Sluis

Feasibility studies of a two-color infrared interferometer/polarimeter system for measurements of electron density and plasma current profiles in the Compact Ignition Tokamak (CIT) were continued. During the past year, the proposed $28\text{-}\mu\text{m}$ system was investigated both theoretically and experimentally. A prototype water vapor laser was successfully designed, constructed, and tested. The maximum output power of 30 mW was achieved at a wavelength of $27.972\ \mu\text{m}$. A photograph of the laser is shown in Fig. 2.13. The laser is of the waveguide type and is operated in the

ORNL PHOTO 603-89

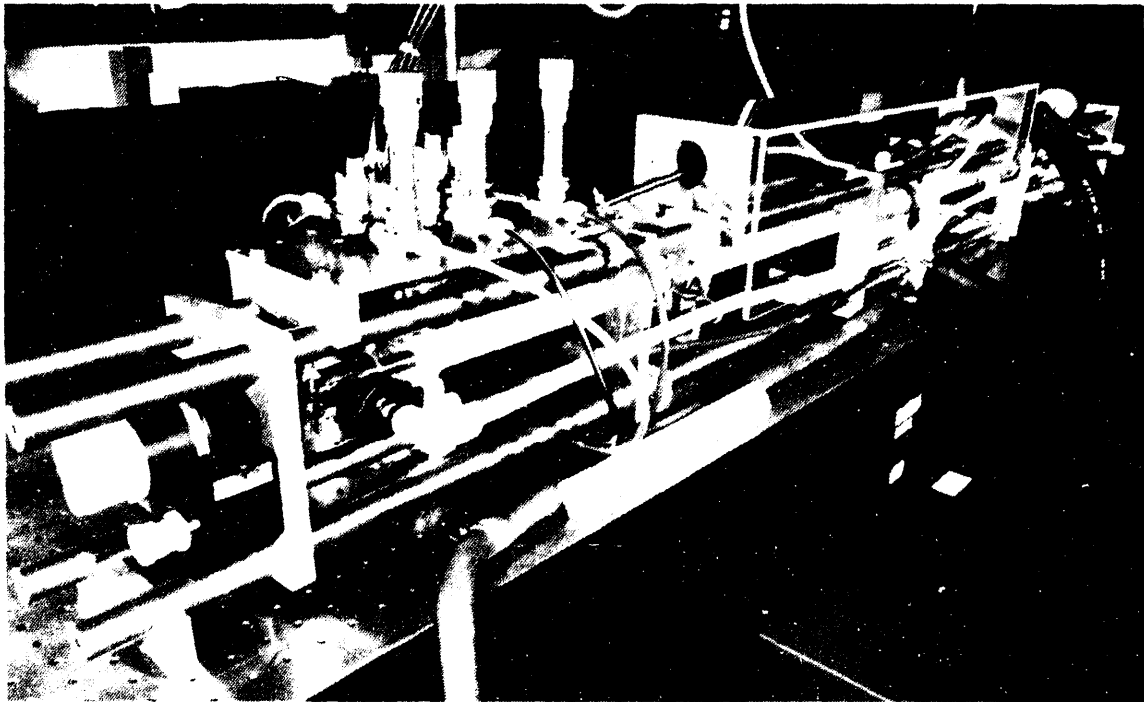


Fig. 2.13. Photograph of the continuous wave $28\text{-}\mu\text{m}$ water vapor laser.

TEM₀₀ mode. The total length of the laser tube is 2 m, and the inside diameter of the tube is 0.9 cm. A cooling jacket is provided outside the tube for ethylene glycol cooling at 5°C. Two cathodes are located at the center of the tube, and the anodes are at either end. The distance between the anodes and the cathodes is approximately 74 cm. The laser operates with the ends at ground potential and only the center section at high voltage. This configuration makes high-voltage shielding easier and removes the electrical hazard from the regions where the operator works. The semi-confocal resonator is formed by a flat mirror and a concave mirror with radius of curvature of 3 m. The concave mirror is mounted in a piezoelectric translator. The concave mirror has a 0.75-mm-diam coupling hole at the center. The position of the flat mirror can be adjusted manually by a micrometer. The mirror mounts and the tube supports are connected by Invar rods for temperature stability. A KRS-5 window is used to transmit both the 28- μm beam and the HeNe laser beam for alignment. Water vapor in the water reservoir and gas additive are continuously pumped out through the Pyrex glass tube. The flow rate and the pressure are controlled by needle valves. A typical cavity detuning curve obtained by changing the piezoelectric voltage is shown in Fig. 2.14. The operating conditions are water vapor pressure of 1.5 torr, helium pressure of 0.5 torr, H₂ pressure of 0.5 torr, and discharge current of 250 mA. Figure 2.15 illustrates the dependence of the output power as the discharge current is varied.

The feasibility of a 28- μm polarimeter using both the electro-optic and photoelastic polarization-modulation techniques was investigated. A cadmium telluride (CdTe) crystal is used in the electro-optic polarization modulator. The electro-optic modulation technique has an important advantage

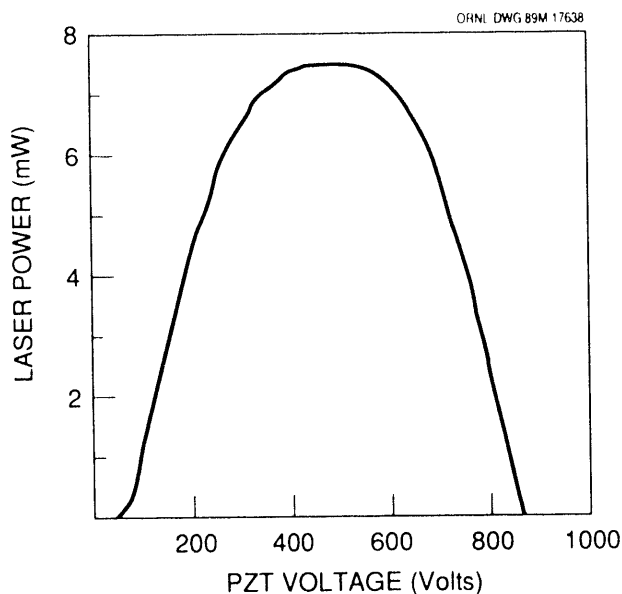


Fig. 2.14. Output power of the water vapor laser vs the piezoelectric voltage under the operating conditions: water vapor pressure of 1.5 torr, He pressure of 0.5 torr, H₂ pressure of 0.5 torr, and discharge current of 250 mA.

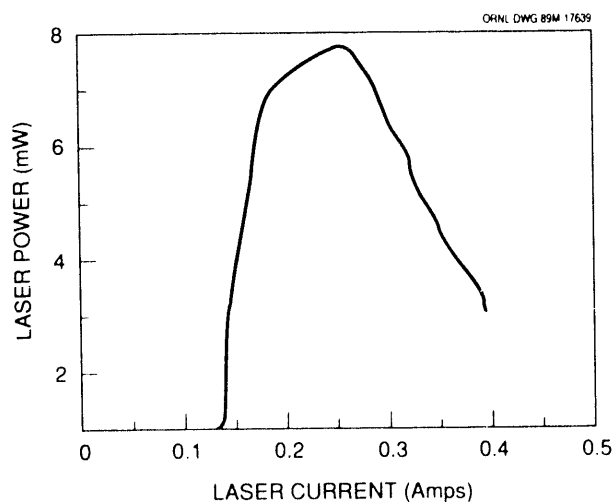


Fig. 2.15. Output power of the water vapor laser vs the discharge current under the operating conditions: water vapor pressure of 1.5 torr, He pressure of 0.5 torr, and H₂ pressure of 0.5 torr.

over the photoelastic technique in fast time response. A modulation frequency of 1 MHz can be easily achieved. The drawback of

electro-optic modulation is the high loss in beam transmission. Even with perfect antireflective coating, the transmission of the 28- μm laser beam through a 3-cm-long CdTe crystal is only 19%. On the other hand, the photoelastic modulation technique offers the advantage of high beam transmission, but the time response is limited by the natural standing wave frequency of the crystal. A rectangular silicon bar is used in the photoelastic modulator. The silicon bar vibrates at its lowest frequency of standing compression waves; thus, a time-varying birefringence is obtained. To sustain these vibrations in the bar, the bar is bonded to a quartz transducer tuned to the same frequency. The amplitude of the vibrations and therefore the magnitude of the birefringence are controlled by the signal generator driving the transducer. The transmission of the water vapor laser beam through a 1-cm-long silicon bar has been measured. A transmission of 45% is observed without any antireflective coating. With perfect coating, transmission of 92% is expected. For a $5 \times 5 \times 1$ -cm silicon bar, the modulation frequency is approximately 42 kHz.

2.4.4 Optics Damage and Irradiation Studies (ODIS)

H. T. Hunter, R. K. Richards, and
D. P. Hutchinson

Optics Damage and Irradiation Studies (ODIS) have as their main goal the screening of high-quality infrared mirrors, windows, and coatings in support of the Advanced Optical Materials and Components Technology Development Program at Martin Marietta Energy Systems, Inc.

Initiated in 1985, the screening was performed by irradiating window samples

with microsecond bursts of fast neutrons from the Health Physics Research Reactor (HPRR) facility at ORNL. Transmission effects at three different laser wavelengths were recorded during and after the irradiations.

Currently, the work effort has shifted to pulsed CO₂ laser damage of both infrared mirrors and windows. For the last two years, we have been measuring the laser-induced damage thresholds (LIDTs) of these optics and their coatings to screen samples for improving manufacturing techniques and developing new coatings with high infrared transmission or reflectance. This work is sponsored by the U.S. Army Strategic Defense Command (USASDC).

To date many types of mirrors, windows, and other optical materials have been successfully tested for their damage threshold. The equipment allows the selection of CO₂ laser pulse widths from 30 ns to 100 ns and spot sizes from approximately 1 mm² to 10 mm². Further sample analysis is provided by other groups at ORNL both before and after ODIS damage testing.

All the test samples are carefully cleaned before damage testing, and all damage tests are conducted in high vacuum. Our capabilities allow for testing all sizes and shapes of test samples from 5 mm² to 8-in.-diam optics. A HeNe laser illuminates the target site on the test optic, and the scattered radiation is collected. Damage of an optic surface, after a pulsed CO₂ laser shot, will be indicated by a change in scattered signal from the HeNe laser. A schematic of the ODIS facility is shown in Fig. 2.16.

Currently, we are capable of damage testing up to ten optics per day with the ability to scan over the surface of a test optic for multiple LIDT measurements. Work is performed under a contract with USASDC.

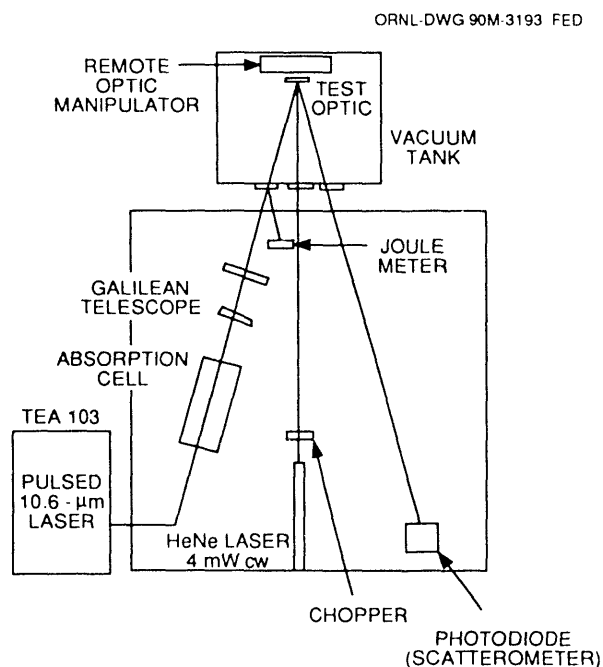


Fig. 2.16. Schematic of Optics Damage and Irradiation Studies facility.

REFERENCES

1. C. C. Havener et al., "Electron Capture by Multicharged Ions at eV Energies," *J. Phys. (Paris)* **50**, Coll. C1, 7-17 (1989).
2. M. S. Huq, C. C. Havener, and R. A. Phaneuf, "Low-Energy Electron Capture by N^{3+} , N^{4+} , and N^{5+} from Hydrogen Atoms using Merged Beams," *Phys. Rev. A* **40**, 1811-16 (1989).
3. R. A. Phaneuf et al., "Electron Capture in Low-Energy Collisions of C^{4+} and O^{4+} with H and H_2 ," *Phys. Rev. A* **26**, 1892-1906 (1982).
4. M. Gargaud, R. McCarroll, and L. Opradole, *Astron. Astrophys.* (in press).
5. S. Bienstock, T. G. Heil, and A. Dalgarno, "Charge Transfer of O^{3+} Ions in Collisions with Atomic Hydrogen," *Phys. Rev. A* **28**, 2741-3 (1983); T. G. Heil, S. E. Butler, and A. Dalgarno, "Charge Transfer of Doubly Charged and Trebly Charged Ions with Atomic Hydrogen at Thermal Energies," *Phys. Rev. A* **27**, 2365-83 (1983).
6. M. Gargaud and R. McCarroll, *J. Phys. B: At. Mol. Opt. Phys.* **21**, 513-20 (1988).
7. A. B. Ehrhardt and W. D. Langer, *Collisional Processes of Hydrocarbons in Hydrogen Plasmas*, PPPL-2477, Princeton Plasma Physics Laboratory, Princeton, N.J., September 1987.
8. D. C. Gregory et al., "Electron-Impact Ionization of Iron Ions: Fe^{11+} , Fe^{13+} , and Fe^{15+} ," *Phys. Rev. A* **35**, 3256-64 (1987).
9. J. K. Swenson et al., "Observation of Coulomb Focusing of Autoionization Electron Produced in Low-Energy $He^+ + He$ Collisions," *Phys. Rev. Lett.* **63**, 35-38 (1989).
10. F. W. Meyer et al., "Observation of Coulomb Focusing of Autoionizing Electrons Produced in Low Energy $He^+ + He$ Collisions," *Bull. Am. Phys. Soc.* **34**, 1367 (1989).
11. R. Morgenstern, A. Niehaus, and U. Thielman, *J. Phys.* **B10**, 1039 (1977).
12. K. Sommer et al., pp. 443-4 in *Abstracts of Contributed Papers, XVI Conference on the Physics of Electronic and Atomic Collisions, New York, July 26-August 1, 1989*, North-Holland, Amsterdam, 1989.
13. A. Bordenave-Montesquieu, A. Gleizes, and P. Benoit-Cattin, *Phys. Rev. A* **25**, 245-67 (1982).
14. K. J. Snowdon et al., "Technique for Determination of the Metastable Fraction of Multicharged Ion Beams," *Rev. Sci. Instrum.* **59**, 902-5 (1988).
15. F. W. Meyer et al., "Inner-Shell Processes as Probes of Multicharged Ions Neutralization at Surfaces," *J. Phys. (Paris)* **50**, Coll. C1, 263-75 (1989).
16. K. J. Snowdon, *Nucl. Instrum. Methods* **B34**, 242 (1987).
17. E. Wählin et al., "Absolute Cross Sections for Electron Impact Excitation of C^+ using Electron Energy Loss," p. 368 in *Abstracts of Contributed Papers, XVI Conference on the Physics of Electronic and Atomic Collisions, New York, July 26-August 1, 1989*, North-Holland, Amsterdam, 1989.
18. To be published in *Journal of the Optical Society of America B*.
19. M. S. Pindzola, D. C. Griffin, and C. Botcher, "Coupling Effects for Electron-Impact Excitation in the Potassium Isoelectronic Sequence," *Phys. Rev. A* **39**, 2385-91 (1989).
20. M. S. Pindzola, D. C. Griffin, and C. Botcher, "Indirect Processes in the Electron Ionization of Atomic Ions," pp. 129-45 in *Electronic and Atomic Collisions*, Elsevier Science Publishers, 1988.
21. Abstract of paper submitted for publication in *Physical Review A*.
22. D. Post et al., *Physics Aspects of the Compact Ignition Tokamak*, PPPL-2389, Princeton Plasma Physics Laboratory, Princeton, N.J., 1986.
23. R. K. Richards et al., " CO_2 Laser Thomson Scattering Diagnostic for Fusion Product Alpha Particle Measurement," *Rev. Sci. Instrum.* **59**, 1556-8 (1988).

24. C. H. Ma et al., "Measurements of Electron Density and Plasma Current Distributions in Tokamak Plasmas," *Int. J. Infrared Millimeter Waves* **3**, 263-77 (1982).

25. C. A. J. Hugenholtz and B. J. H. Meddens, *Rev. Sci. Instrum.* **53**, 171 (1982).

3

FUSION THEORY AND COMPUTING

R. A. Dory

C. L. Alejaldre¹
A. F. Amer²
S. E. Attenberger³
D. B. Batchelor
R. D. Burris³
H. J. Burum
J. D. Callen⁴
B. A. Carreras
M. D. Carter
J. R. Cary⁵
L. A. Charlton³
P. J. Christenson⁶
E. C. Crume, Jr.⁷
P. H. Diamond⁸
N. Dominguez
P. C. Dziurzynski
D. T. Fehling
R. H. Fowler³
L. Garcia⁹

C. E. Gibson
C. A. Giles³
D. C. Giles³
R. C. Goldfinger³
D. E. Greenwood³
J. H. Han⁸
J. D. Hanson¹⁰
C. L. Hedrick
S. P. Hirshman
L. M. Hively
J. T. Hogan
J. A. Holmes³
W. A. Houlberg
H. C. Howe
J. V. Hughes
M. M. Hutchinson
E. F. Jaeger
K. L. Kannan³
J-N. Leboeuf
D. K. Lee³

G. S. Lee
V. E. Lynch³
J. F. Lyon⁷
D. L. Million³
D. R. Overbey
L. W. Owen³
T. C. Patrick
J. A. Rome
K. C. Shaing
D. J. Sigmar¹¹
D. A. Spong
K. A. Stewart³
D. J. Tate
J. S. Tolliver³
N. A. Uckan⁷
W. I. van Rij³
A. G. Varias¹
M. B. Wright³
K. G. Young

-
1. Centro de Investigaciones Energeticas, Medioambientales, y Tecnologicas, Madrid, Spain.
 2. Graduate student, The University of Tennessee, Knoxville.
 3. Computing and Telecommunications Division, Martin Marietta Energy Systems, Inc.
 4. Consultant, University of Wisconsin, Madison.
 5. Consultant, University of Colorado, Boulder.
 6. Graduate student, The University of Michigan.
 7. Toroidal Confinement Section.
 8. Institute for Fusion Studies, University of Texas, Austin.
 9. Universidad Complutense, Facultad de Ciencias Fisicas, Madrid, Spain.
 10. Consultant, Auburn University, Auburn, Alabama.
 11. Massachusetts Institute of Technology, Cambridge.

3. FUSION THEORY AND COMPUTING

SUMMARY OF ACTIVITIES

The most visible progress in fusion theory during 1989 continued to be in the area of turbulence and confinement degradation in toroidal systems—most notably in tokamaks, but also, *mutatis mutandis*, in stellarator devices. As a part of the Tokamak Transport Initiative of the U.S. Department of Energy, detailed modeling was undertaken of turbulent transport phenomena in the outer regions of the Texas Experimental Tokamak (TEXT) at the University of Texas and the Advanced Toroidal Facility (ATF) stellarator at ORNL. The two devices are similar in size, have plasmas of roughly similar characteristics, and are arrayed with sensors for diagnosing fluctuating densities, temperatures, and electric fields. As a result of cooperative work with the Texas group, substantial progress has been made in distinguishing which of several competing models best reproduce experimental data; these are impurity-driven rippling mode turbulence in TEXT and resistive pressure-gradient-driven phenomena in ATF.

Obtaining a picture of the way the radial electric field E_r influences the transition between the L-mode and the H-mode (identified by lower and higher energy confinement times) in tokamaks has remained a major issue in the world fusion program. Data from several experiments give increasing indication that the bifurcation theories proposed by Shaing have pinpointed the key mechanisms. Further work is required, however, to obtain a clear picture of how E_r affects turbulence and, conversely, how turbulence contributes to the development of E_r .

The design and development of new heating and current drive experiments for tokamaks and stellarators place increasing reliance on theoretical modeling of the antenna and Faraday shield regions and the wave propagation and energy deposition processes within the plasma. Results obtained with the ORION and RAYS codes have been used in the International Thermonuclear Experimental Reactor (ITER) and Compact Ignition Tokamak programs, as well as in proposals from the DIII-D group at General Atomics and the Tokamak Fusion Test Reactor group at Princeton Plasma Physics Laboratory.

Understanding the behavior of the ATF stellarator in more general terms is a key part of our activity, with substantial progress made in comparing the results of theoretical calculations with data. During 1989, the primary areas were the study of entry into the second regime of stability and the dependence of the bootstrap current I_b on geometrical factors, which is important in determining the extent to which collisional phenomena dominate I_b ; turbulence effects are much less important than they are for energy transport.

Improving the “tools of the trade” was a key activity, with important progress made in sharpening the existing models and formulating new ones. Examples include expressions for the neoclassical viscosity in the presence of strong rotation and plateau regime collisionality, a hybrid fluid-kinetic model for turbulence, methods for speeding up and improving the convergence of the widely used VMEC equilibrium code, and testing and application of orbit-following models using the symplectic integration technique developed by J. R. Cary of the University of Colorado.

Contributions were also made to the ITER program in the analysis of general confinement physics and the effects on beta limits of nonoptimal profiles influenced by transport and by non-Ohmic current drive schemes.

Specific experiments were undertaken on the Joint European Torus in the U.S.–European Community collaboration to refine the theoretical understanding of the penetration of energetic pellets used to fuel a plasma and modify its distributions. As a result, it has been determined that the velocity dependence of the penetration depth is greater than previously predicted. This improves the likelihood of finding a method to deposit fuel near the center of a device at the ITER and demonstration reactor scales.

Continued improvements were made to the ATF data acquisition system and the associated software for analysis, formation of the overall database, and retrospective analysis of the data. This made possible the rapid assessment of results and modification of the experimental program to capitalize on the resulting understanding. The capabilities of the new workstation computers are being applied to improving the visualization of scientific data and to providing effective analysis at the mesoscale, where massive computers are not required.

3.1 EQUILIBRIUM AND STABILITY

3.1.1 Overview

Magnetohydrodynamic (MHD) equilibrium and stability studies are directed toward the understanding and improvement of the global confinement properties of tokamaks and stellarators. Equilibrium and stability theory is applied to complement configuration optimization studies and used for interpretation of experimental results.

In the area of equilibrium theory, calculation techniques have been improved to provide more efficient computations and a better physics understanding. With the incorporation of the three-dimensional (3-D) Mercier criterion, the resistive interchange stability criterion, and the 3-D ballooning stability solver, the ORNL 3-D spectral code VMEC has become one of the most efficient tools for equilibrium studies of 3-D configurations.¹ These asymptotic criteria are good enough to determine the stability boundaries of stellarators. They lead to the same results as the low- n stability calculations.^{2,3} These criteria have been used in the ATF-II optimization^{4,5} and in the low-aspect-ratio stellarator reactor studies.⁶ The stability properties of other stellarator configurations have been studied in collaboration with other stellarator laboratories:

- With researchers at the Kharkov Physical-Technical Institute, Kharkov, U.S.S.R., we have investigated effect of finite beta on stellarator confinement in the $1/\nu$ regime. The quadrupole magnetic field was used to improve the confinement in this regime for the vacuum magnetic field. However, the finite-beta shift of the magnetic axis reduces the transport optimization done for the vacuum magnetic fields.
 - With the theory group of the Plasma Physics Laboratory at Kyoto University, Kyoto, Japan, we have completed and documented optimization studies of toratron configurations for the design of the Large Helical Device (LHD) to be built in Toki, Japan.^{7,8} We have applied the approach that we followed for ATF-II studies.
 - With the Centro de Investigaciones Energeticas, Medioambientales, y Tecnologicas (CIEMAT), Madrid, Spain, we have continued the stability analysis of the TJ-II experiment, which is under construction in Madrid, and shown that the flexibility built into the device allows access to a broad range of beta values ($\langle\beta\rangle \simeq 0$ to 6%)^{9,10} and that, for some of the configurations, access to the second stability regime is possible.
 - With researchers at the Australian National University in Canberra, we have evaluated the stability properties of the high-transform configuration for the H-1 flexible heliac. The improvements in the VMEC code allow us to study these very strongly shaped configurations.
- We have continued to survey the stability properties of shaped tokamaks with aspect ratios between 3.9 and 2.6 to provide a database for scaling studies for the International Thermonuclear Experimental Reactor (ITER) design. We have included the evaluation of the resistive and alpha particle stability properties for ITER equilibria in the ideal MHD database. We also continued to evaluate the effect of compressibility on global MHD modes,^{11,12} in particular applying it to $m = 1$ instabilities for different q profiles.^{13,14} The linear and nonlinear properties of infernal modes¹⁵ for discharges with pellet injection in the Joint European Torus (JET) have also been investigated.¹⁶ We have shown that the internal disruptions

observed in some of these discharges can be caused by this instability.

An important area of research is the application of equilibrium and stability theory to the analysis of experimental data. A focus of this activity has been the Advanced Toroidal Facility (ATF), which started operation in 1988. In the initial phase of ATF operation in 1988, the plasma minor radius and the edge rotational transform were reduced by field errors. New methods for evaluating the magnetic island width were developed in interpreting the experimental results.¹⁷ The presence of magnetic islands caused an effective change of the magnetic configuration that improved the stability properties, allowing access to the second stability regime, as discussed in Sect. 3.1.2.1.

Discharges with electron cyclotron heating (ECH) in ATF at different settings of the vertical field (VF) coil currents and different plasma positions have been analyzed, and the bootstrap current I_b has been evaluated.^{16,17} The results show very good agreement with the theoretical predictions. The predicted dependence on the quadrupole and dipole moments of the VF coils has been demonstrated. This analysis of the experimental results shows that the bootstrap current in a stellarator can be externally controlled and reduced to zero for proper stellarator operation.

Some of the efforts in the MHD group were dedicated to code development. Two main areas were investigated.

First, a stellarator stability code, CHAFAR, was implemented using the stellarator expansion approach in flux coordinates.²⁰⁻²² The averaging is done directly from a 3-D equilibrium calculated with the VMEC code. This method eliminates the need for calculating an averaged equilibrium independently of the full 3-D calculation and reduces the number of codes involved in the stability evaluations for stellarators.

Second, a 3-D drift wave code²³ was implemented; it uses the results from VMEC as input. This code has been used to study trapped-electron instabilities in stellarators. The trapping in the helical wells can have important effects, such as lowering the collisionality threshold and increasing the radial width of the instability. On the other hand, the external magnetic controls in the stellarator permit external control of the shear length and the fraction of confined trapped particles. Therefore, stellarators in general and ATF in particular are excellent devices in which to study these instabilities.

3.1.2 Highlights of 1989

3.1.2.1 ATF operation in the second stability regime

ATF was designed to have stable access to the second stability regime. For the design conditions, this access should occur at beta values of $\beta_0 \simeq 5\%$. In the initial phase of operation, the plasma minor radius \bar{a} and the edge rotational transform $\epsilon(a)$ were reduced by field errors, which have since been repaired. This reduction of \bar{a} and $\epsilon(a)$ caused a large increase in the Shafranov shift and, as a consequence, a reduction in the beta value needed to access the second stability regime.²⁴⁻²⁶ From low- n and high- n stability analysis using experimentally measured profiles,²⁷ the threshold to second stability was found to be as low as $\beta_0 \simeq 1.0\%$. The beta values reached in the experiment, up to $\beta_0 \simeq 3.0\%$, are well above this threshold value (Fig. 3.1). The magnetic fluctuation measurements showed a reduction of the fluctuation level for $\beta_0 \simeq 1\%$. These fluctuation levels are in reasonable agreement with the theoretical calculations based on the resistive pressure-gradient-driven turbulence and support the

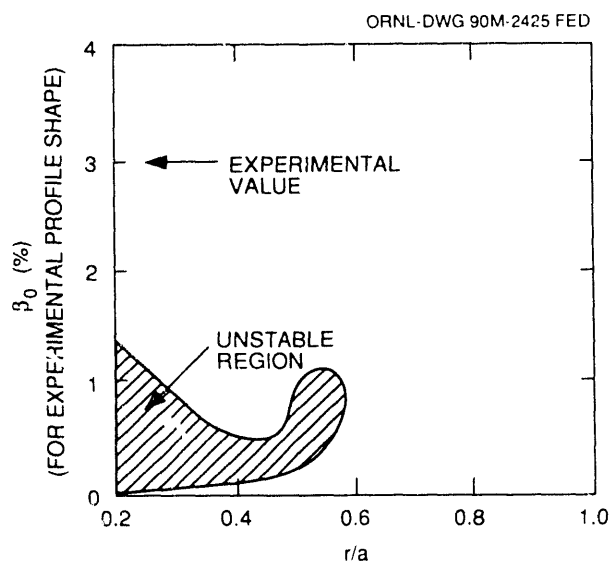


Fig. 3.1. Mercier stability results for a fixed profile equilibrium sequence corresponding to the highest beta value accessed in ATF ($\beta_0 \approx 3.0\%$).

evidence that ATF has already operated in the second stability regime.²⁸

3.1.2.2 Stability of helical-axis stellarators

The stability of flexible heliac configurations for confining toroidal fusion plasmas

has been surveyed. Use of a hardcore central conductor with separately controllable axisymmetric and helical windings provides flexibility to modify the rotational transform and the magnetic well. For the parameters of TJ-II, the Mercier criterion can be used to vary the beta limits almost continuously from 0 to 4%, and a path in parameter space has been found that provides access to the second stability region. This flexibility in controlling the threshold for instabilities by varying the external parameters will provide means for correlating theoretical stability predictions with the behavior of the experiment (Fig. 3.2). The work was done in conjunction with the CIEMAT group.^{9,10}

3.1.3 Advanced VMEC Equilibrium Analysis

During the past year, the ORNL 3-D equilibrium code VMEC has come to be widely used, both within the United States (primarily as a tokamak equilibrium code, with and without ripple) and internationally at various stellarator laboratories. At the Institut für Plasmaphysik (IPP), Garching, Federal Republic of Germany, VMEC forms

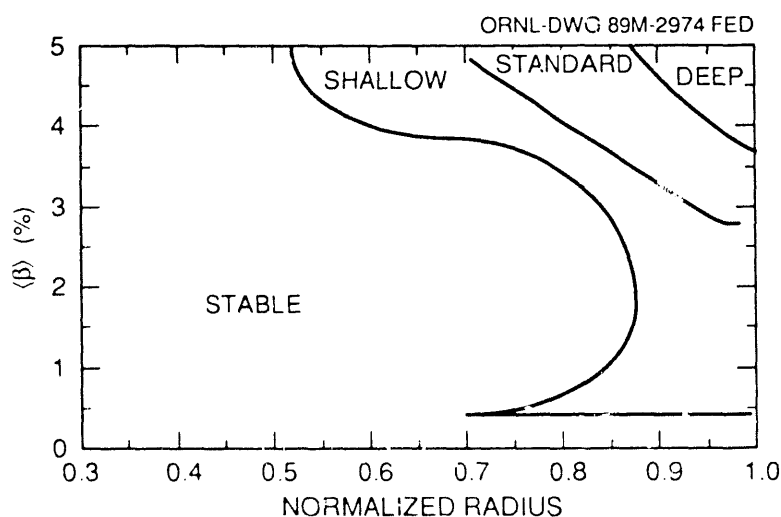


Fig. 3.2. Mercier stability diagram for the TJ-II heliac with different settings of the helical hardcore current, giving various depths for the vacuum magnetic well.

the core of the effort to optimize the so-called "Helias" configuration for both MHD and transport performance.²⁹ At Kharkov, a version of VMEC that runs on a personal computer is installed but not yet fully operational. In the United States, Princeton Plasma Physics Laboratory (PPPL) is a major customer for the two-dimensional (2-D) version of VMEC. Analyses of discharges in the Tokamak Fusion Test Reactor (TFTR) use VMEC in its fixed-boundary mode, and preliminary efforts are under way to adapt the TRANSP code to use the free-boundary mode. The ability of VMEC to treat finite-beta rippled tokamak fields has led to collaborations with the Texas Experimental Tokamak (TEXT) and ITER groups. Work at ORNL to analyze ATF equilibria in the presence of various shaping fields and to determine the effects of these fields on bootstrap current control constitutes a major impetus for further development of this code.

Continuing numerical improvement of VMEC was done in conjunction with several physics projects. The Green's function formulation for the vacuum region has been coupled with the free-boundary version of VMEC to predict the external magnetic signals that Rogowski loops will measure at arbitrary positions and for various pressure and iota profiles.³⁰ We have collaborated with our Russian colleagues to compare our numerical computations with analytic calculations based on the method of averaging. This work was completed in December 1989, during a visit by the Russians.

Improved convergence for the free-boundary version of VMEC has led to a number of useful applications. VMEC is now used in its fixed-boundary form as the main equilibrium solver in the PPPL discharge analysis code, TRANSP. Efforts are under way to compute the correct free-

boundary equilibrium, which is especially important for the discharges with very high poloidal beta that are of present interest. The correct interpretation of these data is important, for example, in analyzing the effect of bootstrap currents at high pressures.

We have also participated in a number of collaborations to assess the effects of 3-D ripple on self-consistent tokamak equilibria for both TEXT and ITER. The ITER work was begun over two years ago; the recent numerical improvements in VMEC have made possible the computation of equilibria for this device. In the course of this work, a simple numerical procedure was developed for checking the integrity of the magnetic field data arising from the external coils (these data are used as input to VMEC, and its numerical convergence is adversely affected if they are not accurate enough to preserve the assumed stellarator symmetry of the magnetic field).

VMEC is also being used for analyzing the effects of field shaping in ATF. The comparison of VMEC-generated vacuum configurations with field line tracings for various combinations of dipole and quadrupole fields has proved to be a valuable tool in improving the free-boundary convergence of VMEC equilibria.

We have collaborated with Japanese researchers to aid them in computing finite-beta effects on free-boundary equilibria for the Compact Helical System (CHS).

A collaboration was begun with M. Wakatani (Kyoto University) and J. L. Johnson (PPPL) to use the VMEC equilibrium as input to a stability code for analyzing long-wavelength modes using the method of averaging.

A fruitful collaboration with O. Betancourt of New York University has resulted in a significant improvement in the convergence time of VMEC.³¹ With a modification

of the preconditioning algorithm developed by Betancourt for his BETAS code, convergence acceleration factors of 10 or more can be achieved in VMEC. This has a significant impact on equilibrium and stability calculations for stellarators and could lead to a much more rapid determination of optimized stellarator configurations in the future.³²

3.2 TURBULENCE

3.2.1 Overview

Plasma turbulence research at ORNL is characterized by the parallel use of analytical and numerical fluid models to study the behavior of magnetically confined plasmas. Calculations are also made of nonlinearly evolved fluctuation levels and their consequences for particle and heat transport. Research is carried out on two strongly interconnected levels. First, fundamental physics research is performed, generally in a simplified geometry, to unveil the basic mechanisms that underlie plasma behavior. This work establishes a sound basis for further theoretical development. Theoretical results are then applied to specific devices, providing basic physics understanding and tools for configuration optimization and for plasma modeling.

During the last eight years, this continued effort has led to the development of a turbulence theory for resistive pressure-gradient-driven turbulence, resistivity-gradient-driven turbulence, and current-gradient-driven turbulence. This year, under the Tokamak Transport Initiative (TTI),³³ new efforts were directed toward modeling plasma edge fluctuations in TEXT and ATF. Another important part of the TTI is the exploration of the role of the electric field in reducing the turbulence level.³⁴ Progress

continued this year with increased accuracy in the numerical calculations³⁵ and with the derivation of the electron thermal conduction coefficient induced by the resistive pressure-gradient-driven turbulence.³⁶ The results of resistive pressure-gradient-driven turbulence have been applied to the interpretation of ATF fluctuation data, revealing similarities between the experimental and calculated spectra.^{24,28} This calculation indicates the importance of the beta self-stabilization effect, which has been confirmed experimentally.

In the first part of this year, as part of the TTI, code development was a major portion of our effort. We have developed codes for tokamak edge turbulence calculations by integrating some of the models studied independently in the past. The basic models include resistivity gradient drive, line radiation drive, and the effect of impurities. Results of these calculations show good agreement with the resonance-broadening mechanism for the saturation of the turbulence. These codes have been intensively applied to the TEXT edge parameters, as discussed in Sect. 3.2.2.3.

A code based on the fluid approach has been developed to study dissipative trapped-electron (DTE) mode turbulence. The basic equations follow a model developed by Catto and Tsang to include the toroidal trapping in real space. The code has been benchmarked in the linear regime using analytical models, and application to tokamak geometry has started.

As turbulence calculations become more sophisticated, there is an increasing need to improve the analysis tools. We have adapted some of the analysis codes to produce Macintosh files and now transfer a great deal of the analysis work from the Crays to Macintoshes. An important step in this direction has been the implementation

of software from the National Center for Supercomputer Applications (NCSA) for visualization (Fig. 3.3). Because the amount of information to handle is large, we plan to transfer part of this analysis to workstations.

3.2.1 Highlights of 1989

3.2.2.1 The hybrid fluid-kinetic model

The fluid approach to the study of turbulence in plasmas has been effective

because detailed numerical calculations are possible with present computer capabilities. When kinetic effects have to be included, the gyrokinetic equation offers a potential approach, but future-generation computers will be required to provide the range of time and space scales necessary for turbulence calculations. We have successfully developed an approach that bridges the fluid and kinetic descriptions and can serve as the solution for the immediate future while more sophisticated computers are

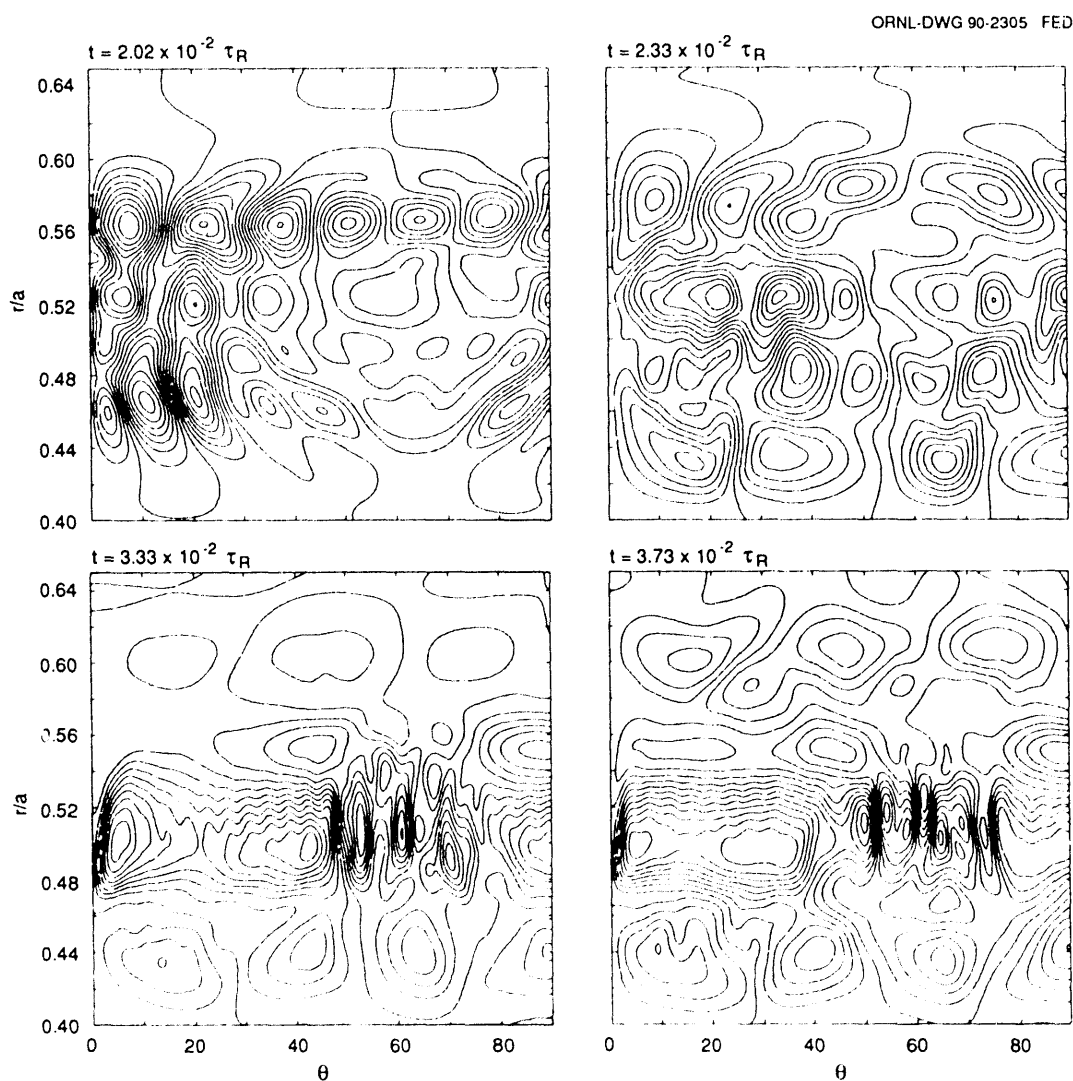


Fig. 3.3. Contours of the electrostatic potential fluctuations at different times during the nonlinear evolution of the resistive pressure-gradient-driven turbulence.

developed. The hybrid fluid-kinetic model treats the ions with fluid equations but follows the electrons as particles obeying the drift kinetic equation. In the hybrid model, the low-frequency wave resonances of the electrons are described exactly. In slab geometry, the hybrid model accurately reproduces sound waves as well as density and ion temperature gradient drift waves. Nonlinear studies of the latter show that the nonlinear kinetic electron response significantly alters the features of the turbulence in the saturated state. Kinetic electrons are currently being imported into our higher-dimensional fluid turbulence parameters and geometries characteristic of fluid models and a direct assessment of electron transport in the presence of fluid turbulence. Trapped-electron modes can play an important role in enhancing losses in a toroidal confinement device. They could be one of the causes for the deterioration of confinement with beta in tokamaks. For straight stellarators, it has been shown that the helical ripple and short connection lengths allow for strongly localized solutions to the drift wave equation. Therefore, in shearless stellarators trapped-electron modes may be more unstable than in tokamaks.

3.2.2.2 Trapped-electron modes

In contrast to tokamaks, stellarators have the advantage that the vacuum magnetic field can be changed substantially by modifying the currents in the VF coils. In ATF, for example, changing the dipolar or quadrupolar moment of the VF coils changes $|B|$ along the field lines, therefore changing the trapping regions and local curvature. This presents the opportunity of changing the ratio

of helically trapped and toroidally trapped particles. In ATF it is possible to study DTE modes and to evaluate and test their role in plasma confinement. In this way, some of the fundamental physics of these modes can be better understood and the theoretical results validated.

3.2.2.3 Edge turbulence modeling

The turbulence at the edge of the TEXT tokamak is characterized by a high level of density and potential fluctuations that do not obey the adiabaticity condition, since $e\phi/kT_e$ can be larger or smaller than \tilde{n}/n . We have incorporated impurity line radiation in our 3-D nonlinear resistive MHD computer model of impurity-driven rippling mode turbulence.^{35,36} Experimental TEXT edge parameters were used as input for the model equilibrium profiles. The radiation function was taken to be a shifted coronal one, with a rate enhancement of a factor of 4 over the nominal coronal rate for carbon impurities. Results of the computer calculations in the nonlinearly saturated state (the equilibrium profiles and radiation source were held fixed throughout the calculation) show excellent agreement with the analytical predictions for $e\phi/kT_e$, provided the average poloidal wave number m at each radial position is taken into account (Fig. 3.4). The nonlinear computer calculations are also in good agreement with the experimentally measured levels and radial variation for $e\phi/kT_e$, \tilde{T}/T_e , and B_r , with $e\phi/kT_e$ larger than \tilde{n}/n . Finally, the average m is measured to range from 12 to 50, which yields an average poloidal wave number of $0.8\text{--}1.8\text{ cm}^{-1}$, compared to the experimentally measured $2\text{--}3\text{ cm}^{-1}$.

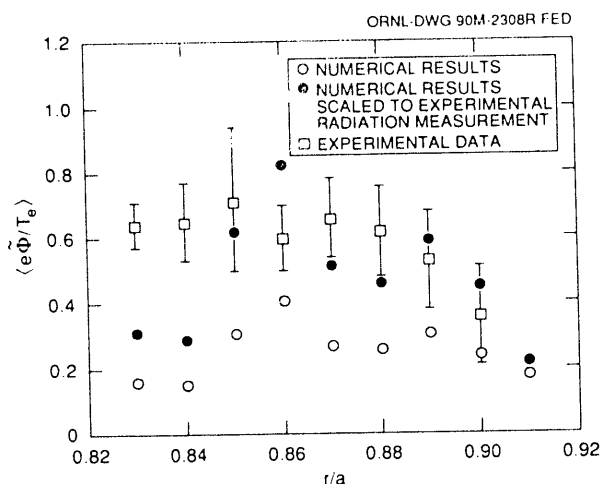


Fig. 3.4. Potential fluctuation levels from the TEXT experimental results, compared with the numerical results of modeling the edge plasma turbulence using a thermal convective cell driven by line radiation plus resistivity-gradient-driven turbulence.

3.3 KINETIC THEORY

3.3.1 Cause and Effect of Electric Fields in Toroidal Devices

We summarize a sequence of calculations that establish the cause and effect of dc electric fields in toroidal devices. These calculations were originally motivated by the observation that the edge radial electric fields in the Impurity Study Experiment (ISX-B), ATF, and TEXT had similar properties. Because of their greater simplicity, we have initially limited ourselves to symmetric tokamaks.

Guided by the experimental measurements, we carried out nonlocal orbit analyses numerically and analytically to see what effect such dc electric fields had on particle orbits. Reasonably compact analytic expressions were developed that allowed us to determine the region in phase space of unconfined orbits. This in turn allowed development of analytic expressions for the direct convective loss of ions in the presence

of dc electric fields like those observed experimentally.

It was found, not surprisingly, that dc electric fields have a strong effect on direct convective losses near the plasma edge. This effect lessens for direct convective losses nearer the plasma center. Direct convective losses can penetrate a considerable distance toward the plasma center, causing a large volume of the plasma to be dominated by direct convection. Interestingly, a key parameter for this penetration is $(a/r)^2$, which occurs in an exponential, rather than as $(r/a)^2$ as in local diffusive losses.

The magnitude of the direct convective losses was determined at about the same time that the magnitude of the fluctuating edge electric field measurements from TEXT became available. A natural question was what effect these locally strong fluctuations had on particle orbits and direct convective losses. By making the approximation that $k_{\parallel} = k_{\phi} = 0$, and using the frequency and wavelength properties of the observed fluctuations, we were able to extend the previous analysis for dc electric fields to include fluctuating electric fields. Several points followed from this orbit analysis.

First, the localized fluctuating electric field, while strongly affecting orbits and direct convective losses at the very edge, did not substantially affect direct convective losses from points nearer the plasma center. Thus, the relevance of the calculations for purely dc electric fields was established.

Second, fluctuating electric fields nonlinearly affect ion orbits more than they do electron orbits. As a consequence, nonlinear fluctuations should not lead to intrinsic or automatic equality of the ion and electron losses. That is, nonlinear fluctuations play a role in the formation of the dc radial electric field. At the same time, other ORNL theorists observed that advection ($\mathbf{v}_E \cdot \nabla \mathbf{v}_E$, where \mathbf{v}_E is the $\mathbf{E} \times \mathbf{B}$ drift velocity) was

nonlinear, leading to dc radial electric fields in their numerical modeling of tokamak edge fluctuations. Thus, further understanding of the role of edge fluctuations in the formation of dc electric fields should receive increased emphasis in the near future.

3.3.2 Ripple Losses of Alpha Particles in ITER

The prompt loss of alpha particles in ITER resulting from toroidal field (TF) ripple effects has been studied by numerous ITER participants. Generally, losses near the 3.5-MeV alpha birth energy have been found to be negligible. The next opportunity for alpha loss is when the alphas start pitch-angle scattering below the critical energy, where they begin to interact with the background ions.

We have studied alpha losses in this range by starting an alpha distribution at the critical energy (which is a function of radius) and using a Monte Carlo code to follow the alpha particles until they have thermalized.³⁹ To model the ripple, we used an axisymmetric ITER equilibrium and the ripple fields due to filamentary models for the 14 TF coils.

About 6% of the alphas were lost owing to a combination of neoclassical and ripple losses. This corresponds to only 0.6% of the initial alpha energy.

For future calculations, we expect to use the free-boundary version of the VMEC equilibrium code to obtain self-consistent finite-beta equilibria, which will be used to further study the ITER ripple effects.

3.3.3 Benchmark Studies of Neutral Beam Injection for Stellarators/Heliotrons

In conjunction with K. Hanatani of the Kyoto Plasma Physics Laboratory, we

have been engaged in a long series of benchmarks of neutral beam injection (NBI) into stellarators.⁴⁰ For the purposes of this investigation, we studied perpendicular injection into Heliotron E, which reveals more types of fast-ion orbit topology than does tangential injection into ATF.

Two Oak Ridge codes and one Kyoto code were benchmarked. If all codes solved exactly the same problem, they all obtained the same answers. However, we were surprised at the sensitivity of the answer to some of the physical models. If two codes used slightly different models, they could obtain significantly different answers.

The birth deposition profiles were carefully calculated, including the effects of beam shape and divergence and of aperture losses. They agreed quite well when the same parameters were used.

The location of the loss boundary caused the most sensitive differences. If the loss boundary was assumed to be the last closed flux surface, almost 50% of the fast ion energy was lost. However, if the actual Heliotron E vacuum vessel was used as the loss boundary, this loss dropped to <1% for the high-density case and about 7% for the low-density case. To obtain the correct answer, it is also necessary to include the effects of charge-exchange losses in this outer region. Although it is difficult to accurately model the neutral density profile (we used the PROCTR code), the charge-exchange losses were estimated to be about 10% for the high-density case and about 22% for the low-density case.

3.3.4 Beam Deposition and TF Ripple in TEXT

In TEXT, a vertically injected beam is used as a target for the charge-exchange diagnostic. Because the TEXT TF coils

are constructed as pancakes, there is a large amount of TF ripple. Simple calculations showed that the injected (perpendicular) fast ions were very close to being ripple trapped, even in the center of the plasma.

If an injected fast ion is ripple trapped, it will drift upward along the path of the beam and have a high probability of charge exchanging with the remaining beam neutrals. The true state of affairs must be

known in order to accurately interpret the charge-exchange diagnostic.

The previous model for the TEXT field was a set of values located on a relatively coarse grid. This did not provide enough information for accurately following guiding-center orbits. To provide better data for the coil fields, we modeled the TEXT TF coils using a series of filamentary coils arranged in a pancake (Fig. 3.5). The interlayer

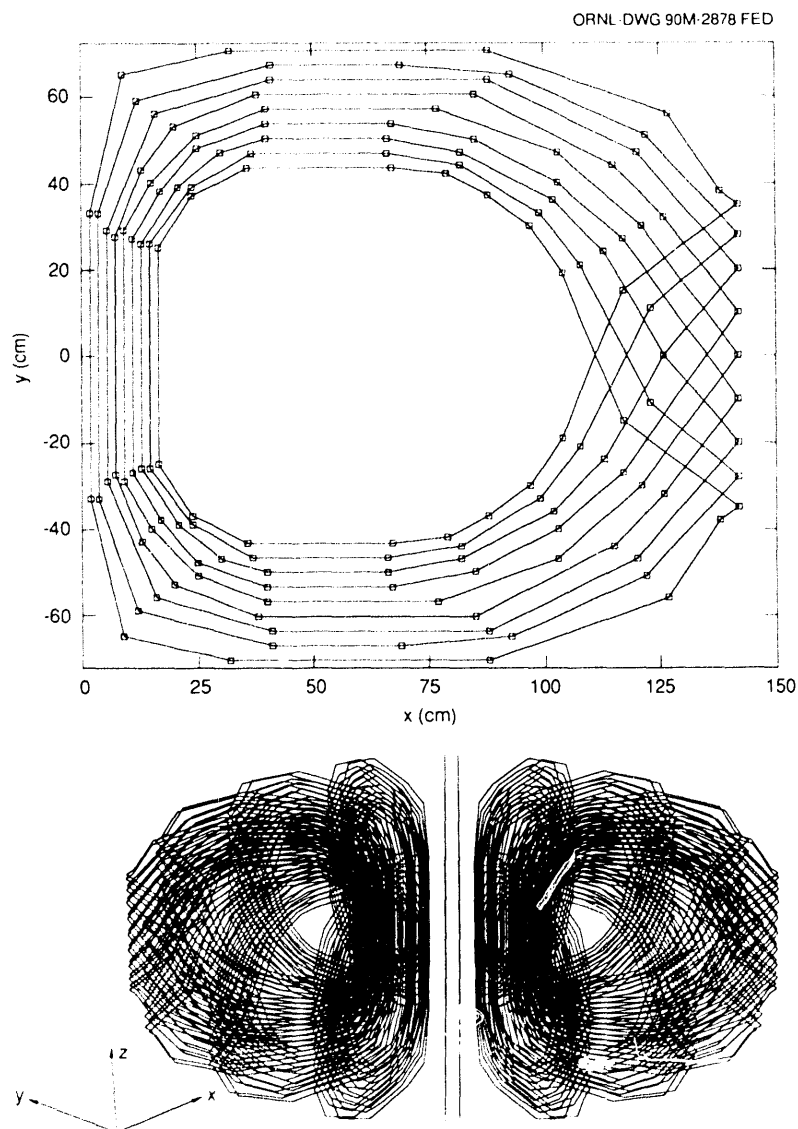


Fig. 3.5. Modeling of TEXT coils. (a) The filamentary model used to describe the current flow in each layer of the pancake coils. (b) Model of the TEXT field, created by modeling each coil with two of the pancakes in (a).

connections of the coil occur only at the outer edge of the coil, and this is reflected by the fact that each filament goes to the outer edge and back in again. The locations of the filaments were determined by using finite element models. We used several pancakes arranged so that the ripple on the inner edge was minimized (although it is still overestimated in our model). The resulting ripple contours for TEXT are shown in Fig. 3.6.

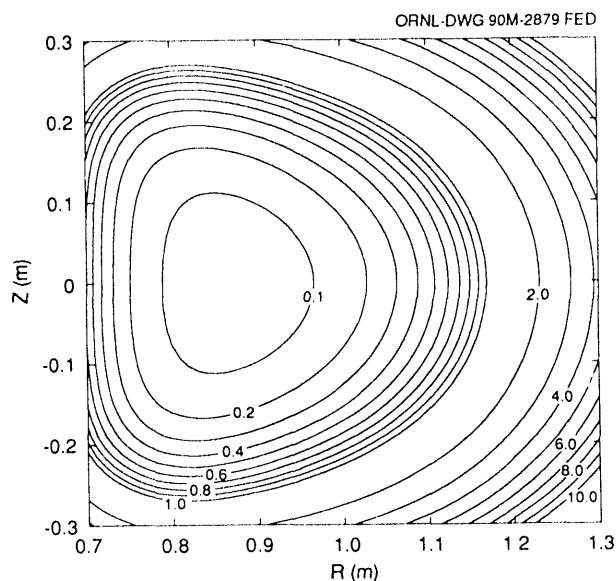


Fig. 3.6. The ripple contours that result from the 10-filament model of Fig. 3.5. $R_{\max} = 16.58$; $R_{\min} = 0.05$.

We also needed a representation for the TEXT equilibrium so that we could properly account for the poloidal fields due to the current in the plasma. Because TEXT has an iron core, this presents a difficult modeling problem. We obtained reasonable results by using the experimental TEXT profiles for rotational transform and pressure, together with our TF model and a uniform vertical field to provide in/out centering of the equilibrium. Using the free-boundary VMEC equilibrium code, we obtained the first self-

consistent rippled tokamak equilibria at finite (but low) beta for TEXT. The resulting flux surfaces (Fig. 3.7) were almost circular and showed a distinct poloidal bulge on the midplane, which is caused by the interlayer connections of the TF coils. There was also a toroidal bulge between the TF coils of about 1 cm due to the TF ripple. Both of these results seem to be consistent with TEXT experimental data, although it is very difficult to measure the profiles with this accuracy.

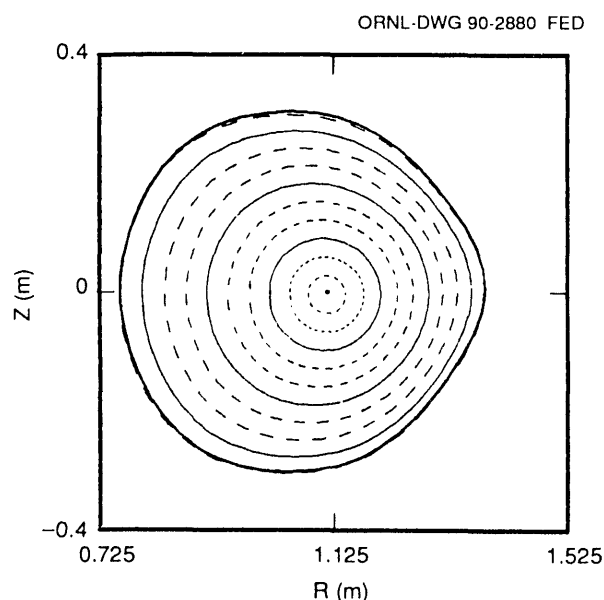


Fig. 3.7. The free-boundary, finite-beta, self-consistent TEXT equilibrium calculated using the experimentally obtained q and pressure profiles and the field model of Fig. 3.6.

We then converted the output of VMEC to Boozer coordinates and followed the beam orbits. The result was that, indeed, those ions born in the outer half of the TEXT plasma are ripple trapped. Figure 3.8 shows the orbit of a typical 25-keV injected ion in TEXT. Because this plot is in Boozer coordinates, the bounce points (which lie along a vertical $|B|$ contour) do not appear to be on a vertical line. In this plot, the

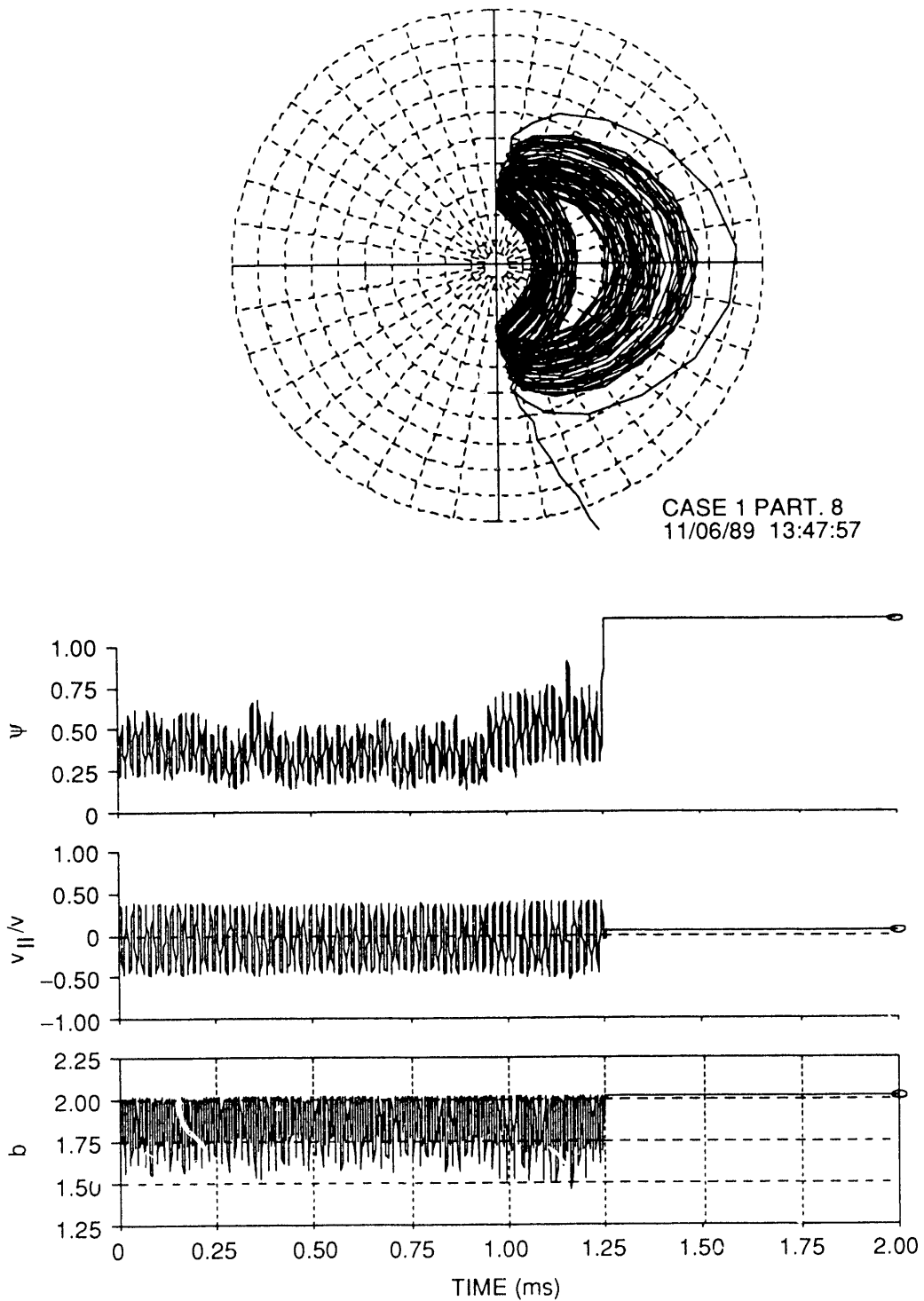


Fig. 3.8. Orbit of a downward-injected, 25-keV ion from the diagnostic neutral beam in TEXT, which eventually becomes ripple trapped and leaves the system.

beam is injected downward. The ion is born at $\psi = 0.22$ but eventually becomes ripple trapped at about $\psi = 0.5$.

3.4 TRANSPORT AND CONFINEMENT MODELING

3.4.1 General Transport Studies

Work continued on the development of a model for the L-H transition. An expression for neoclassical viscosity that is valid for high poloidal rotation velocity was derived; it exhibits a maximum as the rotation speed is increased.⁴¹ As collisionality decreases and ion orbit losses increase at the plasma boundary, the radial electric field E_r becomes more negative and poloidal rotation increases to drive a radial current (through the viscosity) to balance the nonambipolar ion loss. At low enough collisionality, the balance between the orbit and viscosity-driven currents exhibits a bifurcation that appears as an abrupt increase in the poloidal rotation (or, equivalently, an even more negative value of E_r), as observed experimentally in DIII-D.⁴² Shear in the toroidal rotation introduces an additional decorrelation mechanism for turbulence, reducing fluctuation amplitudes and transport.^{43,44} An assessment of the status and issues of transport modeling was completed as part of the TTI.⁴⁵ A set of major program recommendations was also issued.⁴⁶

The relationship between global confinement and local thermal conductivity was evaluated in work that required generation of a LOCUS database for WHIST runs.⁴⁷ This approach to testing transport models was shown to be very efficient and should help in future testing of theoretical models against experimental data.

3.4.2 ITER Studies

ORNL physicists actively participated in the ITER Conceptual Design Joint Work during the winter (February–March 1989) and summer (July–October 1989) sessions at IPP Garching and played a key role in the evolution of the ITER physics design. The primary areas of ORNL contributions to ITER physics studies were in MHD stability and beta limits, confinement assessment, fast-wave current drive (FWCD), and pellet fueling. Work was also carried out on axisymmetric magnetics, alpha particle effects, helium ash accumulation and exhaust, and plasma-wall interactions. Details are described in Sect. 6 of this report. Brief highlights from these areas are as follows: (1) physics design guidelines and physics specifications for the design information document were prepared and published;^{48,49} (2) limitations to the operational space arising from MHD instabilities (ideal and resistive, linear and nonlinear, fluid and kinetic) were estimated;^{50–52} (3) the MHD database for current drive and peaked pressure and current density profiles was extended;⁵³ (4) various transport models were compared with the ITER L-mode database, and the confinement capability of ITER was assessed using these models;^{54,55} (5) DIII-D and TFTR databases for volt-second consumption during the current ramp phase, especially with regard to MHD-influenced (fast ramp) scenarios, were analyzed;⁵⁶ (6) particle transport and fueling (gas puffing vs pellet fueling) issues were assessed;⁵⁷ and (7) detailed estimates of FWCD efficiency were made using a 2-D, full-wave code.⁵⁸

3.4.3 CIT Studies

An assessment of NBI parameters for the Compact Ignition Tokamak (CIT) showed

the influences of beam energy, geometry, and orientation and plasma density on heating profiles and shine-through. Tangential injection gives the widest range of operating densities but requires roughly twice the energy of normal injection and presents more difficult access requirements.⁵⁹

The impact of the uncertainty in the velocity scaling of pellet penetration on CIT operation was evaluated. If the velocity scaling of recent JET experiments holds, then deep penetration in the plasma burn stage with pellets at a nominal velocity of 5 km/s may be possible.⁶⁰ See Sect. 6.1.4 for more details on CIT studies.

3.4.4 ATF Studies

The PROCTR-MOD database system was extended by addition of a LOCUS database that contains scalar machine parameters from ATF for input to the profile analysis code PROCTR-MOD. Previous analysis of measured ATF temperature profiles indicated a region of poor energy confinement in the outer half of the plasma that was attributed to field errors. After repair of the field errors, further profile analysis showed that the region of enhanced energy loss in the peripheral region is still present, although at a reduced level.⁶¹

A geometry database was created that allows online display of the ATF flux surface geometry for a given ATF shot. The geometry is calculated on one of the Cray computers at the National Magnetic Fusion Energy Computer Center (NMFEECC) at Lawrence Livermore National Laboratory (LLNL) with either a field-line-following code (for vacuum surfaces) or VMEC (for finite-beta surfaces). The calculated geometry is then stored in a database on the local VAXcluster. A utility called PLOTG displays the geometry for the coil currents measured for a given shot. This capability

is used extensively by the ATF experimental staff to define the plasma position relative to the vacuum vessel, limiters, and diagnostic chords. The geometry database also forms the starting point for Thomson scattering and far-infrared (FIR) profile fitting and analysis with the PROCTR-MOD code set.⁶²

Several additions were made to PROCTR-MOD to allow analysis of CHS plasmas in Nagoya, Japan. This work was performed in collaboration with Dr. Yamada during a visit to ORNL. Dr. Yamada took a copy of the PROCTR-MOD code set back to Nagoya, where it will be the primary profile analysis tool for CHS. Thus, PROCTR-MOD is being used for analysis of data from both Japanese toratrons (Heliotron E and CHS), and it may be adapted for analysis of the future LHD experiment in Toki.

The predictive transport code PROCTR is being used for specialized studies involving temporal discharge evolution. During the past year, PROCTR continued to be used to understand the collapse of the plasma temperature in NBI-heated discharges in ATF. To this end, the following additions were made to PROCTR. (1) A source term was added to the multispecies impurity source terms for modeling laser-blowoff impurity pulses. (2) The atomic physics database package ALADDIN, supported by the International Atomic Energy Agency, was added as the source of atomic physics coefficients for ionization, recombination, and line emission in the multispecies impurity model. (3) The fast ion Fokker-Planck (FIFPC) routine was revised to allow the detailed treatment of injected fast ions in the presence of loss cones.^{63,64} Further discussion of the ATF modeling studies is contained in Sect. 1.1.4.

3.4.5 Pellet Injection Studies on JET

The shielding physics in present pellet ablation models was re-examined. A series

of experiments at varying pellet velocities (0.4–1.4 km/s) was performed on JET using the ORNL-supplied multiple-pellet injector. The results showed a definite velocity dependence in the penetration depth that confirmed the scaling of the original neutral gas shielding model but indicated higher shielding factors. The present model with combined neutral and plasma shielding had exhibited no scaling with velocity because of the way in which the plasma shield was incorporated, but it had yielded good agreement with experimental results at full pellet velocity over a wide range of plasma conditions and pellet sizes. Leading candidates for increasing the shielding of the neutral gas shielding model while maintaining the scaling with velocity are elongating the neutral shield along the magnetic field (rather than using a spherical approximation for the shield) and/or including magnetic shielding.⁶⁰

Analysis of transport properties in the core of JET plasmas showed that the local particle diffusivity and thermal diffusivity are highly correlated. When the density profile is highly peaked following pellet injection, core diffusivity is significantly reduced well into the following ion cyclotron resonant frequency (ICRF) heating phase. There appeared to be no evidence of an anomalous particle pinch in the core under any operating conditions; the neoclassical Ware pinch could be used to explain both the modest peaking of the density profile in nonpellet cases and the decay of peaked density profiles from pellet injection. This work illustrated the need to consider a full transport matrix, with both neoclassical and turbulence-driven transport processes contributing to the fluxes.^{65,66}

Other aspects of JET experimental analysis are described in Sec. 4.1.2.

3.5 RF HEATING

The task of rf heating and current drive theory is to develop and test theories of (1) plasma wave generation, (2) propagation, (3) absorption, and (4) plasma response in all frequency regimes relevant to fusion (Alfvén, ion cyclotron, lower hybrid, and electron cyclotron). These theories are incorporated into analytical and numerical predictive models that are used to interpret experimental results from tokamaks, stellarators, and other devices; to develop means for enhancing the effectiveness of plasma heating; and to evaluate and optimize designs for future experiments and technologies. By definition, the objective of rf heating or current drive is to modify the plasma distribution function in a specific way. Therefore, the rf theory efforts are closely coupled to kinetic theory, to transport theory, and to stability and are closely allied with experimental, engineering, and technology studies.

In the past year the rf program has been heavily involved in modeling ICRF heating on TFTR, JET, ATF, and CIT; in interpreting electron cyclotron resonance heating (ECRH) experiments on the ATF and L-2 stellarators; in design and optimization of antennas for TFTR and DIII-D; and in assessment of ICRF current drive scenarios for ITER. Significant progress was made in our capability to model the deposition of fast ICRF wave power using 2-D full-wave codes, to calculate rf-driven currents, and to study in detail the fields in the vicinity of realistic ICRF antennas. We have also begun to develop an understanding of the mechanisms by which ICRF power perturbs the plasma edge and produces added impurities.

3.5.1 Global ICRF Wave Propagation in Edge Plasma and Faraday Shield Regions

One of the major issues in the theoretical modeling of high-power ion cyclotron resonance heating (ICRH) experiments is the effect of wave fields on the low-density surface plasma, especially the influence of these fields on impurity generation. Such issues have stimulated interest in calculations of global ICRH wave fields in the surface and antenna regions. Therefore, we extended the ORION code to include finite E_{\parallel} and made detailed calculations of the wave field structure in the low-density edge plasma immediately surrounding the antenna and Faraday shield structure. The magnetic field model is general enough to allow applications to both axisymmetric tokamak and helically symmetric stellarator geometries. The equation solved is the so-called “reduced-order” wave equation in which the value of k_{\perp} (the perpendicular wave number) that appears in the warm-plasma dielectric tensor does not come self-consistently from the wave solution but rather comes from an independent solution of the warm-plasma dispersion relation. Both fast-wave and Bernstein wave roots are calculated, but the Bernstein root is discarded, thus “reducing the order” of the resulting differential equation from fourth to second order. This differential system retains warm-plasma effects such as cyclotron damping, Landau damping, and transit-time magnetic pumping (TTMP) while avoiding the numerical difficulties associated with the short-wavelength ion Bernstein wave (IBW). While such warm-plasma effects are of little consequence in the edge region, they are included for convenience in benchmarking against previous calculations for the warm central plasma in the $E_{\parallel} \sim 0$ limit.

Our numerical approach introduces the electromagnetic potentials \mathbf{A} and ϕ with the Coulomb gauge $\nabla \cdot \mathbf{A} = 0$. This formulation properly includes electrostatic effects, which we find to be important in the region surrounding the Faraday shield. Special care is taken to devise a “conservative” numerical scheme that is consistent with the gauge conditions ($\nabla \cdot \mathbf{A} = 0$). An alternative approach would be to solve the wave equation directly in terms of \mathbf{E} rather than potentials. This approach has proved useful in the $E_{\parallel} = 0$ limit, but we encounter numerical difficulties when it is applied to problems in which electrostatic effects are dominant. As expected, applications to high-density plasmas agree with previous calculations in the $E_{\parallel} = 0$ limit. More interesting is the application to the edge plasma and Faraday shield region, where the parallel electric field is found to peak strongly in the gaps between the Faraday shield blades. Scaling with rotational transform shows that $|E_{\parallel}|$ is directly proportional to the electrostatically induced electric field in the gap between the blades (Fig. 3.9). The constant of proportionality depends on the edge density as well as the parallel wave number.

3.5.2 Fast-Wave Current Drive Modeling for ITER and DIII-D

It is widely recognized that a key element in the development of an attractive tokamak reactor, and in the successful achievement of the mission of ITER, is the development of an efficient steady-state current drive technique. The use of ICRF fast waves is being studied as a technique for steady-state current drive in large tokamaks such as ITER and fusion reactors. A simple slab model has been developed to design and optimize phased antenna arrays to achieve

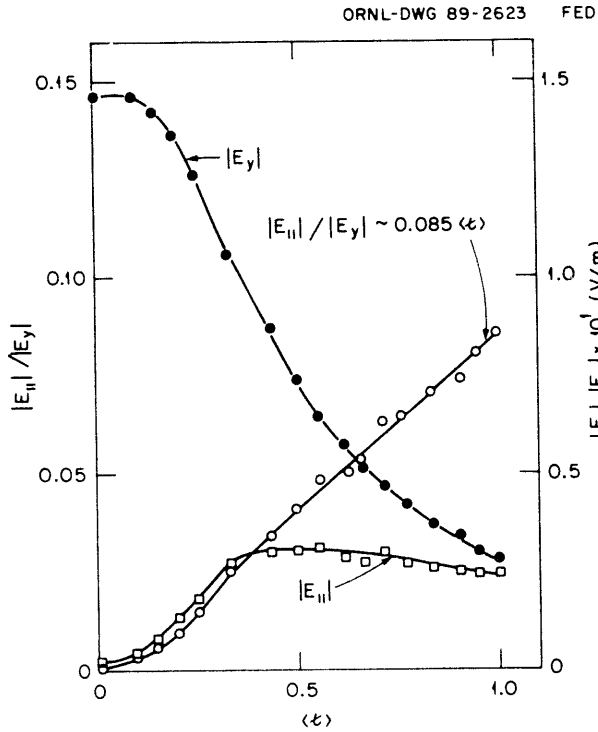


Fig. 3.9. Numerical survey showing parametric dependence of $|E_{||}|$, $|E_y|$, and $|E_{||}|/|E_y|$ on rotational transform. Here $x = 0.425$ m, $y = 0.065$ m, $k_z = 9.84$ m $^{-1}$, $n_{edge} = 3 \times 10^{12}$ cm $^{-3}$.

the required directivity and concentration of high parallel phase velocity components in the power launched into the plasma. Various designs are being evaluated for the individual antenna elements, including multiple-loop, recessed-cavity antennas. Also, the full-wave ICRF heating code ORION is being used to calculate power deposition in the various plasma species and to calculate driven current profiles produced by fast waves in large, noncircular tokamaks such as ITER. The primary current drive mechanism in these cases is TTMP. Wave damping processes that are included are ion cyclotron damping by the fuel components, electron Landau damping, TTMP, and absorption by fusion decay products such as energetic alpha particles. Two primary issues are to be determined:

1. Can an acceptable antenna be designed to produce a $k_{||}$ spectrum with most of the power in the phase velocity range where the efficiency of current drive is high?
2. Will the rf power be efficiently absorbed by electrons in the desired velocity range without unacceptable parasitic damping by fuel ions and alpha particles?

An important figure of merit in this context is

$$\gamma = \frac{n_e}{10^{20} \text{ m}^{-3}} I_{rf} \frac{R}{P_{rf}} = 1.6 \times 10^{-3} T_e \bar{j} / \bar{p} \quad (3.1)$$

Ehst has provided a simple algebraic expression for \bar{j}/\bar{p} obtained as a fit to the Fokker-Planck results of Karney and Fisch, employing a momentum-conserving collision operator including trapped-particle effects.

To address these issues we have employed the slab model for rapid comparison of various antenna designs and phasings to show trends of obtainable current drive efficiency under various assumptions. The ORION 2-D full-wave code gives power absorption and current drive profiles. This code realistically models the launched antenna spectrum with radial focusing, includes toroidal eigenmode effects (multiple-pass absorption) if present, and includes the effects of ion cyclotron harmonic and alpha particle damping.

Results have been computed for ITER for both the 60-MHz and 20-MHz scenarios and for the DIII-D proof-of-principle experiment. In ITER the most promising results are obtained with the low-frequency option, where parasitic ion resonances are absent. Since damping is relatively weak for this case, eigenmode effects are very important. The current drive figure of merit γ and loading resistance per unit length per strap R_L are sensitively dependent on density. By careful matching of the $k_{||}$ spectrum to the

eigenmode structure we have obtained γ up to 0.6 and R_L up to 17 Ω/m .

These results are very encouraging, although there are uncertainties in the calculations. The high values of γ are obtained by phasing the array so as to produce a spectrum near $n_{\parallel} = 1$ where \bar{j}/\bar{p} is favorable and trapped particle effects are minimized, and by relying on a high-Q cavity mode to enhance the comparatively low electron absorption. Relativistic effects are not included in the model, although this is not thought to be a significant source of error. The ORION code, being a straight tokamak model, does not accurately treat the variation of n_{\parallel} across the plasma cross section. If significant upshifts in N_T occur in multiple reflections, the favorable n_{\parallel} spectrum will not be maintained. Also, if additional parasitic loss mechanisms appear, such as collisional absorption or losses due to the shear Alfvén resonance, the current drive efficiency will decrease.

3.5.3 Electron Heating and Static Sheath Enhancement in Front of Energized RF Antennas

The generation of impurities from the Faraday shield and surrounding structures is a commonly observed phenomenon when an ICRF antenna is energized. One of the more interesting experimental observations is the heating of electrons in the region near the antenna. We have developed an analytic model that considers rf near-field effects that occur within a plasma rf skin layer of the Faraday shield in the limit that the rf plasma response is linear. The heating of electrons by the rf near fields is treated by using a quasi-linear electron heating model. The production of high-energy ions can then be understood in terms of an enhanced

time-independent (static) sheath near the shield when electrons are strongly heated by evanescent rf electric fields parallel to the static magnetic field \mathbf{B} , at the locations where the field line intersects a grounded structure. The sheath enhancement results from the fact that the rf-excited electron distribution can be far from a collisional Maxwellian. This model demonstrates that the production of impurities in this region can easily result from the high-energy ions that are produced in the low-density plasma near the front face of the Faraday shield.

Meaningful electron excitation occurs only when some phase decorrelation mechanism exists such that electrons can be heated rather than simply oscillating in the rf fields. One decorrelation mechanism that can give rise to electron heating is analogous to Fermi acceleration when observed in a frame that is oscillating with the electron in the parallel rf electric field E_{\parallel} . In contrast to previous works, where the amplitude of the sheath oscillates within a few Debye lengths λ_D of the wall, we considered an electron that is free to oscillate in the rf electric field except when it reaches a wall, where a strong, localized static potential can force the electron to turn before completing an rf cycle. In the oscillating frame, the static sheath that occurs within a few λ_D of the grounded structure appears to be oscillating in space rather than amplitude. An electron will be reflected by this static sheath if its parallel energy at the time of impact is less than the static sheath potential. Decorrelation can occur on an electron transit time scale, and the electrons are heated either until they overcome the static sheath potential at the end of the field line or until an adiabatic heating limit is reached.

We have used the ORION code to solve for the rf fields in the vicinity of a Faraday shield with plasma present. The code

includes both rf electrostatic and electromagnetic effects and uses a linear warm-plasma dielectric response for specified plasma profiles. Calculations using the code show that, for frequencies near 30 MHz in geometries like that of the Princeton Large Torus (PLT), the electric fields parallel to \mathbf{B} are small enough to produce a linear plasma response. That is, the electrons in the near-field region are able to freely carry oscillatory rf currents and reduce E_{\parallel} . Results of the ORION code indicate that these plasma currents may not be neglected in the calculation of E_{\parallel} unless the plasma density is very low, in which case the rf electric fields approach the expected vacuum limit. E_{\parallel} decays away from the Faraday shield and extends into the plasma in the x -direction, as shown in Fig. 3.10. The evanescent scale length of this near-field region is of the order of the plasma skin depth modified by perpendicular profile effects. For the case of PLT-type parameters, these near fields can extend into the plasma for distances of the order of 1 cm. E_{\parallel} in the gaps at the front face of the Faraday shield reaches values of 10–20 V/cm for power levels comparable to the experimental values. Significant electron excitation in the near-field region has been observed experimentally with these relatively low values of E_{\parallel} .

These estimates can now be used to determine the importance of these processes, assuming that the grounded wall in the perpendicular direction represents the metallic bars of the Faraday shield. Sheath potentials in the range from 200 to 500 V are obtained for deuterium with $E_{\parallel} = 10$ –20 V/cm. Note that in a deuterium plasma, deuterium energies on the order of 500 eV would be capable of sputtering a few wall atoms such as nickel. These sputtered nickel

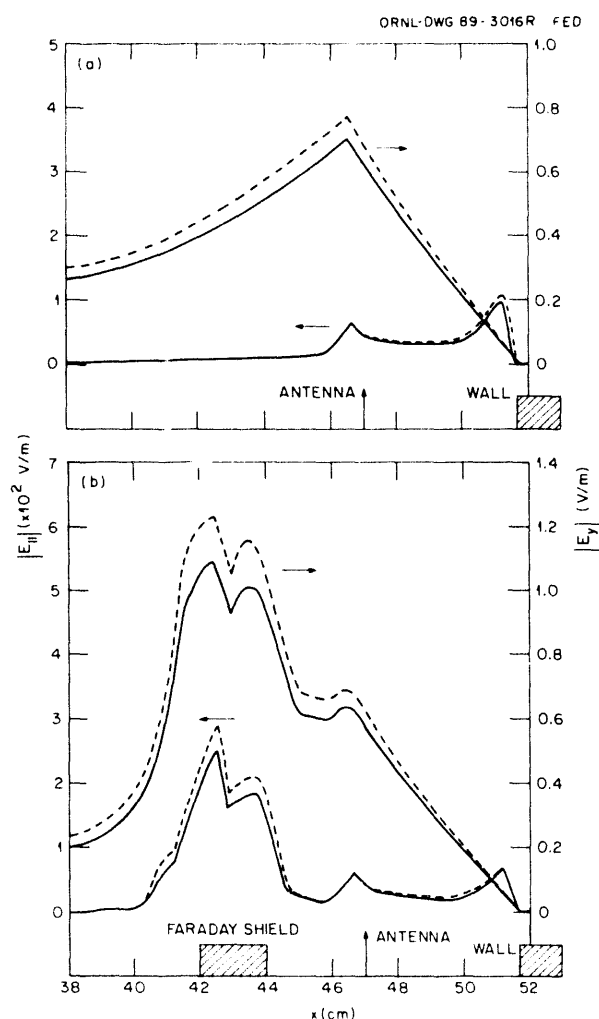


Fig. 3.10. Magnitudes of E_y and E_{\parallel} along a chord (a) without a Faraday shield and (b) with a Faraday shield. Solid curves: uniform antenna current. Dashed curves: nonuniform antenna current.

atoms could then be ionized and fall through a similar potential drop, hitting the screen with energies in the 500-eV range (if only singly charged), where the self-sputtering yield exceeds unity. Thus, the experimentally observed sputtering phenomena at the Faraday shield of an energized rf antenna may be explained by using realistic values for the pertinent parameters in this model.

3.6 COMPUTING AND OPERATIONS

Computing in the Fusion Energy Division can be roughly divided into three categories: the User Service Center (USC), experimental data acquisition, and support of personal computers (PCs). Funding restrictions have placed a considerable premium on developing methods of providing support in these areas with fewer people. The USC now operates with only partial operator coverage, and many labor-intensive activities have been automated or shifted to hardware that can operate almost unattended. Examples include an ion-deposition printer, which requires far less manual paper handling and operator intervention than the Versatec printers; a helical-scan tape unit purchased last year for evaluation, which has proved satisfactory and is now used for the routine daily incremental backups (these can now be run as an unattended batch job); and the use of the optical jukebox purchased last year for "near-line" storage of ATF data. This places all ATF data in machine-mountable storage and removes any need for manual tape or disk mounting, which was a continual problem for the data archive systems on earlier fusion experiments at ORNL. In the PC area, the most interesting development was bridging the AppleTalk zones in the building to the Ethernet backbone and connecting them to the VAXcluster with AlisaShare. Finally, in the first move toward creating a fourth category of computing, the division purchased its first workstations this past year. These workstations (two DECStation 3100s and a Silicon Graphics Personal Iris) offer significant advances in dedicated computing power at a very attractive price.

Software development has concentrated in the area of experimental support and data acquisition. A suite of fully automatic migration procedures was developed for the optical jukebox. These procedures stage

ATF data from its initial repository on primary disks to secondary disks and then on to the jukebox. The primary disks (a set of shadowed fast disks) store the data in uncompressed form and thus provide the shortest access time. Before the data are transferred to secondary disk storage, they are compressed and also copied to tape for offsite vault storage. Data compression slightly slows the access time (~30%) but allows the storage of three times as much data on the secondary disks. Finally, the oldest data migrate off the secondary disks to their final repository in the optical jukebox. All disks in the jukebox appear to be on line simultaneously. In reality, the number of disks spinning at the same time is the same as the number of read stations (currently two). Since data appear to "age" fairly quickly (users most often access recent data, sometimes access older data, and only sporadically access the oldest data), the jukebox can provide an illusion that all data are on line as long as there are enough data in secondary storage to meet the moderate-access demands. Data can be read directly from the jukebox or copied back to a recall area on the secondary disk string. Since analyzed data files can be modified while in this area, and since the storage medium in the jukebox can only be written once, data stored there can be superseded but not erased and rewritten. This placed interesting design constraints on the automatic migration software to guarantee that modified files were properly detected, tracked, and archived.

A complete rewrite of the ORNL Fusion Energy Division CAMAC device driver package was completed this year. This rewrite, which has been under consideration for some time, has allowed the internals of the driver to be modernized significantly. The driver is now compatible with symmetric multiprocessing CPUs from Digital

Equipment Corporation (DEC); in addition, all the hardware register dependences are localized to one point in the code. The resulting code can be ported to other branch driver designs with much less work than would have been required in the past.

Additional development has continued in support of the division's involvement with Tore Supra and TEXTOR (see Sects. 1.2.2 and 1.2.3). Communications software was developed for exchanging data files and synchronizing shot information with Tore Supra's host data acquisition computers (which are non-DEC). This software underwent a major upgrade this year to improve its reliability and robustness. Development of basic data acquisition programs continued at both sites.

REFERENCES

1. V. E. Lynch et al., "Three-Dimensional Equilibria and Mercier Stability Calculations," paper PMA5 presented at the 13th Conference on the Numerical Simulation of Plasmas, Santa Fe, N.M., September 17-20, 1989.
2. N. Dominguez et al., "Ideal Low- n and Mercier Mode Stability Boundaries for $l = 2$ Torsatrons," *Nucl. Fusion* **29**, 2079 (1990).
3. N. Dominguez et al., "Ideal Low- n and Mercier Mode Stability Boundaries for $l = 2$ Torsatrons," paper O2-6 in *Proceedings of the Seventh International Stellarator Workshop, Oak Ridge, 1989*, IAEA-TECDOC-558, International Atomic Energy Agency, Vienna, 1990.
4. J. F. Lyon et al., "ATF-II Studies," *Fusion Technol.* **17**, 188 (1990).
5. B. A. Carreras et al., *Confinement Improvement of Low-Aspect-Ratio Torsatrons*, ORNL/TM-11101, Martin Marietta Energy Systems, Inc., Oak Ridge Natl. Lab., 1989.
6. J. F. Lyon et al., "Compact Torsatron Reactors," *Fusion Technol.* **15**, 1401 (1989).
7. Y. Nakamura et al., "Equilibrium, Stability, and Deeply Trapped Particle Orbit Calculations for $\ell = 2$ Torsatron/Heliatron Configurations," *Fusion Technol.* **15**, accepted for publication (1990).
8. Y. Nakamura et al., "Relation Between Mercier Criterion and Low- n Mode Stability," paper 4P-2 in *Proceedings of the Seventh International Stellarator Workshop, Oak Ridge, 1989*, IAEA-TECDOC-558, International Atomic Energy Agency, Vienna, 1990.
9. A. Varias et al., "Ideal Mercier Stability for the TJ-II," *Europhys. Conf. Abstr.* **13B**, 607 (1989).
10. A. Varias et al., "Stability Studies for TJ-II," paper 4P-12 in *Proceedings of the Seventh International Stellarator Workshop, Oak Ridge, 1989*, IAEA-TECDOC-558, International Atomic Energy Agency, Vienna, 1990.
11. L. A. Charlton et al., "Compressible Linear and Nonlinear Resistive MHD Calculations in Toroidal Geometry," *J. Comput. Phys.* **86**, 270 (1990).
12. L. A. Charlton and B. A. Carreras, "The Effect of Compressibility on Magnetohydrodynamic Instabilities in Toroidal Tokamak Geometry," *Phys. Fluids B* **2**, 539-47 (1990).
13. J. A. Holmes, B. A. Carreras, and L. A. Charlton, "MHD Stability of Shaped Tokamak Plasmas with Low Shear and Inflection Point at the $q = 1$ Surface," presented at the Workshop on Resistive MHD Instabilities in Tokamaks with Emphasis on the Effect on Noncircularity and Finite Beta, Princeton, N.J., November 7-9, 1989.
14. J. A. Holmes, B. A. Carreras, and L. A. Charlton, "MHD Stability and Nonlinear Evolution of the $m = 1$ Mode in Toroidal Geometry for Safety Factor Profiles with an Inflection Point," *Phys. Fluids B* **1**, 788 (1989).
15. L. A. Charlton et al., "Linear and Nonlinear Infernal Modes in Shaped Plasmas," presented at the Workshop on Resistive MHD Instabilities in Tokamaks with Emphasis on the Effect on Noncircularity and Finite Beta, Princeton, N.J., November 7-9, 1989.
16. L. A. Charlton et al., "MHD Analysis of Peaked-Density Profiles Produced by Pellet Injection in JET," presented at the Annual Controlled Fusion Theory Conference: 1989 Sherwood Meeting, San Antonio, Tex., April 3-5, 1989.
17. J. D. Hanson et al., "A Simple Method for Calculation of Magnetic Island Widths," paper 5P7 in *Proceedings of the Seventh International Stellarator Workshop, Oak Ridge, 1989*, IAEA-TECDOC-558, International Atomic Energy Agency, Vienna, 1990; also presented at the Annual Controlled Fusion Theory Conference: 1989 Sherwood Meeting, San Antonio, Tex., April 3-5, 1989.
18. K. C. Shaing et al., "Bootstrap Current Control and the Effects of the Radial Electric Field in Stellarators," paper O5-7 in *Proceedings*

of the Seventh International Stellarator Workshop, Oak Ridge, 1989, IAEA-TECDOC-558, International Atomic Energy Agency, Vienna, 1990.

19. K. C. Shaing et al., "Bootstrap Current Control in Stellarators," *Phys. Fluids B* **1**, 1663-70 (1989).

20. L. Garcia et al., "Low- n Stability Calculations for Three-Dimensional Stellarator Configurations," *Phys. Fluids B* **2**, 2162 (1990).

21. L. Garcia, B. A. Carreras, and N. Dominguez, "Stability of Local Modes in Low-Aspect-Ratio Stellarators," *Europhys. Conf. Abstr.* **13B**, 611 (1989).

22. L. Garcia, B. A. Carreras, and N. Dominguez, "Averaged Equilibrium and Stability in Low-Aspect-Ratio Stellarators," paper 4P-1 in *Proceedings of the Seventh International Stellarator Workshop, Oak Ridge, 1989*, IAEA-TECDOC-558, International Atomic Energy Agency, Vienna, 1990.

23. B. A. Carreras et al., "Dissipative Trapped Electron Modes in Stellarators," paper 4P-9 in *Proceedings of the Seventh International Stellarator Workshop, Oak Ridge, 1989*, IAEA-TECDOC-558, International Atomic Energy Agency, Vienna, 1990; a related paper was presented at the Annual Controlled Fusion Theory Conference: 1989 Sherwood Meeting, San Antonio, Tex., April 3-5, 1989.

24. J. H. Harris et al., "Second Stability in the ATF Torsatron," *Phys. Rev. Lett.* **63**, 1249-52 (1989).

25. M. Murakami et al., "Second Stability Studies in the ATF Torsatron," *Europhys. Conf. Abstr.* **13B**, 575 (1989); also published as ORNL/TM-11138, Martin Marietta Energy Systems, Inc., Oak Ridge National Laboratory, 1989.

26. B. A. Carreras et al., "Access to Second Stability in ATF," presented at the Annual Controlled Fusion Theory Conference: 1989 Sherwood Meeting, San Antonio, Tex., April 3-5, 1989.

27. V. E. Lynch et al., "Equilibrium and Ideal Stability Studies for ATF," paper 4P-10 in *Proceedings of the Seventh International Stellarator Workshop, Oak Ridge, 1989*, IAEA-TECDOC-558, International Atomic Energy Agency, Vienna, 1990.

28. B. A. Carreras et al., *A First Glance at the Initial ATF Experimental Results*, ORNL/TM-11102, Martin Marietta Energy Systems, Inc., Oak Ridge National Laboratory, 1989.

29. J. Nührenberg and R. Zille, "Optimization of Helias for Wendelstein VII-X," p. 17 in *Proceedings of the 2nd Workshop on Wendelstein VII-X, Schloss Ringberg, 1988*, EUR 11705 EN, Commission of the European Communities, Brussels, 1988.

30. R. N. Morris et al., "Finite-Beta Equilibrium Magnetic Field Perturbations in Stellarator Plasmas," *Nucl. Fusion* **29**, 2115 (1989).

31. S. P. Hirshman and O. Betancourt, "Preconditioned Descent Algorithm for Rapid Calculations of Magnetohydrodynamic Equilibria," *J. Comput. Phys.*, accepted for publication (1990).

32. S. P. Hirshman et al., "Low-Aspect-Ratio Optimization Studies for ATF-II," paper O4-6 in *Proceedings of the Seventh International Stellarator Workshop, Oak Ridge, 1989*, IAEA-TECDOC-558, International Atomic Energy Agency, Vienna, 1990.

33. A. J. Wootton et al., *Fluctuations and Anomalous Transport in Tokamaks*, FRCR-340 (DOE-ER/53267-52), Fusion Research Center, University of Texas, Austin, 1989.

34. K. C. Shaing et al., "Radial Electric Field and Enhanced Confinement Regimes in Tokamaks and Stellarators," presented at the Annual Controlled Fusion Theory Conference: 1989 Sherwood Meeting, San Antonio, Tex., April 3-5, 1989.

35. G. S. Lee, B. A. Carreras, and L. Garcia, "Fluctuation Spectrum of Resistive Pressure-Gradient-Driven Turbulence," *Phys. Fluids B* **1**, 119-133 (1989).

36. B. A. Carreras and P. H. Diamond, "Thermal Diffusivity Induced by Resistive Pressure-Gradient-Driven Turbulence," *Phys. Fluids B* **1**, 1011-17 (1989).

37. D. R. Thayer, P. H. Diamond, B. A. Carreras, J. A. Holmes, J. N. Leboeuf, Ch. P. Ritz, and A. J. Wootton, "Drift-Rippling Theory of Edge Turbulent Transport," presented at the Annual Controlled Fusion Theory Conference: 1989 Sherwood Meeting, San Antonio, Tex., April 3-5, 1989.

38. D. K. Lee et al., "Modeling of Fluctuations in the Edge of the TEXT Tokamak," presented at the Annual Controlled Fusion Theory Conference: 1989 Sherwood Meeting, San Antonio, Tex., April 3-5, 1989.

39. L. M. Hively and J. A. Rome, "TF Ripple Losses of Alphas Below the Critical Energy in ITER," *Nucl. Fusion* **30**, 1129-35 (1990).

40. R. H. Fowler et al., "Neutral Beam Injection Benchmark Studies for Stellarators/Heliotrons," *Nucl. Fusion* **30**, 997-1010 (1990).

41. K. C. Shaing and E. C. Crume, Jr., "A Bifurcation Theory of Poloidal Rotation in Tokamaks: A Model for the L-H Transition," *Phys. Rev. Lett.* **63**, 2369 (1989).

42. K. C. Shaing, E. C. Crume, and W. A. Houlberg, "Bifurcation of Poloidal Rotation and Suppression of Turbulent Fluctuations: A Model for the L-H Transition in Tokamaks," *Phys. Fluids B* 2, 1492 (1990).
43. K. C. Shaing, G. S. Lee, B. A. Carreras, W. A. Houlberg, and E. C. Crume, Jr., "A Model for the L-H Transition in Tokamaks," p. 13 in *Plasma Physics and Controlled Nuclear Fusion Research 1988: Twelfth Conference Proceedings, Nice, 12-19 October 1988*, vol. 2, International Atomic Energy Agency, Vienna, 1989.
44. K. C. Shaing, "Suppression of Turbulent Fluctuations by Radial Electric Fields and Confinement Enhancement in Toroidal Plasmas," *Comments Plasma Phys. Controlled Fusion*, submitted for publication (1990).
45. W. A. Houlberg et al., "Modeling Transport in Toroidal Plasmas: Status and Issues," *Phys. Fluids B* 2, accepted for publication (1990).
46. J. D. Callen et al., "Transport Task Force Issues and Recommendations," May 1989.
47. W. A. Houlberg et al., "The Relationship Between Local Transport and Global Confinement," presented at the Annual Controlled Fusion Theory Conference: 1989 Sherwood Meeting, San Antonio, Tex., April 3-5, 1989.
48. N. A. Uckan and ITER Physics Group, *ITER Physics Design Guidelines: Version 1*, ITER-TN-PH-8-7, International Atomic Energy Agency, Vienna, January 1989.
49. ITER Team, *ITER Concept Definition Phase Report*, vols. 1 and 2, ITER Documentation Series 3, International Atomic Energy Agency, Vienna, 1989.
50. J. T. Hogan, *Stability of ITER Profiles with $q(0) < 1$* , ITER-IL-PH-12-9-U-4, International Thermonuclear Engineering Reactor Activity, Garching, Federal Republic of Germany, September 1989.
51. J. A. Holmes, *Resistive MHD Beta Limits*, ITER-IL-PH-12-9-U-3, International Thermonuclear Engineering Reactor Activity, Garching, Federal Republic of Germany, September 1989.
52. D. A. Spong, P. Christenson, and J. A. Holmes, *Modification of ITER Ballooning Stability by an Energetic Alpha Population*, ITER-IL-PH-1-9-U-3, International Thermonuclear Engineering Reactor Activity, Garching, Federal Republic of Germany, September 1989.
53. J. T. Hogan, *Stability of ITER Current-Driven Profiles with $q(0) > 1.5$* , ITER-IL-PH-12-9-U-5, International Thermonuclear Engineering Reactor Activity, Garching, Federal Republic of Germany, September 1989.
54. N. A. Uckan, "Tokamak Confinement Projections and Performance Goals," *Fusion Technol.* 15, 391 (1989).
55. S. E. Attenberger, W. A. Houlberg, and N. A. Uckan, "Transport Analysis of Ignited and Current-Driven ITER Designs," *Fusion Technol.* 15, 629-36 (1989).
56. J. T. Hogan and T. Taylor, *Preliminary Examination of DIII-D Volt-Second Database*, ITER-IL-PH-2-9-U-5, International Thermonuclear Engineering Reactor Activity, Garching, Federal Republic of Germany, September 1989.
57. W. A. Houlberg, *ITER Pellet Fueling*, ITER-IL-PH-9-9-U-1, International Thermonuclear Engineering Reactor Activity, Garching, Federal Republic of Germany, March 1989.
58. D. B. Batchelor et al., "Fast Wave Current Drive Modeling for ITER and Prospects for a Near-Term Proof-of-Principle Experiment," *AIP Conf. Proc.* 190, 218 (1989).
59. R. A. Dory, W. A. Houlberg, and S. E. Attenberger, "Energy Requirements for Neutral Beam Current Drive in a Large Tokamak," *Comments Plasma Phys. Controlled Fusion* 13, 29-44 (1989).
60. W. A. Houlberg, L. R. Baylor, and S. L. Milora, "Velocity Dependence of Pellet Penetration in JET," *Bull. Am. Phys. Soc.* 34, 2057 (1989).
61. M. Murakami et al., "Magnetic Configuration Studies in the ATF Torsatron," *Bull. Am. Phys. Soc.* 34, 1946 (1989).
62. D. A. Rasmussen et al., "Electron Temperature and Density Profile Analysis in ATF," *Bull. Am. Phys. Soc.* 34, 1947 (1989).
63. L. D. Horton et al., "Modeling of Radiation and Density Limits in ATF," *Bull. Am. Phys. Soc.* 34, 1949 (1989).
64. H. C. Howe et al., "Transport Modeling of ECH and Neutral-Beam-Heated Plasmas in the Advanced Toroidal Facility," *Europhys. Conf. Abstr.* 13B, 683 (1989).
65. L. R. Baylor et al., "Particle Transport Analysis of Pellet-Fueled JET Plasmas," pp. 107-12 in *Pellet Injection and Toroidal Confinement: Proceedings of the Technical Committee Meeting, Gut Ising, 1988*, IAEA-TECDOC-534, International Atomic Energy Agency, Vienna, 1989.
66. W. A. Houlberg et al., "WHIST Transport Analysis of High-Neutron-Production, ICRF-Heated, Pellet-Fueled JET Plasmas," pp. 137-42 in *Pellet Injection and Toroidal Confinement: Proceedings of the Technical Committee Meeting, Gut Ising, 1988*, IAEA-TECDOC-534, International Atomic Energy Agency, Vienna, 1989.

4

PLASMA TECHNOLOGY

H. H. Haselton, Section Head
D. W. Swain, Assistant Section Head

B. E. Argo	M. J. Gouge	P. F. Rice
S. E. Attenberger ¹	R. H. Goulding	K. E. Rothe ¹
M. Bacal ²	G. R. Haste	P. M. Ryan
F. W. Baity	P. P. Helton	D. E. Schechter
G. C. Barber	D. J. Hoffman	A. Schempp ¹⁷
L. R. Baylor ³	W. A. Houlberg ⁷	G. L. Schmidt ¹⁸
W. R. Becraft ⁴	G. E. Isham ⁹	R. C. Shanlever ³
P. Berlemont ²	T. C. Jernigan ¹⁰	T. D. Shepard
T. S. Bigelow	L. M. Johnson ¹¹	D. W. Simmons
R. A. Brown ³	R. L. Johnson ³	D. A. Skinner ²
J. Bruneteau ²	C. C. Jones ¹¹	F. Sluss
J. B. O. Caughman ⁵	H. D. Kimrey	C. W. Sohns ¹⁹
L. A. Charlton ¹	J. F. King ¹²	D. O. Sparks
M. J. Cole ³	M. Kwon ¹³	R. A. Stern ²⁰
S. K. Combs	R. Leroy ²	W. L. Stirling
J. F. Cox	R. L. Livesey	K. D. St. Onge ³
K. R. Crandall ⁶	P. S. Meszaros ¹	D. J. Taylor ³
W. K. Dagenhart	G. E. McMichael ¹⁴	C. C. Tsai
E. G. Elliott	S. L. McNair ¹²	J. M. Walters ³
A. Fadnek	S. L. Milora	T. P. Wangler ²¹
D. T. Fehling ⁷	K. Moses ¹⁵	D. J. Webster ³
P. W. Fisher ⁸	B. D. Murphy ¹	J. H. Whealton
S. C. Forrester	P. L. Nguyen ⁵	G. A. White
C. A. Foster	J. L. Ping ³	T. L. White
C. R. Foust	A. L. Qualls ¹⁶	R. E. Wright
W. L. Gardner	R. J. Raridon ¹	R. B. Wysor ³
P. L. Goranson ³		J. J. Yugo ²²

-
1. Computing and Telecommunications Division, Martin Marietta Energy Systems, Inc.
 2. Ecole Polytechnique, Palaiseau, France.
 3. Engineering Division, Martin Marietta Energy Systems, Inc.
 4. Grumman Corporation, Bethpage, N.Y.
 5. University of Illinois, Champaign-Urbana.
 6. AccSys Technology, Inc.
 7. Plasma Theory Section.
 8. Chemical Technology Division.
 9. Finance and Materials Division, Martin Marietta Energy Systems, Inc.
 10. Toroidal Confinement Section.
 11. Management Services Group.
 12. Metals and Ceramics Division.

13. Georgia Institute of Technology, Atlanta.
14. Chalk River Nuclear Laboratories, Chalk River, Ontario, Canada.
15. Plasma Technology Division, JAYCOR.
16. The University of Tennessee, Knoxville.
17. University of Frankfurt, Frankfurt, Federal Republic of Germany.
18. Princeton Plasma Physics Laboratory, Princeton, N.J.
19. Instrumentation and Controls Division.
20. University of Colorado, Boulder.
21. Los Alamos National Laboratory, Los Alamos, N.M.
22. Fusion Engineering Design Center and TRW, Inc., Redondo Beach, Calif.

4. PLASMA TECHNOLOGY

SUMMARY OF ACTIVITIES

During 1989, the Plasma Technology Section continued its activities in development and application of fusion technology. Work in related nonfusion research areas is described in Sect. 9 of this report.

In the plasma fueling program, the long-pulse pellet fueling system for the superconducting Tore Supra tokamak in Cadarache, France, was successfully tested and installed on the facility, with the first pellets injected in December. Tests of the tritium proof-of-principle injector in the Tritium Systems Test Assembly at Los Alamos National Laboratory were completed.

The development of advanced pellet acceleration methods continued with the successful testing of the proof-of-principle e-beam rocket accelerator in February and the development of a repetitive two-stage light gas gun facility, concluding with the first demonstration of repetitive operation at 0.7 Hz. Conceptual designs for pellet injection systems for the Compact Ignition Tokamak and the International Thermonuclear Engineering Reactor (ITER), based on the single-stage pneumatic and two-stage light gas gun approaches, are described in Sect. 6 of this report.

Pellet fueling experiments included the construction and commissioning of an eight-shot pneumatic injector system for the Advanced Toroidal Facility, with the first pellet experiments performed in May. A conceptual design for a four-pellet impurity pellet injector, based on the ORNL two-stage light gas gun, was completed for the Tokamak Fusion Test Reactor (TFTR) in support of the U.S. Tokamak Transport Initiative. In the continuing collaboration on the Joint European Torus (JET) in the area of pellet fueling, the fusion product, $n_D(0)T_i(0)\tau_E$, was increased to $5 \times 10^{20} \text{ m}^{-3} \cdot \text{kV} \cdot \text{s}$, which represents one of the highest fusion products obtained to date on JET.

In the rf technology program, new methods of attaching graphite tiles to Faraday shield tubes were devised; computational methods of quantitatively determining the effect of the Faraday shield geometry on antenna parameters were developed; and the rf power dissipation distribution on the shield was calculated. Experimental studies on the Radio Frequency Test Facility with the development antenna showed increased electron temperatures, plasma potentials, and ion impact energies on the Faraday shield during high-power ion cyclotron resonance heating (ICRH) operation.

Current drive technology efforts included optimizing the geometry of the multiple-strap launcher array and developing control circuitry and tuning algorithms to adjust and maintain proper phasing between the straps. The folded waveguide successfully completed its high-power vacuum testing, and the double-strap ICRH antenna for Tore Supra was completed,

tested, and shipped to France. Design work for a single-strap antenna for Alcator C-Mod continued, and fabrication of a four-strap fast-wave current drive (FWCD) phased-array launcher for the DIII-D experiment began. In the experimental collaboration with Princeton Plasma Physics Laboratory (PPPL), a combined 4.5 MW of ICRH power was injected into TFTR using both the PPPL and ORNL antennas.

In the neutral beam development area, the collaborative work on the rf quadrupole concept for high-energy neutral beams continued. An architecture was produced for an ITER-relevant beam line, and an experimental proof-of-principle demonstration proposal was developed. In the development of the volume negative ion source, diagnostics were developed to measure ion temperature within the source plasma. Atomic processes were analyzed to establish operating points and directions for optimization, and experiments and analyses were performed to evaluate techniques used to reduce the electron density near the extraction sheath. The Lawrence Berkeley Laboratory volume negative ion source was also analyzed, and an explanation of rms transverse emittance of the extracted ion beam was provided.

In summary, the Plasma Technology Section continued to expand its leading role in the development and implementation of the technology needed for fusion.

4.1 PLASMA FUELING PROGRAM

4.1.1 Pellet Injector Development

S. L. Milora

In 1989 the Plasma Fueling Group of the Plasma Technology Section participated in a broad range of research activities in support of the magnetic fusion program in the United States and abroad. Research and development (R&D) activities of the group continued in the general areas of pneumatic and centrifugal pellet injector development to support the present and near-term applications and advanced development in support of more demanding applications anticipated for the Compact Ignition Tokamak (CIT) and International Thermonuclear Engineering Reactor (ITER) devices.

In the area of centrifugal pellet injector development, ORNL completed testing of a long-pulse pellet fueling system for the Tore Supra tokamak and installed the system at the Tore Supra facility in Cadarache, France, in October 1989. The injector, which has been under development since 1986, was designed to fuel Tore Supra plasmas for up to 30 s. In qualification tests at ORNL, the system demonstrated the capability of reliably forming up to 100 pellets at 10 Hz and accelerating them to velocities in the range of 600 to 900 m/s. The first pellets were injected into Tore Supra in December.

In the area of pneumatic injector development, ORNL completed testing of the tritium proof-of-principle (TPOP) experiment on the Tritium Systems Test Assembly (TSTA) at Los Alamos National Laboratory (LANL). In the course of the experimental program, nearly 1500 pellets were fired from the gun, and about a third of these were tritium or mixtures of deuterium and tritium. Pure tritium pellets 4 mm in diameter were successfully accelerated to 1500 m/s in

a conventional 1-m-long single-stage gas gun system using hydrogen propellant gas. During the work, the gun received several modifications, which were performed on the contaminated system through the glove-box ports. This demonstrated that maintenance of future tritium injectors could be carried out using similar techniques.

In the area of more advanced development of higher-speed pellet injectors, ORNL continued the development of the electron-beam (e-beam) rocket pellet accelerator and the two-stage light gas gun concepts, with the following highlights:

- The proof-of-principle (POP) e-beam rocket accelerator was completed and successfully tested in February 1989. Cylindrical hydrogen and deuterium pellets, 4 mm in diameter by 12 mm long, were accelerated to a speed of 300 m/s by high-power pulsed electron beams at various e-beam currents and pulse lengths in a 0.6-m-long acceleration column. Preliminary results indicate that the burn velocity is consistent with theoretical estimates and that extrapolations to higher speeds would be feasible with a multistage accelerator.
- The ORNL two-stage light gas gun facility successfully operated at velocities of up to 4.5 km/s with 35-mg plastic pellets and velocities of 2.85 km/s with 4-mm deuterium pellets. The efforts in 1989 concentrated on the development of the repetitive two-stage device, concluding with the first demonstration of repetitive operation at 0.7 Hz. This was made possible by the addition of an automatic loading mechanism that can easily load pellets at the rate of 1 Hz.

ORNL was also responsible for completion of conceptual designs for pellet injection systems for CIT and ITER based on the single-stage pneumatic and two-stage light gas gun approaches.

ORNL staff members participated in pellet fueling experiments on a number of plasma confinement devices in the United States and abroad. An eight-shot pneumatic injector system was built and commissioned on the Advanced Toroidal Facility (ATF) device, and the first pellet experiments were performed in May 1989. A conceptual design was completed for a four-pellet impurity pellet injector, based on the ORNL two-stage light gas gun, for the Tokamak Fusion Test Reactor (TFTR) at Princeton Plasma Physics Laboratory (PPPL) in support of the U.S. Tokamak Transport Initiative. ORNL staff also participated in major international collaborations between the U.S. Department of Energy (DOE) and the French Commissariat à l'Énergie Atomique (CEA) on the superconducting Tore Supra tokamak and between DOE and the European Atomic Energy Community (EURATOM) on the continuation of the collaboration on the Joint European Torus (JET) in the area of pellet fueling. In 1989 the JET device underwent extensive modifications to allow it to operate with beryllium as a first-wall material. During the brief run period from June to September 1989, pellet injection operations were extensive as the JET program was directed toward an early evaluation of the effects of the beryllium modifications on high-power discharges. The experimental program primarily emphasized the fueling of high-performance discharges. The fusion product, $n_D(0)T(0)\tau_E$, was increased to $5 \times 10^{20} \text{ m}^{-3} \cdot \text{V}\cdot\text{s}$ for electron and ion temperatures in the 7- to 9-keV range. This represents one of the highest fusion products obtained to date on JET. Analysis of the data from the 1988 campaign was completed, and a major new result was the determination of particle diffusivity profiles for peaked-density-profile target plasmas with high-power ion cyclotron range of frequencies (ICRF) heating.

4.1.1.1 Electron-beam rocket pellet injector

C. A. Foster, D. E. Schechter, and
C. C. Tsai

The e-beam rocket pellet injector concept is being developed for injecting ultrahigh-speed pellets to fuel ITER-class fusion confinement devices.¹⁻³ This research is partially supported by U.S. ITER R&D funds. A theoretical evaluation indicates that a practical injector can be developed to deliver deuterium or tritium pellets at speeds of several kilometers per second. Significant results from a POP device⁴ are summarized here, including a brief description of a conceptual design for an ultrahigh-speed pellet injector.

A POP device, shown in Fig. 4.1, has been designed, fabricated, and assembled. It was first operated to demonstrate pellet acceleration by means of e-beam heating in February 1989. Figure 4.2 shows preliminary results from this study. Cryogenic cylindrical (4-mm-diam) pellets of frozen hydrogen (12 mm long) and of frozen deuterium (18 mm long) were reliably injected from the cryostat where they were formed into accelerator guide rails and detected by optical pellet monitors. Pellets are accelerated by partially ablating the back of the pellet with high-power pulsed electron beams at various electron energies, beam currents, and pulse lengths. A typical speed increment of up to 300 m/s is observed, increasing with the beam power. The preliminary results of the experimental study reveal an estimated burn velocity consistent with theoretical estimates.^{3,4} The exhaust velocity and acceleration efficiency are being studied in the ongoing experiments.

The POP device consists of a pellet cryostat, an electron gun, and a pellet accelerating column that includes guide rails and

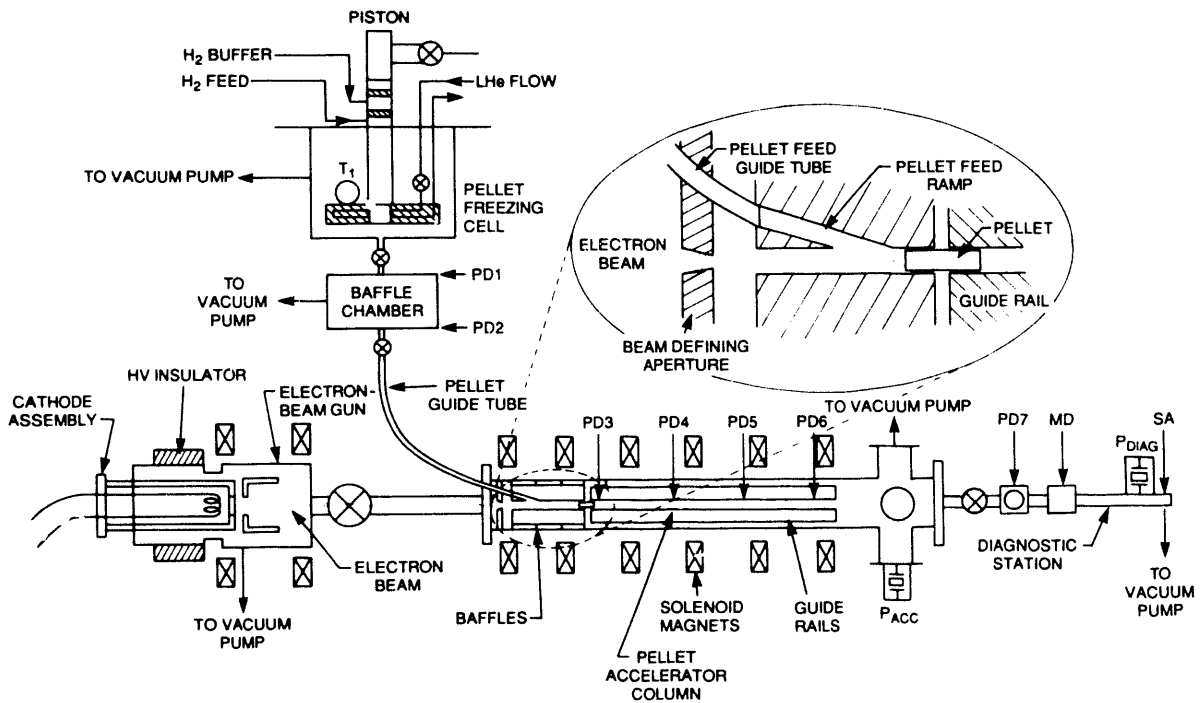


Fig. 4.1. Experimental setup for the e-beam rocket pellet accelerator.

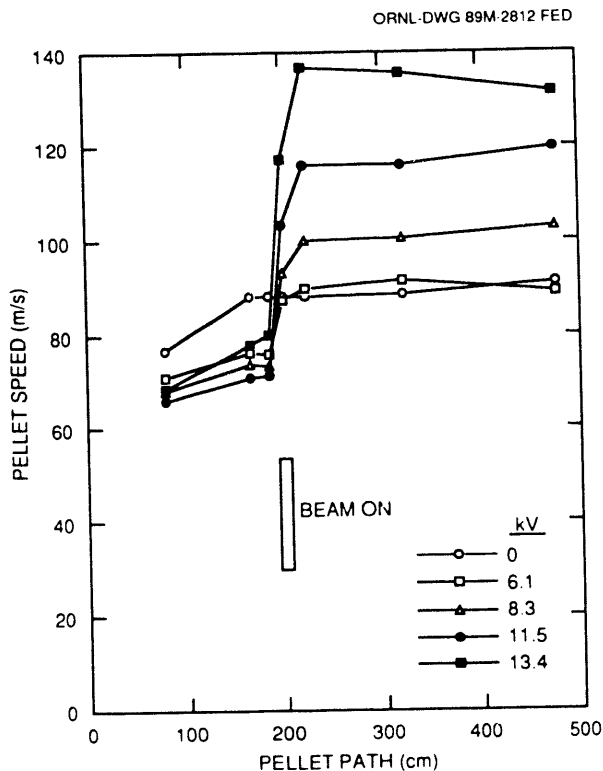


Fig. 4.2. Acceleration of pellets with e-beam rocket pellet accelerator.

a set of axial magnets for beam compression and confinement. The pellet maker can produce hydrogen or deuterium pellets by condensing a fixed amount of gas on a liquid-helium-cooled copper block, punching out the resulting frozen pellet with a mechanical plunger, and injecting the pellet through a baffle chamber and a guide tube into a pellet feed ramp. The innovative design of the pellet feed ramp loads the pellet from an off-axis trajectory in the guide tube into the accelerator guide rails. The pellet is constrained to travel down a set of three 0.6-m-long graphite guide rails. In this acceleration column, the pellet is ablated and accelerated by the electron beam.

The pellet monitors (see Fig. 4.1) include a television (TV) camera station at PD7 for imaging the accelerated pellet and light trip detectors PD1 to PD6, a microwave mass detector MD, and a shock accelerometer SA for measuring the pellet speed before and during e-beam acceleration. The distances of

the monitors from PD1 are as follows: PD2, 78 cm; PD3, 165 cm; PD4, 186 cm; PD5, 202 cm; PD6, 221.7 cm; PD7, 320.7 cm; MD, 356.3 cm; and SA, 475.7 cm. Detector PD7 triggers a nitrogen laser to illuminate the accelerated pellet. The TV camera then records the pellet shadow, thus measuring the pellet size. The microwave mass detector and the target impact shock transducer are also used to measure the pellet speed and size. The gate valves between chambers are closed to isolate the chambers after the pellet passes through. The measured pressures in the accelerator chamber and the diagnostic chamber can be used to determine the amount of pellet mass ablated during acceleration and the size of the accelerated pellet.

The initial results of the POP device indicate that:

1. The intense electron beam can accelerate pellets efficiently.
2. The solenoid magnet can compress, confine, and guide the electron beam during pellet acceleration.
3. Graphite is the appropriate material for all electrodes adjacent to the trajectory of the intense electron beam.
4. The baffle chamber between the pellet maker and the guide tube increases electron gun reliability during pellet acceleration.
5. The pellet feed ramp is suitable for repetitive pellet acceleration.

To enhance the acceleration efficiency and the accelerated pellet integrity, encased-shell pellets produced from a upgraded pellet cryostat will be used to improve e-beam/exhaust gas coupling efficiency and to strengthen the pellet to allow higher acceleration forces. This acceleration technique can be scaled up simply by increasing the length of the acceleration column for injecting ultrahigh-speed pellets. Alternatively, a multistage accelerator with an axial pellet feed and an off-axis electron gun could be used. Figure 4.3 shows a conceptual ultrahigh-speed pellet injector that could use either a single-stage or a multistage e-beam acceleration scheme. It offers the flexibility of accelerating pellets of different lengths and reduces the transverse scattering angles of the accelerated pellets. With pumping modules distributed along the accelerator path and a differentially pumped drift tube, ultrahigh-speed injectors could be developed and used for continuous fueling of reactor plasmas.

4.1.1.2 CIT and ITER fueling

M. J. Gouge

Plasma fueling work in support of CIT and ITER is carried out in collaboration with the division's Fusion Engineering Design Center (FEDC) and is described in Sect. 6 of this report.

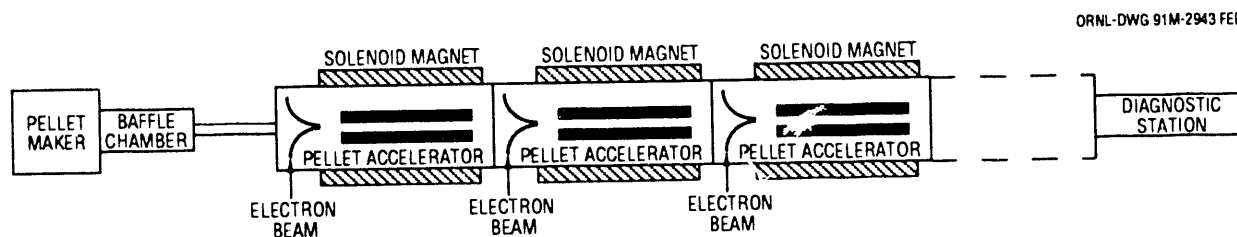


Fig. 4.3. Schematic diagram of e-beam pellet accelerator.

4.1.1.3 Tritium injector

P. W. Fisher

The TPOP experiment was built by ORNL to demonstrate the feasibility of forming solid tritium pellets and accelerating them to high velocities for fueling future fusion reactors. The TPOP injector used a pneumatic pipe gun with a 4-mm-ID, 1-m-long barrel. Nearly 1500 pellets were fired by the gun during the course of the experiment; about a third of these were tritium or mixtures of deuterium and tritium. The system also contained a cryogenic ^3He separator that reduced the ^3He level to $<0.005\%$. Pure tritium pellets were accelerated to 1500 m/s. Experiments evaluated the effect of cryostat temperature and fill pressure on pellet size, the production of pellets from mixtures of tritium and deuterium, and the effect of aging on pellet integrity. The tritium phase of these experiments was performed on the TSTA at LANL from January 1988 to August 1989.

The injector is now in temporary storage at TSTA until the next phase of experiments is ready.

The key to making good tritium pellets in a pipe gun such as that used in the present experiments is to produce tritium with very low ^3He levels. Good-quality pellets that could be accelerated without fracture to velocities of 1400 m/s (Fig. 4.4) had ^3He concentrations of $<0.005\%$. Each time fresh tritium was received from TSTA, or whenever a long period of time had passed without purification, a ^3He separation was performed. Tritium obtained from TSTA ranged from 3% to 13% ^3He . About 100 kCi of tritium was processed through the TPOP system during the course of tritium operations.

In over a year of tritium operation at TSTA, the pellet injector was operated safely with the support of TSTA systems and personnel. The offgas produced by the injector was purified and separated into its constituents for recycle by the TSTA system. This shows that pneumatic pellet

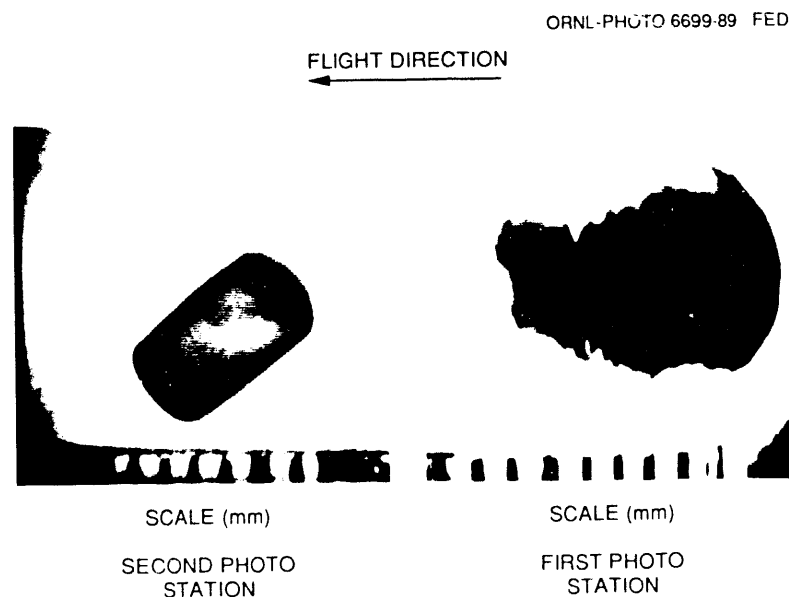


Fig. 4.4. 1400-m/s pellets formed by the TPOP injector.

injectors can be readily integrated into future reactor fueling systems. No failures or detrimental effects because of tritium, or any other operational parameter, were observed in the TPOP hardware during the life of the experiment. During the course of the work, the gun received several modifications (e.g., removing the collar heaters and lengthening the cooled section of barrel). These operations were performed on the contaminated system through the gloves. Maintenance of future tritium pellet injectors should be possible using similar techniques. Although tritium pellets can be routinely produced in a pipe gun with properly prepared tritium, continuous injectors will be required for future reactors. TPOP has clearly demonstrated the feasibility of producing and accelerating tritium pellets. However, the properties of tritium appear to be different enough from those of deuterium that any continuous injector design should probably undergo a prototype test with tritium before it is adopted for fueling a fusion reactor. Injectors with extruders may not require as low a ^3He level as the pipe gun. However, the extrudability of tritium and the design of continuous tritium-compatible extruders should be addressed in future phases of the TPOP experiment.

4.1.1.4 Two-stage light gas gun

S. K. Combs

As reported in last year's annual progress report and in several papers,⁵⁻⁷ speeds of up to 4.5 km/s have been recorded with 35-mg plastic projectiles (4 mm in diameter) in a small two-stage light gas gun, and the pipe-gun technique for freezing hydrogen isotopes in situ in the gun barrel has been used to accelerate deuterium pellets (nominal diameter of 4 mm) to velocities of

up to 2.85 km/s. However, experimental results indicate that the use of sabots to encase the cryogenic pellets and protect them from the high peak pressures will be required to reliably attain intact pellets at speeds of ≈ 3 km/s or greater. In 1989, efforts concentrated on the development of a repetitive two-stage device, concluding with the first demonstration of repetitive operation (ten plastic pellets fired at 0.7 Hz). The pellet frequency of 0.7 Hz is the design repetition rate for the ITER baseline pellet fueling system. In some limited tests, lithium hydride (LiH) pellets were accelerated to speeds of up to 4.2 km/s. The equipment and operation are described briefly, and experimental results and some comparisons with a theoretical model are presented.

Figure 4.5 is a schematic of the ORNL upgraded two-stage device; a facility photograph is shown in Fig. 4.6. Physical parameters of the guns and operating test ranges are listed in Table 4.1. Experimental data are summarized in Table 4.2, along with comparisons to a theoretical model. A 4-mm-diam pellet size was chosen for these tests since it is applicable to large present-day tokamak experiments; in fact, ORNL-supplied pellet fueling systems on both TFTR and JET are equipped with this pellet size. Thus, the projectile mass of interest is in the range of 5–20 mg (hydrogen, deuterium, and tritium ice have densities of 0.087, 0.20, and 0.32 g/cm³, respectively). The use of the sabot technique dictates heavier projectiles, depending on the specific design. As shown in Fig. 4.5, a 2.2-L reservoir provides the gas (typically helium) to accelerate the piston in a 1-m-long pump tube. The downstream gas is compressed as the piston travels down the pump tube and, thus, is driven to high pressure, which propels the projectile in the second driving stage. The projectile does not start to move

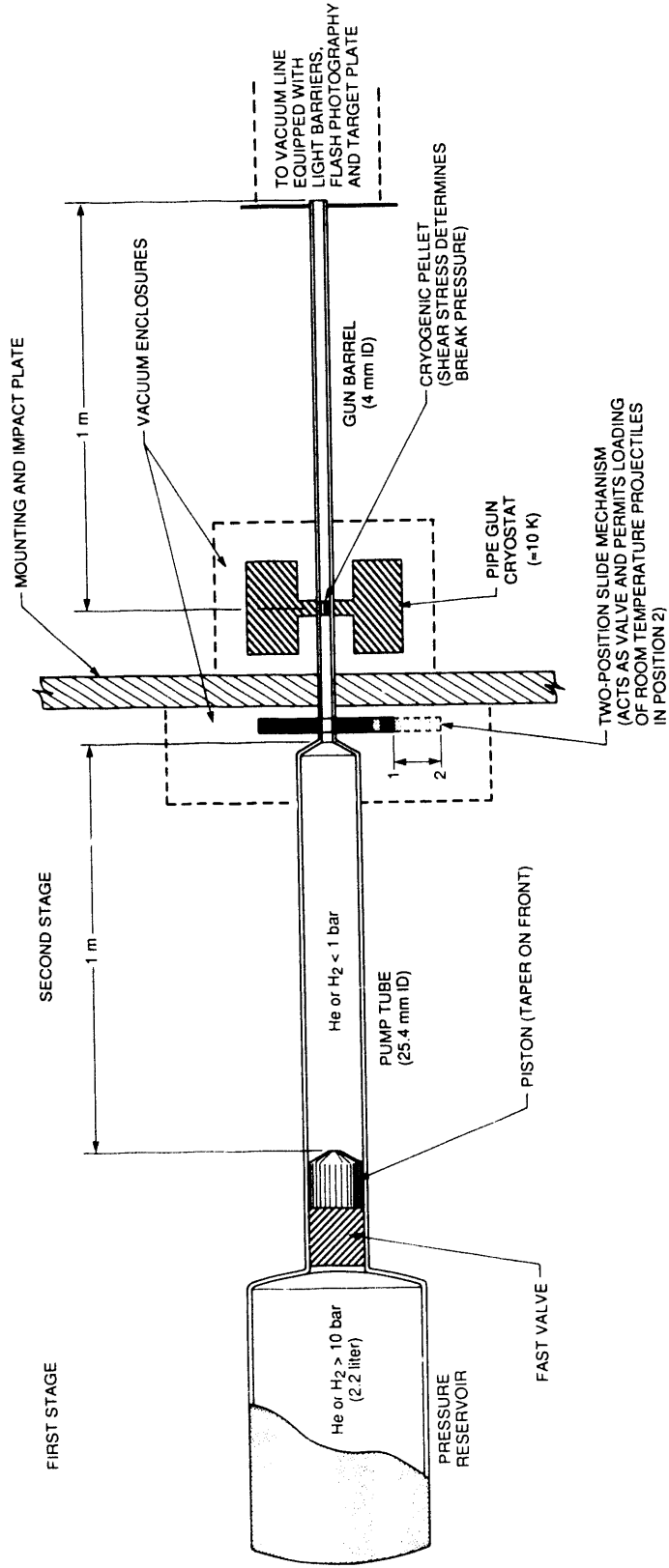


Fig. 4.5. Schematic of upgraded two-stage light gas gun.

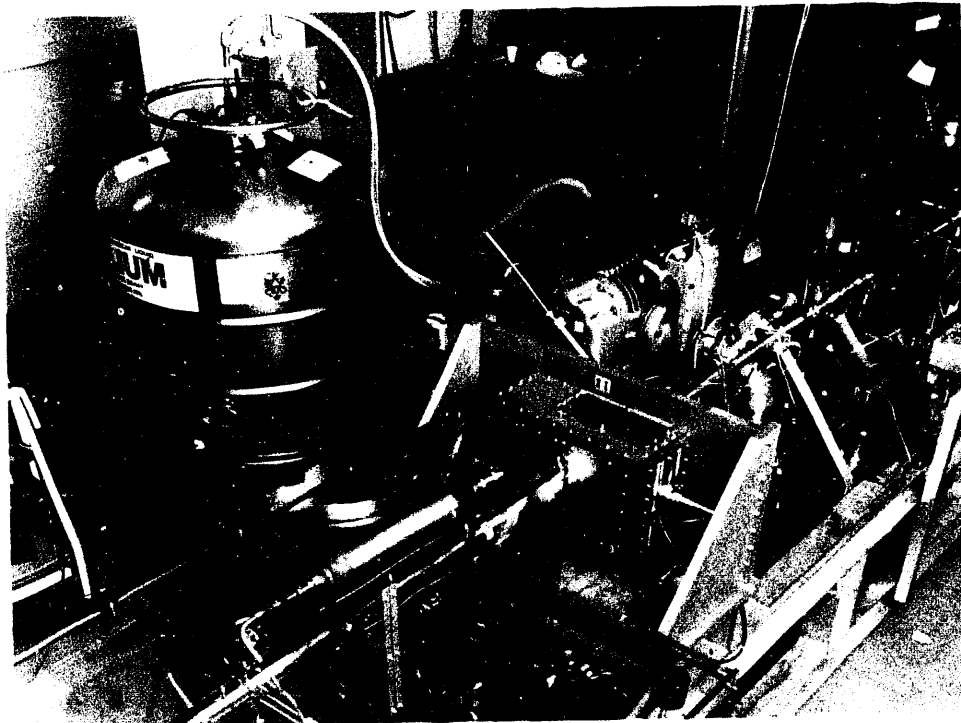


Fig. 4.6. Two-stage light gas gun facility.

Table 4.1. Parameters for ORNL two-stage light gas guns

First stage	
Volume, cm ³	2250
Length, m	≈0.42
Inside diameter, mm	≈82
Initial pressure, ^a bar	10–110
Activation mechanism	Burst disk or fast valve
Second stage	
Volume, cm ³	500
Length, m	1
Inside diameter, mm	25.4
Initial pressure, bar	<1
Gun barrel	
Length, m	1
Inside diameter, mm	3.9
Piston mass, ^b g	10–50

^aPressure in the first-stage reservoir before triggering of activation mechanism.

^bIncludes all piston weights tested in the ORNL experiments.

until the pressure is high enough to overcome the wall shear stress of the tightly fitting pellet (≈70 bar for nylon projectiles and 20 bar for hydrogen pellets); the pellet is then accelerated through the 1-m-long gun barrel into a vacuum injection line. A high-flow-type fast valve separates the two stages and acts to initiate the acceleration process.

The upgraded version of the gun incorporates some new design elements and offers operating options not commonly found on traditional two-stage light gas guns. In addition to the use of a fast valve in place of a rupture disk, a cryostat (inside a vacuum enclosure) was added to the gun barrel. Liquid helium flowing through the cooling channels of the cryostat, which surrounds the gun barrel, provides the capability of freezing hydrogen or deuterium pellets in situ. Another modification is a pneumatically activated, two-position slide

Table 4.2. Experimental data for test shots and results from gas dynamics model
Values in parentheses are inputs for or results from code calculations

	Shot number					
	1210	5041	5064	5088	5089	5165
Projectile	Nylon	Deuterium	Deuterium	Deuterium	Deuterium	LiH
Temperature, K	295	10	10	10	10	295
Projectile mass, mg	35	— (10)	— (10)	— (10)	— (10)	26
Piston mass, g	19.6	25.5	25.5	25.5	25.5	51.0 ^a
First-stage pressure, ^b bar	72.0 (51.7) ^c	13.8 (13.8) ^c	39.9 (34.8) ^c	38.3 (34.8) ^c	42.0 (34.8) ^c	66.4 (81.1) ^c
Second-stage pressure, bar	0.8	0.8	0.8	0.8	0.8	0.8
Peak pump tube pressure, bar	3670 ^d (4690)	— (180)	— (1600)	— (1600)	— (1600)	— (3350)
Piston travel time, ms	3.20 (3.24)	8.20 (8.00)	5.10 (4.85)	4.90 (4.85)	5.10 (4.85)	5.15 (5.14)
Maximum piston speed, m/s	— (391)	— (152)	— (265)	— (265)	— (265)	— (269)
Peak pellet acceleration, m/s ²	— (5.6 × 10 ⁷)	— (4.3 × 10 ⁶)	— (6.7 × 10 ⁶)	— (6.7 × 10 ⁶)	— (6.7 × 10 ⁶)	— (2.3 × 10 ⁷)
Pellet velocity, km/s	4.50 (4.88)	1.60 (1.63)	2.60 (2.75)	2.70 (2.75)	2.85 (2.75)	4.20 (4.00)

^aTwo 25.5-g pistons were used in pump tube for this shot; they were modeled as a single piston.

^bThis is not the reservoir pressure but the maximum pressure estimated from the output of the transducer located at the upstream end of the pump tube.

^cFirst-stage pressure for the code calculation; it was adjusted so that the calculated piston travel time closely matched the experimentally measured value; for shots 5064, 5088, and 5089, the same pressure was used, so the code results are the same.

^dFlat profile of pressure pulse at peak on this shot suggested that instrument or data acquisition may have missed maximum value.

mechanism (located inside a second vacuum enclosure). This mechanism essentially separates the pump tube and the gun barrel. For cryogenic operation, the slide acts as a shutoff valve in position 2 (Fig. 4.5) and separates the cryostat and pellet from the room-temperature helium propellant gas. It is moved into position 1 immediately before the gun is fired; the open hole in the slide bar is accurately aligned with the gun barrel. For room-temperature operation with plastic pellets, single projectiles can be loaded manually into the hole when the slide bar is in position 2, and the gun can be fired after the slide bar is returned to position 1.

A recent addition is an automatic loading mechanism that can be used to remotely load a pellet into the slide mechanism when it is in position 2. This loading mechanism can hold up to 36 4-mm-diam pellets (it could easily be modified to accommodate hundreds of pellets) and can be reloaded manually

within a few minutes. The automatic loading mechanism can easily load pellets at a rate of 1 Hz. O-ring-type seals and a pneumatic clamp provide adequate sealing at the interface between the pump tube, the slide mechanism, and the gun barrel during the firing phase, when high peak pressures are generated in the gun. The pneumatic clamp releases when the slide is moved to minimize the possibility of damage to the O-rings. Details of the mechanical design are not shown in Fig. 4.5.

Another two-stage gun using a bigger pump tube (41.3-mm ID) was also constructed in 1989 and will be used to evaluate the performance of a larger second-stage volume. Both experiments are equipped with instrumentation (not shown in figures) to evaluate gun performance. A programmable logic controller (PLC) and a CAMAC data acquisition system are used for precise control of the systems, for accurate timing,

and for recording and archiving the transient data for each shot.

In preliminary experimental tests, repetitive operation of the two-stage gun was demonstrated with 50-mg plastic pellets (3.9 mm in diameter by 3.5 mm long). The weight of these test pellets is probably close to the combined mass of a hydrogen isotope pellet and a sabot. The automatic loading mechanism was used to fire ten pellets at 0.7 Hz. The first-stage reservoir pressure was 100 bar for this series of shots; the second-stage initial pressure was 0.8 bar. Pellet velocities were consistent, ranging from 2.3 to 2.5 km/s. The equivalent speed of lighter deuterium pellets is 3.0 km/s, or greater, at similar operating conditions. In these tests, each pellet was remotely loaded and fired in an automatically controlled sequence. The preliminary results are encouraging and suggest that operation at ≥ 1 Hz is attainable.

In some limited tests, 3.9-mm-diam, 2.8-mm-long LiH pellets were shot with the gun. These pellets were machined from stock material at the Oak Ridge Y-12 Plant. The density of the material is 0.78 g/cm³; thus, the LiH projectiles weighed ≈ 26 mg. In shots 5164 and 5165, speeds of 3.2 and 4.2 km/s, respectively, were recorded. The corresponding pressures in the first-stage reservoir for these shots were 69 and 110 bar. The information for shot 5165 is summarized in Table 4.2. High-speed "impurity injection" of such materials has been proposed for studying transport phenomena in tokamak plasmas.

A two-stage Lagrangian gas dynamics code⁷ is used to model the interior ballistics of the two-stage light gas gun. Extensive computer modeling runs have been made for both nylon pellets (mass of 35 mg) and deuterium pellets (mass of 10 mg). Experimental data and some inputs to and outputs from the code are shown in Ta-

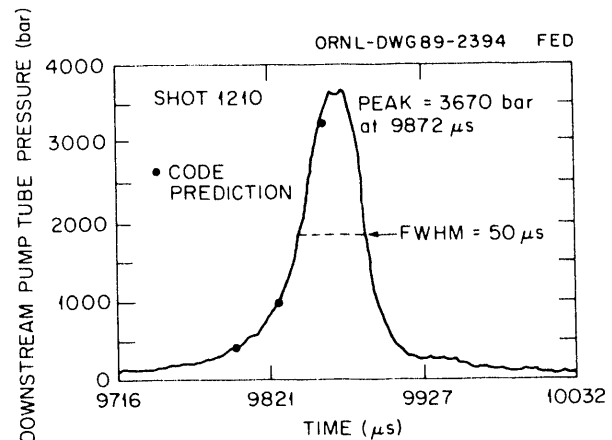


Fig. 4.7. Pressure measured at downstream end of pump tube during a high-speed shot of a 35-mg nylon projectile; calculated predictions from a gas dynamics code are also shown.

ble 4.2. As noted, the velocity in shot 1210 is the highest recorded to date (4.5 km/s). The code indicates that the gas is driven to temperatures approaching 10,000 K during the compression. Figure 4.7 is a comparison of the downstream pump tube pressure from the code calculations with the experimentally measured values. The estimated peak acceleration for this shot is 4.5×10^7 m/s².

In general, the code predicts the gun performance for deuterium pellets very well; calculated speeds are within 6% of the measured values, as shown in Table 4.2. For operation with higher pump tube pressures (as in shots 5064, 5088, and 5089), the maximum acceleration indicated by the code is 6.7×10^6 m/s². The pellet velocity and acceleration rate calculated from the code are shown in Fig. 4.8 as a function of the pellet position in the gun barrel. For many shots at these conditions and even at slightly lower first-stage pressures, broken pellets were observed at the gun muzzle. This is consistent with the acceleration limit of $(5-6) \times 10^6$ m/s² reported by other researchers.^{8,9} For reliable operation at

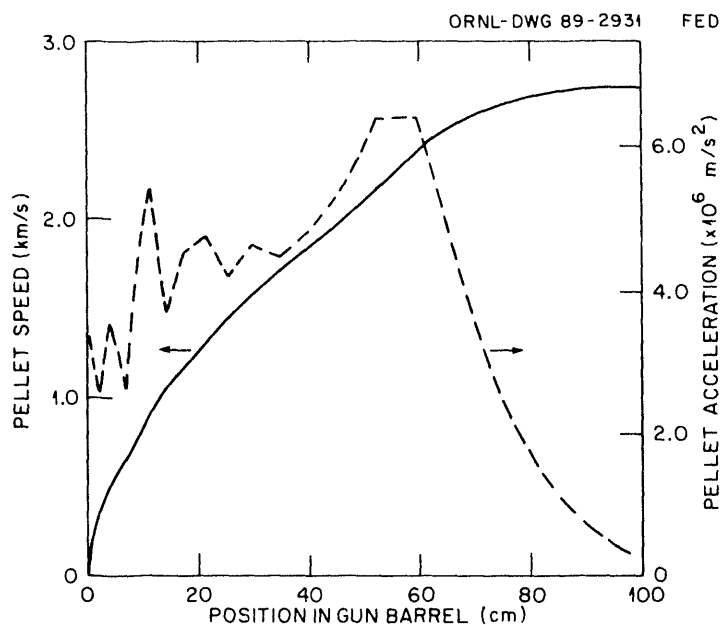


Fig. 4.8. Pellet velocity (solid lines) and acceleration (dashed lines) calculated from a gas dynamics model for a high-speed deuterium test shot.

higher speeds, protective sabots to encase the hydrogenic pellets will probably be required, as noted previously.

The code indicates that gas friction is the dominant nonideal effect, with heat transfer and piston friction accounting for only 10–30% of the total energy loss. This conclusion agrees with recent theoretical work at the Risø National Laboratory in Denmark.¹⁰ For the calculations presented here, the gas friction was determined by measuring the actual surface roughness e of the pump tube and gun barrel and then calculating a friction factor based on the local Reynolds number and the measured e/D , where D is the relevant pipe diameter.

The next major step in this development effort is to combine the two-stage gun with a cryogenic extruder for hydrogen ice. These components form the basis for a repetitive gun that can perform at rates of ≈ 1 Hz or greater and accommodate sabots.

4.1.2 Pellet Injector Applications

4.1.2.1 ATF pellet injector

P. W. Fisher

An eight-shot pellet injector was installed on ATF during May 1989, and the first injection experiments were performed on May 15, 1989. Pellets were injected into ATF plasmas on six days in 1989. Injection experiments have been performed under a variety of operating conditions, including fields of 0.95 and 1.9 T. Hydrogen pellets have been injected into hydrogen plasmas. Deuterium pellets have been injected into plasmas heated with one and two neutral beams, into plasmas heated with ion cyclotron resonance heating (ICRH), and into plasmas heated with electron cyclotron heating (ECH) only.

A record stored energy was achieved with pellet injection on ATF for 0.95-T operation. A simultaneous stored energy of 10.5 kJ and a line-averaged electron number density of $3 \times 10^{13} \text{ cm}^{-3}$ were obtained using pellet injection with gas puffing at 0.95 T. A stored energy of 23 kJ has been obtained with pellet injection at 1.9 T. Multiple-pellet injection has been performed with up to three pellets injected during one discharge.

4.1.2.2 Tore Supra pellet injector

C. A. Foster

A centrifuge pellet injector was completed and delivered to the Tore Supra superconducting tokamak at Cadarache, France, as part of a cooperative research program between DOE and the French CEA. The pellet injector, which has been under development since 1986, was designed to fuel Tore Supra for 30 s. Cryogenic pellets of frozen deuterium are fabricated by a unique device (based on a liquid-helium-cooled rotating disk) and injected into a high-speed rotating arm made of a graphite epoxy composite. An acceleration track molded into the arm guides the pellet to the tip of the arm, where it is ejected at twice the peripheral speed of the rotor, which has been tested to tip speeds of 800 m/s. During 1989, the acceleration system and the pellet feed systems, individually developed and tested in previous years, were integrated; initial pellet acceleration tests were undertaken; several minor but important adjustments and improvements were made; reliability tests were performed; acceptance tests by the French staff were made; and the equipment was packed and shipped to Cadarache, installed on Tore Supra, and put into operation.

The improvements included a timing electronics modification, which adjusted for

changes in the critical feed timing; enlargements in the rotor entrance aperture and guide tube entrance aperture, which also increase the fraction of pellets accelerated; an ice scraper to improve the formation of the deuterium ice rim and eliminate a previous problem of the ice disk locking, which had prevented long-pulse operation; and the implementation of an extrusion system to rapidly reload the ice disk.

The system, as delivered, could make up to 100 pellets of variable mass at rates up to 10 Hz and accelerate them to a speed of 600 to 900 m/s. The reliability of the injector was improved so that, on a given shot, from 60% to 90% of the pellets were delivered. Further improvements in this parameter are envisioned, and a special circuit that detects a missing pellet and fires a replacement has been successfully implemented since the equipment was installed on Tore Supra.

A highlight of the year was the rapid and efficient installation of the equipment on Tore Supra. The equipment was designed as a complete package and constructed on a metal pallet. Therefore, a minimum amount of disassembly and reassembly was required for shipping. During a period of six weeks, the apparatus, which weighs two tons, went from an operational state in Oak Ridge, through crating and shipment to France, to setup on Tore Supra and operation from the Tore Supra control room under control of the Tore Supra computer system.

During 1990, the pellet injector will be used for combined long-pulse fueling and exhaust studies on Tore Supra. Initial experiments show promise for both the pellet injector and the pump limiter systems, which are also part of the DOE-CEA exchange program. Figure 4.9 shows a 9-s plasma discharge, which was fueled by four pellets, one of the first deuterium discharges made on Tore Supra.

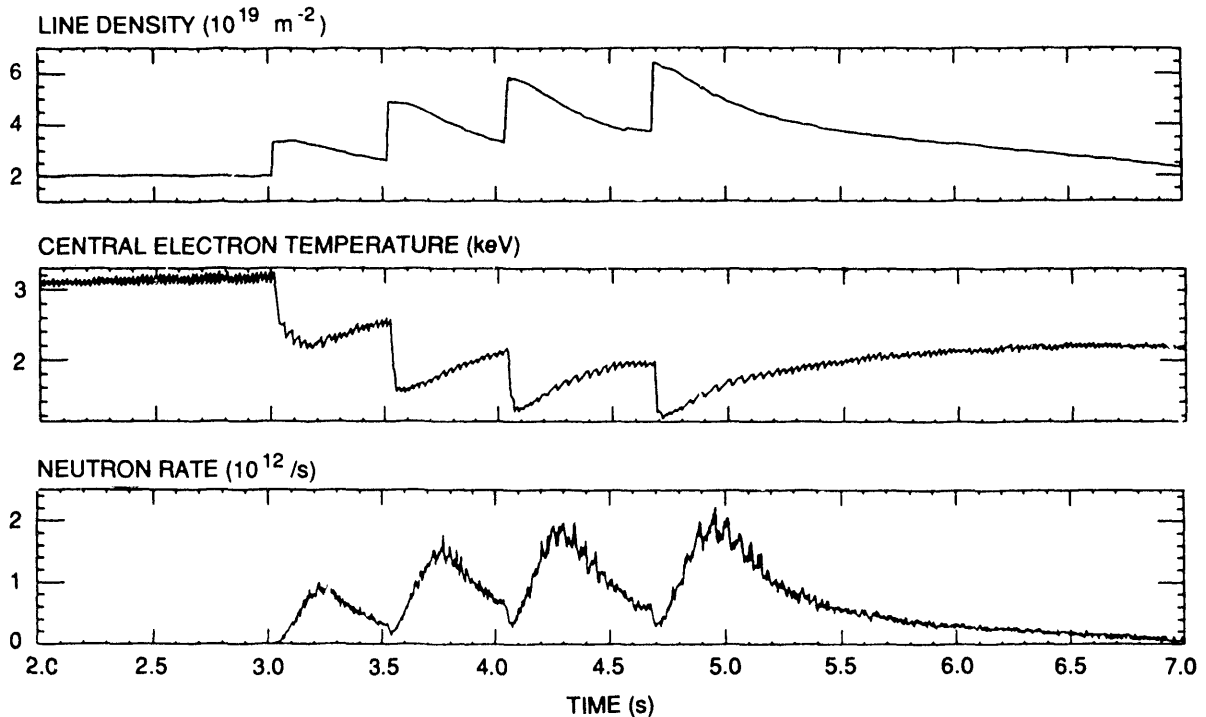


Fig. 4.9. Parameters of one of the first deuterium discharges on Tore Supra, fueled with four pellets from the ORNL centrifuge pellet injector.

4.1.2.3 JET

S. L. Milora

In 1989 ORNL was represented by permanent on-site members in the first phase of the U.S. DOE-EURATOM collaboration on pellet fueling on JET. Additional members of the ORNL physics team included members of the Plasma Technology Section and the Plasma Theory Section.

The initial phase of the experimental program (i.e., the first operational period from June through October 1988) concentrated on the physics associated with peaked plasma density profiles obtained with rf and neutral beam heating at total heating powers of up to 20 MW in primarily 3-MA discharges. The objective of these experiments was to compare energy and par-

ticle transport during strong central heating with the results of edge heating experiments performed earlier on TFTR. A new regime of transient enhancement in performance in limiter plasmas (lasting up to 1.3 s) was obtained by fueling the discharge early in the current ramp phase by injecting multiple 2.7-mm or single 4-mm pellets. This technique produced plasma density peaking factors in the range of 2.6 to 5 with central densities of $(0.8-2) \times 10^{20} \text{ m}^{-3}$. At a power level of 20 MW and a central density of $6 \times 10^{19} \text{ m}^{-3}$, central ion and electron temperatures of 10.5 and 12 keV were achieved in 3-MA, 3.1-T discharges. Values of the fusion product $n_D(0)T_i(0)\tau_E$ in the enhanced confinement phase are in the range of $(1-2) \times 10^{20} \text{ m}^{-3} \cdot \text{kV} \cdot \text{s}$. The improved confinement has been associated with a reduction in transport coefficients in

the plasma core region, where the density profile peaking is most pronounced.

In 1989 the JET device underwent extensive modifications to provide a capability for beryllium evaporation on internal vacuum vessel surfaces and to install a full toroidal beryllium belt limiter. Plasma operations during the abbreviated physics campaign amounted only to about 50% of the 1988 level, but significant scientific progress was achieved, thanks in large part to the ease of operation with beryllium-gettered and limited discharges (resulting in reductions of the effective plasma charge by approximately a factor of two). During the brief run period from June to September 1989, pellet injection operations were extensive as the JET program was directed toward an early evaluation of the effects of the beryllium modifications on high-power discharges. Pellet injection was used in a total of 33 experimental sessions by the Limiter, H-Mode, and Beryllium Assessment Task Forces. For the most part, the experimental program emphasized fueling of high-performance discharges and attempts to extend the pellet-enhanced mode discovered in the 1988 campaign to the H-mode and higher current regimes. The density limit was increased substantially by the lower oxygen and carbon content of beryllium limiter discharges, and for the first time it was possible to inject pellets from the 6-mm gun. This was accomplished in both 4-MA X-point and 5-MA limiter discharges in which peak plasma densities of $3.4 \times 10^{20} \text{ m}^{-3}$ and $2.7 \times 10^{20} \text{ m}^{-3}$, respectively, were measured immediately after pellet injection. Pellet fueling of high-power discharges with auxiliary heating was also demonstrated for the first time on JET during experiments in which a series of 4-mm pellets was injected into a 10-MW neutral-beam-heated limiter discharge. By raising the power gradually as the density

was increased, it was possible to maintain relatively deep pellet penetration and central plasma densities in excess of $1 \times 10^{14} \text{ m}^{-3}$ during a 4-s fueling pulse.

One of the goals of the physics program in FY 1989 was to produce and heat peaked density profiles in H-mode discharges. Although a successful technique was not found to accomplish this in the short time available, good results were obtained in pellet-fueled H-mode discharges. The fusion product, $n_D(0)T_i(0)\tau_E$, was increased to $5 \times 10^{20} \text{ m}^{-3} \cdot \text{kV} \cdot \text{s}$ for electron and ion temperatures in the 7- to 9-keV range. This represents one of the highest fusion products obtained on JET to date.

ORNL assumed the lead role in two areas on JET: pellet ablation physics and particle transport modeling. In the former, a unique experiment was performed in which the pellet velocity was varied by a factor of three to determine the dependence on pellet velocity of pellet penetration. The penetration was found to vary according to the one-third power of the velocity, which is in agreement with the original neutral gas shielding model (as compared with the more recent plasma and neutral gas shielding model, which predicts a much weaker velocity dependence). This result has obvious important consequences for the CIT and ITER pellet injector development programs.

Several transport codes were used to analyze particle and heat transport during the decay phase of Ohmic and rf-heated JET discharges studied in the 1988 campaign. The PTRANS code was written by to interpret particle diffusivity from the six-channel interferometer and edge H_α data. Particle diffusivity D in the core of the plasma was found to depend on the density profile shape. For peaked density profiles (peaking factor > 2), a value of $D = 0.08 \text{ m}^2/\text{s}$ was inferred in the core region;

for peaking factors of ≈ 1.5 , D was found to be in the range of 0.2 to 0.3 m²/s. The shape of D is similar in Ohmic discharges and during the enhanced confinement phase of the auxiliary heating pulse. This is characterized by a low value (0.08 m²/s) in the central core that increases abruptly at $r/a \approx 0.5$ to ≈ 0.3 m²/s. No evidence was found for an anomalous inward particle pinch.

4.1.3 Pellet Projects: High-Speed Injector

M. J. Gouge

In 1989 a conceptual design for a high-speed impurity pellet injector to be used on TFTR was performed for PPPL. The basic device consists of up to four two-stage light-gas-gun injectors with tandem mounts on each side of the present deuterium pellet injector (DPI) on TFTR. The new single-shot injectors would use as much of the existing DPI subsystems as is practical, including vacuum pumping, control, and data acquisition systems. The injectors would inject carbon pellets (0.7 to 1.2 mm in diameter) and lithium/LiD pellets (1 to 2.0 mm in diameter) at speeds of 4 to 5 km/s for plasma perturbation experiments in high-temperature TFTR supershot plasmas. The baseline approach is to use a 4-mm-diam sabot with a C, Li, or LiD pellet payload of variable size from 0.7 to 2.0 mm. The present two-stage light gas gun used in the ORNL high-velocity development program has a 4-mm-ID barrel with a 25.4-mm-ID pump tube, so the performance extrapolation would be modest. A development issue is reliable separation of the plastic sabot from the impurity pellet payload before the pellet enters the tokamak. A backup approach is to use a small-diameter barrel sized for the actual pellet outer diameter,

which eliminates the complexity of sabot separation but requires smaller barrel sizes than have been used previously on two-stage light gas guns. Each gun will have at least a 30-shot magazine to allow about one day of remote operations. This design was presented to PPPL staff at a conceptual design review in September 1989; the design approach was endorsed, but the project was later deferred because of budget constraints.

4.1.4 Work for Others

M. J. Gouge

Several projects were undertaken in non-fusion areas or for external customers as summarized below:

- A four-shot pneumatic injector, previously used on the Princeton Large Torus (PLT) and the Texas Experimental Tokamak (TEXT), was loaned to Lawrence Livermore National Laboratory (LLNL) for use on the Microwave Test Experiment (MTX) tokamak (formerly Alcator-C). This injector was modified by LLNL to use the simpler pipe-gun geometry for pellet fabrication. We provided consultation and conducted a design review of this modification based on our successful eight-shot pipe-gun design used on the Princeton Beta Experiment (PBX) and ATF.
- Occasionally throughout the year, the two-stage pneumatic injectors were used to accelerate projectiles to high velocity for exploratory component damage and armor studies.
- A pneumatic fast valve and power supply were provided to the ORNL Metals and Ceramics Division to upgrade the velocity capability of its light gas gun for material erosion studies. A design for

a new single-shot, light gas gun capable of velocities in the range from 300 to 500 m/s was completed.

4.2 RF TECHNOLOGY

In the rf technology basic development program, new methods of attaching graphite tiles to Faraday shield tubes were developed and tested. Computational methods of quantitatively determining the effect of the Faraday shield geometry on magnetic shielding, change in antenna inductance, and reduction in phase velocity were developed, and the rf power dissipation distribution on the shield was calculated. Experimental studies on the Radio Frequency Test Facility (RFTF) with the development antenna showed increased electron temperatures, higher plasma potentials, and enhanced ion impact energies on the Faraday shield during high-power ICRH operation.

Significant advances in rf current drive technology were made by optimizing the geometry of the multiple-strap launcher array and by developing control circuitry and tuning algorithms to adjust and maintain proper phasing between the straps. The folded waveguide (FWG) successfully completed its high-power vacuum testing.

The two-strap ICRH antenna for Tore Supra was completed, tested, and shipped to Cadarache, France. Design work for a single-strap antenna for Alcator C-Mod continued, and design work was completed and fabrication begun for a four-strap fast-wave current drive (FWCD) phased-array launcher for the DIII-D experiment. We continued our experimental collaboration with PPPL, injecting a combined 4.5 MW of ICRH power into TFTR using both the PPPL (Bay M) and the ORNL (Bay L) antennas.

4.2.1 Basic Development

4.2.1.1 Faraday shield studies

T. D. Shepard, F. W. Baity, and
D. J. Hoffman

Faraday shield with nonbrazed graphite armor

A new, simpler method for attaching graphite tiles to Faraday shield tubes was investigated. Rather than brazing the tiles directly to the tubes, small radial holes were drilled through the tiles. Small metal rods were inserted through the holes, tack-welded directly to the surface of the tube, and then cut flush with the surface of the graphite. The method has two principal advantages: a broken tile may be easily replaced without disassembling the antenna at all, and the loose mechanical connection eliminates thermal stresses in both the tile and the tube. The primary disadvantage is that the thermal contact between the tile and the tube is poor, so this method might not be usable for long-pulse applications without some kind of modification to improve the thermal contact.

A sample consisting of a single, hollow, stainless steel tube (water-cooled) with six tiles attached was constructed. The sample was placed under vacuum and exposed to a hydrogen ion beam with a peak power density of 200 W/cm². The sample was exposed to 5000 2-s pulses at 10-s intervals and then to 333 3-s pulses, also at 10-s intervals. The beam power absorbed by the sample was 670 W. The graphite tiles glowed brightly when struck by the beam but were not damaged in any way. The graphite did not fracture, nor did it separate from the tube, and there was no evidence of thermal stress in the tube. We have not yet performed tests to determine the maximum pulse length that

this configuration can withstand. It is clear at this point that this configuration can be quite useful, at least in relatively short-pulse applications.

Effects of Faraday shields on ICRH antenna coupling

In a continuation of earlier work,¹¹ the transmission characteristics of Faraday shields composed of elements with triangular cross sections were investigated. The overall emphasis of this work is to understand how the shape of the current strap and the geometry of the Faraday shield affect the currents and voltages generated on an antenna for a given power, in order to provide guidance for antenna design optimization. A key issue in this study is the nonideal magnetic transmission property of Faraday shields, which reduces the amplitude of the coupled magnetic field in front of an antenna from that in the case where no Faraday shield is present. The motivation for studying shields with triangular cross sections is that such a geometry was recently proposed by Perkins¹² as a means for reducing impurity generation by ICRH antennas and is being considered for use in the antennas for the Alcator C-Mod tokamak.

A prototype shield was constructed and attached to the same antenna that was previously used to test a large variety of different strap/shield configurations.¹¹ The triangular shields were set up in a single layer with tips pointing inward (toward the current strap), in a double layer with tips of both tiers pointing inward (the Perkins configuration), and also in a single layer with alternating tip direction (the Alcator C-Mod configuration). Variation in the spacing between shield elements was also studied. In all cases, the measured magnetic field transmission coefficients were among

the lowest for all the shields we have tested. While this may seem disconcerting, in any particular antenna design there is a range of allowable shield transmission coefficients, depending on the maximum tolerable voltages and currents in the device. A particular shield design should not be ruled out because of low transmission coefficients unless the overall design of the antenna is considered. In fact, the actual design process involves a trade-off between the shield's transparency and its ability to protect the interior of the antenna against plasma bombardment. In general, the interior of an antenna is better protected by dense shield structures, and one would intuitively expect such structures to have low magnetic field transmission.

In a related study,¹³ we investigated the interaction between variation in current strap shape and variation in Faraday shield geometry, to see if the current strap and the Faraday shield geometry could be optimized separately. It was found that the optimization could indeed be done separately, in spite of the fact that the current distribution on the current strap was affected by the Faraday shield. This current redistribution effect was explained intuitively in terms of the diamagnetic eddy currents that flow in the surface of the shield elements in response to the component of the applied rf field normal to the surface of the element. These diamagnetic eddy currents have previously been cited to explain the nonideal magnetic shielding effect.¹⁴ An important observation that is particularly relevant to this study is that, given a fixed "density" of the Faraday shield (in terms of the fraction of the antenna surface area obstructed from view by the shield), the eddy current effect is reduced by using a large number of small shield elements rather than a small number of large elements. This consideration favors simple tubular Faraday shield elements like those

generally used for ORNL antennas. Larger shields would be needed to take advantage of the triangular shaping because of the need to avoid sharp corners for electrical breakdown and thermal and plasma erosion considerations.

In the Alcator C-Mod design, the shield elements are actually somewhat smaller than were the elements in our prototype. Also, the alternating orientation of the elements allows the Faraday shield to be relatively thin in overall dimension, so that the current strap can be closer to the plasma surface than with a two-tier structure. Thus, we expect that the C-Mod shield will have a somewhat low transmission coefficient, but that the trade-off between transmission and protection from plasma bombardment has been appropriately chosen, given the relatively harsh environment expected for high-density plasmas in C-Mod.

4.2.1.2 Plasma-materials interactions

J. B. O. Caughman and D. J. Hoffman

The plasma-materials interaction experiments on the RFTF for the single-strap antenna were concluded this year with some fascinating results. In 1988, measurements with a capacitive probe showed that the rf electric fields in the plasma were typically equal in magnitude to the electric field between Faraday shield elements. A sheath model of the modification in the ion velocity distributions of the edge plasma showed that these fields could result in substantially enhanced ion energies and increased ion temperatures. The principal work this year was to measure the plasma potentials and ion velocity distributions in front of the antenna and, through implantation techniques, the ion impact energy on the Faraday shield.

The experimental measurements¹⁵ largely confirmed the model's predictions. Figure 4.10 shows that the ion energy distribution of the plasma in front of the antenna had an upward shift and a broader profile as the rf power increased. The electron temperature increased commensurately. Figure 4.11 shows that the increased energy spread and upshift in average energy caused by the addition of rf power, as measured with a

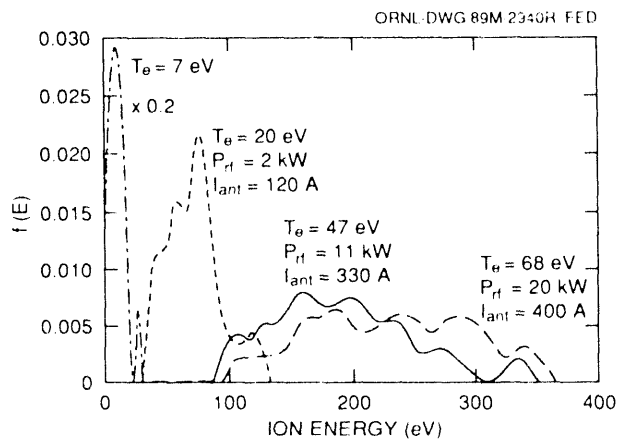


Fig. 4.10. The measured perpendicular ion energy distributions for various rf powers and antenna currents at a gas pressure of 1.5×10^{-4} torr.

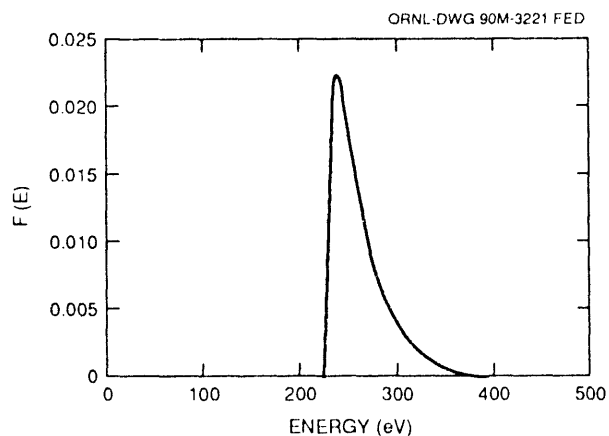


Fig. 4.11. Calculated ion energy distribution at the surface for a dc plasma potential of 189 V, an rf potential of 50 V, an electron temperature of 52 eV, and an ion temperature of 17.3 eV. This corresponds to the $P_{RF} = 11$ -kW case shown in Fig. 4.10.

gridded electrostatic energy analyzer, are in good agreement with the model.

While the plasma near the antenna could have enhanced ion energies from the rf power, one of the important parameters is the actual ion impact energy on the shield itself. This is the source of sputtering and antenna erosion. These ion energies were measured by placing samples of silicon on the Faraday shield and operating the antenna in a deuterium plasma. The trapped deuterium as a function of impact energy can be measured by using $D(^3\text{He},p)^4\text{He}$ nuclear reaction analysis. Figure 4.12 shows theoretical curves of fluence vs trapped fluence of deuterium in the shield. Sample biases vs a given fluence are in agreement with the curves. For the highest-power case, shown in Fig. 4.10, the impact energy was measured in the 500-V range, comparable to the measured ≈ 300 -eV average ion energy. Thus, the impact energies do relate to the measured and predicted ion temperature increases that are the result of the rf interaction with the electron and ion velocity distributions.

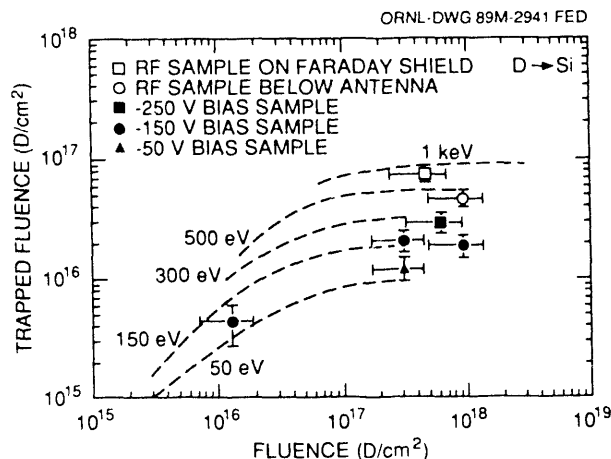


Fig. 4.12. Nuclear reaction analysis data for the experiment. Monoenergetic results (dotted lines) are also shown.

4.2.1.3 Fast-wave current drive

R. H. Goulding, F. W. Baity, W. L. Gardner, D. J. Hoffman, and P. M. Ryan

A series of proof-of-principle FWCD experiments in the ion cyclotron range of frequencies will begin soon on the DIII-D tokamak at General Atomics.^{16,17} These experiments will use a four-strap, 2-MW phased antenna array designed and constructed at ORNL (see Sect. 4.2.2.3). The elements in the array are phased in such a way as to couple to waves traveling in a single toroidal direction. Development work in support of this project included (1) an examination of the effect of changes in antenna geometry on the power spectrum generated by the array and (2) the design of a feed circuit for the array.

A full-scale mock-up of the DIII-D FWCD antenna array was constructed in order to determine the wave spectrum produced by the actual design geometry. It has also been used to determine the electrical characteristics of the array from a transmission line standpoint and to test the proposed configurations of the feed circuit for the array. In the drawing of the DIII-D antenna array shown in Fig. 4.13, the outer septa (between straps 1 and 2 and between straps 3 and 4) are not shown for reasons of clarity. The inner septum between straps 2 and 3, which is formed by the inner walls of the two antenna cavities, is shown, and horizontal slots can be seen that extend from the front of the septum to 1 cm behind the current strap. As reported previously, the slots act to increase the effective distance between the plasma and the return currents in the septa, which are 180° out of phase with the currents on the straps. This reduces the fraction of power coupled to waves traveling opposite to the desired direction.

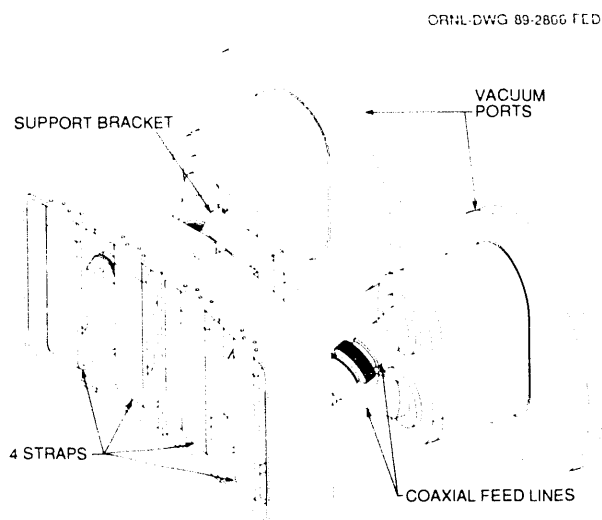


Fig. 4.13. The DIII-D antenna.

Measurements of the toroidal component of the rf magnetic field produced by the mock-up array were made in air using a loop probe scanned in the toroidal direction at a fixed distance (6 cm in front of the Faraday shield), corresponding to the approximate distance from the antenna surface to the nominal location of the magnetic field separatrix. The antenna was driven at 91 MHz with the currents on neighboring straps phased 90° apart. Figure 4.14 compares the power spectra calculated from the rf magnetic field measurements for cases in which the outer septa are either solid or slotted. When the outer septa are slotted, the fraction of total power in the positive-going peak increases from 43.6% to 53.0%, a significant increase. On the basis of this measurement, we decided to slot the outer septa on the actual antenna array.

An undesired feature of the slots in the septa is that they allow increased inductive coupling between straps, causing power transfer from one strap to another, which tends to unbalance the current amplitudes on the straps and increases the difficulty

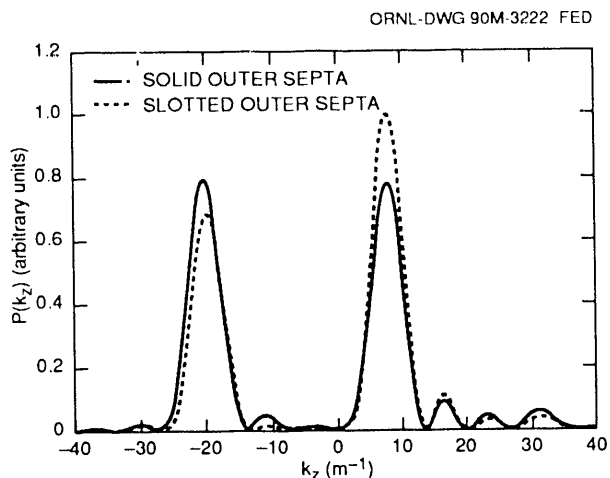


Fig. 4.14. Comparison of k_z power spectra for DIII-D mock-up with solid and slotted outer septa.

of tuning the system. We developed a feed circuit that produces arbitrary phasing between straps and equal current amplitudes on all straps despite strong coupling between them. A principal feature of the circuit is that the straps are fed using unmatched tees, allowing power transfer at the tees to compensate for power transfer between straps due to coupling. In this circuit, straps 1 and 4 are fed by a single tee and straps 2 and 3 are fed by a second tee. Single stub tuners placed between the current straps and the tees are used for prematching. They reduce the standing wave ratios in the lines, allowing the use of phase shifters to obtain the desired phasing between straps (Fig. 4.15). By properly setting these tuners and the accompanying line stretchers, equal currents are also produced on the straps and a $50\text{-}\Omega$ match is obtained at the inputs to the tees. The tees are fed in turn by a power splitter, using a "corporate" or parallel feed arrangement,¹⁸ and a third phase shifter is used to ensure proper phasing between the two tees. This circuit has been constructed using 3-in. rigid coaxial

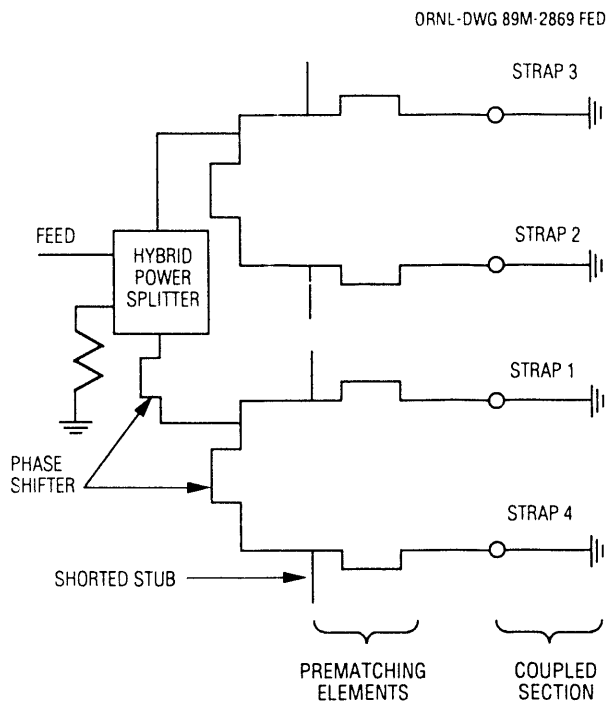


Fig. 4.15. Feed circuit schematic for the DIII-D FWCD array. The circuit allows arbitrary phasing between current straps.

transmission line and attached to the full-scale mock-up antenna. It has been operated successfully in air with no external loading, which produces the largest possible power transfer between straps and is thus the most stringent possible test.

Figure 4.16 shows measurements that were obtained in a test in which only the two central straps on the mock-up were powered using half of the circuit pictured in Fig. 4.15. At the desired operating frequency of 60 MHz, the desired current ratio of 1.0 and phasing of 90° are obtained. For the usual feed system in which each strap is matched separately and equal powers are fed to each, the current produced in strap 2 is measured to be a factor of five higher than that in strap 1 under the conditions in which the results of Fig. 4.16 were obtained. This system is unsatisfactory for

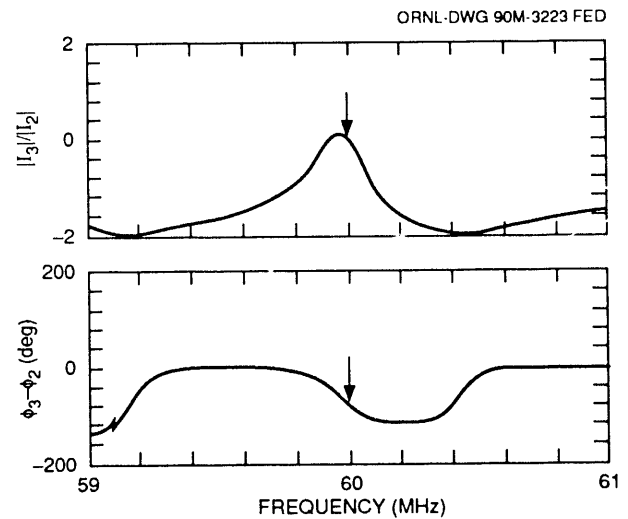


Fig. 4.16. (a) Current amplitude ratio and (b) relative phase as functions of operating frequency for straps 2 and 3 driven by the feed circuit in Fig. 4.15.

cases in which coupling between straps is large and/or plasma loading is low.

In conjunction with the development and testing of this feed circuit, a coupled lossy transmission line model has been developed to calculate tuner settings and aid in circuit design. This model has allowed accurate prediction of circuit behavior and can calculate required settings for all tuning components to within ~ 2 cm.

4.2.1.4 Folded waveguide

G. R. Haste, G. C. Barber, D. J. Hoffman, T. D. Shepard, and D. O. Sparks

Two types of probes, a magnetic pickup and an ionization detector, were mounted in the movable back plate of the FWG antenna for the low-power tests. The former was a simple loop, the latter merely a coaxial center conductor that could be biased to attract ionized particles. The magnetic

probe was used as an aid in tuning the FWG to the applied frequency. Figure 4.17 shows the probe signal as a function of the applied frequency. The frequency width of the resonance curve from this probe is useful in coarse tuning; once the waveguide is approximately resonant at the applied frequency, the reflected power signal is used for the final fine tuning.

One of the advantages that the FWG enjoys over the normal loop antenna is the low electric field at the front face of the launcher. The FWG and the normal loop antenna were compared with a capacitive probe that is sensitive to the rf electric field. Figure 4.18 shows that the electric

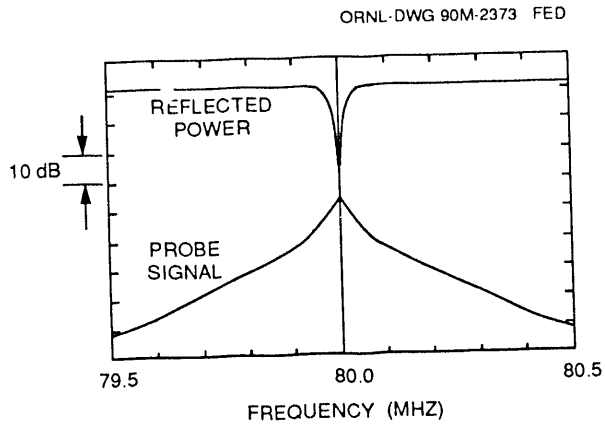


Fig. 4.17. Frequency scan of the folded waveguide, which has been tuned to 80 MHz. The upper trace is the reflected power signal, while the lower trace is the signal from the magnetic probe installed in the rear of the cavity.

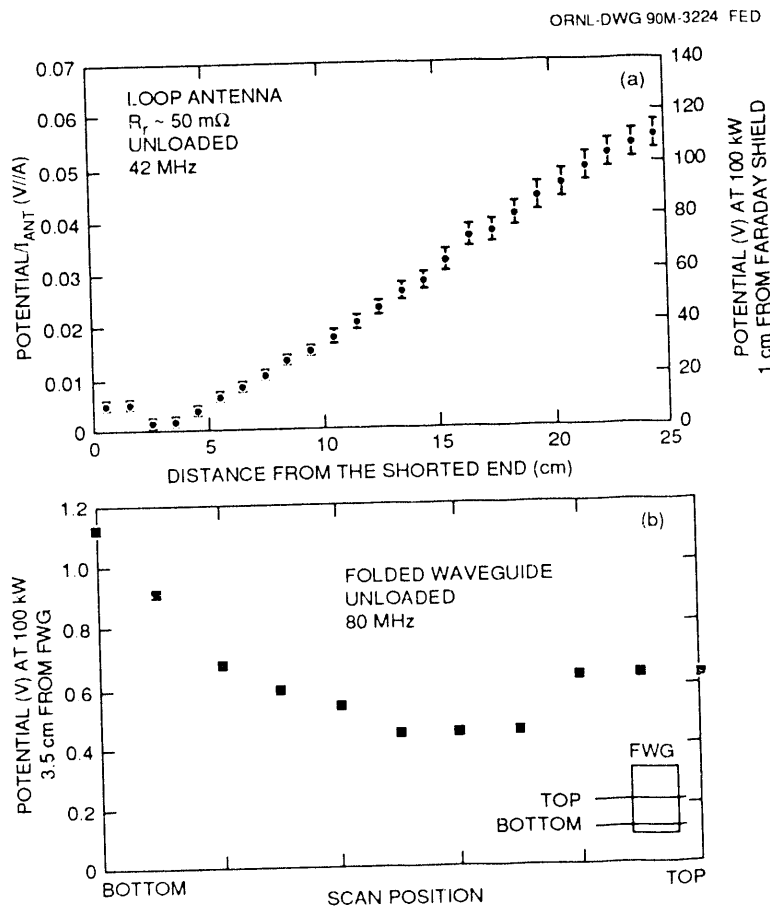


Fig. 4.18. Electric potential distribution developed (a) by a loop antenna and (b) by a FWG, each with 100 kW of input power. The capacitive probe is scanned in the poloidal direction, 1 cm from the Faraday shield of the loop antenna and 3.5 cm from the face of the FWG. For the FWG, the scan is from a position 7 cm above the edge of the FWG (bottom) to the middle of the FWG (top).

field is roughly two orders of magnitude lower for the FWG under comparable power conditions.

High-power testing in the separate vacuum chamber, discussed in the 1988 annual report, continued. Up to 13 kW continuous wave (cw) was applied to the FWG, but at that power level the waveguide temperature increased rapidly, necessitating termination of testing after 30 min. The FWG was moved to RFTF to continue testing to higher power levels. Multipacting was observed there as well as in the separate vacuum chamber, but it could be overcome with continued operation. After conditioning eliminated interior multipacting, visual observation of the front of the waveguide showed that exterior discharges were occurring. Again, continued operation caused this external multipacting to disappear.

Repetitive pulsing at successively higher power allowed operation at 140 kW for 50-ms pulses with a duty cycle of 6% and operation at 200 kW for 12-ms pulses with a duty cycle of 1.2%. For comparison, testing of the Tore Supra loop antenna was terminated at 500-ms pulses of 200 kW. The difference between the two was the lack of cooling for the FWG.

4.2.1.5 RF modeling

P. M. Ryan, K. E. Rothe, and
J. H. Whealton

Faraday shield rf power transmission

The Faraday shield is an integral part of an ICRH antenna, and its design has fundamental consequences for the antenna performance. The purpose of the Faraday shield is essentially threefold: (1) to protect the antenna from line-of-sight radiation from the plasma; (2) to exclude plasma from the immediate environment of the current

strap; and (3) to reduce the electrostatic coupling between the current strap and the antenna. The antenna designer needs to know the effect of a Faraday shield design on the antenna performance: its power transmission, its power dissipation, and its effect on the antenna inductance and capacitance.

A three-dimensional (3-D) magnetostatic analysis¹⁹ was developed to calculate the electromagnetic transmission properties of representative Faraday shield designs, particularly those intended for application on the ICRF antennas for Alcator C-Mod and CIT. The analysis uses the long-wavelength approximation to obtain a 3-D Laplace solution for the magnetic scalar potential over one poloidal period of the Faraday shield, from which the complete magnetic field distribution may be obtained. Once the magnetic field distributions in the presence and absence of a Faraday shield are known, the flux transmission coefficient can be found, as well as any change in the distributed inductance of the current strap. The distributed capacitance of the strap can be found from an analogous 3-D electrostatic calculation, enabling the phase velocity of the slow-wave structure to be determined.

Figure 4.19 shows a typical geometry for a double-tier Faraday shield mounted in front of a current strap in a recessed cavity. Magnetic scalar potentials of $\Psi_m = \mu_0 I_{\text{strap}}/2$ and 0 are applied to the plane of toroidal symmetry; these determine the magnitude of the strap current I_{strap} , although the distribution of this current around the strap is determined self-consistently from the boundary conditions. All other surfaces (metallic walls, Faraday shield elements, conducting "plasma," and poloidal symmetry surfaces) have Neumann boundary conditions on Ψ_m , which force the normal magnetic field component to vanish.

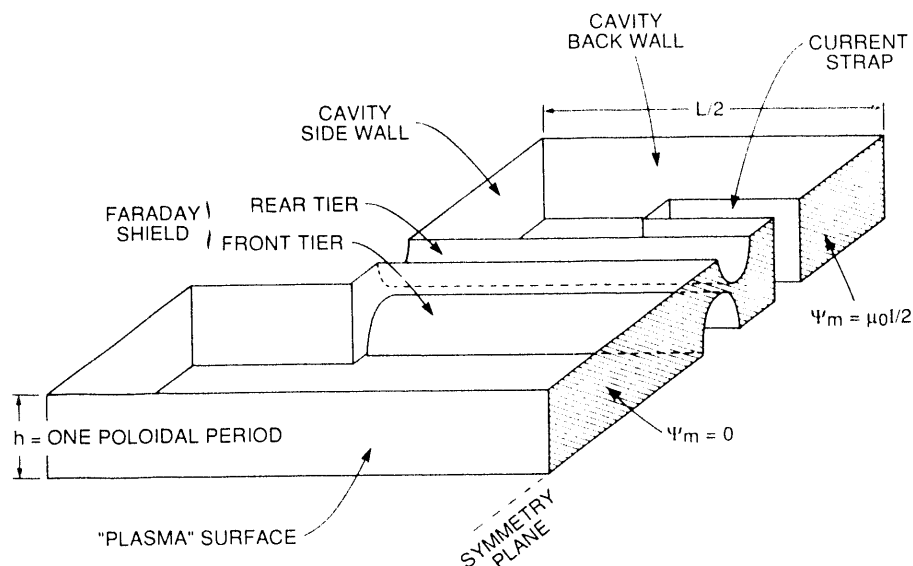


Fig. 4.19. The geometry used in the 3-D magnetostatic analysis, representing the current strap, antenna cavity, and Faraday shield over one poloidal period. The applied boundary conditions are explained in the text.

The flux transmission efficiency is found by comparing the flux to the plasma in the presence of the shield to that in the absence of the shield for the same strap current. This efficiency is dependent on cavity/strap geometry, since the presence of the shield redistributes the strap current toward the front of the strap, which has the effect of lowering the strap inductance and creating more magnetic flux for the same strap current. When this inductance change is taken into account, the result is the flux transmission coefficient, which is dependent only on the shield geometry. The power transmission coefficient is the square of the flux transmission coefficient, since the rf power delivered to the plasma is proportional to the square of the magnetic field.

The presence of the shield also changes the strap capacitance per unit length, much more drastically than the change in inductance per unit length, since the shield is designed to eliminate electrostatic coupling

to the plasma while keeping the electromagnetic coupling as high as possible. The capacitance per unit length can be determined by the same 3-D analysis and the same geometry as in Fig. 4.19, with a change in the boundary conditions. The strap is set to a constant electrostatic equipotential $\Phi = \Phi_0$, all other metallic surfaces are grounded ($\Phi = 0$), and Neumann boundary conditions are applied to all surfaces of symmetry (the normal electric field component vanishes). The capacitance can be determined from the resulting electric field distribution.

Table 4.3 compares calculated and measured power transmission coefficients and the changes in inductance and capacitance per unit length for some representative Faraday shield geometries; these measurements are discussed in Sect. 4.2.1.1. The calculated power transmission coefficients do not take into account the power dissipated in the shield from induced eddy currents, while the measured power transmission does. The

Table 4.3. Calculated and measured power transmission coefficients

	Geometry				
	Single-tier triangular	Double-tier "Perkins"	ORNL C-Mod (shield 10)	MIT C-Mod	"ASDEX"
Dimensions, cm					
Cavity					
Depth	24.4	24.4	10	15	10
Width	20	20	19	16	19
Strap					
Thickness	2.5	2.5	3.5	2	3.5
Width	8	8	5.5	7.2	5.5
Strap to shield	3.9	3.9	1.8	1.0	1.8
Power transmission (T_p)					
Measured	0.672	0.577	0.805	—	0.588
Calculated	0.775	0.697	0.840	0.667	0.687
Effective	0.718	0.583	—	—	—
$\Delta L'/L'$, %					
Measured	-3.0	-3.7	-7.5	—	-9.6
Calculated	-1.3	-1.8	-9.0	-15.7	-8.1
Calculated $\Delta C'/C'$, %	+24.5	+23.4	+109	—	—

calculated power transmission coefficient is modified by this dissipation to give the effective transmission, by a procedure discussed below.

Faraday shield power dissipation

The magnetic field component tangential to the Faraday shield is not compressed as the magnetic flux passes through the shield; it induces surface currents on the shield that flow around the circumference of the tier. The normal or perpendicular component of the magnetic field is compressed as the flux passes through the gaps of the Faraday shield; it induces currents that flow longitudinally along the length of the Faraday shield. This longitudinal current is highest in the narrow gaps, where the flux is most compressed and the surface magnetic fields are thus the highest. Because the total

surface current distribution is essentially divergence free, the divergence of the azimuthal current may be considered the source of this longitudinal current. Flux compression leads to large longitudinal currents and hence large divergences of the azimuthal current; that is, the tangential magnetic field on the plasma side of the shield will be lower than that on the strap side of the shield. It is this mechanism that governs both the flux transmission coefficient and the power dissipated in the Faraday shield.

Figure 4.20 shows an example of flux compression through a double-tier Faraday shield; Figs. 4.21 and 4.22 show the dissipated power distribution along the Faraday shield for an antenna designed for Alcator C-Mod, both without and with compression of the normal field. Clearly, the longitudinal currents flowing primarily along the gaps of the shield are responsible for most of the power dissipated in the Faraday shield.

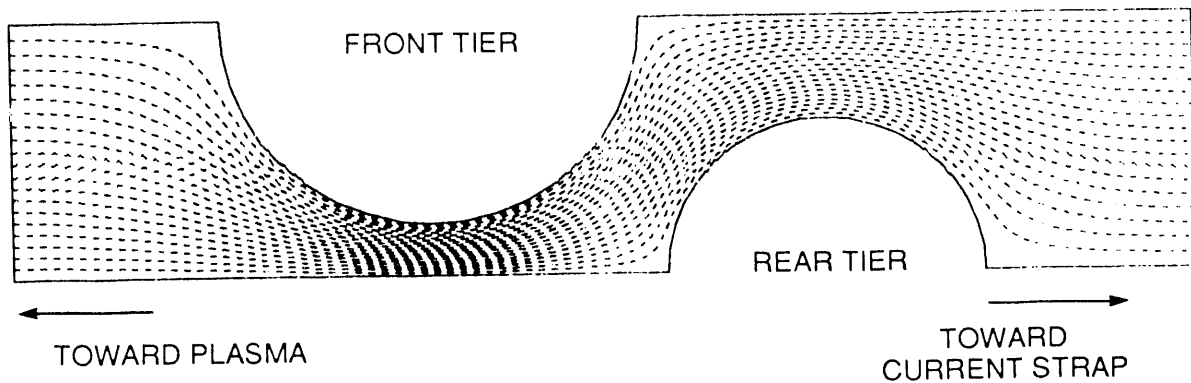


Fig. 4.20. Demonstration of the compression of magnetic flux as it passes through one poloidal period of a double-tier Faraday shield. The more compressed the flux, the higher the magnetic field, leading to larger surface currents in the Faraday shield.

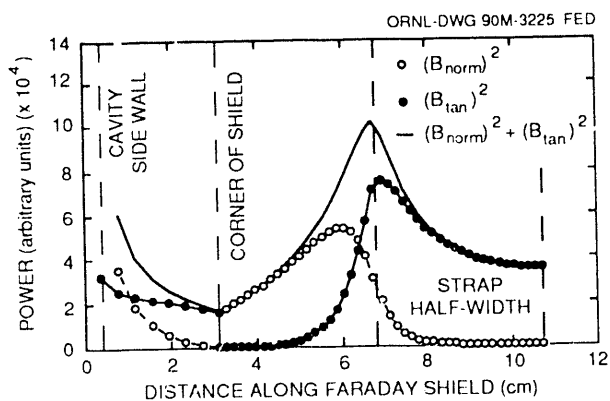


Fig. 4.21. The tangential and normal components of the magnetic field along the Faraday shield at a given poloidal position. The front of the shield extends from 3.1 cm to 10.8 cm (the centerline of the device), the current strap extends from 6.4 to 10.8 cm, and the side of the shield extends from 0.4 cm to 3.1 cm. Both components of the field are peaked near the end of the current strap, where the current distribution is peaked.

Antenna modeling

In 1989 the antenna modeling effort supported the design and evaluation of ICRH antennas for Tore Supra, Alcator C-Mod,

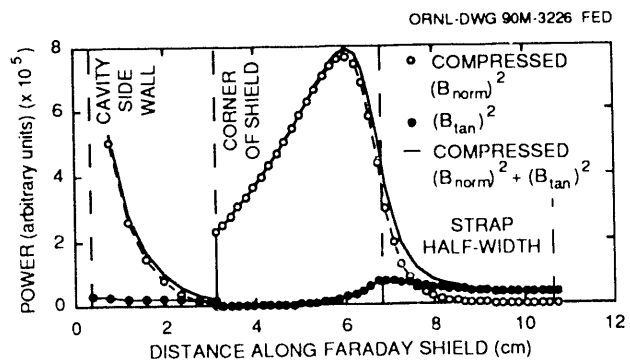


Fig. 4.22. The tangential and normal components of the magnetic field when the flux compression shown in Fig. 4.20 is taken into account. The tangential field is uncompressed and remains unchanged, while the normal field is greatly enhanced by compression and dominates the power dissipation.

ITER, and CIT and of FWCD launchers for DIII-D.

Multiple dielectrics

The two-dimensional analysis used for modeling rf windows and feedthroughs was modified to include multiple dielectrics and arbitrary geometries. In addition to these

areas, this analysis may be applied to rf and microwave sintering of ceramics.

4.2.2 RF Projects

4.2.2.1 Tore Supra antenna

F. W. Baity, G. C. Barber, W. L. Gardner, R. H. Goulding, D. J. Hoffman, R. L. Livesey, T. D. Shepard, and D. J. Taylor

As part of the DOE-CEA collaboration on the Tore Supra tokamak program, ORNL designed and built one high-power, long-pulse ICRF heating antenna for Tore Supra. This antenna, shown in Figs. 4.23 and 4.24, is one of three such antennas, which will be

used to inject up to 12 MW of rf power into Tore Supra for auxiliary heating of plasma ions. The antenna design is described in detail in Refs. 20–22.

Antenna assembly was completed in 1988, and an extensive testing program on the RFTF was begun. During the initial testing period, the Faraday shield incurred some damage during cw operation. This incident demonstrated the integrity of the cooling system design, since no water leak occurred despite the buckling of three Faraday shield tubes. The shield was modified by slotting the corners so that the uncooled top and bottom plates were decoupled from the cooled side plates to reduce the potential stresses in the tubes during long-pulse operation.

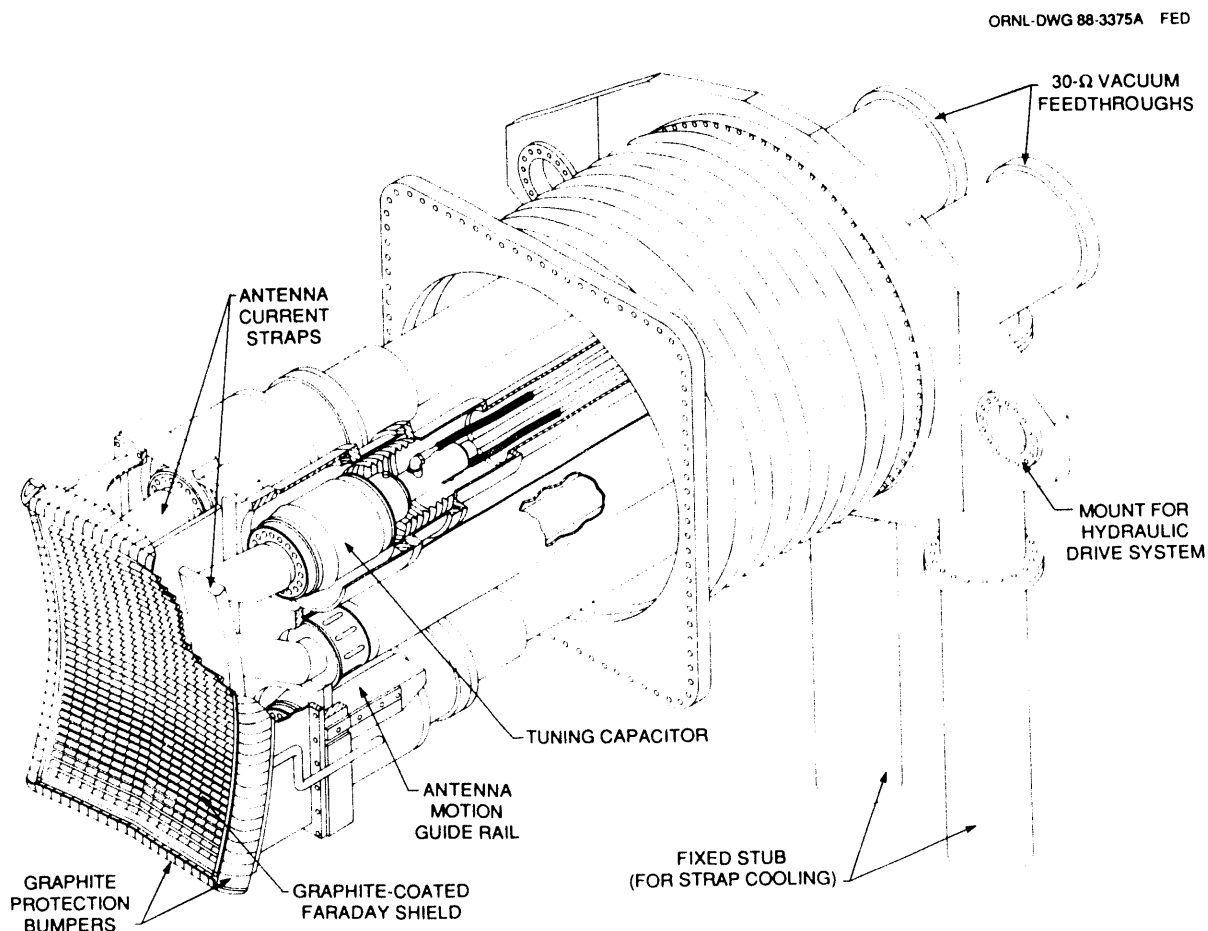


Fig. 4.23. Drawing of the Tore Supra antenna.

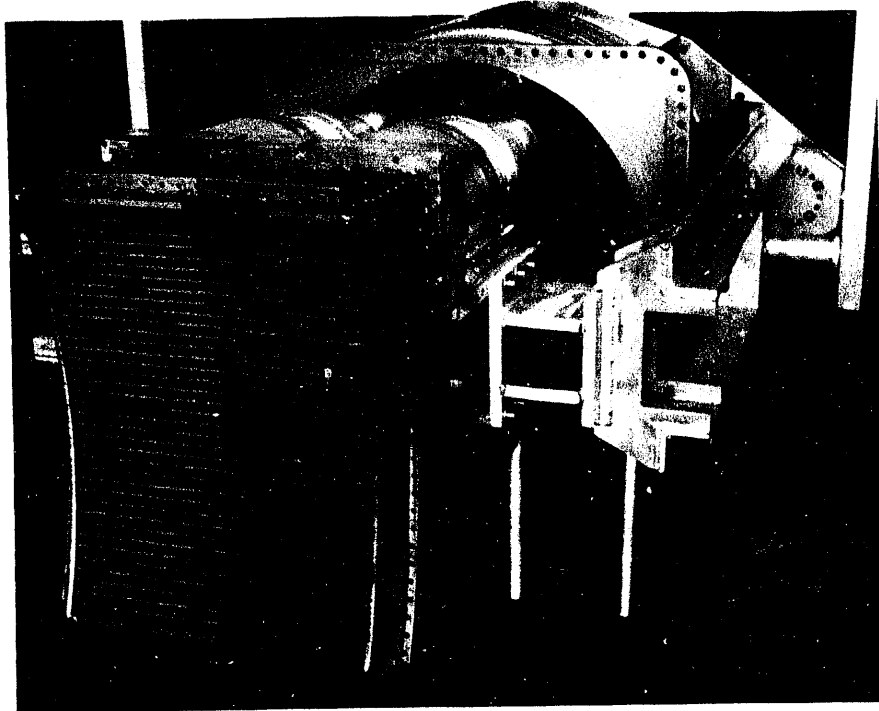


Fig. 4.24. Photograph of the Tore Supra antenna.

Tests showed that the voltage limit in vacuum for short pulses (<0.5 s) was higher than the design value of 50 kV. For long pulses, power was determined to be limited by Ohmic heating of the relatively low-conductivity Inconel septum separating the two antenna halves at the Faraday shield. After several options were examined, plasma sputtering was used to coat the bare part of the septum with copper. Subsequent tests demonstrated improved performance, although the septum heating was still the limiting factor in long-pulse operation of the antenna.

During tests in April and June, a problem developed with the finger contacts used to provide electrical connection between the vacuum capacitors and the antenna housing. The contact rings were modified, and the performance was verified in a final run on RFTF before the antenna was shipped to France in September.

After arrival in France, the antenna was disassembled for installation of new feedthrough ceramics and to have more copper deposited on the septum by plasma spraying. The antenna was then installed on a test sector of the Tore Supra vacuum vessel for final vacuum and rf testing before installation on Tore Supra in 1990.

4.2.2.2 Alcator C-Mod ICRF antenna project

R. H. Goulding, D. J. Hoffman, J. L. Ping, P. M. Ryan, D. J. Taylor, and J. J. Yugo

The preliminary design for a high-power-density, fast-wave ICRF antenna for use on Alcator C-Mod has been completed. The launcher is specifically designed to be prototypical of the launcher currently proposed for use on CIT²³ in as many

aspects as possible, and it incorporates many features of general interest for next-generation tokamaks. The antenna is a single-strap, end-fed configuration with the strap grounded at the center. It is designed to operate at power levels up to 2 MW, for pulse lengths up to 1 s, at a frequency of 80 MHz. It fits entirely within a 20- by 68-cm port and is radially movable over a 15-cm range.

Several notable features of the design make it well suited to application in next-generation tokamaks. It features a disruption support system able to withstand loads generated by a 3-MA, 3-ms disruption at 9 T, while allowing considerable thermal expansion of the antenna box relative to the port in which it is located or, conversely, contraction of the port with respect to the antenna box. The design of the disruption support structure allows installation or removal of the entire launcher, including supports, from outside the port, greatly simplifying remote maintenance.

The Faraday shield elements, which are cylindrical Inconel rods coated with titanium carbide, are designed to have very low primary thermal stresses, facilitating the handling of high power densities. In the CIT Faraday shield, these solid Inconel rods can be replaced by tubes, allowing direct liquid cooling of shield elements without changing the electrical characteristics of the shield design.

Ceramic feedthroughs are located outside the vacuum vessel, where exposure to ionizing radiation, which may enhance rf losses and seriously degrade the feedthrough life expectancy,²⁴ can be limited. There are no ceramic supports between the current strap and these feedthroughs.

The antenna is tuned and matched using an external resonant loop that employs integral capacitors to achieve a match at

the loop feed point. This system can handle power levels up to 2 MW/strap, while being compact enough so that the entire matching system can fit within the CIT shield wall, eliminating spurious resonances and power handling difficulties caused by long unmatched transmission line runs. It also allows tuning in two to three frequency bands without modifying the physical layout of the system.²³

A side view of the launcher, installed in the Alcator C-Mod vacuum vessel, is shown in Fig. 4.25. The primary vacuum feedthroughs and capacitive tuning elements are evident in the figure. A secondary vacuum feedthrough allows the entire external tuning loop to be run either under pressure or in vacuum in order to maximize power handling. A top view is shown in Fig. 4.26. It can be seen that the ends of the Faraday shield elements are bent by 90° before they enter the Faraday shield frame in order to reduce thermal stresses. These bends also form radiating side slots that increase the coupling of power to the plasma. The antenna is cooled by radiation and conduction to the backplane, which is cooled using either water or gas. This system is practical because of the low duty cycle, with 20 min between pulses. At the 2-MW power level, the average rf power flux through the shield is ~ 1600 W/cm². Preliminary calculations indicate that the maximum temperature reached by shield tubes in this case is 620°C.²⁵

Continued design work on this launcher has been suspended owing to budget constraints. However, the novel features in this design, including the low thermal stress, the bent-tube Faraday shield, and the high-performance rf feed and matching system, will very likely be incorporated into later loop antenna designs by the rf development group.

ORNL-DWG 89-2860AR FED

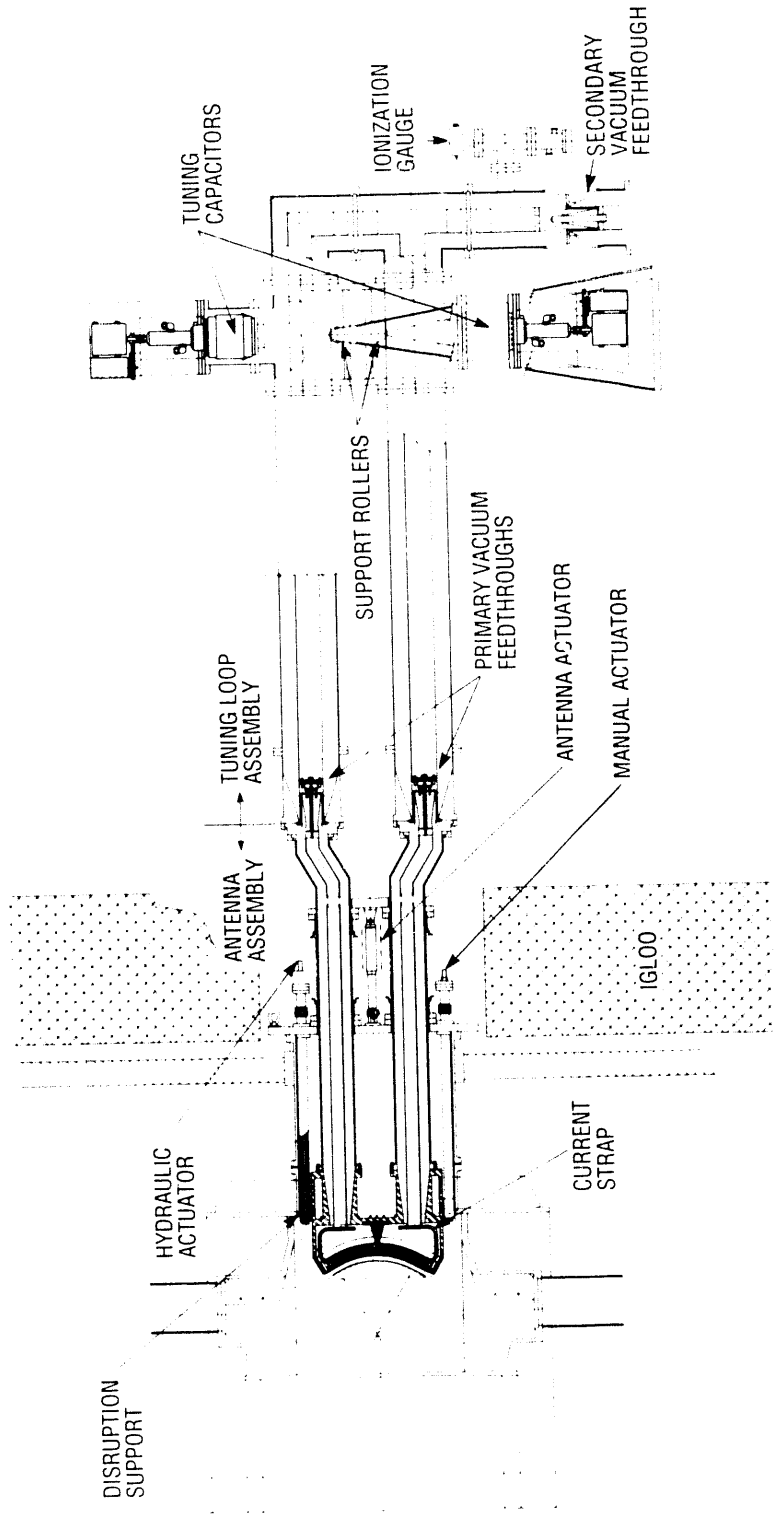


Fig 4.25. The ORNL antenna for Alcator C-Mod.

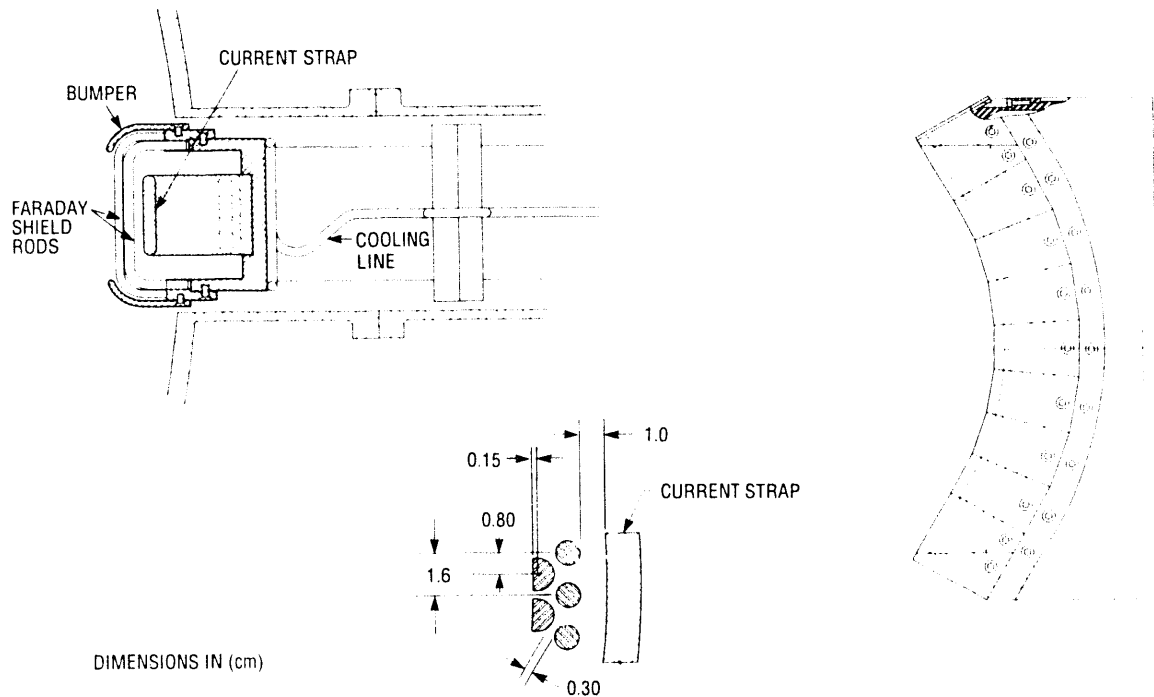


Fig. 4.26. Top view of the Alcator C-Mod antenna, showing the Faraday shield tubes.

4.2.2.3 Fast-wave current drive antenna for DIII-D

F. W. Baity, W. L. Gardner,
R. H. Goulding, D. J. Hoffman, R. L.
Livesey, and P. M. Ryan

Fast-wave current drive with ICRF power is an attractive candidate for driving a steady-state current in a fusion reactor and has recently been proposed for ITER. Fast waves in the ICRF offer the possibility of driving current efficiently in the center of a tokamak plasma, even under reactor conditions, using existing high-power rf sources.²⁶ A four-element loop antenna array for a proof-of-principle test of FWCD is being fabricated by ORNL for installation on the DIII-D experiment at General Atomics in San Diego in the spring of 1990.¹⁶ The array

will be mounted in a 1-m-wide recess in the vacuum vessel wall with poloidal loops oriented side-by-side in the toroidal direction and will be powered from a single 2-MW transmitter at 60 MHz. The mutual coupling between loops and the phase control circuitry have been designed to optimize the wave spectrum launched by the array at arbitrary phase angles.

A schematic drawing of the antenna is shown in Fig. 4.13. The relative phasing of the four straps can be controlled independently. For initial experiments the phasing will be fixed at 90° by the circuit shown in Fig. 4.27. Arbitrary phasing is possible with a different circuit.¹⁷ Algorithms to tune and impedance match the antenna array have been developed by modeling and confirmed on a full-scale mock-up of the DIII-D antenna. The mock-up antenna and 3.125-in. tuners are shown in Fig. 4.28.

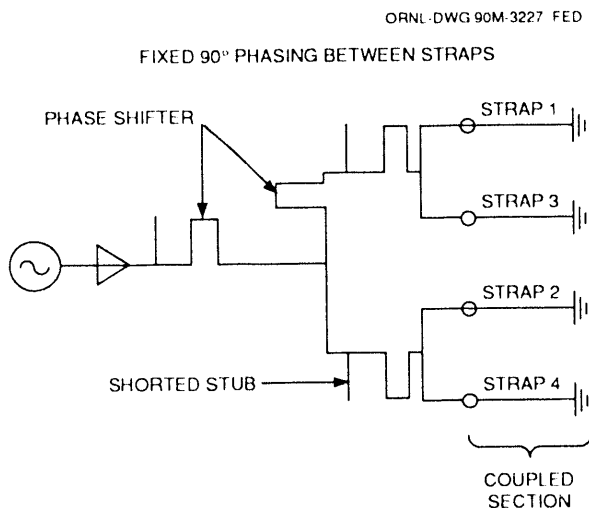


Fig. 4.27. Feed circuit to be used for initial experiments on DIII-D.

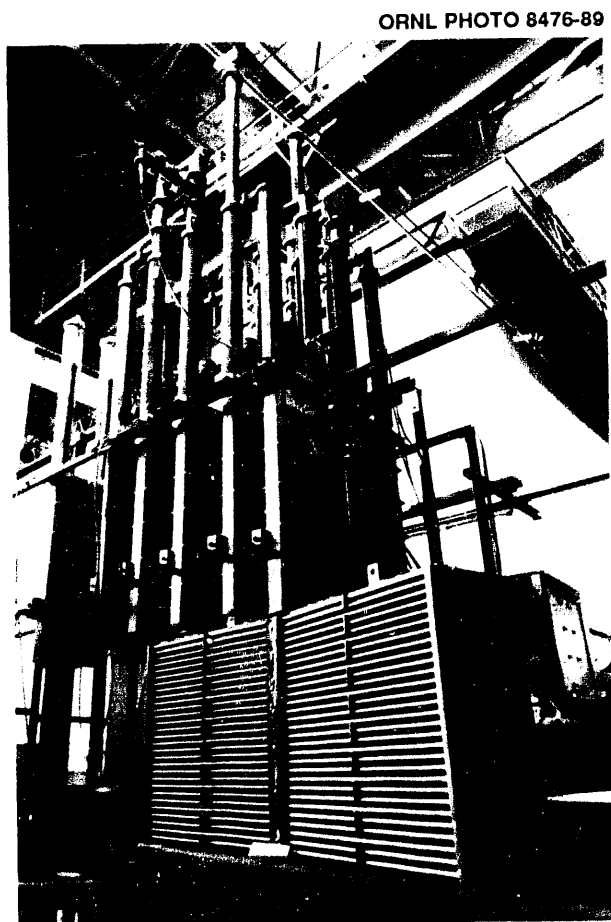


Fig. 4.28. The mock-up antenna and 3.125-in. tuners used for DIII-D modeling.

4.2.2.4 CIT antenna

D. W. Swain, F. W. Baity, R. H. Goulding, D. J. Hoffman, P. M. Ryan, and J. J. Yugo

Responsibility for the design, fabrication, installation, and testing of the ICRH system for CIT is shared by the Plasma Technology Section and the ORNL FEDC. Activities in support of this assignment are described in Sect. 6.1.3 of this report.

4.2.3 ICRH Experiments on TFTR

D. J. Hoffman and W. L. Gardner

The TFTR rf program explored a number of important plasma conditions, including rf heating of Ohmic, pellet-fueled, and beam-heated plasmas. A combined maximum power of 4.5 MW from the two antennas was launched into the tokamak, enough to begin some serious core heating. The target central densities ranged from $1 \times 10^{13} \text{ cm}^{-3}$ to $3 \times 10^{14} \text{ cm}^{-3}$, with electron or ion heating being observed in all cases. The principal physics results for the year were as follows:

1. Central heating was observed at virtually all densities.
2. We could run in a mode where sawteeth were stabilized by the rf power.
3. We achieved significant enhancement of the neutron production when pellets and rf power were combined.
4. Impurities injected from the antennas remained low for these rf power levels.

On the technological side, the details of the Bay L antenna's rf circuit were extensively measured and confirmed that we had indeed been operating at very high voltages. The capacitor system was changed to use high vacuum as the high-voltage insulating medium rather than SF_6 ; this increased the working voltage on the

capacitors to 60 kV, with the breakdown limit as yet untested. As a result of this improvement, we achieved a combined power of 1.7 MW into the antenna's pair of straps and 1.1 MW into a single strap (the second strap was temporarily disabled by an arc protection circuit failure, preventing us from applying power to it). The antenna itself has worked in excess of the design voltage and current, but the power is below the design value of 2 MW per strap because the coupling is low as a result of the very low edge density.

The next area of research will focus on the high-density mode, where we hope to achieve more central heating by increasing the combined power from both antennas to a total of 6–7 MW. Generally, we hope to achieve this by

1. increasing the plasma edge density,
2. moving the antennas closer to the plasma, and
3. increasing the antenna conditioning power.

4.3 NEUTRAL BEAMS

The rf quadrupole (RFQ) concept for high-energy neutral beams was further developed in a collaborative effort by AccSys Technology, Chalk River Nuclear Laboratories in Canada, JAYCOR, the University of Frankfurt in the Federal Republic of Germany, LANL, and ORNL. An architecture was produced for an ITER-relevant beam line that can capitalize on the highly developed volume negative ion source, and an experimental proof-of-principle demonstration proposal was developed. The proposal features a >1-MW, 2-MeV RFQ ion accelerator, using existing test facilities and power supplies for economy.

Further progress in the development of the volume negative ion source was made in

our collaboration with its inventor, M. Bacal. Diagnostics were developed to measure ion temperature within the source plasma. Analyses considering numerous atomic processes were made to establish operating points and directions for optimization. Experiments and analyses were performed to evaluate techniques used to reduce the electron density near the extraction sheath. These techniques, pioneered in the course of this three-year collaboration, are now used worldwide to improve the negative ion sources.

A volume negative ion source was also analyzed, and an explanation of rms transverse emittance of the extracted ion beam was provided. The anomalously high emittance at high currents was previously attributed to ion temperature in the source itself.

4.3.1 Ion Sources

M. Bacal, J. Bruneteau, R. Leroy, R. A. Stern, P. Berlemont, and J. H. Whealton

4.3.1.1 Enhancement of negative ion extraction and electron suppression by a magnetic field

Experiments on extracting negative and positive ions and electrons from a multicusp volume ion source were carried out. The effect of a transverse magnetic field in front of the plasma electrode was evaluated for three extracted species when the bias of the plasma electrons was changed. Also, the effects of the discharge current and of the pressure were determined. The experiments indicate that the magnetic field enhances the negative ion current and suppresses a great part of electrons from the extracted current. An explanation based on electron behavior in the magnetic field was proposed.²⁷

4.3.1.2 Measurement of the H^- thermal energy by two-laser photodetachment

The negative ion thermal energy was systematically measured using a new two-laser beam facility (see Sect. 4.3.1.3). The dependences of the negative ion temperature on discharge current (at constant pressure) and on pressure (at constant discharge current) were measured. The relationship between the negative ion temperature and the electron temperature was established using the data obtained in the center of the plasma at various pressures and discharge currents.

New results on negative ion extraction and electron suppression were obtained under higher transverse magnetic field conditions in the source extraction region by applying a method that we proposed in 1986. It was shown that with a transverse magnetic field of 60 G in front of the plasma electrode, and a suitable bias of this electrode, the electron component can be reduced to a small fraction ($\sim 20\%$) of the extracted negative ion current.²⁸

4.3.1.3 Analysis of the initial stages of H^- evolution

A study was conducted to establish the theory underlying the laser photodetachment technique for measuring the negative ion velocity in ion sources.²⁹ Results on H^- ion thermal velocities were obtained with a new two-laser beam facility (see Fig. 4.29). This facility consists of two identical laser oscillators, synchronized with a jitter of less than 1 ns and capable of generating laser pulses with variable delays ranging from 30 ns to 10 ms. We described an apparent effect of laser intensity, which turns out to be due to reflected laser light, and several data reduction problems. It was shown that the

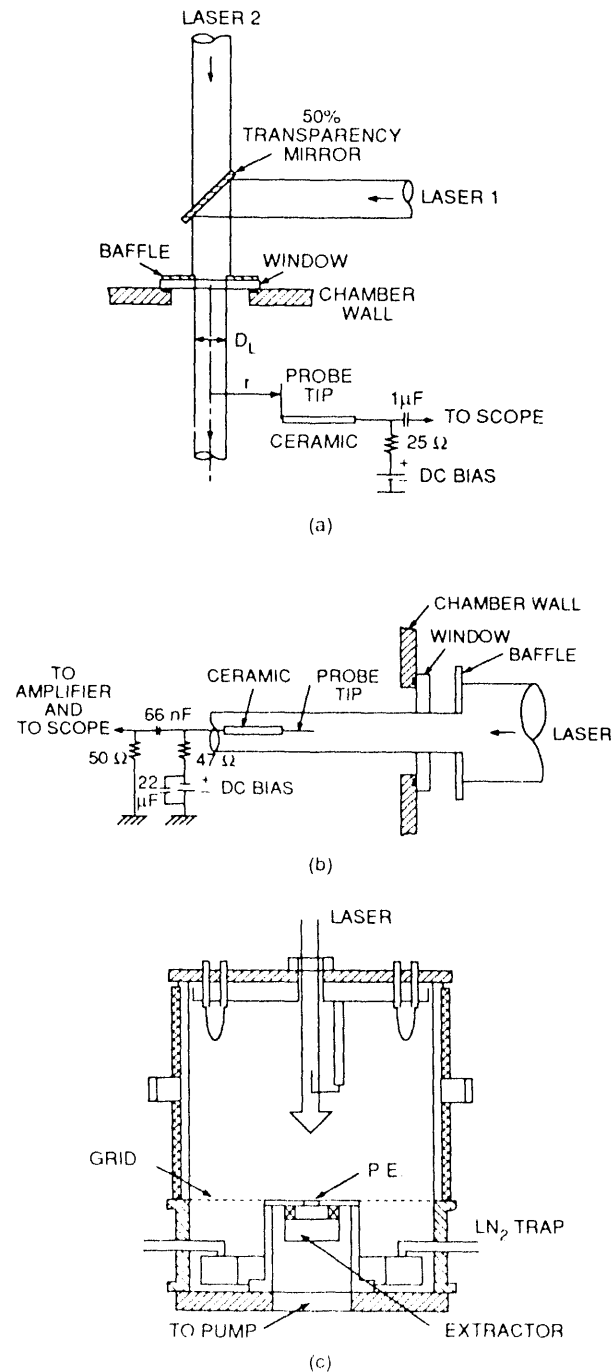


Fig. 4.29. The two-laser photodetachment experiment. In these experiments, the cylindrical probe, which was movable along the source radius, was coaxial with the laser beams. (a) Top view. (b) Side view. (c) Hybrid multicusp source, pumped through a single extraction aperture, with an area of 0.5 cm^2 .

H^- ion thermal velocity determined using this technique is independent of the laser beam diameter, and its value was reported for a particular source operating condition.³⁰

The causes of observed saturation of hydrogen negative ion current at high power in tandem volume sources were investigated using a zero-dimensional time-dependent model, which assumes that dissociative electron attachment to highly vibrationally

excited molecules is the main formation mechanism of hydrogen negative ions. It was found that saturation resulted from a reduction in the density of molecular hydrogen as a result of dissociation.³¹ The mean free path of the vibrationally excited molecules for various destruction processes was evaluated during high-power operation of the source. The reactions of Table 4.4 are described and analyzed in Refs. 30 and 31.

Table 4.4. Production and destruction processes for vibrationally excited molecular populations

$H_2(v'')$ Production and destruction
$e + H_2(v'') \leftrightarrow e + H_2(v')$
$e + H_2(v = 0) \rightarrow e + H_2^* (B^1 \Sigma_u^+, C^1 \pi_u) \rightarrow e + H_2(v'') + h\gamma$
$H_2^+ + e(\text{surface}) \rightarrow H_2(v'')$
$H + H + \text{wall} \rightarrow H_2(v'') + \text{wall}$
$H_2(v'') + \text{wall} \rightarrow H_2(v') + \text{wall}$
$H_2(v'') + H_2(v') \leftrightarrow H_2(v'' - 1) + H_2(v' + 1)$
$H_2(v'') + H_2 \leftrightarrow H_2(v'' - 1) + H_2$
$H_2(v'') + H \leftrightarrow H_2(v') + H$
$e + H_2(v'') \rightarrow e + H_2 \times (b^3 \Sigma_u^+, C_u^3, a^3 \Sigma_g^+) \rightarrow e + 2H$
$e + H_2(v'') \rightarrow e + H_2^+$
$e + H_2(v'') \rightarrow H + H^-$
$H_2(v'') + H_2^+(v) \rightarrow H_3^+ + H$
$H_2(v'' = 0) + H_3^+(v'' = 0) \rightarrow H_2(v'' = 5) + H_3^+$
Positive ion production and destruction
$H_2(v'') + e \rightarrow H_2^+ + 2e$
$H + e^- \rightarrow H^+ + 2e$
$H_2^+ + H_2(v'') \rightarrow H_3^+ + H$
$H^+ + e(\text{wall}) \rightarrow H$
$H_2^+ + e(\text{wall}) \rightarrow H_2(v'')$
$\rightarrow 2H$
$H_3^+ + e(\text{wall}) \rightarrow H_2(v = 0) + H$
$H_2^+ + e \rightarrow 2H$
$H_3^+ + e \rightarrow 3H$

Two negative ion sources (FOM³² and LBL³³) for which H₂(*v*'') vibrational spectra have been reported were studied with a numerical model. The model gives reasonably good agreement with available experimental measurements, with the notable exception of the vibrational spectra. There are significant quantitative differences at the higher *v*'' levels, but also some intriguing qualitative

similarities. Some results are shown in Table 4.5.³⁴

The scaling of high-power sources was also studied. Gas dissociation and possibly vibrational cooling by thermal electrons appear to explain the saturation in negative ion production with increasing input power. The surface-to-volume ratio becomes an important parameter for high-power sources,

Table 4.5. Experimentally measured and calculated parameters for the FOM and LBL sources

	FOM		LBL	
	Measured	Calculated	Measured	Calculated
P_{fill} , mtorr	4.5	—	8	—
I_d , A	10	20	25	25
V_d , V	105/115	115	120	120
T_{mol} , K	390	500	—	500
T_{atom} , K	—	4000	700/7000 ^a	5400
$b(v'' = 1)$	—	2	—	2
γ_{H}	0.06	0.05	0.025 ^b	0.1
n_e , $\times 10^{12}$ cm ⁻³	0.26 ^c	0.39	1.6	2.0
$n_{\text{fe}}(\epsilon > V_{\text{dis}}/3)$, %	1.0 ^c	0.85	—	0.4
T_e , eV	1.3 ^c	1.6	2.5	2.0
V_{plasma} , V	2.9	4.6	—	1.8
Density, cm ⁻³				
H ⁺	—	1.1×10^{10}	—	4.6×10^{10}
H ₂ ⁺	—	10×10^{11}	—	3.1×10^{11}
H ₃ ⁺	—	0.28×10^{12}	—	17×10^{12}
H ⁻	8.5×10^9	6.8×10^9	—	5.2×10^{10}
H	1.0×10^{13}	1.1×10^{13}	1.0×10^{13}	1.0×10^{13}
H ₂	8.3×10^{13}	8.2×10^{13}	—	1.5×10^{14}
$T_{\text{vib}}(v'' = 0:1)$, K	2360	2500	—	4671
Density, cm ⁻³				
H ₂ (<i>v</i> '' = 0)	7.5×10^{13}	7.3×10^{13}	—	1.0×10^{14}
H ₂ (<i>v</i> '' = 1)	6.9×10^{12}	6.7×10^{12}	2.4×10^{13}	2.8×10^{13}
H ₂ (<i>v</i> '' = 2)	7.3×10^{11}	1.5×10^{12}	6.5×10^{12}	1.1×10^{13}
H ₂ (<i>v</i> '' = 3)	1.6×10^{11}	4.4×10^{11}	1.8×10^{12}	4.7×10^{12}
H ₂ (<i>v</i> '' = 4)	4.0×10^{10}	1.7×10^{11}	3.8×10^{11}	2.2×10^{12}
H ₂ (<i>v</i> '' = 5)	1.1×10^{10}	8.5×10^{10}	1.4×10^{11}	9.7×10^{11}
H ₂ (<i>v</i> '' = 6)	—	—	6.7×10^{10}	3.9×10^{11}
H ₂ (<i>v</i> '' = 7)	—	—	2.5×10^{10}	1.6×10^{11}
H ₂ (<i>v</i> '' = 8)	—	—	9.1×10^9	9.5×10^{10}

^aTwo temperatures distribution.

^bPostdischarge γ_{H} .

^cElectron measurements in a lengthened source.

since it affects the atomic recombination rate and the plasma density.³⁴

4.3.2 RFQ-Accelerated High-Energy Beams

W. L. Stirling, J. H. Whealton, and
W. R. Becraft

A conceptual design was developed for an RFQ-based neutral beam system for ITER (see Fig. 4.30). The 2-MeV beam energy was within the range of ITER specifications when the work was carried out. In addition, the prevailing experimental database demonstrates that ion acceleration to the 2-MeV level has been achieved, which may be applicable to future reactor-grade tokamaks. The beam line design takes advantage of preaccelerator pumping and a configuration that does not require a line-of-sight arrangement of the ion source to provide enough power density, so only one

port of ITER is used. Special features of the components are described here.

4.3.2.1 Ion source

An ion source based on existing technology can be used in this system. Future improvements may help but are not necessary. Existing sources can be used because pumping panels are placed immediately next to the exit of the ion source with low conductance limitations (see Fig. 4.31). This is possible because the source exit is at ground potential, thus permitting a large plasma transport region between the ion source and the RFQ entrance. Two points must be immediately acknowledged. First, existing ion sources do not meet the pulse length requirement. However, their current density and gas efficiency are sufficient. Second, opening up the region between the ion source and RFQ to permit adequate pumping places more severe requirements on

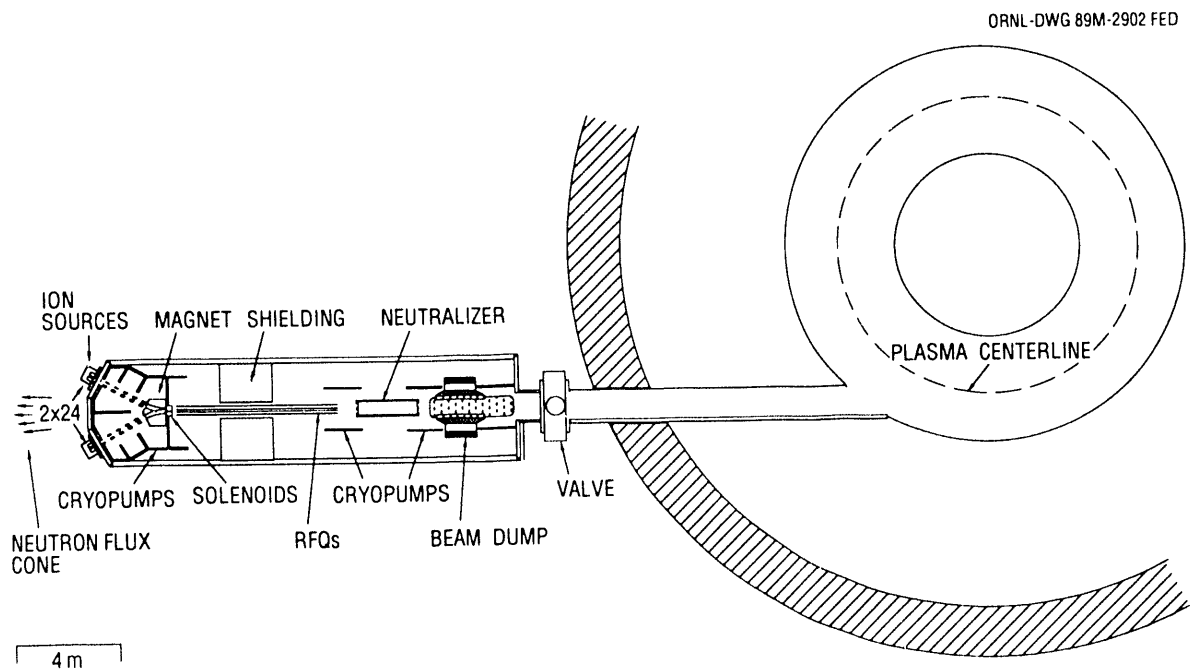


Fig. 4.30. Plan view of proposed 2-MeV, 40-MW rf beam line for ITER.

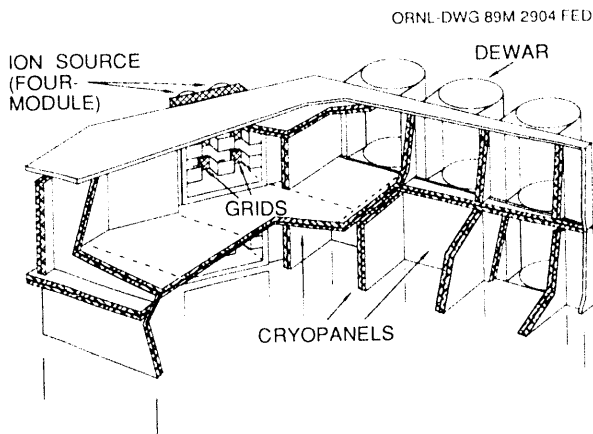


Fig. 4.31. Pumping panels for the ITER ion source.

the source beam optics than for a closely coupled system. However, the ion source is located out of the line of sight of backstreaming neutrons, thus protecting insulators and permitting (1) a shorter distance from the ITER shield to the ion source and (2) relatively close packing of the sources.

4.3.2.2 Low-energy beam transport system

The plasma low-energy beam transport (LEBT) system envisioned has an experimentally established database. Beam bending by the magnet uses well-known principles and permits removal of the ion source from the line of sight of the backstreaming neutrons. The magnet design must be capable of bending the beam and matching it to the focusing solenoid. The solenoids in turn must match the admittance requirement of each beamlet to its RFQ. The magnetic field required is less than 1 kG, and there is ample space to locate the magnet. Emittance growth in this region is an issue.

4.3.2.3 RF accelerator

The efficiency of the RFQ-based system—about 64% from wall plug to accelerated ion—is acceptable. The greatest uncertainties in the RFQ itself are the scaling of operating time from millisecond pulses to dc and the scaling of current capability from tens of milliamperes to hundreds of milliamperes. The design codes in use have been well validated in the current operating ranges, and these codes predict the operating scenario for the accelerator system described here. The issues of pulse length and beam current are addressed by the relaxation of the output beam emittance requirement and the high-current beam capability of the proposed four-rod system. The latter is possible since adiabatic bunching with simultaneous strong focusing is used.

Another important characteristic of the RFQ accelerator is the virtual immunity of the accelerator system (insulators) to damage from X-ray production. X rays degrade and destroy insulators and rf windows. However, these elements are (1) small, (2) located around bends, (3) far from the accelerator, (4) at low voltage points in the transmission line, and (5) located where they can be shielded.

4.3.2.4 Neutralizer

The plasma neutralizer is uniquely suitable for the RFQ because of the high current density achieved in this system. This high current density permits relatively small openings into the neutralizer, thereby minimizing the loss of plasma and gas. An issue with the plasma neutralizer is the degradation of the material used to confine the plasma, which can produce magnetic fields. It may be possible to locate this magnetic material outside the primary neutron flux volume.

4.3.2.5 Beam dump

The main issue for the beam dump is the neutron interaction with materials that produce a magnetic field—in this case, most likely an electromagnet. Depending upon size, required field, and stray field effects, it may be possible to locate the sensitive components outside the neutron flux cone.

4.3.3 Negative Ion Beams

J. H. Whealton and P. S. Meszaros

A preliminary analysis was made of an ion extractor/electron trap configuration;

results are shown in Fig. 4.32. This is apparently the only electron trap proposed for a low-field volume negative ion source that provides a transverse space-charge limit higher than the desired operating range (19 mA/cm^2 vs $10\text{--}15 \text{ mA/cm}^2$). It also appears from these calculations that the image charges in the electron trap produce aberrations in the beam that cause the beam rms emittance to grow sharply at the highest available (emission-limited) beam currents between 10 and 15 mA/cm^2 (Fig. 4.33). This observation is consistent with the experimental observations.

In contrast to the experimental findings, a self-consistent sheath analysis, validated

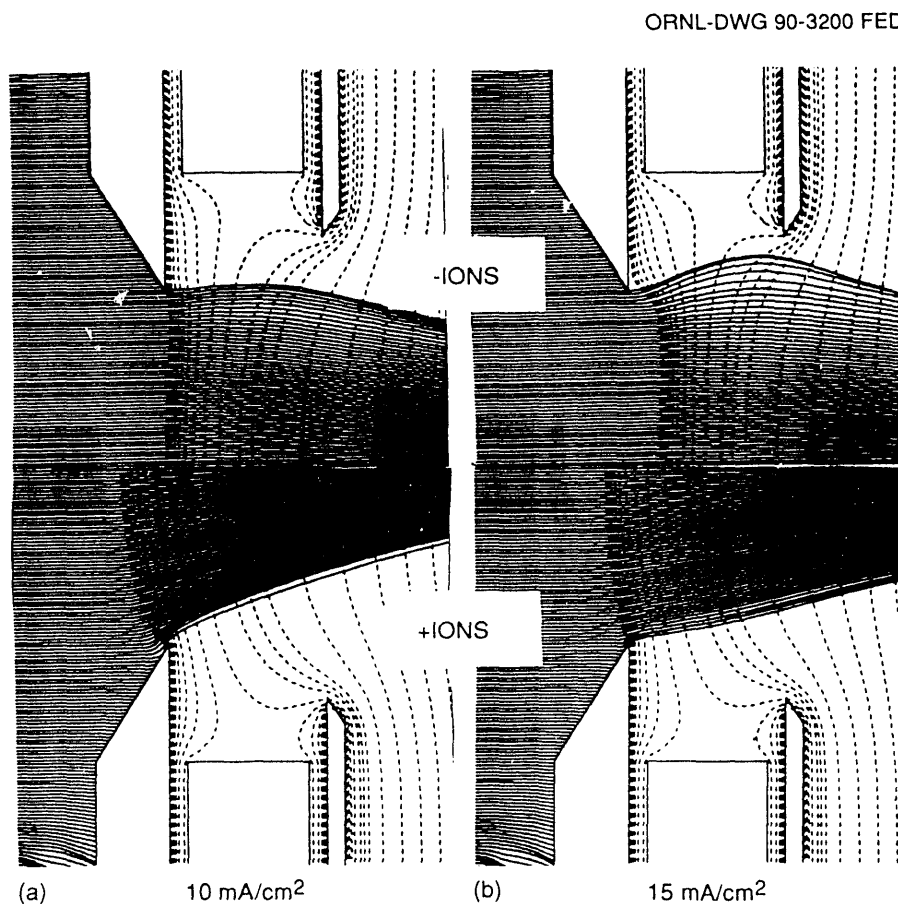


Fig. 4.32. Ion optics for validated positive and negative analysis at current densities of (a) 10 mA/cm^2 and (b) 15 mA/cm^2 . There are significant differences in sheath position and shape for positive and negative ions. Also, the negative ion beam is much closer to the nonlinear fringe fields of the electron trap for negative ions than for positive ions at the same current. This proximity produces significant rms beam emittance growth.

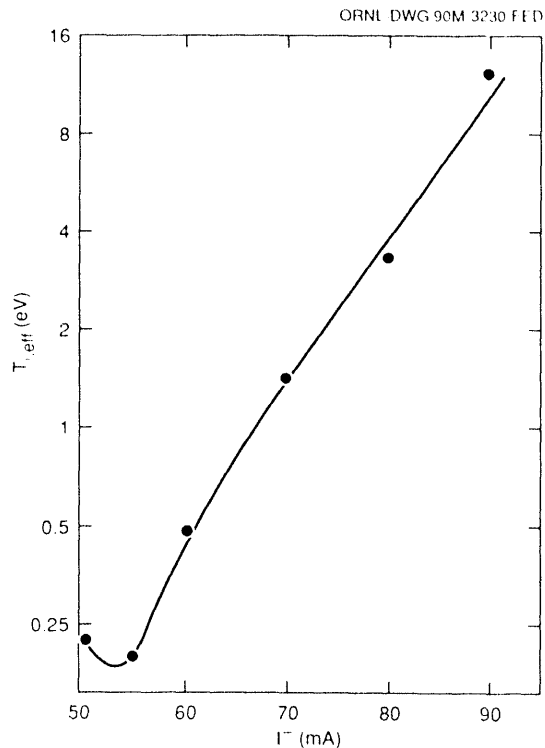


Fig. 4.33. Effective ion temperature vs beam current.

only for positive ions, shows that the beam emittance drops sharply in the same region (10–15 mA/cm²) and is little affected by

the electron trap fringe fields. The striking difference is shown in Fig. 4.32. Further analysis and optimization of this source might prove fruitful.

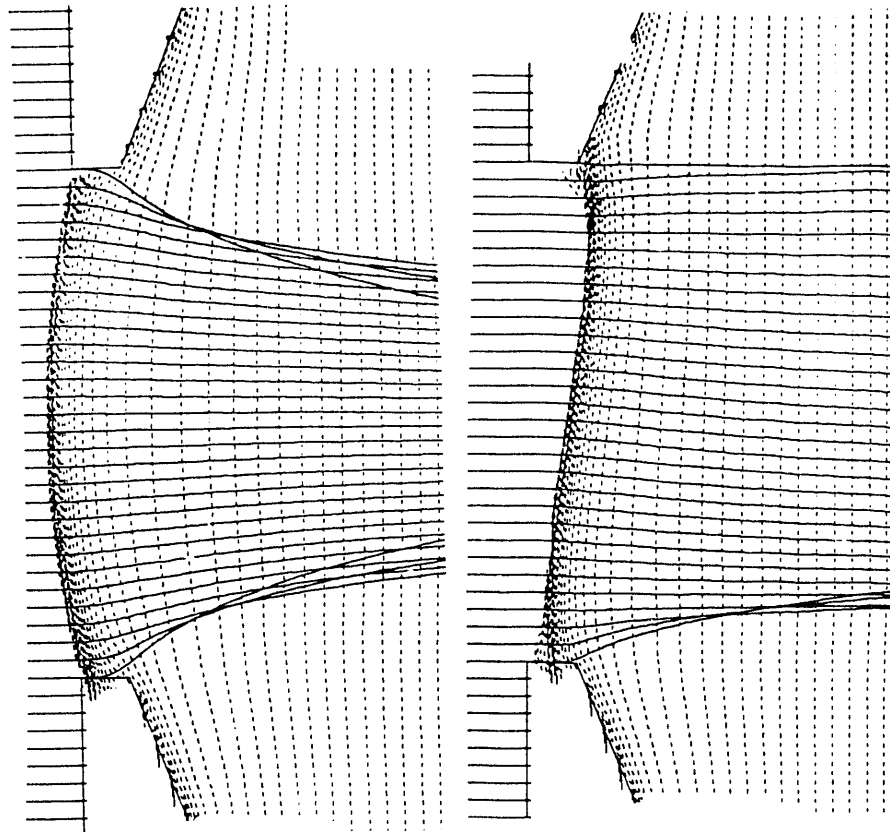
An example of a full 3-D calculation of a negative ion extraction sheath is shown in Fig. 4.34. Including the effect of $\mathbf{E} \times \mathbf{B}$ electrons ($B \sim 100$ G) makes the sheath oblique and nonaxisymmetric, as shown in Fig. 4.34(b).

4.3.4 Upgrade of the T-15 Long-Pulse Ion Source

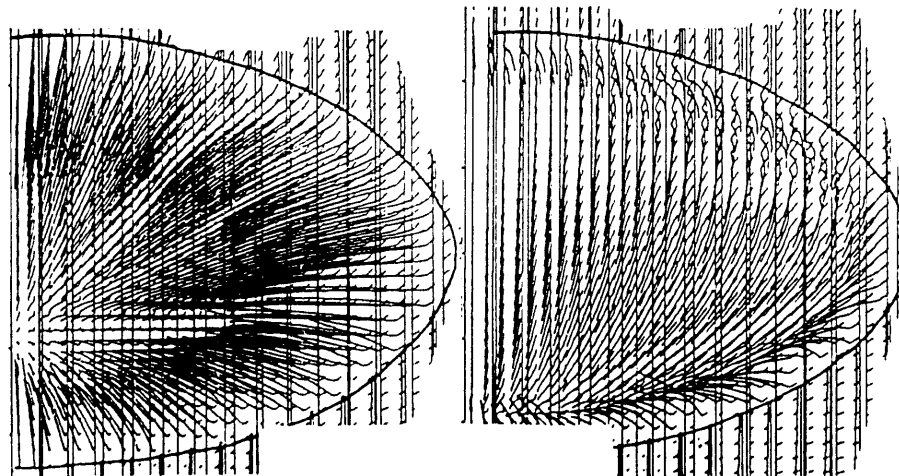
J. H. Whealton and P. S. Meszaros

Calculations for the long-pulse T-15 positive ion source, which represents a step toward optimization of the extractor, have been carried out.

Theoretical results for rms divergence as a function of current have been obtained for a short-pulse injector and the original long-pulse design. Other scenarios are also represented. The optics at the minimum divergence for the two cases are shown in Figs. 4.35 and 4.36.



(a) SIDE VIEW



(b) END VIEW

Fig. 4.34. Three-dimensional calculation of a negative-ion extraction sheath (a) without and (b) with the effect of $\mathbf{E} \times \mathbf{B}$ electrons ($B \sim 100$ G). These electrons make the sheath oblique and nonaxisymmetric.

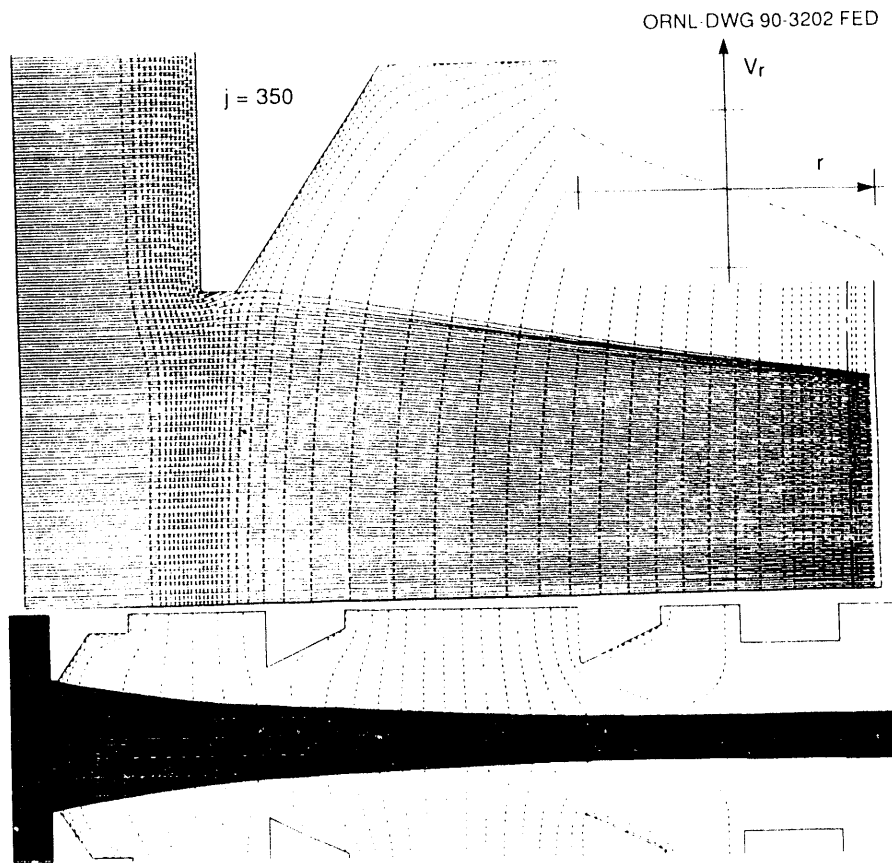


Fig. 4.35. The optics at the minimum divergence for the short-pulse injector. At bottom is the extractor geometry. Above it is an enlargement of the extractor at the minimum divergence. In the upper right corner, the ideal emittance diagram, corresponding to the right-hand side of the enlargement, shows the degree of linearity of the optics halfway down the accelerator.

ORNL-DWG 90-3203 FED

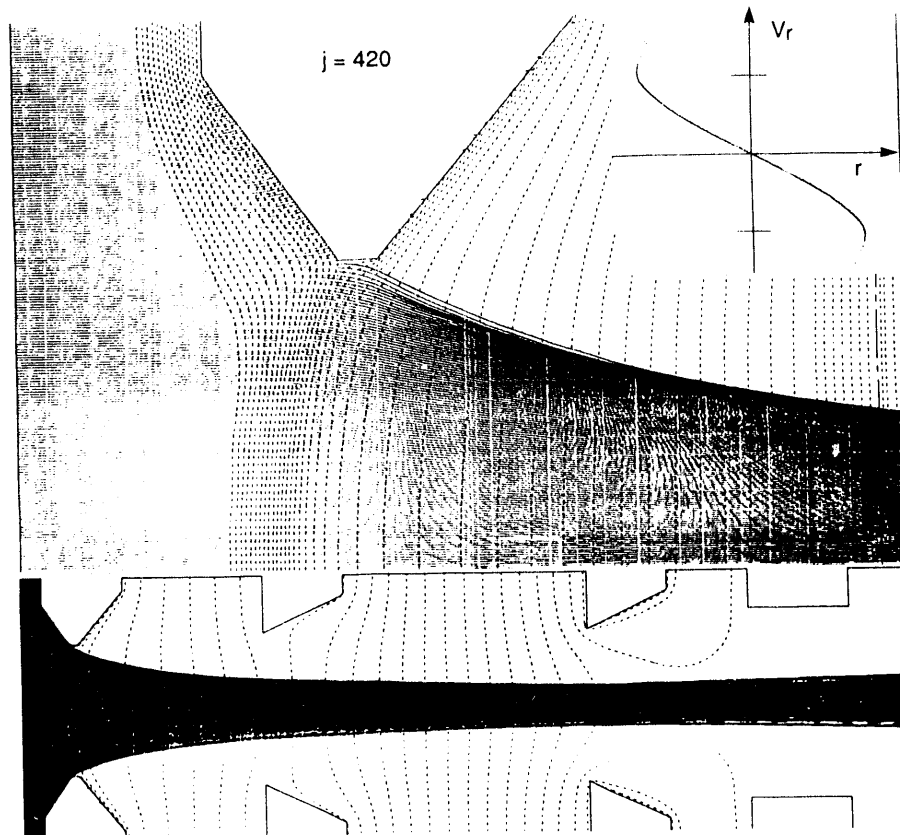


Fig. 4.36. The optics at the minimum divergence for the long-pulse design. At bottom is the extractor geometry. Above it is an enlargement of the extractor at the minimum divergence. In the upper right corner, the ideal emittance diagram, corresponding to the right-hand side of the enlargement, shows the degree of linearity of the optics halfway down the accelerator.

REFERENCES

1. C. A. Foster et al., "The ORNL/Tore Supra Pellet Injector and The E-Beam Rocket Pellet Accelerator," in *Pellet Injection and Toroidal Confinement (Proceedings of the IAEA Technical Committee Meeting, Gut Ising, 1988)*, IAEA-TECDOC-534, IAEA, Vienna, 1989.
2. C. A. Foster et al., "Electron Beam Rocket Pellet Accelerator," presented at the International Pellet Fueling Workshop, La Jolla, California, October 30–November 3, 1985.
3. C. A. Foster, C. C. Tsai, and D. E. Schechter, "Electron-Beam Rocket Pellet Accelerator," presented at the 36th Annual Symposium of the American Vacuum Society, Boston, Massachusetts, October 23–27, 1989.
4. C. C. Tsai, C. A. Foster, and D. E. Schechter, "Characteristics of Electron-Beam Rocket Pellet Accelerator," pp. 1230–35 in *Proceedings of the IEEE 13th Symposium on Fusion Engineering*, ed. M. S. Lubell, M. B. Nestor, and S. F. Vaughan, Vol. 2, IEEE, New York, 1990.
5. S. K. Combs et al., "Development of a Two-Stage Light Gas Gun to Accelerate Hydrogen Pellets to High Speeds for Plasma Fueling Applications," *J. Vac. Sci. Technol. A* **7** (3), 963–7 (1989).
6. S. K. Combs et al., "Acceleration of Small, Light Projectiles (Including Hydrogen Isotopes) to High Speeds Using a Two-Stage Light Gas Gun," *J. Vac. Sci. Technol. A* **8**, 1814 (1990).
7. M. J. Gouge et al., "Design Considerations for Single-Stage and Two-Stage Pneumatic Pellet Injectors," *Rev. Sci. Instrum.* **60** (4), 570–5 (1989).
8. A. Reggiori et al., *J. Vac. Sci. Technol. A* **6** (4), 2556 (1983).
9. K. Sonnenberg et al., "Prototype of a High Speed Pellet Launcher for JET," p. 715 in *Fusion Technology 1988*, Vol. 1, ed. A. M. Van Ingen, A. Nijssen-Vis, and H. T. Klippel, Elsevier Science Publishers B.V., North-Holland, Amsterdam, 1989.
10. Ming-Lun Xue, M-2663, Risø National Laboratory, Roskilde, Denmark, October 1987.
11. D. J. Hoffman et al., "Experimental Measurements of Ion Cyclotron Antennas' Coupling and RF Characteristics," *Fusion Technol.* **8**, 411 (1985).
12. F. W. Perkins, *Nucl. Fusion* **29**, 583 (1989).
13. M. Kwon et al., "Measurement of the Effects of Faraday Shields on ICRH Antenna Coupling," *IEEE Trans. Plasma Sci.* **P3-18**, 184 (1990).
14. D. W. Faulconer, *J. Appl. Phys.* **54**, 3810 (1983).
15. J. B. O. Caughman, D. N. Ruzic, and D. J. Hoffman, "Experimental Evidence of Increased Electron Temperature, Plasma Potential, and Ion Energy Near an ICRF Antenna Faraday Shield," *Fusion Eng. Des.* **12**, 179 (1990).
16. M. J. Mayberry et al., "60-MHz Fast Wave Current Drive Experiments for DIII-D," p. 298 in *Radio-Frequency Power in Plasmas*, R. McWilliams, ed., *AIP Conf. Proc.* **190**, American Institute of Physics, New York, 1989.
17. F. W. Baity et al., "Spectral Shaping and Phase Control of a Fast-Wave Current Drive Antenna Array," p. 214 in *Radio-Frequency Power in Plasmas*, R. McWilliams, ed., *AIP Conf. Proc.* **190**, American Institute of Physics, New York, 1989.
18. W. L. Stutzman and G. A. Thiele, *Antenna Theory and Design*, John Wiley & Sons, New York, 1981.
19. P. M. Ryan et al., "Determination of ICRF Antenna Fields in the Vicinity of a 3-D Faraday Shield Structure," *Fusion Eng. Des.* **12**, 37 (1990).
20. U.S. Patent 4,755,345.
21. D. J. Hoffman et al., "The Design of High-Power ICRF Antennas for TFTR and Tore Supra," in *Applications of Radio-Frequency Power to Plasmas*, ed. S. Bernabei and R. W. Motley, *AIP Conf. Proc.* **159**, American Institute of Physics, New York, 1987.
22. *Fusion Energy Division Annual Progress Report for the Period Ending December 31, 1988*, ORNL-6528, Martin Marietta Energy Systems, Inc., Oak Ridge National Laboratory, 1989, pp. 112–4.
23. R. H. Goulding et al., "ICRF Antenna Designs for CIT and Alcator C-Mod," pp. 250–3 in *Radio Frequency Power in Plasmas*, ed. R. McWilliams, *AIP Conf. Proc.* **190**, American Institute of Physics, New York, 1989.
24. S. N. Buckley and P. Agnew, "Radiation-Induced Changes in the Dielectric Properties of Insulating Ceramics at ICRH Frequencies," *J. Nucl. Mater.* **155–157**, 361–5, 1988.
25. R. H. Goulding et al., "Design of a CIT Prototypical Fast-Wave ICRF Antenna for Alcator C-Mod," *Bull. Am. Phys. Soc.* **34**, 2095 (1989).
26. D. A. Ehst, *Fast-Wave Current Drive: Experimental Status and Reactor Prospects*, ANL/FPP/TM-219, Argonne National Laboratory, Argonne, Ill., March 1988.

27. J. Bruneteau et al., "Enhancement of Negative Ion Extraction and Electron Suppression by a Magnetic Field," presented at the 5th International Symposium on the Production and Neutralization of Negative Ions and Beams, Brookhaven National Laboratory, October 30–November 3, 1989.

28. M. Bacal et al., *Volume Negative Hydrogen Ion Beam Production: Thirteenth Quarterly Technical Report, July 1–September 30, 1989*, Laboratoire de Physique des Milieux Ionisés, Ecole Polytechnique, under Subcontract No. 19X-91351V with Martin Marietta Energy Systems, Inc., for the U.S. Department of Energy.

29. M. Bacal and R. A. Stern, *Volume Negative Hydrogen Ion Beam Production: Twelfth Quarterly Technical Report, April 1–June 30, 1989*, Laboratoire de Physique des Milieux Ionisés, Ecole Polytechnique, under Subcontract No. 19X-91351V with Martin Marietta Energy Systems, Inc., for the U.S. Department of Energy.

30. M. Bacal et al., *Volume Negative Hydrogen Ion Beam Production: Eleventh Quarterly Technical Report, January 1–March 31, 1989*, Laboratoire de Physique des Milieux Ionisés, Ecole Polytechnique,

under Subcontract No. 19X-91351V with Martin Marietta Energy Systems, Inc., for the U.S. Department of Energy.

31. M. Bacal et al., *Volume Negative Hydrogen Ion Beam Production: Tenth Quarterly Technical Report, October 1–December 31, 1988*, Laboratoire de Physique des Milieux Ionisés, Ecole Polytechnique, under Subcontract No. 19X-91351V with Martin Marietta Energy Systems, Inc., for the U.S. Department of Energy.

32. P. J. Eenshuistra, A. W. Kleyn, and J. H. Hopman, *Europhys. Lett.* **8**, 423 (1989); P. J. Eenshuistra et al., *Phys. Rev.* **A40**, 3613 (1980).

33. G. C. Stutzin et al., *Chem. Phys. Lett.* **155**, 475 (1989); G. C. Stutzin et al., *Rev. Sci. Instrum.* **61** (1), 619–21 (1990).

34. M. Bacal, P. Berlemont, and D. A. Skinner, *Volume Negative Hydrogen Ion Beam Production: Ninth Quarterly Technical Report, July 1–September 30, 1988*, Laboratoire de Physique des Milieux Ionisés, Ecole Polytechnique, under Subcontract No. 19X-91351V with Martin Marietta Energy Systems, Inc., for the U.S. Department of Energy.

5

**SUPERCONDUCTING MAGNET
DEVELOPMENT**

M. S. Lubell, Magnetics and Superconductivity Section Head

L. Dresner
W. A. Fietz¹
P. N. Haubenreich²
W. J. Kenney
J. W. Lue
J. S. Luton
S. W. Schwenterly
S. F. Vaughan³

-
1. On assignment to the Office of Fusion Energy, U.S. Department of Energy, Washington.
 2. On assignment to the International Atomic Energy, Agency, Vienna.
 3. Section secretary.

5. SUPERCONDUCTING MAGNET DEVELOPMENT

SUMMARY OF ACTIVITIES

The Magnetics and Superconductivity Section carries out experimental and theoretical research in applied superconductivity. Activities this year focused on new applications for technology developed in support of fusion research and on mathematical techniques for designing and understanding superconducting magnets. Analysis of the extensive data from the international Large Coil Task continued.

5.1 EXPERIMENTAL WORK

5.1.1 Superconducting Magnet Design

It is now possible to design superconducting magnets that use forced-flow cooling of cable-in-conduit NbTi superconductor and operate at high fields (8–12 T) and high current densities (5–15 kA/cm²) in a stable manner (margins of 50–300 mJ/cm³). High current density leads to smaller, lighter, and thus less expensive coils. Forced-flow cooling provides confined helium, full conductor insulation, and a rigid winding pack for better load distribution. The cable-in-conduit conductor configuration ensures a high stability margin for the magnet. The NbTi superconductor has reached a good engineering material standard, and its strain-insensitive critical parameters are particularly well suited to complicated coil windings like those needed for stellarators.

A procedure for optimizing the design of such a conductor, based on the theoretical and experimental work at ORNL over the past decade, has been developed. The database for such coils is still very sparse, and a few issues remain to be addressed. These include the amount of cyclic loading that NbTi cable can withstand and normal-zone propagation in cable-in-conduit conductor. Work is in progress to address these issues and to incorporate the results into designing coils for fusion experiments and for other applications.

5.1.2 Quench Propagation, Pressure Rise, and Thermal Expulsion of Helium from a Cable-in-Conduit, Forced-Flow Superconductor

The quench behavior of a forced-flow, cable-in-conduit superconductor is being investigated on a sample consisting of a

single triplex of 1.25-mm-diam NbTi wires in a circular 3.9-mm-diam conduit.¹ The total sample length is 50 m, wound in a bifilar coil. Heaters of several different lengths are provided, both at the center and at one end of the sample, and the heated end can be closed off to simulate a normal zone centered in a 100-m conductor. Heaters are mounted on the triplex wires and on the outside of the conduit to ascertain the effect of heating the wires directly vs heating the helium. The sample coil is mounted in vacuum so that heat flow occurs only along the conductor. The propagation rates, pressure and temperature profiles, and expulsion flow rates vs time are being measured for initial normal zones of various lengths. The results will be compared with theoretical calculations.

5.1.3 Magnetic Heat Pump Test

A magnetic heat pump test was performed with a gadolinium sample in a water column inserted into an 18-in. dewar containing the NbTi, forced-flow-cooled, cable-in-conduit coil built at ORNL 10 years ago. The coil was refurbished and installed in the dewar, which was modified to make a 3-in. room-temperature access bore for the test sample. The magnet was cooled by two-phase helium at 1 to 1.4 atm. Although the magnet was originally designed and built for dc operation, it was successfully charged to 7.5 T (at the winding) in 18 s. Cyclic runs in triangular waveform were performed to 5.1 T in a 20-s period and to 6.8 T in a 30-s period for more than 15 min each. The ramp rates in all tests were limited by the power supply voltage. Use of the overhead crane to raise and lower the water column was not successful in establishing a desirable temperature gradient from the temperature

swing in the gadolinium generated by the field sweep.

5.1.4 Large Coil Task

The Large Coil Task (LCT) was a multinational cooperative research and development program, carried out under the auspices of the International Energy Agency, to demonstrate the feasibility of building and operating large superconducting coils in a toroidal array. The goals of the LCT were to obtain experimental data, to demonstrate reliable operation of large superconducting coils, and to prove design principles and fabrication techniques under consideration for the toroidal magnets of thermonuclear reactors.

Six coils, three contributed by the United States and one each from Japan, Switzerland, and the European Community, were tested in the International Fusion Superconducting Magnet Test Facility (IFSMTF) at ORNL. The test facility was placed under vacuum in October 1985 and operated until September 1987. The main test results are summarized in Ref. 2; analysis of the extensive data acquired during the 22 months of operation continues. The performance of the refrigerator compressors was described in discussions of compressor experience during U.S.-U.S.S.R. exchange I.8 during November 1989.

One of the six coils tested as part of the LCT was built by Westinghouse Electric Corporation; it was the only coil to use Nb_3Sn conductor, which was in a loose cable form rather than a rigid monolith, and it used aluminum alloy plates to provide a distributed coil structure rather than a lumped case structure. Analysis of the LCT data showed that the distributed structure of the Westinghouse coil was useful in eliminating large stress concentrations.

Unintentional shorting of the plates caused large eddy currents when the coil was rapidly discharged, extending the cooling time needed between tests. However, the shorted plates absorbed some of the coil energy and thus reduced the possible hot-spot temperature in the conductor. The coil withstood high voltages (maximum of 2.44 kV), despite the need to insulate every turn of the conductor from the ground potential because of the plate scheme. Not potting the conductor to the plates resulted in local stick-slip under mechanical loads and poor thermal contact between conductor and plates. The results demonstrated the feasibility of manufacturing a long (4.7-km), helium-tight, stainless steel conduit for a force-cooled magnet, even without a hermetic case. Auxiliary cooling channels to remove heat (e.g., nuclear heating) from the conductor would be desirable, and separate cooling for the structure appears prudent.

5.2 THEORETICAL RESEARCH

5.2.1 The Gorter-Mellink Pulsed-Source Problem in Cylindrical and Spherical Geometry

The diffusion of heat in turbulent superfluid He-II is described by the nonlinear equation $C_t = \nabla \cdot (\nabla C)^{1/3}$, sometimes called the Gorter-Mellink diffusion equation. The pulsed-source problem was solved earlier in plane geometry³ and has now been solved for cylindrical and spherical geometry.⁴ After a pulse, the central temperature falls with time t faster than $(t_0 - t)^{9/2}$ in spherical geometry and faster than $\exp(-2\beta t)$ in cylindrical geometry (with t_0 and β constants that depend on the initial heat distribution). This contrasts with its $t^{-3/2}$ behavior in plane geometry.

5.2.2 Propagation of Normal Zones of Finite Size in Large, Composite Superconductors

Very large composite superconductors of the type proposed for use in energy storage magnets⁵ can sustain normal zones of finite size that travel at a uniform velocity along the conductor. A simple analytical model has been developed⁶ to determine the conditions under which such zones can exist and the size and velocity of these zones. The transport current has a threshold value below which finite normal zones cannot exist, and the propagation velocity corresponding to this current, though not zero, is the smallest possible. The results of the model show that in a typical energy storage magnet, with 1000 km of conductor, a finite normal zone could take 3.17 d to traverse the entire winding, releasing a steady power of more than 8.22 kW that would have to be removed. Thus, conductors in energy storage magnets should be designed to operate in the stable region that does not permit the propagation of normal zones of finite size.

REFERENCES

1. S. W. Schwenterly, J. W. Luc, and L. Dresner, "Quench Propagation, Pressure Rise, and Thermal Expulsion of Helium from a Cable-in-Conduit Forced-Flow Superconductor," presented at CEC89: The 1989 Cryogenic Engineering Conference, Los Angeles, July 24–28, 1989 [to be published in *Adv. Cryog. Eng.* **35** (1990)].
2. D. S. Beard et al., eds., "The IEA Large Coil Task: Development of Superconducting Toroidal Field Magnets for Fusion Power," *Fusion Eng. Des.* **7**, 1–232 (1988).
3. L. Dresner, "Transient Heat Transfer in Superfluid Helium," *Adv. Cryog. Eng.* **29**, 323–33 (1984).
4. L. Dresner, "The Gorter-Mellink Pulsed-Source Problem in Cylindrical and Spherical Geometry," presented at CEC89: The 1989 Cryogenic Engineering Conference, Los Angeles, July 24–28, 1989 [to be published in *Adv. Cryog. Eng.* **35** (1990)].
5. J. Waynert, Y. Eyssa, and X. Huang, "The Transient Stability of Large Scale Superconductors Cooled in Superfluid Helium," *Adv. Cryog. Eng.* **33**, 187–94 (1988).
6. L. Dresner, "Propagation of Normal Zones in Finite Size in Large, Composite Superconductors," presented at MT11: The 11th International Conference on Magnet Technology, Tsukuba, Japan, August 28–September 1, 1989 (to be published in the proceedings).

6

ADVANCED SYSTEMS PROGRAM

T. E. Shannon¹

M. K. Bullock²
T. W. Burgess³
L. S. Dale⁴
F. C. Davis¹
C. A. Flanagan⁵
P. J. Fogarty¹
J. D. Galambos⁶
I. Gomes⁷
L. D. Gomes⁷
P. L. Goranson¹
M. J. Gouge⁸
J. T. Hogan⁹
H. W. Jernigan
G. H. Jones¹
D. P. Kuban¹
V. D. Lee¹⁰

D. J. Lousteau¹
T. J. McManamy¹
J. F. Monday¹
G. H. Neilson¹¹
B. E. Nelson¹
Y-K. M. Peng
R. L. Reid¹
R. O. Sayer⁶
D. J. Strickler⁶
D. W. Swain
S. L. Thomson¹²
N. A. Uckan¹¹
J. C. Whitson⁶
J. J. Yugo¹³
K. L. Zell⁴

-
1. Engineering Division, Martin Marietta Energy Systems, Inc.
 2. AG & Associates.
 3. Robotics and Process Systems Division.
 4. Section secretary.
 5. Westinghouse Electric Corporation, Madison, Pa.
 6. Computing and Telecommunications Division, Martin Marietta Energy Systems, Inc.
 7. The University of Tennessee, Knoxville.
 8. Plasma Technology Section.
 9. Plasma Theory Section.
 10. McDonnell Douglas Astronautics Corporation, St. Louis.
 11. Toroidal Confinement Section.
 12. Bechtel National, Inc., San Francisco.
 13. TRW, Inc., Redondo Beach, Calif.

6. ADVANCED SYSTEMS PROGRAM

SUMMARY OF ACTIVITIES

The Advanced Systems Program has been organized as a focal point for design studies of future fusion experiments. The Fusion Engineering Design Center is the major engineering resource for the program. This group of 20 to 25 persons consists of both ORNL and outside industrial participants. Since its formation in 1979, the Design Center has played a leading role in the design of next-generation devices. In 1989, the Advanced Systems Program comprised two principal activities, the Compact Ignition Tokamak (CIT) project and the International Thermonuclear Experimental Reactor (ITER) project.

The CIT project, led by Princeton Plasma Physics Laboratory, was begun in 1985. As part of the national CIT design team, ORNL has made major contributions to this project. In 1989, these contributions included lead responsibility for design integration and for six Work Breakdown Structure (WBS) elements: ex-vessel remote maintenance, vacuum systems, ion cyclotron resonance heating, shielding, external structure, and fueling.

The ITER design study continued from its 1988 beginning as an outgrowth of a U.S.-U.S.S.R. summit agreement that was formalized by the International Atomic Energy Agency (IAEA). The purpose of this activity is to cooperate in the international conceptual design of a fusion test reactor under the auspices of the IAEA. The ITER concept includes reactor-relevant features such as superconducting magnets, steady-state or extended-burn capability, and testing of nuclear components and materials. In the United States, the program is organized as a national study under the direction of Lawrence Livermore National Laboratory. In 1989, the program involved international participation in a program for research, development, and conceptual design that will continue through 1990. The major participants in the program are the United States, the U.S.S.R., Japan, and the European Community.

The Design Center led the U.S. effort in configuration development, design integration, mechanical design of the plasma-facing components and blankets, facilities, reliability and availability analysis, remote maintenance, design and analysis of heating and current drive, and cost estimating. Support was provided in the design of poloidal field systems and in structural analysis. Several members of the Design Center staff participated in the five-month-long Joint Work Session in Garching, Federal Republic of Germany, and in numerous specialists' meetings.

The Design Center also led the national effort to develop and maintain the tokamak systems code TETRA. The Design Center was responsible for performance of numerous systems and trade studies required to support the evolution of the ITER design concept and provided support in poloidal plasma magnetics, plasma control analysis, and disruption analysis.

A three-year tokamak reactor study, the Advanced Reactor Innovation and Evaluation Study (ARIES) program, was initiated in January 1988. The Design Center played a key role in several aspects of this project, including the ARIES equilibrium and stability evaluation and the poloidal field system design. Work to evaluate the potential of pellet fueling and of rf heating and current drive in ARIES was initiated at the end of the year.

6.1 CIT

6.1.1 Ex-Vessel Remote Maintenance

The use of deuterium-tritium (D-T) fuel in the Compact Ignition Tokamak (CIT) will require remote handling technology for ex-vessel maintenance and replacement of machine components. Highly activated and contaminated components of the fusion device's auxiliary systems, such as diagnostics and rf heating, must be replaced using remotely operated maintenance equipment in the test cell. The development of the ex-vessel remote maintenance (XVRM) concept for CIT has been the prime responsibility of ORNL for Princeton Plasma Physics Laboratory (PPPL) and the U.S. Department of Energy.¹

The CIT fusion device is located in the center cell of the test cell facility. The machine will operate initially in a nonactivating hydrogen phase for approximately one year. This will permit hands-on repair of equipment that fails during shakedown runs and demonstration of remote maintenance operations. Thereafter, limited access to the test cell may still be possible after deuterium-deuterium (D-D) operations commence; however, once D-T fuel is introduced, personnel access into the center cell will be prohibited, and repair and replacement of machine components will be accomplished by remotely operated equipment. Virtually all machine components that interface with the vertical and horizontal ports of the vacuum vessel will be designed for remote replacement and handling. These components will be repaired or packaged for disposal in the hot repair cell.

6.1.1.1 Remote maintenance systems

The key element of the test cell maintenance system is a pair of bilateral, force-

reflecting, servomanipulator arms mounted on a telescoping boom supported from an overhead transporter to provide dexterous manipulation throughout the test cell. This equipment provides the primary means for remote operations on the upper vertical ports and the horizontal ports of the machine and on the floor area of the center cell. Replacing equipment in the center cell requires opening the sliding shield roof, decoupling components, and enclosing them in a container to prevent the spread of contamination before removing them to the hot repair cell for repair or disposal. These operations are performed remotely using the servomanipulator and crane hook reaching down from their high bay bridges.

The manipulator configuration will be similar to that shown in Fig. 6.1. It consists of a dual-arm master-slave manipulator with camera positioners and a hoist at the slave. Collision avoidance capability is planned for the manipulator system (including the transporter, the manipulator, and the auxiliary equipment) to protect the system during motion from one work location to another.

Several maintenance tasks have been identified in the pit area under the machine. The use of a mobile telerobot to perform these tasks is under consideration. The mobile robot must be operated in a very confining, constricted environment. Compact size, maneuverability, and collision avoidance are paramount requirements for operation in this confined space without damage to the vehicle or to the equipment.

6.1.1.2 Graphic modeling

Throughout the CIT remote maintenance studies, computer modeling has been used extensively to investigate manipulator access. Three-dimensional (3-D) kinematic computer models of the CIT machine are

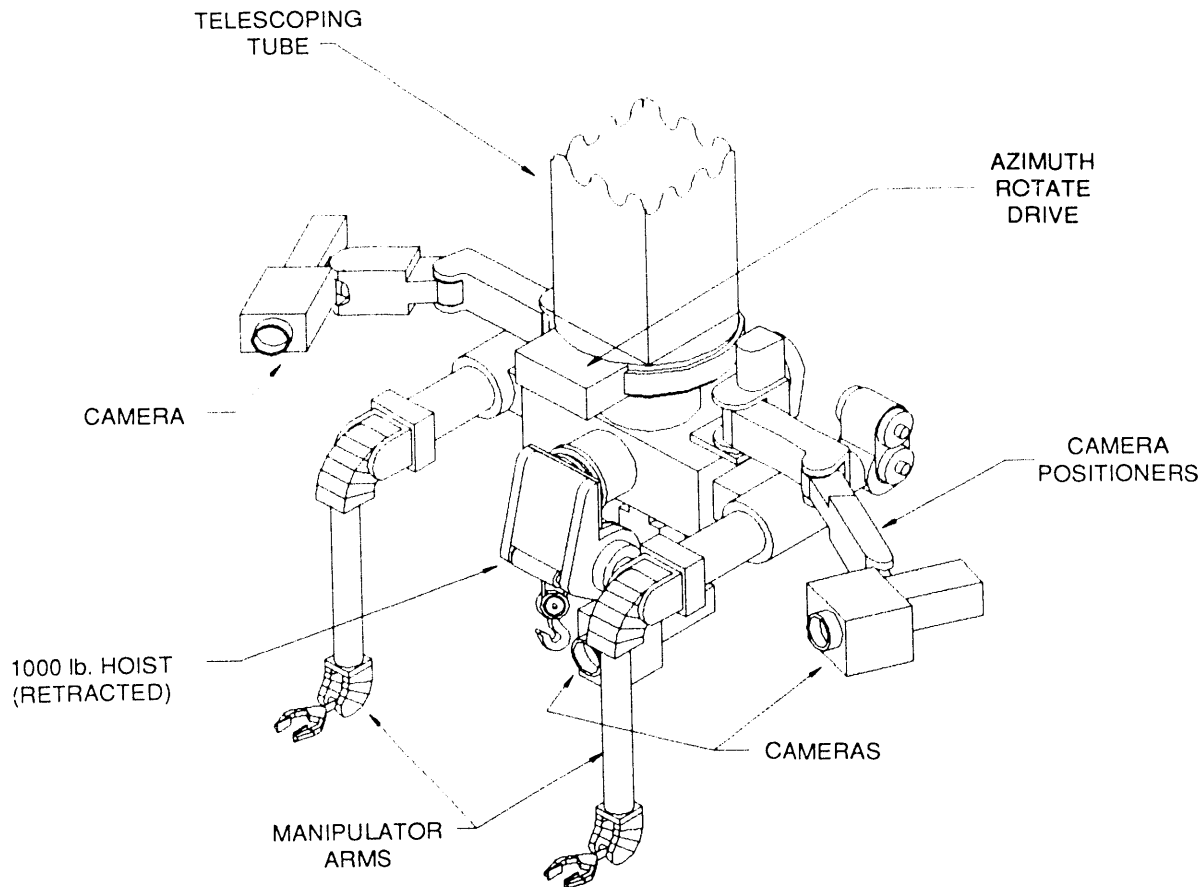


Fig. 6.1. Manipulator system configuration.

proving to be powerful tools in our efforts to evaluate remote maintenance requirements. A recent refinement of computer modeling involves the use of an intelligent engineering workstation called IGRIP (Interactive Graphics Robot Instruction Program) for real-time interactive display of task simulations. It can be used to model work spaces and kinematic geometry used within a remote facility (manipulators, cranes, transporters, etc.). IGRIP's collision detection and "near miss" detection features are proving to be excellent tools for remote maintenance. Simulation of an activity or process is a powerful feature of the software; programs can be written

for IGRIP devices to perform tasks within the work space. This feature allows remote maintenance designers to perform detailed maintenance studies in true 3-D geometry.

A large portion of the CIT facility has already been modeled in IGRIP, and the entire facility will eventually be included. Shown in Fig. 6.2, the current facility model includes the center test cell, north and south cells, high bay, hot and contact repair cells, operating gallery, and loading area. The model contains a moderate level of detail such as passageways, doorways, and roof hatches. Details will be added continuously as the project matures.

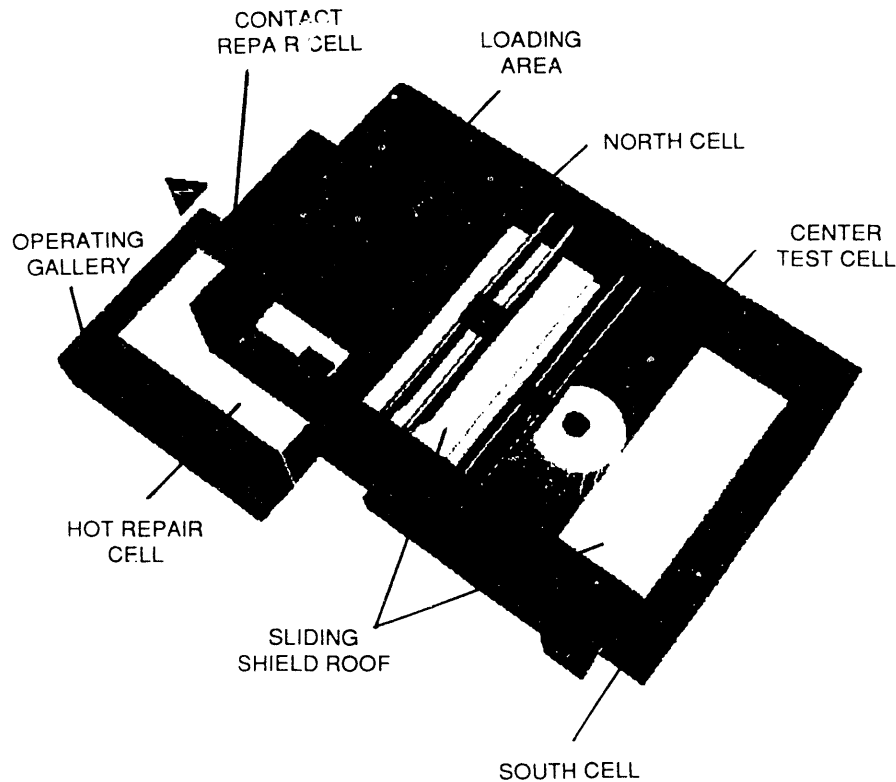


Fig. 6.2. Shielded cell configuration.

6.1.1.3 Task evaluations

The simulation capabilities of IGRIP have been used with the CIT model to depict XVRM activities. In conjunction with IGRIP's interference detection, the simulations have allowed the evaluation of access constraints and problems that might otherwise have gone unnoticed until hardware mock-ups were constructed.

The removal of a plasma/infrared television (IRTV) diagnostic was completely simulated, as described in ref. 2. A presentation describing this simulation included a videotape of the remote replacement of a plasma viewing assembly. The simulation illustrates some of the constraints associated with typical remote maintenance activities

and the ways in which computer modeling enhances the design process. Remote maintenance designers have incorporated several design features to facilitate remote maintenance for the plasma/IRTV diagnostic (Fig. 6.3).

The remote handling needs for the replacement of the central solenoid have been studied. This task presents several concerns, primarily because of the solenoid's weight (100 tons) and size (22.5 ft long by 5.5 ft in diameter). Various scenarios were developed for extracting the "hot" cylindrical solenoid from the center of the machine and transporting it to a suitable location for disposal. A special lifting fixture consisting of a strongback fitted with two 50-ton ball screwjacks was designed.

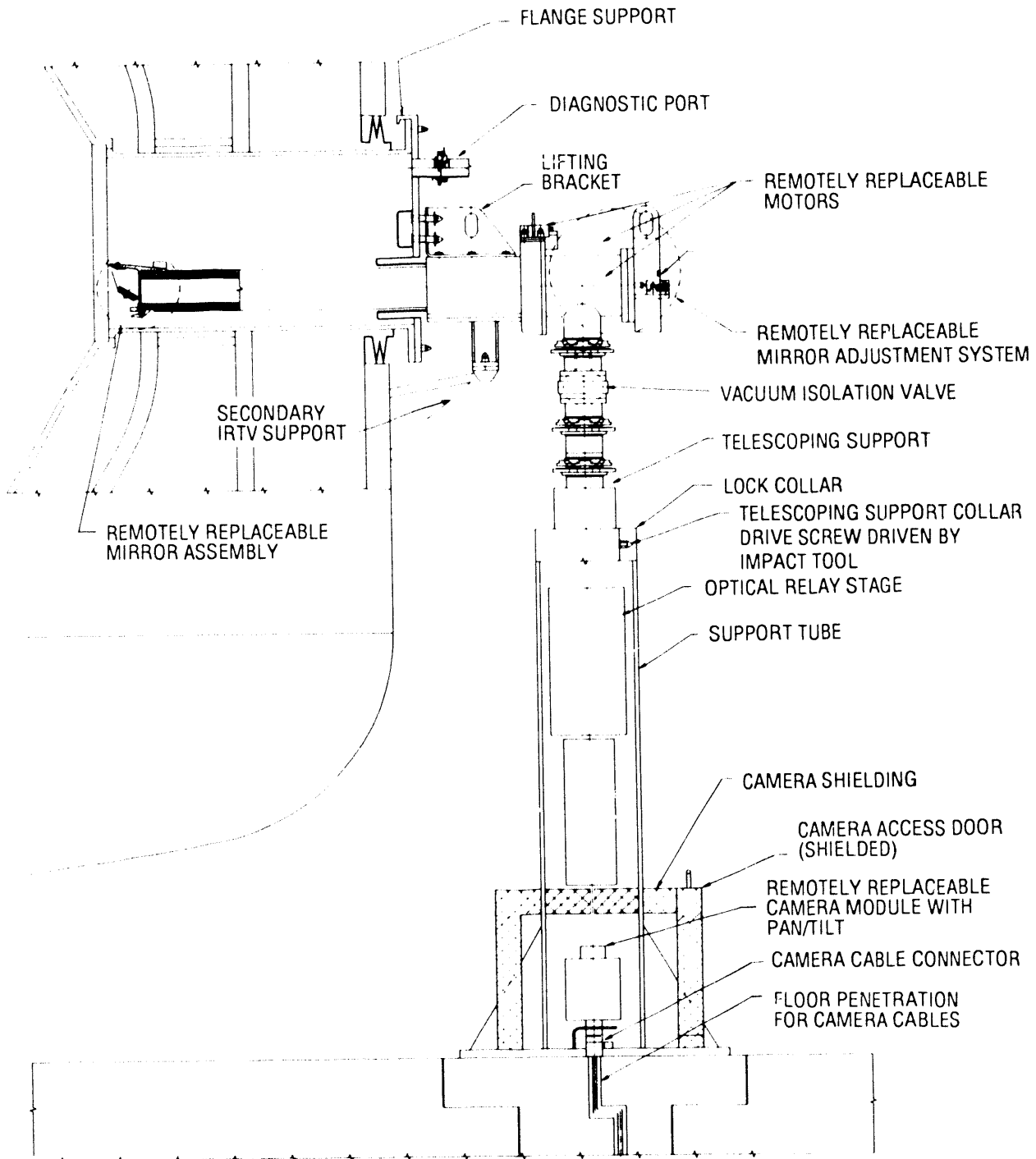


Fig. 6.3. Plasma/IRTV design for remote maintenance.

This fixture provides the 4-ft vertical travel needed to supplement the maximum crane hook height so that the solenoid can be lifted clear of the test cell roof hatch.

A remotely maintainable ion cyclotron resonance heating (ICRH) concept was developed. The special design features include

- vertical removal of higher-maintenance items such as vacuum feedthroughs,
- in-place capacitor maintenance with manipulator,
- manipulator access between neighboring ICRH units,
- relatively short radial length (about 8 ft), and
- placement of the vacuum feedthrough out of the direct line of the neutron flux.

6.1.1.4 Special tools

T. W. Burgess, a member of the CIT remote maintenance design team, remained on assignment to the ex-vessel mock-up program of the Joint European Torus (JET) Joint Undertaking. During this assignment, Mr. Burgess has participated in the major shutdown activities associated with the replacement of the failed toroidal field (TF) coil in octant 3. In September 1989, four members of the CIT remote maintenance design team visited the JET facility to discuss the remote maintenance problems that have been addressed to date (e.g., vacuum flange couplings and seals, fluid and mechanical couplings, decontamination of components, pipe cutting and welding, manipulator design) and may be applicable to CIT. JET staff members presented design drawings and specifications for prototypes of several welding and cutting tools and a remote connector that provides for several hydraulic, pneumatic, and electrical supplies in a single connector.

6.1.2 Vacuum System and Shield

6.1.2.1 Vacuum system

CIT will require an ultrahigh-vacuum pumping system to evacuate the plasma chamber from atmospheric pressure to low pressure and to maintain the required vacuum levels during bakeout, discharge cleaning, and pulsed burn operation. The base partial pressure requirements are 1.34×10^{-6} Pa (1×10^{-7} torr) for fuel gases and 1.34×10^{-8} Pa (1×10^{-9} torr) total for all other constituents. These pressure requirements are very stringent for a system of this size, with a volume of over 80 m^3 and a surface area of 300 m^2 . In addition, the presence of tritium in the pumped stream prevents the use of lubricants or organic seal materials anywhere in the system.

The present CIT vacuum pumping system design calls for six 2000-L/s magnetic bearing turbomolecular pumps backed by two $600\text{-m}^3/\text{h}$ mechanical scroll pumps. Earlier concepts included diaphragm pumps to back up the scroll pumps, but further investigations have indicated that the diaphragm pumps are not necessary. One of the turbomolecular pumps and one of the two scroll pumps are provided for redundancy. The pumps are located in a shielded vault below the experimental enclosure and are connected to the torus via a vertical duct and a single radial duct. The low conductance of the radial duct into the torus restricts the net pumping speed of the system and may require changing the configuration to include a second radial duct. The shielding of the vacuum pumps is sufficient to prevent neutron activation.

Experience in operating the scroll pumps is necessary to ensure that they will reliably pump fusion gases (H_2 , D_2 , T_2) and perform according to the assumptions of

the analysis. A research and development (R&D) program is planned to procure representative pumps, install them in a test stand, and run performance characterization tests. Communication and collaboration with other laboratories and programs [including Kernforschungszentrum Karlsruhe (KfK) and JET] will continue to be beneficial.

In summary, calculations and design studies indicate that an oil-free, ultrahigh-vacuum pumping system can be provided for CIT. The major uncertainties include (1) the ability to provide sufficient pumping speed through a single pumping duct and (2) the performance of the scroll pumps as backing pumps for pumping fusion gases. These issues will be resolved as the design and R&D programs progress.

6.1.2.2 Thermal shield

CIT will require a thermal shield to insulate the coil set, which is cooled with liquid nitrogen to 77 K before each operating pulse. The liquid nitrogen coolant is introduced through piping into the coil set and then vented from the coils directly into the space formed by the thermal shield. Some of the nitrogen does not change phase during cooldown, so the thermal shield must form a container, or cryostat, to collect the liquid. In addition, the nitrogen left in the system during a pulse becomes activated by the high neutron fluence, which imposes a strict leak rate requirement on the system.

The original cryostat design consisted of a double-wall, all-welded sandwich structure with thermal insulation between the walls. This design offered good stiffness, low thermal mass for cooldown, and double containment for the nitrogen. However, this approach limits access to the coil set and structure and is very difficult from a remote maintenance viewpoint. The new design

philosophy that has evolved requires access to any part of the device with a minimum amount of interference from the cryostat. A new, modular approach to the cryostat design will be undertaken in FY 1992 when funds become available.

An R&D program is in place to identify thermal insulation materials that will remain effective after exposure to the high neutron flux. Several candidate materials have been identified through a literature search, and these materials will be irradiated and tested for deterioration of thermal and mechanical properties during FY 1991 and 1992.

6.1.3 Ion Cyclotron Resonance Heating System

On the basis of experimental results from several tokamaks worldwide [primarily the Tokamak Fusion Test Reactor (TFTR) and JET], the CIT antenna geometry was modified. Dual current straps in the toroidal direction replaced the single current strap. Experimentally, dual-strap antennas driven out of phase have shown smaller impedance variations, smaller edge density and temperature increases, and higher breakdown voltages than in-phase antennas. As shown in Table 6.1, antenna dimensions were reduced to accommodate the additional straps in the port. Calculations of the system's plasma coupling and electrical characteristics showed that with dual-strap antennas a launched power of approximately 4.0 MW/port would be feasible. The ICRH system would occupy five of the large horizontal ports to launch 20 MW to the plasma during initial operations and would be expandable to a 28-MW system using seven ports. The antenna power limit was determined by a peak voltage in the antenna and transmission line system of 50 kV for a plasma loading impedance of 4 Ω /m.

Table 6.1. Single- and dual-strap antenna dimensions

	Antenna	
	Single-strap	Dual-strap
Strap width, cm	14	7.5
Strap length, cm	45	45
Cavity width, cm	31	15
Cavity depth, cm	15	10

The dual-strap antenna was designed to be inserted into a large horizontal port so that it could be completely removed for maintenance and replacement with the XVRM equipment. A significant effort was devoted to refining the remote maintenance aspects of the antenna design and to defining the installation and removal procedures.

A key requirement of the antenna is to withstand forces induced in the Faraday shield, antenna housing, and current strap by a plasma disruption. A finite element model of the ICRH launcher was developed, and an analysis of the disruption-induced forces on the antenna was completed for two potential disruption scenarios. Neglecting thermal stresses, the peak stress in the Faraday shield tube was found to be within the allowable limits for Inconel 718.

6.1.4 Fueling System

CIT will use an advanced, high-velocity pellet injection system to achieve and maintain ignited plasmas. Two pellet injectors are provided: a moderate-velocity (1- to 1.5-km/s), single-stage pneumatic injector with high reliability, which incorporates three light gas guns, and a high-velocity (4- to 5-km/s), two-stage pellet injector that uses frozen hydrogenic pellets encased in sabots. Both pellet injectors are qualified for oper-

ation with tritium feed gas. Performance, neutron activation of injector components, maintenance, design of the pellet injection vacuum line, gas loads to the reprocessing system, and equipment layout have been addressed.

Performance requirements for the pellet injection system were developed in collaboration with CIT physics and project staff to ensure sufficient performance for the ignition mission while minimizing the system's impact on the isotope reprocessing system and local tritium inventory levels. Table 6.2 gives the specifications of the CIT pellet injection system, and Table 6.3 gives the parameters of the pellet injectors.

Table 6.2. CIT pellet injection system specifications

Pellet diameter, mm	2–4 (20–40% $\Delta n/n$)
Pellet species	H, D, T, D-T
Pellet velocity, km/s	
Minimum	1.5
Goal	5
Pellet frequency, Hz	0–10
Total pellets	40
System reliability, %	95

The moderate-velocity pellet injector is similar to the JET pellet injector and consists of three single-stage, light gas guns in a common vacuum enclosure. The three different barrel sizes, repetition rates, and total pellets listed in Table 6.3 for the moderate-velocity pellet injector are for the three different light gas guns. The range of pellet diameters is provided to accommodate the range in plasma perturbation $\Delta n/n$ from Table 6.2, as well as a range in plasma operating densities. The ramp-up to ignition will have a continuously increasing plasma density, and the ignition density will be different with different plasma temperatures

Table 6.3. CIT pellet injector parameters

	Moderate-velocity injector	High-velocity injector
Pellet speed, km/s	1-1.5	4.0-5.0
Pellet diameter, mm	2.8, 3.5, 4.0	4.0
Pellet type	H, D, T, D-T	H, D, T, D-T
Repetition rate, Hz	8, 4, 2	2
Total pellets	40, 30, 20	20
Reliability, %	90, 90, 90	80

and heating profiles. The largest (4-mm-diam) pellet results in a 40% perturbation to a CIT plasma with an average density of $2 \times 10^{20} \text{ m}^{-3}$.

The reliability figures in Table 6.3 should be achievable. The JET pellet injector has operated for sustained periods at reliabilities well over 90%.³ The overall system reliability of 95% will be achieved through improvements to existing designs and through the redundancy in the different pellet sizes and repetition rates. That is, the smaller pellets can provide fueling rates equivalent to those of the nominal 4-mm pellet if higher pellet repetition rates are used. Penetration of the pellet into a hot plasma is a strong function of pellet initial diameter (proportional to $d^{5/3}$), and the largest possible pellet, given perturbation limits, should be used to provide the most leverage on plasma density profile peaking, which can increase the ignition margin even if plasma transport is unchanged because of the increased fusion rate with peaked profiles.

The high-velocity pellet injector is based on the two-stage light gas gun concept. A piston is pneumatically accelerated in a high-pressure pump tube and provides adiabatic compression of a second stage of propellant gas between the piston and the pellet/sabot. The resulting high pressures (up to 6,000 bar) and, more importantly,

high temperatures (up to 8,000-10,000 K) can accelerate the pellet/sabot payload to muzzle velocities in the range of 4-5 km/s. For the pellet/sabot combinations used for CIT, the accelerated mass is less than 0.1 g, and the mass per unit area is less than 0.5 g/cm^2 . This permits consideration of repetitive operation, as the pump tube conditions are moderate enough to allow multiple shots with a single piston. The sabots are separated from the hydrogenic pellets in the injection line to the torus and allowed to hit a target plate. Two-stage light gas gun pellet injectors are under development at ORNL and in Europe.

A preliminary layout of the CIT pellet injection system in the CIT central and north cells is shown in Fig. 6.4. To conserve floor area, the injectors are stacked with the heavier high-velocity injector beneath the moderate-velocity injector. Since both injectors will have tritium or D-T mixtures in the gas fuel supply, three layers of containment throughout the pellet injection system are proposed. The primary level of containment will be the pellet injector itself, which will have tritium-compatible materials throughout. The second level of containment is a glove box, or tritium isolation boundary, inside the north cell and double-walled piping for all penetrations of this boundary. The third level of containment is the north and center cells themselves.

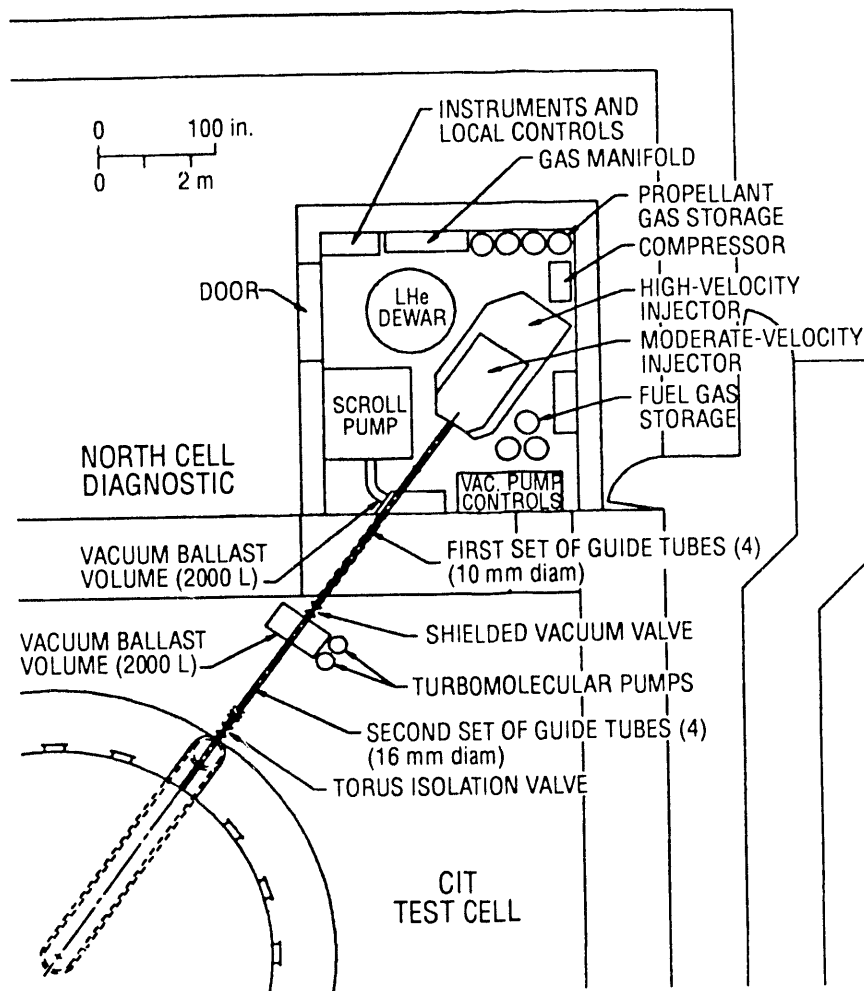


Fig. 6.4. Layout of pellet injection system in CIT north diagnostic cell.

6.1.5 Insulation for the TF Coils

Insulation samples from a variety of commercial vendors were tested for interlaminar shear strength with simultaneous compression. All demonstrated good mechanical properties. Three boron-free types were selected for irradiation in the Advanced Technology Reactor at Idaho National Engineering Laboratory. The three materials were Spaulrad-S and two 3-D weave materials from Shikishima Canvas Co. Two materials (PG5-1 and Spaulrad-S) used a

bismaleimide resin. The third (PG3-1) used an aromatic amine hardened, bisphenol-A resin.

A lead shield was employed to limit the gamma dose fraction to 60%. Flexure samples and shear/compression samples were irradiated and tested.

In general, all three insulation systems performed well and showed apparently adequate margins of mechanical strength and electrical resistance for use in CIT. The results are encouraging. However, further

testing is required and planned to include bonded samples and cryogenic testing. The results are summarized in Table 6.4. All materials were tested at 5 kV for 3 min and did not break down. The resistance was too high to measure for control groups and for groups from both dose levels.

Table 6.4. Results of insulation tests

Values quoted are the average of all samples tested

Material	Dose (rad)	Shear strength ^a (ksi)	Flexure strength ^b (ksi)
Spaulrad	0	18.2	97.9
	4×10^9	18.7	77.0
	3×10^{10}	17.4	52.5
PG5-1	0	19.5	137
	4×10^9	19.4	120
	3×10^{10}	19.2	105
PG3-1	0	17.9	102
	4×10^9	17.2	79.5
	3×10^{10}	19.8	101

^a50-ksi compression applied.

^bExtreme fiber stress.

Fatigue testing was performed by cycling the shear stress with a constant compression. The peak stress levels were 16.2 ksi for Spaulrad, 17.0 ksi for PG5-1, and 11.6 ksi for PG3-1. After 30,000 cycles at 5 Hz, the testing was stopped and the static strength was measured. No significant loss of strength was observed for the control or irradiated groups. The epoxy PG3-1 system failed after approximately 1000 cycles when tested at 15-ksi shear stress with the control group. This material appears to be more sensitive to fatigue damage than either bismaleimide system.

In addition to the irradiation study, a manufacturing study was performed by the ORNL Applied Technology Division (ATD).

The ATD group completed laboratory testing for seven different resin and hardener combinations with two different cure schedules for each combination. The most severe test was a cryogenic shock test of a disk of resin with a copper disk embedment. Other testing included viscosity vs time, wet-out, and compressive strength measurement. The two systems that performed best in the laboratory testing were a highly flexibilized aromatic amine hardened system from Shell and a cycloaliphatic amine cured system.

6.1.6 MHD Equilibrium and Poloidal Field System Studies

Free-boundary magnetohydrodynamic (MHD) equilibria with constrained major and minor radii, magnetic X-point position, and flux linkage are obtained efficiently using a control matrix method.⁴ Plasma shape control matrices \mathbf{A} relating changes in the poloidal field (PF) coil currents dI to errors in the plasma shape and volt-seconds e , $dI = \mathbf{A}e$, are computed as part of the inner loop of the iterative solution of the nonlinear equilibrium equation and used to determine the consistent external field. A least-squares method is used to compute the control matrix when the number of independent coil currents is greater than the number of constraints. The result is an order of magnitude decrease in CPU time from previous methods, making new applications in the areas of CIT divertor equilibrium optimization and PF system design possible.

The control matrix equilibrium code is used in the CIT PF system design process to (1) produce shape control matrices used in the PPPL Tokamak Simulation Code (TSC),⁵ (2) examine alternative CIT plasma configurations (Fig. 6.5), and (3) develop CIT shape control feedback algorithms.

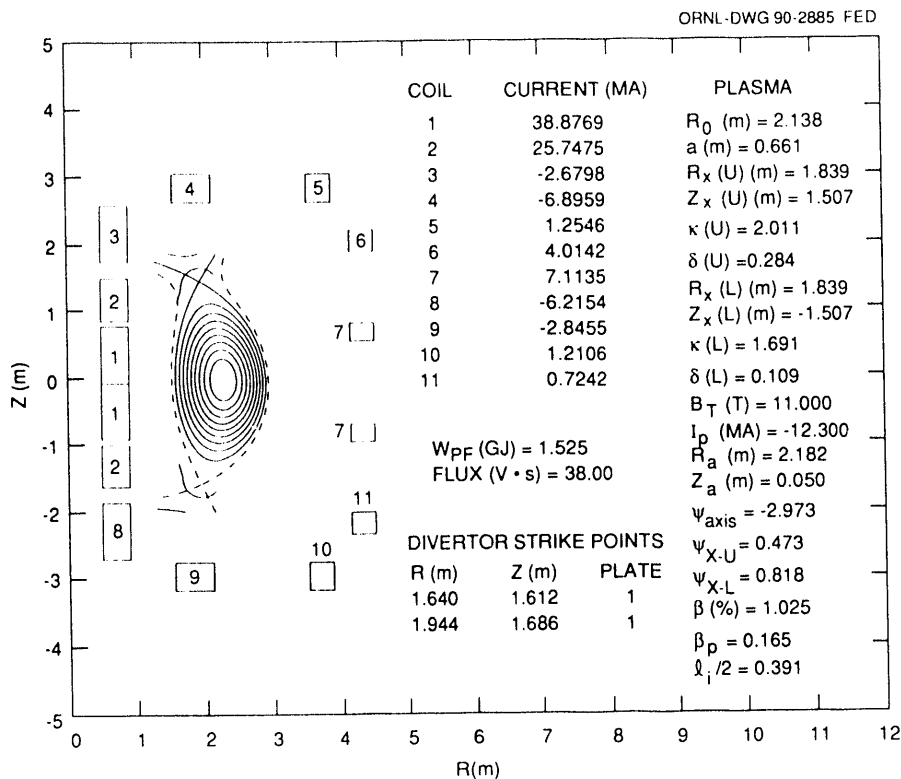


Fig. 6.5. Asymmetric CIT equilibrium at start of flattop. The upper and lower X-points are symmetric about $Z = 0$.

6.1.7 Plasma Disruption Simulations

R. O. Sayer, Y-K. M. Peng, and
S. C. Jardin*

The design of the CIT vacuum vessel (VV) is driven strongly by the disruption-induced forces produced by plasma motion and current decay. It is, therefore, particularly important to model disruption effects as accurately as possible. Our basic tool for computation of plasma disruptions is TSC,⁵ a numerical model of a free-boundary axisymmetric tokamak plasma interacting in a self-consistent manner with a set of conductors that obey circuit equations with active feedback amplifiers included. For both disruptive and nondisruptive discharges, TSC simulations have given excellent agree-

ment with experiment for the evolution of plasma current and profiles.

Several TSC disruption scenarios for the CIT design with magnetic field $B = 11$ T and plasma current $I_p = 12.3$ MA have led to estimates of the effects produced by variations in plasma parameters and initial conditions. These include the initial magnetic field B , a hyperresistive term in the mean field Ohm's law, and the vertical plasma position before a thermal quench.

Let F_R and F_Z be the extreme net radial and vertical VV forces. Two "slow vertical" disruptions were simulated by allowing the plasma to drift before thermal quench until the magnetic axis, Z_{mag} , was 35 or 45 cm below the midplane. The magnitude of F_Z was about 15% larger for the case with $Z_{mag} = -45$ cm at thermal quench time.

Fast ($\langle dI_p/dt \rangle \simeq -3.0$ MA/ms) radial and vertical disruptions were simulated with and without a hyperresistive term. Inclusion of hyperresistivity gave a 10% increase in plasma current and 10% higher magnitude for the inboard radial VV force at thermal quench time.

Fast radial disruptions with high initial beta ($\beta = 0.051$) and low initial beta ($\beta = 0.003$) yielded nearly identical extreme net radial VV forces. This rather unexpected result is due to the contribution from “diamagnetic” poloidal VV currents produced by plasma paramagnetism changes. Figure 6.6 illustrates the evolution of the

net radial VV force F_R and contributions to F_R from diamagnetic poloidal and toroidal VV currents as functions of time for radial disruptions with $\langle dI_p/dt \rangle \simeq -3.0$ MA/ms. For the case with low (high) initial beta, the diamagnetic poloidal VV current acts to increase (decrease) the magnitude of F_R . For the case with low initial beta, at peak F_R , the contributions from toroidal and poloidal currents are -10.5 MN/rad and -4.9 MN/rad, respectively. Poloidal VV currents substantially alter the distribution of VV forces and must be taken into account in simulations of major disruptions for tokamak VV design. The relative magnitudes of poloidal and toroidal components are quite sensitive to the initial beta value.

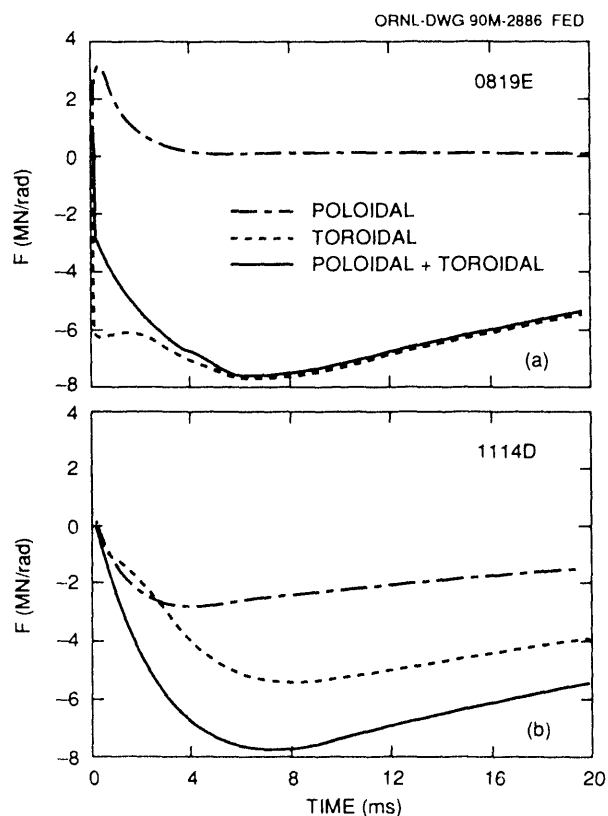


Fig. 6.6. Net radial VV force F_R and contributions to F_R from diamagnetic poloidal and toroidal VV currents as functions of time for radial disruptions with $\langle dI_p/dt \rangle \simeq -3.0$ MA/ms. Initial $I_p = 12.3$ MA, $B_{\text{tor}} = 11$ T. (a) Troyon beta (0.051). (b) Low beta (0.003).

*Princeton Plasma Physics Laboratory, Princeton, N.J.

6.1.8 Structural Materials

Research aimed at developing structural materials for CIT is carried out as part of the Fusion Materials Program, which is described in Sect. 7 of this report.

6.2 ITER

6.2.1 Plasma Engineering

The plasma engineering effort for the International Thermonuclear Experimental Reactor (ITER) was primarily involved with systems and disruption analysis. The systems analysis provided operational scenarios for the steady-state and technology testing phases. This information is used as input for design work on a wide range of topics (heat loads, plasma current levels, etc.). The disruption simulations provided detailed analysis of the plasma current decay process and the associated eddy currents induced

in the vacuum vessel. The high level of sophistication in this modeling procedure allows these results to be used as a basis of comparison for other calculations. These results are also used in the mechanical design of the first wall and vacuum vessel.

6.2.1.1 Systems analysis

The primary emphasis of the 1989 ITER systems analysis was the identification of operational scenarios for the ITER technology phase. These studies were done using the TETRA systems code, and the operational points identified with TETRA are used as the baseline design points.⁶

The ITER program has mission goals of demonstrating both an ignited plasma with steady-state operation and extended-burn technology testing. Accomplishing the second of these goals, called the technology phase, is complicated by the need to inject large amounts of power into the plasma to drive the plasma current noninductively. This injection power exacerbates an already troublesome divertor heat load. In order to identify desirable technology-phase operation points that satisfy the divertor limits, the Harrison-Kukushkin analytic divertor model was incorporated into TETRA.

The divertor constraint prohibits steady-state operation at high neutron wall loads (>0.5 MW/m²). Typically, the steady-state plasma operation is optimal at low density ($n_e < 0.7 \times 10^{20}$ m⁻³), high temperature ($T_e > 15$ keV), and plasma current levels lower than those in the ignition phase.

To satisfy the technology testing mission statement, a hybrid operation scenario, which uses a combination of inductive and noninductive current drive, was identified. With this approach, operational points with high wall loads (>0.8 MW/m²) and long pulse times (thousands of seconds) were

found. Hybrid operation is characterized by medium density (10^{20} m⁻³) and temperature (T_e near 15 keV) and by reduced plasma current levels (near 15 MA).

Another approach to alleviating the divertor heat load problem is to seed the plasma with impurities, in order to radiate large fractions of the power deposited in the plasma. This would permit operation at higher wall loads but requires more confinement capability than the nonseeded case.

Sensitivity studies indicate that increasing the installed injection power allows operation at higher wall loads. This option could be used if performance is not satisfactory with the initial installed power capability (near 100 MW).

6.2.1.2 Plasma disruption simulations

R. O. Sayer, Y-K. M. Peng, and
D. J. Strickler

Design of ITER tokamak conducting structures is driven strongly by the disruption-induced forces produced by plasma motion and current decay. TSC has been used to model ITER disruptions and to predict the time evolution of currents and forces on the vacuum vessel, internal control (IC) coil, and passive stabilizing (PS) structures.⁵ Both inward-shifting and vertically moving disrupting plasmas and a range of current decay rates were studied.

Conducting structures were represented by groups of filamentary wires of specified resistivity. Figure 6.7(a) illustrates the filamentary models for the vacuum vessel, IC coil, and PS structures, all of which were located within the computational grid. Also shown in Fig. 6.7(a) is an overlay plot of plasma boundaries during the disruption phase of a vertical disruption simulation.

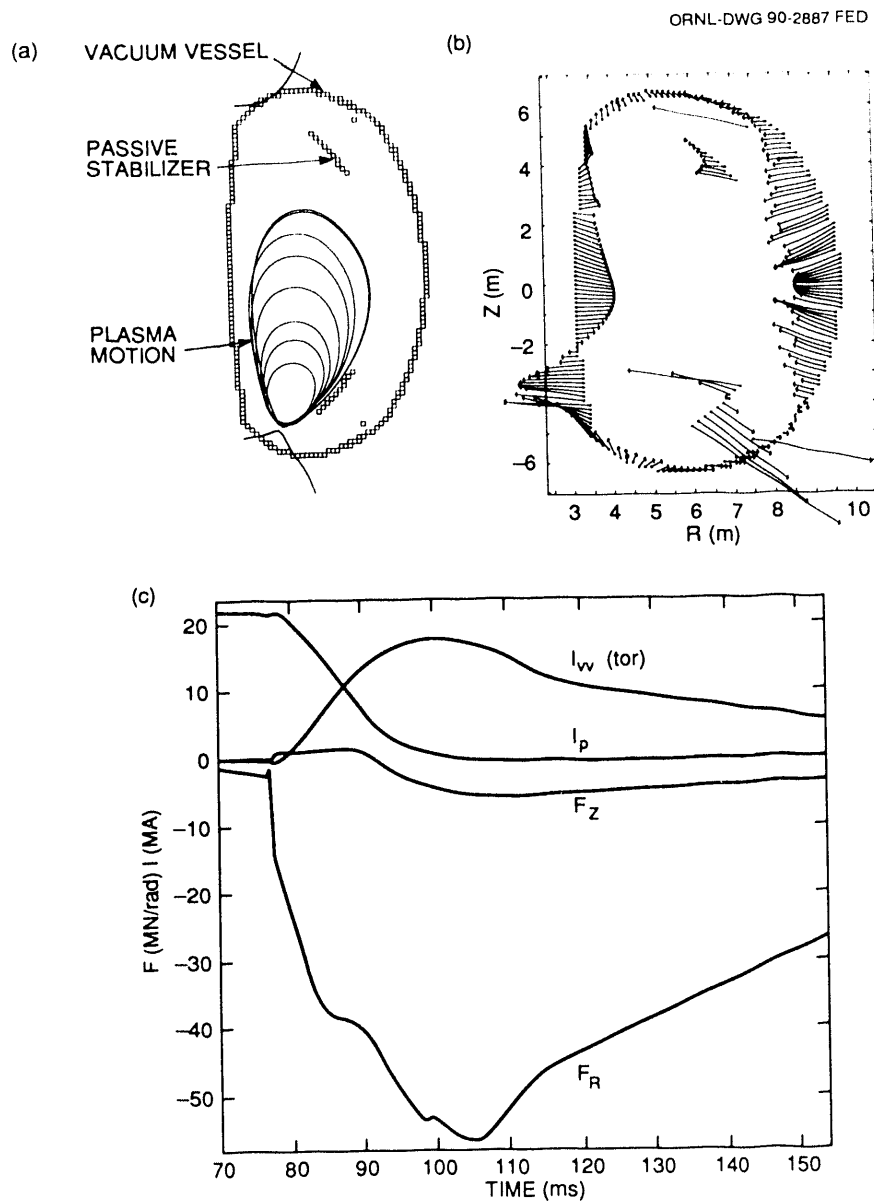


Fig. 6.7. ITER vertical disruption simulation. (a) Filamentary models for vacuum vessel, IC coil, and PS structures and plasma boundaries during the disruption phase. (b) Snapshot of forces. (c) Forces and current history.

The vacuum vessel was represented as a continuous 2-cm-thick structure of type 316 stainless steel. The effective toroidal resistance was $20 \mu\Omega$, and the L/R time was 98 ms.

The IC coil was represented by copper wires at $R = 7.00$ m and $Z = \pm 5.00$ m,

connected up-down anti-series (equal and opposite currents in upper and lower members).

The PS plates were modeled as wires at $R = 6.55$ m and $Z = \pm 3.90$ m, connected up-down anti-series with resistivity adjusted⁷ to give a vertical instability growth rate

equivalent to that for a realistic PS plate with 48 vertical legs.

PF coil currents for the initial equilibrium were determined with the ORNL equilibrium code.⁸ Typical initial plasma parameters were $I_p = 22$ MA, $B_t = 5.00$ T, $R_0 = 5.80$ m, $a = 2.20$ m, $\kappa_{95} = 1.89$, $\delta_{95} = 0.32$, $l_i/2 = 0.30$, $\beta = 3.2I/aB$, and $\beta_{pol} = 0.70$. For the vertical disruption simulations, a TSC initial equilibrium was achieved with the plasma magnetic axis, Z_{mag} , displaced 0.04 m from the midplane. The plasma was then allowed to drift downward until $Z_{mag} = 1.0$ m. After drift, the thermal quench was initiated by enhancing the plasma thermal conductivity by a large factor, producing an increase in plasma resistivity and the subsequent current quench.

Example results from a typical simulation are shown in Fig. 6.7(b), a snapshot of the force distributions for the vacuum vessel, PS structures, and IC coil for a vertically moving plasma during the current quench ($I_p = 14.7$ MA). Figure 6.7(c) shows the time behavior of the plasma current I_p , the toroidal VV eddy current $I_{VV}(tor)$, the net radial VV force F_R , and the net vertical VV force F_Z for a vertical disruption with $\langle dI_p/dt \rangle \simeq -1.0$ MA/ms.

Plasma disruptions have been modeled with TSC for the ITER physics phase. The time evolution of currents and forces on the vacuum vessel, IC coil, and PS structures was determined.

For a vertically moving disrupting plasma with $Z_{mag} = -1.0$ m at thermal quench and $\langle dI_p/dt \rangle \simeq -1.0$ MA/ms, the peak vacuum vessel total current is 18 MA. The extreme F_R is 56 MN/rad, and the extreme F_Z is 6.0 MN/rad. For the PS structure closer to the vertically moving plasma, the extreme net radial and vertical forces are 5.2 MN/rad and 3.6 MN/rad, respectively. Similarly, the extreme IC coil forces are 1.8 MN/rad (radial) and 0.5 MN/rad (vertical).

Outboard vacuum vessel forces are typically twice as large as inboard forces. Including forces due to the “diamagnetic” poloidal vacuum vessel current and toroidal fields increases F_R by about 6%. The maximum vacuum vessel disruption pressure is 1.0 MPa. Variations in vacuum vessel resistance (20–160 $\mu\Omega$) and dI_p/dt (1–2.5 MA/ms) do not change F_R significantly.

6.2.2 Engineering

An electrically segmented vacuum vessel with a 30-cm-thick wall was established as the reference ITER design on the basis of its apparent ability to withstand the maximum calculated value of loads transferred to it by the blanket during a plasma disruption. The reference value of these loads, for the most dramatic plasma disruption event, was set at 20 MN for each blanket octant, pending identification of methods to achieve electrical segmentation in blanket modules. The wall thickness was set at 30 cm to allow for 50 cm of shielding between the field weld joints and the plasma. This amount of shielding was determined to be required to allow rewelding of the joints between the parallel and wedge segments of the vacuum vessel.

Future work will be directed at identifying methods of reducing the loads transmitted to the vacuum vessel. More analysis is required to obtain a better understanding of the distribution of the loads and to identify design modifications of the blanket modules that reduce their size. Parallel design efforts will be directed toward identifying feasible methods to compensate for these loads within a module and/or between adjacent modules. If these efforts are successful, the much simpler alternative design proposed by the Design Center will be adopted.

The reference design for the cryostat was chosen on the basis of the structural, electromagnetic, and nuclear shielding requirements. A continuous stainless steel vessel with structural ribs (700-mm maximum thickness) with an equivalent electrical thickness of 70 mm satisfies both the mechanical and electrical requirements. Bucking criteria are dominant in determining the required mechanical strength. The Nuclear Engineering Group determined that space inside the cryostat vacuum vessel was adequate for shielding that would allow personnel access, if required, to the outer surface of the cryostat vessel 24 h after operation shutdown. Consequently, there is no special nuclear shielding requirement on the cylindrical section of the cryostat vessel other than penetration shielding, which must be provided independently of cryostat vessel design options. A simple full-welded, single-sheet structure with welded vertical and toroidal ribs has been chosen as the reference design. The cylindrical wall has an inner radius of 13 m, with the ribs extending to an outer radius of 13.7 m. The continuous sheet has a thickness of 35 mm.

6.2.2.1 Configuration and maintenance

The general arrangement of the ITER configuration is shown in Fig. 6.8. The main interior reactor components are contained within an assembly 13.7 m in radius and approximately 25 m high.

A double vacuum vessel arrangement, combined at the access ports, is used. The outer cylindrical vessel, constructed of rib-reinforced stainless steel plate, provides both a vacuum environment for the included cryogenic coils and secondary confinement for tritium located within the primary vacuum region. The interior toroidal vessel provides the vacuum quality needed

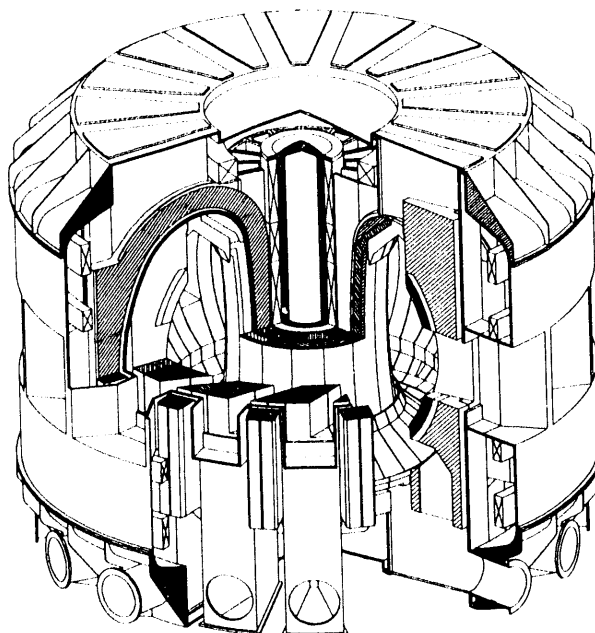


Fig. 6.8. General arrangement of the ITER configuration.

for successful plasma operation, forms the primary tritium boundary, and serves as the mechanical/structural support for the included nuclear components. At each of the 16 reactor toroidal sections, 4 large ducts connect the vessels. The upper duct is used for the installation of and service routing to the included nuclear components. The centerline ports provide access to the plasma for the required auxiliary heating, diagnostic, and maintenance equipment. The lower vertical port provides service routing to the lower portion of the included components and acts as the interface to the vacuum pumping duct, the fourth port, which extends horizontally off the lower port in Fig. 6.9.

As shown in Fig. 6.10, the components inside the vacuum vessel are configured into modules for insertion. Each toroidal sector is an assembly of inboard shield/blanket modules, outboard modules, additional local shield pieces, and upper and lower divertor

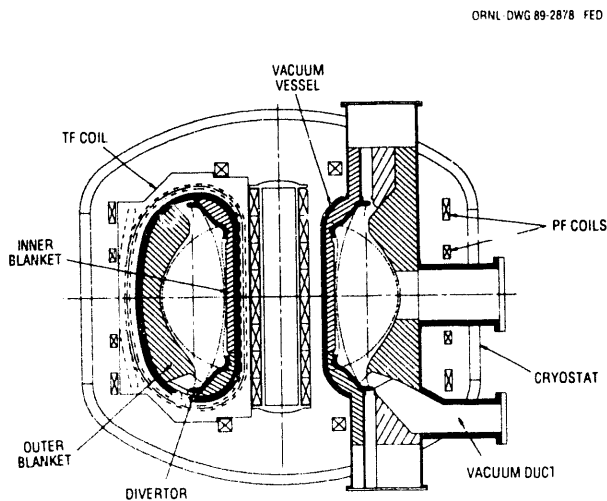


Fig. 6.9. Cross section of ITER showing double vacuum vessel arrangement and connecting ports.

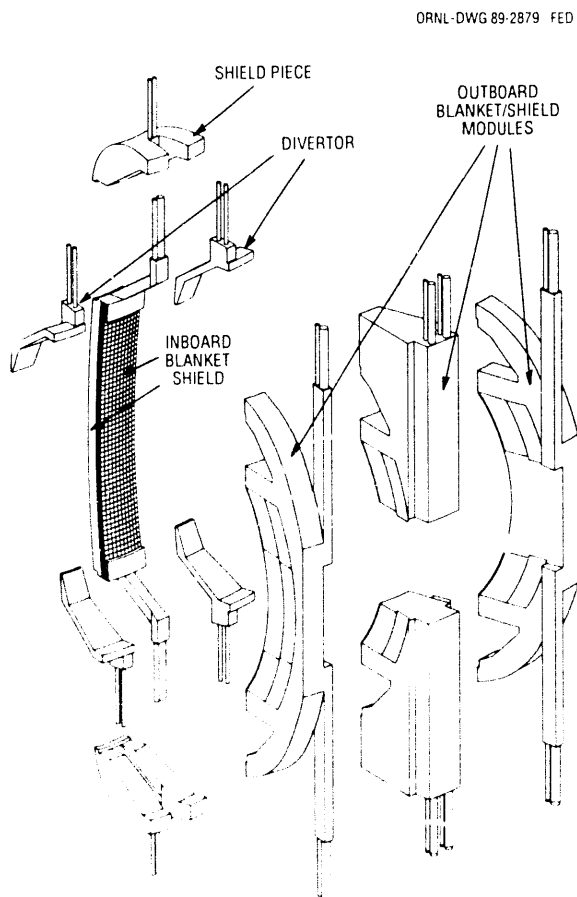


Fig. 6.10. Modular configuration.

assemblies. A breeding blanket is included on all the inboard and outboard modules and is backed with enough additional shielding to provide radiation protection to the TF coils. The first wall structure is also included in the module assembly. Passive stability loops are incorporated into the outboard modules. Independently removable divertor modules are mounted to the top and bottom of the inboard shield modules after they are installed. A principal feature of the revised configuration is that it maintains a fixed blanket/shield geometry for both the physics phase and the technology phase, meaning that modules will be removed only for maintenance following failures.

The magnetic configuration consists of 16 TF coils, a central solenoid (CS), and 3 sets of up-down symmetrical PF coils. All of these coils are superconducting. For ease of maintenance, all PF coils are located outside the TF coils: one pair in the inboard knuckle region and two pairs in a vertical stack outboard of the TF coil outer legs. Additional saddle loop resistive coils are used to provide active control of plasma stability; they are located within the vacuum vessel.

6.2.2.2 Electromagnetic and structural analysis

Efforts were begun to develop a self-consistent method of calculating both the plasma behavior and the induced loads in the structure. TSC is used to calculate the current distribution in the plasma volume for a set of axisymmetric coils and conducting structures. The resulting plasma behavior is used as the driver for a finite element eddy-current calculation using the SPARK or FDDYCUFF program and 3-D representations of the conducting structure. The

eddy currents in the conducting structure that are computed by the finite element method and TSC are compared, and appropriate adjustments are made in the TSC model. The process is repeated until the two calculations agree.

Initial results were presented to the ITER team and were instrumental in establishing the following project guidelines:

1. The effects of the size of the electrical gaps and surface resistivity are important.
2. Electromagnetic loads should be specified as a function of the electrical segmentation of the in-vessel components. Typical values for the inboard blankets are:
 - 20 MN for one electrical segment per sector,
 - 10 MN for three electrical segments per sector, and
 - 4 MN for nine electrical segments per sector.
 Values for the outboard blanket are:
 - 20 MN for one electrical segment per sector, and
 - 10 MN for three electrical segments per sector.
3. Since the electromagnetic loads are not up-down antisymmetric in the case of a vertical disruption, they are not self-compensated within the sector. In general, the loads from a vertical disruption are more severe than those from a symmetric disruption.
4. Maximizing electrical segmentation, while minimizing mechanical segmentation, seems most desirable for inboard blanket design.
5. The maximum forces occur at the electrical breaks, so separation of the electrical and mechanical breaks seems promising from the viewpoint of supporting the electromagnetic loads.
6. The divertor must be highly segmented and electrically isolated from its support plate.

6.2.2.3 Fast-wave current drive system

Members of the Design Center and the RF Development Group continued their work on the conceptual design of a fast-wave current drive (FWCD) system for ITER. Two designs were carried out: in one, all antennas are mounted in the midplane horizontal ports; in the second, the antenna elements are mounted in the blanket modules. Members participated in a specialists' meeting on FWCD at Garching, Federal Republic of Germany, August 21–September 1, 1989, at which a common design approach among the four participating parties was obtained. This design features

- an operating frequency of 15–60 MHz; FWCD can be done at 17 MHz (and possibly at 55 MHz), and plasma heating using ICRH can be done at intermediate frequencies;
- an array of 30–60 antenna elements mounted in blanket modules, with constant spacing and phase difference between antennas;
- rf coaxial lines embedded in the blanket module and emerging through the top of the blanket module;
- up to 60 2-MW rf power units, each connected by a separate transmission line and tuning/matching network to an antenna.

An elevation view of this system is shown in Fig. 6.11. The most critical element of this assembly is the antenna and Faraday shield system. The present design has two antennas mounted in each blanket module. With 96 blanket modules surrounding the machine, 30 antennas extend approximately one-third of the way around the torus, and 60 go two-thirds of the way around.

Calculations by the Plasma Theory Group yield a current drive efficiency factor $\gamma = (0.3\text{--}0.4) \times 10^{20}$ A/W·m² for this design.

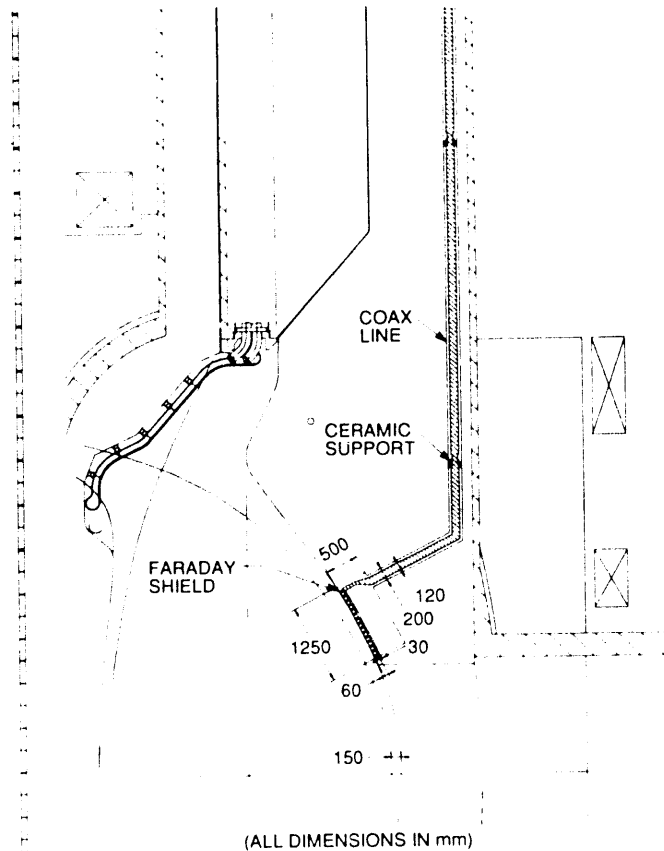


Fig. 6.11. ICRF launcher elevation view.

While this is not quite as high as the efficiencies calculated for the present baseline neutral beam system in ITER, the fact that the FWCD system does not contribute to the plasma beta by injecting high-energy particles (as the neutral beam system does) yields overall current drive efficiencies for FWCD that are comparable to those of the neutral beam system.

In the ITER design, the FWCD system is at present an alternative to the neutral beam current drive system. The most critical issue for the FWCD system is the experimental demonstration of FWCD at efficiencies suitable for ITER. Other engineering problems that will be addressed by the Design Center include the forces and thermal stresses that

the Faraday shield and the rest of the antenna structure will experience during a plasma disruption, the viability of using ceramic insulators in the transmission line near the antenna (in particular, the expected lifetime in the presence of the ITER neutron fluences), and the range of load resistances that the antennas are likely to see, given a realistic range of L-mode and H-mode plasma scenarios in ITER.

6.2.2.4 Pellet injection system

Overview

An advanced, high-velocity pellet injection system will be used to achieve and

maintain ignited plasmas on ITER. Staff members participated in a series of meetings of fuel cycle experts at Garching and have developed a conceptual design description for a flexible plasma fueling system, which includes three pellet injectors in addition to the traditional gas puffing system. For ramp-up to ignition, a highly reliable, moderate-velocity (1- to 1.5-km/s), single-stage pneumatic injector and a high-velocity (4- to 5-km/s), two-stage pneumatic pellet injector using frozen hydrogenic pellets encased in sabots will be used. For the steady-state burn phase, a continuous, single-stage pneumatic injector is proposed; this injector will provide a flexible source of fuel that penetrates to well beyond the edge region to aid in decoupling the plasma edge (constrained by divertor requirements) from the high-temperature burning plasma. All three pellet injectors are designed for operation with tritium and D-T feed gas. Issues such as performance, neutron activation of injector components, maintenance, design of the pellet injection vacuum line, gas loads to the reprocessing system, and equipment layout have been addressed.

Staff members are also conducting R&D in support of ITER fueling requirements, as described in Sect. 4 of this report. Tritium single-pellet fabrication and acceleration experiments have been conducted on the Tritium Systems Test Assembly at Los Alamos National Laboratory, and a program has been initiated to develop tritium-compatible extruders for long-pulse fueling. High-velocity pellet accelerators are under development, including a repetitive two-stage pneumatic injector (4–5 km/s) and, in the longer term, an electron-beam-heated, mass-ablation system. ORNL is also operating and maintaining state-of-the-art pellet fueling systems on TFTR, Tore Supra, and JET. This experience is providing an operational and reliability database for

extrapolation to ITER, in addition to its contribution to the understanding of the physics of pellet-fueled high-temperature plasmas.

Performance requirements for the ITER pellet injection system were developed in collaboration with ITER physics and engineering staff to ensure sufficient performance for the ITER mission while minimizing impact on the isotope reprocessing system and local tritium inventory levels. Other aspects considered are the need to develop the supporting technology in time for design, fabrication, and testing of the ITER pellet injection system, followed by installation on ITER, to meet the first plasma milestone and the need for technology that is adequate for accelerating repetitive pellets (repetition rate of order 1 Hz) for long pulses (100 to 1000 s) at high component reliability (of order 90 to 95%). These considerations eliminated some of the more advanced methods of plasma fueling, such as electron-beam pellet ablation and compact toroid fueling, from further consideration.

System description

The specifications of the ITER pellet injection system are summarized in Table 6.5. These specifications are met by a system with three pneumatic pellet injectors: a high-velocity (two-stage light gas gun) injector and two moderate-velocity (single-stage light gas gun) injectors. The parameters of these injectors are summarized in Table 6.6. Their arrangement in ITER is shown in Figs. 6.12 and 6.13, with components identified in Table 6.7.

The design of the moderate-velocity injectors is similar to that of the JET pellet injector. Each injector consists of two single-stage light gas guns in a vacuum enclosure. The diameters of the formed pellets (and of the gun barrels) may have to be 10 to 15%

Table 6.5. ITER pellet injection system specifications

Pellet diameter, mm	5–7.4
Pellet species	
Normal	D-T (in 50:50 ratio)
Alternative	H, D, T
Pellet velocity, km/s	1.0–5
Maximum pellet frequency, Hz	3
Total pellets	
During ramp-up	60
During burn phase	Continuous
System reliability, %	97

larger than the pellet sizes listed in Table 6.5 because of erosion of pellet material in the barrel during acceleration. For the moderate-velocity injector (operated without sabots), the diameter of the larger pellets at formation (and the barrel size) is 8.3 mm to account for a 30% mass loss by erosion. Erosion is a concern with tritium and D-T pellets because of the tritium lost through erosion. However, this effect increases with pellet velocity and should not be a problem in the velocity range (1 to 1.5 km/s) of the moderate-velocity injector.

The design of the high-velocity pellet injector is based on the two-stage light gas gun concept, in which a piston is pneumatically accelerated in a high-pressure pump tube to provide adiabatic compression of a second stage of propellant gas between the piston and the pellet/sabot. The resulting high pressures (up to 6000 bar) and, more importantly, high temperatures (4000 to 8000 K) can accelerate the pellet/sabot payload to muzzle velocities in the 4- to 5-km/s range.

The plasma perturbation limit, $\Delta n/n \leq 15\%$, sets the maximum pellet diameter of 7.4 mm and also, in combination with the range in plasma operating densities, dictates the range of pellet diameters specified in Table 6.5. During the ramp-up to ignition, the plasma density will continuously increase, and the density at ignition will be different with different plasma temperatures and heating profiles. The different pellet sizes are obtained by using two different barrel sizes on the moderate-velocity injectors and by using sabots of different designs on the high-velocity injector. The largest (7.4-mm-diam) pellet results in a 15% perturbation to an ITER plasma at an average density of $1.2 \times 10^{20} \text{ m}^{-3}$.

Table 6.6. ITER pellet injection parameters

	Moderate-velocity injectors	High-velocity injectors
Barrel diameter, mm	6.0, 8.3 ^a	9.0 ^b
Pellet velocity, km/s	1.0–1.5	2.0–5.0
Pellet species	H, D, T, D-T	H, D, T, D-T
Repetition rate, Hz	0–5	0–2
Total pellets	Continuous	30 (minimum) to continuous (goal)
Reliability, %	95	90

^a Accounts for erosion loss in barrel.

^b Accounts for 2.0-mm radial growth for sabot.

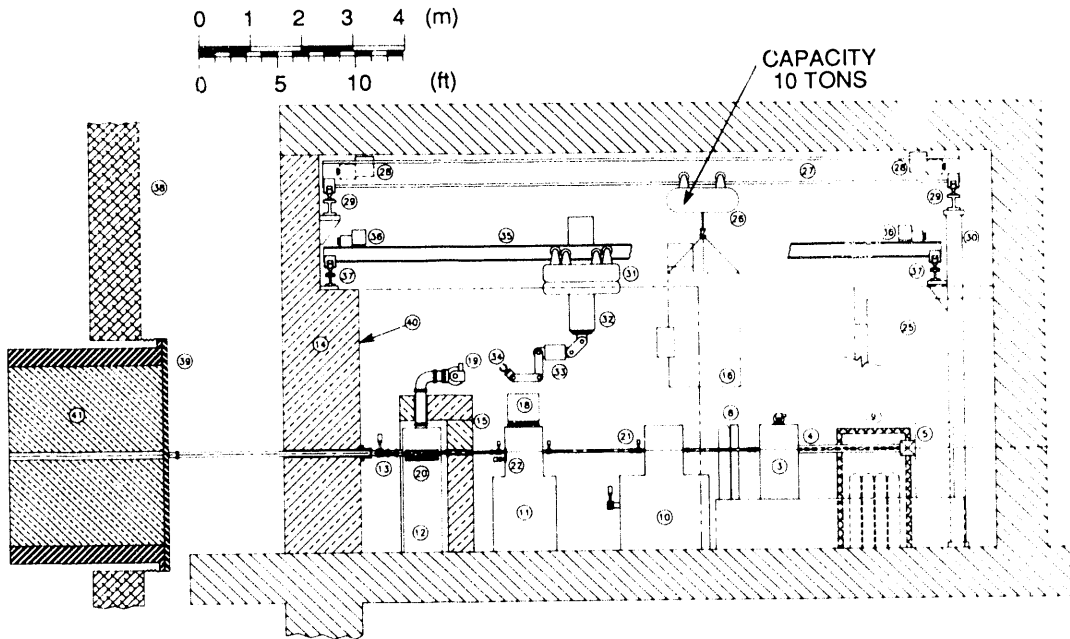


Fig. 6.12. Elevation view of ITER pellet injectors. Components are identified in Table 6.7.

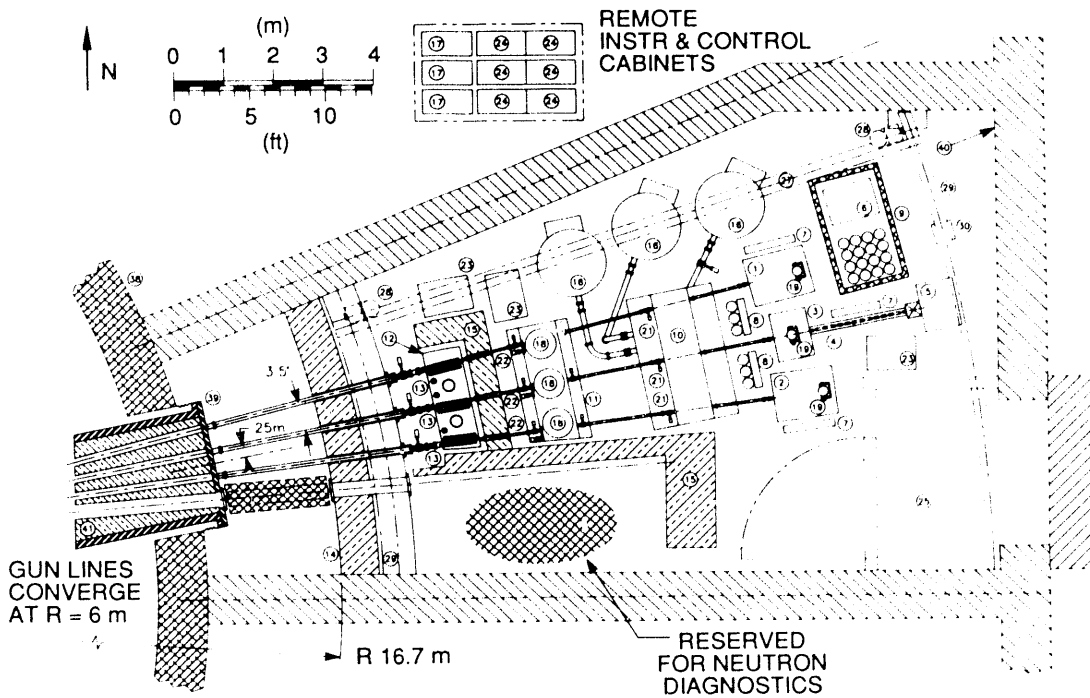


Fig. 6.13. Plan view of ITER pellet injectors. Components are identified in Table 6.7.

Table 6.7. Components of the ITER pellet injectors
Numbers refer to Figs. 6.12 and 6.13

1. Moderate-velocity injector	22. Rotatable targets
2. Moderate-velocity injector	23. Backing pumps
3. High-velocity injector (HVI)	24. Instrumentation cabinets
4. HVI pump tube	25. Airlock
5. HVI propellant reservoir	26. Crane, 10-ton capacity
6. HVI propellant compressor	27. Crane beam
7. Propellant gas manifolds	28. Crane beam gearmotors
8. Fuel gas manifolds	29. Crane rails
9. High-pressure cage	30. Crane rail columns
10. Low-vacuum chamber	31. Manipulator turret
11. Mid-vacuum chamber	32. Telescoping boom
12. High-vacuum chamber	33. Manipulator and camera
13. Torus isolation valves, breaks, bellows	34. Dual replaceable end effectors
14. Structural shielding wall	35. Manipulator bridge
15. Modular shielding	36. Manipulator bridge gearmotors
16. Normetex 1300-m ³ /h scroll pumps	37. Manipulator bridge rails
17. Normetex control cabinets	38. ITER cryostat
18. Turbopumps, 5000 L/s	39. ITER vacuum vessel port 16
19. Turbopumps, 500 L/s	40. Metal room liner
20. Rotatable shielding drums and motors	41. In-port shielding
21. Flow-limiting fast valves	

As discussed in Sect. 6.1.4, the reliability figures in Table 6.6 should be achievable. Also, during the ramp-up to ignition, the high-velocity injector and one of the two moderate-velocity injectors will be used. Having two moderate-velocity injectors that can be used interchangeably increases the system reliability.

The second moderate-velocity injector will be used for continuous fueling, with penetration significantly beyond the edge region, during the burn phase. The high-velocity injector can also be used during the burn phase if piston lifetimes of 100 to 1000 cycles can be achieved.

A plan view of the pellet injector installation is shown in Fig. 6.13. The two-stage high-velocity injector is located on the

centerline of vacuum vessel port 16, approximately 24.5 m from the center of the ITER machine. The moderate-velocity injectors are on either side of the two-stage pneumatic injector; the centerlines of the three injectors converge in the midplane at the ITER major radius of 6.0 m. To prevent the propellant gas from reaching the torus, the injectors are isolated from the vacuum vessel by a series of three separately pumped vacuum chambers connected by conductance-limiting pellet guide tubes and fast-acting flow-limiting valves. The pellet injector bay is shielded by the structural shielding wall; by a rotating, eccentrically bored shielding drum in each injection line (to limit line-of-sight exposure of the injectors); and by modular shielding around the high-vacuum

isolation chamber. The bay also serves as a redundant containment boundary and is sealed by bellows at the shielding wall and by an airlock at the entrance. Equipment in the pellet injector bay is serviced by a 10-ton crane and a bridge-mounted articulated manipulator supported on curved rails at machine radii of approximately 15.7 m and 29.5 m.

6.2.3 ITER Physics

N. A. Uckan, J. T. Hogan, D. B. Batchelor,* B. A. Carreras,* J. A. Holmes,[†] W. A. Houlberg,* E. F. Jaeger,* D. A. Spong,* and D. W. Swain

ORNL physicists actively participated in the ITER Conceptual Design Joint Work during the winter (February–March 1989) and summer (July–October 1989) sessions at the Max Planck Institut für Plasmaphysik (IPP) Garching and played a key role in the evolution of the ITER physics design. The primary areas of ORNL contributions to ITER physics studies were in MHD stability and beta limits, confinement assessment, FWCD, and pellet fueling. In addition, work has been carried out on axisymmetric magnetics, alpha particle effects, helium ash accumulation and exhaust, and plasma-wall interactions.

Physics design guidelines and physics specifications for the design information document were prepared and published. Limitations to the operational space arising from MHD instability (ideal and resistive, linear and nonlinear, fluid and kinetic) were estimated, and the MHD databases for current drive and for peaked pressure and current density profiles were extended. Various transport models were compared with the ITER L-mode database, and the confinement capability of ITER was assessed using these

models. The DIII-D and TFTR databases for volt-second consumption during the current ramp-up phase, especially as they apply to MHD-influenced (fast ramp) scenarios, were analyzed. Particle transport and fueling (gas puffing vs pellet fueling) issues were assessed. Detailed estimates of FWCD efficiency were made with a two-dimensional, full-wave code. Finally, the ITER physics R&D contributions received from various experimental groups were coordinated.

*Plasma Theory Section.

[†]Computing and Telecommunications Division, Martin Marietta Energy Systems, Inc.

6.2.3.1 ITER physics design guidelines

N. A. Uckan and ITER Physics Group*

The physics requirements for the ITER design have been set to provide reasonable assurance that the plasma performance will be sufficient to meet the goals of ITER in both the physics phase and the technology phase of operation. Considerations for an adequate level of energy confinement with a stable plasma, a satisfactory power and particle control system, an efficient heating and current drive scheme, a suitable plasma control system, a sufficient level of volt-seconds, a need for high-fluence burn, etc., along with several engineering and technology constraints, set the machine parameters (size, field, current, etc.). The physics specifications and guidelines for the ITER design are based on reasonable extrapolations of the tokamak physics database as assessed during the ITER Joint Work sessions. The original guidelines, covering the period up to 1989, were summarized in a recent publication.⁹

*ITER Physics Group members: K. Borrass, S. Cohen, F. Engelmann, N. Fujisawa, M. Harrison,

J. Hogan, H. Hopman, S. Krasheninnikov, T. Mizoguchi, V. Mukhovatov, W. Nevins, G. Pacher, H. Pacher, V. Parail, D. Post, S. Putvinskij, M. Sugihara, D. Swain, T. Takizuka, T. Tsunematsu, N. Uckan, J. G. Wegrowe, J. Wesley, S. Yamamoto, R. Yoshino, and K. Young.

6.2.3.2 ITER confinement capability

N. A. Uckan and J. T. Hogan

The confinement capability of ITER physics and technology phase plasmas was examined for a number of operational scenarios, using the ITER physics design guidelines.⁹ The impact of changes in these guidelines on ITER performance projections was investigated. Both empirically based confinement scaling expressions (deduced from the ITER L- and H-mode databases) and several theoretical models were used in the analyses. Areas considered were the effect of changes in density and temperature (pressure) profiles that can be realized from various fueling and heating scenarios (subject to sawtooth and MHD stability considerations), operational boundaries, impurity and helium ash concentrations, current drive efficiency, bootstrap current fraction, and allowable fusion power (P_{fus}) levels. Achievement of adequate energy confinement time (τ_E) for ignition (or energy multiplication factor $Q \geq 10$) in ITER requires attainment of an H-mode level of enhanced confinement with $\tau_E(\text{H-mode}) \sim 2 \times \tau_E(\text{L-mode})$. The reference scenario for the physics phase ($I = 22$ MA with capability up to 25–28 MA, $P_{\text{fus}} \sim 1.1$ GW, average neutron wall loading ~ 1 MW/m²) has substantial ignition (or $Q \geq 10$) capability. The ignition capability of ITER can be further improved if some of the limits on operational boundaries can be relaxed and if centrally peaked density and heat deposition profiles

with favorable MHD stability properties can be realized. It is found that peaking the density profile (from nominal square-root parabolic form to parabolic squared) in the reference ITER scenario yields about the same results as lowering the helium ash concentration by about a factor of 2 (from the baseline value of 10% to 5%) or increasing the plasma current by about 20% (from the baseline value of 22 MA to 25 MA). The ITER technology phase accommodates several operational scenarios (ranging from long-pulse to steady-state operation) with $Q \geq 5$ and $I \approx 15$ –22 MA. Access to high- Q operation depends sensitively on the MHD beta limits, current drive efficiency, and bootstrap current fraction. Representative results are given in Figs. 6.14 and 6.15.

6.2.3.3 ITER global stability limits

J. T. Hogan and N. A. Uckan

The stability-related limits to the operational space of ITER physics and technology phase plasmas have been examined using the PEST 2 code (furnished by J. Manickam of PPPL). Experimental results cannot be

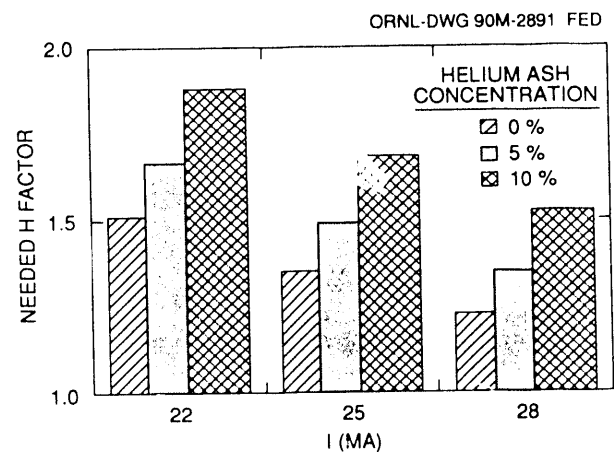


Fig. 6.14. ITER ignition capability at 1 MW/m² (ITER-P scaling).

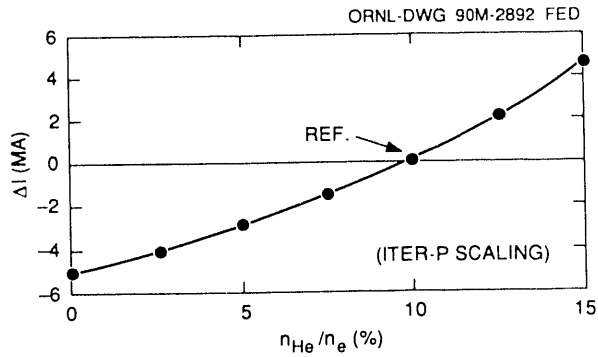


Fig. 6.15. Impact of helium concentration on required plasma current for equivalent performance. Reference point: $I = 22$ MA at an average neutron wall loading of 1 MW/m^2 .

directly adopted because the close-fitting shell-like PF systems in present experiments are not similar to the ITER PF system. An ITER database of calculated results ($\sim 20,000$ cases) enables prediction of the characteristics of the overall operational space. This technique is preferable to relying on a stability study of a few (perhaps atypical) profiles. The theoretically predicted ITER operational space has many features in common with that observed in present strongly shaped tokamaks [magnitude of the maximum Troyon factor (g), and g -dependence on current density profile (l_i) and safety factor q_ψ]. Stability limits are strongly affected by pressure and current density profiles, and the impact of profile variation on ITER performance projections was investigated. Studies of the beta limits for edge current drive [$q(0) > 1.5$], current density profile peaking [$q(0) < 1.0$], and central pressure profile peaking have been carried out, as well as examination of the feasibility of operation at values of $q_\psi < 3.1$ (the present physics phase specification), as could be required for divertor operation. Study of edge-current-driven scenarios

shows that Troyon factors $g \leq 2.5$ can be attained (with a conducting wall at infinity) for $q_\psi \sim 3.1$, and $g \sim 3$ for higher q_ψ (up to 6). Stability of $n = 1$ modes is found with the proper shear distribution for profiles with $q(0) \sim 0.85$, allowing $g \sim 2.5$. Strongly peaked pressure profiles can lead to a degradation in stability limits.

The predicted ITER operational space in g - q_ψ space is shown in Fig. 6.16. Some restriction in the available space is apparent for operation with $g > 3$, and the zero-beta limitation due to external kinks is evident for low values of l_i .

6.3 ARIES

6.3.1 MHD Equilibrium and Stability

The plasma equilibrium and stability analysis carried out for the Advanced

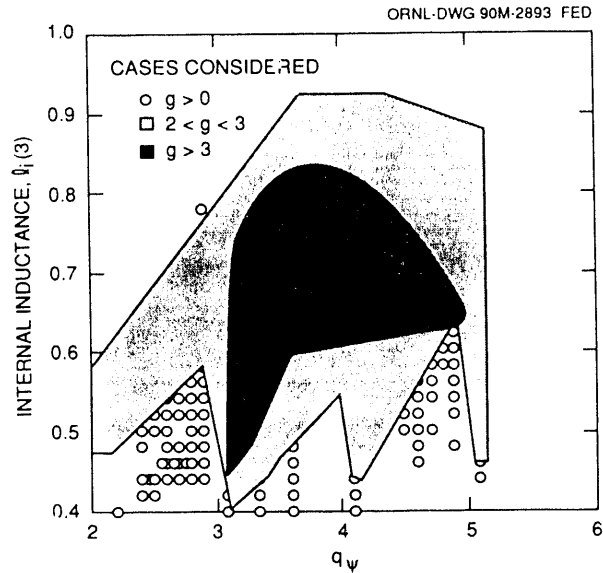


Fig. 6.16. ITER operational space in g - q_ψ space, predicted from the ITER database, for $A = 2.64 \rightarrow 3.1$, $1.8 < \kappa < 2.2$, $0.2 < \delta < 0.6$. Stability to $n = 1$ ($a_\psi/\alpha = \infty$) ballooning modes is found.

Reactor Innovation and Evaluation Study (ARIES) program employs assumptions consistent with those of the ITER design. Distinguishing features of the ARIES-I design include

1. limiting the plasma current I_p to about 10 MA to reduce the steady-state current drive power while assuming H-mode plasma confinement with an enhancement factor $H \geq 2$ over the L-mode;
2. raising the plasma $\epsilon\beta_p$ to about 0.6 to increase the bootstrap fraction to about 0.7, which further reduces the current drive power; and
3. enhancing the plasma beta in the first stability regime using plasma current profiles characterized by $q_0 \simeq 1.5$ and $q_{95} \leq 5$, and produced by ion cyclotron resonant frequency or neutral beam current drive. Here q_{95} refers to the flux surface at 95% of the poloidal flux toward the divertor X-point.

Two other design requirements unique to the ARIES-I concept have a direct bearing on the plasma equilibrium:

1. The distance between the PF coils and the plasma edge is about 2.5 times the plasma minor radius a , leading to large PF coil stored energy (up to about 25 GJ).
2. The distance between the plasma edge and a passive conductor (located between the blanket and the shield) is about $0.6a$. This reduces the X-point elongation ($\kappa_X = 1.8$) needed to maintain vertical stability and increases the triangularity ($\delta_X = 0.7$), which minimizes PF coil stored energy.

Key results in the areas of PF coil placement, plasma equilibrium and stability are now summarized. The placement of the PF coil set is determined by the need to provide the basic multipolar fields so as to meet the overall design requirements:

1. a dipole (vertical) field to center the plasma at $R_0 = 6.75$ m,
2. a quadrupole (elongating) field to maintain $\kappa_X = 1.8$,
3. a hexapole (triangulating) field to maintain $\delta_X = 0.7$, and
4. an octupole field to provide some plasma current induction and to further reduce stored energy.

The reference MHD equilibria for ARIES-I are computed using the VEQ code, which provides free-boundary solutions for a given plasma position, shape, and linked poloidal flux while minimizing the stored energy. The plasma pressure and current profiles are consistent with the first stability regime and a steady-state current profile produced by bootstrap current and active drive. Trade-offs among these requirements lead to a choice of profiles,

$$p(\chi) = p_0 \left(\frac{\epsilon^{\alpha\chi} - \epsilon^\alpha}{\epsilon^\alpha - 1} \right),$$

$$ff'(\chi) = \mu_0 R_0^2 \rho_0 \left(\frac{1}{\beta_J - 1} \right) \times \left(\frac{\epsilon^{\gamma\chi} - \epsilon^{-\gamma}}{\epsilon^{-\gamma} - 1} \right),$$

where p is the pressure, f is the poloidal current, and χ is the poloidal flux, which is normalized to 1 within the plasma. The toroidal plasma current density is

$$J_t = Rp' + \frac{ff'}{\mu_0 R},$$

where R is the major radius. The poloidal flux distribution of a reference equilibrium assuming $\alpha = -3$, $\gamma = -3$, and $\beta_J = 2.75$ is provided in Fig. 6.17. Parameters of this

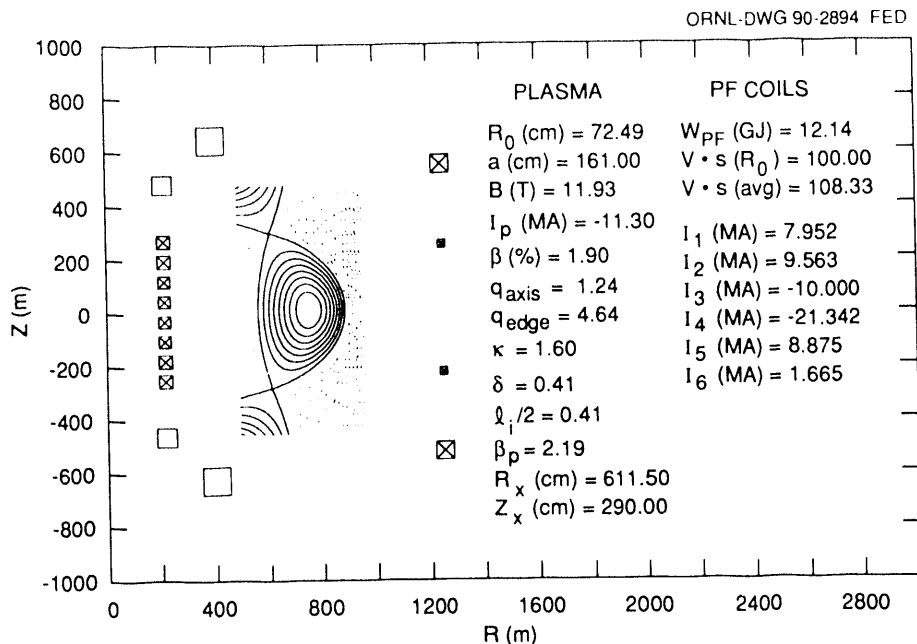


Fig. 6.17. Plasma equilibrium flux configuration and the placement of the PF coils for the ARIES-I reactor.

reference equilibrium that are relevant to stability and current drive analysis are given in Table 6.8.

This reference case provides an adjustment to the conditions that relate I_p to q , a , B_t , and the plasma shape parameters:

$$I_p q = 5aB_t \frac{\epsilon(1.15 - 0.65\epsilon)}{(1 - \epsilon^2)^2} \left(\frac{1 + \kappa_X^2}{2} \right),$$

where q is the average-field safety factor using the averaged poloidal field at the plasma edge. For the reference equilibrium,

$$\frac{\delta_X}{\delta_{95}} = 1.59, \quad \frac{\kappa_X}{\kappa_{95}} = (1.13 - 0.08\epsilon),$$

$$\frac{q_{95}}{q} = 1.09$$

are also used to relate the edge and 95% flux surface quantities. The maximum PF coil currents of up to 35 MA occur in the elongating and triangulating coils PF3 and PF4.

The first stability regime implies that all ideal MHD modes are at least marginally

Table 6.8. Parameters of a reference divertor MHD equilibrium for the ARIES-I reactor

Major radius R_0 , m	6.75
Minor radius a , m	1.50
External toroidal field on axis B_t , T	11.3
Plasma current I_p , MA	10.2
Safety factor on axis q_0	1.45
Average-field safety factor q	4.40
Safety factor at 95% flux q_{95}	4.75
Average beta β , %	1.92
Poloidal beta β_p	2.18
Elongation at X-point κ_X	1.80
Elongation at 95% flux κ_{95}	1.62
Triangularity at X-point δ_X	0.70
Triangularity at 95% flux δ_{95}	0.44
X-point location, m	
R_X	5.70
Z_X	2.70
Internal inductance l_i	0.74

stable in the absence of a conducting shell beyond the plasma edge. While this requirement is broad in scope, it is usually adequate to examine only the high- n ballooning modes and the low- n ($n = 1$) kink modes to determine the stability beta limit. As an input to design trade-offs involving plasma shaping, profile, aspect ratio, and the beta limit, our study emphasizes clarifying the dependences of beta on A , κ_{95} , q_0 , and q_{95} . Only the traditionally successful profile functions have been used for the analysis, such as those used for ITER and in reviews of the large body of information in the literature. Calculations are carried out for high- A ($A = 4.5$ and 6.0) ARIES-I plasmas using the PEST equilibrium and stability codes to "fill in" data where needed. The combined database of the stability analysis covers a range of $A = 2.6$ – 6.0 , $\kappa_{95} = 1.6$ – 3.2 , $q_0 = 1.05$ – 2.0 , and $q_{95} \leq 5$.

The dependence of the beta limit on κ_{95} and ϵ ($\equiv 1/A$), expressed in terms of the Troyon factor limit ($C_T = \beta a B_t / I_p$, in %·m·T/MA) is

$$C_T = 2.8 \frac{1 - 0.4(\kappa_{95} - 1)^2}{(1 - \epsilon)^{1.5}},$$

which gives $C_T \sim 3.4$ and $\beta \sim 2.1\%$ for the reference plasma parameters in Table 6.8. It has also been shown that for $A \geq 3$, this beta limit remains relatively unchanged as long as l_i remains below 0.75. Additional studies of the beta limit have been carried out for plasmas using polynomial profiles and parameters encompassing the reference case: I_p ranging from 16 to 8 MA, q_{95} from 3 to 6, and β_p from 1.4 to 3. The value of C_T is 3.1 to 3.2 as long as q_{95} is above 3.7. This result is considered conservative relative to the preceding indication. Design values of $C_T = 3.2$ (corresponding to $\beta = 1.9\%$) and $l_i = 0.74$ are therefore adopted for ARIES-I (see Table 6.8).

6.3.2 Pellet Fueling

An advanced pneumatic pellet injection system was developed for the ARIES-I fusion reactor study. The flexible system will use three pneumatic pellet injectors based on existing or near-term technology to achieve and maintain ignited D-T plasmas. During the density ramp-up to ignition, a moderate-velocity (1- to 1.5-km/s), single-stage pneumatic injector and a high-velocity (4- to 5-km/s), two-stage pneumatic pellet injector using frozen hydrogenic pellets encased in sabots will be used. For the continuous-burn phase, a single-stage pneumatic injector is proposed. This injector will provide a flexible fueling source beyond the edge region to allow decoupling the edge region (constrained by divertor requirements) from the high-temperature burning plasma. All three pellet injectors are qualified for operation with tritium feed gas. Issues such as performance, neutron activation of injector components, maintenance, design of pellet injection vacuum line, gas loads to the reprocessing system and equipment layout have been addressed.

REFERENCES

1. D. Macdonald, "Maintenance Concept Development for the CIT," presented at the ANS Third Topical Meeting on Robotics and Remote Systems, Charleston, S.C., March 1989.
2. R. E. DePew and D. Macdonald, "Remote Maintenance of Compact Ignition Tokamak Ex-Vessel Systems," pp. 593–6 in *Proceedings of the IEEE 13th Symposium on Fusion Engineering, Knoxville, 1989*, vol. 1, IEEE, New York, 1990.
3. S. K. Combs et al., "Performance of a Pneumatic Hydrogen-Pellet Injection System on the Joint European Torus," *Rev. Sci. Instrum.* **60**, 2697–2700 (1989).
4. D. J. Strickler et al., "MHD Equilibrium Using Free-Boundary Control Matrix," *Bull. Am. Phys. Soc.* **34**, 1972 (1989).

5. S. C. Jardin, N. Pomphrey, and J. Delucia, "Dynamic Modeling of Transport and Positional Control of Tokamaks," *J. Comput. Phys.* **66**, 481 (1986).
6. ITER Systems Group and ITER Physics Group, *ITER Operational Scenarios for Ignition, Steady-State and Hybrid Modes: Final Performance for the New Impurity Specifications*, ITER-IL-SA-1-9-36, International Thermonuclear Experimental Reactor Joint Working Group, Garching, Federal Republic of Germany, 1989.
7. J. Leuer, private communication.
8. D. J. Strickler et al., *Equilibrium Modeling of the TFCX Poloidal Field Coil System*, ORNL/FEDC-83/10, Martin Marietta Energy Systems, Inc., Oak Ridge National Laboratory, April 1984.
9. N. A. Uckan and the ITER Physics Group, *ITER Physics Design Guidelines 1989*, IAEA/ITER/DS-10, IAEA, Vienna, February 1990.

7

FUSION MATERIALS RESEARCH

E. E. Bloom¹
Fusion Materials Program Manager

D. J. Alexander¹
G. E. C. Bell¹
D. N. Braski¹
T. D. Burchell¹
M. L. Grossbeck¹
T. Inazumi²
R. L. Klueh¹
A. W. Longest³
L. K. Mansur¹

P. J. Maziasz¹
A. F. Rowcliffe¹
T. Sawai²
R. L. Senn³
I. I. Siman-Tov³
R. E. Stoller¹
K. R. Thoms³
P. F. Tortorelli¹
S. J. Zinkle¹

-
1. Metals and Ceramics Division.
 2. Japan Atomic Energy Research Institute, Ibaraki-ken, Japan.
 3. Engineering Technology Division.

7. FUSION MATERIALS RESEARCH

SUMMARY OF ACTIVITIES

The Fusion Materials Program at ORNL is active in three areas of materials research and development: structural materials for the first wall and blanket, graphite and carbon-carbon composites for plasma-interactive and high-heat-flux components, and ceramics for electrical, optical, and possible structural applications. About 75% of our work directly supports the Compact Ignition Tokamak and the International Thermonuclear Experimental Reactor (ITER). The remainder is focused on longer-term issues associated with the development of structural materials for fusion power reactors. Research on Fe-Cr-Ni austenitic steels, leading candidates for ITER structural applications, is conducted collaboratively with the Japan Atomic Energy Research Institute. This research will provide the major portion of the database on structural materials for first wall and blanket design. Research on irradiation-induced stress-corrosion cracking of austenitic steels, effects of irradiation on low-temperature fracture toughness, development of low-activation Fe-Cr-Mn austenitic steels, mechanical behavior of copper and copper alloys, irradiation performance of ceramics, and irradiation effects in graphite and carbon-carbon composites also addresses critical questions identified in the initial phases of the ITER project. In the longer term, the economic and environmental acceptability of fusion will depend in large measure on the development of materials that minimize the radioactive waste burden and have adequate properties from the viewpoints of systems engineering, safety, and lifetime capability. To address this question, we are pursuing the development of low-activation austenitic and ferritic steels, vanadium alloys, and structural ceramics.

7.1 STRUCTURAL MATERIALS

7.1.1 Austenitic Stainless Steels: The U.S.-Japan Collaborative Program

The austenitic stainless steels have occupied a central position in structural materials programs worldwide for the past decade. A vast amount of commercial experience exists on fabrication, welding, and mechanical and corrosion behavior. Irradiation behavior in fast breeder reactor environments has been extensively studied. It has been shown that alloys such as D9 and prime candidate alloy (PCA) maintain swelling resistance and favorable mechanical behavior at neutron doses approaching 100 displacements per atom (dpa) for temperatures in the range from 400 to 650°C.

The U.S.-Japan collaborative program is focused on determining the behavior of austenitic stainless steels under irradiation conditions that are more typical of the fusion environment. Irradiation experiments are conducted in the mixed-spectrum fission reactors [the Oak Ridge Research Reactor (ORR) and the High-Flux Isotope Reactor (HFIR)]. The two-step reaction between the nickel component of the steel and thermal neutrons results in the generation of helium; the rate of helium generation can be adjusted either by modifying the ratio of thermal to fast neutrons (spectral tailoring) or by adjusting the ratio of ^{58}Ni and ^{60}Ni isotopes in the steel (isotopic tailoring). The collaborative program embraces three sets of irradiation experiments. The first set of experiments was conducted in HFIR target positions and explored the effects of high concentrations of helium (>2000 appm) on the tensile, fatigue, and swelling properties of austenitic stainless steels at temperatures in the range from 300 to 600°C; this work was completed in 1988. The second set of experiments was designed to reproduce the temperatures,

damage rate, helium generation rate, and neutron fluence characteristic of the first wall and blanket (FWB) structure of the International Thermonuclear Experimental Reactor (ITER). These spectrally tailored experiments completed their initial dose increment of 8 dpa in the ORR and have been re-encapsulated for further irradiation in the HFIR RB* positions. The third set of experiments consists of a set of eight HFIR target capsules containing isotopically tailored alloys. These experiments will explore the swelling resistance of advanced austenitic steels that have been compositionally and microstructurally adjusted to improve the swelling resistance of the PCA in the fusion environment. These experiments will explore doses up to 70 dpa at temperatures ranging from 300 to 600°C and will provide information relevant to the design of advanced FWB module concepts for ITER.

During the past year, data were obtained from the ORR 6J/7J spectrally tailored experiments on swelling, tensile, and creep properties of U.S. and Japanese alloys. It is concluded that void swelling will not be a problem for AISI 316 or PCA under ITER conditions, provided FWB temperatures remain below 400°C. Swelling could be significant at 300°C, however, if a low-carbon version of AISI 316 is used. For temperatures up to 500°C, tensile properties are not very sensitive to spectral or damage rate variations. At temperatures below 400°C, the spectrally tailored experiments have shown that the most significant effect of neutron irradiation is radiation hardening coupled with a severe reduction in work hardening capacity. The possible impact of this phenomenon on fracture toughness is being studied under a further collaborative experiment.

Using miniature pressurized tubes, it was shown that irradiation creep is a significant

deformation mechanism under ITER FWB temperatures and stress conditions. Creep strains were found to be linear with stress; surprisingly, it was found that creep rates for a variety of austenitic steels were higher at 60°C than at 330 to 400°C (Fig. 7.1). A mechanism based on transient climb-enabled glide was proposed to explain this behavior. Creep rates at 330 and 400°C for the ferritic alloys HT-9 and Fe-16Cr were somewhat lower than those for austenitics; for both ferritic alloys, creep rates at 60°C were higher by factors of 10 to 15 than those at 330 to 400°C.

The possibility that radiation-assisted stress-corrosion cracking may be significant under ITER conditions is being investigated. Electrokinetic potential reactivation measurements combined with analytical electron microscopy (AEM) have demonstrated that neutron irradiation to ~10 dpa at 400°C induces susceptibility to intergranular stress-corrosion cracking (IGSCC). No evidence could be found for IGSCC susceptibility following irradiation at 330 and 200°C. However, measurements do indicate a radiation-

assisted increase in overall corrosion rates at these temperatures, resulting from localized chromium segregation within the grains and consequent destabilization of passive films. Irradiation to 8 dpa at 60°C does not appear to have any effect on corrosion behavior or susceptibility to cracking. The possibility of radiation-assisted corrosion phenomena related to phosphorus segregation is being investigated by alternative electrochemical measurements on irradiated materials.

7.1.2 ITER Design Database

A multinational effort is in place to provide a common source of data for the design of ITER. Such a database will enable designers to compare component and system designs for the relative merits of the designs themselves. The database project is guided by an international steering committee, and operations are handled by a database coordinator. The effort on austenitic stainless steels is coordinated at Oak Ridge.

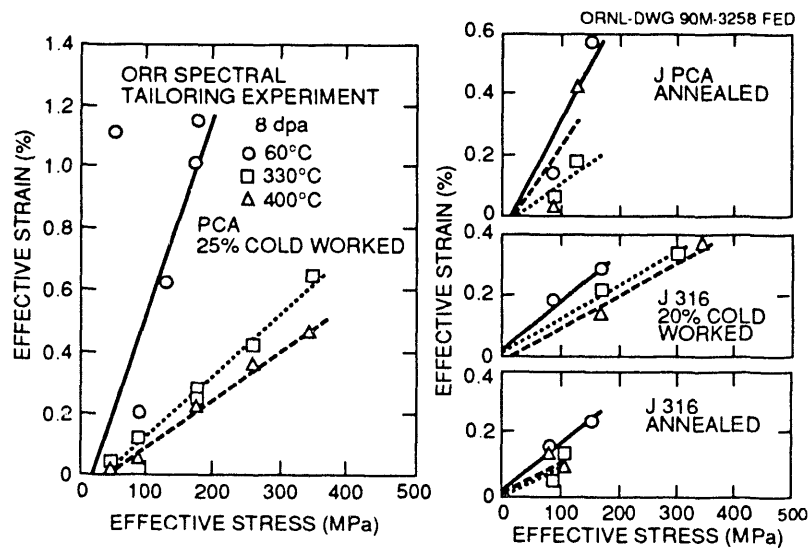


Fig. 7.1. Irradiation creep strain as a function of stress for various austenitic stainless steels irradiated under simulated ITER conditions.

During the last reporting period, the effort on tensile properties was discussed. In the past year, minor refinements were made to the equations for tensile properties.¹ In addition, preliminary equations for swelling were developed and submitted to the committee for evaluation and modification.

7.1.2.1 Tensile properties

Most of the effort in the study of tensile properties was directed toward the analysis of new data on the properties of irradiated, annealed type 316 stainless steel and irradiated welds in stainless steels. The experiment that made the major contribution to the database was ORR-MFE-6J-7J, conducted in the ORR. This spectrally tailored experiment was designed to achieve the ratio of transmutation-produced helium to atomic displacements (He:dpa) characteristic of a fusion reactor. In addition to this important feature, the temperatures were in the range from 60 to 400°C to address ITER operating conditions. The experiment was a joint effort between the United States and Japan, enabling the U.S. program to benefit from the strengths of the Japanese efforts in welding and in characterization of annealed austenitic stainless steels. The strength properties of the materials were slightly lower than predicted by the equation from the database effort, as expected from the lower atomic displacement level: 7 dpa as opposed to 10 dpa. This can be clearly seen in Fig. 7.2.

Perhaps the most important and interesting result of the experiment is the precipitous drop in uniform elongation observed in annealed type 316 stainless steel, which is shown in Fig. 7.3. Cold-worked (CW) austenitic stainless steels have a characteristically low uniform elongation at temperatures below 400°C, as seen in Fig. 7.4. This was considered a disadvantage that

had to be accounted for in design but was compensated for by higher strength and swelling resistance. It had been previously

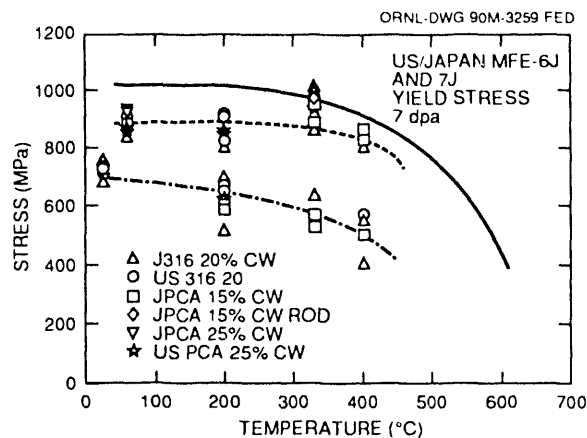


Fig. 7.2. Yield strength of irradiated cold-worked austenitic stainless steels. The solid line is the proposed ITER database equation; the dashed line is for data from the 7-dpa ORR-MFE-6J-7J experiment; the dash-dot line is for corresponding unirradiated material.

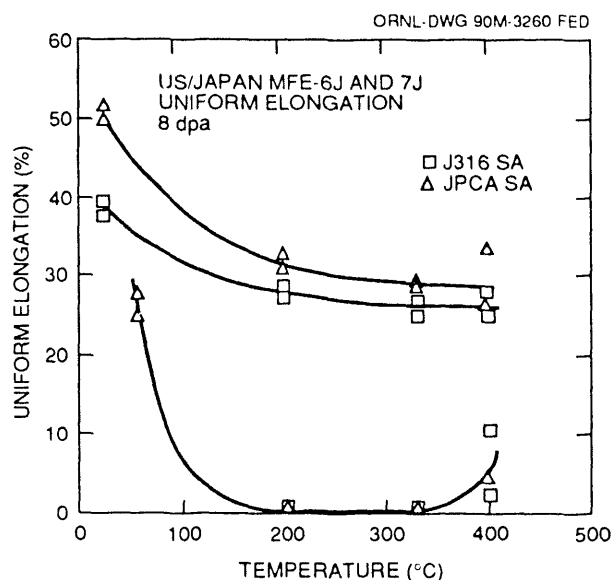


Fig. 7.3. Uniform elongation of annealed austenitic stainless steels, showing the low ductility of irradiated material between 200 and 300°C. The two upper curves are for unirradiated alloys.

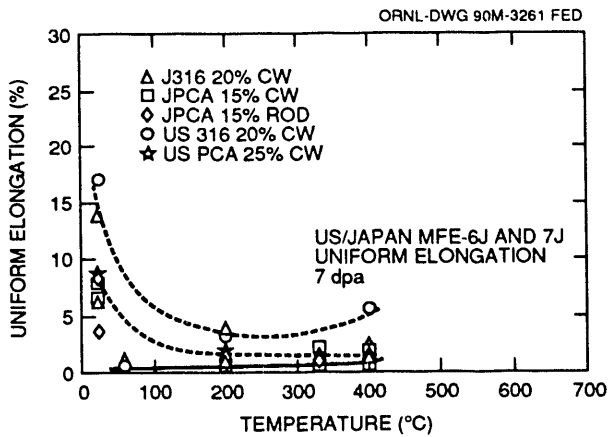


Fig. 7.4. Uniform elongation for cold-worked austenitic stainless steels. The dashed curves are for unirradiated alloys; the solid curve is for corresponding alloys irradiated in the ORR-MFE-6J-7J experiment.

thought that annealed material did not suffer this premature plastic instability leading to low uniform elongation. As a result of the ORR experiment, it is now known that this is an incorrect perception.

The reason for this behavior is not yet understood. However, analysis of the fracture surfaces and transmission electron microscopy (TEM) studies are both planned to help determine the mechanism of this behavior. Some possible mechanisms that can contribute to the observed behavior are discussed here.

As can be seen from Fig. 7.3, even the unirradiated alloy experiences decreasing uniform elongation as temperature increases from 60 to 200°C. This behavior has been previously observed in austenitic stainless steels, as shown by the data in Fig. 7.5, which were obtained as part of the U.S. Breeder Reactor Program.² The first step in understanding the very precipitous drop in uniform elongation in irradiated material is to understand the mechanism active in the unirradiated material. The first observation

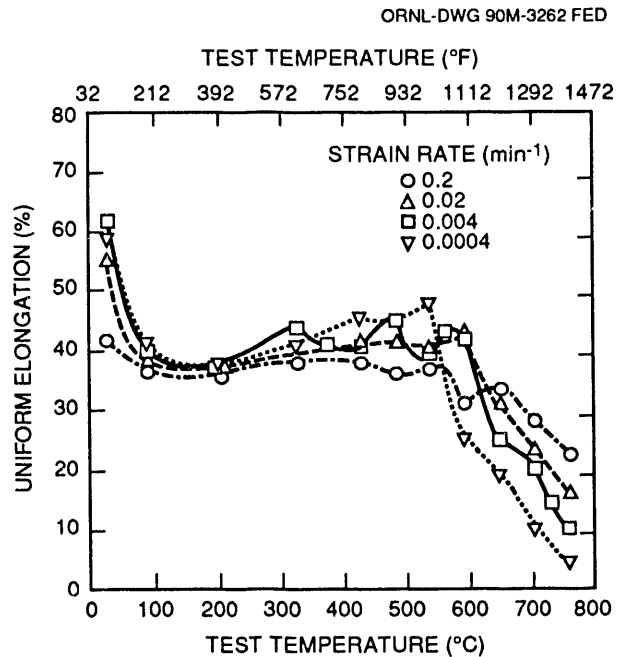


Fig. 7.5. Uniform elongation as a function of test temperature at several strain rates for 16-mm (0.625-in.) plate of the reference heat (8092297) of type 316 stainless steel in the reannealed condition.

relevant to this behavior is the presence of a yield point at temperatures below 400°C. This alone suggests the involvement of dislocation barriers that diffuse too slowly at low temperatures to remain with the dislocations. The next question to ask is whether any interstitial impurities are sufficiently mobile at temperatures of 200°C to cause a change in behavior as temperature decreases in this range. Diffusivity data for carbon, nitrogen, and boron were used to construct the plot in Fig. 7.6 (ref. 3). Boron is not considered a major impurity in these alloys but was included for completeness in the analysis. Carbon is, of course, the most likely candidate, and it is seen that the diffusion distance $(Dt)^{1/2}$, where D is the diffusivity and t is the time available, is on the order of ten atomic diameters for a 1-min time interval at 200°C. At

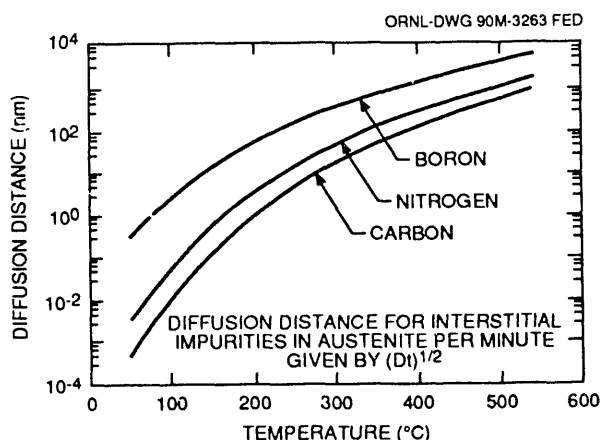


Fig. 7.6. Diffusion distances for boron, nitrogen, and carbon in austenite. The curves are plots of $(Dt)^{1/2}$ for a time interval of 1 min as a function of temperature.

60°C, the diffusion distance is three orders of magnitude lower, the difference between reasonable mobility and negligible mobility.

This effect could account for the disappearance of a yield point at higher temperatures. It could also account for higher strength at low temperatures and for a less rapid drop in strength with increasing temperatures, since the trapping impurities can remain in the lower-energy positions along dislocations as they move. Reasoning further, perhaps having the dislocations break away from the pinning impurities results in enhanced plastic deformation at the low temperatures. At higher temperatures, the pinning points remain with the dislocations, causing the low uniform elongation. Any crack that is initiated can propagate in a more brittle matrix rather than be blunted in a soft defect-free environment. In irradiated material, additional defect clusters generated from irradiation could contribute to the effect, making ductility still lower. At still higher temperatures, sufficient thermal energy is available to dissociate the impu-

rity atoms and dislocations; thus, ductility returns above 400°C.

Another effect that is being considered is localized deformation. Yield points in bcc metals are associated with local deformation, Luders bands, where deformation advances in a wave or band of work hardening.⁴ As the deformation proceeds, the strength remains constant until the whole stressed region has been hardened; then strength increases. In irradiated materials, a local deformation mechanism is believed to be responsible for channel fracture, where dislocation motion sweeps a band free of strengthening defects.⁵ In this case, the band is softer than the surrounding material, and immediate fracture results.

The present state of understanding of limited ductility in irradiated, annealed austenitic alloys considered for FWB structures in ITER is being incorporated into the ITER database equations. As this behavior becomes better understood, the alloy development effort will seek ways to improve ductility.

7.1.2.2 Swelling

A preliminary swelling equation, primarily based on fast reactor data for 20% CW type 316 stainless steel,⁶ has been formulated:

$$\frac{\Delta V}{V} = \frac{D}{1 - D}, \quad (7.1)$$

$$D = \frac{\rho_f - \rho_0}{\rho_0}, \quad (7.2)$$

$$D = 0.01 R \left(\phi t + \frac{1}{\alpha} \times \ln \left\{ \frac{1 + \exp[\alpha(\tau - \phi t)]}{1 + \exp(\alpha\tau)} \right\} \right), \quad (7.3)$$

$$R = \exp(0.5 + 1.62\beta - 0.1\beta^2 + 0.2\beta^3) , \quad (7.4)$$

$$\beta = \frac{T - 500}{125} , \quad (7.5)$$

$$\tau = 1.47 - 0.127\beta , \quad (7.6)$$

$$\alpha = 0.75 , \quad (7.7)$$

where ρ_0 and ρ_f are the initial and final densities, respectively; T is the irradiation temperature in degrees Celsius; and (ϕt) is the radiation exposure in units of 10^{22} neutrons-cm⁻² ($E > 0.1$ MeV). This design equation for the swelling of austenitic stainless steel (AISI 316, PCA type) under deuterium-tritium (D-T) fusion conditions is intended for use only at $\leq 500^\circ\text{C}$ and for doses up to 50 dpa.

Data from spectrally tailored experiments in the ORR were also used in the formulation, since these experiments are designed to achieve the fusion reactor He:dpa ratio.⁷ Because of the relevance of these data, they were weighted heavily in the equation. Theoretical considerations also predict a strong dependence on the helium concentration and the He:dpa ratio. Based on these data, shown with the proposed equations and breeder reactor data in Fig. 7.7, the incubation parameter in the breeder reactor equation has been adjusted in proportion to the square root of the He:dpa ratio and the rate parameters further adjusted to accommodate the spectrally tailored experiment data.

At this point it is not possible to distinguish between CW and annealed material or between PCA and type 316 stainless steel; there are insufficient data. As the ORR-MFE-6J and 7J experiments continue, data at higher fluences will become available and perhaps enable the determination of differences in alloy variations. It should be noted, however, that even at 7 dpa, the low-carbon versions of PCA swell significantly

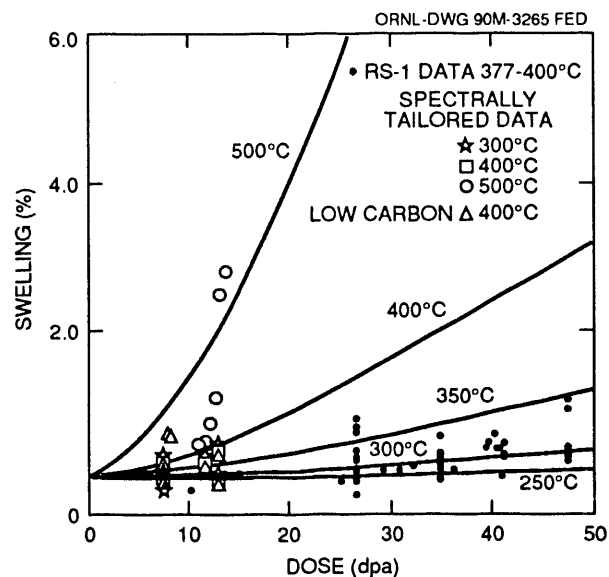


Fig. 7.7. Swelling in austenitic stainless steels. The curves are a recommended approximation to fusion conditions based on data from spectrally tailored experiments in which the He:dpa ratio is characteristic of a fusion reactor with a liquid-metal blanket.

more than the conventional versions at 330 and 400°C . The equation will be modified as data from other committee members become available.

7.1.3 Reduced-Activation Steels

A program is in progress to develop reduced-activation ferritic and austenitic steels for fusion reactor applications. After service, the induced radioactivity of such alloys would meet the criteria for shallow land burial set forth in Nuclear Regulatory Commission Guidelines 10 CFR 61, as opposed to the deep geologic disposal required for conventional steels. In accordance with 10 CFR 61, we are developing these steels without the use of Nb, Ni, Mo, Cu, and N. Reduced-activation steels are

being developed to replace the conventional steels that are now considered fusion reactor candidate alloys. Ferritic steel candidates to be replaced are Cr-Mo steels that include 2¼Cr-1Mo, 9Cr-1MoVNb, and 12Cr-1MoVW steels; austenitic steels to be replaced are type 316 stainless steel and PCA.

Studies on the ferritic steels are oriented toward developing steels analogous to the present Cr-Mo candidates (similar chromium concentration), but with molybdenum replaced by tungsten and niobium replaced by vanadium and tantalum. Eight experimental steels were produced. These included steels with 2¼, 5, 9, and 12 wt % Cr, each containing 2% W and 0.25% V (designated 2¼Cr-2WV, 5Cr-2WV, 9Cr-2WV, and 12Cr-2WV). To determine the effect of tungsten and vanadium, 2¼Cr steels were produced with 2% W and 0% V (2¼Cr-2W) and with 0.25% V and 0% W (2¼CrV) and 1% W (2¼Cr-1WV). A 9Cr steel containing 2% W, 0.25% V, and 0.07% Ta (9Cr-2WVTa) was also studied. All alloys contained 0.1% C.

Two of these steels, the 2¼Cr-2WV and the 9Cr-2WVTa, were shown to have strengths similar to those of the strongest Cr-Mo steels, the 9Cr-1MoVNb and 12Cr-1MoVW. Although the 9Cr-2WVTa steel had toughness properties better than those of the Cr-Mo steels (as measured in a Charpy impact test), the 2¼Cr-2WV steel had inferior properties. All of the high-chromium steels (5 to 12% Cr) had impact properties comparable to those of the Cr-Mo steels, as did the 2¼Cr-2W steel. The other two 2¼Cr steels had impact properties comparable to the 2¼Cr-2WV. The inferior properties of these three steels were attributed to the duplex microstructure of bainite and polygonal ferrite (the 2¼Cr-2W was 100% bainite). Therefore, it was postulated that the toughness of these three

steels could be improved if the microstructure were completely bainite.

To verify that the microstructure was the determining factor on the impact properties of the low-chromium steels, all eight steels were heat treated in two section sizes, the smaller size being chosen so that the low-chromium steels were entirely bainitic after a typical normalizing-and-tempering heat treatment. Indeed, it was found that the impact properties of the three low-chromium steels previously having low toughness depended critically on microstructure, which was affected by cooling rate after austenitization. By heat treating to change the microstructure from one containing 20 to 75% ferrite to 100% bainite, the ductile-to-brittle transition temperature (DBTT) for these three steels was reduced substantially. On the other hand, cooling rate had no effect on the high-chromium steels, which were 100% martensite regardless of the cooling rate. No change was observed for the 2¼Cr-2W, which was entirely bainite in both section sizes.

The type of bainite formed also affects the toughness. In particular, two morphological variations of bainite could be detected, depending on the hardenability of the steel. These different morphologies, termed granular and acicular bainite, were affected differently by tempering. For the acicular bainite, acceptable toughness could be achieved by a relatively mild temper (low temperature or short time), whereas a more severe temper was required for granular bainite. With the more severe temper, the strength was decreased more for the granular bainite. Thus it appears that if an acicular bainite could be developed, it would have a higher combination of strength and toughness (toughness is the most important mechanical property for fusion reactor applications). The development of acicular bainite depends on the hardenability of

the low-chromium steel, and we are now attempting to develop a steel with improved hardenability to provide optimum strength and toughness.

Irradiation of ferritic steels with neutrons in the range between room temperature and $\sim 450^\circ\text{C}$ results in lattice hardening, which causes an increase in strength and a decrease in ductility. Some investigators had concluded that reduced-activation ferritic steels with 2 to 3% Cr would harden more than high-chromium steels. To examine this possibility, the eight reduced-activation Cr–W steels and 9Cr–1MoVNb and 12Cr–1MoVW steels were irradiated to ~ 7 dpa at 365°C in the Fast Flux Test Facility (FFTF). All of the steels hardened. Observations on the Cr–W steels indicated that steels containing 2.25% Cr and a combination of vanadium and tungsten hardened less than those to which only vanadium or tungsten had been added. Of the steels containing 2% W, 0.25% V, and 2.25, 5, 9, or 12% Cr, the steel with 12% Cr hardened the most. The other three steels hardened less, with the $2\frac{1}{4}\text{Cr}$ –2WV steel hardening somewhat less than the others. The 9Cr–2WVTa steel developed the smallest amount of hardening of all of the reduced-activation steels. In a comparison of hardening behavior of the Cr–W and Cr–Mo steels, it was found that analogous steels hardened by similar amounts: the 9Cr–2WVTa and 9Cr–1MoVNb steels showed similar amounts of hardening, as did the 12Cr–2WV and the 12Cr–1MoVW steels. These results indicate that low-chromium steels should not be eliminated as fusion reactor materials because of excessive hardening, since they offer some advantages for this application.

The approach to developing a reduced-activation austenitic steel involves the replacement of nickel by manganese in conventional Fe–Ni–Cr stainless steels. As the first part of this effort, the austenite-

stable region in the Fe–Mn–Cr–C system was determined. A base composition of Fe–20%Mn–12%Cr–0.25%C was chosen, and this steel was shown to have tensile properties as good as or better than those for type 316 stainless steel in both the solution-annealed (SA) and CW conditions. On the basis of this work, the base composition was alloyed for strength and irradiation resistance. Heats of the base composition were produced to which Ti, W, V, B, and P were added in various combinations to determine the effects of these elements on precipitate formation and strength. TEM studies showed that, by the proper combination of these elements, fine MC precipitate similar to that found in the titanium-modified Fe–Cr–Ni PCA could be produced.

These experimental alloys were tested for strength. Figure 7.8 shows a comparison of the yield strength of an Fe–20Mn–12Cr–0.25C–1W–0.1Ti–0.1V–0.04P–0.005B alloy with type 316 stainless steel in an SA condition. The low-activation steel is considerably stronger than the conventional stainless steel. Similarly, the ultimate tensile strength of the high-manganese steel exceeded that of type 316 stainless steel. Despite its higher strength, the ductility of the high-manganese steel was comparable to that of the type 316 stainless steel. This observation on ductility is important, because it means that these new steels represent a significant gain in strength that does not come at the expense of ductility. The superior strength and ductility of the high-manganese steels were also observed when the steels were tested in the 20% CW condition.

7.1.4 Conventional Ferritic Steels

Work continued on the conventional steels that are candidates for fusion reactor applications. Conventional ferritic steels

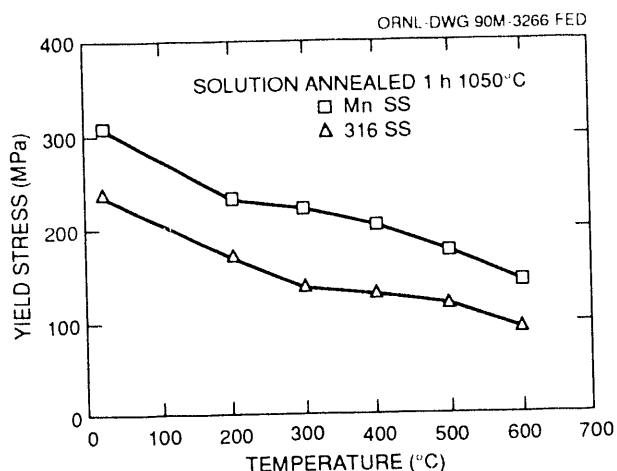


Fig. 7.8. Yield stress as a function of temperature for an experimental reduced-activation high-manganese stainless steel and type 316 stainless steel.

of interest are $2\frac{1}{4}\text{Cr-1Mo}$, 9Cr-1MoVNb , and 12Cr-1MoVW . Although these steels have excellent radiation resistance in fast reactor irradiation, information about their performance when irradiated under conditions where displacement damage occurs and transmutation helium forms is needed because the high-energy neutrons generated in the fusion reaction can produce large amounts of helium in a fusion reactor FWB structure. Information on irradiation damage developed on the conventional steels will also be of interest for the reduced-activation steels, because they are expected to behave similarly.

One way to study both displacement damage and helium effects is to irradiate nickel-containing steels in a mixed-spectrum reactor, such as HFIR. Displacement damage is produced by the fast neutrons in the spectrum, while helium is produced by a two-step (n,α) reaction of ^{58}Ni with the thermal neutrons in the spectrum. This technique has been used on the ferritic steels by irradiating the standard steels and samples of these steels doped with up to 2% Ni. Helium was shown to affect

the swelling behavior of 9Cr-1MoVNb and 12Cr-1MoVW steels. Helium also affects the tensile behavior in the temperature range of 300 to 450°C and the tensile and impact properties with irradiation at a temperature as low as $\sim 50^\circ\text{C}$. Preliminary work also indicated that helium affects the impact properties of standard 12Cr-1MoVW steel irradiated at 300 and 400°C in HFIR to 4–9 dpa. During the past year, we published data for conventional 9Cr-1MoVNb and 12Cr-1MoVW steels that support this observation.

Charpy impact tests were conducted on half-size specimens of standard 9Cr-1MoVNb and 12Cr-1MoVW steel irradiated at 300 and 400°C in HFIR. Specimens irradiated at 400°C had damage levels of 38 to 42 dpa, while those irradiated at 300°C had levels of 20 to 34 dpa. Helium concentrations were considerably different in the 9Cr-1MoVNb and 12Cr-1MoVW steels, because the 12Cr-1MoVW has a higher nickel content than the 9Cr-1MoVNb (0.43% Ni compared to 0.11% Ni). Irradiation in HFIR produced up to ~ 110 appm He in the 12Cr-1MoVW and ~ 35 appm He in the 9Cr-1MoVNb . The shifts in DBTT (Δ_{DBTT}) for the 9Cr-1MoVNb were 167°C at 300°C and 204°C at 400°C ; the shifts for the 12Cr-1MoVW steel were 105°C at 300°C and 242°C at 400°C . These increases in DBTT were accompanied by large decreases in upper-shelf energy. The Δ_{DBTT} values for the 9Cr-1MoVNb and 12Cr-1MoVW steels irradiated at 400°C in HFIR were the largest ever observed for these steels.

Results from these experiments at 400°C are significantly different from those obtained when these steels were irradiated at 390°C in the Experimental Breeder Reactor-II (EBR-II), a fast reactor in which little helium formed during irradiation. In the EBR-II experiments, steels were irradiated to 13 and 26 dpa, and a saturation in Δ_{DBTT} was observed. That is, when specimens

were irradiated to 26 dpa, there was no further increase in the Δ_{DBTT} over that obtained by irradiation to 13 dpa. Saturation values of ~ 54 and 144°C were observed for the 9Cr-1MoVNb and 12Cr-1MoVW steels, respectively. This compared with 242 and 204°C for these steels when irradiated to 40 dpa in HFIR. Thus, the saturation indicated after irradiation in EBR-II does not apply to specimens irradiated in HFIR. Furthermore, the Δ_{DBTT} is considerably higher for steels irradiated in HFIR.

Differences were previously observed between HFIR and EBR-II for the only other Charpy specimens irradiated in HFIR. In that experiment, capsules that contained half-size specimens of a different heat of 12Cr-1MoVW steel were irradiated to 4-9 dpa at 400°C . A Δ_{DBTT} value of 195°C was obtained, again considerably larger than the 144°C observed in EBR-II. This value is also quite a bit lower than the 242°C observed in the present experiment. Therefore, no saturation in Δ_{DBTT} in HFIR has yet been observed, and irradiations to higher dpa levels are required.

These observations led to the tentative conclusion that helium affected the impact properties, although the mechanisms by which helium affects strength are not yet understood. When helium is in an interstitial position, it can readily diffuse through an alloy. However, interstitial helium can become immobilized when trapped by a vacancy into a substitutional position. De-trapping occurs either directly (replacement by a self-interstitial) or by irradiation (by a neutron collision or by the knock-on process). Helium-vacancy clusters can form when the helium and vacancies are mobile. There are also indications that helium refines the scale of loop nucleation and prolongs loop stability to high fluences.

To the extent that helium preempts vacancies from recombining with mobile self-interstitials, either more self-interstitials will be present at a given time or more self-interstitials will migrate and cluster to form and grow sinks (i.e., loops). Such a process would cause additional hardening as helium builds up. Excess self-interstitials could cause more loop nucleation and/or growth relative to lower helium concentrations. Helium-enhanced loop formation and growth and a buildup of helium-vacancy clusters in the matrix could cause additional strengthening over that caused by displacement damage alone.

Regardless of the cause of the loss of toughness, these experiments demonstrated that fracture properties are more seriously degraded in a mixed-neutron-spectrum environment than in a fast neutron environment. Further experimental evidence on hardening and microstructure fractography are required before the origins of this difference can be reliably defined. However, it has already been established that helium bubble and void development is enhanced in a mixed-spectrum environment, indicating that helium plays a role. Although the role of solid transmutants cannot be ignored, increased helium generation must be considered the most likely cause of the worsening fracture behavior. If this is true, then even more serious degradation of properties can be expected to occur in steels doped with sufficient nickel to attain the fusion He:dpa ratio. Such data will become available during the next year. It must be concluded, therefore, that the occurrence of transition temperatures as high as 242°C in these experiments, coupled with the drastic reduction in upper-shelf energy, confirms that radiation-induced loss of toughness is a serious problem. Clearly, this phenomenon

must be understood and controlled before the ferritic/martensitic steels can be considered viable FWB structural alloys.

7.1.5 Copper

The ORNL fusion research program on copper incorporates both fundamental and applied studies. On the fundamental side, the barrier strength of defect clusters to dislocation motion in 14-MeV neutron-irradiated copper was measured to be 25% of the Orowan (impenetrable obstacle) value. These measurements are important for radiation hardening models. Grain boundaries were found to modify the radiation hardening behavior in a manner that was not directly additive to the hardening component associated with dislocation loops. This was interpreted to result from grain boundaries blocking the transmission of dislocation slip bands and could be important for interpreting radiation hardening in numerous materials.

The temperature-dependent void swelling behavior of neutron-irradiated copper was accurately determined for the first time in a study that utilized the ORR. Specimens of copper and a dilute copper-boron alloy were irradiated to ~ 1.2 dpa at 180 to 550°C. The peak void swelling temperature was $\sim 325^\circ\text{C}$ for both copper and Cu-B (which produced ~ 100 appm He during the irradiation). Figure 7.9 shows the temperature-dependent void swelling for copper and Cu-B as determined by density measurements.

On the applied side, the tensile and fatigue properties of copper and of the commercial dispersion-strengthened copper alloy Glidcop Al-15 were measured over the temperature range from 20 to 600°C. The mechanical properties of Glidcop were distinctly superior to those of copper and are suitable for some anticipated applications in near-term fusion devices. Figure 7.10 compares the fatigue behavior of copper and Glidcop. Attempts to furnace braze Glidcop using conventional techniques proved

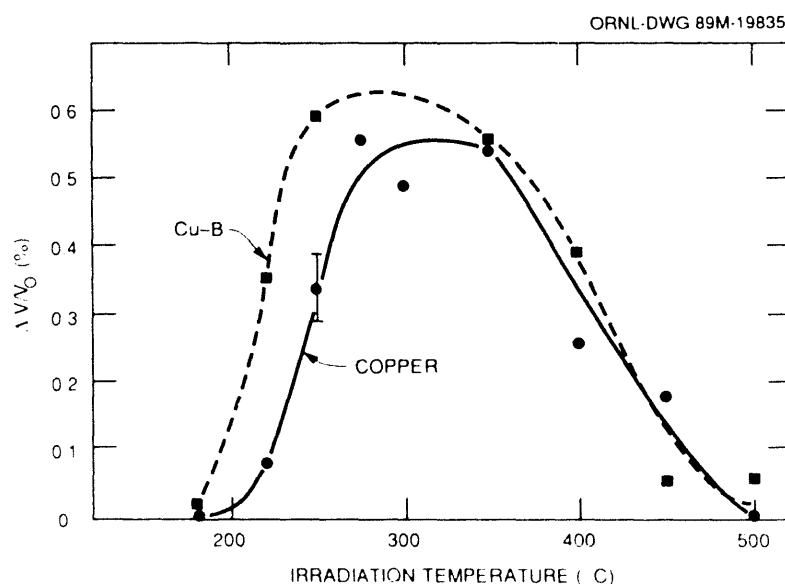


Fig. 7.9. Density changes measured in copper and Cu-20 wt ppm ^{10}B following irradiation to ~ 1.2 dpa in ORR.

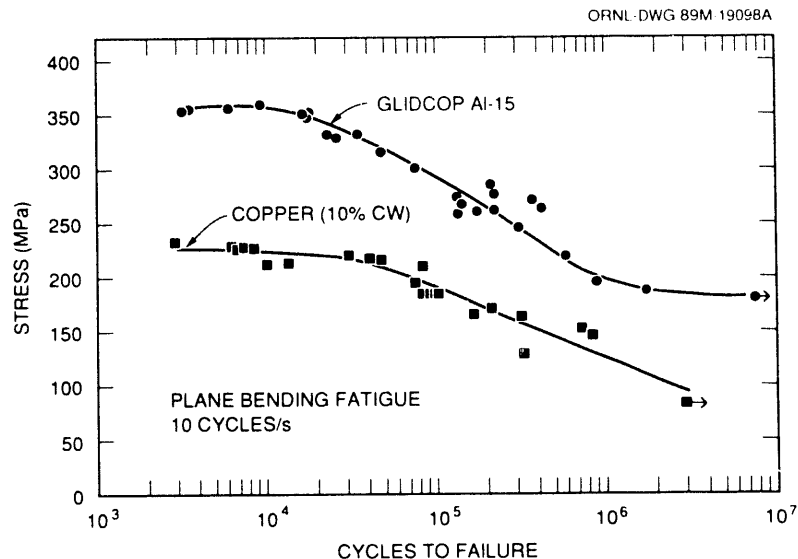


Fig. 7.10. Fatigue strength of copper and Glidcop Al-15 sheet tensile specimens (modified Grodzynski cantilever beam bending fatigue).

unsuccessful because of the migration of the braze filler metal along grain boundaries (away from the braze joint). A novel rapid brazing technique using an induction furnace (~5-s braze time) was investigated. Preliminary results indicate that a pore-free, high-strength braze joint can be achieved and that the short induction furnace brazing time inhibits migration of the filler metal away from the braze joint.

7.1.6 Vanadium Alloys

The first structural wall of a magnetic fusion reactor will be subjected to radiation damage and the effects of helium gas induced by the energetic neutrons from the plasma. These effects invariably harden and embrittle the wall material. Although vanadium alloys offer some advantages over other candidate materials for this application, they are not immune to these two basic radiation effects.

Recent studies have centered on several simple vanadium alloys based on the V-Ti-C and V-Ti-Zr-C systems. These alloys have demonstrated better resistance to helium embrittlement than any other previously investigated vanadium alloys, without sacrificing elevated-temperature strength or ductility. The approach taken to achieve this goal was the same as that used in the past for austenitic stainless steels: to create high densities of small MC-type precipitate particles throughout the microstructure to trap helium and keep it from embrittling the grain boundaries.

Eight experimental alloys were melted and fabricated into small sheet tensile specimens, injected with approximately 300 appm ³He using a modified tritium trick procedure, and tensile tested at 420, 520, and 600°C. All of the experimental alloys exhibited lower losses in ductility due to the presence of helium than V-15Cr-5Ti, Vanstar-7, V-3Ti-1Si, and V-5Cr-5Ti under similar test

conditions. In addition, several of the experimental vanadium alloys exhibited tensile properties (larger differences between yield and ultimate strengths) which indicate that they might demonstrate better resistance to irradiation hardening than the earlier alloys.

7.1.7 Corrosion Studies

Corrosion studies have the objective of (1) establishing compatible combinations of structural material, coolant, and tritium breeder and (2) understanding the mechanisms of corrosion to provide a basis for alloy development and for predicting corrosion and mass transfer kinetics in a fusion reactor system. In 1989, such studies were focused on two key fusion-relevant aqueous corrosion issues: the potential for radiation-induced sensitization of stainless steel (and accompanying intergranular corrosion) and the thermal sensitization behavior of developmental manganese-based austenitic stainless steels. In addition, further mass transfer analysis for steels in molten lithium and Pb-17 at. % Li was conducted.

One of the major environmental degradation mechanisms of austenitic stainless steels in water-cooled nuclear power systems is irradiation-assisted stress-corrosion cracking (IASCC). Changes in grain boundary composition caused by radiation-induced segregation (RIS) can play an important role in increasing the IASCC susceptibility of stainless steels. Chromium depletion from grain boundaries (sensitization) is one of the major phenomena caused by RIS and has been suggested as a cause of IASCC: the chromium concentration at grain boundaries can be reduced by RIS to below 12 wt %, the minimum chromium level for formation of a protective film on austenitic steel surfaces. In the case of water-cooled stainless steel components for fusion reactors, IASCC is a

possible degradation mechanism. Therefore, in collaboration with the Japan Atomic Energy Research Institute, an electrochemical facility for corrosion studies of irradiated materials was established at ORNL to evaluate the degree of sensitization associated with chromium depletion along grain boundaries in neutron-irradiated austenitic stainless steels. The electrochemical potentiokinetic reactivation (EPR) test technique was then applied to the determination of sensitization in a neutron-irradiated (420°C, 10 dpa), titanium-modified austenitic stainless steel (PCA). Miniaturized specimens (3 mm in diameter by 0.25 mm thick) in SA and 25% CW conditions were tested. Results indicated the occurrence of radiation-induced sensitization; they are compared to results for control specimens thermally aged at the irradiation temperature in Fig. 7.11. Ongoing work is defining the range of irradiation conditions and steel compositions for which this effect of radiation on corrosion resistance will be observed.

Standard chemical immersion (modified Strauss) tests and AEM showed that reduced-activation austenitic Fe-Mn-Cr steels based

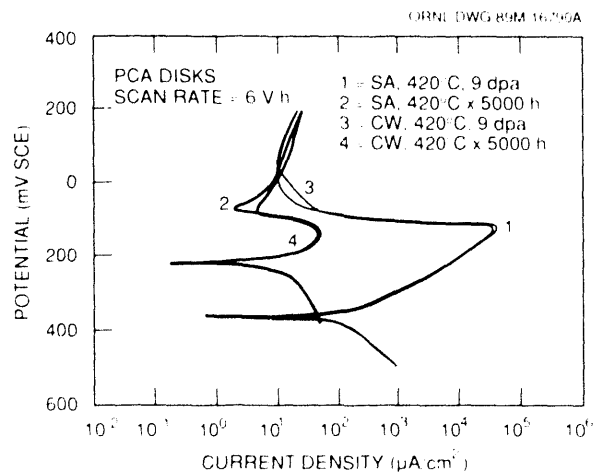


Fig. 7.11. Reactivation curves for thermally treated (2, 4) and irradiated (1, 3) PCA.

on Fe-20Mn-12Cr-0.25 (wt %) are extremely prone to thermal sensitization and resulting intergranular corrosion because of their high carbon contents and low chromium concentrations. Therefore, this susceptibility to sensitization after appropriate thermal aging, fabrication, or irradiation makes their use in aqueous and certain other environments problematical. Excellent correlation between intergranular corrosion induced by immersion in the acidified CuSO_4 solution and the presence of narrow chromium-depleted zones around grain boundaries, as determined by AEM, was found. Because of the need to meet reduced-activation requirements, the opportunities to increase the sensitization resistance of fully austenitic Fe-Mn-Cr steels by alloy design are limited.

Weight losses as a function of time were analyzed for austenitic and ferritic steels exposed to molten Pb-17 at. % Li and lithium at temperatures of $\geq 500^\circ\text{C}$ under thermal convection conditions. In both liquid-metal environments, parabolic weight loss kinetics were observed for type 316 stainless steel, while dissolution losses of Fe-12Cr-1MoVW steel rapidly became linearly proportional to time. The difference between the kinetic behavior for these two types of steel can be explained on the basis of the contribution of preferential dissolution (of nickel) to the corrosion of the austenitic steel and the resultant surface destabilization process during the first few thousand hours of exposure. After extended exposures (>3000 h), both types of steels exhibited linear weight loss kinetics indicative of the dissolution of Fe-Cr surfaces.

7.2 GRAPHITE AND CARBON-CARBON COMPOSITES

Research on bulk graphite and carbon-carbon (C/C) composites has been carried

out in support of plasma-interactive (PI) and high-heat-flux (HHF) materials. The interest in carbon-based materials stems from carbon's low atomic number, which minimizes radiative heat losses from the plasma. The eventual practical application of these materials to plasma-facing components requires control of erosion and excellent resistance to thermal shock and irradiation damage.

There is an extensive database on neutron damage in bulk graphites. However, continuing research on C/C materials is required. There is extensive evidence that the thermal shock resistance of properly designed C/C composite structures is adequate for fusion reactor applications. Thus, the problems to be solved for C/C composites lie in improving their resistance to erosion and to neutron irradiation damage. C/C composites have other desirable attributes; they may be fabricated in large sizes and to near net shape, and their mechanical and physical properties may be tailored through appropriate selection of fiber type, weave architecture, and processing parameters.

The problems of neutron damage can probably be solved by using (1) small unit cell size to permit semicontinuous design characteristics; (2) three-dimensional architecture, with fiber fractions and directions favoring the physical property geometry requirements; and (3) highly crystalline filaments (pitch-based fibers) and matrices. To verify these assumptions, a test matrix of C/C composite materials (pitch and PAN fibers) of differing architecture has been assembled and will be irradiated at ORNL. Additionally, pitch fibers of varying elastic modulus and degree of crystallinity will be irradiated. Some C/C composite materials have been heat treated to above normal processing temperatures to improve their crystallinity.

Neutron irradiations will be performed in the target region of the HFIR reactor at ORNL. Four target capsules are planned. One (HTFC 3) will be irradiated at 900°C to maximum fluences of 20 dpa. The remaining three (HTFC 1, 2, and 4) will be irradiated at 600°C to maximum fluences of 8, 16, and 32 dpa, respectively. Capsules HTFC 1 and 2 contain materials from the test matrix (C/C composites and fibers) and samples of a reference graphite (H-451). Capsule HTFC 3 contains samples of GraphNOL N3M, a fine-grained, high-strength aerospace graphite developed at ORNL (N3M is the current backup option to C/C composites for ITER), in addition to materials from the test matrix. Capsules HTFC 1 and 2 have been constructed and are expected to be loaded into HFIR in June 1990. Capsule HTFC 3 is currently in construction and irradiation is planned to commence during summer 1990. Capsule HTFC 4 will not commence assembly until the postirradiation examination of materials from HTFC 1 and 2 has been completed. This will allow the substitution of improved C/C materials and the removal of those materials whose performance in HTFC 1 and 2 is deemed unsatisfactory.

One further irradiation experiment is planned. Its purpose is to determine the effect of neutron damage on the thermal conductivity of C/C composite materials. The experiment will run to a peak fluence of <1 dpa in either the Buffalo Materials Test Reactor or the Bulk Shielding Reactor at ORNL.

7.3 CERAMICS

Ion cyclotron resonance heating (ICRH) has been proposed as a major heating source for the Compact Ignition Tokamak (CIT), and ceramic vacuum windows are a critical

component of ICRH systems. It is important for these windows to remain transparent to the rf energy, in part because excessive rf absorption could lead to their mechanical failure. The rf power absorbed in these ceramics is proportional to the so-called loss tangent. The loss tangent, $\tan \delta$, is defined as the ratio of the imaginary part to the real part of the dielectric constant, $\tan \delta = \epsilon''/\epsilon'$. Typical values for the loss tangent in unirradiated ceramics of interest to the fusion program are from 10^{-4} to 10^{-3} , with 10^{-3} being near the maximum tolerable value.

Postirradiation measurements have shown that ionizing and displacive irradiation can increase the value of the loss tangent, but there have been no relevant measurements of dielectric properties during irradiation. There is some concern that the losses may be higher during irradiation because of the higher density of charge carriers that will exist. To address this concern, a series of irradiation experiments has been planned to measure the dielectric properties of typical ceramics in situ. The experiments call for the use of two facilities. The first is the Spent Core Facility of HFIR. Decay of fission products in HFIR spent cores leads to an ionizing damage rate of 10^8 rad/h, which is comparable to that expected in CIT. Since the HFIR spent cores do not provide a component of displacive irradiation, TRIGA, a small research reactor at the University of Illinois, will be used to obtain data on the influence of displacive irradiation. A beam tube that runs adjacent to the core of TRIGA will be used for these experiments. When TRIGA is operated in a pulsed mode, both the displacive and ionizing damage rates are near those expected in the CIT.

Alumina (Al_2O_3) is a prime candidate material for use in rf heating systems. Therefore, the initial measurements will focus on this material. The experimental matrix includes the use of oriented single-

crystal and commercial-grade polycrystalline alumina. The commercial products include several different purity levels because postirradiation measurements have shown a significant influence of impurities. The dielectric measurements will be made using a capacitively loaded resonant cavity. The initial experiments in HFIR will measure the loss tangent at 100 MHz. The geometry of TRIGA will provide more flexibility in the cavity dimensions, thus permitting lower frequencies to be probed. The dimensions of a prototype cavity that has been built to bench-test the design are shown in Fig. 7.12.

The cavity method is well suited to measurement of the loss tangent because the power dissipation is maximized in the ceramic relative to other structures. In addition, losses in the feed line can be accounted for without the need for prior calibration, which would be extremely difficult to accomplish in situ. The loss tangent can be measured by determining the cavity quality factor Q , which is the ratio of the stored energy to the energy dissipated per field period, and is

$$\tan \delta = \left[\frac{\beta l}{\sin(2\beta l)} + \frac{1}{2} \right] \left(\frac{1}{Q} - \frac{1}{Q_0} \right), \quad (7.8)$$

where β is the angular frequency divided by the speed of light, l is the length of

the coaxial cavity center conductor, Q is the quality factor with the ceramic in place, and Q_0 is the quality factor at the same frequency when the ceramic is absent. In Eq. (7.8), both Q and Q_0 refer to the so-called "unloaded Q ," for which only the energy stored and dissipated in the cavity itself is taken into account. They can be determined by measuring the ratio of reflected power to transmitted power as a function of frequency over a ~ 1 -MHz range centered at the resonant frequency for the case of a tuned cavity. Relative changes in the dielectric constant can also be measured using the resonant cavity technique with an accuracy of $1/Q$, or less than 1% for the highest values of the loss tangent expected here.

The microstructures of spinel and alumina have been examined following ion irradiation to assess their microstructural stability during operation in a fusion radiation environment. A high density of dislocation loops and small cavities was observed in both materials following dual-beam irradiation (He^+ and Al^+) at conditions close to the fusion He:dpa ratio. The amount of cavity swelling in the matrix of both materials was very low ($\Delta V/V < 0.1\%$). However, the grain boundaries of spinel developed large cavities that led to complete separation

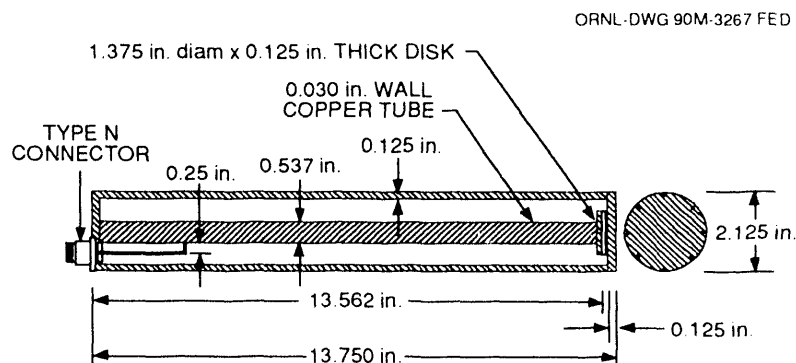


Fig. 7.12. Capacitively loaded cavity.

of the grains. These results suggest that polycrystalline spinel cannot be used in a fusion irradiation environment, whereas alumina and single-crystal spinel may be suitable materials.

A program was initiated to study the irradiated behavior of SiC/SiC composite ceramic. This material is a possible first wall material and has attractive (low) levels of induced long-lived radioactivity in a fusion environment. The interfacial friction between the SiC fiber and matrix is considered to be a key factor that will control the mechanical properties of the irradiated composite. The Nanoindenter mechanical properties microprobe was used to make initial measurements of the fiber-matrix friction on nonirradiated material, and specimens were implanted with helium at temperatures between 25 and 800°C in preparation for further measurements that will examine helium effects. In addition, plans were developed for in situ measurement of the electrical conductivity of SiC and SiC/SiC composites in an ionizing radiation field.

TEM disks of numerous advanced structural ceramics were obtained for an upcoming irradiation in HFIR. This irradiation will provide the first data on the irradiated properties of a wide range of technologically important ceramics that may be useful for a number of fusion reactor applications. The materials collected include toughened ceramics, whisker and fiber-reinforced ceramics, and chemical vapor deposition (CVD) diamond films.

7.4 HFIR EXPERIMENTS

Numerous irradiation experiments have been assembled in support of the Fusion Materials Program at ORNL and are awaiting full-power operation of the HFIR. For

the U.S.-Japan collaborative program on development of austenitic stainless steels, two highly complex, instrumented, and spectrally tailored capsules have been assembled for irradiation in the HFIR reflector region, and eight smaller uninstrumented capsules were assembled for irradiation in the target region. The reflector region capsules contain specimens previously irradiated to about 8 dpa in ORR. These specimens were retrieved and reloaded into newly designed and fabricated capsules. During irradiation, the capsules will be surrounded by a 4.2-mm-thick hafnium tube, which will reduce the thermal neutron flux by about 85%, permitting the specimens to achieve the correct He:dpa ratio after an additional 8-dpa exposure.

The eight target capsules contain a variety of mechanical specimens that will be irradiated to damage fluences as high as 70 dpa. Included in these experiments are the first specimens to use the isotopically tailored technique to achieve the correct He:dpa ratio at the completion of irradiation. In this technique the nickel content in the steel is made up of the appropriate isotopic ratios such that the two-step nickel reaction produces the correct helium level at the end of irradiation.

Two experiments have been assembled, and a third has been designed, to irradiate a variety of state-of-the-art and advanced C/C composite materials in the HFIR target region.

Two additional experiments have been designed to irradiate a variety of ceramic materials using isotopic tailoring to study the effects of helium in neutron-irradiated ceramics. Irradiation of these experiments in the HFIR target region is expected to begin next year.

In support of the ITER program, three experiments are being designed to irradiate fracture toughness specimens in the HFIR

target region at temperatures of about 100 and 250°C. These experiments are to be assembled and irradiation is to begin next year.

REFERENCES

1. M. L. Grossbeck, "Empirical Relations for Tensile Properties of Austenitic Stainless Steels Irradiated in Mixed Spectrum Reactors," *J. Nucl. Mater.*, accepted for publication (1990).
2. V. K. Sikka, B. L. P. Booker, M. K. Booker, and J. W. McEnerney, *Tensile and Creep Data on Type 316 Stainless Steel*, ORNL/TM-7110, Union Carbide Corp., Nuclear Div., Oak Ridge National Laboratory, January 1980.
3. M. A. Krishtal, *Diffusion Processes in Iron Alloys*, U.S. Dept. of Commerce, Springfield, Va., 1970.
4. J. Weertman and J. R. Weertman, "Mechanical Properties, Mildly Temperature-Dependent," pp. 735-92 in *Physical Metallurgy*, ed. R. W. Cahn, North Holland, Amsterdam, 1965.
5. M. L. Grossbeck, J. O. Stiegler, and J. J. Holmes, "Effects of Irradiation on the Fracture Behavior of Austenitic Stainless Steels," presented at the International Conference on Breeder Reactor Structural Materials, Scottsdale, Ariz., June 1977.
6. J. F. Bates and M. K. Korenko, *Nucl. Technol.* **48**, 303-14 (1990).
7. R. E. Stoller, P. J. Maziasz, A. F. Rowcliffe, and M. P. Tanaka, "Swelling Behavior of Austenitic Stainless Steels in a Spectrally Tailored Reactor Experiment: Implications for Near-Term Fusion Machines," *J. Nucl. Mater.* **155-157**, 1328-34 (1988).

8

NEUTRON TRANSPORT

R. G. Alsmiller, Jr.¹

J. M. Barnes²
J. Bartley¹
C. Y. Fu¹

D. M. Hetrick²
D. C. Larson¹
R. A. Lillie¹
R. W. Roussin¹

R. T. Santoro¹
D. K. Trubey¹
J. E. White¹

-
1. Engineering Physics and Mathematics Division.
 2. Computing and Telecommunications Division, Martin Marietta Energy Systems, Inc.

8. NEUTRON TRANSPORT

SUMMARY OF ACTIVITIES

The neutron transport program includes three elements: the work of the Radiation Shielding Information Center (RSIC), cross-section evaluation and processing, and analyses.

Staff members of the RSIC serve as technical consultants to the fusion energy research community, as well as a variety of other research communities, on all matters relating to neutron transport. The evaluation and processing program is directed at producing accurate cross-section data for materials that are of specific interest to fusion reactor designers. The analysis program at present is part of a joint U.S.-Japan neutronics program and is directed at validating available computer codes and cross-section data by comparing calculated results with experimental data obtained from the Fusion Neutron Source Facility at the Japan Atomic Energy Research Institute.

8.1 RADIATION SHIELDING INFORMATION CENTER

R. W. Roussin, D. K. Trubey,
J. E. White, and J. Bartley

The Radiation Shielding Information Center (RSIC) serves an international community by responding to inquiries about radiation transport problems. Staff members provide guidance by drawing on a technical database that includes a computerized literature file, a collection of complex computer programs, and a substantial body of nuclear data libraries pertinent to the solution of such problems.

Acquiring the needed computer-based technology base requires the collaboration of the neutronics community with RSIC staff members to collect, organize, process, evaluate, and package relevant technology developed in the community. This technology is disseminated to the community with a mechanism for feedback of experience through use, which results in an improved product. The resulting technology base provides an advancement of the state of the art.

A sample of some recent products of this information cycle process shows the international character of the RSIC community. The National Committee for Nuclear and Alternative Energies (ENEA), Bologna, Italy, contributed PSR-271/MILER for converting NJOY-produced cross-section libraries into AMPX format. A multigroup cross-section library, DLC-135/SHAMSI, for fusion neutronics analysis was provided by the Joint Research Centre of the European Atomic Energy Community (EURATOM) in Ispra, Italy. A version of the University

of Wisconsin DKR radioactivity and dose rate code system for fusion reactors was extended for fission and hybrid systems, denoted CCC-541/FDKR, and submitted by the Southwestern Institute of Physics, Leshan, People's Republic of China. The Japan Atomic Energy Research Institute (JAERI), Tokai Establishment, provided the CCC-430/EDMULT 2.1 electron depth dose code system, and the Tokyo Institute of Technology submitted the CCC-535/MORSE-CV multigroup Monte Carlo system for calculating the covariance of mean spectral values. The PSR-146/ALICE-87 nuclear model code was contributed by the International Atomic Energy Agency, Vienna, Austria, via the Organisation for Economic Co-operation and Development (OECD) Nuclear Energy Agency, Saclay, France. From the University of California at Los Angeles came the CCC-537/TRIPOS ion transport code. Los Alamos National Laboratory provided CCC-200/MCNP-3B, a general-purpose Monte Carlo system; PSR-171/NJOY89, a cross-section processing system for ENDF/B-VI; and PSR-27/ZOTT, an evaluator of correlated data. Oak Ridge National Laboratory contributed the DLC-146/HUGO 86 photon interaction library, the PSR-273/FERD-PC spectrum unfolding code (PC version), and the CCC-543/TORT three-dimensional discrete ordinates system.

This selection represents a small portion of the total activity of the center. Information processing (including evaluation and packaging) is a daily function. In addition to a comprehensive literature database, RSIC-packaged products include 146 data packages (DLC), 545 neutronics and shielding code packages (CCC), and 277 data processing and other miscellaneous code packages (PSR).

8.2 DATA EVALUATION AND PROCESSING FOR FUSION NEUTRONIC DATA NEEDS

D. C. Larson, C. Y. Fu, D. M. Hetrick, and J. E. White

Evaluated and processed neutron cross-section data are produced to meet the needs of fusion reactor designers. Nuclear data needs for the magnetic fusion energy program are given in ref. 1 and include evaluated cross sections for copper, nickel, and chromium. This year, isotopic evaluations for chromium, copper, and nickel were accepted for ENDF/B-VI. Also accepted for ENDF/B-VI were isotopic evaluations for iron and lead and an evaluation for natural carbon. Several of the evaluations were selected by an international committee for inclusion in the Fusion Evaluated Nuclear Data Library (FENDL). This will be the first version of ENDF in which special attention has been paid to data of priority to fusion energy. All of this work has been jointly funded by the Offices of Fusion Energy, Basic Energy Sciences, and Nuclear Physics in the U.S. Department of Energy (DOE) and the Defense Nuclear Agency.

Evaluated cross sections must be processed into forms that can be used in radiation transport computer codes. The focus of this effort has been the development of VITAMIN-E,² a 174-neutron, 38-gamma-ray group cross-section library. It can be used in conjunction with the AMPX-II system³ to derive cross-section data suited to a particular application.

A continuing effort is under way to maintain VITAMIN-E and the relevant AMPX-II computing technology on the National Magnetic Fusion Energy Computing Center

at Lawrence Livermore National Laboratory. The VITAMIN-E data and AMPX-II computing technology are also available from the RSIC.

8.3 REACTION RATE DISTRIBUTIONS AND RELATED DATA IN THE FUSION NEUTRON SOURCE PHASE II EXPERIMENTS: COMPARISON OF MEASURED AND CALCULATED DATA

R. T. Santoro, R. G. Alsmiller, Jr., and J. M. Barnes

Neutronics parameters including the source neutron spectrum, activation rates, and the tritium breeding in the Li₂O test zone of the phase II experiment performed on the Fusion Neutron Source Facility at JAERI have been calculated using the Monte Carlo code MORSE with ENDF/B-V transport and reaction cross sections. Favorable comparisons between the measured and calculated results have been achieved for the ²⁷Al(n, α), ⁵⁸Ni(n, p), ⁹³Nb(n, 2n), and ¹⁹⁷Au(n, 2n) reactions. Calculated ⁵⁸Ni(n, 2n) and ¹⁹⁷Au(n, γ) reactions did not agree with measured values within 10–40%. For the nickel reaction the differences may result from poor data in the ORACT files; discrepancies for the gold data may result from unknown quantities of hydrogen-rich epoxy used to coat the Li₂CO₃ blocks used in the test assembly walls. The calculated tritium breeding in the Li₂O agreed with experimental values within ±10% for ⁶Li and ±15–20% for ⁷Li.

REFERENCES

1. *Proceedings of the Fifth Coordination Meeting of Participants in the Office of Basic Energy Sciences Program to Meet High Priority Nuclear Data Needs of the Office of Fusion Energy, Argonne, Illinois, September 17-19, 1986, Appendix D, DOE/ER/02490-4, Ohio State University, Columbus, 1986.*
2. R. W. Roussin et al., *VITAMIN-E: A Coupled 174-Neutron, 38-Gamma-Ray Multigroup Cross-Section Library for Deriving Application-Dependent Working Libraries for Radiation Transport Calculations* [computer program], available from the Radiation Shielding Information Center, Engineering Physics and Mathematics Division, Oak Ridge National Laboratory, as DLC-113/VITAMIN-E.
3. N. M. Greene et al., *AMPX: A Modular Code System for Generating Coupled Multigroup Neutron Gamma Libraries from ENDF/B*, ORNL-3706, Union Carbide Corp. Nuclear Div., Oak Ridge National Laboratory, 1976.

9

NONFUSION APPLICATIONS

H. H. Haselton

G. D. Alton¹
M. Bacal²
F. W. Baity
G. C. Barber
R. L. Beatty³
W. R. Becraft⁴
L. A. Berry
T. S. Bigelow
S. K. Combs
J. F. Cox
W. K. Dagenhart
E. G. Elliott
C. A. Foster

W. L. Gardner
S. M. Gorbatkin⁵
M. J. Gouge
R. H. Goulding
D. J. Hoffman
G. E. Isham⁶
M. A. Janney³
R. L. Johnson⁷
C. C. Jones⁸
J. O. Kiggans³
H. D. Kimrey
R. L. Livesey
G. E. McMichael¹⁰
S. L. McNair³

P. S. Meszaros⁹
B. D. Murphy⁹
R. J. Raridon⁹
J. B. Roberto⁵
K. E. Rothe⁹
P. M. Ryan
D. E. Schechter
W. B. Snyder¹¹
D. O. Sparks
C. C. Tsai
J. H. Whealton
G. A. White
T. L. White

-
1. Physics Division.
 2. Ecole Polytechnique, Palaiseau, France.
 3. Metals and Ceramics Division.
 4. Grumman Corporation, Bethpage, N.Y.
 5. Solid State Division.
 6. Finance, Materials, and Services Division, Y-12 Plant.
 7. Engineering Division, Martin Marietta Energy Systems, Inc.
 8. Management Services Group.
 9. Computing and Telecommunications Division, Martin Marietta Energy Systems, Inc.
 10. Chalk River Nuclear Laboratories, Chalk River, Ontario, Canada.
 11. Engineering Technology Division.

9. NONFUSION APPLICATIONS

SUMMARY OF ACTIVITIES

During recent years, fusion technology development programs have been broadened to include nonfusion applications. The technologies that have been central to the fusion mission have been found by other sponsors to be appropriate matches for their future needs. Many fusion-related, challenging, and important research and development (R&D) program opportunities have been identified. It is expected that fusion technology will continue to contribute to critical advancements needed by the country.

The concentration of program initiation and development efforts in the nonfusion area follows two basic guidelines: the technology to be advanced is related to fusion in that the majority of advances (e.g., microwave and rf developments) expected to result from the work will directly benefit future fusion system designs, and the technology is expected to be applicable to fusion, although the initial application may not be directly fusion related. An example is plasma processing work for others that will eventually provide the potential of diamond coatings for critical fusion reactor components.

The nonfusion technology applications are concentrated in four main technical fields: (1) energy, (2) U.S. Department of Energy facility environmental restoration and waste management, (3) defense, and (4) technology transfer to industry through which the U.S. competitive position in the world can be improved.

The R&D efforts conducted to date address all of these areas. The highlights of the past year's work are presented in this section. Some of the endeavors apply to more than one field.

9.1 MICROWAVE PROCESSING OF RADIOACTIVE WASTES

T. L. White

The ORNL Waste Handling and Packaging Plant (WHPP) is developing a microwave process to reduce and solidify remote-handled transuranic (RH-TRU) liquids and sludges that are now stored in large tanks at ORNL. The microwave expertise and equipment of the Fusion Energy Division are being used in this development effort, which has focused on drying RH-TRU liquids and sludges in the final storage container and then melting the salt residues to form a solid monolith.

A proprietary microwave applicator at one-third scale was designed and fabricated to demonstrate the essential features of the microwave design and to provide input into the design of a full-scale applicator. Testing recently began on an in-drum process using nonradioactive RH-TRU surrogates.

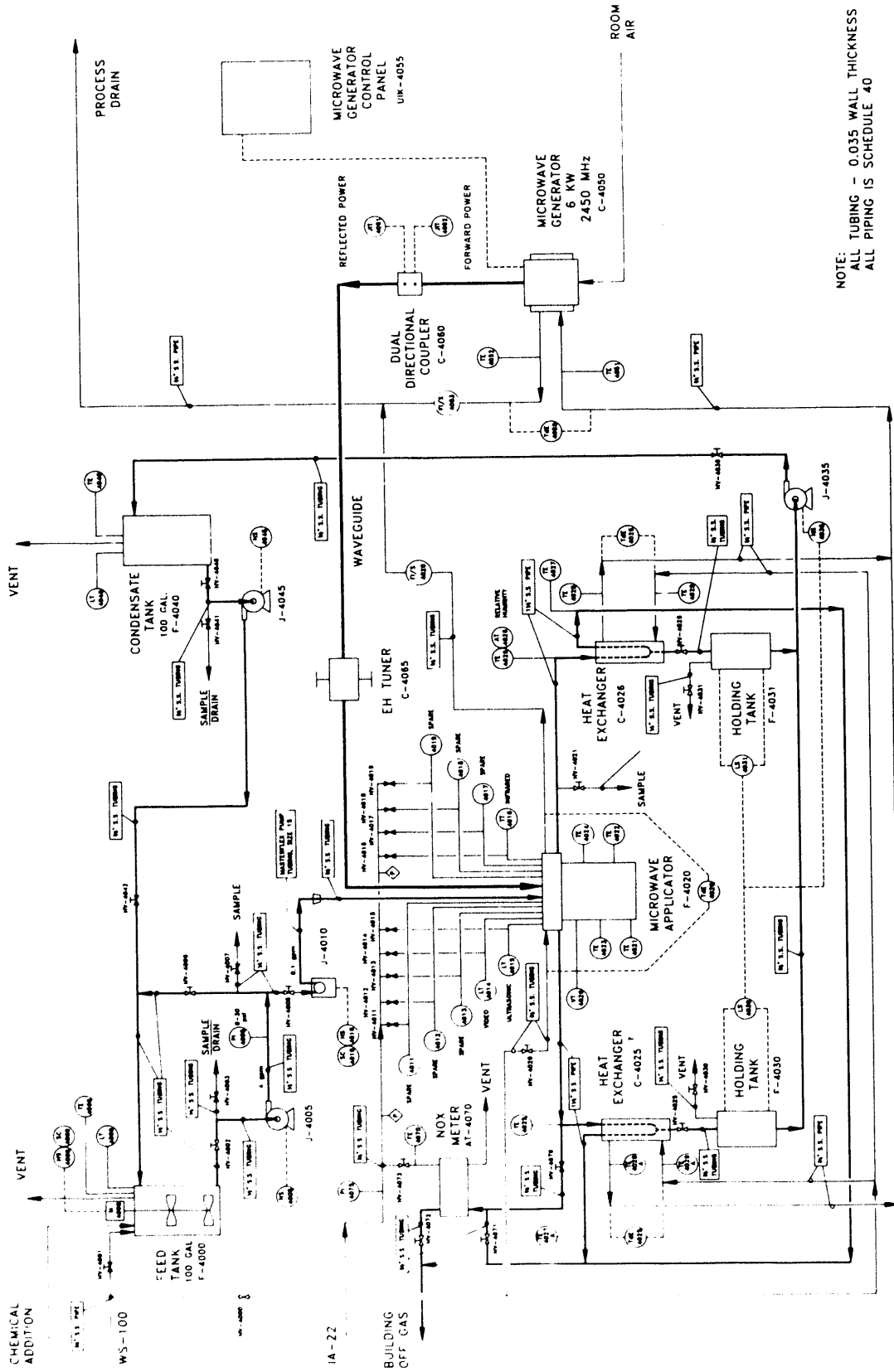
In the conceptual design stage, the WHPP process required the use of conventional wiped-film evaporators or extruders to perform the liquid evaporation and melting; microwaves would have been used only to maintain the temperature in a drum during filling operations. These evaporators and extruders require separate heating elements or heat transfer surfaces and moving parts to wipe a thin film across the heat transfer surfaces. The moving parts are subject to wear, especially if small hard particles are present in the waste (ORNL records indicate that some of the RH-TRU storage tanks may contain hard particles such as grout and other hard deposits). Frequent maintenance of wiped-film evaporators or extruders would be very complicated in a hot cell environment.

Last year, however, we showed that microwaves can be used to process the RH-TRU liquids over the entire temperature range in a batch microwave oven. The wasteform produced satisfied the Waste Isolation Pilot Plant waste acceptance criteria and was similar to wasteforms produced by conventional evaporation technologies. Because of this success, we are developing a more aggressive microwave processing flow sheet with the potential to greatly simplify the conceptual WHPP liquid processing flow sheet by replacing the wiped-film evaporator/microwave drum heater with a single microwave in-drum process.

Microwave energy heats the RH-TRU liquid waste directly because the oscillating electric fields directly couple to the molecular bonds of the chemicals in the waste, causing frictional heating. This direct heating eliminates the need for separate heating elements or heat transfer surfaces. The microwave process that we are developing contains no moving parts and is designed to heat the liquid waste in the final storage container, thus eliminating the need to transport hot chemicals from the heated casing of the wiped-film evaporator or extruder into the storage container. Another possibility is using a conventional evaporator (e.g., a wiped-film evaporator) to concentrate the liquid, which would then be melted by the in-drum microwave process.

The 1/3-scale microwave system is shown in Fig. 9.1. The surrogate RH-TRU liquid is stored in a mixing tank and pumped through a slurry transport loop to keep solids from clogging the loop. A smaller metering pump taps off a small portion of the loop flow near the applicator to control the amount of surrogate that is fed to the applicator. The line from the metering pump to the applicator is kept as short as possible to

ORNL DWG 89A-1242



NOTE:
ALL TUBING - 0.035 WALL THICKNESS
ALL PIPING IS SCHEDULE 40

Fig. 9.1. Prototype 1/3-scale microwave evaporation system.

avoid clogging. The metering pump is reversible so that surrogate in this short line can be drawn back out of the applicator feed pipe. The applicator feed pipe is located above the stainless steel waste container, which is 18 cm in diameter and 23 cm deep, with a 4.6-L usable volume. The applicator is powered by a 6-kW, 2450-MHz microwave generator. Forward and reflected microwave power levels are monitored by a dual-directional waveguide coupler (50 dB coupling, 30 dB directivity) so that net absorbed microwave power can be measured. An *E-H* tuner matches the applicator to the waveguide system to maximize the power absorbed by the applicator. The offgases from the waste are removed through evenly spaced openings around the sides of the applicator. These openings are connected by a manifold that feeds a pair of heat exchangers used to remove water vapor from the offgases. The distillate is collected and stored for later analysis and/or recycling to the mixing tank. An NO_x meter is connected to the offgas system to monitor the amount of NO_x gases produced during processing. A humidity/temperature probe is being procured to monitor the drying of the wasteform during processing.

Early tests have verified the correct applicator mode, and further testing is under way. The microwave process is much less developed than conventional technologies; the goal is to develop a full-scale microwave process so that all technologies can be at the pilot plant stage before the WHPP is built.

9.2 MICROWAVE SINTERING

H. D. Kimrey, R. L. Beatty, M. A. Janney, J. O. Kiggans, and W. B. Snyder

The microwave sintering effort is directed toward developing ceramics with improved

strength, toughness, reliability, and uniformity of properties for energy conversion systems, using microwave processing to engineer and control critical component microstructures. For oxide ceramics, the objective is to develop the mechanical properties and reliability of zirconia-toughened alumina to levels beyond those currently obtainable with conventional sintering.

9.2.1 Background

Microwave sintering has unique attributes and has the potential to be developed as a new technique for controlling microstructure to improve the properties of advanced ceramics. Because microwave radiation penetrates most ceramics, uniform volumetric heating is possible. Thermal gradients, which are produced during conventional sintering by conductive and radiative heat transfer to and within the part, can be minimized. This makes it possible to reduce internal stresses that contribute to the cracking of parts during sintering and to create a more uniform microstructure, which may lead to improved mechanical properties and reliability. With uniform volumetric temperatures, the nonuniform particle/grain growth caused by temperature gradients and associated sintering gradients can be regulated.

Recent investigations have identified additional benefits of microwave sintering. Using 28-GHz radiation, we demonstrated that alumina could be densified at temperatures 300–400°C below those used in conventional processing and that a uniform, fine-grained microstructure could be obtained. Lower-temperature processing should reduce grain growth, vaporization, and interactions between phases, which are often significant in the fabrication of advanced ceramics.

One class of composites, in which microstructural control in conjunction with microwave processing is expected to yield improved properties, is transformation-toughened ceramics. The retention of the tetragonal zirconia phase ($t\text{-ZrO}_2$) has previously been shown to control the mechanical properties of composites that contain dispersed ZrO_2 particles. The amount of $t\text{-ZrO}_2$ retained in the body and the microstructure of a composite significantly affects the composite's mechanical properties. Limitations of currently produced zirconia-toughened alumina are related to (1) variations in the composition of the stabilizing additive and (2) the location, grain size, and morphology of the dispersed tetragonal zirconia second phase. The high sintering temperature of $\sim 1600^\circ\text{C}$ required by conventional heating processes often leads to rapid diffusion and variation in the stabilizer content of the zirconia phase from grain to grain. Compositional variations lead directly to decreases and variations in the strength and toughness of the composite. In addition, there is a critical size of the zirconia-dispersed phase above which the zirconia particles transform to the monoclinic structure. Particles that are already transformed limit the magnitude of the mechanical properties that can be achieved.

Microwave sintering, which produces uniform temperatures and more rapid densification, is expected to produce the degree of control of the densification and microstructural development required to produce composites with optimum toughness. It should produce a finer grain size in the matrix alumina phase as well as finer zirconia particles of more uniform size in the matrix. These features will contribute to improved strength, fracture toughness, and mechanical reliability in the composite. Improved mechanical properties and reliability would make zirconia-toughened alumina an

attractive material for use in fuel metering systems, turbine housings, and applications requiring thermal shock resistance better than that of alumina.

9.2.2 Technical Progress

In preparing for the start of the composites work it was necessary to better understand the nature of the microwave effect. During FY 1989, grain growth in dense, hot-pressed alumina was shown to be structurally similar for microwave and conventional annealing conditions. We performed an extensive study of kinetics and microstructural evolution during grain growth for conventional and microwave heating of alumina. Our starting material was dense, hot-pressed alumina with a grain size of $1.1\ \mu\text{m}$ in coupons of $<1\ \text{cm}^3$. The small size of the samples necessitated the development of a ballasting crucible arrangement, as shown in Fig. 9.2. The ballast was a dense alumina body that acted to moderate the microwave-material interactions by simulating a sintering sample. The grain growth experiments could then be compared directly to our earlier sintering results. We observed that the evolution of microstructure was identical for both cases by all of the available quantitative

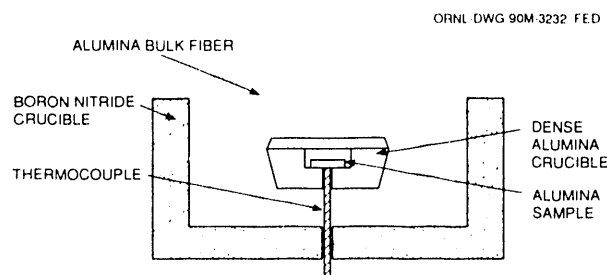


Fig. 9.2. The ballast/crucible arrangement developed to permit running small ($<5\text{-g}$) samples in the 28-GHz microwave furnace.

stereological measures (grain size, grain size distribution, grain boundary area, aspect ratio, etc.). The grain growth kinetics follow a power-law form in both cases; a power-law form is typical for normal grain growth in dense metals and ceramics. In addition, the kinetics of grain growth are much higher for microwave heating than for conventional heating; the rate of grain growth for microwave heating at 1500°C is the same as that for conventional heating at 1700°C.

We used these data to calculate an activation energy for grain growth in the two cases. An activation energy of 590 kJ/mol has been determined for conventional grain growth, which is typical for kinetic processes in alumina. The 480-kJ/mol activation energy for microwave grain growth represents a 20% decrease in activation energy, as shown in Fig. 9.3.

While both sintering of alumina powder compacts and grain growth in dense hot-

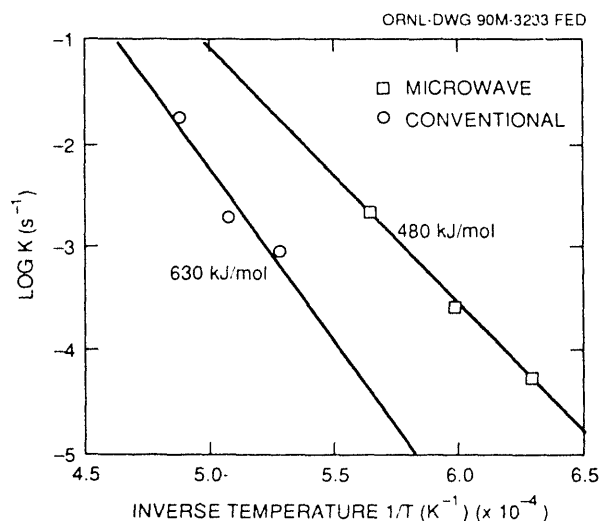


Fig. 9.3. Grain growth rate K as a function of temperature T , shown as an Arrhenius plot of $\log K$ vs $1/T$. The activation energy for grain growth is higher for firing in a conventional furnace than for firing in a microwave furnace.

pressed alumina are accelerated by processing in a microwave field, there are significant differences in the behavior of the two processes. For sintering, the apparent activation energies for microwave and conventional firing differed by a factor of 3 (170 vs 575 kJ/mol), as reported in FY 1988. For grain growth, the differences were only $\approx 20\%$ (480 vs 590 kJ/mol). The differences in the pre-exponential factors for microwave vs conventional sintering suggest that the processes going on during sintering are dissimilar. The difference in the evolution of the pore structure for microwave and conventional sintering provides additional support for this hypothesis. In contrast, the pre-exponential factors for microwave and conventional grain growth are similar. The pre-exponential factor can be interpreted in terms of an entropy of activation, which implies that the structural changes that occur during grain growth under microwave and conventional heating are similar. That the same kinetic process is operating in the two cases is supported by the similarity in microstructural development demonstrated by the quantitative microstructural parameters and the kinetic forms presented. Therefore, the differences in activation energies for grain growth probably represent the differences in diffusional processes for microwave and conventional processing better than do those for sintering. That is, the activation energy for diffusion is probably reduced by $\approx 20\%$, rather than by 300%, by the microwave field. We then interpret the increased rate of grain growth as the result of enhanced volume diffusion in the sample. From this standpoint, the results reported here are consistent with those obtained from previous sintering experiments. Finally, it was shown that a microwave effect can manifest itself in a dense ceramic body and that no free pore-solid interface is necessary.

Several developments in microwave technology occurred this year. An optical pyrometer system has been procured and used as a nonintrusive measurement technique to verify sintering temperature data. This system provides an independent confirmation of temperature. Also, modifications to a microwave-compatible dilatometer to make it compatible with alumina and zirconia-toughened alumina have been made and tested. This system is now in use to verify the interrupted-run alumina data. It will be quite valuable in reducing the number of runs required to characterize sintering behavior in subsequent activities.

The composites work was initiated. Based on a literature search, a partially stabilized zirconia powder (TOSOH TZ2Y) was selected and incorporated into an alumina matrix (Sumitomo AKP-50). The composite has been sintered at 28 GHz and in a conventional tube furnace. Initial results are quite encouraging, as shown in Fig. 9.4. The sintering temperature of the composite can

be greatly reduced by firing in the microwave field, perhaps to as low as 1050°C. The sintering temperature is so low, in fact, that it may be possible to eliminate grain growth of the zirconia phase.

9.3 PLASMA PROCESSING

C. C. Tsai, L. A. Berry, S. M. Gorbatkin, H. H. Haselton, and J. B. Roberto

The ORNL plasma processing program has had a productive year, with significant progress made in both plasma technology and applications. The technical progress is described in refs. 1 and 2. The ORNL invention of a microwave electron cyclotron resonance (ECR) multicusp plasma source has been licensed to SEMATECH for evaluating plasma etching concepts that are being pursued for high-density submicrometer features for very large silicon integrated (VLSI) circuits. The collaboration between ORNL and SEMATECH has also led to the establishment of a plasma etching research center at ORNL for the development of new manufacturing equipment and materials for the semiconductor industry.

The ORNL ECR multicusp plasma source (Fig. 9.5) has been developed by feeding a multicusp bucket arc chamber with a compact ECR plasma source. Linearly polarized microwaves at $f = 2.45$ GHz are launched from a rectangular S-band waveguide. Saturation current profiles for this source are shown in Fig. 9.6 for a hydrogen plasma. This novel source produces large (about 25-cm-diam), uniform (to within $\pm 10\%$), dense ($>10^{11}$ -cm³) plasmas of argon, helium, hydrogen, and oxygen. Based on electrical probe measurements, the source plasmas normally are characterized by cold electron temperatures of 2 to 5 eV

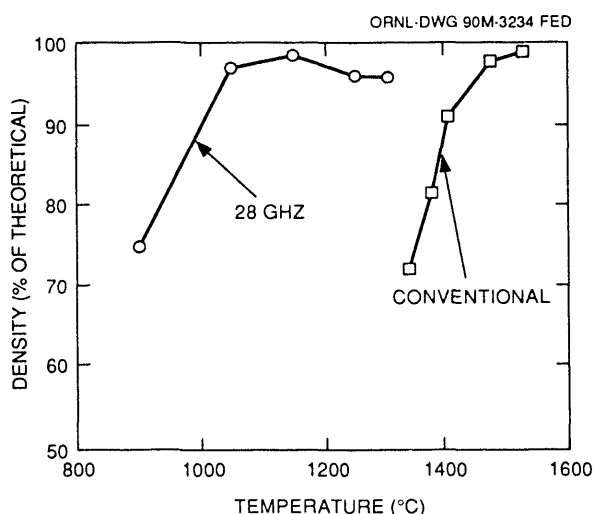


Fig. 9.4. Density of alumina + 20 wt % zirconia sintered for 1 h in 28-GHz microwave and conventional furnaces.

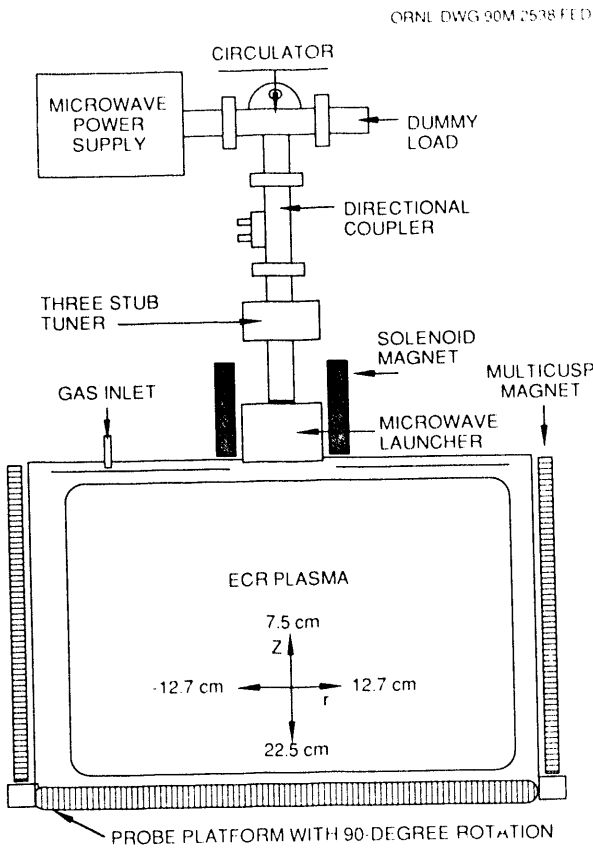


Fig. 9.5. Schematic of the ECR multicusp plasma source, showing the experimental arrangement with the probe position platform used for studying plasma properties.

and ion energies of about 20 eV. Here the ion energy is equivalent to the potential difference of the plasma sheath through which the ions are accelerated. With the weak magnetic field, this ion impact energy is expected to be directed normal to the probe scanning plane.

This source has been operated to produce an oxygen plasma for etching 12.7-cm positive photoresist-coated silicon wafers with a uniformity within $\pm 8\%$, as shown in Fig. 9.7. The potential applications of this plasma source technology for developing new manufacturing equipment are myriad. In addition to the collaboration with SEM-

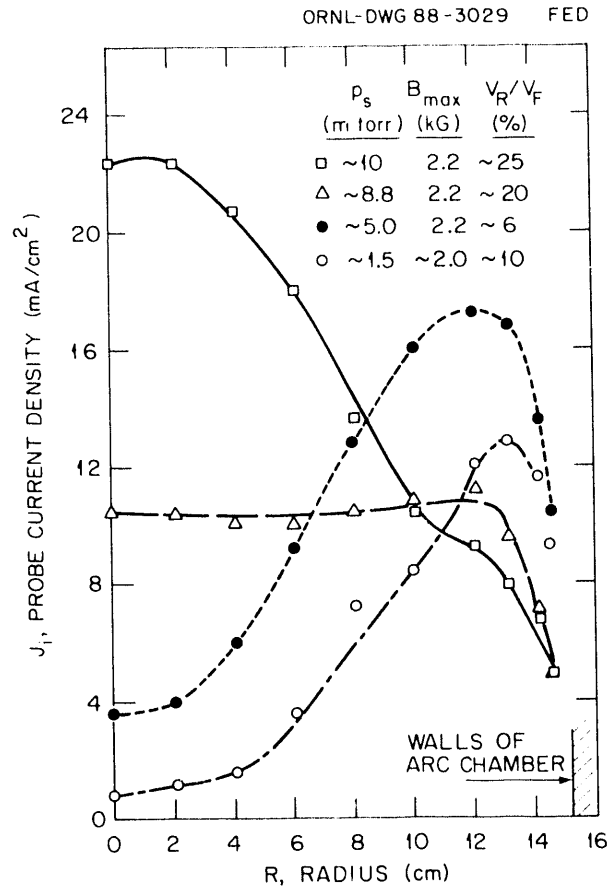


Fig. 9.6. Effect of pressure on a hydrogen plasma produced by the ECR multicusp plasma source.

ATECH, LAM Research Corporation, one of the main U.S. suppliers of wafer etching and deposition equipment, is interested in pursuing a collaborative program with ORNL, with the goal of advancing U.S. ECR technology for processing 300-mm wafers.

The capability of plasma reactors is substantially enhanced when the plasma is produced by a hybrid scheme that uses both microwave and rf power. In these plasma reactors, the plasma constituents are hot and cold electrons, positive and negative ions, metastable and radical atoms and molecules, and photons. Such plasmas are ideal for plasma processing. Ions can

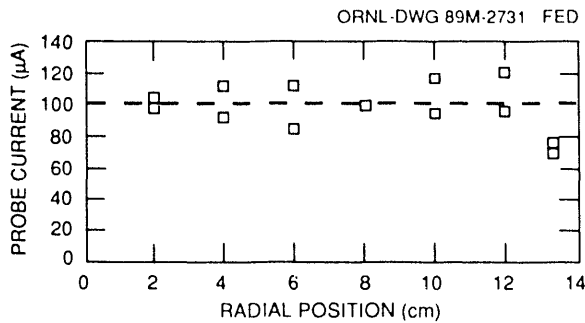


Fig. 9.7. Etching profiles of photoresist/silicon in an oxygen plasma.

be accelerated to form broad (20- to 30-cm-diam), low-energy (about 1000-eV) ion beams for ion-beam processing, including sputtering, milling, surface modification, etc. If ion energies are controlled to about 100 eV or lower, such plasma reactors can have wide applications in plasma etching, thin-film deposition, surface cleaning, waste management, and other areas.

9.4 DIAMOND FILMS

W. L. Gardner

Diamond film growth is being investigated as a part of a program for fundamental studies of chemical vapor deposition (CVD) materials growth processes. The goal of this program is to develop the diagnostics and advanced deposition techniques necessary to establish a program for fundamental studies of film growth by CVD processes. The program is a collaboration of three ORNL divisions: Fusion Energy, Metals and Ceramics, and Analytical Chemistry. Diamond film growth was chosen for study because diamond is a material with broad technological applications, there is local expertise for film growth, simple growth reactors are possible, the spectroscopy of hydrocarbon

species is well established (combustion), and no toxic gases are required. To gain knowledge of the molecular and/or plasma dynamics and the corresponding interrelation of the film microstructure with the material properties required to model the growth and to optimize film properties, various diagnostics and materials characterization techniques for CVD growth will be developed. The Fusion Energy Division is providing basic plasma diagnostics as well as a plasma-based reactor. Initially a high-pressure, rf-based technique is to be used to decompose the molecular hydrogen and hydrocarbon gases required for diamond formation. Support is also being provided by the division's RF Technology Group to develop diamond coatings for Faraday shields.

9.5 EHD ION SOURCE

J. H. Whealton, R. J. Raridon,
P. S. Meszaros, and P. M. Ryan

The disparate scales present in an electrohydrodynamic (EHD) ion source make it difficult to model accurately. Extending our previous work,³ we developed a method to accurately analyze the scale change. An example is shown in Fig. 9.8, where several blowups are analyzed, leading to fractional-angstrom resolution [Fig. 9.8(d)]. More than 1016 nodes (reduced by symmetry from 1027 nodes) for the finite difference solution to the Laplace equation would be needed to get the level of resolution in Fig. 9.8(d). Ion trajectories are calculated accurately in Figs. 9.8(d) and 9.9. The procedure can be repeated iteratively to account for space charge in a self-consistent manner. Quasi-plasma liquid models, such as that considered in refs. 3 and 4, can be incorporated. Use of this analysis

should provide an enhanced understanding of emission physics, since macroscopic beam parameters can now be connected to an emission scenario. Also, it should be possible to begin optimization of conditions leading to exploitation of the brightness possibilities previously conjectured for an EHD ion source.

sible to begin optimization of conditions leading to exploitation of the brightness possibilities previously conjectured for an EHD ion source.

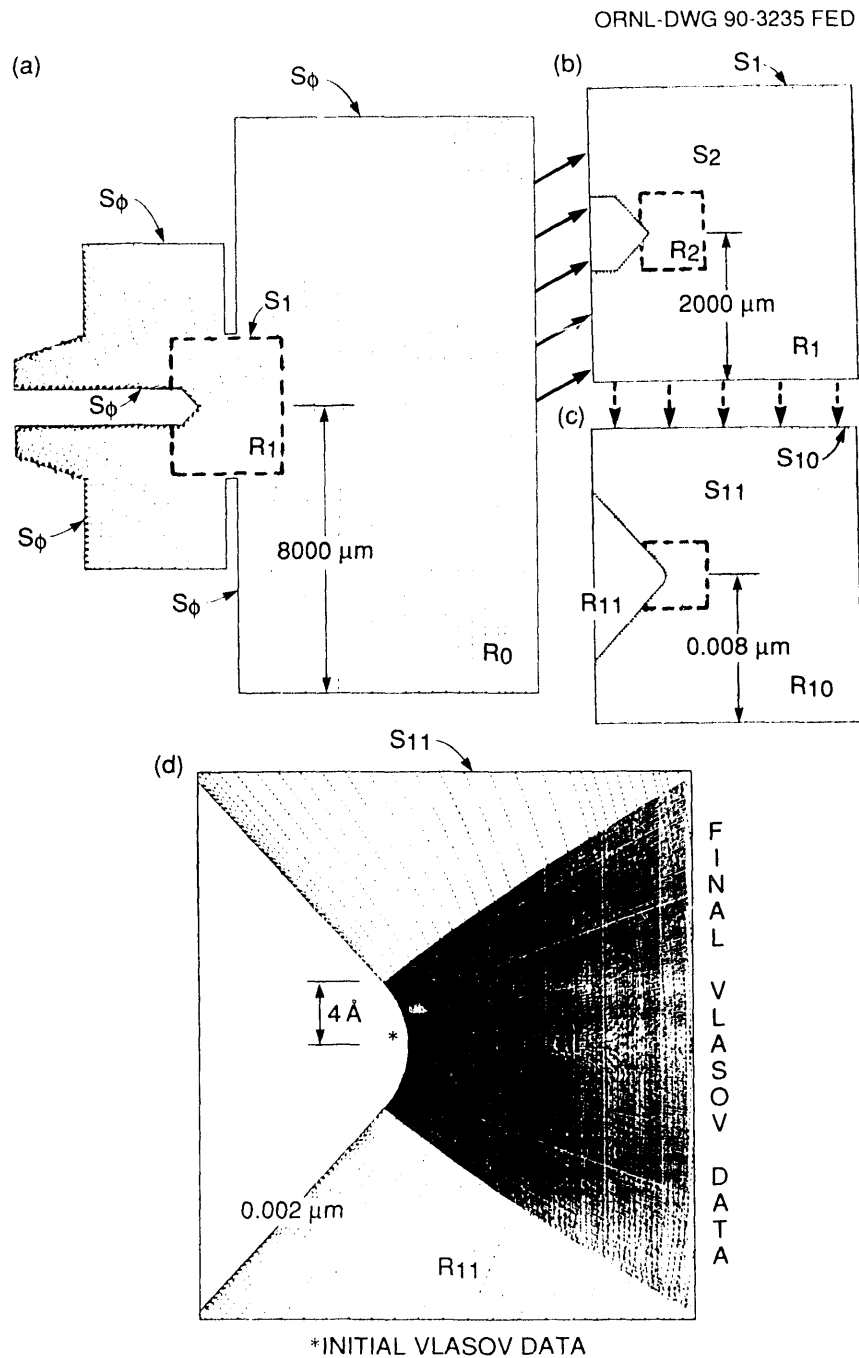


Fig. 9.8. EHD ion source (a) actual size and enlarged (b) $\times 4$, (c) $\times 4^{10}$, and (d) $\times 4^{11}$ with trajectories of extracted ions.

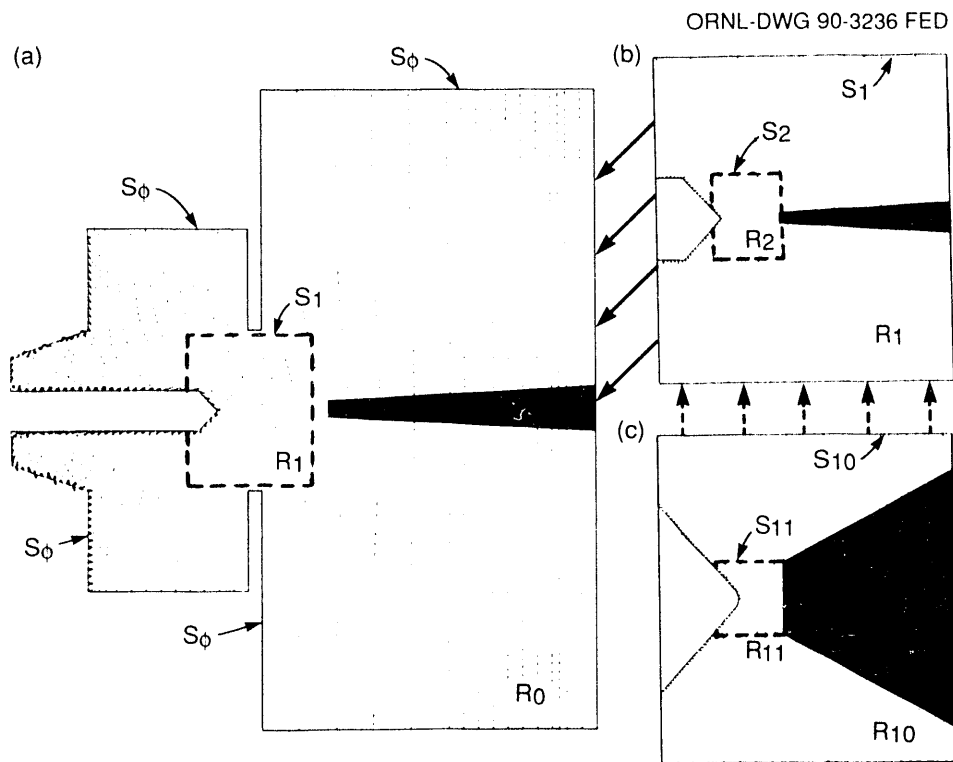


Fig. 9.9. EHD ion source with trajectories of extracted ions (a) actual size and enlarged (b) $\times 4$ and (c) $\times 4^{10}$.

REFERENCES

1. L. A. Berry et al., "Characteristics of the ORNL ECR Multicusp Plasma Source," presented at the SRC Topical Research Conference on Plasma Etching, Cambridge, Mass., February 1-2, 1989.
2. C. C. Tsai et al., "Potential Applications of an Electron Cyclotron Resonance Multicusp Plasma Source," *J. Vac. Sci. Technol. A* **8**, 2900 (1990); also published as ORNL/TM-11442, Martin Marietta Energy Systems, Inc., Oak Ridge National Laboratory, March 1990.
3. J. H. Whealton et al., "Extraction Induced Emittance Growth for Negative Ion Sources," *Rev. Sci. Instrum.* **61**, 568 (1990).
4. J. H. Whealton et al., "Electrohydrodynamic Ion Source Extraction," pp. 122-3 in *Fusion Energy Division Annual Progress Report for Period Ending December 31, 1988*, ORNL-6528, Martin Marietta Energy Systems, Inc., Oak Ridge National Laboratory, 1990.

10

MANAGEMENT SERVICES, QUALITY ASSURANCE, AND SAFETY

Management Services

F. E. Gethers*/E. R. Wells*

D. R. Alford	J. M. Finger	J. C. Parrott ³
L. R. Ballard	J. R. Jernigan ^{1,4}	J. O. Richardson
B. J. Beem ¹	C. H. Johnson ³	G. G. Ross ^{3,4}
J. B. Booth ²	D. Y. Johnson ³	E. M. Ruckart
D. P. Brooks	L. M. Johnson ⁵	S. R. Schwartz ³
S. H. Buechler ³	C. C. Jones	D. G. Sharp
J. L. Burke	I. A. Kunkel	B. J. Smith ³
M. W. Darnell ³	J. C. Neeley ³	P. A. Sumner ³
A. G. Evers	M. B. Nestor	M. S. Thompson ¹

Quality Assurance

E. J. Byrnes⁶

Safety

F. E. Gethers*/E. R. Wells*

*Dual capacity.

1. Group secretary.
2. Information Services Division, Administrative Services Organization, Martin Marietta Energy Systems, Inc.
3. Publications Division, Administrative Services Organization, Martin Marietta Energy Systems, Inc.
4. Part-time.
5. Finance and Materials Division, Martin Marietta Energy Systems, Inc.
6. Quality Department.

10. MANAGEMENT SERVICES, QUALITY ASSURANCE, AND SAFETY

SUMMARY OF ACTIVITIES

Broad technical and administrative support for the programmatic research and development activities of the Fusion Energy Division is provided by the Management Services Group and by the division's Quality Assurance (QA) and Safety programs.

The Management Services Group provides support in the following areas:

- General personnel administration, material and service procurement, subcontracting, and coordination of national and international agreements.
- Nonprogrammatic engineering services for support systems and equipment; identification, planning, and coordination of general plant project and facility improvements; coordination of maintenance and production shop work; labor relations; and telecommunications.
- Financial management.
- Library services and resources.
- Publications services.

Support is provided through effective communication with division programmatic staff and through the coordination of resources from disciplines outside the division.

The QA activity in the division emphasizes the development and documentation of a QA program that conforms to national standards, the review and approval of engineering documents, supplier surveillance, identification and documentation of nonconforming items, audits, and QA assessments/plans.

The division's safety activities include a formal safety program and environmental protection services. A safety resource team was established to improve the environmental, safety, and health upgrade program in the division, and a hazard communication program was established.

10.1 MANAGEMENT SERVICES

10.1.1 General Administration Services

10.1.1.1 Personnel

On December 31, 1989, the Fusion Energy Division had 135 employees, compared with 152 on December 31, 1988. Figure 10.1 shows the composition of the division's scientific staff. Attrition from the division during 1989 consisted of 2 retirements, 3 resignations, and 16 transfers to other divisions. Two employees joined the division during the year.

The University and College Co-Op Program sponsored two students from the University of Tennessee, both in electrical engineering; three from the Georgia Institute of Technology, two in nuclear engineering and one in physics; and one student from Tennessee Technological University in physics. Seven students were here under university subcontracts. Nine technical students participated in summer programs; six of them were sponsored by Oak Ridge Associated Universities. The division was host to 19 foreign scientific guests and 10 subcontractor personnel.

Division personnel on long-term foreign assignments included three staff members at the Joint European Torus (JET) Joint Undertaking, Abingdon, United Kingdom, for the JET project; one at the Centre d'Etudes Nucléaires, Cadarache, France, for the Tore Supra project; and one at the Max-Planck-Institut für Plasmaphysik, Garching, Federal Republic of Germany, for the International Thermonuclear Engineering Reactor project. One staff member was on a long-term domestic assignment to General Atomics in San Diego, California. Three division employees were on relocation assignments.

10.1.1.2 Procurement

During 1989, the division's procurement group processed 1510 requisitions with a total value of about \$2.0 million. Throughout the year, this group actively monitored an average of 200 to 400 open purchase orders. In addition, 220 shipping orders were processed.

Industrial participation through subcontracts to the division approximated \$1.7 million in 1989. Almost all of the subcontract

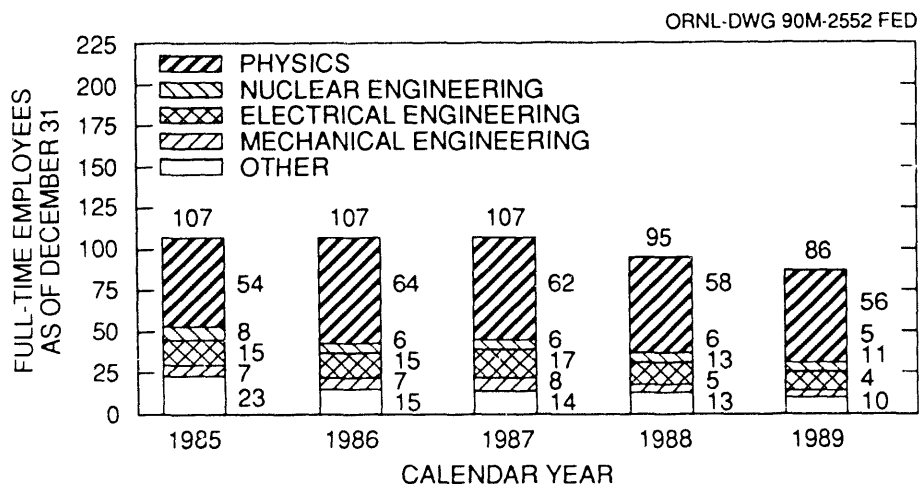


Fig. 10.1. Fusion Energy Division professional staff by discipline.

cost (\$1.2 million) was applicable to the ORNL Fusion Program.

The procurement status database provides users with the status of individual procurements and serves as an effective tool for cost control.

10.1.1.3 International agreements and collaboration

The division participated in several personnel exchanges and collaborations during 1989. The Management Services Group (MSG) played a key role in organizing these activities, with responsibility for coordinating administrative, legal, and protocol matters for outbound Fusion Program representatives and inbound foreign guests.

In this capacity, MSG staff members interacted with the ORNL Foreign National Office, the ORNL and Y-12 Plant security organizations, the Office of General Counsel and the Office of the Comptroller and Treasurer of Martin Marietta Energy Systems, and the Washington and Oak Ridge Operations offices of DOE, as well as other support and service organizations. Responsibilities included ensuring adherence to general laboratory and company policies and to federal procedures and laws, monitoring the processing of paperwork to ensure timeliness and accuracy, obtaining the necessary approvals, and generally supporting the satisfactory implementation of exchanges, cooperative programs, and collaborations.

10.1.2 Engineering Services

The Engineering Services Group coordinates all engineering work performed on general facilities additions, modifications, and repairs in the division. Active work to improve the physical plant facilities, despite

limited resources, continued during 1989. The Engineering Services Group worked closely with the Engineering Division of Martin Marietta Energy Systems, Inc., and with Fusion Energy Division researchers to install needed improvements. In this reporting period, construction was nearing completion on phase 4 of a six-phase effort to improve the air-handling systems in Bldg. 9201-2. Engineering is complete for the first and second phases of an upgrade for the 480-V electrical distribution system.

The demineralized water system in Bldg. 9201-2 provides cooling water for the Advanced Toroidal Facility (ATF), the Radio-Frequency Test Facility (RFTF), and other test facilities and for the building air conditioners. During 1989, the Engineering Services Group provided data for a quality investigation report on pump problems. New and improved polypropylene filters and pressure drop indicators were installed. Water quality was improved dramatically. Cost reductions through electrical power savings were accomplished by the Performance Improvement Process (PIP) program.

The liquid nitrogen tank installed in 1988 as part of a PIP project continued to save the division an estimated \$90,000 yearly.

Housekeeping and safety of building and grounds have been brought to a new level of consciousness, including active industrial hygiene work to eliminate chemical problems and industrial safety work to eliminate other hazards.

10.1.3 Financial Services

The Finance Office is a functional part of the MSG and provides financial management support for administrative, engineering, and research personnel in areas that include budget preparation, cost scheduling, and variance analysis. The office also provides

meaningful and appropriate accounting and cost control. Interaction with division management is an essential part of administering the budget, accounting policies, and procedures. Table 10.1 and Fig. 10.2 show the funding trends for the ORNL Fusion Program.

10.1.4 Library Services

The Fusion Energy Library maintains a specialized collection in plasma physics and fusion technology and is a branch of the

Information Services Division (ISD) library system that serves Energy Systems. Library staff members select materials for acquisition, circulate library materials, provide reference assistance and online literature searching, and retrieve information in support of research activities.

During 1989, the Fusion Energy Library acquired an NCR PC810 computer to serve as a CD-ROM workstation, which now provides access to Business Periodicals Index, PC-SIG (shareware), and the National Technical Information Service reports database. The library also acquired a LaserJet printer

**Table 10.1. Fusion Program expense funding
(in thousands of dollars)—budget outlay**

Activity	FY 1987 Actual cost	FY 1988 Actual cost	FY 1989 Actual cost	FY 1990 Funding as of April 1990	FY 1991 Budget submission	FY 1992 Budget submission
Applied plasma physics						
Fusion plasma research	\$2,303	\$2,606	\$2,591	\$2,179	\$2,686	\$2,825
TEXT collaboration	0	0	0	250	263	276
Experimental plasma research	1,194	1,277	1,128	1,596	1,482	1,564
National MFE computer network	370	373	353	290	300	315
Technical program support	168	104	0	0	0	0
	\$4,035	\$4,360	\$4,072	\$4,315	\$4,731	\$4,980
Confinement systems						
Research operations	\$16,212	\$17,218	\$17,256	\$14,398	\$15,305	\$16,697
Major device fabrication	1,960	466	0	0	0	0
Magnetic mirror research operations	1,953	0	0	0	0	0
Compact Ignition Tokamak support	835	2,340	2,315	2,360	2,387	2,402
Technical program support	0	89	281	0	0	0
Doublet III-D	0	0	922	800	1,000	1,085
TEXT collaboration	0	0	409	0	0	0
	\$20,960	\$20,113	\$21,183	\$17,558	\$18,692	\$20,184
Development and technology						
Magnetic systems	\$7,450	\$2,216	\$471	\$24	\$0	\$0
Plasma engineering	5,672	7,342	5,045	3,887	3,758	3,768
Reactor systems	310	648	1,185	447	443	224
Environment and safety	69	242	215	135	181	196
Reactor materials	5,193	4,264	3,763	5,440	4,337	4,368
Fusion Engineering Design Center	3,285	2,202	2,773	2,430	2,410	2,625
	\$21,979	\$16,914	\$13,452	\$12,363	\$11,129	\$11,181
TOTAL ORNL FUNDING	\$46,974	\$41,387	\$38,707	\$34,236	\$34,552	\$36,345

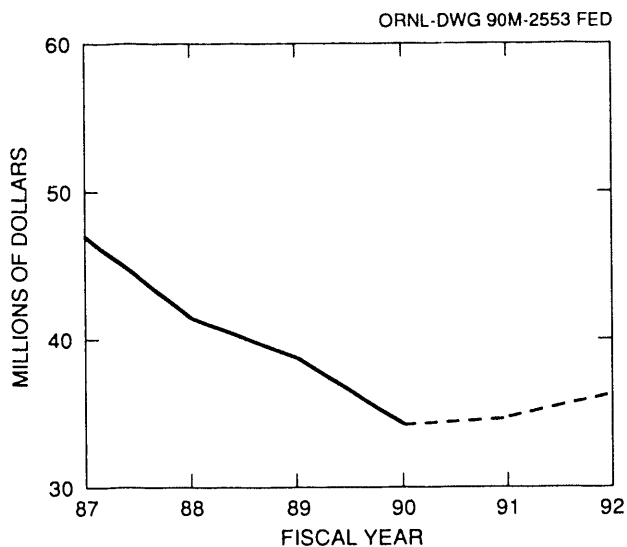


Fig. 10.2. Fusion Program expense funding (budget outlay).

and underwent refurbishing with new signs and new carpeting.

Library activity was affected by the intense controversy worldwide for several months of the year concerning claims that the major breakthrough of cold fusion had been achieved. During this exciting and busy time, standard library services were augmented by acquiring daily news updates from the online news services and displaying them in the library.

10.1.5 Publications Services

The Fusion Energy Division Publications Office (FEDPO) provides the division with editing, writing, composition, conventional and computer graphics, document makeup, and reproduction services. It also serves as liaison with the Laboratory Records Department of ISD for clearance processing of all documents prepared by division staff.

Throughout 1989, the FEDPO staff processed a total of 230 jobs (a 30% increase over the previous year), including

journal articles, conference papers, reports, preprints, and one thesis. In addition, 310 presentations (abstracts and viewgraph packages) were cleared. Much of this material is listed in Appendix 1.

Electronic publishing—preparation of text, graphics, and sometimes complete documents using computers—made steady advances in the division in 1989. Continuing its support of the division's commitment to electronic publishing, FEDPO updated several packages of word processing and either upgraded or purchased graphics software for both the Macintoshes and the IBM PC ATs. The editor in the publications office uses a Macintosh and the division's computer system for much of her editing and writing. During the year, compositors continued to expand their knowledge and skill in using the \TeX formatter available on the division's VAX cluster, WordPerfect 5.0 software for support of Fusion Engineering Design Center projects, and a number of new word processing packages for the Macintosh.

The Graphics Section of the publications office produced 1,605 drawings and revisions, 95 visuals, 5,291 Pos prints and viewgraphs, and 925 miscellaneous items during 1989. During the year, the section's illustrators continued to train in new software packages for the Macintosh computers, and 1989 saw a majority of the work being produced on the Macintosh as compared to the more expensive and time-consuming online production of previous years.

Seven members of the FEDPO staff won awards in the Society for Technical Communications (STC) East Tennessee Chapter annual competition (including an award for Best of Show). In addition, one member won an award at the STC international art competition for conceptual renderings of equipment being developed and/or operated by the division.

In December 1989, FEDPO merged with the Engineering Technology Division Publications Office (ETDPO) to form the Engineering Technology/Fusion Energy Division Publications Office (ET/FE DPO). The ET/FE DPO is committed to providing high-quality, cost-effective publications support to both of its host divisions.

10.2 QUALITY ASSURANCE

10.2.1 QA Program Development and Training

During the year, one new procedure was added to the division quality assurance (QA) manual. The NQA-1 orientation and portions of the QA training program were completed. The 213 participants included division staff; Y-12 Plant supervisors, planners, and craft workers; staff of other ORNL divisions supporting Fusion Energy Division; staff of the Energy Systems Engineering and Publications divisions; and DOE staff.

10.2.2 QA Program Implementation

The division's QA engineer reviewed engineering and procurement documents, including drawings and specifications defining technical requirements for items to be fabricated, to ensure that they clearly defined the QA requirements to be met. Five nonconformance reports, four quality inspection reports, and one unusual occurrence report were written to document problems, produce corrective action, and disseminate information to other organizations. One vendor surveillance was performed during the year. The Princeton Plasma Physics

Laboratory Quality Department performed an audit of the division.

10.3 SAFETY AND ENVIRONMENTAL PROTECTION

10.3.1 Safety

In an effort to improve the environment, safety, and health (ES&H) upgrade program in the division, a safety resource team was established in 1989. The team included a member from each section in the division. Its purpose was to identify safety hazards in division facilities and develop plans of action to correct or resolve the issues. The team successfully initiated activities such as the identification of 400 safety-related issues, planned and executed a division-wide safety work day, prepared the division for audits preceding the Technical Safety Appraisal (TSA) and for the actual TSA, and continued to monitor the division's safety and health policies. The team also assisted in the improvement of safety documentation and records, which included safety assessments, operating procedures, and safety study reports.

In general, the division has continued to recognize the need for its safety awareness program and housekeeping efforts. The monthly safety meetings are being used as a training forum to address these issues. With the increased emphasis on these programs, division staff are expected to develop a safer attitude and improve the division's performance in 1990.

10.3.2 Environment

The division implemented new activities and programs to address environmental

concerns, compliance issues, and improved employee communications in 1989. These activities included a hazard communication program, which enables employees to determine the hazardous level of the chemicals in laboratories, and noise level and asbestos survey programs. An area of concern in Bldg. 9201-2 is the basement; this area was

evaluated, and a restoration plan is being prepared.

New procedures and directives are being implemented in areas of air and water pollution, polychlorinated biphenyl (PCB) contamination, radiation controls, etc. These initiatives will assist the division in improvement and protection of the environment.

Appendix 1

PUBLICATIONS AND PRESENTATIONS

BOOKS AND JOURNAL ARTICLES	233
PRESENTATIONS	245
CONGRESSIONAL TESTIMONY	267
SEMINARS	269
REPORTS	271
ORNL Reports	271
ORNL Technical Memoranda	271
ORNL Fusion Engineering Design Center Reports	272
Reports Prepared by ORNL for the U.S. Department of Energy	272
Reports Published by Other Institutions	272
THESES AND DISSERTATIONS	275

BOOKS AND JOURNAL ARTICLES

- F. S. B. Anderson, F. Middleton, R. J. Colchin, and D. Million, "Accurate Electron Gun-Positioning Mechanism for Electron Beam-Mapping of Large Cross-Section Magnetic Surfaces," *Rev. Sci. Instrum.* **60**, 795–7 (1989)
- S. E. Attenberger, W. A. Houlberg, and N. A. Uckan, "Transport Analysis of Ignited and Current-Driven ITER Designs," *Fusion Technol.* **15**, 629–36 (1989)
- D. B. Batchelor, E. F. Jaeger, B. A. Carreras, V. E. Lynch, H. Weitzner, K. Imre, D. C. Stevens, V. Fuchs, and A. Bers, "Full-Wave Modeling of Ion Cyclotron Heating in Tokamaks," p. 611 in *Plasma Physics and Controlled Nuclear Fusion Research 1988: Twelfth Conference Proceedings, Nice, 12–19 October 1988*, vol. 1, International Atomic Energy Agency, Vienna, 1989
- D. B. Batchelor, E. F. Jaeger, and P. L. Colestock, "Ion Cyclotron Emission from Energetic Fusion Products in Tokamak Plasmas—A Full-Wave Calculation," *Phys. Fluids B* **1**, 1174–84 (1989)
- D. B. Batchelor, E. F. Jaeger, and H. Weitzner, "2D Full Wave Modeling of ICRF with Finite E_{\parallel} ," pp. 691–8 in *Theory of Fusion Plasmas: Proceedings of the Joint Varenna-Lausanne Workshop Held at Hotel du Signal, Chexbres (near Lausanne), Switzerland, October 3–7, 1988*, ed. J. Vaclavik, F. Troyon, and E. Sindoni, Editrice Compositori, Bologna, Italy, 1989
- L. R. Baylor, W. A. Houlberg, G. L. Schmidt, S. L. Milora, and the JET/U.S. Pellet Team, "Particle Transport Analysis of Pellet-Fueled JET Plasmas," pp. 107–12 in *Pellet Injection and Toroidal Confinement: Proceedings of the Technical Committee Meeting, Gut Ising, 1988*, IAEA-TECDOC-534, International Atomic Energy Agency, Vienna, 1989
- W. R. Becraft, J. H. Whealton, T. P. Wangler, A. Schempp, G. E. McMichael, M. A. Akerman, G. C. Barber, W. K. Dagenhart, H. H. Haselton, R. J. Raridon, K. E. Rothe, B. D. Murphy, and W. L. Stirling, "RF Accelerated High Energy (1–3 MeV) Neutral Beams for Tokamak Plasma Heating, Current Drive and Alpha Diagnostics," *Fusion Technol.* **15**, 734 (1989)
- G. E. Bell, M. A. Abdou, and P. F. Tortorelli, "Experimental and Analytical Investigation of Mass Transport Processes of 12Cr-1MoVW Steel in Thermally Convected Lithium Systems," *Fusion Eng. Des.* **8**, 421–7 (1989)
- M. G. Bell, V. Arunasalam, C. W. Barnes, M. Bitter, H.-S. Bosch, N. L. Bretz, R. Budny, C. E. Bush, A. Cavallo, T. K. Chu, S. A. Cohen, P. L. Colestock, S. L. Davis, D. L. Dimock, H. F. Dylla, P. C. Efthimion, A. B. Ehrhardt, R. J. Fonck, E. D. Fredrickson, H. P. Furth, G. Gammel, R. J. Goldston, G. J. Greene, B. Grek, L. R. Grisham, G. W. Hammett, R. J. Hawryluk, H. W. Hendel, K. W. Hill, E. Hinnov, J. C. Hosea, R. B. Howell, H. Hsuan, R. A. Hulse, K. P. Jaehnig, A. C. Janos, D. L. Jassby, F. C. Jobses, D. W. Johnson, L. C. Johnson, R. Kaita, C. Kieras-Phillips, S. J. Kilpatrick, V. A. Krupin, P. H. LaMarche, W. D. Langer, B. LeBlanc, R. Little, A. Lysojvan, D. M. Manos, D. K. Mansfield, E. Mazzucato, R. T. McCann, M. P. McCarthy, D. C. McCune, K. M. McGuire, D. H. McNeill, D. M. Meade, S. S. Medley, D. R. Mikkelsen, R. W. Motley, D. Mueller, Y. Murakami, J. A. Murphy, E. B. Nieschmidt, D. K. Owens, H. K. Park, A. T. Ramsey, M. H. Redi, A. L. Roquemore, P. H. Rutherford, T. Saito, N. R. Sauthoff, G. Schilling, J. Schivell, G. L. Schmidt, S. D. Scott, J. C. Sinnis, J. E. Stevens, W. Stodiek, B. C. Stratton, G. D. Tait, G. Taylor, J. R. Timberlake, H. H. Towner, M. Ulrickson, S. Von Goeler, R. M. Wieland, M. D. Williams, J. R. Wilson, K.-L. Wong, S. Yoshikawa, K. M. Young, M. Zarnstorff, and S. J. Zweben, "An Overview of TFTR Confinement with Intense Neutral Beam Heating," p. 27 in *Plasma Physics and Controlled Nuclear Fusion Research 1988: Twelfth Conference Proceedings, Nice, 12–19 October 1988*, vol. 1, International Atomic Energy Agency, Vienna, 1989
- C. A. Bennett and D. P. Hutchinson, "Far Field Propagation of the Truncated EH_{11} Dielectric Waveguide Mode," *Appl. Opt.* **28**, 2581–83 (1989)
- H. Biglari, P. H. Diamond, M. N. Rosenbluth, R. E. Waltz, R. R. Dominguez, P. W. Terry, N. Mattor, P. Lyster, J. N. Leboeuf, B. A. Carreras, G. S. Lee, L. Garcia, N. Dominguez, and J. H. Han, "Advances in the Theory of Ion-Temperature-Gradient-Driven Turbulence," p. 261 in *Plasma Physics*

and *Controlled Nuclear Fusion Research 1988: Twelfth Conference Proceedings, Nice, 12–19 October 1988*, vol. 2, International Atomic Energy Agency, Vienna, 1989

- A. Boileau, M. von Hellermann, L. D. Horton, J. Spence, and H. P. Summers, "The Deduction of Low-Z Ion Temperatures and Densities in the JET Tokamak Using Charge Exchange Recombination Spectroscopy," *Plasma Phys. Controlled Fusion* **31**, 779 (1989)
- A. Boileau, M. von Hellermann, L. D. Horton, H. P. Summers, and P. D. Morgan, "Analysis of Low-Z Impurity Behaviour in JET by Charge Exchange Measurements," *Nucl. Fusion* **29**, 1449 (1989)
- K. H. Burrell, S. L. Allen, G. Bramson, N. H. Brooks, R. W. Callis, T. N. Carlstrom, M. S. Chance, M. S. Chu, A. P. Colleraine, D. Content, J. C. DeBoo, R. R. Dominguez, S. Ejima, J. Ferron, R. L. Freeman, H. Fukumoto, P. Gohil, N. Gottardi, C. M. Greenfield, R. J. Groebner, G. Haas, R. W. Harvey, W. W. Heidbrink, F. J. Helton, D. N. Hill, F. L. Hinton, R.-M. Hong, N. Hosogane, W. Howl, C. L. Hsieh, G. L. Jackson, G. L. Jahns, R. A. James, A. G. Kellman, J. Kim, S. Kinoshita, L. L. Lao, E. A. Lazarus, P. Lee, T. LeHecka, J. Lister, J. M. Lohr, P. J. Lomas, T. C. Luce, J. L. Luxon, M. A. Mahdavi, K. Matsuda, M. Mayberry, C. P. Moeller, Y. Neyatani, T. Ohkawa, N. Ohyabu, T. H. Osborne, D. O. Overskei, T. Ozeki, W. A. Peebles, S. Perkins, M. Perry, P. I. Petersen, T. W. Petrie, K. Philipono, J. C. Phillips, R. Pinsker, G. D. Porter, R. Prater, D. B. Reimsen, M. E. Rensink, K. Sakamoto, M. J. Schaffer, D. P. Schissel, J. T. Scoville, R. P. Seraydarian, M. Shimada, T. C. Simonen, R. T. Snider, G. M. Staebler, B. W. Stallard, R. D. Stambaugh, R. D. Stav, H. St. John, R. E. Stockdale, E. J. Strait, P. L. Taylor, T. T. Taylor, P. K. Trost, A. Turnbull, U. Stroth, R. E. Waltz, and R. Wood, "Energy Confinement in Auxiliary Heated Divertor and Limiter Discharges in the DIII-D Tokamak," p. 193 in *Plasma Physics and Controlled Nuclear Fusion Research 1988: Twelfth Conference Proceedings, Nice, 12–19 October 1988*, vol. 1, International Atomic Energy Agency, Vienna, 1989
- J. D. Callen, Y. B. Kim, A. K. Sundaram, B. A. Carreras, L. Garcia, K. C. Shaing, D. A. Spong, H. Biglari, P. H. Diamond, and O. J. Kwon, "Neoclassical MHD Description of Tokamak Plasmas," p. 33 in *Plasma Physics and Controlled Nuclear Fusion Research 1988: Twelfth Conference Proceedings, Nice, 12–19 October 1988*, vol. 2, International Atomic Energy Agency, Vienna, 1989
- B. A. Carreras and P. H. Diamond, "Thermal Diffusivity Induced by Resistive Pressure-Gradient-Driven Turbulence," *Phys. Fluids B* **1**, 1011–17 (1989)
- B. A. Carreras, N. Dominguez, L. Garcia, J. F. Lyon, S. L. Painter, V. E. Lynch, J. R. Cary, and J. D. Hanson, "Low-Aspect-Ratio Torsatrons," p. 397 in *Plasma Physics and Controlled Nuclear Fusion Research 1988: Twelfth Conference Proceedings, Nice, 12–19 October 1988*, vol. 2, International Atomic Energy Agency, Vienna, 1989
- M. D. Carter, D. B. Batchelor, and C. L. Hedrick, "Drift Loss Transport Driven by Radiofrequency Heating," *Nucl. Fusion* **29**, 729–44 (1989)
- M. D. Carter, E. F. Jaeger, and D. B. Batchelor, "Non-Linear Core Plasma Response to ICRF Heating with Transport," *Nucl. Fusion* **29**, 2141 (1989)
- J. B. O. Caughman II, D. N. Ruzic, and D. J. Hoffman, "Floating Potential Measurements in the Near Field of an Ion Cyclotron Resonance Heating Antenna," *J. Vac. Sci. Technol. A* **7**, 1092–98 (1989)
- L. A. Charlton, R. J. Hastie, and T. C. Hender, "Ideal and Resistive Infernal Modes," *Phys. Fluids B* **1**, 798 (1989)
- R. J. Colchin, F. S. B. Anderson, A. C. England, R. F. Gandy, J. H. Harris, M. A. Henderson, D. L. Hillis, R. R. Kindsfather, D. K. Lee, D. L. Million, M. Murakami, G. H. Neilson, M. J. Saltmarsh, and C. M. Simpson, "Electron Beam and Magnetic Field Mapping Techniques Used to Determine Field Errors in the ATF Torsatron," *Rev. Sci. Instrum.* **60**, 2680 (1989)
- S. K. Combs, C. A. Foster, S. L. Milora, D. D. Schuresko, M. J. Gouge, P. W. Fisher, B. E. Argo, G. C. Barber, L. R. Baylor, M. J. Cole, D. T. Fehling, C. R. Foust, F. E. Gethers, H. H. Haselton, T. C. Jernigan, N. S. Ponte, A. L. Qualls, D. E. Schechter, D. W. Simmons, C. W. Sohns, D. O. Sparks, C. C. Tsai, and J. C. Whitson, "Pellet Injector Research at ORNL," p. 709 in *Fusion Technology 1988: Proceedings of the 15th Symposium on Fusion Technology, Utrecht, The Netherlands, 19–23*

September 1988, Vol. 1, edited by A. M. Van Ingen, A. Nijssen-Vis, and H. T. Klippel, North-Holland, Amsterdam, 1989

- S. K. Combs, T. C. Jernigan, L. R. Baylor, S. L. Milora, C. R. Foust, P. Kupschus, M. Gadeberg, and W. Bailey, "Performance of a Pneumatic Hydrogen-Pellet Injection System on the Joint European Torus," *Rev. Sci. Instrum.* **60**, 2697-2700 (1989)
- S. K. Combs, S. L. Milora, C. R. Foust, M. J. Gouge, D. T. Fehling, and D. O. Sparks, "Development of a Two-Stage Light Gas Gun to Accelerate Hydrogen Pellets to High Speeds for Plasma Fueling Applications," *J. Vac. Sci. Technol. A* **7**, 963-7 (1989)
- W. A. Cooper, S. P. Hirshman, and D. K. Lee, "The Beta Limit in the Advanced Toroidal Facility due to Local Ideal MHD Instabilities," *Nucl. Fusion* **29**, 617 (1989)
- N. Dominguez, J. N. Leboeuf, B. A. Carreras, and V. E. Lynch, "Ideal Low- n and Mercier Mode Stability Boundaries for $\ell = 2$ Torsatrons," *Nucl. Fusion* **29**, 2079 (1989)
- D. G. Doran and R. L. Klueh, "Reduced Activation Alloy Development for Fusion," *MRS Bull.* **XIV**, 45-57 (1989) R. A. Dory, "Matrices and Contour Plots," *Comput. Phys.* **3** (3), 84 (1989)
- R. A. Dory, "Ordinary Differential Equations," *Comput. Phys.* **3** (5), 88 (1989)
- R. A. Dory, "WingZ as a Scientific Aid," *Comput. Phys.* **3** (3), 93 (1989)
- R. A. Dory, W. A. Houlberg, and S. E. Attenberger, "Energy Requirements for Neutral Beam Current Drive in a Large Tokamak," *Comments Plasma Phys. Controlled Fusion* **13**, 29-44 (1989)
- L. Dresner, "Bubble Growth in Superheated He-II," *Cryogenics* **29**, 509 (1989)
- L. Dresner, "Quench Pressure, Thermal Expulsion, and Normal Zone Propagation in Internally Cooled Superconductors," *IEEE Trans. Magn.* **MAG-25**, 1710 (1989)
- C. L. Dunford, D. C. Larson, and P. G. Young, "ENDF/B-VI Nuclear Data Evaluations for Fusion Applications," *Fusion Technol.* **15**, 429 (1989)
- C. L. Easterly, G. S. Hill, and J. B. Cannon, "Environmental Effects of Fusion Power Plants. Part III: Potential Radiological Impact of Environmental Releases," *Fusion Technol.* **16**, 125 (1989)
- A. C. England, O. C. Eldridge, S. F. Knowlton, M. Porkolab, and J. R. Wilson, "Power Transmission and Coupling for RF Heating of Plasmas," *Nucl. Fusion* **29**, 1527-1632 (1989)
- P. W. Fisher, M. L. Bauer, L. R. Baylor, S. K. Combs, L. E. Deleanu, D. T. Fehling, C. A. Foster, M. J. Gouge, S. L. Milora, D. D. Schuresko, D. O. Sparks, and J. C. Whitson, "Tritium Pellet Injector Results," *J. Vac. Sci. Technol. A* **7**, 938-43 (1989)
- J. D. Galambos, Y-K. M. Peng, R. L. Reid, M. S. Lubell, L. Dresner, and J. R. Miller, "Comparison of Nb₃Sn and NbTi Superconducting Magnets for ITER Devices," *Fusion Technol.* **15**, 1046 (1989)
- J. D. Galambos, D. J. Strickler, Y-K. M. Peng, and R. L. Reid, "Plasma Elongation Studies for ITER-Like Tokamaks," *Fusion Technol.* **15**, 483 (1989)
- L. Garcia, C. Alejandre, A. L. Fraguas, J. Guasp, A. Varias, B. A. Carreras, N. Dominguez, and V. E. Lynch, "Equilibrium and Stability Studies for Low-Aspect-Ratio Stellarator Configurations," p. 389 in *Plasma Physics and Controlled Nuclear Fusion Research 1988: Twelfth Conference Proceedings, Nice, 12-19 October 1988*, vol. 2, International Atomic Energy Agency, Vienna, 1989
- R. C. Goldfinger and D. B. Batchelor, "A Numerical Model for Electron Cyclotron Heating Profiles in Stellarator Geometry," *Nucl. Fusion* **29**, 1743 (1989)
- M. J. Gouge, S. K. Combs, P. W. Fisher, and S. L. Milora "Design Considerations for Single-Stage and Two-Stage Pneumatic Pellet Injectors," *Rev. Sci. Instrum.* **60**, 570-75 (1989)
- D. L. Grekov, M. D. Carter, and A. I. Pyatak, "Ion Trapping Effect on Cyclotron Fast Magnetosonic Wave Absorption in a Tokamak," *Fiz. Plasmy* **15**, 1143 (1989).
- D. C. Griffin, M. S. Pindzola, and P. Krylstedt, "Distorted-Wave Calculations of Dielectronic Recombination for C³⁺ and O⁵⁺ in Small Electric Fields," *Phys. Rev. A* **40**, 6699-6701 (1989)
- S. P. Grotz, N. M. Ghoniem, TITAN Research Group, J. R. Bartlit, C. G. Bathke, J. P. Blanchard, E. T. Cheng, Y. Chu, R. W. Conn, P. I. H. Cooke, R. L. Creedon, A. Dabiri, W. P. Duggan, O. Fischer,

- P. J. Gierszewski, G. E. Gorker, M. Z. Hasan, C. G. Hoot, D. C. Keeton, W. P. Kelleher, C. E. Kessel, R. A. Krakowski, O. Kveton, D. C. Lousteau, R. C. Martin, R. L. Miller, F. Najmabadi, R. A. Nebel, G. E. Orient, A. K. Prinja, K. R. Schultz, S. Sharafat, D. Steiner, D. K. Sze, S. L. Thomson, S. G. Visser, E. L. Vold, K. A. Werley, and C. P. C. Wong, "Overview of the TITAN-I Fusion-Power Core," *Fusion Eng. Des.* **9**, 357–73 (1989)
- J. H. Harris, M. Murakami, B. A. Carreras, J. D. Bell, G. L. Bell, T. S. Bigelow, L. A. Charlton, N. Dominguez, J. L. Dunlap, J. C. Glowienka, L. D. Horton, H. C. Howe, R. C. Isler, H. Kancko, R. R. Kindsfather, J. N. Leboeuf, V. E. Lynch, M. M. Menon, R. N. Morris, G. H. Neilson, V. K. Paré, D. A. Rasmussen, J. B. Wilgen, and W. R. Wing, "Second Stability in the ATF Torsatron," *Phys. Rev. Lett.* **63**, 1249–52 (1989)
- P. N. Haubenreich, S. Shimamoto, P. Komarek, and G. Vécsey, "International Development of Superconducting Magnets for Fusion Power," *Fusion Technol.* **15**, 909 (1989)
- C. C. Havener, M. S. Huq, F. W. Meyer, and R. A. Phaneuf, "Electron Capture by Multicharged Ions at eV Energies," *J. Phys. (Paris)* **50**, Coll. C1, 7–17 (1989)
- C. C. Havener, M. S. Huq, H. F. Krause, P. A. Schulz, and R. A. Phaneuf, "Merged-Beams Measurements of Electron-Capture Cross Sections for $O^{5+} + H$ at Electron-Volt Energies," *Phys. Rev. A* **39**, 1725–40 (1989)
- C. C. Havener, K. J. Reed, K. J. Snowdon, N. Stolterfoht, D. M. Zehner, and F. W. Meyer, "Evidence for Production of Inner-Shell Vacancies in Slow Multicharged F Ions Interacting with a Cu Surface," *Surf. Sci.* **216**, L357–L365 (1989)
- C. C. Havener, K. J. Reed, K. J. Snowdon, D. M. Zehner, and F. W. Meyer, "Interaction of Multiple Charged Ions with Solid Surfaces," *Radiat. Eff. Defects Solids* **109**, 99–109 (1989)
- D. M. Hetrick, C. Y. Fu, and D. C. Larson, "ENDF/B-VI Evaluations for Isotopes of Cr, Fe, Ni, Cu, and Pb," *Fusion Technol.* **15**, 453 (1989)
- D. L. Hillis, P. K. Mioduszewski, R. H. Fowler, J. A. Rome, O. Motojima, T. Mizuuchi, N. Noda, T. Mutoh, H. Zushi, R. Takahashi, T. Obiki, A. Iiyoshi, and K. Uo, "Experimental Investigation of the Natural Divertor Configuration in Heliotron-E," *J. Nucl. Mater.* **162–164**, 629 (1989)
- D. J. Hoffman and G. C. Barber, "The Technology of the Ion Cyclotron Range of Frequencies," *Fusion Technol.* **15**, 719 (1989)
- J. T. Hogan, C. C. Klepper, D. L. Hillis, and T. Uckan, "Modeling of Spectroscopic Measurements of Edge Recycling," *J. Nucl. Mater.* **162–164**, 469 (1989)
- J. A. Holmes, B. A. Carreras, and L. A. Charlton, "Magnetohydrodynamic Stability and Nonlinear Evolution of the $m = 1$ Mode in Toroidal Geometry for Safety Factor Profiles with an Inflection Point," *Phys. Fluids B* **1**, 788–97 (1989)
- J. A. Holmes, L. A. Charlton, J. T. Hogan, B. A. Carreras, and E. A. Lazarus, "Maximum Beta for a Small-Aspect-Ratio Tokamak," *Phys. Fluids B* **1**, 358–63 (1989)
- W. A. Houlberg, S. L. Milora, C. K. Phillips, J. S. Tolliver, and the JET/U.S. Pellet Team, "WHIST Transport Analysis of High-Neutron-Production, ICRF-Heated, Pellet-Fueled JET Plasmas," pp. 137–42 in *Pellet Injection and Toroidal Confinement: Proceedings of the Technical Committee Meeting, Gut Ising, 1988*, IAEA-TECDOC-534, International Atomic Energy Agency, Vienna, 1989
- M. S. Huq, C. C. Havener, and R. A. Phaneuf, "Low-Energy Electron Capture by N^{3+} , N^{4+} , and N^{5+} from Hydrogen Atoms Using Merged Beams," *Phys. Rev. A* **40**, 1811–16 (1989)
- R. C. Isler, E. C. Crume, L. D. Horton, H. C. Howe, and G. S. Voronov, "Spectroscopic Studies of Plasma Collapse in the Advanced Toroidal Facility," *Nucl. Fusion* **29**, 1384–90 (1989)
- R. C. Isler, L. D. Horton, G. S. Voronov, E. C. Crume, G. L. Bell, R. F. Gandy, J. H. Harris, J. C. Glowienka, M. Murakami, G. H. Neilson, D. A. Rasmussen, J. B. Wilgen, and W. R. Wing, "Temperature Behaviour During Neutral Beam Injection in a Torsatron (ATF) with Field Errors," *Nucl. Fusion* **29**, 1391–97 (1989)

- JET Team (ORNL staff members: L. R. Baylor, W. A. Houlberg, T. C. Jernigan, and S. L. Milora), "High Temperature Experiments and Fusion Product Measurements in JET," p. 247 in *Plasma Physics and Controlled Nuclear Fusion Research 1988: Twelfth Conference Proceedings, Nice, 12-19 October 1988*, vol. 1, International Atomic Energy Agency, Vienna, 1989
- JET Team (ORNL staff members: L. R. Baylor, W. A. Houlberg, T. C. Jernigan, and S. L. Milora), "Heating of Peaked Density Profiles Produced by Pellet Injection in JET," p. 215 in *Plasma Physics and Controlled Nuclear Fusion Research 1988: Twelfth Conference Proceedings, Nice, 12-19 October 1988*, vol. 1, International Atomic Energy Agency, Vienna, 1989
- JET Team (ORNL staff members: L. R. Baylor, W. A. Houlberg, T. C. Jernigan, and S. L. Milora), "The JET H-Mode at High Current and Power Levels," p. 159 in *Plasma Physics and Controlled Nuclear Fusion Research 1988: Twelfth Conference Proceedings, Nice, 12-19 October 1988*, vol. 1, International Atomic Energy Agency, Vienna, 1989
- JET Team (ORNL staff members: L. R. Baylor, W. A. Houlberg, T. C. Jernigan, and S. L. Milora), "Latest JET Results and Future Prospects," p. 41 in *Plasma Physics and Controlled Nuclear Fusion Research 1988: Twelfth Conference Proceedings, Nice, 12-19 October 1988*, vol. 1, International Atomic Energy Agency, Vienna, 1989
- E. A. Kenik, P. J. Maziasz, and R. L. Klueh, "Phase Stability of a Manganese-Stabilized Austenitic Stainless Steel," pp. 284-5 in *Proceedings of the 47th Annual Meeting of the Electron Microscopy Society of America, San Antonio, Texas, August 6-11, 1989*, ed. G. W. Bailey, San Francisco Press, Inc., San Francisco, 1989
- J. F. King, F. W. Baity, D. J. Hoffman, J. C. Walls, and D. J. Taylor, "Materials Tests and Analyses of Faraday Shield Tubes for ICRF Antennas," *Fusion Technol.* **15**, 1093-5 (1989)
- C. C. Klepper, L. W. Owen, P. I. Mioduszewski, and A. Grosman, "Modeling of Neutral Transport and Impurity Generation in the Core Supra Pump Limiter," *J. Nucl. Mater.* **162-164**, 696 (1989)
- R. L. Klueh, "Heat Treatment Behavior and Tensile Properties of Cr-W Steels," *Metall. Trans.* **20A**, 463-70 (1989)
- R. L. Klueh, "Impact Behavior of Cr-W Steels," *J. Mater. Eng.* **11**, 169-75 (1989)
- R. L. Klueh, "Tensile Property Behavior of Irradiated Martensitic Alloys," *Trans. Am. Nucl. Soc.* **60**, 296-7 (1989)
- R. L. Klueh and P. J. Maziasz, "The Microstructure of Chromium-Tungsten Steels," *Metall. Trans.* **20A**, 373-82 (1989)
- R. L. Klueh and J. M. Vitek, "Fluence and Helium Effects on the Tensile Properties of Ferritic Steels at Low Temperatures," *J. Nucl. Mater.* **161**, 13-23 (1989)
- H. W. Kugel, G. M. Gammel, L. R. Grisham, R. Kaita, J. Kamperschroer, R. A. Langley, C. W. Magee, S. S. Medley, T. J. Murphy, A. L. Roquemore, and M. D. Williams, "Measurements of Neutral Beam Species, Impurities, Spatial Divergence, Energy Dispersion, Pressure, and Reionization Using the TFTR U.S. Common Long Pulse Ion Source," *Rev. Sci. Instrum.* **60**, 37-52 (1989)
- R. A. Langley, "Helium-Ion-Induced Release of Hydrogen from Graphite," *J. Nucl. Mater.* **162-164**, 1030 (1989)
- R. A. Langley, "Initial Results for Ion-Induced Release of Hydrogen and Deuterium from AXF-5Q Graphite by Hydrogen and Deuterium," *J. Vac. Sci. Technol. A* **7**, 1060-4 (1989)
- R. A. Langley, J. W. Halliwell, G. R. Dyer, and J. L. Yarber, "Gas Injection System for the Advanced Toroidal Facility," *J. Vac. Sci. Technol. A* **7**, 2423-6 (1989)
- LCT Team, L. Dresner, W. A. Fietz, S. Gauss, P. N. Haubenreich, B. Jakob, T. Kato, P. Komarek, M. S. Lubell, J. W. Lue, J. N. Luton, W. Maurer, K. Okuno, S. W. Schwenterly, S. Shimamoto, Y. Takahashi, A. Ulbricht, G. Vecsey, F. Wuechner, and J. A. Zichy, "The Results of the International 'Large Coil Task': a Milestone for Superconducting Magnets in Fusion Power," p. 381 in *Plasma Physics and Controlled Nuclear Fusion Research 1988: Twelfth Conference Proceedings, Nice, 12-19 October 1988*, vol. 3, International Atomic Energy Agency, Vienna, 1989

- G. S. Lee, B. A. Carreras, and L. Garcia, "Fluctuation Spectrum of Resistive Pressure-Gradient-Driven Turbulence," *Phys. Fluids B* **1**, 119-33 (1989)
- G. S. Lee, P. H. Diamond, and Z. G. An, "Dynamics of Magnetic Relaxation in a High-Temperature, Current-Carrying Plasma," *Phys. Fluids B* **1**, 99-108 (1989)
- D. C. Lousteau, "Impact of Maintainability on the International Thermonuclear Experimental Reactor (ITER) Configuration Options," *Fusion Technol.* **15**, 649 (1989)
- G. E. Lucas, G. R. Odeh, and A. F. Rowcliffe, "Innovations in Testing Methodology for Fusion Reactor Materials Development," *MRS Bull.* **XIV**, 29-35 (1989)
- V. E. Lynch and B. A. Carreras, "Fusion Calculations on Cray Supercomputers," *ORNL Review* **21**, 17 (1989)
- J. F. Lyon, B. A. Carreras, V. E. Lynch, J. S. Tolliver, and I. N. Sviatoslavsky, "Compact Torsatron Reactors," *Fusion Technol.* **15**, 1401-19 (1989)
- J. Manickam, V. Arunasalam, C. W. Barnes, M. G. Bell, M. Bitter, H.-S. Bosch, N. L. Bretz, R. Budny, C. E. Bush, A. Cavallo, T. K. Chu, S. A. Cohen, P. L. Colestock, S. L. Davis, D. L. Dimock, H. F. Dylla, P. C. Efthimion, A. B. Ehrhardt, R. J. Fonck, E. D. Fredrickson, H. P. Furth, G. Gammel, R. J. Goldston, G. J. Greene, B. Grek, L. R. Grisham, G. W. Hammett, R. J. Hawryluk, H. W. Hendel, K. W. Hill, E. Hinnov, J. C. Hosea, R. B. Howell, H. Hsuan, R. A. Hulse, K. P. Jaehnig, A. C. Janos, D. L. Jassby, F. C. Jobs, D. W. Johnson, J. L. Johnson, L. C. Johnson, R. Kaita, C. Kieras-Phillips, S. J. Kilpatrick, V. A. Krupin, G. Kuo-Petravic, P. H. LaMarche, W. D. Langer, B. LeBlanc, R. Little, A. Lysojvan, D. M. Manos, D. K. Mansfield, E. Mazzucato, R. T. McCann, M. P. McCarthy, D. C. McCune, K. M. McGuire, D. H. McNeill, D. M. Meade, S. S. Medley, D. R. Mikkelsen, A. Miller, D. A. Monticello, R. W. Motley, D. Mueller, Y. Murakami, J. A. Murphy, E. B. Nieschmidt, D. K. Owens, H. K. Park, W. Park, A. T. Ramsey, M. H. Redi, A. L. Roquemore, P. H. Rutherford, T. Saito, N. R. Sauthoff, G. Schilling, J. Schivell, G. L. Schmidt, S. D. Scott, J. C. Sennis, J. E. Stevens, W. Stodiek, B. C. Stratton, G. D. Tait, G. Taylor, J. R. Timberlake, H. H. Towner, M. Ulrickson, S. Von Goeler, R. M. Wieland, M. D. Williams, J. R. Wilson, K.-L. Wong, S. Yoshikawa, K. M. Young, M. Zamstorff, and S. J. Zweben, "Stability of TFTR Plasmas," p. 395 in *Plasma Physics and Controlled Nuclear Fusion Research 1988: Twelfth Conference Proceedings, Nice, 12-19 October 1988*, vol. 1, International Atomic Energy Agency, Vienna, 1989
- P. J. Maziasz, "Developing an Austenitic Stainless Steel for Improved Performance in Advanced Fossil Power Facilities," *J. Met.* **41**, 14-20 (1989)
- P. J. Maziasz, "Formation and Stability of Radiation-Induced Phases in Neutron-Irradiated Austenitic and Ferritic Steels," *J. Nucl. Mater.* **169**, 95-115 (1989)
- P. J. Maziasz, "Microstructural Evolution of Martensitic Steels During Fast Neutron Irradiation," *Trans. Am. Nucl. Soc.* **60**, 297-9 (1989)
- P. J. Maziasz, R. L. Klueh, and A. F. Rowcliffe, "Using Analytical Electron Microscopy to Design Radiation Resistant Steels for Fusion Applications," *MRS Bull.* **XIV**, 36-44 (1989)
- T. J. McManamy, R. D. Benson, R. L. Brown, G. H. Henkel, E. A. Lazarus, D. E. Williamson, and C. T. Wilson, Jr., "STX Magnet Fabrication and Testing to 16 T," *Fusion Technol.* **15**, 1064 (1989)
- F. W. Meyer, C. C. Havener, S. H. Overbury, K. J. Reed, K. J. Snowdon, and D. M. Zehner, "Inner-Shell Processes as Probes of Multicharged Ion Neutralization at Surfaces," *J. Phys. (Paris)* **50**, Coll. C1, 263-75 (1989)
- S. L. Milora, "Review of Hydrogen Pellet Injection Technology for Plasma Fueling Applications," *J. Vac. Sci. Technol. A* **7**, 925-37 (1989)
- P. K. Mioduszewski, J. D. Bell, T. S. Bigelow, R. J. Colchin, E. C. Crume, J. L. Dunlap, G. R. Dyer, A. C. England, J. C. Glowienka, J. W. Halliwell, J. H. Harris, G. R. Haste, D. L. Hillis, S. Hiroe, L. D. Horton, H. C. Howe, R. C. Isler, T. C. Jernigan, R. R. Kindsfather, R. A. Langley, J. F. Lyon, M. M. Menon, T. Mizuuchi, O. Motojima, M. Murakami, G. H. Neilson, V. K. Paré, D. A. Rasmussen, M. J. Salimmarsh, F. Sano, J. E. Simpkins, T. Uekan, T. L. White, J. B. Wilgen, and

- W. R. Wing, "Initial Operation and Edge Plasma Studies in ATF," *J. Nucl. Mater.* **162–164**, 825 (1989)
- R. N. Morris, J. C. Glowienka, G. H. Neilson, S. P. Hirshman, and P. Merkel, "Finite-Beta Equilibrium Magnetic Field Perturbations in Stellarator Plasmas," *Nucl. Fusion* **29**, 2115 (1989)
- D. W. Mueller, L. J. Wang, and D. C. Gregory, "Electron-Impact Double-Ionization Cross Sections for Xe^{8+} ," *Phys. Rev. A* **39**, 2381–4 (1989)
- B. D. Murphy, J. H. Whealton, G. E. McMichael, W. R. Becraft, and H. H. Haselton, "High-Current Radio Frequency Quadrupole Accelerators for Current Drive in Tokamaks," *Nucl. Instrum. Methods Phys. Res.* **A275**, 157 (1989)
- M. Nakagawa, T. Mori, K. Kosako, T. Nakamura, M. Z. Youssef, Y. Watanabe, C. Y. Gung, R. T. Santoro, R. G. Alsmiller, Jr., J. Barnes, and T. A. Gabriel, "Analysis of Neutronics Parameters Measured in Phase-II Experiments on the JAERI/US Collaborative Program on Fusion Blanket Neutronics, Part I: Source Characteristics and Reaction Rate Distributions," *Fusion Eng. Des.* **9**, 315–22 (1989)
- B. E. Nelson for the ATF Team, "Final Assembly and Initial Operation of the Advanced Toroidal Facility," pp. 391–97 in *Fusion Technology 1988: Proceedings of the 15th Symposium on Fusion Technology, Utrecht, The Netherlands, 19–23 September 1988*, Vol. 1, edited by A. M. Van Ingen, A. Nijssen-Vis, and H. T. Klippel, North-Holland, Amsterdam, 1989
- H. Noguchi, C. L. Easterly, and M. R. Bennett, "Conversion of Low-Concentration Tritium Gas to Tritiated Water," *Fusion Technol.* **16**, 137 (1989)
- S. L. Painter and J. F. Lyon, "Alpha-Particle Losses in Compact Torsatron Reactors," *Fusion Technol.* **16**, 157–71 (1989)
- R. R. Parker, G. Bateman, P. L. Colestock, H. P. Furth, R. J. Goldston, W. A. Houlberg, D. Ignat, S. C. Jardin, J. L. Johnson, S. Kaye, C. Kieras-Phillips, J. Manickam, D. B. Montgomery, R. Myer, M. Phillips, R. Pillsbury, N. Pomphrey, M. Porkolab, D. E. Post, P. H. Rutherford, R. Sayer, J. Schmidt, G. Sheffield, D. J. Sigmar, D. Stotler, D. Strickler, R. Thome, R. Weiner, and J. C. Wesley, "Compact Ignition Tokamak Physics and Engineering Basis," p. 341 in *Plasma Physics and Controlled Nuclear Fusion Research 1988: Twelfth Conference Proceedings, Nice, 12–19 October 1988*, vol. 3, International Atomic Energy Agency, Vienna, 1989
- R. R. Parker, J. Sheffield, M. Wakatani, J-P. Watteau, and G. Grieger, "Plasma Physics and Controlled Nuclear Fusion Research (Summaries of the 12th International Conference, Nice, France, 12–19 October 1988)," *Nucl. Fusion* **29**, 489 (1989)
- R. A. Phaneuf, P. Defrance, D. C. Griffin, Y. Hahn, M. S. Pindzola, L. Roszman, and W. Wiese, "Review of Spectroscopic and Electron-Impact Collision Data Base for Fusion Plasma Research," *Phys. Scr.* **T28**, 5–7 (1989)
- M. W. Phillips, M. H. Hughes, A. M. M. Todd, J. T. Hogan, R. A. Dory, F. J. Helton, J. M. Greene, J. W. Helton, S. Jardin, J. L. Johnson, J. Manickam, R. R. Parker, and N. Pomphrey, "Effect of Shaping on the Equilibrium and Stability of High Current, High Beta Tokamaks," p. 65 in *Plasma Physics and Controlled Nuclear Fusion Research 1988: Twelfth Conference Proceedings, Nice, 12–19 October 1988*, vol. 2, International Atomic Energy Agency, Vienna, 1989
- M. S. Pindzola, D. C. Griffin, and C. Bottcher, "Coupling Effects for Electron-Impact Ionization in the Potassium Isoelectronic Sequence," *Phys. Rev. A* **39**, 2385–91 (1989)
- M. S. Pindzola, D. C. Moores, and D. C. Griffin, "Electron-Impact of Highly Charged Ions in Lowest-Order QED Theory," *Phys. Rev. A* **40**, 4941–46 (1989)
- A. E. Pontau, D. K. Brice, D. A. Buchenauer, R. A. Causey, B. L. Doyle, W. L. Hsu, S. R. Lee, R. T. McGrath, B. Mills, W. R. Wampler, K. L. Wilson, R. Langley, H. F. Dylla, D. B. Heifetz, S. Kilpatrick, P. H. LaMarche, R. A. P. Sisingh, M. Ulrickson, and J. N. Brooks, "TFTR Tritium Inventory Analysis," *Fusion Eng. Des.* **10**, 365–71 (1989)
- R. L. Reid, Y-K. M. Peng, and J. D. Galambos, "System Studies for ITER," *Fusion Technol.* **15**, 605 (1989)

- B. W. Riemer, "Estimation of Toroidal Field Coil Stresses from Magnetic Loads in FER and NET by Analytic Methods," *Fusion Technol.* **15**, 1051 (1989)
- A. F. Rowcliffe, E. E. Bloom, D. G. Doran, D. L. Smith, and T. C. Reuther, "Low-Activation Materials for Fusion," p. 429 in *Plasma Physics and Controlled Nuclear Fusion Research 1988: Twelfth Conference Proceedings, Nice, 12-19 October 1988*, vol. 3, International Atomic Energy Agency, Vienna, 1989
- J. A. Rome, "An Improved Method of Calculating Flux Coordinates," *J. Comput. Phys.* **82**, 348-61 (1989)
- M. J. Saltmarsh, F. S. B. Anderson, G. L. Bell, J. D. Bell, T. S. Bigelow, M. D. Carter, R. J. Colchin, E. C. Crume, Jr., J. L. Dunlap, G. R. Dyer, A. C. England, R. F. Gandy, J. C. Glowienka, R. C. Goldfinger, R. H. Goulding, J. W. Halliwell, J. H. Harris, D. L. Hillis, S. Hiroe, L. D. Horton, H. C. Howe, R. C. Isler, T. C. Jemigan, H. Kaneko, R. R. Kindsfather, R. A. Langley, D. K. Lee, J. F. Lyon, M. Kwon, M. M. Menon, P. K. Mioduszewski, T. Mizuuchi, O. Motojima, M. Murakami, G. H. Neilson, V. K. Paré, N. F. Perepelkin, D. A. Rasmussen, F. Sano, J. Sheffield, J. E. Simpkins, C. E. Thomas, T. Uckan, G. S. Voronov, M. R. Wade, T. L. White, J. B. Wilgen, and W. R. Wing, "Initial Experimental Results from the ATF Torsatron," p. 349 in *Plasma Physics and Controlled Nuclear Fusion Research 1988: Twelfth Conference Proceedings, Nice, 12-19 October 1988*, vol. 2, International Atomic Energy Agency, Vienna, 1989
- M. Sataka, S. Ohtani, D. Swenson, and D. C. Gregory, "Experimental Cross Sections for Electron-Impact Ionization of Chromium Ions: Cr^{6+} , Cr^{7+} , Cr^{8+} , and Cr^{10+} ," *Phys. Rev. A* **39**, 2397-2403 (1989)
- J. Schivell, C. E. Bush, D. K. Mansfield, S. S. Medley, H. K. Park, and F. J. Stauffer, "Survey of Features in Radiative Power Loss Profiles in the Tokamak Fusion Test Reactor," *Fusion Technol.* **15**, 1520 (1989)
- G. L. Schmidt, L. R. Baylor, G. Hammett, the JET/U.S. DOE Pellet Collaboration, R. Hulse, and D. K. Owens, "Pellets in Large Tokamaks: TFTR and JET," in *Pellet Injection and Toroidal Confinement: Proceedings of the Technical Committee Meeting, Gut Ising, 1988*, IAEA-TECDOC-534, International Atomic Energy Agency, Vienna, 1989
- D. D. Schnack, D. S. Hamed, J. McBride, H. Biglari, P. H. Diamond, F. Y. Gang, E. J. Caramana, R. A. Nebel, B. A. Carreras, E. Hamieri, H. R. Strauss, Y. L. Ho, and S. C. Prager, "Advances in Reverse-Field Pinch Theory and Computations," p. 467 in *Plasma Physics and Controlled Nuclear Fusion Research 1988: Twelfth Conference Proceedings, Nice, 12-19 October 1988*, vol. 2, International Atomic Energy Agency, Vienna, 1989
- T. Schober and D. N. Braski, "The Microstructure of Selected Annealed Vanadium-Base Alloys," *Metall. Trans.* **20A**, 1927-32 (1989)
- K. R. Schultz, R. Gallix, C. Baxi, B. Bourque, L. Creedon, D. Vance, W. Barr, W. Neff, J. Haines, J. A. Koski, R. McGrath, R. Causey, G. Listvinsky, and C. Carson, "Divertor and First Wall Armor Design for the TIBER-II Engineering Test Reactor," *Fusion Eng. Des.* **9**, 15-23 (1989)
- D. D. Schuresko, M. J. Cole, P. W. Fisher, A. L. Qualls, M. L. Bauer, R. B. Wysor, P. Lickliter, D. J. Webster, B. E. Argo, S. K. Combs, S. L. Milora, C. A. Foster, C. R. Foust, A. Fadnek, H. Takahashi, and T. Kozub, "Simplified Eight-Shot Pneumatic Pellet Injector for Plasma Fueling Applications on the Princeton Beta Experiment and on the Advanced Toroidal Facility," *J. Vac. Sci. Technol. A* **7**, 949-54 (1989)
- S. D. Scott, M. Bitter, R. J. Fonck, R. J. Goldston, R. B. Howell, H. Hsuan, K. P. Jaehnig, G. Pautasso, G. Schilling, B. C. Stratton, M. Zarnstorff, C. W. Barnes, M. G. Bell, H.-S. Bosch, C. E. Bush, A. Cavallo, H. F. Dylla, A. B. Ehrhardt, E. D. Fredrickson, G. Gammel, B. Grek, L. R. Grisham, G. W. Hammett, R. J. Hawryluk, H. W. Hendel, K. W. Hill, A. C. Janos, D. L. Jassby, F. C. Jobes, D. W. Johnson, S. J. Kilpatrick, B. LeBlanc, D. K. Mansfield, R. T. McCann, D. C. McCune, K. M. McGuire, D. H. McNeill, S. S. Medley, D. Mueller, J. A. Murphy, D. K. Owens, H. K. Park, A. T. Ramsey, A. L. Roquemore, J. Schivell, J. E. Stevens, G. D. Tait, G. Taylor, J. R. Timberlake, H. H. Towner, M. Ulrickson, R. M. Wieland, M. D. Williams, K.-L. Wong, S. J. Zweben, and the TFTR Group, "Current Drive and Confinement of Angular Momentum in TFTR," p. 655 in *Plasma*

Physics and Controlled Nuclear Fusion Research 1988: Twelfth Conference Proceedings, Nice, 12–19 October 1988, vol. 1, International Atomic Energy Agency, Vienna, 1989

- K. C. Shaing and E. C. Crume, Jr., "A Bifurcation Theory of Poloidal Rotation in Tokamaks: A Model for the L-H Transition," *Phys. Rev. Lett.* **63**, 2369–72 (1989)
- K. C. Shaing, B. A. Carreras, N. Dominguez, V. E. Lynch, and J. S. Tolliver, "Bootstrap Current Control in Stellarators," *Phys. Fluids B* **1**, 1663–70 (1989)
- K. C. Shaing, E. C. Crume, Jr., J. S. Tolliver, S. P. Hirshman, and W. I. van Rij, "Bootstrap Current and Parallel Viscosity in the Low Collisionality Regime in Toroidal Plasmas," *Phys. Fluids B* **1**, 148–52 (1989)
- K. C. Shaing and S. P. Hirshman, "Relaxation Rate of Poloidal Rotation in the Banana Regime in Tokamaks," *Phys. Fluids B* **1**, 705–7 (1989)
- K. C. Shaing, G. S. Lee, B. A. Carreras, W. A. Houlberg, and E. C. Crume, Jr., "A Model for the L-H Transitions in Tokamaks," p. 13 in *Plasma Physics and Controlled Nuclear Fusion Research 1988: Twelfth Conference Proceedings, Nice, 12–19 October 1988*, vol. 2, International Atomic Energy Agency, Vienna, 1989
- T. E. Shannon, "Design and Cost Evaluation of a Generic Magnetic Fusion Reactor Using the D-D Fuel Cycle," *Fusion Technol.* **15**, 1245 (1989)
- J. Sheffield, "Summary on Alternative Concepts," p. 577 in *Plasma Physics and Controlled Nuclear Fusion Research 1988: Twelfth Conference Proceedings, Nice, 12–19 October 1988*, vol. 3, International Atomic Energy Agency, Vienna, 1989
- J. Sheffield, "Tokamak Transport in the Presence of Multiple Mechanisms," *Nucl. Fusion* **29**, 1347 (1989)
- J. E. Simpkins, R. A. Strehlow, P. K. Mioduszewski, and T. Uckan, "Control of Water Absorption by Gas Purification of Graphite," *J. Nucl. Mater.* **162–164**, 871 (1989)
- C. J. Sofield, L. B. Bridwell, C. D. Moak, P. D. Miller, D. C. Gregory, C. M. Jones, G. D. Alton, P. L. Pepmiller, and J. Hall, "Charge-Exchange Cross Sections for 445 MeV Cl Ions in Solid C Targets," *Phys. Rev. A* **40**, 59–68 (1989)
- W. M. Stacey, Jr., D. A. Ehst, C. A. Flanagan, Y-K. M. Peng, N. Pomphrey, D. E. Post, D. L. Smith, and P. T. Spampinato, "U.S. Contribution to the International Tokamak Reactor Workshop, Phase 2A, Part 3, 1985–1987," *Fusion Technol.* **15**, 1485 (1989)
- N. Stolterfoht, K. Sommer, D. C. Griffin, C. C. Havener, M. S. Huq, J. K. Swenson, and F. W. Meyer, "Studies of Electron Correlation Effects in Multicharged Ion-Atom Collisions Involving Double Capture," *Nucl. Instrum. Methods. Phys. Res.* **B40/41**, 28–32 (1989)
- E. J. Strait, L. L. Lao, T. S. Taylor, M. S. Chu, J. K. Lee, A. D. Turnbull, S. L. Allen, N. H. Brooks, K. H. Burrell, R. W. Callis, T. N. Carlstrom, M. S. Chance, A. P. Colleraine, D. Content, J. C. DeBoo, J. Ferron, J. M. Greene, R. J. Groebner, W. W. Heidbrink, F. J. Helton, D. N. Hill, R.-M. Hong, N. Hosogane, W. Howl, C. L. Hsieh, G. L. Jackson, G. L. Jahns, A. G. Kellman, J. Kim, S. Kinoshita, E. A. Lazarus, P. J. Lomas, J. L. Luxon, M. A. Mähdavi, Y. Neyatani, T. Ohkawa, T. H. Osborne, D. O. Overskei, T. Ozeki, M. Perry, P. I. Petersen, T. W. Petrie, J. C. Phillips, G. D. Porter, D. P. Schissel, J. T. Scoville, R. P. Seraydarian, M. Shimada, T. C. Simonen, R. T. Snider, R. D. Stambaugh, R. D. Stav, H. St. John, R. E. Stockdale, U. Stroth, and R. Wood, "Stability of High Beta Discharges in the DIII-D Tokamak," p. 83 in *Plasma Physics and Controlled Nuclear Fusion Research 1988: Twelfth Conference Proceedings, Nice, 12–19 October 1988*, vol. 1, International Atomic Energy Agency, Vienna, 1989
- J. K. Swenson, C. C. Havener, N. Stolterfoht, K. Sommer, and F. W. Meyer, "Observation of Coulomb Focusing of Autoionization Electrons Produced in Low-Energy $\text{He}^+ + \text{He}$ Collisions," *Phys. Rev. Lett.* **63**, 35–38 (1989)
- D. K. Sze, J. Gordon, S. Piet, E. T. Cheng, J. DeVan, and A. Klein, "Engineering, Safety, and Economic Evaluations of ASPIRE," *Fusion Eng. Des.* **9**, 471–475 (1989)

- D. J. Taylor, F. W. Baity, R. A. Brown, W. E. Bryan, A. Fadneck, D. J. Hoffman, J. F. King, R. L. Livesey, and R. L. McIlwain, "Resonant Double Loop Antenna Development at ORNL," *Fusion Technol.* **15**, 1088 (1989)
- D. R. Thayer, P. H. Diamond, H. Biglari, Ch. P. Ritz, A. J. Wootton, B. A. Carreras, G. G. Craddock, T. S. Hahm, S. J. Zweben, O. J. Kwon, P. W. Terry, J. K. Lee, N. Ohyabu, and F. Wagner, "Resistive Fluid Turbulence and Tokamak Edge Plasma Dynamics," p. 277 in *Plasma Physics and Controlled Nuclear Fusion Research 1988: Twelfth Conference Proceedings, Nice, 12-19 October 1988*, vol. 2, International Atomic Energy Agency, Vienna, 1989
- K. Tinschert, A. Müller, G. Hoffman, K. Huber, R. Becker, D. C. Gregory, and E. Salzborn, "Experimental Cross Sections for Electron Impact Ionization of Hydrogen-Like Ions Li^{2+} ," *J. Phys.* **B22**, 531-40 (1989)
- N. A. Uckan, "Ignition and Steady-State Current Drive Capability of INTOR Plasma," *Fusion Technol.* **15**, 1076 (1989)
- N. A. Uckan, "Tokamak Confinement Projections and Performance Goals," *Fusion Technol.* **15**, 391 (1989)
- M. Ulrickson, M. G. Bell, R. Budny, C. E. Bush, H. F. Dylla, A. B. Ehrhardt, J. Gilbert, R. Goldston, O. Griesbach, R. J. Hawryluk, D. B. Heifetz, K. W. Hill, A. C. Janos, F. C. Jobes, S. Kilpatrick, P. H. LaMarche, W. D. Langer, D. Mansfield, S. S. Medley, D. Mueller, D. K. Owens, H. Park, A. T. Ramsey, J. Schivell, J. E. Stevens, B. C. Stratton, G. Tait, K.-L. Wong, M. Zamstorff, TFTR Group, R. Bastasz, D. A. Buchenauer, R. A. Causey, W. L. Hsu, B. E. Mills, A. E. Pontau, K. L. Wilson, D. Brice, B. L. Doyle, R. T. McGrath, S. R. Lee, W. R. Wampler, J. N. Brooks, Y. Hirooka, and R. A. Langley, "Tritium Retention and Conditioning of Graphite Limiters in TFTR," p. 419 in *Plasma Physics and Controlled Nuclear Fusion Research 1988: Twelfth Conference Proceedings, Nice, 12-19 October 1988*, vol. 3, International Atomic Energy Agency, Vienna, 1989
- W. I. van Rij and S. P. Hirshman, "Variational Bounds for Transport Coefficients in Three-Dimensional Toroidal Plasmas," *Phys. Fluids B* **1**, 563-9 (1989)
- R. E. Waltz, R. R. Dominguez, F. W. Perkins, J. C. Wiley, W. H. Miner, D. W. Ross, P. W. Terry, P. M. Valanju, P. H. Diamond, and J. Sheffield, "Theoretical Models for Tokamak Ignition Projections," p. 369 in *Plasma Physics and Controlled Nuclear Fusion Research 1988: Twelfth Conference Proceedings, Nice, 12-19 October 1988*, vol. 3, International Atomic Energy Agency, Vienna, 1989
- H. Weisen, M. von Hellerman, A. Boileau, L. D. Horton, W. Mandl, and H. P. Summers, "Charge Exchange Spectroscopy Measurements of Ion Temperature and Toroidal Rotation in JET," *Nucl. Fusion* **29**, 2187 (1989)
- J. H. Whealton, W. R. Becraft, W. L. Stirling, K. E. Rothe, R. J. Raridon, B. D. Murphy, P. S. Meszaros, H. H. Haselton, P. M. Ryan, G. E. McMichael, T. P. Wangler, A. Schempp, M. A. Akerman, G. C. Barber, and W. K. Dagenhart, "Technology of Megavolt-Multiampere Negative Ion Beam Acceleration with Application to ITER Neutral Beam Current Drive," p. 534 in *Fusion Technology 1988: Proceedings of the 15th Symposium on Fusion Technology, Utrecht, The Netherlands, 19-23 September 1988*, Vol. 1, edited by A. M. Van Ingen, A. Nijsen-Vis, and H. T. Klippel, North-Holland, Amsterdam, 1989
- J. H. Whealton, P. S. Meszaros, R. J. Raridon, K. E. Rothe, M. Bacal, J. Bruneteau, and P. Devynck, "Validation and Comparison of Nonlinear Negative Extraction Theory for Two Experimental Configurations," *Rev. Phys. Appl.* **24**, 945-49 (1989)
- J. R. Wilson, M. G. Bell, A. Cavallo, P. L. Colestock, W. Dorland, W. Gardner, G. J. Greene, G. W. Hammett, R. J. Hawryluk, H. W. Hendel, D. J. Hoffman, J. C. Hosea, K. P. Jaehnig, F. C. Jobes, R. Kaita, C. Kieras-Phillips, A. Lysojvan, D. K. Mansfield, S. S. Medley, D. Mueller, D. K. Owens, D. Smithe, J. E. Stevens, D. Swain, G. D. Tait, G. Taylor, M. Ulrickson, K.-L. Wong, S. J. Zweben, and the TFTR Group, "ICRF Heating on the TFTR Tokamak for P_{rf} up to 2.5 MW," p. 691 in *Plasma Physics and Controlled Nuclear Fusion Research 1988: Twelfth Conference Proceedings, Nice, 12-19 October 1988*, vol. 1, International Atomic Energy Agency, Vienna, 1989

- J. J. Yugo, S. Bernabei, P. Bonoli, R. S. Devoto, M. Fenstermacher, M. Porkolab, and J. Stevens, "Lower Hybrid Waves for Current Drive and Heating in Reactors," p. 485 in *Fusion Technology 1988: Proceedings of the 15th Symposium on Fusion Technology, Utrecht, The Netherlands, 19-23 September 1988*, Vol. 1, edited by A. M. Van Ingen, A. Nijsen-Vis, and H. T. Klippel, North-Holland, Amsterdam, 1989
- M. C. Zarnstorff, V. Arunasalam, C. W. Barnes, M. G. Bell, M. Bitter, H.-S. Bosch, N. L. Bretz, R. Budny, C. E. Bush, A. Cavallo, T. K. Chu, S. A. Cohen, P. L. Colestock, S. L. Davis, D. L. Dimock, H. F. Dylla, P. C. Efthimion, A. B. Ehrhardt, R. J. Fonck, E. D. Fredrickson, H. P. Furth, G. Gammel, R. J. Goldston, G. J. Greene, B. Grek, L. R. Grisham, G. W. Hammett, R. J. Hawryluk, H. W. Hendel, K. W. Hill, E. Hinnov, J. C. Hosea, R. B. Howell, H. Hsuan, R. A. Hulse, K. P. Jaehnig, A. C. Janos, D. L. Jassby, F. C. Jobses, D. W. Johnson, L. C. Johnson, R. Kaita, C. Kieras-Phillips, S. J. Kilpatrick, V. A. Krupin, P. H. LaMarche, B. LeBlanc, R. Little, A. Lysojvan, D. M. Manos, D. K. Mansfield, E. Mazzucato, R. T. McCann, M. P. McCarthy, D. C. McCune, K. M. McGuire, D. H. McNeill, D. M. Meade, S. S. Medley, D. R. Mikkelsen, R. W. Motley, D. Mueller, Y. Murakami, J. A. Murphy, E. B. Nieschmidt, D. K. Owens, H. K. Park, A. T. Ramsey, M. H. Redi, A. L. Roquemore, P. H. Rutherford, T. Saito, N. R. Sauthoff, G. Schilling, J. Schivell, G. L. Schmidt, S. D. Scott, J. C. Sinnis, J. E. Stevens, W. Stodiek, J. D. Strachan, B. C. Stratton, G. D. Tait, G. Taylor, J. R. Timberlake, H. H. Towner, M. Ulrickson, S. Von Goeler, R. M. Wieland, M. D. Williams, J. R. Wilson, K.-L. Wong, S. Yoshikawa, K. M. Young, and S. J. Zweben, "Transport in TFTR Supershots," p. 183 in *Plasma Physics and Controlled Nuclear Fusion Research 1988: Twelfth Conference Proceedings, Nice, 12-19 October 1988*, vol. 1, International Atomic Energy Agency, Vienna, 1989
- S. J. Zinkle, "Hardness and Depth Dependent Microstructure of Ion-Irradiated Magnesium Aluminate Spinel," *J. Am. Ceram. Soc.* **72**, 1343-51 (1989)
- S. J. Zinkle, "Ion Irradiation Studies of Oxide Ceramics," pp. 219-29 in *Structure-Property Relationships in Surface-Modified Ceramics*, Kluwer Academic Publishers, 1989
- S. J. Zinkle, "Microstructural Characterization of Al₂O₃ Following Simultaneous Triple Ion Bombardment," *Mat. Res. Soc. Symp. Proc.* **128**, 363-8 (1989)
- S. J. Zinkle and K. Farrell, "Void Swelling and Defect Cluster Formation in Reactor-Irradiated Copper," *J. Nucl. Mater.* **168**, 262-7 (1989)

PRESENTATIONS

January

ITER Nuclear Group Meeting, San Diego, California, January 1, 1989

B. E. Nelson, G. H. Jones, J. A. Mayhall, and D. E. Williamson, "Solid Breeder Blanket Mechanical Design and Configuration"

Transport Task Force: Enhanced Confinement Subcommittee Meeting, Austin, Texas, January 11-13, 1989

H. Howe and N. A. Uckan, "A Method for Comparison of Local Transport Models with Tokamak Experimental Results"

J. N. Leboeuf, "Kinetic/Fluid Hybrid Approach to Modeling of Low Frequency Plasma Turbulence"

K. C. Shaing, G. S. Lee, B. A. Carreras, W. A. Houlberg, and E. C. Crume, "Role of Radial Electric Field in Enhancing Confinement in Tokamaks and Stellarators"

International Society for Optical Engineering Meeting and Exhibition on Optoelectronics and Laser Applications in Science and Engineering (OE/LASE 89), Los Angeles, California, January 15-20, 1989. Proceedings to be published in *Proc. SPIE*.

W. L. Stirling, M. A. Akerman, G. C. Barber, W. R. Becraft, W. K. Dagenhart, A. Fadnek, D. E. Schechter, T. D. Steckler, C. C. Tsai, and J. H. Whealton, "Production of Intense Negative Ion Beams in Strong Magnetic Field Ion Sources: VITEX and Ringatron"

J. H. Whealton, P. S. Meszaros, R. J. Raridon, K. E. Rothe, W. R. Becraft, and B. D. Murphy, "Nonlinear Dynamics of Negative Ion Extraction From a Plasma, Acceleration and Transport"

U.S.-Japan Workshop on the Role of Edge Physics and Particle Control in Core Plasma Characteristics, San Diego, California, January 17-19, 1989

M. M. Menon, J. T. Hogan, P. K. Mioduszewski, and L. W. Owen, "Conceptual Studies of Divertor Pumping in DIII-D"

Japan/U.S. Workshop on Radiation Damage: Theory and Calculation, Tsukuba, Japan, January 18-20, 1989

L. K. Mansur, "On Theoretical Modeling of Radiation-Induced Deformation Relevant to Fusion Reactor Materials"

Conference on Particle Simulation of the Edge Plasma for ICRF Heating, January 26-27, 1989

J. H. Whealton and P. M. Ryan, "ICRF/Faraday Shield Antenna Plasma Sheath Physics"

J. H. Whealton and P. M. Ryan, "3D Quasistatic Antenna Field Model Using Magnetic Scalar Potential"

February

Semiconductor Research Corporation Topical Research Conference on Plasma Etching, Cambridge, Massachusetts, February 1-2, 1989

L. A. Berry, S. M. Gorbalkin, J. B. Roberto, C. C. Tsai, W. Holber, and J. Yeh, "Characteristics of the ORNL ECR Multipole Plasma Source"

IEA Workshop on the International Fusion Materials Irradiation Facility, February 14-17, 1989

S. Ishino, P. Schiller, and A. F. Rowcliffe, "Need for and Requirements for Neutron Irradiation Facility for Fusion Materials Testing"

Sixteenth Annual WATtec Interdisciplinary Technical Conference and Exhibition, Knoxville, Tennessee, February 14-17, 1989

E. E. Bloom, "Materials for Fusion Reactors"

M. S. Lubell, "Niobium-Based Superconductors and Their Application in Magnets"

ITER Working Session, Garching, Federal Republic of Germany, February 20–April 30, 1989

D. B. Batchelor, E. F. Jaeger, and M. D. Carter, "Fast Wave Current Drive Modeling for ITER"

J. Yugo, R. Goulding, and D. Batchelor, "Fast Wave Current Drive System for ITER"

IEA Low-Activation Workshop, Los Angeles, California, February 21–22, 1989

R. L. Klueh, "The Development of Low-Activation Alloys at ORNL"

Workshop on Internal Magnetic Structure, Austin, Texas, February 22–24, 1989

B. A. Carreras, N. Dominguez, J. N. Leboeuf, V. E. Lynch, L. A. Charlton, J. H. Harris, M. Murakami, J. D. Bell, V. K. Paré, and J. L. Dunlap, "Magnetic Fluctuations and Access to Second Stability in ATF"

C. H. Ma, C. A. Bennett, D. P. Hutchinson, and K. L. Vander Sluis, "A Two-Wavelength Infrared Interferometer System for CIT"

15th Symposium on Waste Management, Tucson, Arizona, February 26–March 2, 1989. Proceedings published as *Waste Management '89* by the Arizona Board of Regents, Tucson, 1989.

T. L. White, R. D. Peterson, and A. J. Johnson, "Microwave Processing of Remote-Handled Transuranic Wastes at Oak Ridge National Laboratory," vol. 1, p. 263

Transport Task Force Meeting, Germantown, Maryland, February 28–March 1, 1989

W. A. Houlberg, D. W. Ross, G. Bateman, S. C. Cowley, P. C. Efthimion, W. W. Pfeiffer, G. D. Porter, D. E. Shumaker, L. E. Sugiyama, and J. C. Wiley "Transport Modeling: Status, Issues, Recommendations"

March**IAEA Specialists' Meeting on Alpha Particle Ripple Loss, Garching, Federal Republic of Germany, March 8–10, 1989**

J. A. Rome, S. P. Hirshman, and L. M. Hively, "Distortion of ITER Flux Surfaces Due to TF Ripple"

3rd American Nuclear Society Topical Meeting on Robotics and Remote Systems, Charleston, South Carolina, March 13–16, 1989

D. Macdonald, "Maintenance Concept Development for the Compact Ignition Tokamak"

J. D. Snider, "Development of a Remotely Maintainable Radio Frequency Module for the Compact Ignition Tokamak"

16th European Conference on Controlled Fusion and Plasma Physics, Venice, Italy, March 13–17, 1989. Contributed papers published by the European Physical Society in *Europhys. Conf. Abstr.* 13B, parts I–IV (1989).

C. O. Beasley, C. L. Hedrick, and W. I. van Rij, "Optimization of Transport and Direct High-Energy Losses in Stellarators and Torsatrons," part II, p. 671

W. R. Becraft, J. H. Whealton, T. P. Wangler, H. Klein, A. Schempp, G. E. McMichael, M. A. Akerman, G. C. Barber, W. K. Dagenhart, R. A. Dory, H. H. Haselton, W. A. Houlberg, P. M. Ryan, and W. L. Stirling, "Advantages of High Energy RF Accelerated Neutral Beams for Tokamak Plasma Current Drive, Heating, and Profile Control"

R. Carrera, G. Y. Fu, J. Helton, L. Hively, E. Montalvo, C. Ordonez, M. N. Rosenbluth, S. Tamor, and J. W. Van Dam, "Analysis of the Ignition Experiment IGNITEX," part I, p. 375

M. Chatelier, C. C. Klepper, P. Chapuis, C. Gil, D. Guilhem, M. Lipa, L. Rodriguez, J. C. Vellet, D. VanHoutte, and J. G. Watkins, "First Pump Limiter Experiments in Tore Supra"

R. J. Colchin, J. H. Harris, F. S. B. Anderson, A. C. England, R. F. Gandy, J. D. Hanson, M. A. Henderson, D. L. Hillis, T. J. Jernigan, D. K. Lee, V. E. Lynch, M. Murakami, G. H. Neilson, J. A. Rome, M. J. Saltmarsh, and C. M. Simpson, "Correction of Field Errors in the ATF Torsatron," part II, p. 615

- L. Garcia, B. A. Carreras, and N. Dominguez, "Stability of Local Modes in Low-Aspect-Ratio Stellarators," part II, p. 611
- W. L. Gardner, D. J. Hoffman, F. W. Baity, T. S. Bigelow, R. H. Goulding, G. R. Haste, P. M. Ryan, and D. W. Swain, "Technology Development in the U.S. ICRF Heating Program"
- H. C. Howe, L. D. Horton, E. C. Crume, J. H. Harris, R. C. Isler, M. Murakami, D. Rasmussen, J. B. Wilgen, and W. R. Wing, "Transport Modeling of ECH and Neutral-Beam-Heated Plasmas in the Advanced Toroidal Facility," part II, p. 683
- R. C. Isler, L. D. Horton, E. C. Crume, H. C. Howe, and G. Voronov, "Impurity Studies in the Advanced Toroidal Facility," part II, p. 619
- C. C. Klepper, W. R. Hess, T. Fall, J. T. Hogan, A. Grosman, and D. Guilhem, "Spectroscopic Studies of Plasma-Surface Interactions in Tore Supra," part III, p. 1007
- J. B. Lister, J. M. Moret, E. A. Lazarus, A. Kellman, T. S. Taylor, and J. R. Ferron, "High Decay Index Plasmas in DIII-D," part I, p. 107
- S. L. Milora, D. V. Bartlett, L. R. Baylor, K. Behringer, D. J. Campbell, L. Charlton, A. Cheetham, J. G. Cordey, S. Corti, M. Gadeberg, R. Galvao, A. Gondhalekar, N. A. Gottardi, R. Granetz, G. Hammett, M. von Hellermann, K. Hirsch, J. T. Hogan, W. A. Houlberg, O. N. Jarvis, T. C. Jernigan, P. Kupschus, G. S. Lee, P. Morgan, C. K. Phillips, J. O'Rourke, G. Sadler, G. L. Schmidt, J. Snipes, P. Stubberfield, A. Taroni, B. Tubbing, and H. Weisen, "Summary of Energy and Particle Confinement in Pellet-Fuelled, Auxiliary-Heated Discharges on JET," part I, p. 91
- P. K. Mioduszewski, T. Uckan, D. L. Hillis, J. A. Rome, R. H. Fowler, J. C. Glowienka, M. Murakami, and G. H. Neilson, "Edge Plasma and Divertor Studies in the ATF Torsatron," part II, p. 623
- M. Murakami, B. A. Carreras, J. H. Harris, F. S. B. Anderson, G. L. Bell, J. D. Bell, T. S. Bigelow, R. J. Colchin, E. C. Crume, N. Dominguez, J. L. Dunlap, A. C. England, J. C. Glowienka, L. D. Horton, H. C. Howe, R. C. Isler, H. Kaneko, R. R. Kindsfather, J. N. Leboeuf, V. E. Lynch, M. M. Menon, R. N. Morris, G. H. Neilson, V. K. Paré, D. A. Rasmussen, J. B. Wilgen, and W. R. Wing, "Second Stability Studies in the ATF Torsatron," part II, p. 575
- A. Pospieszczyk, J. Hogan, Y. Ra, Y. Hirooka, R. W. Conn, D. Goebel, B. LaBombard, and R. E. Nygren, "Spectroscopic Determination of Molecular Fluxes and the Breakup of Carbon-Containing Molecules in PISCES-A," part III, p. 987
- D. W. Swain, D. B. Batchelor, M. D. Carter, E. F. Jaeger, P. M. Ryan, and D. J. Hoffman, "Fast-Wave Ion Cyclotron Current Drive for ITER and Prospects for Near-Term Proof-of-Principle Experiments," part IV, p. 1311
- T. Taylor, E. Strait, L. Lao, A. Turnbull, J. Lee, M. Chu, J. Ferron, G. Jackson, A. Kellman, E. Lazarus, T. Osborne, M. Schaffer, and R. Stambaugh, "Ideal and Resistive Stability near the Beta Limit in DIII-D," part II, p. 521
- A. Varias, A. L. Fraguas, L. Garcia, B. A. Carreras, N. Dominguez, and V. E. Lynch, "Ideal Mercier Stability for the TJ-II," part II, p. 607
- IAEA Technical Committee Meeting on H-Mode Physics, Gut Ising, Federal Republic of Germany, March 20-22, 1989**
- W. A. Houlberg, "CIT Pellet Fueling"
- W. A. Houlberg, "ITER Density Profile with Pellet Injection"
- W. A. Houlberg, "ITER Pellet Fueling"
- W. A. Houlberg, "ITER Transport Analysis"
- W. A. Houlberg, "Pellet Ablation and Ablation Model Development"
- K. C. Shaing, W. A. Houlberg, G. S. Lee, B. A. Carreras, and E. C. Crume, Jr., "L-H Transition Model Based on Turbulence Processes"

April

Sherwood Controlled Fusion Theory Conference, San Antonio, Texas, April 3–5, 1989

- R. Carrera, G. Fu, J. Helton, L. M. Hively, E. Montalvo, C. Ordonez, M. N. Rosenbluth, S. Tamor, and J. W. Van Dam, "Plasma Physics Considerations in the Fusion Ignition Experiment IGNITEX"
- B. A. Carreras, N. Dominguez, J. N. Leboeuf, V. E. Lynch, L. A. Charlton, J. H. Harris, M. Murakami, J. D. Bell, V. K. Paré, and J. L. Dunlap, "Access to Second Stability in ATF"
- M. D. Carter, D. B. Batchelor, and E. F. Jaeger, "Nonlinear Core Plasma Response to RF Power Absorption and Transport in Tokamaks"
- L. A. Charlton, L. R. Baylor, B. A. Carreras, J. T. Hogan, G. S. Lee, S. L. Milora, A. Edwards, and J. O'Rourke, "MHD Analysis of Peaked Density Profiles Produced by Pellet Injection in JET"
- N. Dominguez, K. C. Shaing, and B. A. Carreras, "Dissipative Trapped Electron Modes in $\ell = 2$ Toroidal Plasmas"
- R. C. Go'dfinger and D. B. Batchelor, "Analytic Model for Electron Cyclotron Heating Profiles"
- J. D. Hanson, J. R. Cary, B. A. Carreras, and V. E. Lynch, "A Simple Method for Calculation of Magnetic Island Widths"
- C. L. Hedrick, "Edge Electric Field Effects on Orbits in Tokamaks and Stellarators"
- S. P. Hirshman, R. N. Morris, J. A. Rome, C. L. Hedrick, and J. F. Lyon, "Low Aspect Ratio Stellarator Optimization"
- L. M. Hively, S. P. Hirshman, and J. A. Rome, "TF-Rippled Equilibrium for ITER"
- J. A. Holmes, "Nonlinear Interaction of Resistive Modes for $q < 1$ Tokamaks"
- W. A. Houlberg, S. E. Attenberger, H. C. Howe, and N. A. Uckan, "The Relationship Between Local Transport and Global Confinement"
- E. F. Jaeger, D. B. Batchelor, M. D. Carter, and D. W. Swain, "Fast Wave Current Drive in Large Noncircular Tokamaks—A Global Wave Calculation"
- J. N. Leboeuf, B. A. Carreras, and P. H. Diamond, "Three-Dimensional Fluid Computer Calculations of Ion Temperature Gradient Driven Instabilities"
- D. K. Lee, B. A. Carreras, R. H. Fowler, J. A. Holmes, J. N. Leboeuf, Ch. P. Ritz, A. J. Wootton, D. R. Thayer, and P. H. Diamond, "Modeling of Fluctuations in the Edge of the TEXT Tokamak"
- G. S. Lee and B. A. Carreras, "Study of the Magnetic Fluctuations in Resistive Pressure-Gradient-Driven Turbulence"
- Y-K. M. Peng, " $Tn\tau_E$ Comparisons of Tokamak Reactors of Different Aspect Ratios"
- J. A. Rome, R. H. Fowler, and P. K. Merkel, "Coil Realization for Low Aspect Ratio Stellarators"
- K. C. Shaing, W. A. Houlberg, G. S. Lee, B. A. Carreras, and E. C. Crume, Jr., "Radial Electric Field and Enhanced Confinement Regimes in Tokamaks and Stellarators"
- D. A. Spong, K. C. Shaing, and B. A. Carreras, "Extension of Braginskii Fluid Equations to the Banana-Plateau Regime and Application to Resistive Instabilities"
- A. Sykes, P. S. Haynes, T. C. Hender, T. N. Todd, Y-K. M. Peng, and J. C. Whitson, "Theoretical Studies of Tight Aspect Ratio Tokamaks"
- D. R. Thayer, P. H. Diamond, B. A. Carreras, J. A. Holmes, J. N. Leboeuf, Ch. P. Ritz, and A. J. Wootton, "Drift-Rippling Theory of Edge Turbulent Transport"
- J. S. Tolliver, E. F. Jaeger, B. A. Carreras, V. E. Lynch, D. B. Batchelor, P. L. Colestock, and D. N. Smithe, "Comparison of RF Codes: ORION, HYPERION, and SHOOT"
- A. Varias, C. Alejandre, L. Garcia, A. López-Fraguas, B. A. Carreras, N. Dominguez, and V. Lynch, "Stability Beta Limit of Local Modes for the TJ-II Flexible Helical"

- AVS Topical Conference on Surface Conditioning of Vacuum Systems, Los Angeles, California, April 3–7, 1989.** Proceedings published in *Surface Conditioning of Vacuum Systems*, American Institute of Physics, New York (*AIP Conf. Proc.* 199), 1990.
- R. A. Langley, T. L. Clark, J. C. Glowienka, R. H. Goulding, P. K. Mioduszewski, D. A. Rasmussen, T. F. Rayburn, C. R. Schaich, T. D. Shepard, J. E. Simpkins, and J. L. Yarber, "Recent Results on Cleaning and Conditioning the ATF Vacuum System"
- R. A. Langley and J. M. McDonald, "A Technique for Efficiently Cleaning and Conditioning Low- and Medium-Energy Accelerators"
- Division of Environmental Chemistry, American Chemical Society, Dallas, Texas, April 9–14, 1989**
- T. L. White and J. B. Berry, "Microwave Processing of Radioactive Materials—I"
- IAEA Technical Committee Meeting, 7th International Workshop on Stellarators, Oak Ridge, Tennessee, April 10–14, 1989.** Proceedings published as *Stellarator Physics*, IAEA-TECDOC-558, by the International Atomic Energy Agency, Vienna, 1990.
- F. S. B. Anderson, A. C. England, R. J. Colchin, J. H. Harris, D. L. Hillis, M. Murakami, G. H. Neilson, J. A. Rome, M. J. Saltmarsh, M. A. Henderson, and C. M. Simpson, "Electron Beam Mapping of the ATF Vacuum Magnetic Surfaces," p. 389
- J. D. Bell, J. H. Harris, J. L. Dunlap, V. K. Paré, M. Murakami, and H. Kaneko, "Fluctuation Studies in ATF," p. 307
- T. S. Bigelow, C. R. Schaich, and T. L. White, "Measurements of ECH Absorption on ATF using a Polarization-Controlled Beam Launcher," p. 243
- B. A. Carreras, N. Dominguez, J. N. Leboeuf, V. E. Lynch, and P. H. Diamond, "Dissipative Trapped Electron Modes in $\ell = 2$ Torsatrons," p. 329
- M. D. Carter, "Plasma Production Using Microwave and Radio Frequency Sources," p. 275
- J. R. Cary, J. D. Hanson, B. A. Carreras, and V. E. Lynch, "Simple Method for Calculating Island Widths," p. 413
- L. A. Charlton, B. A. Carreras, J. N. Leboeuf, and V. E. Lynch, "Magnetic Fluctuations Due to Pressure Driven Instabilities in ATF," p. 313
- R. J. Colchin, A. C. England, J. H. Harris, D. L. Hillis, T. C. Jernigan, M. Murakami, G. H. Neilson, J. A. Rome, M. J. Saltmarsh, F. S. B. Anderson, R. F. Gandy, J. D. Hanson, M. A. Henderson, D. K. Lee, V. E. Lynch, and C. M. Simpson, "ATF Flux Surfaces and Related Plasma Effects," p. 369
- N. Dominguez, J. N. Leboeuf, B. A. Carreras, and V. E. Lynch, "Ideal Low- n and Mercier Mode Stability Boundaries for $\ell = 2$ Torsatrons," p. 225
- L. Garcia, B. A. Carreras, and N. Dominguez, "Averaged Equilibrium and Stability in Low-Aspect-Ratio Stellarators," p. 289
- R. C. Goldfinger and D. B. Batchelor, "An Analytic Model for Electron Cyclotron Heating Profiles," p. 281
- J. H. Harris, M. Murakami, B. A. Carreras, J. D. Bell, G. L. Bell, T. S. Bigelow, L. A. Charlton, N. Dominguez, J. L. Dunlap, J. C. Glowienka, H. C. Howe, H. Kaneko, R. R. Kindsfather, J. N. LeBoeuf, V. E. Lynch, M. M. Menon, R. N. Morris, G. H. Neilson, V. K. Paré, N. F. Perepelkin, D. A. Rasmussen, J. B. Wilgen, and W. R. Wing, "Second Stability Studies in ATF," p. 223
- C. L. Hedrick, C. O. Beasley, and W. I. van Rij, "Optimization of Transport in Stellarators," p. 93
- S. Hiroe, R. R. Kindsfather, J. B. Wilgen, D. B. Batchelor, T. S. Bigelow, W. R. Wing, G. L. Bell, R. F. Gandy, and R. C. Goldfinger, "Bolometric Measurements in ATF," p. 167
- S. P. Hirshman, R. N. Morris, C. L. Hedrick, J. F. Lyon, J. A. Rome, S. L. Painter, and W. I. van Rij, "Low-Aspect-Ratio Optimization Studies for ATF-II," p. 493
- L. D. Horton, E. C. Crume, H. C. Howe, and R. C. Isler, "Impurity Studies and Transport in ATF," p. 333

- H. C. Howe, L. D. Horton, E. C. Crume, J. H. Harris, R. C. Isler, M. Murakami, D. Rasmussen, J. B. Wilgen, and W. R. Wing, "Transport Modeling of ECH and Neutral-Beam-Heated Plasmas in the Advanced Toroidal Facility," p. 79
- R. A. Langley, T. L. Clark, J. C. Glowienka, R. H. Goulding, P. K. Mioduszewski, D. A. Rasmussen, T. F. Rayburn, C. R. Schaich, T. D. Shepard, J. E. Simpkins, and J. L. Yarber, "Wall Conditioning in ATF," p. 127
- D. K. Lee, J. H. Harris, R. J. Colchin, A. C. England, G. S. Lee, V. E. Lynch, G. H. Neilson, M. J. Saltmarsh, F. S. B. Anderson, and J. D. Hanson, "Field Error Modeling Studies in ATF," p. 393
- J. W. Lue, L. Dresner, and M. S. Lubell, "High-Field, High-Current-Density, Stable Superconducting Magnets for Fusion Machines," p. 551
- V. E. Lynch, B. A. Carreras, N. Dominguez, and J. N. Leboeuf, "Equilibrium and Ideal Stability Studies for ATF," p. 333
- J. F. Lyon, S. C. Aceto, F. S. B. Anderson, G. L. Bell, J. D. Bell, T. S. Bigelow, B. A. Carreras, M. D. Carter, R. J. Colchin, K. A. Connor, E. C. Crume, N. Dominguez, J. L. Dunlap, G. R. Dyer, A. C. England, R. H. Fowler, R. F. Gandy, J. C. Glowienka, R. C. Goldfinger, R. H. Goulding, J. W. Halliwell, J. D. Hanson, J. H. Harris, M. A. Henderson, D. L. Hillis, S. Hiroe, L. D. Horton, H. C. Howe, D. P. Hutchinson, R. C. Isler, T. C. Jernigan, H. Kaneko, R. R. Kindsfather, M. Kwon, R. A. Langley, D. K. Lee, J. N. Leboeuf, V. E. Lynch, C. H. Ma, M. M. Menon, F. W. Meyer, P. K. Mioduszewski, T. Mizuuchi, R. N. Morris, O. Motojima, M. Murakami, G. H. Neilson, V. K. Paré, N. F. Perepelkin, D. A. Rasmussen, R. K. Richards, P. S. Rogers, J. A. Rome, M. J. Saltmarsh, F. Sano, P. L. Shaw, J. Sheffield, T. D. Shepard, J. E. Simpkins, C. M. Simpson, Y. Takeiri, C. E. Thomas, T. Uckan, K. L. Vander Sluis, G. S. Voronov, M. R. Wade, T. L. White, J. B. Wilgen, W. R. Wing, and J. J. Zielinski, "Overview of the ATF Program," p. 33
- C. H. Ma, D. P. Hutchinson, Y. Fockedey, K. L. Vander Sluis, and C. A. Bennett, "FIR Interferometer and Scattering Measurements on ATF," p. 155
- P. K. Mioduszewski, T. Uckan, D. L. Hillis, J. A. Rome, R. H. Fowler, J. C. Glowienka, M. Murakami, and G. H. Neilson, "Edge Plasma and Divertor Studies in the ATF Torsatron," p. 121
- R. N. Morris, C. L. Hedrick, S. P. Hirshman, J. F. Lyon, and J. A. Rome, "Numerical Methods for Stellarator Optimization," p. 539
- Y. Nakamura, K. Ichiguchi, H. Sugama, M. Wakatani, H. Zushi, J. L. Johnson, G. Rewoldt, B. A. Carreras, N. Dominguez, J. N. Leboeuf, J. A. Holmes, and V. E. Lynch, "Relation between Mercier Criterion and Low- n Mode Stability," p. 295
- S. L. Painter and J. F. Lyon, "Alpha-Particle Losses in Compact Torsatron Reactors," p. 557
- S. L. Painter and J. F. Lyon, "Transport Survey Calculations using the Spectral Collocation Method," p. 567
- D. A. Rasmussen, A. C. England, M. Murakami, H. C. Howe, T. L. Clark, R. R. Kindsfather, T. M. Rayburn, P. S. Rogers, K. A. Stewart, G. L. Bell, P. L. Shaw, and C. E. Thomas, "Recent Electron Temperature and Density Results from the ATF Thomson Scattering System," p. 159
- J. A. Rome, R. N. Morris, S. P. Hirshman, R. H. Fowler, and P. Merkel, "Coil Configurations for Low Aspect Ratio Stellarators," p. 545
- K. C. Shaing, "The Role of the Radial Electric Field in Enhanced Confinement Regimes in Stellarators," p. 97
- K. C. Shaing, B. A. Carreras, E. C. Crume, N. Dominguez, S. P. Hirshman, V. E. Lynch, J. S. Tolliver, and W. I. van Rij, "Bootstrap Current Control and the Effects of the Radial Electric Field in Stellarators," p. 611
- A. Varias, C. Alejaldre, A. Lopez-Fraguas, B. A. Carreras, N. Dominguez, and V. Lynch, "Stability Studies for TJ-II," p. 341

ARIES Project Meeting, Los Angeles, California, April 12–14, 1989

- R. L. Reid, "Economics of Alternative Current Drive Systems for the ARIES-I Concept"

- R. L. Reid, "TETRA-R/ARIES System Codes Cost Comparison"
- Y-K. M. Peng, "Low Aspect Ratio Tokamak as an Optimum Reactor: Spherical Torus"
- 91st Annual Meeting of the American Ceramics Society, Indianapolis, Indiana, April 23–27, 1989**
- H. D. Kimrey, M. K. Ferber, and M. A. Janney, "Sintering Dilatometry in a High-Frequency Microwave Field"
- CIT Physics Workshop, Princeton, New Jersey, April 27, 1989**
- W. A. Houlberg, "CIT Pellet Fueling Issues"

May

- American Physical Society 1989 Spring Meeting: Special Sessions on Cold Fusion, Baltimore, Maryland, May 1–2, 1989.** Abstracts published in *Bull. Am. Phys. Soc.* **34**, No. 8 (1989).
- D. P. Hutchinson, R. K. Richards, C. A. Bennett, C. C. Havener, C. H. Ma, F. G. Perey, R. R. Spencer, J. K. Dickens, B. D. Rooney, J. Bullock IV, and G. L. Powell, "A Search for Cold Fusion Neutrons at ORELA," p. 1860
- 8th Topical Conference on Radio Frequency Power in Plasmas, Irving, California, May 1–3, 1989.** Proceedings published as *AIP Conf. Proc.* **190** by the American Institute of Physics, New York, 1989.
- F. W. Baity, D. B. Batchelor, W. L. Gardner, R. H. Goulding, D. J. Hoffman, P. M. Ryan, and J. J. Yugo, "Spectral Shaping and Phase Control of a Fast-Wave Current Drive Antenna Array," p. 214
- D. B. Batchelor, E. F. Jaeger, M. D. Carter, and D. W. Swain, "Fast Wave Current Drive Modeling for ITER and Prospects for a Near-Term Proof of Principle Experiment," p. 218
- T. S. Bigelow, C. R. Schaich, and T. L. White, "Polarization Controlled Beam Launch for the ATF ECH System"
- J. B. O. Caughman, II, D. N. Ruzic, and D. J. Hoffman, "Ion Energy and Plasma Measurements in the Near Field of an ICRF Antenna," p. 226
- P. Colestock, A. Cavallo, W. Dorland, J. Hosea, G. Greene, G. Hammett, H. W. Hendel, B. Howell, K. Jaehnig, R. Kaita, S. S. Medley, C. K. Phillips, A. L. Roquemore, G. Schilling, J. Stevens, B. Stratton, D. Smithe, A. Ramsey, G. Taylor, J. R. Wilson, S. J. Zweben, TFTR Group, W. Gardner, and D. Hoffman, "ICRF and ICRF Plus Neutral Beam Heating Experiments on TFTR," p. 189
- R. H. Goulding, F. W. Baity, P. L. Goranson, D. J. Hoffman, P. M. Ryan, D. J. Taylor, and J. J. Yugo, "ICRF Antenna Designs for CIT and Alcator C-MOD," p. 250
- G. J. Greene, P. L. Colestock, J. C. Hosea, C. K. Phillips, D. N. Smithe, J. E. Stevens, J. R. Wilson, W. Gardner, and D. Hoffman, "ICRF Coupling on TFTR Using the PPPL Antenna," p. 254
- G. R. Haste and D. J. Hoffman, "High-Power Testing of the Folded Waveguide," p. 266
- D. J. Hoffman, W. L. Gardner, G. J. Greene, J. C. Hosea, P. M. Ryan, J. R. Wilson, and J. E. Stevens, "ICRF Heating on TFTR with the ORNL Antenna," p. 274
- J. Hosea, P. Bonanos, P. Colestock, G. Greene, S. Medley, C. Phillips, J. Stevens, J. Wilson, TFTR Group, W. Gardner, D. Hoffman, and D. Swain, "ICRF Antenna Designs and Relative Performances on TFTR," p. 278
- K. Imre, H. Weitzner, D. C. Stevens, and D. B. Batchelor, "ICRH in Large Tokamaks with Poloidal Magnetic Field," p. 282
- C. K. Phillips, A. Cavallo, P. L. Colestock, D. M. Smithe, G. J. Greene, G. W. Hammett, J. C. Hosea, J. E. Stevens, J. R. Wilson, D. J. Hoffman, and W. L. Gardner, "Sawtooth Mixing Effects on ICRF Power Deposition in Tokamaks," p. 310
- P. M. Ryan, K. E. Rothe, J. H. Whealton, and D. W. Swain, "Determination of Fields near an ICRH Antenna Using a 3D Magnetostatic Laplace Formulation," p. 322

- T. D. Shepard, M. D. Carter, R. H. Goulding, and M. Kwon, "Loading, Absorption, and Fokker-Planck Calculations for Upcoming ICRF Experiments on ATF," p. 334
- J. Stevens, C. Bush, P. Colestock, G. J. Greene, K. W. Hill, J. Hosea, C. K. Phillips, P. Stratton, S. von Goeler, J. R. Wilson, W. Gardner, D. Hoffman, and A. Lysojvan, "Metal Impurity Behavior During ICRF Heating on TFTR," p. 342
- J. H. Whealton, P. M. Ryan, and R. J. Raridon, "ICRF Faraday Shield Plasma Sheath Physics: The Perkins Paradigm," p. 366
- J. R. Wilson, P. L. Colestock, G. J. Greene, J. C. Hosea, C. K. Phillips, J. E. Stevens, D. J. Hoffman, and W. L. Gardner, "The TFTR ICRF Antenna-Power Feed and Phase Control of Two Mutually Coupled Antenna Elements," p. 370
- J. J. Yugo, D. B. Batchelor, P. L. Goranson, R. H. Goulding, E. F. Jaeger, and P. M. Ryan, "A Fast-Wave Current Drive System Design for ITER," p. 378
- J. J. Yugo, P. Colestock, P. L. Goranson, R. H. Goulding, D. J. Hoffman, E. F. Jaeger, and P. M. Ryan, "ICRH Antenna for the Compact Ignition Tokamak"
- American Chemical Society, Environmental Chemistry Division Winter Symposium on Emerging Technologies for Hazardous Waste Treatment, Atlanta, May 1-4, 1989**
- T. L. White and J. B. Berry, "Microwave Processing of Radioactive Materials—II"
- 6th Annual Conference on Real-Time Computer Applications in Nuclear, Particle and Plasma Physics, Williamsburg, May 16-19, 1989.** Proceedings to be published in *IEEE Trans. Nucl. Sci.*
- K. A. Stewart, R. R. Kindsfather, and D. A. Rasmussen, "The Data Acquisition and Control System for Thomson Scattering on ATF"
- Initial Workshop on Tokamak Improvement, University of California, Los Angeles, California, May 22-23, 1989**
- Presented by:* J. Sheffield *Contributors:* C. C. Baker, W. R. Becraft, L. A. Berry, E. E. Bloom, R. A. Dory, H. H. Haselton, D. J. Hoffman, M. S. Lubell, and S. L. Milora, "Advances in Technology and Design for Tokamak Improvement"
- Presented by:* N. A. Uckan *Contributors:* D. Batchelor, L. A. Berry, B. A. Carreras, R. Dory, J. Hogan, W. Houlberg, G. S. Lee, S. Milora, M. Murakami, Y-K. M. Peng, K. Shaing, J. Sheffield, J. Callen, and C. Baker, "Tokamak Physics Improvements: Operational Boundaries and Ways to Extend Them"
- 16th IEEE International Conference on Plasma Science, Buffalo, New York, May 22-24, 1989**
- R. Carrera, M. Barrington, R. Bickerton, D. Booth, Y. Chen, J. Dong, M. Driga, S. Eways, G. Fu, J. Gully, G. Hallock, J. Helton, N. Hertel, L. Hively, J. Howell, K. Hsieh, J. Ling, G. Miller, E. Montalvo, C. Ordonez, D. Palmrose, T. parish, M. Rosenbluth, S. Tamor, D. Tesar, J. Van Dam, P. Varghese, A. Walls, W. Weldon, M. Werst, and H. Woodson, "IGNITEX Experiment"
- A. C. England, F. S. B. Anderson, R. J. Colchin, R. F. Gandy, J. D. Hanson, J. H. Harris, M. A. Henderson, D. L. Hillis, T. C. Jernigan, D. K. Lee, V. E. Lynch, D. L. Million, M. Murakami, G. H. Neilson, J. A. Rome, M. J. Saltmarsh, and C. M. Simpson, "Measurements of Flux Surfaces in the ATF Torsatron"
- G. Fu, R. Bickerton, R. Carrera, J. Dong, J. Helton, L. Hively, E. Montalvo, C. Ordonez, M. Rosenbluth, S. Tamor, and J. Van Dam, "Ohmic and Alpha Heating in the High-Field IGNITEX Tokamak"
- D. A. Rasmussen, F. S. B. Anderson, G. L. Bell, J. D. Bell, R. D. Bengtson, T. S. Bigelow, B. A. Carreras, K. R. Carter, R. J. Colchin, E. C. Crume, N. Dominguez, J. L. Dunlap, A. C. England, R. H. Fowler, R. F. Gandy, J. C. Glowienka, S. Hiroe, J. H. Harris, D. L. Hillis, L. D. Horton, H. C. Howe, R. C. Isler, T. C. Jernigan, H. Kaneko, R. R. Kindsfather, J. N. Leboeuf, V. E. Lynch, J. F. Lyon, C. H. Ma, M. M. Menon, P. K. Mioduszewski, R. N. Morris, M. Murakami, G. H. Neilson, V. K. Paré, T. L. Rhodes, R. K. Richards, C. P. Ritz, J. A. Rome, C. E. Thomas, T. Uckan, M. R. Wade, J. B. Wilgen, and W. R. Wing, "The Role of Stellarators in Understanding Toroidal Transport Physics"

- P. M. Ryan, K. E. Rothe, J. H. Whealton, and D. W. Swain, "Determination of Field Structure Near an ICRH Antenna Using a 3D Magnetostatic Laplace Formulation"
- J. H. Whealton, R. J. Raridon, and P. M. Ryan, "Plasma Sheath Modeling Near an ICRF Faraday Shield"
Engineering Test Reactor Technical Oversight Committee (ETOC) Meeting, Livermore, California, May 25, 1989
- J. Sheffield, "A Different Logic for ITER"

June

- Fusion Power Associates Symposium, Washington, D.C., June 1-2, 1989**
- J. Sheffield, "Recent Progress in Fusion Research at the Oak Ridge National Laboratory"
- International Thermonuclear Experimental Reactor Specialists' Meeting on Electromagnetics, Garching, Federal Republic of Germany, June 22, 1989**
- R. O. Sayer, "ITER Disruption Modeling with TSC"
- 5th Conference on Radiation Effects in Insulators, Crystalline Oxides and Ceramics Session, Hamilton, Ontario, Canada, June 19-23, 1989**
- S. J. Zinkle and S. Kojima, "Microstructural Changes in $MgAl_2O_4$ Induced by Ion Irradiation"

July

- International Conference on Ion Sources, Berkeley, California, July 10-14, 1989.** Proceedings published in *Rev. Sci. Instrum.* **61** (1990).
- C. C. Tsai, M. A. Akerman, W. R. Becraft, W. K. Dagenhart, J. J. Donaghy, H. H. Haselton, D. E. Schechter, W. L. Stirling, and J. H. Whealton, "Factors Affecting Emittance Measurements of Ion Beams," pp. 783-7
- J. H. Whealton, P. S. Meszaros, R. J. Raridon, and K. E. Rothe, "Extraction Induced Emittance Growth for Negative Ion Sources," p. 436
- J. H. Whealton, P. S. Meszaros, K. E. Rothe, R. J. Raridon, and P. M. Ryan, "Beam Dynamics of a Liquid Metal Ion Source," pp. 568-70
- Workshop on High-Intensity Electro-Magnetic and Ultrasonic Effects on Inorganic Materials Behavior and Processing, Raleigh, North Carolina, July 16-17, 1989**
- H. D. Kimrey and M. A. Janney, "Effects Other Than Heating by High-Intensity, High-Frequency Microwaves in Materials Processing"
- Cryogenic Engineering Conference, Los Angeles, California, July 24-28, 1989.** Proceedings published in *Adv. Cryog. Eng.* **35** (1990).
- W. A. Fietz, "Experience in the Operation of the International Fusion Superconducting Magnet Test Facility"
- S. W. Schwenterly, J. W. Lue, and L. Dresner, "Quench Propagation, Pressure Rise, and Thermal Expulsion of Helium From a Cable-in-Conduit Forced-Flow Superconductor"
- NSF Workshop on Future Directions in Electromagnetics Research, Cambridge, Massachusetts, July 25-26, 1989**
- T. S. Bigelow, "High-Power Microwave Transmission and Launching Systems for Fusion Plasma Heating Systems"

August

- Neutron Calibration Techniques Workshop, Princeton, New Jersey, August 1-3, 1989**
- A. C. England, J. N. Sumner, and K. G. Young, "Calibration of Neutron Detectors at the ORNL Advanced Toroidal Facility"

- 47th Annual Meeting of the Electron Microscopy Society of America, San Antonio, Texas, August 6–11, 1989.** Proceedings published by San Francisco Press, Inc., San Francisco, 1989.
- E. A. Kenik, P. J. Maziasz, and R. L. Klueh, "Phase Stability of a Manganese-Stabilized Austenitic Stainless Steel," pp. 284–5
- 1989 Faculty Workshop for Nuclear Engineers, Oak Ridge, Tennessee, August 7–18, 1989**
- P. J. Maziasz, "Development of New Austenitic Steels and Alloys for Advanced Nuclear and Fossil Energy Applications"
- M. J. Saltmarsh, "Fusion and Cold Fusion R&D"
- 10th International Conference on Structural Mechanics in Reactor Technology (SMiRT-10), Anaheim, California, August 14–18, 1989**
- J. W. Lue, L. Dresner, M. S. Lubell, J. N. Luton, and T. J. McManamy, "Experience with the Plate Structure of the Westinghouse Coil for the Large Coil Task"
- 24th Microwave Power Symposium, Stamford, Connecticut, August 20–23, 1989**
- H. D. Kimrey, "Progress in Microwave Sintering Technology at Oak Ridge National Laboratory"
- Tokamak Transport Initiative Meeting, San Diego, August 21, 1989**
- B. A. Carreras, "Resistive MHD and Anomalous Transport"
- B. A. Carreras, N. Dominguez, R. H. Fowler, L. Garcia, J. N. Leboeuf, and P. H. Diamond, "Trapped Electron Modes in Stellarators and Tokamaks"
- J. H. Harris, "Edge Fluctuations in ATF"
- J. H. Harris, "Second Stability in ATF"
- G. H. Neilson, "Stellarator Contributions to Toroidal Transport Understanding"
- K. C. Shaing, "The Effects of Rotations on Plasma Confinement and the L-H Transition"
- International Thermonuclear Experimental Reactor Fast Wave Current Drive Workshop, Garching, Federal Republic of Germany, August 21–September 1, 1989**
- J. J. Yugo, "Design and Analysis of a FWCD Antenna for ITER"
- Workshop on Magnetic Confinement Fusion, Universidad Internacional Menendez Pelayo, Santander, Spain, August 28, 1989**
- B. A. Carreras, "Equilibrium and Stability of Toroidal Confinement Systems"
- 11th International Conference on Magnet Technology, Tsukuba, Japan, August 28–September 1, 1989**
- L. Dresner, "Propagation of Normal Zones of Finite Size in Large, Composite Superconductors"
- September**
- IAEA Specialists' Meeting on Superconducting Materials and Magnets, Tokyo, Japan, September 4–6, 1989**
- L. Dresner, "Rational Design of High-Current Cable-in-Conduit Superconductors"
- Third European Fusion Theory Conference, Oxford, England, September 11–13, 1989**
- C. Alejandre, A. Varias, A. Lopez Fraguas, L. Garcia, B. Carreras, N. Dominguez, and V. E. Lynch, "Second Stability Studies for TJ-II"
- L. Garcia, B. Carreras, N. Dominguez, and V. E. Lynch, "Low-n Stability Calculations for Three-Dimensional Stellarator Configurations"
- A. Varias, C. Alejandre, A. Lopez Fraguas, L. Garcia, B. Carreras, N. Dominguez, and V. E. Lynch, "Mercier Stability Limits of Some TJ-II Configurations"
- First International Youth School on Plasma Physics and Controlled Fusion, Narva, U.S.S.R., September 11–25, 1989**
- B. A. Carreras, "Fluid Approach to Plasma Turbulence"

13th Conference on the Numerical Simulation of Plasmas, Santa Fe, New Mexico, September 17–20, 1989

- J.-N. Leboeuf, R. H. Fowler, J. H. Han, and P. M. Lyster, "Hybrid Particle-Fluid Approach to Low Frequency Turbulence in Magnetically Confined Plasmas"
- V. E. Lynch, N. Dominguz, B. A. Carreras, A. Varias, C. Alejandre, and A. L. Fraguas, "Three-Dimensional Equilibria and Mercier Stability Calculations"

ITER R&D Specialists' Meeting on Density Limits, Garching, Federal Republic of Germany, September 20–22, 1989

- L. D. Horton, E. C. Crume, H. C. Howe, and R. C. Isler, "Modeling of Radiative Collapse and Density Limits in ATF"

1989 European Workshop on Lead Lithium and Lithium Corrosion and Chemistry, Seibersdorf, Austria, September 20–22, 1989

- P. F. Tortorelli, "Kinetic Analysis of Corrosion in Pb-17 at. % Li and Comparison to Pure Lithium"
- P. F. Tortorelli and G. E. Bell, "A Lower Temperature Lithium Purification Process Incorporating Warm Trapping"
- P. F. Tortorelli and G. E. Bell, "Mass Transport Processes in Li/Fe-12Cr-1MoVW Systems"

ITER Technical Committee Meeting, Garching, Federal Republic of Germany, September 27, 1989

- L. M. Hively and J. A. Rome, "TF-Rippl: Loss of Suprathermal Alphas in ITER"

Workshop on Radiation Damage Correlation for Fusion Conditions, Silkeborg, Denmark, September 27–October 3, 1989

- M. L. Grossbeck, K. Ehrlich, and C. Wassilew, "An Assessment of Tensile, Irradiation Creep, Creep Rupture, and Fatigue Behavior in Austenitic Stainless Steels with Emphasis on Spectral Effects"

October

ICRH/Edge Physics, Garching, Federal Republic of Germany, October 2–5, 1989. Proceedings published in *Fusion Eng. Des.* **12** (1990).

- M. D. Carter, D. B. Batchelor, and E. F. Jaeger, "Electron Heating and Static Sheath Enhancement in Front of Driven RF Antennas," pp. 105–10
- J. B. O. Caughman, II, D. N. Ruzic, and D. J. Hoffman, "Experimental Evidence of Increased Electron Temperature, Plasma Potential, and Ion Energy Near an ICRF Antenna Faraday Shield," p. 179
- P. M. Ryan, K. E. Rothe, J. H. Whealton, and T. D. Shepard, "Determination of ICRF Antenna Fields in the Vicinity of a 3-D Faraday Shield Structure," pp. 37–42
- J. H. Whealton, P. M. Ryan, and R. J. Raridon, "ICRF Faraday Shield Plasma Sheath Models: Low and High Conductivity Limits," pp. 121–6

7th American Physical Society Topical Conference on Atomic Processes in Plasmas, Gaithersburg, Maryland, October 2–5, 1989

- J. T. Hogan, A. Pospieszczyk, Y. Ra, Y. Hirooka, and R. Conn, "Modeling Hydrocarbon Fueling of Tokamak Edge Plasma," invited
- L. D. Horton, H. C. Howe, E. C. Crume, Jr., and R. C. Isler, "Application of Quantitative Spectroscopic Data to Modeling of Global Plasmas Evolution in ATF"
- R. C. Isler, L. D. Horton, E. C. Crume, and C. B. Brooks, "Charge-Exchange Excitation of He-Like Ions in ATF"

13th Symposium on Fusion Engineering, Knoxville, Tennessee, October 2–6, 1989. Proceedings published by IEEE, New York, 1990.

- S. E. Attenberger and W. A. Houlberg, "Transport Simulation of ITER Startup," vol. 1, p. 99
- L. R. Baylor, T. C. Jernigan, and K. A. Stewart, "The Control System for the Multiple-Pellet Injector on the Joint European Torus," vol. 2, p. 1474

- L. Bromberg, J. Wei, D. B. Montgomery, D. R. Cohn, and T. J. McManamy, "Upgrade Possibilities for the Central Solenoid in CIT," vol. 1, p. 605
- R. Buende, G. Ollivier, and C. A. Flanagan, "ITER Guide for Reliability Analysis," vol. 2, p. 816
- J. B. O. Caughman, II, D. N. Ruzic, D. J. Hoffman, R. A. Langley, M. B. Lewis, and P. M. Ryan, "An Assessment of the Lifetime of Faraday Shield Elements," vol. 2, p. 921
- S. K. Combs, T. C. Jernigan, L. R. Baylor, S. L. Milora, C. R. Foust, P. Kupschus, M. Gadeberg, and W. Bailey, "Operation and Reliability of a Pneumatic Hydrogen Pellet Injection System on the Joint European Torus," vol. 2, p. 1305
- F. C. Davis and D. P. Kuban, "Remote Maintenance for Fusion: Requirements vs Technology Gap," vol. 1, p. 251
- R. E. DePew and D. Macdonald, "Remote Maintenance of Compact Ignition Tokamak Ex-Vessel Systems" vol. 1, p. 593
- S. E. Eways, W. D. Booth, R. Carrera, M. E. Oakes, and E. F. Jaeger, "Cavity Resonance Mode Plasma Breakdown for the IGNITEX Experiment," vol. 2, p. 838
- P. W. Fisher, D. T. Fehling, M. J. Gouge, and S. L. Milora, "Tritium Proof-of-Principle Pellet Injector Results," vol. 2, p. 1236
- J. D. Galambos and Y-K. M. Peng, "Accomplishing Dual Missions of the International Thermonuclear Experimental Reactor (ITER), Bi-Modal or Retrofitting?" vol. 1, p. 243
- Y. Gohar, H. Attaya, M. C. Billone, P. Finn, S. Majumdar, L. R. Turner, C. C. Baker, B. E. Nelson, and R. Raffray, "Solid Breeder Blanket Option for the ITER Conceptual Design," vol. 1, p. 53
- M. L. Goins, "Preliminary Design of the CIT Cryostat," vol. 2, p. 1168
- M. J. Gouge, S. K. Combs, P. W. Fisher, and S. L. Milora, "The CIT Pellet Injection System: Description and Supporting Research and Development," vol. 2, p. 1240
- M. J. Gouge, S. L. Milora, C. A. Foster, S. K. Combs, P. W. Fisher, C. C. Tsai, B. E. Argo, G. C. Barber, L. R. Baylor, D. T. Fehling, C. R. Foust, T. C. Jernigan, A. L. Qualls, D. E. Schechter, D. W. Simmons, C. W. Sohns, and D. O. Sparks, "The ORNL Plasma Fueling Program," vol. 2, p. 1299
- R. H. Goulding, D. J. Hoffman, S. N. Golovato, C. J. Hammonds, P. M. Ryan, D. J. Taylor, and J. J. Yugo, "The ORNL Fast-Wave ICRF Antenna for Alcator C-MOD," vol. 1, p. 215
- S. P. Grotz, F. Najmabadi, the ARIES Team, D. K. Sze, Y-K. M. Peng, R. L. Creedon, C. P. C. Wong, R. L. Miller, and D. Bromberg, "Design Integration of the ARIES-I Tokamak Reactor," vol. 2, p. 1031
- J. W. Halliwell, G. R. Dyer, and J. E. Simpkins, "Design and Development of a Fast-Response Ionization Gauge Controller," vol. 1, p. 178
- C. J. Hammonds, B. E. Nelson, J. C. Walls, D. J. Hoffman, and F. W. Baity, "Thermal and Stress Analysis of the Faraday Shield for the ORNL/TFTR RF Antenna," vol. 1, p. 1432
- D. J. Hoffman, F. W. Baity, W. L. Gardner, R. H. Goulding, G. R. Haste, P. M. Ryan, D. J. Taylor, D. W. Swain, M. J. Mayberry, and J. J. Yugo, "The Technology of Fast-Wave Current Drive Antennas," vol. 1, p. 1267
- T. A. Kozub, J. M. Carson, P. W. Fisher, K. T. Frank, G. J. Gibilisco, D. D. Schuresko, H. Takahashi, and R. W. Yager, "Initial Performance and Characteristics of the PBX-M Pellet Injector," vol. 2, p. 1256
- R. A. Langley, "Graphite as a First Wall Material in Fusion Experiments," vol. 1, p. 522
- D. C. Lousteau, B. E. Nelson, V. D. Lee, and J. N. Doggett, "The International Thermonuclear Engineering Reactor Configuration Evolution," vol. 1, p. 247
- T. J. McManamy, J. Brasier, and P. Snook, "Insulation Interlaminar Shear Strength Testing with Compression and Irradiation," vol. 1, p. 342
- M. M. Menon and P. K. Mioduszewski, "Particle Exhaust Schemes in the DIII-D Advanced Divertor Configuration," vol. 1, p. 542

- E. Montalvo, R. Carrera, G. Y. Fu, J. Helton, L. Hively, H. Howe, C. Ordonez, M. N. Rosenbluth, D. Sigmar, S. Tamor, and J. Van Dam, "Fusion Physics Study of the IGNITEX Experiment," vol. 2, p. 1226
- F. Najmabadi, R. W. Conn, and the ARIES Team (ORNL staff members: W. R. Becraft, J. T. Hogan, Y-K. M. Peng, R. L. Reid, D. J. Strickler, and J. W. Whitson), "The ARIES Tokamak Fusion Reactor Study," vol. 2, p. 1021
- G. H. Neilson, S. C. Aceto, E. Anabitarte, F. S. B. Anderson, G. L. Bell, J. D. Bell, R. D. Benson, T. S. Bigelow, B. A. Carreras, T. L. Clark, R. J. Colchin, E. C. Crume, W. R. DeVan, J. L. Dunlap, G. R. Dyer, A. C. England, J. C. Glowienka, J. W. Halliwell, G. R. Hanson, J. H. Harris, C. L. Hedrick, C. Hidalgo, D. L. Hillis, S. Hiroe, L. D. Horton, H. C. Howe, R. C. Isler, T. C. Jernigan, R. A. Langley, D. K. Lee, J. W. Lue, J. F. Lyon, C. H. Ma, C. H. Ma, P. K. Mioduszewski, R. N. Morris, M. Murakami, D. A. Rasmussen, Ch. P. Ritz, P. S. Rogers, S. W. Schwenterly, P. L. Shaw, T. D. Shepard, J. E. Simpkins, C. E. Thomas, T. Uckan, M. R. Wade, J. A. White, J. B. Wilgen, C. T. Wilson, W. R. Wing, H. Yamada, and J. J. Zielinski, "Studies of Plasma Performance and Transport in the Advanced Toroidal Facility (ATF)," invited paper, vol. 1, p. 7
- C. A. Ordonez, R. Carrera, P. H. Edmonds, J. Howell, G. Rodin, and H. C. Howe, "Impurity Release Disruption Effects and Thermomechanical Stress Analysis of the First Wall System for the IGNITEX Experiment," vol. 2, p. 927
- S. L. Painter and J. F. Lyon, "Transport Studies of Low-Aspect-Ratio Stellarator Reactors," vol. 1, p. 102
- Y-K. M. Peng, D. J. Strickler, J. T. Hogan, J. C. Whitson, C. G. Bathke, S. C. Jardin, M. Klasky, K. Evans, J. A. Leuer, and the ARIES Team, "MHD Equilibrium and Stability Considerations for High-Aspect-Ratio ARIES-I Tokamak Reactors," vol. 1, p. 1278
- A. L. Qualls, P. W. Fisher, J. B. Wilgen, D. D. Schuresko, D. T. Fehling, and M. J. Gouge, "Eight-Shot Pneumatic Pellet Injector for the Advanced Toroidal Facility," vol. 2, p. 1244
- R. L. Reid and Y-K. M. Peng, "Parameter Trade-Offs and Optimization of ITER-Like Reactors," vol. 1, p. 258
- J. F. Santarius, J. P. Blanchard, G. A. Emmert, I. N. Sviatoslavsky, L. J. Wittenberg, N. M. Ghoniem, M. Z. Hasan, T. K. Mau, E. Greenspan, J. S. Herring, W. Kernbichler, A. C. Klein, G. H. Miley, R. L. Miller, Y-K. M. Peng, M. J. Schaffer, C. P. C. Wong, D. Steiner, D. K. Sze, and the ARIES Team, "Energy Conversion Options for ARIES-III—A Conceptual D-³He Tokamak Reactor," vol. 2, p. 1039
- S. W. Schwenterly, W. A. Gabbard, C. R. Schaich, and J. L. Yarber, "Location and Repair of Air Leaks in the ATF Vacuum Vessel," vol. 2, p. 978
- R. T. C. Smith, J. Booth, P. S. Haynes, T. C. Hender, J. B. Hicks, A. Sykes, K. Thompson, T. N. Todd, Y-K. M. Peng, and J. C. Whitson, "Design of the START Experiment," vol. 2, p. 866
- W. L. Stirling, W. R. Becraft, J. H. Whealton, and H. H. Haselton, "A Neutral Particle Beam System for ITER with RF Acceleration," vol. 2, p. 1448
- D. J. Strickler, N. Pomphrey, and S. C. Jardin, "Equilibrium Shape Control in CIT PF Design," vol. 2, p. 898
- S. L. Thomson, "ITER Reactor Building Design Study," vol. 1, p. 424
- C. C. Tsai, C. A. Foster, and D. E. Schechter, "Characteristics of an Electron-Beam Rocket Pellet Accelerator," vol. 2, p. 1230
- N. A. Uckan, "Confinement Projections for the Compact Ignition Tokamak"
- N. A. Uckan and the ITER Physics Group, "Physics Design Guidelines for ITER"
- J. H. Whealton, P. M. Ryan, and R. J. Raridon, "ICRF Faraday Shield Plasma Sheath Physics"
- J. H. Whealton, W. R. Becraft, W. L. Stirling, and H. H. Haselton, "Prospects for High-Energy Neutral Beams for Current Drive"
- J. J. Yugo, D. W. Swain, D. B. Batchelor, P. L. Goranson, R. H. Goulding, D. J. Hoffman, E. F. Jaeger, and P. M. Ryan, "Design and Analysis of a Fast-Wave Current Drive Antenna for the International Thermonuclear Experimental Reactor (ITER)"

- J. J. Yugo, D. W. Swain, D. B. Batchelor, P. L. Goranson, R. H. Goulding, D. J. Hoffman, E. F. Jaeger, and P. M. Ryan, "Ion Cyclotron Heating Antenna for the Compact Ignition Tokamak"
- NSF-EPRI Workshop on Anomalous Effects in Deuterated Metals, Washington, D.C., October 16–18, 1989**
- D. P. Hutchinson, C. A. Bennett, R. K. Richards, J. Bullock IV, and G. L. Powell, "Initial Calorimetry Experiments in the Physics Division of ORNL"
- Optical Society of America Annual Meeting, Orlando, Florida, October 16–20, 1989**
- R. C. Isler, "Spectroscopic Techniques for Studying Magnetic Fusion Plasmas"
- U.S.-Japan Workshop on Theoretical Problems with Non-Axisymmetric Toroidal Configurations, Plasma Physics Laboratory, Kyoto University, Uji, Kyoto, Japan, October 16–20, 1989**
- S. P. Hirshman, "Preconditioned Descent Algorithm for Computation of MHD Equilibria"
- DOE/PNC Technical Specialists' Meeting, Mito City, Japan, October 17, 1989**
- T. L. White, "Microwave Process Development Status for ORNL TRU Waste"
- IAEA Technical Committee Meeting on Alpha Particles/Confinement and Heating, Kiev, U.S.S.R., October 23–26, 1989**
- D. A. Spong, J. A. Holmes, J.-N. Leboeuf, and P. J. Christenson, "Destabilization of Tokamak Pressure-Gradient Driven Instabilities by Energetic Alpha Populations"
- D. A. Spong, J.-N. Leboeuf, J. A. Holmes, and P. J. Christenson, "Alpha Modification of Tokamak Ballooning Instabilities"
- 36th National Vacuum Symposium and Topical Conference of the American Vacuum Society, Boston, Massachusetts, October 23–27, 1989.** Proceedings published in *J. Vac. Sci. Technol. A* **8** (1990).
- J. B. O. Caughman, II, D. N. Ruzic, D. J. Hoffman, R. A. Langley, and M. B. Lewis, "Ion Energy and Erosion Measurements at the Surface of an ICRF Antenna Faraday Shield"
- S. K. Combs, C. R. Foust, M. J. Gouge, and S. L. Milora, "Acceleration of Small, Light Projectiles (Including Hydrogen Isotopes) to High Speeds Using a Two-Stage Light Gas Gun," pp. 1814–19
- C. A. Foster, C. C. Tsai, and D. E. Schechter, "Electron-Beam Rocket Pellet Accelerator"
- D. J. Hoffman, F. W. Baity, W. L. Gardner, R. H. Goulding, D. J. Taylor, P. M. Ryan, and J. C. Hosea, "The Impact of Experimental ICRF Results from Tokamaks and Tests on Antenna Development for CIT"
- R. A. Langley, J. C. Glowienka, P. K. Mioduszewski, T. F. Rayburn, J. E. Simpkins, and J. L. Yarber, "Wall Conditioning in ATF"
- R. A. Langley, J. C. Glowienka, P. K. Mioduszewski, M. Murakami, T. F. Rayburn, J. E. Simpkins, S. W. Schwenterly, and J. L. Yarber, "Wall Conditioning and Leak Localization in the Advanced Toroidal Facility," pp. 3058–62
- R. L. Livesey, F. W. Baity, R. A. Brown, A. Fadneck, W. L. Gardner, D. J. Hoffman, and D. J. Taylor, "Vacuum Issues Encountered During Design Construction and Testing of the Tore Supra Resonant Double Loop Antenna"
- J. E. Simpkins, G. R. Dyer, and J. W. Halliwell, "A Fast Response Ionization Gauge Controller"
- C. C. Tsai, L. A. Berry, S. M. Gorbatkin, H. H. Haselton, J. B. Roberto, and W. L. Stirling, "Potential Applications of An Electron Cyclotron Resonance Multicusp Plasma Source," pp. 2900–2903
- U.S.-Japan Workshop on Comparison of Theoretical and Experimental Transport in Toroidal Systems, Nagoya, Japan, October 23–27, 1989**
- W. A. Houlberg, S. E. Attenberger, H. C. Howe, and N. A. Uckan (presented by S. P. Hirshman), "Numerical Analysis of the Relationship Between Local Transport and Global Confinement in Tokamaks"
- K. C. Shaing (presented by S. P. Hirshman), "The Role of the Radial Electric Field in Producing Confinement Enhancement in Tokamaks"

5th International Symposium on Production and Neutralization of Negative Ions and Beams, Upton, New York, October 29–November 3, 1989

J. H. Whealton, "Extraction Induced RMS Emittance Growth for Volume Negative Ion Source"

November

Workshop on Resistive MHD Instabilities in Tokamaks with Emphasis on the Effect on Noncircularity and Finite Beta, Princeton, New Jersey, November 7–9, 1989

L. A. Charlton, B. A. Carreras, J. A. Holmes, R. J. Hastie and T. C. Hender, "Linear and Nonlinear Infernal Modes in Shaped Plasmas"

J. A. Holmes, B. A. Carreras, and L. A. Charlton, "MHD Stability of Shaped Tokamak Plasmas with Low Shear and Inflection Point at the $q = 1$ Surface"

ETOC Meeting, Cambridge, Massachusetts, November 8–9, 1989

J. Sheffield, "ORNL Contributions to ITER in the Engineering Design Phase"

Symposium on Charpy Impact Test: Factors and Variables, Orlando, Florida, November 8–9, 1989

D. J. Alexander and R. L. Klueh, "Specimen Size Effects in Charpy Impact Testing"

Southeastern Section of the American Physical Society, Tuscaloosa, Alabama, November 9–11, 1989

J. H. Harris, "Plasma Confinement Experiments in the ATF Torsatron"

Thirty-first Annual Meeting of the American Physical Society Division of Plasma Physics, Anaheim, California, November 13–17, 1989. Abstracts published in *Bull. Am. Phys. Soc.* 34, No. 9 (1989).

S. C. Aceto, K. A. Connor, P. E. McLaren, J. G. Schatz, J. J. Zielinski, G. H. Henkel, and J. C. Glowienka, "Analyzer Calibration for the ATF Heavy Ion Beam Probe," p. 1950

C. Alejandre, L. Garcia, A. Lopez-Fraguas, A. Varias, B. Carreras, N. Dominguez, and V. Lynch, "Second Stability Studies in the TJ-II Flexible Helic," p. 1930

F. W. Baity, W. L. Gardner, R. H. Goulding, D. J. Hoffman, and P. M. Ryan, "60-MHz Fast-Wave Current Drive Antenna for DIII-D," p. 2093

L. R. Baylor, W. A. Houlberg, S. L. Milora, and the JET/U.S. Pellet Injection Team, "Particle Confinement and Transport in Pellet Fueled JET Discharges," p. 2057

G. L. Bell, J. B. Wilgen, R. F. Gandy, T. S. Bigelow, and D. A. Rasmussen, "ECE Electron Temperature Measurements on ATF," p. 1947

J. D. Bell, J. H. Harris, J. L. Dunlap, and V. K. Paré, "Magnetic Fluctuations in ATF," p. 1948

T. S. Bigelow, J. B. Wilgen, and C. R. Schaich, "ECH Absorption Measurements on ATF Using Polarization Controlled Beam Launch," p. 1949

C. E. Bush, J. Schivell, R. J. Goldston, M. G. Bell, B. Grek, D. W. Johnson, J. H. Kamperschroer, K. McGuire, H. K. Park, S. D. Scott, E. Synakowski, G. Taylor, and R. M. Wieland, "Studies of H-Mode Plasmas on TFTR," p. 2012

R. Carrera, G. Y. Fu, L. Hively, G. Miley, E. Montalvo, M. N. Rosenbluth, D. Sigmar, S. Tamor, and J. Van Dam, "Description of Alpha Physics Phenomena in the IGNITEX Experiment," p. 2146

B. A. Carreras, N. Dominguez, P. H. Diamond, and L. Garcia, "Dissipative Trapped Electron Modes in Toroidal Confinement Devices," p. 2046

M. D. Carter, D. B. Batchelor, and E. F. Jaeger, "RF Field Estimates and Particle Orbits Near Antenna Structures," p. 2035

J. B. O. Caughman II, D. N. Ruzic, and D. J. Hoffman, "Measurements of Increased Electron Temperature and Ion Energies Near the Surface of an ICRF Antenna Faraday Shield," p. 2035

L. A. Charlton, J.-N. Leboeuf, B. A. Carreras, and V. E. Lynch, "MHD Analysis of the ATF Second Stability Behavior," p. 2059

P. J. Christenson, D. A. Spong, J. A. Holmes, and T. Kammash, "Trapped Alpha Effects on Ballooning Stability," p. 2145

- R. J. Colchin, "Overview of Results from the ATF Torsatron," invited paper, p. 1999
- R. J. Colchin, A. C. England, J. H. Harris, D. L. Hillis, M. Murakami, F. S. B. Anderson, R. F. Gandy, M. A. Henderson, D. K. Lee, and C. M. Simpson, "Flux Surface Measurements in ATF Following Field Error Repair," p. 1950
- E. C. Crume, Jr., R. C. Isler, L. D. Horton, H. C. Howe, and C. B. Brooks, "Impurity Behavior in ATF," p. 1949
- K. H. Dippel, K. H. Finken, J. G. Watkins, R. A. Moyer, D. S. Gray, and D. L. Hillis, "Thermographic Measurements at TEXTOR," p. 2166
- N. Dominguez, B. A. Carreras, L. A. Charlton, J.-N. Leboeuf, and V. E. Lynch, "Stability Beta Limit from Ballooning Modes for the ATF Device," p. 1951
- J. C. Dooling, K. G. Moses, and J. H. Wheaton, "Diagnostic Neutral Beam Generated with a Compact RF-Driven Ion Source—Experimental and Numerical Results," p. 2067
- D. A. Ehst, D. B. Batchelor, E. F. Jaeger, M. D. Carter, T. K. Mau, and C. F. F. Karney, "Fast Wave Heating/Current Drive Options for ITER," p. 1968
- A. C. England, D. A. Rasmussen, T. L. Clark, H. C. Howe, R. R. Kindsfather, K. C. Klos, M. Murakami, T. M. Rayburn, P. S. Rogers, P. L. Shaw, K. A. Stewart, and C. E. Thomas, "Electron Temperature and Density Results from the ATF Thomson Scattering System," p. 1947
- T. E. Evans, C. C. Klepper, and the Tore Supra Group, "A Survey of Ergodic Divertor Experimental Results in Tokamak TORE SUPRA," p. 2168
- S. E. Eways, W. D. Booth, R. Carrera, M. E. Oakes, and E. F. Jaeger, "Cavity-Resonance-Mode Plasma Breakdown for the IGNITEX Experiment," p. 2146
- K. H. Finken, D. L. Hillis, A. Hardtke, K. H. Dippel, R. A. Moyer, D. S. Gray, J. G. Watkins, K. Akaishi, and S. Sengoku, "Helium Detection in the Pump Limiter ALT-II at TEXTOR," p. 2167
- C. A. Foster, D. E. Schechter, and C. C. Tsai, "Characteristics of an Electron-Beam Rocket Pellet Accelerator"
- R. H. Fowler, J.-N. Leboeuf, B. A. Carreras, P. H. Diamond, and P. M. Lyster, "Studies of Trapped Electron Modes Using a Particle-Fluid Model," p. 2046
- J. D. Galambos, Y.-K. M. Peng, and L. J. Perkins, "Hybrid Current Drive to Insure Long Pulse ITER Operation," p. 1968
- W. L. Gardner, D. J. Hoffman, R. H. Goulding, F. W. Baity, and P. M. Ryan, "Spectral Shaping and Phase Control of a Fast-Wave Current Drive Antenna," p. 1093
- J. C. Glowienka, T. S. Bigelow, G. R. Dyer, P. W. Fisher, J. W. Halliwell, R. A. Langley, J. W. Lue, M. Murakami, B. E. Nelson, G. H. Neilson, A. L. Qualls, J. E. Simpkins, J. A. White, and W. R. Wing, "Operating Window Enhancement of the ATF Torsatron," p. 1946
- R. C. Goldfinger and D. B. Batchelor, "Fast Wave Current Drive Calculations Using the Geometrical Optics Code RAYS," p. 1950
- R. H. Goulding, D. J. Hoffman, C. J. Hammonds, P. M. Ryan, D. J. Taylor, and J. J. Yugo, "Design of a CIT Prototypical Fast-Wave ICRF Antenna for Alcator C-Mod," p. 2095
- D. S. Gray, R. A. Moyer, R. P. Doerner, R. W. Conn, K. H. Dippel, K. H. Finken, D. Reiter, D. L. Hillis, C. C. Klepper, S. Sengoku, J. G. Watkins, and M. Ciotti, "Particle Exhaust Performance of the ALT-II Pump Limiter with Neutral Beam Heating in TEXTOR," p. 2166
- D. J. Guilhem, J. A. Koski, J. G. Watkins, M. Chatelier, C. Klepper, P. Chappuis, and I. Fleury, "Power Deposition to the Pumped Limiters in Tore-Supra with Ohmic Plasmas," p. 2168
- J. H. Han, J. N. Leboeuf, R. H. Fowler, and P. M. Lyster, "Particle and Hybrid Simulations of Finite β Interchange Modes in Sheared Slab Geometry," p. 2043
- G. R. Hanson, C. E. Thomas, E. Anabitarte, J. H. Harris, and J. B. Wilgen, "Microwave Reflectometry System for ATF," p. 1948
- J. H. Harris, "Second Stability in the ATF Torsatron—Experiment and Theory," invited paper, p. 1992

- G. R. Haste, P. L. Nguyen, D. J. Hoffman, and T. D. Shepard, "Folded Waveguide Development," p. 2093
- C. L. Hedrick, "Radial Electric Field Effects on Tokamak Orbits"
- F. J. Helton, J. M. Greene, L. L. Lao, E. A. Lazarus, and T. S. Taylor, "Ideal MHD Properties of Elongated DIII-D Shots," p. 2118
- D. L. Hillis, R. C. Isler, C. C. Klepper, J. T. Hogan, P. K. Mioduszewski, A. Pospieszczyk, D. Rusbüldt, R. Schorn, K. H. Dippel, K. H. Finken, R. Moyer, and the ALT-II Team, "Helium Removal Studies with a Pump Limiter in TEXTOR," p. 2166
- S. Hiroe, C. E. Bush, J. B. Wilgen, P. W. Fisher, T. S. Bigelow, A. L. Qualls, G. Renda, and J. Schivell, "Bolometric Measurements in ATF," p. 1949
- S. P. Hirshman and O. Betancourt, "SPEC: Spectral Preconditioned Equilibrium Code," p. 1975
- L. M. Hively, J. A. Rome, and S. P. Hirshman, "Suprathermal Alpha Loss Due to Ripple in ITER," p. 1971
- D. J. Hoffman, F. W. Baity, W. L. Gardner, R. H. Goulding, D. J. Taylor, P. M. Ryan, and J. C. Hosea, "The Impact of Experimental ICRF Results from Tokamaks and Tests on Antenna Development for CIT," p. 2035
- J. T. Hogan, C. C. Klepper, D. L. Hillis, R. Schorn, D. Rusbüldt, A. Pospieszczyk, K.-H. Dippel, R. Moyer, and R. P. Doerner, "Analysis of Recycling Energy Distributions from H_α Measurements on TEXTOR," p. 2169
- J. T. Hogan and P. K. Mioduszewski, "Global Modeling of the Particle Balance in DIII-D with a Pumped Divertor," p. 2121
- J. A. Holmes, B. A. Carreras, J. N. Leboeuf, D. K. Lee, C. P. Ritz, A. J. Wootton, D. R. Thayer, and P. H. Diamond, "Thermally Driven Convective Cell Turbulence at the Edge of TEXT," p. 2158
- L. D. Horton, H. C. Howe, E. C. Crume, Jr., and R. C. Isler, "Modeling of Radiation and Density Limits in ATF," p. 1949
- J. Hosea, P. Colestock, G. J. Greene, J. Stevens, J. R. Wilson, and D. Hoffman, "TFTR ICRF Antenna Configuration Circuit Models," p. 2013
- W. A. Houlberg, L. R. Baylor, S. L. Milora, and the JET/U.S. Pellet Injection Team, "Velocity Dependence of Pellet Penetration in JET," p. 2057
- R. C. Isler, L. D. Horton, E. C. Crume, and C. B. Brooks, "Ion Temperatures and Plasma Rotation in ATF," p. 1948
- ITER Physics Team and N. A. Uckan, "Confinement Capability of ITER," p. 1966
- E. F. Jaeger, D. B. Batchelor, P. M. Ryan, and J. S. Tolliver, "Fast Wave Current Drive with Recessed Antenna Arrays," p. 2035
- T. C. Jernigan, T. S. Bigelow, R. J. Colchin, A. C. England, D. L. Hillis, S. Hiroe, R. C. Isler, L. A. Massengill, M. M. Menon, M. Murakami, D. A. Rasmussen, W. L. Stirling, T. Uckan, M. R. Wade, and W. R. Wing, "Power Accountability in ATF," p. 1949
- C. C. Klepper, J. E. Simpkins, P. K. Mioduszewski, M. Chatelier, J. L. Bruneau, A. Grosman, and J. G. Watkins, "Measurements of Pressure Buildup and particle Fluxes in the Tore Supra Pump Limiter," p. 2168
- M. Kwon, R. H. Goulding, T. D. Shepard, and C. E. Thomas, Jr., "Edge Plasma and RF Field Measurements during Fast-Wave ICRH Experiments on ATF," p. 1950
- E. A. Lazarus, A. G. Kellman, J. A. Leuer, A. D. Turnbull, E. J. Strait, J. F. Helton, and T. S. Taylor, "Axisymmetric Stability in DIII-D," p. 1940
- J. N. Leboeuf, B. A. Carreras, J. A. Holmes, D. K. Lee, C. P. Ritz, A. J. Wootton, D. R. Thayer, and P. H. Diamond, "Resistivity Gradient Driven Turbulence at the Edge of TEXT," p. 2159
- D. K. Lee, J. H. Harris, and G. S. Lee, "Calculation of Magnetic Island Widths due to Field Errors in a Toroidal Stellarator Device," p. 1950

- G. S. Lee, "Characterization of the Magnetic Fluctuations in Resistive Pressure-Gradient-Driven Turbulence," p. 1926
- B. Lloyd, G. L. Jackson, E. Lazarus, T. Luce, R. Prater, and T. S. Taylor, "Low Voltage Start-Up with ECH in DIII-D," p. 1967
- C. H. Ma, C. A. Bennett, D. P. Hutchinson, and K. L. Vander Sluis, "FIR Interferometer and Scattering Measurements on ATF," p. 1947
- M. M. Menon, and P. K. Mioduszewski, "Pumping Schemes for the DIII-D Collaborative Advanced Divertor Program," p. 2121
- D. R. Mikkelsen, M. G. Bell, C. E. Bush, R. J. Goldston, B. Grek, T. S. Hahm, K. W. Hill, D. W. Johnson, D. K. Mansfield, H. K. Park, A. T. Ramsey, M. H. Redi, G. Rewoldt, G. Schilling, J. Schivell, B. C. Stratton, E. J. Synakowski, W. M. Tang, G. Taylor, H. H. Towner, M. Zarnstorff, and S. J. Zweben, "Comparison of Predicted and Measured Temperature Profiles in TFTR Plasmas," p. 2011
- P. K. Mioduszewski and L. W. Owen, "Particle Exhaust Studies for the DIII-D Collaborative Advanced Divertor Program," p. 2121
- R. N. Morris, J. F. Lyon, and J. A. Rome, "Effect of Finite Drift Orbit Size on Interpretation of Neutral Particle Analyzer Spectra," p. 1948
- M. Murakami, G. L. Bell, T. S. Bigelow, A. C. England, J. C. Glowienka, J. H. Harris, H. C. Howe, D. K. Lee, R. N. Morris, G. H. Neilson, D. A. Rasmussen, and W. R. Wing, "Magnetic Configuration Studies in the ATF Torsatron," p. 1946
- C. A. Ordonez, R. Carrera, J. Howell, G. Rodin, and H. C. Howe, "Operation of the Ignition Experiment IGNITEX with a Limiterless First Wall System," p. 2146
- L. W. Owen, P. K. Mioduszewski, J. T. Hogan, and M. Rensink, "Neutral Particle Modeling of the DIII-D Advanced Divertor Performance," p. 2121
- Y-K. M. Peng, J. C. Whitson, and A. H. Glasser, "Access to Second Ballooning Stability in Divertor Plasmas," p. 1971
- Y-K. M. Peng, D. J. Strickler, J. T. Hogan, J. C. Whitson, C. G. Bathke, K. Evans, Jr., S. C. Jardin, M. Klasky, and J. A. Leuer, "MHD Equilibrium and Stability for ARIES-I"
- L. J. Perkins, D. T. Blackfield, and J. D. Galambos, "The Impact of Confinement on the Design of ITER and Reactors: Why ITER Is Where It Is Today," p. 1966
- A. L. Qualls, P. W. Fisher, M. J. Cole, A. C. England, D. T. Fehling, M. J. Gouge, W. A. Houlberg, T. C. Jernigan, S. L. Milora, and J. B. Wilgen, "Pellet Ablation Studies on ATF," p. 1947
- D. A. Rasmussen, G. L. Bell, T. L. Clark, A. C. England, R. F. Gandy, H. C. Howe, R. R. Kindsfather, K. C. Klos, R. N. Morris, M. Murakami, T. M. Rayburn, P. S. Rogers, P. L. Shaw, K. A. Stewart, C. E. Thomas, and J. B. Wilgen, "Electron Temperature and Density Profile Analysis in ATF," p. 1947
- Ch. P. Ritz, C. Hidalgo, H. Lin, M. Meier, T. L. Rhodes, A. J. Wootton, T. Uckan, J. D. Bell, J. L. Dunlap, J. H. Harris, and G. H. Neilson, "Comparison of Edge Turbulence of TEXT and ATF," p. 2153
- J. A. Rome and A. Ouroua, "Diagnostic Neutral Beam Calculations for TEXT," p. 2156
- P. M. Ryan, K. E. Rothe, J. H. Whealton, and T. D. Shepard, "Determination of ICRF Antenna Fields in the Vicinity of a 3-D Faraday Shield Structure," p. 2036
- R. O. Sayer, Y-K. M. Peng, J. C. Wesley, and S. C. Jardin, "ITER Disruption Modeling Using TSC," p. 1969
- K. C. Shaing, "Bifurcation Theory of Poloidal Rotation and L-H Transition in Tokamaks," invited paper, p. 2162
- K. C. Shaing and R. D. Hazeltine, "Enhanced Trapped Particle Pinch from Asymmetric Electrostatic Potentials in Tokamaks," p. 2084

- T. D. Shepard, R. H. Goulding, M. Kwon, M. R. Wade, and C. E. Thomas, "Fast-Wave ICRF Heating Experiments on the ATF Torsatron," p. 1949
- D. A. Spong and K. C. Shaing, "Neoclassical MHD Modifications of Resistive Instabilities in the Banana-Plateau Regime," p. 2058
- J. E. Stevens, P. L. Colestock, G. J. Greene, J. C. Hosea, C. K. Phillips, D. J. Hoffman, and W. L. Gardner, "ICRF Phasing Experiments on TFTR," p. 2013
- W. L. Stirling, J. H. Whealton, W. R. Becraft, P. M. Ryan, and W. K. Dagenhart, "An RF Linear Accelerator Beam Line Design for ITER," p. 2066
- D. P. Stotler, C. E. Bush, and D. E. Post, "Applications of Radiation-Dominated and Density Limit Simulations to ITER," p. 1969
- E. J. Strait, J. R. Ferron, L. L. Lao, T. S. Taylor, M. S. Chu, F. J. Helton, W. L. Howl, A. G. Kellman, E. Lazarus, J. K. Lee, T. H. Osborne, R. D. Stambaugh, and A. D. Turnbull, "High Beta Discharges in DIII-D," p. 1939
- D. J. Strickler, Y.-K. M. Peng, S. C. Jardin, and N. Pomphrey, "MHD Equilibrium Using Free-Boundary Control Matrix," p. 1972
- D. W. Swain, D. B. Batchelor, M. D. Carter, R. H. Goulding, D. J. Hoffman, E. F. Jaeger, P. M. Ryan, and J. J. Yugo, "Fast Ion Cyclotron Wave Current Drive System for ITER," p. 2095
- D. R. Thayer, P. H. Diamond, B. A. Carreras, J. A. Holmes, J. N. Leboeuf, Ch. P. Ritz, and A. J. Wootton, "Tokamak Edge Turbulent Transport," p. 2085
- J. S. Tolliver and D. B. Batchelor, "A 2D Model for Recessed Phased Antenna Arrays," p. 2035
- C. C. Tsai, L. A. Berry, S. M. Gorbalkin, H. H. Haselton, J. B. Roberto, and D. E. Schechter, "Potential Applications of ORNL Multicusp Plasmatron," p. 2128
- N. A. Uckan, "Tokamak Physics Improvements: Implications for CIT and ITER," p. 1967
- T. Uckan, J. D. Bell, J. L. Dunlap, G. R. Dyer, J. H. Harris, D. L. Million, P. K. Mioduszewski, G. H. Neilson, J. B. Wilgen, C. P. Ritz, K. R. Carter, and C. Hidalgo, "ATF Edge Plasma Studies Using a Fast Reciprocating Langmuir Probe (FRLP)," p. 1948
- A. Varias, C. Alejaldre, A. L. Fraguas, L. Garcia, B. A. Carreras, N. Dominguez, and V. E. Lynch, "Stability of Local Modes of High Rotational Transform TJ-II Configurations," p. 1931
- M. R. Wade, R. J. Colchin, J. F. Lyon, and C. E. Thomas, "Neutral Particle Measurements on ATF," p. 1948
- J. H. Whealton, P. M. Ryan, and R. J. Raridon, "ICRF Faraday Shield Plasma Sheath Physics," p. 2036
- J. C. Whitson, Y.-K. M. Peng, A. Sykes, T. N. Todd, and T. C. Hender, "Spherical Torus Production by Major Radius Compression in the START Experiment," p. 2166
- J. B. Wilgen, G. L. Bell, J. D. Bell, A. C. England, P. W. Fisher, H. C. Howe, D. P. Hutchinson, C. H. Ma, M. Murakami, A. L. Qualls, D. A. Rasmussen, R. K. Richards, T. Uckan, and W. R. Wing, "Pellet Injection into ATF Plasmas," p. 1947
- J. R. Wilson, P. L. Colestock, G. J. Greene, J. C. Hosea, C. K. Phillips, J. E. Stevens, D. J. Hoffman, and W. L. Gardner, "High Power ICRF Heating on TFTR," p. 2012
- W. R. Wing, G. R. Dyer, J. C. Glowienka, J. H. Harris, J. W. Halliwell, and G. H. Neilson, "ATF Diamagnetic Measurements," p. 1946
- J. J. Zielinski, S. C. Aceto, K. A. Connor, J. F. Lewis, J. C. Glowienka, G. H. Henkel, W. R. DeVan, K. D. St. Onge, D. K. Lee, and A. Carnevali, "Initial Operation of the HIBP Primary Beamline on ATF," p. 1950
- American Nuclear Society 1989 Winter Meeting, San Francisco, California, November 26–30, 1989.**
Proceedings published as *Trans. Am. Nucl. Soc.* 60 (1989).
- M. L. Grossbeck, L. L. Horton, and L. K. Mansur, "An Investigation of Irradiation Creep in Ferritic Alloys in the Oak Ridge Research Reactor at 60 to 400°C"
- R. L. Klueh, "Tensile Property Behavior of Irradiated Martensitic Alloys," pp. 296–7

- P. J. Maziasz, "Microstructural Evolution of Martensitic Steels During Fast Neutron Irradiation," pp. 297-9
Materials Research Society Symposium, Boston, Massachusetts, November 30-December 5, 1989.
 Proceedings published as *Mat. Res. Soc. Symp. Proc.* **128** (1989).
- S. J. Zinkle, "Microstructural Characterization of Al₂O₃ Following Simultaneous Triple Ion Bombardment,"
 pp. 363-8

December

- First International Toki Conference on Plasma Physics and Controlled Nuclear Fusion Research, Toki, Japan, December 4-8, 1989.** Proceedings published as NIFS-PROC-3, by the National Institute for Fusion Science, Nagoya, Japan, 1990.
- B. A. Carreras, N. Dominguez, J. N. Leboeuf, V. E. Lynch, and P. H. Diamond, "Dissipative Trapped Electron Modes in $\ell = 2$ Torsatrons," p. 118-21
- L. A. Charlton, J. N. Leboeuf, B. A. Carreras, N. Dominguez, and V. E. Lynch, "Resistive MHD Studies for ATF Plasmas During Operation in the Second Stability Regime," pp. 41-44
- R. L. Dewar, H. J. Gardner, G. J. Cooper, S. M. Hamberger, L. E. Sharp, B. D. Blackwell, T. Y. Tou, G. D. Conway, X-H. Shi, D-F. Zhou, J. Howard, B. A. Carreras, N. Dominguez, and V. E. Lynch, "The ANU Helic Program"
- R. F. Gandy, G. L. Bell, J. B. Wilgen, T. S. Bigelow, and D. A. Rasmussen, "ECE Electron Temperature Measurements on ATF"
- J. F. Lyon, B. A. Carreras, L. Dresner, S. P. Hirshman, R. N. Morris, S. L. Painter, and J. A. Rome, "Overview of the ATF-II Studies"
- M. Murakami, E. Anabitarte, F. S. Anderson, G. L. Bell, J. D. Bell, T. S. Bigelow, B. A. Carreras, L. A. Charlton, T. L. Clark, J. Colchin, E. C. Crume, Jr., N. Dominguez, J. L. Dunlap, G. R. Dyer, A. C. England, P. W. Fisher, R. F. Gandy, J. C. Glowienka, R. H. Goulding, G. R. Hanson, J. H. Harris, G. R. Haste, C. Hidalgo-Vera, D. L. Hillis, S. Hiroe, L. D. Horton, H. C. Howe, D. E. Hutchinson, R. C. Isler, T. C. Jernigan, K. L. Kannan, H. Kaneko, M. Kwon, R. A. Langley, J-N. Leboeuf, D. K. Lee, J. W. Lue, V. E. Lynch, J. F. Lyon, C. H. Ma, M. M. Menon, P. K. Mioduszewski, R. N. Morris, G. H. Neilson, A. L. Qualls, D. A. Rasmussen, Ch. P. Ritz, P. S. Rogers, S. W. Schwenterly, K. C. Shaing, P. L. Shaw, T. D. Shepard, J. E. Simpkins, K. A. Stewart, S. Sudo, C. E. Thomas, J. S. Tolliver, T. Uckan, M. R. Wade, J. B. Wilgen, W. R. Wing, H. Yamada, and J. J. Zielinski, "Overview of Recent Results from the Advanced Toroidal Facility," pp. 77-80
- 4th International Conference on Fusion Reactor Materials (ICFRM-4), Kyoto, Japan, December 4-8, 1989**
- G. E. C. Bell, P. F. Tortorelli, T. Inazumi, and R. L. Klueh, "An Investigation of the Stress Corrosion Cracking Behavior of Fe-Cr-Mn Austenitic Steels"
- G. E. C. Bell, P. F. Tortorelli, E. A. Kenik, and R. L. Klueh, "An Investigation of the Sensitization Behavior of Fe-Cr-Mn Austenitic Steels"
- T. D. Burchell and W. P. Eatherly, "The Effects of Radiation Damage on the Properties of Graphnol N3M"
- M. L. Grossbeck, "Empirical Relations for Tensile Properties of Austenitic Stainless Steels Irradiated in Mixed Spectrum Reactors"
- T. Inazumi, G. E. C. Bell, A. Hishinuma, and R. L. Klueh, "Electrochemical Evaluation of Sensitization in Austenitic Stainless Steels Using Miniaturized Specimens"
- S. Jitsukawa, M. L. Grossbeck, and A. Hishinuma, "Stress-Strain Relations of HFIR-Irradiated Austenitic Stainless Steels"
- R. L. Klueh, "Irradiation Hardening of Ferritic Steels: Effects of Composition"
- R. L. Klueh and D. J. Alexander, "Impact Behavior of 9Cr-1MoVNb and 12Cr-1MoVW Steels Irradiated in HFIR"

- R. L. Klueh, D. J. Alexander, and P. J. Maziasz, "Heat Treatment Effects on Impact Properties of Reduced-Activation Steels"
- S. Kojima and S. J. Zinkle, "Contributions to Radiation Hardening in Neutron Irradiated Polycrystalline Copper"
- H. T. Lin and B. A. Chin, "The Feasibility of Welding Irradiated Materials"
- T. J. Miller, S. J. Zinkle, and B. A. Chin, "Strength and Fatigue of Dispersion-Strengthened Copper"
- T. Sawai, P. J. Maziasz, and A. Hishinuma, "Microstructural Evolution of Welded Austenitic Stainless Steels Irradiated in Spectrally Tailored ORR Experiment"
- T. Sawai, M. Suzuki, P. J. Maziasz, and A. Hishinuma, "The Thickness Measurement of Reactor Irradiated TEM Specimens by Contamination Spot Separation Method"
- S. J. Zinkle, "Microstructural Analysis of a Neutron-Irradiated Copper-Boron Alloy"
- S. J. Zinkle and S. Kojima, "Microstructural Evaluation of Ion-Irradiated Ceramics"
- IEA/U.S.-Japan Workshop on Next-Generation Experiments, National Institute for Fusion Science, Nagoya, Japan, December 8-9, 1989**
- J. F. Lyon, "ATF-II Optimization Studies"
- J. F. Lyon, "ATF-II Compact Torsatron Studies"
- J. F. Lyon, "Status of the ATF-II Studies"
- J. F. Lyon, "Orbit Confinement and Transport in Large Stellarators"
- Workshop on Reactor Fuel-Materials Interactions, Tokyo, Japan, December 11-12, 1989**
- W. P. Eatherly and T. D. Burchell, "The Fundamental Understanding of the Physical Properties of Graphite—A Review"
- P-149 Workshop on Evaluation of Radiation Damage in Ceramics and Graphite, Tokyo, Japan, December 12-13, 1989**
- T. D. Burchell and W. P. Eatherly, "Radiation Damage in Graphite—Physical and Chemical Aspects"
- ITER Nuclear Group Meeting, Argonne, Illinois, December 13, 1989**
- B. E. Nelson, "Vacuum Vessel Configuration Studies"

CONGRESSIONAL TESTIMONY

- L. A. Berry, "Magnetic Fusion Research at Oak Ridge National Laboratory," Subcommittee on Energy Research and Development, House Committee on Science, Space and Technology, February 21, 1989
- M. J. Saltmarsh, "Cold Fusion Investigations at ORNL," House Committee on Science, Space, and Technology, April 26, 1989
- J. Sheffield, "Magnetic Fusion Energy," Subcommittee on Investigations and Oversight, House Committee on Science, Space, and Technology, October 4, 1989

SEMINARS

- B. A. Carreras, "Access to the Second Stability Regime in ATF," Kyoto University, Kyoto, Japan, May 12-14, 1989
- B. A. Carreras, "Stability Studies for the TJ-II Helic," " $M = 3$ Helic Evaluation Studies," Tohoku University, Sendai, Japan, June 6, 1989
- S. K. Combs, Kiwanis Club, Oak Ridge, June 1989
- J. G. Delene, "An Economic Study of Fusion Energy," Department of Electrical and Computer Engineering, University of Tennessee, Knoxville, March 31, 1989
- J. C. Glowienka, "Fusion," Meeting of the East Tennessee Chapter of the Health Physics Society, Oak Ridge, Tennessee, June 14, 1989
- D. C. Gregory, "Electron Impact Ionization of Ions: What Is and Is Not Important," Lawrence Livermore National Laboratory, Livermore, California, June 29, 1989
- C. C. Havener, "Cold Fusion or ConFusion," Catholic University of Louvain, Belgium, May 10, 1989
- C. C. Havener, "Ion-Atom Collisions," Catholic University of Louvain, Belgium, May 1989
- C. C. Havener, "Ion-Surface Collisions," Utrecht, The Netherlands, May 25, 1989; KVI Groningen, May 26, 1989
- C. C. Havener, "Low Energy Multicharged Ion-Atom Collisions," Physics Department, University of Louisville, Louisville, Kentucky, November 1989
- P. J. Maziasz and R. W. Swindeman, "Development of New Austenitic Steels and Alloys for Advanced Nuclear and Fossil Energy Applications," Department of Engineering Physics, School of Engineering, Air Force Institute of Technology, Wright-Patterson Air Force Base, Dayton, Ohio, August 30, 1989
- F. W. Meyer, "Multicharged Ion Collision Studies at the ORNL ECR Source Facility," Physics Department, North Carolina State University, April 3, 1989
- F. W. Meyer, "Recent Experiments at the ORNL ECR Source Facility," Chemical Physics Seminar, ORNL, March 27, 1989
- M. Murakami, "Recent ATF Results," Plasma Physics Laboratory, Kyoto University, Uji, Japan, December 11, 1989
- M. Murakami (with K. Matsuoka), "Recent Results from ATF and CHS," National Institute for Fusion Science, Nagoya, Japan, December 14, 1989
- R. A. Phaneuf, "Laboratory Experimental Atomic Physics of Highly Charged Ions," Princeton Plasma Physics Laboratory, Princeton, New Jersey, December 6, 1989
- R. A. Phaneuf, "Low Energy Electron Capture by Multiply Charged Ions," Kansas State University, Manhattan, Kansas, April 12, 1989
- J. A. Rome, "Stellarators—A New Twist on an Old Idea," University of Colorado, Boulder, February 27, 1989
- J. Sheffield, "Prospects for Fusion Power," Johns Hopkins University, Baltimore, March 17, 1989
- D. A. Spong, "Neoclassical MHD Effects in Tokamaks," Kurchatov Institute, Moscow, U.S.S.R., October 31, 1989
- P. F. Tortorelli, "Recent ORNL Results on the Development of Fe-Mn-Cr Steels," European Community Joint Research Center, Ispra, Italy, September 25, 1989

REPORTS

ORNL Reports

- ORNL-6551 *Spectroscopic Data for Titanium, Chromium, and Nickel: Vol. 1, Titanium; Vol. 2, Chromium, Vol. 3, Nickel*
W. L. Wiese and A. Musgrove
September 1989

ORNL Technical Memoranda

- ORNL/ATD-23 *Stress Analysis of the Princeton Plasma Physics Laboratory 1/2- × 1/2-in. Shear/Compression Test Fixture*
H. W. Blake
October 1989
- ORNL/TM-10988 *Runaway Studies in the ATF Torsatron*
A. C. England, G. L. Bell, W. R. DeVan, C. C. Eberle, and R. H. Fowler
January 1989
- ORNL/TM-11075 *Application of Theta Functions for Numerical Evaluation of Complete Elliptic Integrals of the First and Second Kinds*
D. K. Lee
February 1989
- ORNL/TM-11101 *Confinement Improvement of Low-Aspect-Ratio Torsatrons*
B. A. Carreras, V. E. Lynch, N. Dominguez, J.-N. Leboeuf, and J. F. Lyon
March 1989
- ORNL/TM-11102 *A First Glance at the Initial ATF Experimental Results*
B. A. Carreras, N. Dominguez, J. N. Leboeuf, V. E. Lynch, and L. A. Charlton
May 1989
- ORNL/TM-11138 *Second Stability Studies in the ATF Torsatron*
M. Murakami, B. A. Carreras, J. H. Harris, F. S. B. Anderson, G. L. Bell, J. D. Bell, T. S. Bigelow, R. J. Colchin, E. C. Crume, N. Dominguez, J. L. Dunlap, A. C. England, J. C. Glowienka, L. D. Horton, H. C. Howe, R. C. Isler, H. Kaneko, R. R. Kindsfather, J. N. Leboeuf, V. E. Lynch, M. M. Menon, R. N. Morris, G. H. Neilson, V. K. Paré, D. A. Rasmussen, J. B. Wilgen, and W. R. Wing
March 1989
- ORNL/TM-11158 *Simulation of the Welding of Irradiated Materials*
H. T. Lin
July 1989
- ORNL/TM-11177 *Bibliography of Fusion Product Physics in Tokamaks*
L. M. Hively and D. J. Sigmar
August 1989
- ORNL/TM-11253 *Construction and Initial Operation of the Advanced Toroidal Facility*
J. F. Lyon, G. L. Bell, J. D. Bell, R. D. Benson, T. S. Bigelow, K. K. Chipley, R. J. Colchin, M. J. Cole, E. C. Crume, J. L. Dunlap, A. C. England, J. C. Glowienka, R. H. Goulding, J. H. Harris, D. L. Hillis, S. Hiroe, L. D. Horton, H. C. Howe, R. C. Isler, T. C. Jernigan, R. L. Johnson, R. A. Langley, M. M. Menon, P. K. Mioduszewski, R. N. Morris, M. Murakami, G. H. Neilson, B. E. Nelson, D. A. Rasmussen, J. A. Rome, M. J. Saltmarsh, P. B. Thompson, M. R. Wade, J. A. White, T. L. White, J. C. Whitson, J. B. Wilgen, and W. R. Wing
August 1989
- ORNL/TM-11254 *ATF-II Studies*
J. F. Lyon, B. A. Carreras, N. Dominguez, L. Dresner, C. L. Hedrick, S. P. Hirshman, M. S. Lubell, J. W. Lue, R. N. Morris, S. L. Painter, J. A. Rome, and W. I. van Rij
September 1989

ORNL/TM-11255 *Near-Term Directions in the World Stellarator Program*
 J. F. Lyon
 October 1989

ORNL Fusion Engineering Design Center Reports

ORNL/FEDC-88/7 *MHD Equilibrium Methods for ITER PF Coil Design and Systems Analysis*
 D. J. Strickler, J. D. Galambos, and Y-K. M. Peng
 March 1989

Reports Published by ORNL for the U.S. Department of Energy

- DOE/ER-0313/5 *Fusion Reactor Materials Semiannual Progress Report for Period Ending September 30, 1988*
 A. F. Rowcliffe, comp.
 April 1989
- DOE/ER-0313/6 *Fusion Reactor Materials Semiannual Progress Report for Period Ending March 31, 1989*
 A. F. Rowcliffe, comp.
 1989
- DOE/ER-0313/7 *Fusion Reactor Materials Semiannual Progress Report for Period Ending September 30, 1989*
 R. Price
 September 1989

Reports Published by Other Institutions

- DOE/ER-0421 *Review of Computer Applications in the Magnetic Fusion Energy Theory Program*
 H. R. Lewis, B. A. Carreras, B. I. Cohen, J. P. Freidberg, S. C. Jardin,
 W. Pfeiffer, J. L. Schwarzmeier, and A. B. White
 U.S. Department of Energy, Washington, D.C.
 July 1989
- FRCR-340 *Fluctuations and Anomalous Transport in Tokamaks*
 (DOE/ER 53267-52) A. J. Wootton, B. A. Carreras, H. Matsumoto, K. McGuire, R. McKnight,
 T. Peebles, Ch. Ritz, P. W. Terry, and S. Zweben
 Fusion Research Center, University of Texas, Austin
 1989
- GA-A19581 *Control of the Vertical Instability in Tokamaks*
 E. A. Lazarus, J. B. Lister, and G. H. Neilson
 General Atomics, San Diego, California
 1989
- IFSR-371 *Enhanced Radiation Driven by a DC Electric Field*
 (DOE/ET-53088-371) T. Tajima, A. O. Benz, M. Thacker, and J-N. Leboeuf
 Institute for Fusion Studies, University of Texas, Austin
 May 1989
- ITER-IL-Ph-1-9-1 *Summary Report: ITER Alpha Particle Ripple Loss Meeting*
 S. Putvinskii, N. A. Uckan, K. Borrass, and T. Tsunematsu
 ITER Conceptual Design Activity, Garching, Federal Republic of Germany
 1989
- ITER-IL-Ph-4-9-U8 *ITER Transport Analysis*
 W. A. Houlberg
 ITER Conceptual Design Activity, Garching, Federal Republic of Germany
 1989

- ITER-IL-Ph-9-9-U1 *ITER Pellet Fueling*
W. A. Houlberg
ITER Conceptual Design Activity, Garching, Federal Republic of Germany
1989
- ITER-IL-Ph-9-9-U2 *ITER Density Profile with Pellet Injection*
W. A. Houlberg
ITER Conceptual Design Activity, Garching, Federal Republic of Germany
1989
- ITER-TN-PH-8-7 *ITER Physics Design Guidelines: Version 1*
N. A. Uckan and ITER Physics Group
ITER Conceptual Design Activity, Garching, Federal Republic of Germany
January 1989
- ITER-TN-PH-9-7 *ITER Physics Design Guidelines: Version 2*
N. A. Uckan and ITER Physics Group
ITER Conceptual Design Activity, Garching, Federal Republic of Germany
1989
- SAND89-0863 *A Technique for Efficiently Cleaning and Conditioning Low- and Medium-Energy Accelerators*
R. A. Langley and J. M. McDonald
Sandia National Laboratories, Albuquerque, New Mexico
1989
- TAERF-47 *Fusion Ignition Experiment (IGNITEX)*
R. Carrera, M. Barrington, W. D. Booth, Y. Chen, B. Daugherty, M. Driga,
G. Fu, J. Gully, G. Hallock, J. Helton, N. Hertel, L. Hively, J. Hopf, K. Hsieh,
M. Kerwick, T. Lovett, J. Ling, G. Miller, E. Montalvo, C. Ordonez, D. Palmrose,
T. Parish, M. N. Rosenbluth, D. Sreevijayan, S. Tamor, D. Tesar, J. Van Dam,
P. Varghese, A. Walls, W. Weldon, M. Werst, and H. Woodson
Fusion Research Center, University of Texas, Austin
1989

THESES AND DISSERTATIONS

L. R. Baylor, "Particle Transport in Pellet Fueled JET Plasmas," Ph.D., The University of Tennessee, Knoxville, December 1989

Appendix 2
ABBREVIATIONS AND ACRONYMS

ABBREVIATIONS AND ACRONYMS

ADP	Advanced Divertor Program
AEM	analytical electron microscopy
ALT-II	Advanced Limiter Test II
amu	atomic mass unit
appm	atomic parts per million
ARIES	Advanced Reactor Innovation and Evaluation Studies
ATF	Advanced Toroidal Facility
bcc	body-centered cubic
C/C	carbon-carbon
CEA	Commissariat à l'Énergie Atomique
CFADC	Controlled Fusion Atomic Data Center
CHS	Compact Helical System
CIEMAT	Centro de Investigaciones Energéticas, Medioambientales, y Tecnológicas
CIT	Compact Ignition Tokamak
CPU	central processing unit
CVD	chemical vapor deposition
CW	cold-worked
cw	continuous wave
CXE	charge-exchange excitation
DBTT	ductile-to-brittle transition temperature
D-D	deuterium-deuterium
DOE	U.S. Department of Energy
dpa	displacements per atom
DPI	deuterium pellet injector
D-T	deuterium-tritium
DTE	dissipative trapped-electron
DIII-D	tokamak experiment at General Atomics
EBR-II	Experimental Breeder Reactor-II
ECE	electron cyclotron emission
ECH	electron cyclotron heating
ECR	electron cyclotron resonance
ECRH	electron cyclotron resonance heating
EHD	electrohydrodynamic
EPPC	Edge Physics and Particle Control
EPR	electrochemical potentiokinetic reactivation
EURATOM	European Atomic Energy Community
FEDC	Fusion Engineering Design Center
FFTF	Fast Flux Test Facility
FIR	far-infrared

FRLP	fast reciprocating Langmuir probe
FWB	first wall and blanket
FWCD	fast-wave current drive
FWG	folded waveguide
FY	fiscal year
GA	General Atomics
GDC	glow discharge cleaning
HF	helical field
HFIR	High-Flux Isotope Reactor
HHF	high heat flux
HIBP	heavy-ion beam probe
IAEA	International Atomic Energy Agency
IASCC	irradiation-assisted stress-corrosion cracking
IBW	ion Bernstein wave
ICRF	ion cyclotron range of frequencies
ICRH	ion cyclotron resonance heating
IFSMTF	International Fusion Superconducting Magnet Test Facility
IGSSC	intergranular stress-corrosion cracking
IPP Garching	Max Planck Institut für Plasmaphysik, Garching, Federal Republic of Germany
ISX-B	Impurity Study Experiment
ITER	International Thermonuclear Experimental Reactor
JAERI	Japan Atomic Energy Research Institute
JET	Joint European Torus
JILA	Joint Institute for Laboratory Astrophysics
KFA	Kernforschungsanlage
KfK	Kernforschungszentrum Karlsruhe
LANL	Los Alamos National Laboratory
LBL	Lawrence Berkeley Laboratory
LCFS	last closed flux surface
LCT	Large Coil Task
LHD	Large Helical Device
LIDT	laser-induced damage threshold
LLNL	Lawrence Livermore National Laboratory
MHD	magnetohydrodynamic
MSG	Management Services Group
MTX	Microwave Tokamak Experiment
NBI	neutral beam injection
NMFECC	National Magnetic Fusion Energy Computer Center
NPA	neutral particle analyzer

ODIS	Optics Damage and Irradiation Studies
ORNL	Oak Ridge National Laboratory
ORR	Oak Ridge Research Reactor
PBX	Princeton Beta Experiment
PC	personal computer
PCA	prime candidate alloy
PCI	postcollision interaction
PF	poloidal field
PI	plasma-interactive
PLC	programmable logic controller
PLT	Princeton Large Torus
POP	proof-of-principle
PPPL	Princeton Plasma Physics Laboratory
QA	quality assurance
QMS	quadrupole mass spectrometer
R&D	research and development
rf	radio frequency
RFQ	radio-frequency quadrupole
RFTF	Radio-Frequency Test Facility
RH-TRU	remote-handled transuranic
RPI	Rensselaer Polytechnic Institute
RSIC	Radiation Shielding Information Center
RTD	resistance temperature detector
SA	solution-annealed
TEM	transmission electron microscopy
TEXT	Texas Experimental Tokamak
TEXTOR	Torus Experiment for Technology Oriented Research
TF	toroidal field
TFTR	Tokamak Fusion Test Reactor
TPOP	tritium proof-of-principle
TSC	Tokamak Simulation Code
TSTA	Tritium Systems Test Assembly
TTI	Tokamak Transport Initiative
TTMP	transit-time magnetic pumping
USASDC	U.S. Army Strategic Defense Command
USC	User Service Center
VF	vertical field
VV	vacuum vessel
WHPP	Waste Handling and Packaging Plant

XVRM	ex-vessel remote maintenance
1-D	one-dimensional
2-D	two-dimensional
3-D	three-dimensional

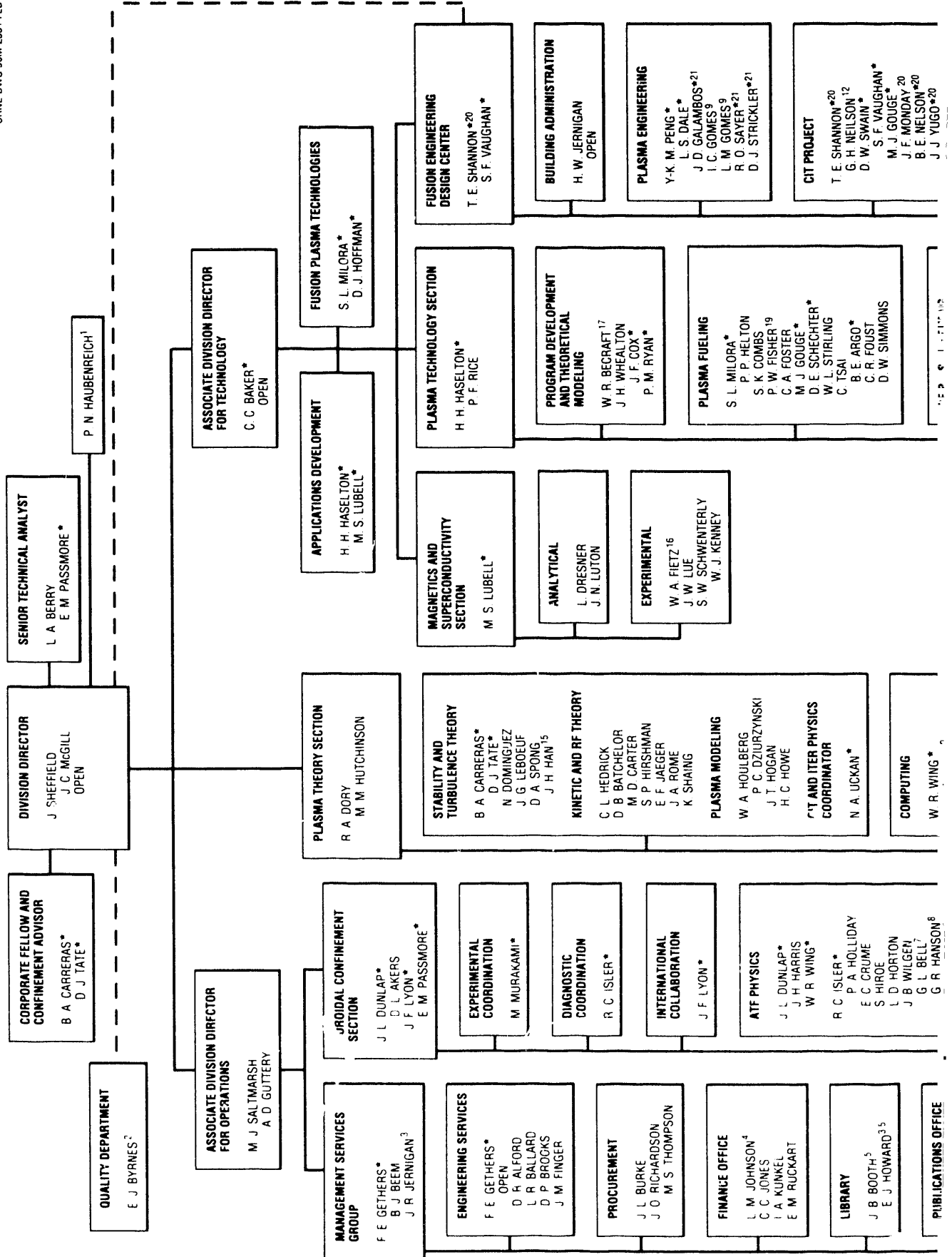
Appendix 3
FUSION ENERGY DIVISION
ORGANIZATION CHART

2

ORNL-DWG 90M-2331 FED

FUSION ENERGY DIVISION

APRIL 1990



S H BUECHLER⁶
 C H JOHNSON⁶
 D Y JOHNSON⁶
 J C NEELEY⁶
 M B NESTOR
 J C PARROTT⁶
 G G ROSS^{3,6}
 D G SHARP
 B J SMITH⁶
 P A SUMMER⁶

A L ZELINSKI¹⁰
 J J ZELINSKI¹⁰
 S C ACETO¹⁰
 J F LYON*
 E M PASSMORE*
 R J COLCHIN
 M R WADE⁸
 A C ENGLAND
 S L PAINTER³
 D A RASMUSSEN
 J M GOSSETT¹¹
 K C KLOS⁸
 T M RAYBURN⁹
 M MURAKAMI*

OPEN
 D R OVERBEY
 K A STEWART
 D T FEHLING
 C E GIBSON
 T C PATRICK

- * DUAL CAPACITY
- ¹ ASSIGNMENT - IAEA VIENNA
- ² QUALITY DEPARTMENT
- ³ PART-TIME
- ⁴ FINANCE AND MATERIALS DIVISION
- ⁵ INFORMATION SERVICES DIVISION
- ⁶ PUBLICATIONS DIVISION
- ⁷ AUBURN UNIVERSITY
- ⁸ GEORGIA INSTITUTE OF TECHNOLOGY
- ⁹ UNIVERSITY OF TENNESSEE
- ¹⁰ RP1
- ¹¹ TENNESSEE TECH
- ¹² ASSIGNMENT - PRINCETON PLASMA PHYSICS LABORATORY
- ¹³ ASSIGNMENT - GENERAL ATOMICS
- ¹⁴ ON LOAN TO PHYSICS DIVISION
- ¹⁵ UNIVERSITY OF TEXAS
- ¹⁶ ASSIGNMENT - DOE/WASHINGTON
- ¹⁷ GRUMMAN AEROSPACE CORPORATION
- ¹⁸ METALS AND CERAMICS DIVISION
- ¹⁹ CHEMICAL TECHNOLOGY DIVISION
- ²⁰ ENGINEERING
- ²¹ COMPUTING AND TELECOMMUNICATIONS DIVISION
- ²² WESTINGHOUSE ELECTRIC CORPORATION

ATF OPERATIONS
 J C GLOWIENKA
 P L FARNSWORTH
 R A LANGLEY
 G H HENKEL
 L A MASSENGILL
 W J REDMOND
 C R SCHAICH
 J L YARBER

ATF PROJECTS
 T C JERNIGAN
 G R DYER

EDGE PHYSICS AND PARTICLE CONTROL
 P K MODUSZEWSKI
 R W JONES
 D L HILLIS
 C C KLEPPER
 M M MENON
 J E SIMPKINS
 T UCKAN
 T F RAYBURN
 C L STOKELY⁸

SPECIAL ASSIGNMENTS
 ES&H UPGRADE - F E GETHERS
 SAFETY OFFICER - F E GETHERS
 ENVIRONMENTAL PROTECTION OFFICER - J M FINGER
 RADIATION CONTROL OFFICER - A C ENGLAND
 COMPUTER SECURITY OFFICER - D R OVERBEY
 AFFIRMATIVE ACTION - P A HOLLIDAY

D J HOFFMAN*
 E G ELLIOTT
 G A WHITE
 F W BAITY
 G C BARBER*
 T S BIGELOW
 W L GARDNER
 R H SOULDING
 G R HASTE
 P M RYAN*
 D E SCHECHTER*
 T D SHEPARD
 T L WHITE*
 B E ARGO*
 A FADNEK
 M KWON⁸
 R L LWESEY
 F SLUSS
 D O SPARKS*

CERAMIC HEATING
 H D KIMREY
 S C FORRESTER
 J O KIGGANS¹⁸

ELECTRICAL ENGINEERING
 G C BARBER*
 R E WRIGHT*
 J F COX*
 B E ARGO*
 D O SPARKS*

WASTE PROCESSING
 T L WHITE*
 S L McNAIR¹⁹

ITER PROJECT
 C C BAKER*
 D C LOUSTEAU²⁰
 D W SWAIN*
 N A UCKAN*
 L S DALE*
 M K BULLOCK²⁰
 C A FLANAGAN²²
 P J FOGARTY²⁰
 J D GALAMBOS*²¹
 M J GOUGE*
 B E NELSON*²⁰
 R O SAYER*²¹
 D J STRICKLER*²¹
 J J YUGO*²⁰

ARIES PROJECT/IST
 Y-K M PENG*

INTERNAL DISTRIBUTION

- 1-5. R. G. Alsmiller
6. F. W. Baity
- 7-11. C. C. Baker
12. L. R. Baylor
13. W. R. Becraft
14. J. D. Bell
15. R. D. Benson
16. L. A. Berry
- 17-21. E. E. Bloom
22. J. L. Burke
23. B. A. Carreras
24. L. A. Charlton
25. R. E. Clausing
26. R. J. Colchin
27. S. K. Combs
28. E. C. Crume, Jr.
29. W. K. Dagenhart
30. W. R. DeVan
31. N. Dominguez
- 32-36. R. A. Dory
37. L. Dresner
- 38-42. J. L. Dunlap
43. G. R. Dyer
44. W. A. Fietz
45. P. W. Fisher
46. S. C. Forrester
47. R. H. Fowler
48. W. Fulkerson
49. W. L. Gardner
- 50-54. F. E. Gethers
55. R. W. Glass
56. J. C. Glowienka
57. R. C. Goldfinger
58. R. H. Goulding
59. D. C. Gregory
- 60-64. H. H. Haselton
65. G. R. Haste
66. G. H. Henkel
67. S. Hiroe
68. D. J. Hoffman
69. J. A. Holmes
70. L. D. Horton
71. W. A. Houlberg
72. D. W. Jared
73. H. W. Jernigan
74. T. C. Jernigan
75. C. C. Klepper
76. J-N. Leboeuf
77. D. K. Lee
78. R. P. Leinius
- 79-83. M. S. Lubell
84. J. N. Luton, Jr.
85. J. F. Lyon
86. M. M. Menon
87. F. W. Meyer
88. S. L. Milora
- 89-93. P. K. Mioduszewski
94. O. B. Morgan
95. R. N. Morris
96. M. Murakami
97. G. H. Neilson
- 98-99. M. B. Nestor
100. D. R. Overbey
101. S. L. Painter
102. V. K. Paré
- 103-104. J. C. Parrott
105. Y-K. M. Peng
106. R. A. Phaneuf
107. D. A. Rasmussen
108. R. K. Richards
109. J. A. Rome
110. M. W. Rosenthal
111. R. W. Roussin
112. P. M. Ryan

- | | | | |
|----------|-------------------|----------|--|
| 113–117. | M. J. Saltmarsh | 141. | T. L. White |
| 118. | C. R. Schaich | 142. | F. W. Wiffen |
| 119. | D. E. Schechter | 143. | J. B. Wilgen |
| 120. | S. W. Schwenterly | 144. | W. R. Wing |
| 121–125. | T. E. Shannon | 145. | R. E. Wright |
| 126–130. | J. Sheffield | 146. | R. B. Wysor |
| 131. | W. L. Stirling | 147. | R. A. Zuhr |
| 132. | D. J. Strickler | 148–149. | Laboratory Records Department |
| 133. | D. W. Swain | 150. | Laboratory Records, ORNL-RC |
| 134. | A. Trivelpiece | 151. | Central Research Library |
| 135. | C. C. Tsai | 152. | Document Reference Section |
| 136. | N. A. Uckan | 153. | Fusion Energy Division Library |
| 137. | T. Uckan | 154–156. | Engineering Technology/Fusion Energy
Division Publications Office |
| 138. | W. I. van Rij | 157. | ORNL Patent Office |
| 139. | J. H. Whealton | | |
| 140. | J. A. White | | |

EXTERNAL DISTRIBUTION

Office of Fusion Energy, Office of Energy Research, Germantown, U.S.
Department of Energy, Washington, DC 20545

- 158. D. S. Beard, ER-531
- 159. S. E. Berk, ER-533
- 160. R. A. Blanken, ER-542
- 161. C. Bolton, ER-55
- 162. M. Cohen, ER-533
- 163. D. H. Crandall, ER-542
- 164. R. Dagazian, ER-55
- 165. N. A. Davies, ER-51
- 166. V. Der, ER-531
- 167. W. F. Dove, ER-543
- 168. R. J. Dowling, ER-53
- 169. S. A. Eckstrand, ER-55
- 170. T. V. George, ER-531
- 171. T. R. James, ER-55
- 172. A. Katz, ER-52
- 173. D. Markevich, ER-55
- 174. W. Marton, ER-55
- 175. R. H. McKnight, ER-542
- 176. G. R. Nardella, ER-533
- 177. D. B. Nelson, ER-54
- 178. E. Oktay, ER-55
- 179. A. Opdenaker, ER-532
- 180. R. E. Price, ER-55
- 181. T. C. Reuther, ER-533

- 182. W. Sadowski, ER-541
- 183. C. Sege, ER-52
- 184. H. S. Staten, ER-531
- 185. J. W. Willis, ER-55

Lawrence Livermore National Laboratory, P.O. Box 5511, Livermore, CA 94550

- 186. J. Denavit, L-18
- 187. F. Coengen
- 188. C. D. Henning, L-644
- 189. B. G. Logan
- 190. L. D. Pearlstein, L-630
- 191. R. F. Post
- 192. K. I. Thomassen, L-637

Los Alamos National Laboratory, P.O. Box 1663, Los Alamos, NM 87545

- 193. J. L. Anderson
- 194. H. Dreicer, MS-F640
- 195. R. A. Krakowski
- 196. R. K. Linford, MS-F646
- 197. J. D. Rogers

National Institute of Standards and Technology, University of Colorado, Campus Box 440, Boulder, CO 80309

- 198. V. D. Arp
- 199. A. Clark
- 200. G. H. Dunn
- 201. A. V. Phelps
- 202. F. R. Fickett

Naval Research Laboratory, Washington, DC 20375

- 203. W. R. Ellis
- 204. B. Hui
- 205. A. Robson, Code 4760

Oak Ridge Associated Universities, P.O. Box 117, Oak Ridge, TN 37831

- 206–286. J. M. Haffey, Information Services
- 287. A. M. Weinberg, IEA
- 288. University Programs Department
- 289. Institute for Energy Analysis

Pacific Northwest Laboratories, Battelle Boulevard, P.O. Box 999, Richland, WA 99352

- 290. D. A. Dingee
- 291. B. F. Gore
- 292. L. L. Schmid

Princeton Plasma Physics Laboratory, P.O. Box 451, Princeton, NJ 08543

- 293. T. K. Chu
- 294. P. L. Colestock
- 295. R. C. Davidson
- 296. J. File
- 297. R. B. Fleming
- 298. J. W. French
- 299. R. J. Goldston
- 300. K. W. Hill
- 301. J. C. Hosea
- 302. S. M. Kaye
- 303. D. M. Meade
- 304. R. G. Mills
- 305. P. H. Rutherford
- 306. J. A. Schmidt
- 307. M. L. Shoaf
- 308. T. H. Stix
- 309. S. Yoshikawa

Sandia National Laboratories, P.O. Box 5800, Albuquerque, NM 87185

- 310. W. B. Gauster, Div. 1837
- 311. F. L. Vook, Org. 1100
- 312. J. B. Whitley, Div. 6248

Bechtel National, Inc., P.O. Box 3965, San Francisco, CA 94119

- 313. E. von Fischer
- 314. H. K. Forsen, Advanced Technology Division

EG&G ORTEC, 100 Midland Road, Oak Ridge, TN 37830

- 315. J. Ayers
- 316. D. A. Gedcke

General Atomics, P.O. Box 85608, San Diego, CA 92138-5608

- 317. R. L. Freeman
- 318. R. Harder
- 319. C. Moeller
- 320. D. O. Overskei
- 321. T. Ohkawa
- 322. J. M. Rawls
- 323. T. Simonen
- 324. R. D. Stambaugh
- 325. T. Tamano

General Dynamics—Convair Division, P.O. Box 85377, San Diego, CA 92138

- 326. R. F. Beuligmann
- 327. D. S. Hackley
- 328. R. A. Johnson, MZ 16-1070

Grumman Corporation, Bethpage, NY 11714

- 329. R. Botwin
- 330. A. Favale
- 331. C. von Keszycski
- 332. F. Thomas

TRW, Inc., 1 Space Park, Redondo Beach, CA 92078

- 333. J. Gordon
- 334. N. H. Lazar
- 335. J. A. Maniscalco

Westinghouse Electric Corporation, Advanced Reactors Division, P.O. Box 158,
Madison, PA 15663

- 336. A. Anderson
- 337. G. G. Gibson

Atlanta University, Atlanta, GA 30314

- 338. C. R. Handy
- 339. R. E. Mickens

Auburn University, Auburn, AL 36849-3511

- 340. M. S. Pindzola, Physics Department
- 341. D. G. Swanson
- 342. R. F. Gandy, Physics Department

Denison University, Granville, OH 43032

- 343. W. A. Hoffman
- 344. R. R. Winters

University of California at Los Angeles, Los Angeles, CA 90024

- 345. M. Abdou
- 346. R. W. Conn, Mechanical, Aerospace, and Nuclear Engineering Department

University of California at San Diego, La Jolla, CA 92093

- 347. M. N. Rosenbluth
- 348. P. H. Diamond

Georgia Institute of Technology, Atlanta, GA 30332

- 349. J. N. Davidson
- 350. R. K. Feeney, School of Electrical Engineering
- 351. W. M. Stacey, School of Nuclear Engineering
- 352. C. E. Thomas, School of Nuclear Engineering
- 353. E. W. Thomas, School of Physics

University of Illinois, Urbana, IL 61801

- 354. K. K. Kim, Department of Electrical Engineering
- 355. W. Sutton, Department of Nuclear Engineering

University of Maryland, College Park, MD 20742

- 356. V. L. Granatstein, Electrical Engineering Department
- 357. H. R. Griem, Laboratory for Plasma and Fusion Studies
- 358. C. S. Liu, Department of Physics and Astronomy

Massachusetts Institute of Technology, 77 Massachusetts Ave., Cambridge, MA
02139 .

- 359. G. Bekefi, 36-213
- 360. D. R. Cohn
- 361. B. Coppi, 26-217
- 362. J. P. Freidberg, NW16-240
- 363. K. Molvig, NW16-240
- 364. D. B. Montgomery, NW17-288
- 364. R. R. Parker, NW16-288
- 366. J. Schultz
- 367. R. J. Thome, NW17-223

Rensselaer Polytechnic Institute, P.O. Box 2000, Troy, NY 12181

- 368. R. L. Hickok
- 369. W. C. Jennings
- 370. D. Steiner

The University of Tennessee, Knoxville, TN 37916

- 371. I. Alexeff, Dept. of Electrical Engineering
- 372. E. G. Harris, Dept. of Physics
- 373. J. R. Roth, Dept. of Electrical Engineering
- 374. P. N. Stevens, Dept. of Nuclear Engineering

University of Texas, Austin, TX 78712

- 375. D. Baldwin, Institute for Fusion Studies, RLM 11.222
- 376. H. L. Berk, Institute for Fusion Studies
- 377. K. W. Gentle, Dept. of Physics
- 378. D. W. Ross, Dept. of Physics
- 379. H. H. Woodson, Dept. of Electrical Engineering
- 380. A. J. Wootton, Fusion Research Center

University of Wisconsin, Madison, WI 53706

- 381. J. D. Callen, Nuclear Engineering Department
- 382. J. R. Conrad, Nuclear Engineering Department
- 383. D. W. Kerst
- 384. G. Kulcinski
- 385. D. C. Larbalestier
- 386. J. L. Shohet, Torsatron/Stellarator Laboratory
- 387. J. C. Sprott, Department of Physics

Research School of Physical Sciences, Australian National University, P.O. Box 4, Canberra, A.C.T. 2601, Australia

- 388. S. M. Hamberger, Plasma Research Laboratory
- 389. Plasma Research Laboratory

Plasma Research Section, Physics Division, Forskningscenter, Risø, P.O. Box 49, DK-4000 Roskilde, Denmark

- 390. C. T. Chang
- 391. V. O. Jensen
- 392. O. Kofoed-Hansen

JET Joint Undertaking, Abingdon, Oxon OX14 3EA, United Kingdom

- 393. J. G. Cordey
- 394. K. J. Dietz
- 395. D. Duchs
- 396. A. Gibson
- 397. M. Keilhacker
- 398. P. H. Rebut
- 399. P. E. Stott
- 400. T. E. Stringer
- 401. E. Thompson
- 402. Library

UKAEA, Culham Laboratory, Abingdon, Oxon OX14 3DB, United Kingdom

- 403. R. Hancox
- 404. T. C. Hender
- 405. Library
- 406. M. W. Lomer
- 407. D. C. Robinson
- 408. D. R. Sweetman
- 409. J. B. Taylor

CEN/Cadarache, B.P. 1, F-13108 Saint-Paul-lez-Durance, France

- 410. C. Mercier
- 411. J. Tachon
- 412. Bibliothèque

CEN/Saclay, B.P. No. 2, F-91191 Gif-sur-Yvette, France

- 413. H. Desportes, STIPE
- 414. J. C. Lottin

KFA Jülich, Postfach 1913, D-5170 Jülich 1, Federal Republic of Germany

- 415. Bibliothek
- 416. H. Conrads
- 417. E. Hintz
- 418. A. Rogister
- 419. G. Wolf

Kernforschungszentrum Karlsruhe GmbH, Postfach 3640, D-7500 Karlsruhe 1,
Federal Republic of Germany

- 420. O. Hagen, Nuclear Engineering Institute
- 421. W. Klose, Division of Neutron Technology and Basic Research
- 422. P. Komarek, Institute for Technical Physics
- 423. A. Ulbricht, Institute for Technical Physics
- 424. J. E. Vetter, Nuclear Fusion Project
- 425. Bibliothek

Max-Planck Institut für Plasmaphysik, D-8046 Garching, Federal Republic of
Germany

- 426. Bibliothek
- 427. G. von Gierke
- 428. G. Grieger
- 429. J. Junker
- 430. M. Kaufman
- 431. M. Keilhacker
- 432. A. Knobloch
- 433. K. Lackner
- 434. L. L. Lengyel
- 435. D. Pfirsch
- 436. K. Pinkau
- 437. H. Renner
- 438. A. Schlüter
- 439. R. Toschi
- 440. F. Wagner

ENEA Centro di Frascati, C.P. 65, I-00044 Frascati (Roma), Italy

- 441. A. Bracci, Fusion Department
- 442. H. E. Knoepfel
- 443. Library
- 444. N. Sacchetti, Technology Division
- 445. G. Sacerdoti
- 446. M. Spadoni, Fusion Reactor Engineering Project

International Centre for Theoretical Physics, P.O. Box 586, I-34100 Trieste, Italy

- 447. A. M. Hamende
- 448. Library

National Institute for Fusion Science, Chikusa-ku, Nagoya 464-01, Japan

- 449. T. Amano
- 450. M. Fujiwara
- 451. K. Husimi
- 452. A. Iiyoshi
- 453. H. Ikegami
- 454. S. Okamura
- 455. Research Information Center
- 456. T. Uchida
- 457. Library

Japan Atomic Energy Research Establishment, Naka Fusion Research Establishment, Naka-machi, Naka-gun, Ibaraki-ken 311-02, Japan

- 458. S. Shimamoto
- 459. K. Tomabechi
- 460. M. Yoshikawa
- 461. Library

Plasma Physics Laboratory, Kyoto University, Gokasho, Uji, Kyoto 531, Japan

- 462. Library
- 463. K. Uo
- 464. M. Wakatani
- 465. T. Obiki

Plasma Research Center, University of Tsukuba, Sakura-mura, Niihari-gun, Ibaraki 305, Japan

- 466. Y. Kiwamoto
- 467. S. Miyoshi

FOM-Instituut voor Plasmafysica, Rijnhuizen, Postbus 1207, NL-3430 BE Nieuwegein, The Netherlands

- 468. M. J. van der Wiel
- 469. Library

Division de Fusion Termonuclear, EURATOM/CIEMAT, Avenida Complutense 22, 28040 Madrid, Spain

- 470. J. Alvarez-Rivas
- 471. A. Perez Navarro
- 472. M. Soler
- 473. B. Zurro

Centre de Recherches en Physique des Plasmas, Ecole Polytechnique Fédérale de Lausanne, 21 Avenue des Bains, CH-1007 Lausanne, Switzerland

- 474. Bibliothèque
- 475. F. Troyon

Paul Scherrer Institute, CH-5234 Villigen, Switzerland

- 476. Library
- 477. G. Vécsey

I. V. Kurchatov Institute of Atomic Energy, P.O. Box 3402, 123182 Moscow, U.S.S.R.

- 478. G. A. Eliseev
- 479. V. D. Shafranov

Institute of General Physics, U.S.S.R. Academy of Sciences, Ulitsa Vavilova 38,
1779246 Moscow, U.S.S.R.

- 480. I. S. Danilkin
- 481. L. M. Kovrizhnykh
- 482. I. Shpigel

Kharkov Physico-Technical Institute, Ukrainian S.S.R. Academy of Sciences,
310108 Kharkov, U.S.S.R.

- 483. A. Y. Omelchenko
- 484. O. S. Pavlichenko

- 485. R. E. Aamodt, Lodestar Research Corporation, P.O. Box 4545, Boulder, CO 80306
- 486. E. Anabitarte, Avenida de los Castros s/n, Dpt. Fisica Aplicada, Universidad de Cantabria, 39005 Santander, Spain
- 487. W. D. Ard, McDonnell Douglas Astronautics Company, P.O. Box 516, St. Louis, MO 63166
- 488. M. P. G. Avanzini, NIRA S.p.A., C.P. 1166, 16100 Genova, Italy
- 489. W. Bauer, Dept. 8340, Sandia National Laboratories, P.O. Box 969, Livermore, CA 94550
- 490. P. R. Bell, 132 Westlook Circle, Oak Ridge, TN 37830
- 491. R. A. Berry, Varian Associates, Inc., 611 Hansen Way, Palo Alto, CA 94303
- 492. G. Bohner, Forschungslabororien, Siemens AG, Postfach 325, D-8520 Erlangen 2, Federal Republic of Germany
- 493. R. A. E. Bolton, IREQ Hydro-Quebec Research Institute, 1800 Montée Ste.-Julie, Varennes, P.Q. JOL 2P0 Canada
- 494. M. H. Brennan, Australian Atomic Energy Commission, Lucas Heights Research Laboratories, New Illawara Road, Lucas Heights, Private Mail Bag, Sutherland, N.S.W., Australia 2232
- 495. G. Briffod, CEN/Grenoble, B.P. 85X, F-38041 Grenoble, France
- 496. P. Catto, Lodestar Research Corporation, P.O. Box 4545, Boulder, CO 80306
- 497. R. N. Cherdack, Burns & Roe, Inc., 700 Kinder Kamack Road, Oradell, NJ 07649
- 498. G. Clemens, University Library of Essen, Gustav-Hicking-Strasse 15, D-4300 Essen, Federal Republic of Germany
- 499. E. W. Collings, Battelle Memorial Institute, 505 King Ave., Columbus, OH 43201
- 500. J. G. Crocker, EG&G Idaho, Inc., Idaho National Engineering Laboratory, Idaho Falls, ID 83401
- 501. F. L. Culler, Electric Power Research Institute, P.O. Box 10412, Palo Alto, CA 94303
- 502. R. A. Dandl, Applied Microwave Plasma Concepts, Inc., 2075 N. Portico de Nogal, Carlsbad, CA 92009
- 503. S. O. Dean, Fusion Power Associates, Inc., 2 Professional Drive, Suite 248, Gaithersburg, MD 20879
- 504. H. W. Deckman, Advanced Energy Systems Laboratory, Exxon Research and Engineering Company, P.O. Box 8, Linden, NJ 07306
- 505. Department of Nuclear Engineering Sciences, 202 Nuclear Science Center, University of Florida, Gainesville, FL 32611
- 506. Director, Technical Library, Defense Atomic Support Agency, Sandia Base, Albuquerque, NM 87185

507. D. R. Dobrott, Science Applications International Corporation, P.O. Box 2351, La Jolla, CA 92037
508. T. J. Dolan, Department of Nuclear Engineering, University of Missouri, Rolla, MO 65401
509. G. W. Donaldson, School of Electrical Engineering, University of New South Wales, P.O. Box 1, Kensington, N.S.W., Australia
510. E. Dullni, NB-05/639, Experimentalphysik, Ruhr-Universität Bochum, D-4630 Bochum, Federal Republic of Germany
511. R. W. Fast, Experimental Facilities, National Accelerator Laboratory, P.O. Box 500, Batavia, IL 60510
512. T. K. Fowler, University of California at Berkeley, Berkeley, CA 92740
513. Y. Furuto, Superconducting Group, Central Research Laboratory, Furukawa Electric Company, Ltd., 915, 2-Chome, Futaba, Shinagawaku, Tokyo 141, Japan
514. W. F. Gauster, Neuwaldeggerstrasse 9-2-5, A-1170 Vienna, Austria
515. F. C. Gilbert, Division of Military Applications, U.S. Department of Energy, Washington, DC 20545
516. H. B. Gilbody, Department of Pure and Applied Physics, Queens University, Belfast BT7 1NN, Northern Ireland, United Kingdom
517. R. W. Gould, California Institute of Technology, Building 116-81, Pasadena, CA 91125
518. D. C. Griffin, Rollins College, Winter Park, FL 32789
519. R. A. Gross, Department of Applied Physics & Nuclear Engineering, Columbia University, New York, NY 10027
520. T. G. Heil, Department of Physics and Astronomy, University of Georgia, Athens, GA 30602
521. W. R. Husinsky, Technical University of Vienna, Karlsplatz 13, A-1040 Vienna, Austria
522. S. Ihara, Central Research Laboratory, 8th Department, Hitachi Ltd., Kokubunji, Tokyo 185, Japan
523. M. Iwamoto, Central Research Laboratory, Mitsubishi Electric Corporation, 80 Nakano, Minamishimizu, Amagasaki, Hyogo 661, Japan
524. C. K. Jones, Cryogenic Research Laboratory, Westinghouse Electric Corporation, Research and Development Center, 1310 Beulah Road, Pittsburgh, PA 15235
525. R. W. Jones, Physics Department, Emporia State University, 1200 Commercial, Emporia, KS 66801
526. R. Jones, Department of Physics, National University of Singapore, Bukit Timah Road, Singapore 10.25
527. D. Klein, Westinghouse Electric Corporation, Strategic Operations Division, P.O. Box 598, Pittsburgh, PA 15230
528. A. C. Kolb, Maxwell Laboratories, Inc., 9244 Balboa Avenue, San Diego, CA 92123
529. K. Koyama, Electrotechnical Laboratory, 1-1-4 Umezono, Sakura-mura, Niihari-gun, Ibaraki-ken 305, Japan
530. N. A. Krall, Krall Associates, 1070 America Way, Del Mar, CA 92014
531. A. H. Kritz, 69 Lillie Street, Princeton Junction, NJ 08550
532. K. Kuroda, Central Research Laboratory, 1-280, Higa Shiko Igakubo, Kokubumji, Tokyo 185, Japan

533. Laboratory for Plasma and Fusion Studies, Department of Nuclear Engineering, Seoul National University, Shinrim-dong, Gwanak-ku, Seoul 151, Korea
534. Laser Fusion Group, Department of Mechanical and Aerospace Science, River Campus Station, University of Rochester, Rochester, NY 14627
535. B. Lehnert, Department of Plasma Physics and Fusion Research, Royal Institute of Technology, S-10044 Stockholm 70, Sweden
536. C. M. Loring, EIMAC Division of Varian, 301 Industrial Way, San Carlos, CA 94070-2682
537. V. A. Maroni, CEN 205, Argonne National Laboratory, Argonne, IL 60439
538. E. A. Mason, Brown University, Providence, RI 02912
539. D. G. McAlees, Advanced Nuclear Fuels Corporation, 600 108th Ave., NE, Bellevue, WA 98009
540. O. Mitarai, Department of Electrical Engineering, Kumamoto Institute of Technology, Ikeda 4-22-1, Kumamoto 860, Japan
541. F. Moon, Department of Theoretical and Applied Mechanics, Cornell University, Ithaca, NY 14850
542. T. J. Morgan, Physics Department, Wesleyan University, Middletown, CT 06457
543. K. G. Moses, JAYCOR, 2811 Wilshire Boulevard, Suite 690, Santa Monica, CA 90403
544. C. Oberly, Aero Propulsion Laboratory, Power Distribution Branch, Wright-Patterson Air Force Base, OH 45433
545. T. Ogasawara, Department of Physics, College of Science and Technology, Nihon University, Kanda-Surugadai, Chiyoda-ku, Tokyo 101, Japan
546. H. Ogiwara, Toshiba Research and Development Center, 1 Komukai Tsohiba-cho, Saiwai, Kawasaki, Kanagawa 210, Japan
547. R. J. Onega, Nuclear Engineering Group, College of Engineering, Virginia Polytechnic Institute and State University, Blacksburg, VA 24061
548. B. Outten, Jr., Western Metal Products Company, 1300 Weber Street, Orlando, FL 32803
549. D. Palumbo, via Gabriele d'Annunzio 52, Palermo I-90144, Italy
550. K. Prélec, Brookhaven National Laboratory, Upton, NY 11973
551. F. C. Rock, Plasma Physics Laboratory, Department of Physics and Astronomy, Brigham Young University, Provo, UT 84602
552. R. H. Rohrer, Department of Physics, Emory University, Atlanta, GA 30322
553. P. A. Sanger, Airco, 600 Milik St., Carteret, NJ 07008
554. S. St. Lorant, Stanford Linear Accelerator Center, P.O. Box 4349, Stanford, CA 94305
555. M. M. Satterfield, The Nucleus, 761 Emory Valley Road, Oak Ridge, TN 37830
556. Y. Sawada, Heavy Apparatus Engineering Laboratory, Toshiba Corp., 2-4 Suehiro-cho, Tsurumi-ki, Yokohama 230, Japan
557. J. H. Schneider, Joint Research Centre, Ispra Establishment, I-21020 Ispra (Varese), Italy
558. G. R. Siegel, Tennessee Valley Authority, 25 33A Missionary Ridge Place, Chattanooga, TN 37402
559. Z. J. J. Stekly, Magnetics Corporation of America, 47 Hartz St., No. 2, Gloucester, MA 01930
560. B. P. Strauss, Magnetics Corporation of America, 179 Bear Hill Rd., Waltham, MA 02154

561. U. Stiefel, Eidg. Institut für Reaktorforschung, CH-5301 Würenlingen, Switzerland
562. K. Tachikawa, Chief, Electric Materials Laboratory, National Research Institute for Metals, 3-12, 2-Chome, Nakameguro, Meguru, Tokyo, Japan
563. R. J. Taylor, Center for Plasma Physics and Fusion Engineering, University of California, Los Angeles, CA 90024
564. L. F. Temple, Construction Project Management Support Division, ER-15, U.S. Department of Energy, Washington, DC 20545
565. D. P. Tewari, Department of Physics, Indian Institute of Technology, New Delhi 110016, India
566. M. Thumm, Institut für Plasmaforschung, Pfaffenwaldring 31, D-7000 Stuttgart 80, Federal Republic of Germany
567. J. F. Traexler, Westinghouse Electric Corp., Quadrangle 2WII-203, Orlando, FL 32817
568. G. Vahala, Department of Physics, College of William and Mary, Williamsburg, VA 23185
569. T. C. Varljen, Westinghouse Hanford, P.O. Box 1970, Richland, WA 99352
570. R. Varma, Physical Research Laboratory, Navrangpura, Ahmedabad 380009, India
571. C. Walters, Technology Division, Building R25, Rutherford Laboratory, Chilton, Didcot, Oxon OX11 0QX, United Kingdom
572. C. N. Watson-Munro, University of Sydney, Wills Plasma Project, Sydney, N.S.W., Australia
573. H. Weitzner, Courant Institute for Mathematical Sciences, New York University, 251 Mercer St., New York, NY 10012
574. J. Wong, Supercon, Inc., 9 Erie Drive, Natick, MA 01760
575. S. B. Woo, Department of Physics, University of Delaware, Newark, DE 19711
576. H. Yoshikawa, Manager, Materials Engineering, Hanford Engineering Development Laboratory, P.O. Box 1970, Richland, WA 99352
577. V. A. Glukhikh, Scientific-Research Institute of Electro-Physical Apparatus, 188631 Leningrad, U.S.S.R.
578. D. D. Ryutov, Institute of Nuclear Physics, Siberian Branch of the Academy of Sciences of the U.S.S.R., Sovetskaya St. 5, 630090 Novosibirsk, U.S.S.R.
579. Deputy Director, Southwestern Institute of Physics, P.O. Box 15, Leshan, Sichuan, China (PRC)
580. Director, The Institute of Plasma Physics, P.O. Box 26, Hefei, Anhui, China (PRC)
581. M-L. Xue, Institute of Mechanics, Academia Sinica, Beijing, China (PRC)
582. Office of Assistant Manager for Energy Research and Development, U.S. Department of Energy, Oak Ridge Operations Office, P.O. Box 2001, Oak Ridge, TN 37831-8705
- 583-622. Given distribution as shown in DOE/OSTI-4500/R75, Energy Research (Category UC-420, Magnetic Fusion Energy) (40 copies)

END

**DATE
FILMED**

11 108 191

